

MASARYK UNIVERSITY
FACULTY OF SCIENCE
DEPARTMENT OF EXPERIMENTAL BIOLOGY

**Role of transcription cyclin-dependent
kinases and their cyclins in cellular
processes**

HABILITATION THESIS

Jiří Kohoutek

**MUNI
SCI**

BRNO 2024

ACKNOWLEDGEMENTS

I would like to express my gratitude to my wife Sabina and my two daughters Sara and Sona for their patience, understanding, and continuous support. I would like to dedicate this work to my mom for all her love and support.

My great thank belongs to the previous and current members of our research group. I would like to thank especially prof. Šmarda who was at the beginning of my scientific career and inspired me to pursue science.

CONTENT

LIST OF ABBREVIATIONS	iv
COMMENTARY	vi
1 INTRODUCTION	1
1.1 History of discoveries of cell cycle regulators.....	1
1.2 Atypical cyclin-dependent kinases	3
1.3 Cyclin-dependent kinases regulating transcription.....	3
2 FUNCTION OF P-TEFB IN CONTROL OF ELONGATION PHASE OF TRANSCRIPTION.....	4
2.1 Association of P-TEFb in Small and Large complexes	4
2.2 Regulation of elongation phase of transcription by P-TEFb	9
3 ROLE OF CDK12 AND CDK13 IN THE REGULATION OF TRANSCRIPTION.....	11
3.1 Defining CDK12 and CDK13 complexes	11
4 IMPACT OF TRANSCRIPTION KINASES AND THEIR ASSOCIATED CYCLINS IN DEVELOPMENTAL PROCESSES	16
4.1 Cyclin T2 and its role in early development	16
4.2 Ineffective selection of autoreactive T cells in the absence of cyclin T1.....	17
4.3 Impact of CDK13 loss on development	18
4.4 Role of CDK13 in cranial neurogenesis.....	21
4.5 Function of CDK12 during the oogenesis	24
5 SUMMARY AND FUTURE DIRECTIONS	28
6 CITATIONS	29
7 APPENDICES	42

LIST OF ABBREVIATIONS

4E-BP1	Eukaryotic Translation Initiation Factor 4E Binding Protein 1
7SK snRNA	7SK Small Nuclear RNA
AFF1	ALF Transcription Elongation Factor 1
ATR	Ataxia Telangiectasia and Rad3-Related Protein
BRCA-1	Breast Cancer-Associated Gene 1
BRD4	Bromodomain Containing 4
CDC	Cell Division Cycle
CDK	Cyclin-Dependent Kinase
CHDFIDD	Congenital Heart Defects, Dysmorphic Facial Features and Intellectual Developmental Disorder
CHK1	Check Kinase 1
CLP1	Cardiac Lineage-Associated Protein 1
CTD	C Terminal Domain
Cyc	cyclin
DDR	DNA Damage Repair
DSIF	DRB Sensitivity Inducing Factor
E	Embryonic Day
EDG-1	Estrogen Down-Regulated Gene
GRN	Gene Regulatory Network
GV	Germinal Vesicle
HCT116	Human Colorectal Carcinoma Cell Line
HEK293	Human Embryonic Kidney Cell Line
HER2	Human Epidermal Growth Factor Receptor 2
HEXIM1	Hexamethylene Bis-acetamide Inducible 1
HR	Homologous Recombination
Jak/Stat	Janus Kinase/Signal Transducers and Activators of Transcription
LARP7	La Ribonucleoprotein 7
LPS	Lipopolysaccharide
MAT1	Ménage À Quatre
MDA-MB-231	M D Anderson - Metastatic Breast – 231

MEPCE	7SK Methylphosphate Capping Enzyme
MPF	Mitotic Promoting Factor
NELF	Negative Elongation Factor
NHEJ	Nonhomologous-End Joining
P21	Cyclin Dependent Kinase Inhibitor 1A
PARP1	Poly(ADP-ribose) Polymerase 1
PI3K/Akt	Phosphoinositide 3-Kinase/AKT Serine/Threonine Kinase 1
PIC	Promoter Initiation Complex
PKC	Protein Kinase C
PMA	Phorbol 12-Myristate 13-Acetate
POF	Premature Ovarian Failure
PP1 α	Protein Phosphatase 1 Catalytic Subunit Alpha
P-TEFb	Positive Transcription Elongation Factor b
RNAPII	RNA Polymerase II
TP53	Tumor Protein P53
TRC	Transcription Replication Conflict
ZGA	Zygotic Gene Activation
ZP3	Zona Pellucida Glycoprotein 3
γ H2AX	Phosphorylated histone Histone Family Member X

COMMENTARY

The habilitation proposal aims to introduce the role of cyclin-dependent kinases - CDKs in transcription via posttranslational modification of RNA polymerase II - RNAPII. The role of CDKs in the regulation of transcription was recognized about three decades ago, but the actual *modus operandi* is still a mystery, mainly due to sophisticated control of RNAPII posttranslational modifications at several levels. By phosphorylating RNAPII, the CDKs not only control passage through a particular phase of transcription but also control transition between these phases. Over the years, the transition between the initiation and elongation phases of transcription was recognized as a transcriptional control point, similar to checkpoints in the cell cycle, allowing the cell to postpone or rapidly reactivate paused transcription in response to extracellular or intracellular stimuli.

The reactivation of paused transcription is mediated by the activity of positive transcription elongation factor b – P-TEFb, a heterodimer composed of CDK9 and cyclin T1 or T2. To trigger the elongation phase of transcription, P-TEFb must be released from the multiprotein inhibitory complex where it is bound with its cellular inhibitory factors. The first part of the thesis elucidates the composition of this inhibitory complex and describes the mechanics how this complex is formed through mutually abundant interactions of RNA and proteins. Also, the example of disassembly of this complex in response to interferon gamma stimuli is provided as an example of a regulatory network.

The second section is focused on introducing the fascinating biology of newly identified CDK12 and CDK13 on the regulation of RNAPII. In contrast to CDK9 within P-TEFb the CDK12 and CDK13 do not participate in the release of paused RNAPII, rather they influence various cellular processes including DNA replication, regulation of DNA damage genes and cell cycle genes expression, transcription elongation, pre-mRNA processing, RNA turnover, initiation of translation of mRNA subgroups [1–6]. Among these, the impact of CDK12 on the regulation of DNA-damage repair – DDR pathway will be introduced in more detail. The DDR was recently exploited as a valuable target for targeted therapy, especially in connection with the concept of synthetic lethality. Thus, the susceptibility of tumors with nonfunctional CDK12 to treatment with CHK1 inhibitors will be discussed.

The third part is dedicated to the description of CDKs and their associated partners – cyclins, during the regulation of cell differentiation, tissue formation, and complex embryonic development. By employment of several knock-out and conditional knock-out models we were able to demonstrate essential role of cyclin T2 and cyclin K in early preimplantation development, the function of cyclin T1 in a negative selection of autoreactive T cells, impact of CDK13 loss on formation of craniofacial structures and cleft palate, and involvement of CDK12 in transcription of growing oocytes during oogenesis and meiotic maturation.

The list of ten original research articles and three reviews below denotes selected peer-reviewed articles in support of my contributions to the topic of this thesis. The majority of articles were published in Q1 journals. The table below the article describes my contribution to the given manuscript. All manuscripts are attached, numbered as Appendices, and highlighted in green in the main text.

- 1) BARBORIC, Matjaz, **Jirí KOHOUTEK**, Jason P. PRICE, Dalibor BLAZEK, David H. PRICE and B. Matija PETERLIN. Interplay between 7SK snRNA and oppositely charged regions in HEXIM1 direct the inhibition of P-TEFb. *The EMBO journal*. 2005, 24(24), 4291–4303. (JCR 2005; IF = 10,1; Q1 – Cell Biology)

Experimental work (%)	Supervision (%)	Manuscript preparation (%)	Research design (%)
30	0	15	20

- 2) BLAZEK, Dalibor, Matjaz BARBORIC, **Jiri KOHOUTEK**, Irena OVEN and B. Matija PETERLIN. Oligomerization of HEXIM1 via 7SK snRNA and coiled-coil region directs the inhibition of P-TEFb. *Nucleic Acids Research*. 2005, 33(22), 7000–7010. (JCR 2005; IF = 7,5; Q1 – Biochemistry & Molecular Biology)

Experimental work (%)	Supervision (%)	Manuscript preparation (%)	Research design (%)
20	0	20	10

- 3) **KOHOUTEK, Jiri**, Dalibor BLAZEK and B. Matija PETERLIN. Hexim1 sequesters positive transcription elongation factor b from the class II transactivator on MHC class II promoters. *Proceedings of the National Academy of Sciences*. 2006, 103(46), 17349–17354. (JCR 2006; IF = 9,6; Q1 – Multidisciplinary Sciences)

Experimental work (%)	Supervision (%)	Manuscript preparation (%)	Research design (%)
60	0	70	50

- 4) **KOHOUTEK, Jiri**. P-TEFb- the final frontier. *Cell Division*. 2009, 4, 19. (JCR 2009; IF = 4,0; Q2 – Cell Biology)

Experimental work (%)	Supervision (%)	Manuscript preparation (%)	Research design (%)
0	0	100	100

- 5) BLAZEK, Dalibor, **Jiri KOHOUTEK**, Koen BARTHOLOMEEUSEN, Eric JOHANSEN, Petra HULINKOVA, Zeping LUO, Peter CIMERMANCIC, Jernej ULE and B. Matija PETERLIN. The Cyclin K/Cdk12 complex maintains genomic stability via regulation of expression of DNA damage response genes. *Genes & Development*. 2011, 25(20), 2158–2172. (JCR 2011; IF = 11,6; Q1 – Cell Biology)

Experimental work (%)	Supervision (%)	Manuscript preparation (%)	Research design (%)
30	0	30	40

6) **KOHOUTEK, Jiri** and Dalibor BLAZEK. Cyclin K goes with Cdk12 and Cdk13. *Cell Division*. 2012, 7, 12. (JCR 2012; IF = 3,4; Q2 – Cell Biology)

Experimental work (%)	Supervision (%)	Manuscript preparation (%)	Research design (%)
0	0	50	50

7) PACULOVÁ, Hana, Juraj KRAMARA, Šárka ŠIMEČKOVÁ, Radek FEDR, Karel SOUČEK, Ondřej HYLSE, Kamil PARUCH, Marek SVOBODA, Martin MISTRÍK and **Jiří KOHOUTEK**. BRCA1 or CDK12 loss sensitizes cells to CHK1 inhibitors. *Tumour Biology: The Journal of the International Society for Oncodevelopmental Biology and Medicine*. 2017, 39(10), 1010428317727479. (JCR 2017; IF = 4,6; Q2 – Cell Biology)

Experimental work (%)	Supervision (%)	Manuscript preparation (%)	Research design (%)
10	80	40	50

8) PACULOVÁ, Hana and **Jiří KOHOUTEK**. The emerging roles of CDK12 in tumorigenesis. *Cell Division*. 2017, 12, 7. (JCR 2017; IF = 4,6; Q2 – Cell Biology)

Experimental work (%)	Supervision (%)	Manuscript preparation (%)	Research design (%)
0	30	35	50

9) **KOHOUTEK, Jiri**, Qintong LI, Dalibor BLAZEK, Zeping LUO, Huimin JIANG and B. Matija PETERLIN. Cyclin T2 Is Essential for Mouse Embryogenesis. *Molecular and Cellular Biology*. 2009, 29(12), 3280–3285. (JCR 2009; IF = 6,1; Q1 – Biochemistry & Molecular Biology)

Experimental work (%)	Supervision (%)	Manuscript preparation (%)	Research design (%)
70	0	70	60

10) OVEN Irena, BRDICKOVA Nada, **KOHOUTEK Jiri**, VAUPOTIC Tomas, NARAT M and Peterlin B. Matija. AIRE recruits P-TEFb for transcriptional elongation of target genes in medullary thymic epithelial cells. *Molecular and cellular biology*. 2007, 27(24). (JCR 2007; IF = 6,4; Q1 – Biochemistry & Molecular Biology)

Experimental work (%)	Supervision (%)	Manuscript preparation (%)	Research design (%)
20	0	20	10

11) NOVÁKOVÁ, Monika, Marek HAMPL, Dávid VRÁBEL, Jan PROCHÁZKA, Silvia PETREZSELYOVÁ, Michaela PROCHÁZKOVÁ, Radislav SEDLÁČEK, Michaela KAVKOVÁ, Tomáš ZIKMUND, Jozef KAISER, Hsien-Chia JUAN, Ming-Ji FANN, Marcela BUCHTOVÁ and Jiří KOHOUTEK. Mouse Model of Congenital Heart Defects, Dysmorphic Facial Features and Intellectual Developmental Disorders as a Result of Non-functional CDK13. *Frontiers in Cell and Developmental Biology*. 2019, 7, 155. (JCR 2019; IF = 5,1; Q2 – Cell Biology)

Experimental work (%)	Supervision (%)	Manuscript preparation (%)	Research design (%)
10	80	60	50

12) HAMPL, Marek, Nela JANDOVÁ, Denisa LUSKOVÁ, Monika NOVÁKOVÁ, Tereza SZOTKOWSKÁ, Štěpán ČADA, Jan PROCHÁZKA, Jiří KOHOUTEK and Marcela BUCHTOVÁ. Early embryogenesis in CHDFIDD mouse model reveals facial clefts and altered cranial neurogenesis. *Disease Models & Mechanisms*. 2024, 17(6), dmm050261. (JCR 2023; IF = 4,0; Q2 – Cell Biology)

Experimental work (%)	Supervision (%)	Manuscript preparation (%)	Research design (%)
10	10	10	15

13) JANSOVA, Denisa, Veronika SEDMIKOVA, Fatima J. BERRO, Daria ALESHKINA, Michal DVORAN, Michal KUBELKA, Jitka REZACOVA, Jana RUTAROVA, Jiří KOHOUTEK and Andrej SUSOR. Absence of CDK12 in oocyte leads to female infertility. *Cell Death & Disease*. 2025, 16(1), 213. ISSN 2041-4889. (JCR 2023; IF = 8,1; Q1 – Cell Biology)

Experimental work (%)	Supervision (%)	Manuscript preparation (%)	Research design (%)
0	10	15	10

1 INTRODUCTION

1.1 History of discoveries of cell cycle regulators

The desire of mankind to understand the basic principles of cell division predates the golden era of true pioneers represented by many great scientists of their time. The divine curiosity to observe and understand the mechanism of cell division fascinated many, yet only few succeeded in uncovering the mysteries of cellular processes and molecular factors orchestrating the transition through individual phases of the cell division. Undoubtedly, the work of Robert Hooke, who first observed distinct structures which he named cells, from Latin cellula, resembling the monk's chamber from the convent, is worth mentioning [7]. It took two centuries to define the cell theory, stating that all living organisms are composed of cells, the cell is the smallest structural and functional biological unit, and every cell arises from a former cell [8, 9]. In 1882 Walther Flemming first draw different stages of the cell division in the plant cell, especially the filamentous structures of various size and shapes just before cell division, after he developed new technique to stain plant cells [10].

The drawings prepared by Flemming described the mitotic phase of cell division in unprecedented detail for its time, yet limited information was available to describe the interphase. In 1953 Alma Howard and Stephen Pelc were first to realize and propose four periods for the cell division, latter recognized as phases of the cell cycle – the pre-S phase (G1), the S-phase (DNA synthesis), the pre-miotic period (G2) and mitotic and division period (M) [11, 12]. By studying cell proliferation in bean roots, Howard and Pelc deduced that DNA synthesis takes about six hours, measured by incorporation of p32-labeled isotope in DNA only during interphase, and that cells enter prophase of the next mitosis only eight hours after DNA synthesis is completed. The discovery of cell cycle phases evoked two important questions: 1) what are the molecular determinants or motors of each phase onset, and 2) how is the transition between phases orchestrated? It was clear that drivers of the cell cycle ensure that phases of the cell cycle occur in the correct order, and that the cell cycle should be considered as an organized sequence of events analogous to simple model as phage morphogenesis [13]. This idea led to a concept of checkpoint controls where the cell checks if an early event, the S phase, for instance, has been properly finished before proceeding with a later event, such as the mitosis [14].

Understanding of this concept was complemented by two powerful experimental approaches available at the time the genetic studies in yeast and biochemical studies of cell extracts acquired from amphibian and marine invertebrate oocytes or eggs [15, 16]. Both approaches played a key role in discovering molecular machines driving the cell cycle progression. While biochemists were racing to

purify component of the Mitotic Promoting Factor – MPF, a factor able to cause cell to prematurely enter mitosis even when the cell is in the G1 phase, the geneticists generated series of yeast mutants essential for cell cycle progression, which were called Cell Division Cycle – *cdc* genes [13, 17, 18]. The *CDC28* gene, *Saccharomyces cerevisiae*, and the *cdc2* gene, *Saccharomyces pombe*, were identified, which products are essential for G1/S or G2/M transition, respectively [19]. Later, it was reported that human cells also possess a *cdc*-like gene able to complement a *cdc2* mutant [20]. Importantly, MPF was demonstrated to be composed of two proteins: one of size 34 kDa and the other of size 45 kDa, and the 34 kDa subunit was demonstrated to cross-react with antibody against product of *cdc2* gene [16, 21]. Meanwhile, Tim Hunt observed proteins that were newly synthesized before each division and immediately degraded after each cleavage in sea urchin eggs undergoing cleavage after fertilization [22]. The proteins were called cyclins because of their cyclic appearance. Finally, the molecular engines of progression through the cell cycle were discovered, consisting of a protein kinase and its associated partner, a cyclin. Cyclin is synthesized at a particular phase of the cell cycle and binds to the kinase, which becomes activated. Once the cell phase transition is accomplished, the kinase is inactivated by degradation of the associated cyclin [23].

Over two decades, the delicate control of CDK/cyclin complexes was elaborated by many groups, leading to the identification of upstream signaling pathways, posttranslational modifications, association with cellular factors regulating its activity positively or negatively, cellular CDK inhibitors, and ubiquitin machinery playing a crucial role in the function of these complexes. By completing numerous studies, researchers uncovered principal CDKs and their associated cyclins orchestrating transition through exact cell cycle phases [24]. The CDK4/6 with D-type cyclins are found in G1 phase, replaced by cyclin E with CDK2 at the end of G1 marking the beginning of S phase, exchanged by switch of cyclin E for cyclin A with CDK2 during S phase, followed by substitution of CDK2 for CDK1 with cyclin A, ending the circle by activation of CDK1 with B-type cyclins [25].

Using degenerate oligomers for the catalytic domain of CDK1, Harlow and colleagues were able to identify five new genes related to the *CDK1* gene [26]. The family of CDKs was about to expand with the identification of CDK5 in neurons [27], CDK7 as CDK-activating kinase – CAK [28], CDK8 [29], and CDK9 [30] reviewed in [31]. We now recognize 21 genes encoding 20 CDKs, named CDK1 to CDK20, with two genes, *CDK11A* and *CDK11B*, expressing two isoforms of CDK11 [32]. The family of CDKs with its binding cyclins could be classified in three phylogenetic groups sharing involvement in similar cellular processes, 1) cell cycle – CDK1, CDK2, CDK3, CDK4, CDK6 and CDK7; transcription regulation – CDK7, CDK8, CDK9, CDK10, CDK11, CDK12 and CDK13; various cellular functions, thus are called – atypical – CDK5, CDK14, CDK15, CDK16, CDK17, CDK18, CDK19 and CDK20 [25, 33].

1.2 Atypical cyclin-dependent kinases

Cell cycle-related CDKs were described in the previous text and are not in the scope of the habilitation thesis. The group of atypical CDKs represents CDKs that are studied to a lesser extent, except for CDK5, the kinase expressed in differentiated neurons [34]. The CDK5 with PSSALRE amino acid motif within the catalytically active site is considered the ancestor of the two subfamilies named, as PFTAIREs - CDK14 and CDK15, and PCTAIREs - CDK16, CDK17, and CDK18 families [32]. Atypical CDKs are involved in a broad range of cellular processes and are undoubtedly worth of further detailed studies, but they are not the focus of the habilitation thesis.

1.3 Cyclin-dependent kinases regulating transcription

The CDKs regulating the transcription mediated by RNA polymerase II – RNAPII will be discussed in more detail, especially with an emphasis on the transition from the initiation to the elongation phase of transcription and their role in cellular processes. The eukaryotic transcription can be divided into functionally distinct phases – initiation, elongation, and termination [31, 35]. RNAPII is a multiprotein complex with a unique structure recognized as the carboxy-terminal domain – CTD within the Rpb1, the largest subunit of RNAPII [36, 37]. The CTD is composed of heptapeptide $Y_1S_2P_3T_4S_5P_6S_7$ repeated 57 times in mammals, and posttranslational modifications of specific amino acids within the heptapeptide motif mirror a particular phase of transcription [38, 39].

The CDK7 is a 346 amino acid protein and was among the first CDKs to be implicated in the transcription mediated by RNAPII [40, 41]. At the molecular level, the CDK7 phosphorylates serine at position 5, Ser5, within the CTD of RNAPII, allowing initiation of transcription, [Appendix 4](#) [31]. Phosphorylated RNAPII leaves the promoter and synthesizes the nascent RNA, nevertheless, around 35 - 50 nucleotides pass the transcriptional start site, the RNAPII movement is imposed by the action of two factors [37]. Negative Elongation Factor, NELF, and DRB Sensitivity Inducing Factor, DSIF, in cooperation, they interact with RNAPII and physically block its movement. To overcome stalled RNAPII, the Positive Transcription Elongation Factor b, P-TEFb, comes into place and phosphorylates Ser at position 2, Ser2 within CTD [35]. The CDK9 catalytically active subunit of P-TEFb is responsible for the phosphorylation only if associated with the cyclin, in the case of CDK9, we recognize Cyclin T1 and T2 [31]. Previously, Cyclin K was also assumed to be a CDK9 associating partner [42, 43]. In parallel to CTD phosphorylation, P-TEFb phosphorylates DSIF and NELF, causing release of DSIF from RNAPII and conformational change within the NELF, which then becomes a positive elongation factor. RNAPII is released from its pause, and the elongation phase of transcription is triggered [44]. The newly synthesized RNA undergoes 5' capping, splicing corresponding to posttranslational modifications of

amino acids within the CTD. Once the RNAPII reaches the polyadenylation site, the Ser2 and Thr4 are extensively phosphorylated, converging in the termination of transcription. The Thr4 phosphorylation seems to be obligatory for termination, since CTD phosphorylated on Thr4 is enriched at 3'-ends of protein coding genes in metazoans [45].

The habilitation proposal focuses on the functions of CDKs and their associated partners in various cellular processes which some of them are key to proper embryonic development. The first part discusses the delicate balance of active versus inactive state of P-TEFb through association with its cellular inhibitor, Hexim1. The second part focuses on the new function of CDK12 and CDK13 in cellular processes. The third part illustrates fascinating roles of cyclin T1, T2, K, CDK12, and CDK13 in numerous morphogenetic processes during development.

2 FUNCTION OF P-TEFB IN CONTROL OF ELONGATION PHASE OF TRANSCRIPTION

Earlier studies from 90th of 20th century indicated that transcription is not always controlled at the step of promoter initiation complex, PIC, formation mediated by general and specific transcription factors [31, 46]. Instead, the beginning of the elongation phase is the limiting step, which is not restricted only to mammals but was detected in *Drosophila* or during HIV infection [35, 44]. More detailed studies revealed that elongation control of transcription is typical for 30% of genes in primary human lung fibroblasts and up to 40% of protein coding genes in human embryonic stem cells [47, 48]. The last two decades have brought compelling evidence that regulation of transcription at the elongation phase of transcription is more the rule than the exception. Still, the whole mechanism of P-TEFb recruitment to the promoter occupied by different transcription factors was not completely understood, and the mechanism of P-TEFb inactivation was an intriguing question for researchers to pursue.

2.1 Association of P-TEFb in Small and Large complexes

When we joined the research community studying transcription of RNAPII, the role of P-TEFb in phosphorylation of CTD during transition from initiation to elongation phase of transcription was established, and the association between P-TEFb and prototypical transcription factors was described. Nevertheless, there was an unanswered question: how is the transition between the active and inactive state of P-TEFb achieved? Is P-TEFb permanently active? Is P-TEFb active in all phases of the cell cycle or transcription cycle? How is the association of P-TEFb with various transcription factors accomplished

and regulated? Since the level of CDK9 and its binding cyclins merely changes during the cell cycle or transcription, the activity of P-TEFb must be controlled by other means.

Several groups independently provided compelling evidence of the existence of two intracellular complexes of P-TEFb in cells. The catalytically active complex was recognized as the small

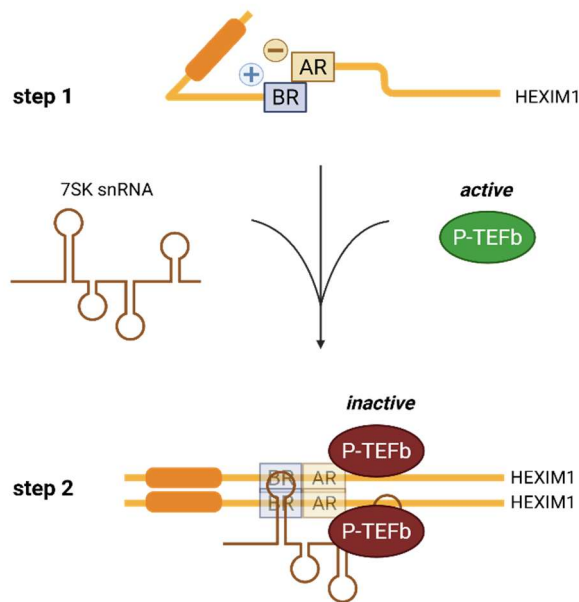


Figure 1: Structure of Hexim1 and assembly of a large complex. Step 1) Hexim1 protein is presented as an orange line. Black and ocher boxes represent basic (BR) and gray acidic (AR) regions, respectively. **Step 2)** By coordinated interactions of two Hexim1 molecules, 7SK snRNA and two P-TEFb (active, green oval) the large complex with inactive P-TEFb (red oval) is formed, adapted from [Appendix 1](#).

complex and consists of a heterodimer of CDK9 bound to cyclin T1 or T2. The catalytically inactive complex was assigned as the large complex, where P-TEFb and cyclins associate with 7SK snRNA and protein called Hexim1 or MAT1. Initially, the 7SK small nuclear RNA, 7SK snRNA, was found to sequester P-TEFb to its inactive complex [49, 50]. Followed by discovery of Hexim1 in the large complex the term Hexim1, hexamethylene bis-acetamid inducible 1, was described as protein induced in vascular smooth muscle cells during differentiation by hexamethylene bis-acetamide [51, 52]. The same protein was recognized by other three groups as Ménage À Quatre – MAT1 [53], Cardiac Lineage-associated Protein 1 – CLP-1 [54,

55], Estrogen Down-regulated Gene – EDG-1 at the same time [56]. The term Hexim1 was accepted by most of the research community and is used to this day. The discovery of active and inactive complexes of P-TEFb was radical since it simply explains the elegant way in which cells modulate transcription activation by the balance of active versus inactive P-TEFb pool. The constituents of the large complex were known, but the mechanism of its assembly was not reconciled. In our initial work, we described how different domains in Hexim1 direct nuclear localization, binding to P-TEFb, and activity of transcription factors, [Appendix 1](#) [57]. First, we demonstrated that the basic region is indispensable for nuclear import of Hexim1. The basic region, BR, spans from 150 – 177 amino acids in Hexim1, and can be divided into two subregions, BR1 and BR2, which contain lysines and arginines and only lysines, respectively, resembling the classical composition for nuclear localization sequences – NLSs. Indeed, when BR was deleted, the nuclear localization of Hexim1 was diminished, and we observed the same result when all lysines or arginines were replaced by alanines. By mutating individual amino acids or

specific regions, we were able to conclude that two monopartite and two bipartite NLSs control the localization of Hexim1 to the nucleus.

Interestingly, the arginines in BR1 were essential for its binding to 7SK snRNA and inhibition of P-TEFb. Next to the BR, there is an adjacent stretch of acidic amino acids we assigned as an acidic region, AR. Similarly, to BR, the AR is subdivided into two clusters AR1 and AR2. From binding studies, we knew that BR and AR can interact together in the absence of RNA, supporting the idea that AR mimics the negative charge of 7SK snRNA and participates in the coordinating assembly of a large complex. Thus, we envisioned that the removal of AR would lead to the release of BR1 and subsequent binding to 7SK snRNA and inhibition of P-TEFb activity. Indeed, the mutation of acidic residues to alanines restored incorporation of Hexim1 to the large complex together with P-TEFb. In summary, our study provided a mechanistic view of how oppositely charged regions within the Hexim1 and 7SK snRNA coordinate binding to P-TEFb, subcellular localization of P-TEFb, and its inhibition of transcription.

In parallel to our effort to understand intramolecular interaction with Hexim1 and its impact on assembly of the large complex, we were also intrigued by the composition of the large complex. We could delineate molecular masses of small and large complexes from glycerol gradient experiments. The size of the small complex fits our prediction, but the molecular mass of the large complex implies the presence of two P-TEFb complexes, one molecule of 7SK snRNA, and two molecules of Hexim1, yet the nature of the Hexim1 protein in the cells was not known. In the following publication, we determined that Hexim1 forms oligomers in cells, and we could define regions within Hexim1 responsible for its oligomerization and binding to P-TEFb, [Appendix 2](#) [58]. First, we analyzed the amino acid sequence of Hexim1 and identified two predicted coiled-coil regions in the C-terminal part of Hexim1, which we assigned as coiled-coil regions 1 and 2, CR1 and CR2. When the evolutionarily conserved leucines were mutated to alanines in both CR1 and CR2, Hexim1 did not form the oligomers in the absence of 7SK snRNA (Fig. 2).

If the 7SK snRNA was available, oligomerization was detected. It pointed us to a scenario where Hexim1 can also oligomerize through the 7SK snRNA bound to BR region of Hexim1. Indeed, the depletion of BR from Hexim1 did not affect oligomerization when the coiled-coil region was intact, but when the CR2 was omitted from Hexim1, the formation of the oligomers was not detected. Moreover, Hexim1 with a mutated CR1 domain could not bind P-TEFb and inhibit transcription. This data suggested the presence of two regions, BR and CR2, coordinating the oligomerization of Hexim1. In our presented model, Hexim1 forms oligomers via the CR1 and CR2 regions, when 7SK snRNA and P-TEFb are available, the CR1 domain serves as a platform for interaction with P-TEFb, and BR, together with CR2, provides oligomerization between two Hexim1 molecules (Fig. 2).

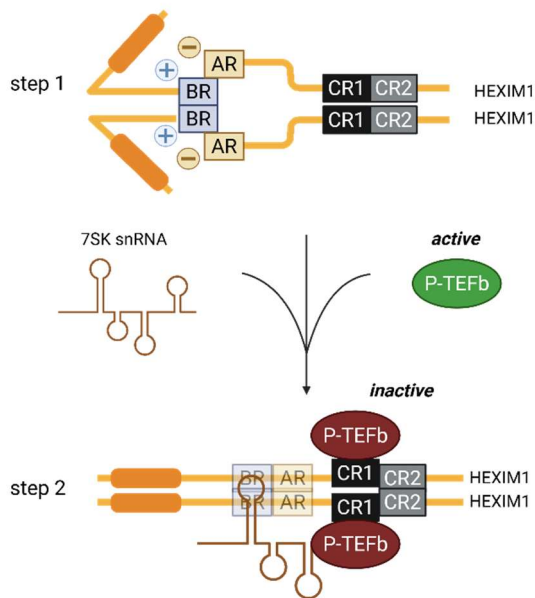


Figure 2: Scheme of Hexim1 and mechanism of assembly of a large complex. Schematic depiction of human Hexim1 protein. Blue and ochre boxes represent the basic and acidic regions – BR and AR. Coiled-coil regions CR1 and CR2 are represented by black and gray boxes, respectively. A model of how the oligomerization of Hexim1 via 7SK snRNA and CR directs the incorporation of P-TEFb into the large complex. **Step1)** In the absence of 7SK snRNA, free Hexim1 proteins are oligomers. This oligomerization is mediated solely by the CR1 and CR2 in the C-terminal domain of Hexim1. The small complex of P-TEFb – green oval is active. **Step 2)** In contrast, when 7SK snRNA binds the BRs in Hexim1, it facilitates the second oligomerization event. Subsequently, P-TEFb is incorporated into the large complex, leading to its inactivation – dark red ovals. In this complex, the CR1 in Hexim1 mediates the binding to P-TEFb, whereas the CR2 facilitates Hexim1 oligomerization, adapted from [Appendix 2](#) [58].

Our data imply a mechanism by which cells can regulate the sequestration or release of P-TEFb in response to intracellular or extracellular stimuli. It became increasingly apparent that shuffling between small and large complexes is generally utilized by cells to regulate the activity of diverse transcription factors.

Based on the knowledge from published literature, it seemed that Hexim1 is recruited to the vicinity of transcription factors and inhibits their function. But it was not apparent how Hexim1 achieved inhibition of transcription mediated by various transcription factors. To examine how Hexim1 inhibits transcription factor, we chose the class II transactivator (CIITA), which is the master integrator of the expression of *MHC class II* genes, and it interacts with a variety of basal transcription factors to orchestrate transcription of these genes, [Appendix 3](#) [59]. CIITA actively recruits P-TEFb to promoters of *MHC class II* genes. As described earlier in the text, P-TEFb is present in the cell in small active or large inactive complexes. In our preliminary experiments, we recognized Hexim1 as a potent inhibitor of the CIITA-mediated transcription [59]. Not only exogenously expressed, but also IFN-gamma-induced CIITA was inhibited by the presence of intracellular Hexim1, [Appendix 3](#). This inhibition depended on the intact Cyclin T1-binding domain in Hexim1. Importantly, Hexim1 sequestered P-TEFb from CIITA, as documented by binding competition and ChIP assays. Conversely, the depletion of Hexim1 from cells by siRNA increased CIITA-mediated transcription.

The regulation based on competition between transcription factor and Hexim1 for the binding to P-TEFb actually provides a dynamic cellular switch to regulate effectively transcription of CIITA-dependent genes in response to cellular demands. In general, the competition of Hexim1 with the given

transcription factor for binding to P-TEFb allows cells to utilize only one negative transcription factor, Hexim1, to efficiently inhibit many transcription factors. There is no need for Hexim1 to accommodate several interaction platforms for various transcription factors. It would be a challenging task to explore what is behind the rule orchestrating competition between transcription factors known to be strong versus weak initiators of transcription, [Appendix 4](#).

The results from introduced publications were intended to uncover some fundamental aspects of the dynamic formation and disassembly of small versus large complexes and how cells can utilize this regulatory circuit to modulate the release of P-TEFb for its transcriptional demands, in response to internal or external stimuli. The main conceptual advances are that signaling pathways activating different transcriptional factors can effectively modulate P-TEFb by releasing its active form from a large complex by modification of Hexim1 or P-TEFb. Even if there is no direct recruitment of P-TEFb by the specific transcription factor, activation of a particular signaling pathway is sufficient to secure the effective elongation phase of transcription by releasing active P-TEFb from the large complex. One can argue that the majority of well-characterized transcription factors recruit P-TEFb to the promoter directly, and there is no imminent need to release P-TEFb from a large complex by the activity of the upstream signaling pathway. Nevertheless, various transcription factors attract P-TEFb to the promoter regions with different efficiency, mainly due to competition with Hexim1 for the same P-TEFb binding site, [Appendix 4](#). Therefore, any additional mechanism strengthening the elongation phase of transcription is crucial during specific cellular responses, differentiation, growth, apoptosis, development, etc. *Vice versa*, posttranslational modifications of Hexim1 or CDK9 could induce attraction of CDK9 to a large complex. Indeed, phosphorylation of CDK9 at Thr-186 is directly involved in Hexim1 binding [60, 61]. The CDK9 is not the only target of posttranslational modification that affects activation or inhibition of P-TEFb. The Phosphorylation of Thr270 and Ser278 relies on the PI3K/Akt pathway and Tyr271 on the Erk1 pathway [62, 63]. Phosphorylation of Ser158 in the basic region of Hexim1 by PKC neutralizes the positive charge, protecting binding of 7SK and impairs Hexim1 association with P-TEFb during T cell activation [64]. Recently, it was shown that PKC activation in T lymphocytes coincides with phosphorylation of Thr-186 in CDK9 and its activation [65]. The pathological activation of Jak/STAT signaling pathway promotes dissociation of P-TEFb from Hexim1 and heart hypertrophy induction [66]. The dephosphorylation of Thr186 in CDK9 by PP1 α phosphatase during UV stress inactivates CDK9 [67, 68].

2.2 Regulation of elongation phase of transcription by P-TEFb

The previous section aimed to understand the composition and assembly/disassembly of large and small P-TEFb complexes. Nevertheless, the composition of the large complex was about to be unveiled. A year later, when our results were published, two groups independently described two additional factors participating in stabilizing the large P-TEFb complex they were LARP7 and MEPCE. The MEPCE is 7SK methyl phosphate capping enzyme, which was demonstrated to post-transcriptionally add a cap to the γ -phosphate of 5' end of 7SK RNA [69]. This modification enhances the stability of 7SK since silencing of MEPCE led to a decrease in the steady-state level of 7SK snRNA *in vivo* [69]. The LARP7 is La-Ribonucleoprotein7, which was identified throughout the proteomics survey of P-TEFb associating partners and later on characterized by Price group as a constituent factor of the large P-TEFb complex [70]. From our understanding, the 7SK snRNA serves as a central scaffold coordinating the assembly of large complexes and maintains P-TEFb in an inactive state (Fig. 3). Large complex is a reservoir of active P-TEFb from which it can be released in response to cellular or developmental cues [71]. Even though our research describing the formation of Hexim1 oligomers and the intramolecular interaction responsible for the sequential assembly of a large complex was published two decades ago, the model has remained unchanged, only enriched for understanding how different intra- or extracellular stimuli control the balance between small and large complexes, [Appendix 4](#) [31].

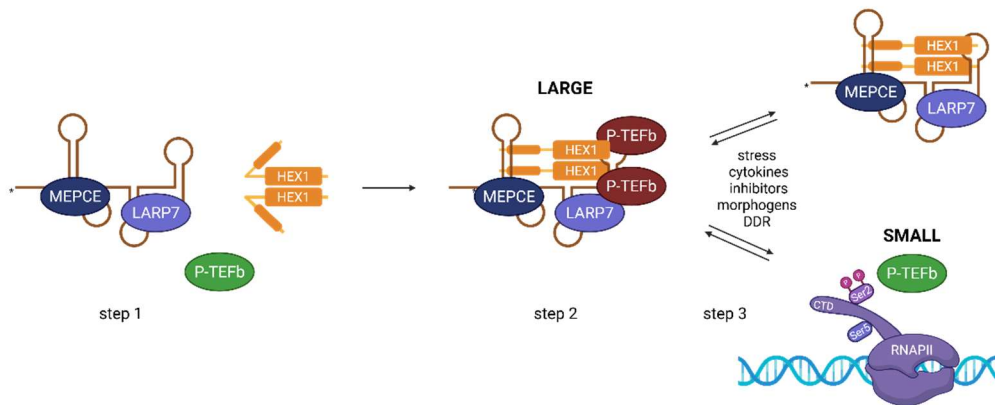


Figure 3: Composition, assembly of a large complex and release of P-TEFb complexes. Step 1) 7SK snRNA contains 5'- and 3'- ends with pppG (triphosphate guanosine) and UUUU-OH (oligouridylate tail), respectively. 7SK snRNA is recognized by MEPCE and LARP7. MEPCE methylates the gamma-phosphate of its first 5'ribonucleotide, depicted by an asterisk, and LARP7 stabilizes 7SK snRNA by binding to its oligouridylate tail. Hexim1 homodimerizes via its coiled-coil domain in the C-terminus, but the N-terminus adopts a conformation that does not allow binding to P-TEFb. **Step 2)** Binding of 7SK snRNA from 7SK snRNA/MEPCE/LARP7 complex to the basic region in the central part of Hexim1 triggers conformational changes of the hexim dimer, leading to exposition of the CycT1-binding domain at the C-terminus of Hexim1 and consequent binding of P-TEFb. The 'LARGE' complex is formed and is stabilized due to multiple protein-protein and protein-RNA contacts within the complex. **Step 3)** Activity of P-TEFb is inhibited in the large complex. Several stimuli have been reported to disrupt the large complex, such as stress, cytokines, inhibitors, morphogens, and DDR stress signals, allowing release of active P-TEFb 'SMALL' complex, adapted from [Appendix 4](#) [31].

There are numerous publications describing how modulation of small versus large P-TEFb complexes participates in various cellular processes. Among them, activation of T cells by phorbol ester – PMA leads to release of P-TEFb from the large complex by induction of phosphorylation of Hexim1 on Ser-158, Tyr-271, and Tyr-274 and CDK9 phosphorylation on Thr-186 [64]. If the T cells are infected by HIV virus then CDK9 is phosphorylated on Ser-175 by CDK7 to promote transcription of HIV genome through association with Tat and super elongation complex [72, 73]. If Ser-175 is dephosphorylated, the interaction between CDK9 and BRD4 is enhanced.

In view of our and others' work, it is sufficient to introduce an additional phase in the transcription cycle based on the novel role of CDKs. It is apparent that CTD of RNAPII represents a central hub for modulation by CDKs and other kinases (Fig. 4), [Appendix 4](#). As evident active P-TEFb can restart paused RNAPII at the transcription start sites of many genes which transcription is activated in response to many intra- or extracellular stimuli.

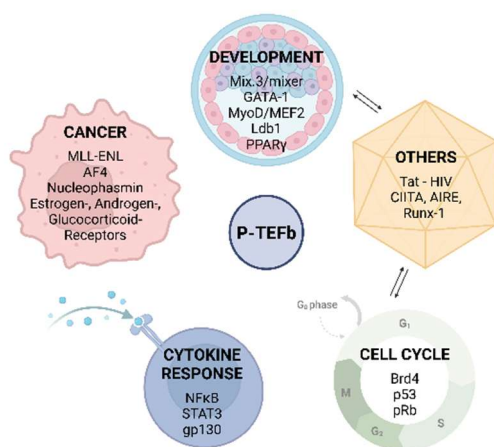


Figure 4: Role of P-TEFb in a broad spectrum of biological processes. P-TEFb (blue oval) participates in many different biological processes, such as development, cancer, cell cycle, cytokine response. Abbreviations in each oval represent particular transcription factors that have been found to employ P-TEFb in given biological process. Significantly, dysregulation of P-TEFb-dependent transcription factors involved in development or cell cycle could also significantly contribute to malignant transformation of normal cells, as depicted by arrows in this figure, adapted from [Appendix 4](#) [31].

For example, the renewal of epidermal progenitors is characterized by inactive CDK9 in complex with Hexim1 and AFF1, when differentiation is triggered, the CDK9 with super elongation complexes activates differentiation-activating transcription factors [74]. Also, activation of primary response genes by LPS during immune response in macrophages is a classic example of release of paused RNAPII by recruitment and activity of P-TEFb [75]. Thus, the stage of pausing RNAPII resembles all necessary characteristics of the inherent phase of the transcription cycle. In this view, the transcription cycle can be described by these stages of transcription – assembly of pre-initiation complex and initiation; proximal promoter pausing and release of RNAPII; elongation accompanied by splicing; termination and release of RNAPII [25]. The CDKs are the principal regulators of these phase transitions, with CDK7 during initiation, CDK9 in elongation, CDK11, CDK12, and CDK13 in splicing coupled with the synthesis of RNA, and the role of CDK8 and CDK19 in PIC assembly is recognized.

3 ROLE OF CDK12 AND CDK13 IN THE REGULATION OF TRANSCRIPTION

3.1 Defining CDK12 and CDK13 complexes

When studying the mechanism of incorporation or release of P-TEFb into the large complex of P-TEFb, we were recapitulating earlier observations of other research groups verifying the association of CDK9 with cyclin K. Despite utilizing many various experimental approaches, we could not detect direct binding between CDK9 and cyclin K, neither *in vitro* nor *in vivo*. Thus, we immunoprecipitated cyclin K from HEK293 cells, followed by mass spectrometry. To our surprise, we did not retrieve any peptides resembling CDK9 kinase, instead, we were able to identify peptides of CDK12 and CDK13 kinases. Similar observation regarding the association of CDK12 and CDK13 with cyclin K in *Drosophila* was published earlier by the Greenleaf group [76]. Nevertheless, this was rather an unexpected result as CDK12 and CDK13 were barely associated with the regulation of transcription before. After cloning both kinases, we first prove an association between cyclin K and both kinases, [Appendix 5](#) [77].

Importantly, CDK12-cyclin K and CDK13-cyclin K heterodimers are present in cells in mutually separate complexes (Fig. 5). We also collected data clearly supporting the role of CDK12 and CDK13 in the phosphorylation of Ser2 within the CTD of RNAPII. Depletion of cyclin K had a specific impact on transcription of a variety of subsets of cellular genes. Among affected genes was a group of genes involved in DNA-damage repair – DDR pathway, such as *BRCA1*, *ATM*, *FANCD2*, and *FANCI*. If the DDR genes are affected by depletion of CDK12-cyclin K, then the impact on the maintenance of genomic stability should be noticeable. When different DNA-damaging agents, etoposide and camptothecin, were applied to the cells, strong and dose-dependent sensitivity of cells to double-strand breaks were detected. When CDK12 and cyclin K were down-regulated in cells, the decreased level of DDR genes was determined by RT-qPCR or nuclear run-on assays, and the occupancy of active Ser2-RNAPII was evaluated by ChIP with specific antibodies.

All these data implied the novel function of CDK12-cyclin K complex and established that the depletion of CycK/Cdk12 does not affect global transcriptional rates, but CycK/Cdk12 is the limiting factor that affects the transcription of a small subset of genes, such as DDR genes [78]. In summary, we demonstrated that CycK-Cdk12 regulates resistance of cells to the exogenous DNA-damaging agents and is essential for maintaining genomic stability in various cellular models of cancer or primary cells (Fig. 5), adapted [Appendix 6](#) [78]. Over the past years, the CDK12 and CDK13 were demonstrated to participate in diverse cellular processes including transcription of DDR genes, splicing and pre-mRNA processing, DNA replication and initiation of translation of mRNA subgroups (Fig. 5) [1–6].

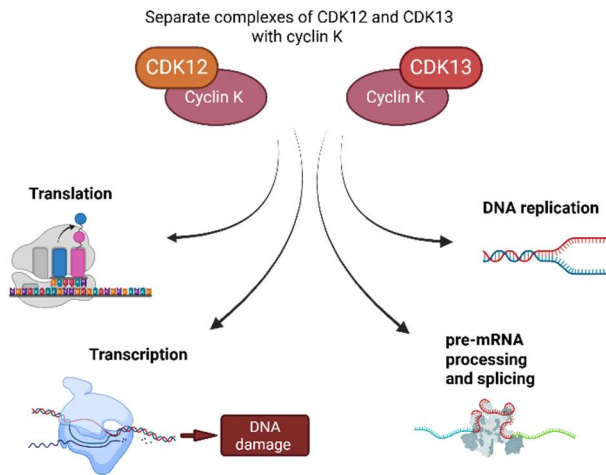


Figure 5: Function of CDK12 and CDK13 in various cellular processes. Both kinases CDK12 and CDK13 actively participate in regulation of transcription of DDR genes, splicing and pre-mRNA processing, DNA replication and initiation of translation of mRNA subgroups. Especially, regulation of transcription of DNA damage genes by CDK12 was novel concept.

Our seminal observation connecting CDK12 with cyclin K to DDR was inspirational for many research groups and led to identifying CDK12 as a promising target for patient treatment (Fig. 7). Mutations of CDK12 were identified in several cancers, but probably the most striking involvement of CDK12 was demonstrated for high-grade serous ovarian cancer and castrate resistant prostate cancer. Over the years, loss of CDK12 function was recognized as the vulnerability of cancer cells due to their impaired homologous recombination - HR, since CDK12 regulates the expression of many factors involved in the HR process, BRCA1 in particular, since it is one of the genes whose expression depends on intact CDK12 activity [77]. The breast cancer-associated gene 1 – *BRCA1*, is a tumor suppressor and is vital to HR-mediated DNA damage repair, cell cycle checkpoints, and transcriptional regulation [79, 80]. The loss of *BRCA1*, caused by homozygous mutations, reduces the ability of cells to carry out HR-mediated DNA repair, resulting in cellular genomic instability mostly imposed by double-stranded breaks. Interestingly, *BRCA1* mutations are mutually exclusive with *CDK12* mutations, which suggests that CDK12 belongs to the same HR-mediated DNA damage repair pathway as BRCA1 [81].

Importantly, homologous recombination deficiency provides an opportunity for cancer treatment, and tumors with loss of BRCA1 or BRCA2 are sensitive to inhibitors of PARP1/2, a protein involved in DDR. The Poly (ADP-ribose) polymerase 1 – PARP1, are DNA damage sensors and they primarily attached branched poly(ADP-ribose) chains on target proteins at the sites of damaged DNA at single strand DNA breaks preferentially [82]. PARP1 is also involved in DDR pathways, such as the single-strand break repair and nonhomologous-end joining - NHEJ pathways. If HR is compromised, for

example, due to loss of BRCA1 or CDK12, the cells employ additional mechanisms to repair damaged DNA, the error-prone NHEJ, typically [83]. Among other factors involved in DDR is the check kinase 1 – CHK1, which responds to DNA damage by activating ATR to block cell cycle, by regulating the G2/M checkpoint by phosphorylation of DDR factors [84, 85]. Since the loss of BRCA1 compromises DDR and leads to replication stress and DNA damage, we hypothesized that BRCA1- or CDK12-deficient cells will extensively rely on the S-phase-related kinase activity of CHK1 for survival [86].

We therefore directly intervened the catalytic activity of CHK1 by specific inhibitors, SCH900776 and LY2603618 and we tested their effect on the cell survival in the presence or absence of BRCA1, CDK12 or CDK13, [Appendix 7](#) [87]. The level of specific protein was downregulated by siRNAs, and a proliferation assay with or without inhibitors was carried out in HCT116 cells with wild-type or mutated TP53. As expected, CDK13 had no measurable effect on proliferation, but silencing BRCA1 and CDK12 sensitized HCT116 cells to CHK1 inhibitors (Fig. 6). Then we assessed the DNA damage marker γ H2AX and CHK1 autophosphorylation at serine 296. Importantly, the γ H2AX signal, which reflects the amount of endogenous DNA damage, was increased after SCH900776 treatment. This effect was exacerbated in CDK12- and BRCA1-depleted cells, but not in CDK13-depleted cells. Further we focused to validate progression through the cell cycle by measuring protein level of endogenous CDK inhibitor p21 (Cip1/Waf1) which blocks progression through the cell cycle and was known to be induced by inhibition of CHK1 catalytic activity [88]. The p21 levels increased proportionally to the concentration of CHK1 inhibitor in BRCA1-depleted cells in comparison to strong induction in CDK12-depleted cells, even without the CHK1 inhibitor (Fig. 6). Since BRCA1 deregulation is a common characteristic of ovarian and breast cancers, we also evaluated whether BRCA1 deficiency can sensitize relevant cancer cells to inhibition of CHK1 kinase [89]. Two cell lines of triple-negative breast cancer cells, MDA-MB-231, with stable expression of shRNA against BRCA1 – shBRCA1, were generated and used in survival assay, clonogenic assay, cell cycle status and activation of DDR pathway. We noticed severe reduction in cell viability after treatment with SCH900776, reduced colony size in both shBRCA1 cell lines accompanied by decrease in cell counts, prominent increase in the S-phase of cell cycle in shBRCA1 clones suggestive of major proliferative arrest and activation of DDR as demonstrated by induction of γ H2AX in comparison to parental cell line. Finally, we assessed the *in vivo* therapeutic effects of CHK1 inhibitors by employing a mouse orthotopic xenograft model of the MDA-MB-231 clones in the fat pads of immunocompromised mice. Treatment with a CHK1 inhibitor did not significantly affect the size of the tumors when compared to tumors from control animals. On the other hand, shBRCA1 MDA-MB-231 cells gave rise to slightly bigger tumors, and treatment with a CHK1 inhibitor significantly decreased their size, [Appendix 7](#). Based on these data, we conclude that the enhanced cytostatic effect of CHK1

inhibition in CDK12- or BRCA1-depleted context results from increased DNA damage followed by a robust induction of p21 and delayed cell cycle progression.

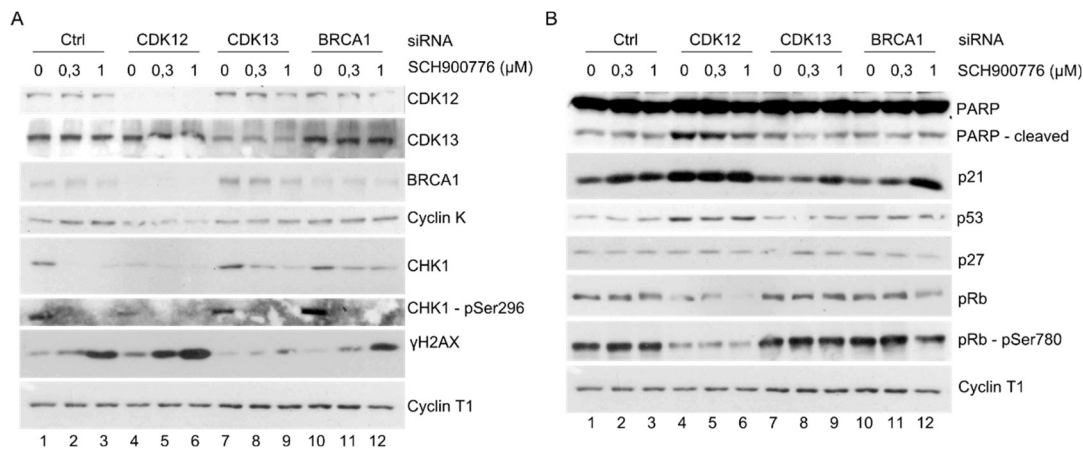


Figure 6: Impact of CDK12 and BRCA1 downregulation on DDR, apoptosis, and cell cycle. (A) The effective knockdown of various proteins after siRNA transfection, CHK1 inhibition, and DNA damage induction was assessed by Western blot analysis. HCT116p53+/+ cells were transfected with control or specific siRNAs (Ctrl, CDK12, CDK13, and BRCA1), and 2 days post-transfection, cells were treated with 0, 0.3, or 1 μM CHK1 inhibitor SCH900776 for an additional 96 h. The protein levels of the studied proteins were elucidated by Western blot with the indicated antibodies. The protein level of Cyclin T1 was used as a loading control. (B) Status of cellular factors participating in the regulation of apoptosis and the cell cycle. The protein levels of PARP, a marker of late apoptosis, tumor suppressor p53, and the cell-cycle regulating proteins p21, p27, pRb, and pRb-pSer780 were elucidated by Western blot with the indicated antibodies. The protein level of Cyclin T1 was used as a loading control, adapted from Appendix 7 [87].

We therefore proposed that simultaneous inhibition of CDK12 with CHK1 or inhibition of CHK1 in the presence of a loss-of-function mutation of the CDK12 gene is beneficial for the patients [90]. Recently, Petropoulos group demonstrated that synthetic lethality of PARP inhibitors in cells with HR deficiency results from transcription replication conflicts – TRC and not from PARP trapping on DNA at the sites of DNA damage [91, 92]. It was previously proposed that PARP inhibitors trap PARPs on DNA, and these trapped complexes block replisome progression, leading to the formation of DNA double-strand breaks that require HR for repair [93]. Notably, the TRC-dependent synthetic lethality was achieved only in BRCA2-/- cells due to the fact that these cells accumulate DNA damage in S-phase. The inhibition of transcription at the early S phase induced resistance of HR-deficient cells to PARP inhibitor, and depletion of PARP1 restored synthetic lethality in HR deficient cells [91]. Thus, developing novel therapeutic agents that selectively inhibit PARP1 without causing PARP trapping could be a promising direction to exploit HR-deficient tumors. Recently, a published manuscript reported that intact CDK12 prevents TRCs and the activation of cytotoxic replicative stress upon upregulation of the MYC oncogene. Depletion of CDK12 enhanced TRCs in MYC-overexpressing cells and led to the accumulation of double-strand DNA breaks [94]. Other publication reported that inactivation of CDK12 mediates genomic instability by inducing TRC in a model of castration-resistant prostate cancer subtype [95]. Therefore, the synergic effect we detected between CDK12 and CHK1 could be at least partially a result

of aberrant TRC. Recently, it was demonstrated that tumors with extrachromosomal DNA - ecDNA intensively rely on CHK1 to manage DNA damage, and that CHK1 inhibition could trigger preferential cell death in ecDNA-containing tumor cells [96].

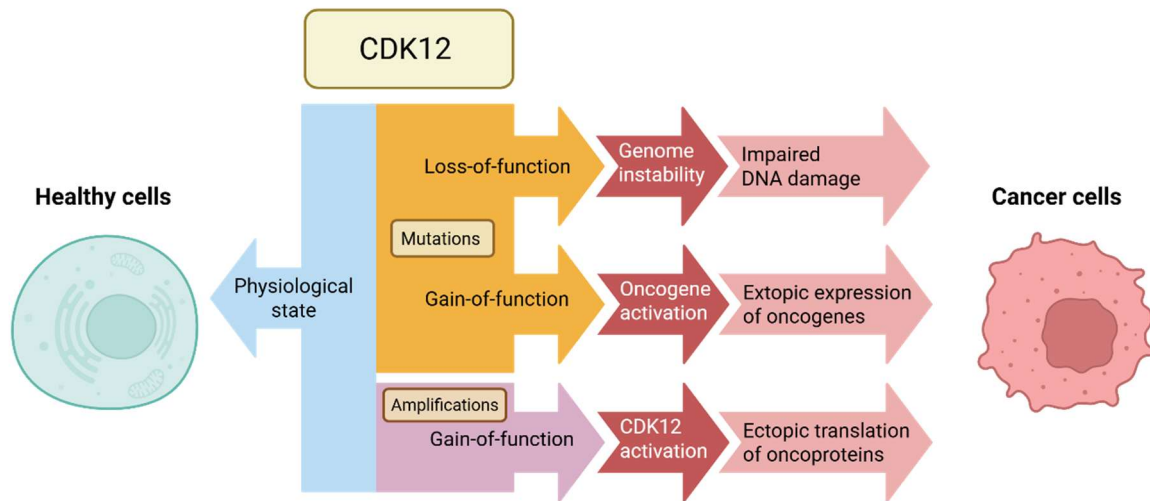


Figure 7: Role of CDK12 in cancer. CDK12 loss-of-function mutations lead to decreased expression of HR genes, resulting in genomic instability and tumorigenesis. CDK12 loss or inhibition sensitizes tumor cells to PARP1/2 inhibitors. CDK12 has oncogenic properties. CDK12 amplification might lead to increased expression of various oncogenes and consequently participate in tumorigenesis. Therefore, targeting CDK12 with specific inhibitors in these tumors could be beneficiary for patient treatment.

CDK12 mutations and amplification have been reported in various types of malignancies, covering loss-of-function mutations in high-grade serous ovarian carcinomas or castration-resistant prostate cancer subtype, and that has led to assumption that CDK12 is a tumor suppressor. On the contrary, CDK12 overexpression was documented in Her2 positive breast carcinomas and additional tumors suggesting the possibility that CDK12 has oncogenic properties, similarly to other transcription-associated kinases. Thus, recently developed CDK12 inhibitors or specific degraders constitute not only powerful research tools but also offer promising anti-cancer drugs for patient therapy. CDK12 inhibitor monotherapy could be useful for patients with tumors overexpressing activated CDK12. In addition, CDK12 inhibition increases sensitivity of cells to PARP1/2 inhibitors, thus presenting a potential strategy for targeting PARP1/2-resistant tumors. The overview of CDK12 loss-of-function or gain-of-function on tumor progression is summarized in Fig. 7, adapted from [Appendix 8](#) [90].

4 IMPACT OF TRANSCRIPTION KINASES AND THEIR ASSOCIATED CYCLINS IN DEVELOPMENTAL PROCESSES

4.1 Cyclin T2 and its role in early development

Function of CDKs in the regulation of transcription has been studied over three decades, primarily in cancer cell lines, but a limited number of studies utilized primary cells or animal models to describe the roles of transcription CDKs and their cyclins during physiological processes such as development. We were among the first groups to examine the impact of loss of CDKs or their cyclins on the regulation of transcription during mouse development. Embryonic development is a complex process by which plants and animals grow and develop from single fertilized eggs to fully grown organisms. The gene regulatory networks - GRN orchestrate diverse cellular and developmental processes such as cell proliferation, differentiation, and morphological movements during embryonic development [98]. The action of GRN is primarily regulated at the level of transcription mediated by RNA polymerase II. As described earlier, the transition between particular phases of transcription is orchestrated by phosphorylation of the CTD of RNAPII by transcription CDKs complexes [31].

Initially, we concentrated on examining the physiological role of CDK9 associating cyclins. For this purpose, we generated three mouse strains with genetically inactivated genes for cyclin T1, *Ccnt1*, cyclin T2, *Ccnt2*, and cyclin K, *Ccnk*, which were all thought to associate with CDK9. When *Ccnt2* or *Ccnk*

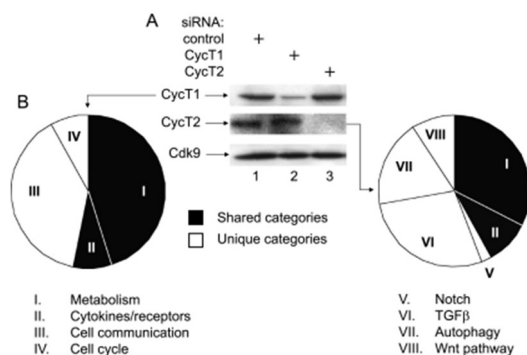


Figure 8: Genes regulated by CycT1 and CycT2 in mouse ES cells. (A) Specific siRNAs were used to decrease the expression of CycT1 and CycT2 in ES cells and western blotting against CycT1, CycT2, and Cdk9 detected the levels of these proteins. (B) Mouse whole-genome RNA expression profiles between ES cells with siRNA species against CycT1 and CycT2. Forty-nine and 43 differentially expressed genes are depicted by pie charts for CycT1 and CycT2 knockdowns, respectively. The black and white slices denote shared and unique categories of proteins, respectively, adapted from Appendix 9 [97].

genes were genetically inactivated, we did not observe any viable embryos beyond the blastocyst stage, Appendix 9 and 10 [97, 99]. The physiological expression of both cyclins was detected in specific regions of developing embryos, especially in the epiblast, which is critical for the formation of all three germ layers and extraembryonic tissues. When the protein level of *Ccnt2* was downregulated utilizing specific siRNAs in embryonic stem cells - ESc, among the most affected were genes essential for early embryogenesis, including transforming growth factor β , Notch, Wnt signaling, and autophagy (Fig. 8).

In contrast, when cyclin T1 was downregulated, genes involved in glucose metabolism, cytokines, cell communication, and cell cycle were decreased.

4.2 Ineffective selection of autoreactive T cells in the absence of cyclin T1

One could conclude that CDK9-cyclin T1 or CDK9-cyclin T2 are mostly redundant in their transcription regulation, but there are subsets of genes which are specifically under the control of either CycT1 or CycT2, some of which are also critical for the early mouse embryonic development. In case of genetic inactivation of the *Ccnt1* gene, we failed to prepare a complete knock-out allele, thus only a hypomorphic *Ccnt1* mouse model was generated, Appendix 10 [99]. Nevertheless, this hypomorphic model allowed us to uncover a rather intriguing role of cyclin T1 during negative selection of autoreactive T lymphocytes in the thymus. The autoimmune regulator - AIRE is a transcriptional activator that mediates central tolerance in the thymus [100]. AIRE is expressed primarily in the subpopulations of medullary thymic epithelial cells - mTECs. The function of mTECs is to ectopically express various tissue-restricted, peripheral, antigens, which allow identification of autoreactive T cells. When AIRE is depleted from the mTEC cells it leads to autoimmunity in periphery manifested by infiltration of autoreactive T cells in periphery tissues, mainly endocrine glands, and production of autoreactive antibodies [101]. In case of a hypomorphic *Ccnt1* allele, lower expression of cyclin T1 led to insufficient selection of autoreactive clones of T lymphocytes in the thymus, leading to the appearance of inflammatory foci in salivary glands (Fig. 9).

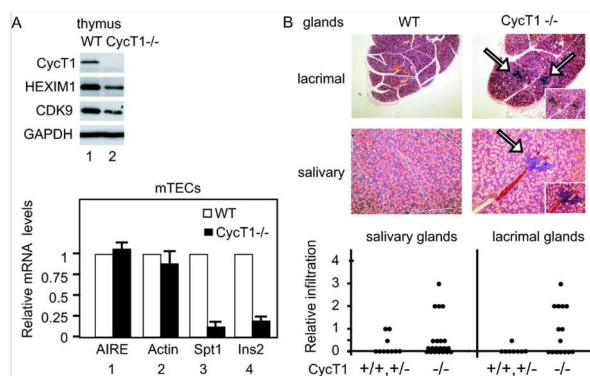


Figure 9: CycT1 mice do not express AIRE-responsive genes in the thymus and display lymphocytic infiltration of lacrimal and salivary glands. (A) Absent expression of CycT1 in the thymus parallels the lack of *Spt1* and *Ins2* transcripts in CycT1^{-/-} mice. The protein levels of CycT1, Hexim1, Cdk9, and GAPDH were evaluated by Western blotting and transcripts for AIRE, actin, *Spt1*, and *Ins2* were determined by RT-qPCR. **(B)** Lack of CycT1 in the mouse results in lymphocytic infiltration of lacrimal and salivary glands. Hematoxylin and eosin staining of formalin-fixed sections of lacrimal and salivary glands from 5- to 7-month-old WT and CycT1^{-/-} mice is presented. Arrows point to lymphocytic infiltrates in these organs, adapted from Appendix 10 [99].

In conclusion, improper negative selection was due to impaired function of transcription factor AIRE, which was responsible for spatio-temporal activation of expression of peripheral epitope antigens, which are presented by antigen-presenting cells during negative thymocyte selection. Of note, the organ with the highest expression of cyclin T1 was the thymus. It is likely to envision that the complete

knock-out of the *Ccnt1* gene would recapitulate the fate of *Ccnt2* or *Ccnk* knock-out mouse models. At the moment, there is no publication addressing the *Ccnt1* complete gene knock-out; the only information retrieved from the search is available from the database of the International Mouse Phenotyping Consortium, where the impact of cyclin T1 on mouse development was assessed (www.mousephenotype.org). Surprisingly, knock-out for the *Ccnt1* gene expressed only mild phenotypic alterations in homeostasis, hematopoietic, and immune systems. The observed phenotype could be attributed either to an inefficient knock-out strategy based on the CRISPR/Cas9 system in comparison to the insertion of a trap vector in the case of *Ccnt1*, *Ccnt2*, and *Ccnk*, or by the virtue of an incomplete truncated form of cyclin T1 as a product of CRISPR/Cas9-mediated mutagenesis. It is also possible that intact cyclin T2 substituted for cyclin T1. In case of the *Cdk9* gene, several significantly impacted phenotypes are reported, among them embryonic lethality prior organ formation, which partially recapitulates phenotypes observed in *Ccnt2* and *Ccnk* mice, yet without detectable preimplantation embryonic lethality in mouse embryos.

The early development is regulated by a very delicate balance of signaling stimuli mediated by prototypical morphogens. The mechanism of action of these morphogens starts with activation of the appropriate receptor and activation of specific signaling pathways, all converging in the modulation of transcription [31]. It has been demonstrated that transcription of many developmental genes is paused just right after initiation of synthesis, tens of nucleotides, and awaits activation by P-TEFb [44]. This type of regulation allows a very quick response to morphogenetic stimuli because phosphorylation of CTD by P-TEFb triggers release from the pause and initiates the productive elongation phase of transcription instantly. This type of regulation is well illustrated from our experiments in embryonic stem cells with down-regulated cyclin T2, when most of the genes with aberrant upregulated or downregulated expression were transcription factors responsible for developmental cues, morphogens, signaling molecules, or signaling pathways. Several research groups supported our observation by identifying specific developmental factors that are dependent on the kinase activity of CDK9-cyclin T2 rather than CDK9-cyclin T1 [44]. In my opinion, the CDK9-cyclin T1 axis is utilized by cells to regulate transcription of genes responsible for basal cellular processes, ranging from replication, movement, to cell division. On the other hand, CDK9-cyclin T2 controls transcription of genes not only implemented in basal cellular processes but also during development.

4.3 Impact of CDK13 loss on development

During our attempt to generate a CDK12 knock-out mouse model, a group of prof. Fann from Taipei, Taiwan, published work describing the impact of CDK12 deficiency on mouse development [102].

Similarly to the cyclin K knock-out model, the early embryonic lethality prior to the preimplantation stage was reported [77]. The ablation of CDK12 induced massive apoptosis in the morula blastocyst transition due to hyperactivated DDR [102]. Observed phenotype recapitulated the earlier described mechanism of CDK12-DDR axis in cancer cells described by our and other research groups. Thus, we shifted our attention to developing the CDK13 knock-out model and to exploring the role of CDK13 during mouse development.

The system of gene-trap technology was chosen to generate a knock-out allele of the *Cdk13* gene in the mouse. The gene-trap technology is based on the use of special viral vectors containing the *LacZ* gene under a very weak promoter. Only if the vector integrates into a genomic locus that provides a functional upstream promoter is the *LacZ* gene expressed. In addition, the vector contains unique homology sequences specific to the intron and exon of the *Cdk13* gene, providing navigation to the genomic locus. Once the vector is delivered to the cell, it integrates into the *Cdk13* gene as a result of a homologous recombination. Upon integration, the new allele *Cdk13^{tm1a}* is generated, which blocks productive transcription due to the presence of two strong PolyA sites in the gene-trap vector. The embryonic stem cells bearing the *Cdk13^{tm1a}* allele were injected into the recipient blastocyst, which was transferred to the pseudopregnant female mouse. The newborn mice were screened for the presence of founder animals, in which the *Cdk13^{tm1a}* allele was present in the germ line. Once we acquired F1 generations of heterozygous *Cdk13^{tm1a}* animals, the breeding of heterozygous animals was initiated.

The newborn mice were obtained, but no knock-out animal with the *Cdk13^{tm1a/tm1a}* combination was observed, [Appendix 11](#) [103]. However, the residual expression of Cdk13 was detected in the embryonic brain of *Cdk13^{tm1a/tm1a}* mice, suggesting generation of a hypomorphic allele of Cdk13, a situation similar to the *Ccnt1* gene [99]. Nevertheless, the embryonic lethality of *Cdk13^{tm1a/tm1a}* mouse was recognized at 16.5 days of embryonic development – E, with numerous visible morphological abnormalities. Apart from later discussed organ abnormalities the loss of Cdk13 caused growth retardation and developmental delay at each stage of gestation. On average, the *Cdk13^{tm1a/tm1a}* embryos appeared to be one embryonic day behind in comparison to their littermate controls as evidenced by the shallow indentation of the footpad at E13.5 in comparison to wild-type littermates exhibiting deep indentations between the developing toes which are characteristic of embryos at E14.5.

The analysis of craniofacial area revealed defective palatal shelves development in several *Cdk13^{tm1a/tm1a}* embryos, resulting in their insufficient horizontal growth and the formation of the cleft palate at E15.5, yet the severity among Cdk13-deficient animals was variable. In addition, the *Cdk13^{tm1a/tm1a}* embryo exhibited nuchal edema and pericardial effusion, most likely caused by

dysfunction of the heart. The heart is one of the first organs to form during mammalian development, and its organ morphology and organization reflect the increasing need of growing embryos for nutrition and oxygen supply. Interestingly, we found that the heart wall of *Cdk13^{tm1a/tm1a}* mice embryos was less compact, with an apparent disruption of tissue architecture, and a reduction of myocardium compared to wild-type embryos. In support of our observation, several miRNAs targeting *Cdk13* mRNA were recently recognized during the acute myocardial infarctions [104]. Recently, a group of prof. Loughna, Nottingham reported that homozygous and heterozygous animals with nonfunctional *Cdk13* allele in heart exhibited a range of congenital heart disease including ventricular septal defects, bicuspid aortic valve, double outlet right ventricle and atrioventricular septal defects accompanied by down-regulation of two genes known to be participating in heart development endothelin 1 and endothelin A receptor in E12.5 *Cdk13* mutant embryos [105].

All these data reflect CDK13 as a strategic molecule for optimal heart function. The brains of *Cdk13^{tm1a/tm1a}* embryos appeared developmentally delayed as demonstrated by reduced size as compared to littermate controls, probably due to a decrease in the number of proliferating cells in *Cdk13^{tm1a/tm1a}* embryos in comparison to *Cdk13* wild-type littermates. When a genome-wide screen was performed to identify factors involved in the formation of the nervous system in *Drosophila*, cyclin K was retrieved [106]. CDK12 and CDK13 kinases were shown to regulate activity of CDK5 and thus participate during the axonal elongation, supported by described function of CDK12 in process of embryonic neural development [107, 108]. Thus, studying CDK12 and CDK13 in the brain development appears as an exciting direction for our further research.

Since all described abnormalities resulted from the hypomorphic *Cdk13^{tm1a}* allele, we decided to generate a *Cdk13* allele with a nonfunctional variant of CDK13 to assess the impact of the complete loss of *Cdk13* gene. Therefore, *Cdk13^{tm1a}* mice were crossed with Flp-deleter mice and Cre-deleter mice to acquire the *Cdk13^{tm1d}* allele with deleted exons 3 and 4. Mice bearing the *Cdk13^{tm1d}* allele displayed undetectable *Cdk13* protein in the developing brain, with severely downregulated protein levels in heterozygous *Cdk13^{tm1d}* mice compared to wild-type littermates. Mice carrying *Cdk13^{tm1d}* alleles exhibited more severe defects in the craniofacial area with profound midline facial cleft, since the prevalence of the midline orofacial deficiency was 60.5% in *Cdk13^{tm1d}* homozygous mice at E12.5-E14.5 in comparison to wild-type littermates with a prevalence of 3% (Fig. 10). In conclusion, *Cdk13^{tm1d/tm1d}* embryos exhibited smaller body with visible growth retardation, prevalent hypoplasia of midfacial structures, smaller undeveloped hearts with severe ventricle, smaller liver with abrogated liver lobes arrangement and abrogated right left symmetry in kidney (Fig. 10). Overall, the developmental abnormalities were similar in animals with complete inactivation of *Cdk13* in comparison to mice with

a hypomorphic allele, yet with a more pronounced phenotype, especially in the case of the development of craniofacial structures.

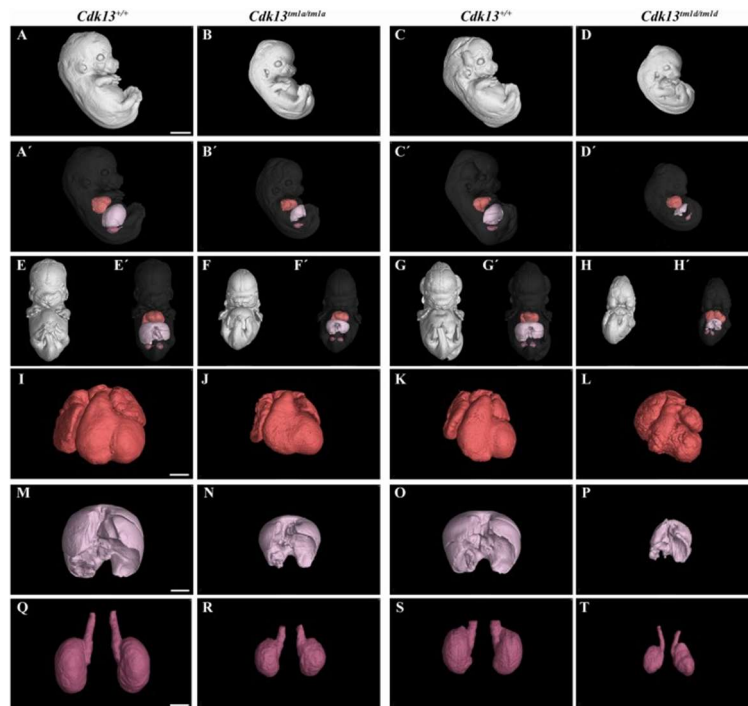
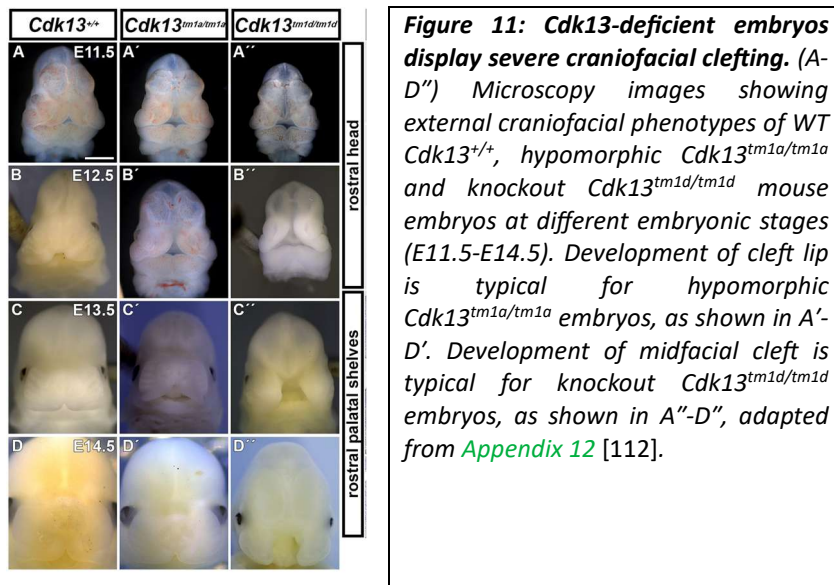


Figure 10: Comparison of $Cdk13^{tm1a}$ and $Cdk13^{tm1d}$ mice at E13.5. High-contrast differentiation resolution by X-ray computed microtomography, where Lugol's staining was used to visualize the soft tissues. The $Cdk13^{tm1a/tm1a}$, $Cdk13^{tm1d/tm1d}$, and their littermate controls, $Cdk13^{C/C}$, were analyzed at E13.5. (A–D) Overall view of $Cdk13^{C/C}$, $Cdk13^{tm1a/tm1a}$, and $Cdk13^{tm1d/tm1d}$ embryos. Both mutants exhibited smaller body size, with severe growth retardation in $Cdk13^{tm1d/tm1d}$ animals. (A'–D') 3D reconstruction of heart (red color), kidney (violet color), and liver (light pink color) in right side view of embryo, with embryo outlined in gray, where segmentation of serial sections was used for the reconstruction. Livers in $Cdk13^{tm1a/tm1a}$ and $Cdk13^{tm1d/tm1d}$ embryos were smaller than in $Cdk13^{C/C}$ embryos. (E–H') Frontal view of embryos with 3D reconstruction of heart, kidneys, and liver. A clear deficiency in the development of midfacial structures in $Cdk13^{tm1d/tm1d}$ embryos, in contrast to $Cdk13^{C/C}$ animals, was observed. (I–L) 3D reconstruction of the heart. The hearts of $Cdk13^{tm1a/tm1a}$ and $Cdk13^{tm1d/tm1d}$ embryos were smaller in comparison to control mice, with severe ventricular deficiency detected in $Cdk13^{tm1d/tm1d}$ animals. (M–P) 3D reconstruction of the liver. Generally, smaller livers were observed in $Cdk13^{tm1a/tm1a}$ and $Cdk13^{tm1d/tm1d}$ embryos in comparison to $Cdk13^{C/C}$ littermate control mice. Liver in $Cdk13^{tm1d/tm1d}$ mice exhibits abrogated liver parts arrangements. (Q–T) 3D reconstruction of kidneys. Kidneys are smaller with abnormal shape in $Cdk13^{tm1a/tm1a}$ and $Cdk13^{tm1d/tm1d}$ embryos. Scale bar (A–H) = 1,5 mm, Scale bar (I–L) = 350 mm, scale bar (M,P) = 500 mm, and scale bar (Q–T) = 250 mm, adapted from Appendix 11 [103].

4.4 Role of CDK13 in cranial neurogenesis

The phenotypic appearance of $Cdk13^{tm1a}$ and $Cdk13^{tm1d}$ homozygous mice recapitulated symptoms of patients with heterozygous mutation of the *CDK13* gene [109–111]. These patients exhibit a plethora of developmental abnormalities such as delayed development, intellectual disorders, heart and kidney defects, and craniofacial anomalies, features that – together – have been recognized as congenital heart defects, dysmorphic facial features, and intellectual development disorder - CHDFIDD. Therefore, we focused to examine mechanism regulating development of craniofacial structures and analyzed

early embryonic stages in CHDFIDD mouse models, with one model comprising a hypomorphic allele in *Cdk13* and exhibiting cleft lip/palate, and another model comprising knockout of *Cdk13*, featuring a stronger phenotype including midfacial cleft, [Appendix 12](#) [112]. Detailed morphological analyses revealed split facial prominences and, thus, a widely opened face in *Cdk13*^{tm1d/tm1d} embryos (Fig. 11).



Measurements of distances between individual facial prominences identified a significantly greater ratio of nasal pits distances and head width in maxillary prominence and lateral nasal prominence levels in both mutant genotypes (Fig. 11). Since the heads of mutant mice were smaller, we decided to validate the protein level of cyclin D1, a cell proliferation marker. The expression of mRNA of cyclin D1 was upregulated in almost all tissues isolated from facial prominences at E11.5 and E12.5 of *Cdk13*-deficient embryos, but no significant changes were detected in the palatal shelves of E12.5 or E14.5 *Cdk13*-deficient embryos. We knew that the development of the craniofacial region is closely associated with the development of cranial nerves, mainly the trigeminal nerve [113]. Interestingly, outgrowth alterations of several cranial nerves were detected in both *Cdk13*-deficient embryos, manifested by reduced length and obvious hypoplasia of maxillary, mandibular, and ophthalmic nerves. The expression profile of 84 neurogenesis-specific genes previously connected to neurogenesis during palatogenesis was evaluated in *Cdk13*^{tm1a/tm1a} embryos at E12.5 and E14.5. In both tested embryonic stages, gene expression was generally downregulated in the caudal compared to the rostral region, whereas in the rostral region, both up- and downregulation of gene expression were detected. Significant changes in the expression of genes involved in neurogenesis (*Ache*, *Dcx*, *Mef2c*, *Neurog1*, *Ntn1*, *Pou4f1*) within the developing palatal shelves were observed, along with changes in the expression pattern of other key face-specific genes (*Fgf8*, *Foxd1*, *Msx1*, *Meis2* and *Shh*). Aberrant

expression of these genes, including their downstream targets, led to similar facial clefts or reduced growth of facial nerves [114–116].

Observed morphological changes might be a result of insufficient development of the neural crest cells (NCCs, which could be the case since we confirmed reduced protein expression of the NCC marker *Sox9* in facial prominences of *Cdk13*-deficient animals. Significantly, conditional downregulation of *Mef2c* in NCCs was associated with craniofacial anomalies and neonatal lethality [117]. Conditional downregulation of *Mef2c* in neural crest cells - NCC, resulted in craniofacial and neonatal lethality, which resembles our observation with significant downregulation of *Mef2c* in all the palatal shelf regions [117]. CDK12 and CDK13 kinases were shown to regulate activity of CDK5 and thus participate during the axonal elongation, supported by described function of CDK12 in process of embryonic neural development [107, 108]. In support of this CDK13-CDK5 functional axis, we detected significant downregulation of genes encoding CDK5 regulatory subunits, such as of *Cdk5rap2* and *Cdk5r1*, in the caudal palatal shelves at E14.5 embryos supporting previous observation with *in vitro* neural cell lines [107, 108]. We also employed the trigeminal ganglia explant - TG *ex vivo* system in combination with THZ531, a specific inhibitor of CDK12 and CDK13 kinase activity. Increasing concentration of THZ531 led to a significant reduction in the formation of neurite outgrowths in TGs. Since the cells with neurite outgrowth did not exhibit noticeable DDR due to inactive CDK12, CDK13 likely participates in this process.

Collectively, these data demonstrate a key role of CDK13 in regulating craniofacial morphogenesis. To address the effect of CDK13 depletion on transcription, we performed chromatin immunoprecipitation - ChIP with an antibody against RNAPII for two genes *Pou4f1* and *Ntn1* selected from the PCR. The relative expressions for *Pou4f1* and *Ntn1* were downregulated and upregulated, respectively. Slight decrease of RNAPII was observed for the *Pou4f1* promoter in contrast to higher occupancy of RNAPII at the *Ntn1* promoter in *Cdk13^{tm1d/tm1d}* MEFs when compared with WT MEFs. Even though the statistical analyses did not prove statistically significant, the pattern of bound RNAPII correlated with different expressions of these genes evaluated by qPCR experiments.

The inactivation, even partial of *Cdk13*, led to embryonic lethality at later stages of mouse development due to multiple organ failures, which is in complete contrast with preimplantation lethality due to deregulated expression of DNA-damage repair genes leading to enhanced genomic instability reported for *Cdk12* deficient mice [102]. This observation nicely correlates with our data describing the same lethal phenotype at the blastocyst stage for mice with inactivated *CcnK* [77]. Cyclin K is abundantly expressed in mouse embryonic stem cells, gonocytes and spermatogonial stem cells during neonatal spermatogenesis [118, 119]. Interestingly, genetic depletion of *Cdk12* in the mouse

resulted in early developmental lethality at the blastocyst stage due to deregulated expression of DDR genes, leading to enhanced genomic instability [102]. When CDK13 was down-regulated in HCT116 cells, gene ontology analysis showed enrichment of genes connected to various extracellular and growth signaling pathways [120, 121]. Based on these observations, it is highly possible to propose that CDK13 controls transcription of unique sets of genes, which are necessary for specific developmental processes orchestrated by versatile signaling pathways and cellular processes such as growth, adhesion, migration, etc.

The expression of Cdk13 was evaluated first by RNAScope and qPCR, and its physiological expression was found to be highly expressed in craniofacial structures, such as the forebrain, nasal epithelium, and maxillary mesenchyme. Cdk13 is considered to localize in the nucleus, but limited information exists regarding the detection of Cdk13 in the cytoplasm. We therefore employed indirect immunofluorescence and uncovered localization of Cdk13 in the nuclear area and the cytoplasm around the nucleus, with a transparent signal for CDK13 within cellular outgrowths where it colocalized with actin filaments. The presence of CDK13 in the cytoplasm was next evaluated by cellular fractionation followed by western blot. As expected, CDK13 was detected in the nuclear fraction of primary MEF cells; however, significant levels of CDK13 were also detected in the cytoplasmic fraction. A similar nuclear versus cytoplasm distribution was proven in the mouse fibroblast cell line NIH3T3. This somewhat puzzling observation seems inconsistent with our understanding of the cellular function of CDK13, but CDK13 was found in the cytoplasm of various cancer cells, and CDK13 phosphorylated the intracellular domain of the transmembrane protein SERINC5 within the cytoplasm [122, 123].

4.5 Function of CDK12 during the oogenesis

For an oocyte to become a fully competent and mature egg, it must undergo through extensive growth and cytoplasmic extension characterized by the synthesis and storage of maternal RNA and proteins in the cytoplasm [124]. During the growth and maturation periods, the oocyte acquires meiotic and developmental competence, which is the ability to orchestrate and maintain early embryonic development [125]. The transcription of RNA throughout oocyte development, fertilization, and the preimplantation stage is orchestrated at the level of posttranslational modification of RNAPII, mainly phosphorylation. The growth of oocytes is accompanied by an extensive transcription burst defined by the active hyperphosphorylated form of RNAPII. The transcription is silenced from the fully grown oocyte, during meiotic maturation, fertilization, and first cell division, manifested by hypophosphorylation of RNAPII [126, 127]. Reactivation of transcription is initiated at the transition from one to two-cell mouse embryo, a process known as zygotic gene activation – ZGA, defined by

massive *de novo* hyperphosphorylation of RNAPII [128]. The hyperphosphorylated form represents phosphorylated CTD at Ser2, Ser5, and Ser7. The CDK9 was demonstrated to play a key role during transcription elongation phase at the 2-cell stage [129]. Thus, the Ser2 phosphorylation of RNAPII by CDK9 in the two-cell stage embryo is crucial for ZGA, nevertheless, the impact of related transcription kinases CDK12 or CDK13, Ser2 phosphorylating kinases, was not examined in growing oocytes.

To elucidate the role of CDK12 in growing and mature oocytes, we generated *Cdk12*^{-/-} by crossing a conditional *Cdk12*^{fl/fl} mouse with the ZP3Cre strain, in which Cre-recombinase expression is driven by the oocyte-specific zona pellucida glycoprotein 3 - Zp3 promoter. To explore the requirement of CDK12 in female fertility, we performed a series of experiments using a conditional CDK12 knockout (cKO) mouse model, [Appendix 13](#) [130]. Immunoblot analysis confirmed the absence of Cdk12 protein in the *CDK12*^{-/-} germinal vesicle - GV oocytes, supported by the absence of Cdk12 in the nucleus, while Cdk12 was present in the WT oocytes. Breeding experiments demonstrated that females lacking CDK12 in their oocytes were completely sterile, suggesting female sterility in *CDK12*^{-/-} animals. The oocytes undergo series of developmental stages before fully meiotically competent and prepare for fertilization, if any of the developmental stage is compromised the female sterility emerges. To understand the main cause of infertility in *CDK12*^{-/-} females, we analyzed the quality of ovaries and oocytes. The ovaries of *CDK12*^{-/-} females were significantly smaller compared to WT females, and their further histological analysis revealed a reduced number of primary follicles and almost no antral follicles, which could be the reason for the observed premature ovarian failure - POF phenotype.

As introduced in previous sections, the CDK12 regulates the activity of RNAPII, and since transcription drives oocyte growth, the impact of CDK12 on transcription was examined. To assess overall transcription, the newly synthesized RNA was labeled with 5-ethynyluridine, and the *CDK12*^{-/-} oocytes exhibited a 71% decrease in 5-ethynyluridine staining compared to *CDK12*^{+/+} oocytes. Importantly, the phosphorylation of Ser2 within the CTD of RNAPII was reduced by 39% in *CDK12*^{-/-} oocytes. These results suggest that the synthesis of RNA is impaired due to abnormal transcription caused by CDK12 deficiency during oogenesis. Next, we examined the expression of developmentally relevant classes of mRNAs encoding translational factors and markers associated with POF. Interestingly, a significant 3.5-fold increase in mRNA of the translational repressor eukaryotic translation initiation factor 4E binding protein 1 - 4E-BP1 was observed while other tested mRNAs, including POF, were significantly decreased in *CDK12*^{-/-} oocytes. Importantly, the mRNAs of *Cdk12* and *Cdk13* were significantly decreased in *CDK12*^{-/-} oocytes, whereas the mRNAs of *Ccnk*, *PolIII*, and *Hprt* were equally expressed in control and *CDK12*^{-/-} groups. The same results were obtained when immunoblotting of selected proteins was carried out. When the expression of Cdk12 was restored by microinjection of mRNA carrying mouse *Cdk12*, the level of 4E-BP1 was reduced to the same degree as

in WT oocytes, and importantly, the Ser2 mark of active RNAPII was reestablished. The stabilization of 4E-BP1 translational repressor in *Cdk12*^{-/-} oocytes led to a 23 % reduction in global protein synthesis compared to WT oocytes.

Considering the effect of CDK12 on RNA polyadenylation, we examined polyadenylation of the mRNA encoding 4E-BP1 [131, 132]. The Poly-A-length assay detected a visible poly(A) shift of the 3'UTR tail of *4E-bp1* mRNA in *CDK12*^{-/-} oocytes, while the poly(A) tail remained unchanged for control *Cnot7* mRNA, which is translated after completion of meiosis I. Moreover, no difference was detected for global polyadenylation by RNA FISH between *CDK12*^{+/+} and *CDK12*^{-/-} oocytes. The results demonstrate that *Cdk12* deficiency leads to a phenotype resembling premature oocyte failure due to aberrant oocyte growth because of impaired maternal transcription and translation.

The 69% decrease in global transcription is the most dramatic effect of CDK12 depletion on transcription previously documented by other research groups (Fig. 12). When both kinases were genetically depleted or chemically inhibited in various cellular systems, the transcription was downregulated by at most 15%. The most likely explanation is that the ablation of CDK12 led to a severe decrease of CDK13 as well, which is normally not detectable in cancer cells. If it is the case, then the CDK12 and CDK13 are major CDKs governing transcription program during oogenesis, and the residual level of transcription in growing oocytes was due to the activity of CDK9, since Ser2 phosphorylation of CTD, the mark of active transcription, was present. Apart from the effect on transcription the depletion of CDK12 led to stabilization of 4E-BP1, which is factor blocking initiation of translation, thus the stabilization of 4E-BP1 could explain 23% reduction in global protein synthesis in KO oocytes (Fig. 12).

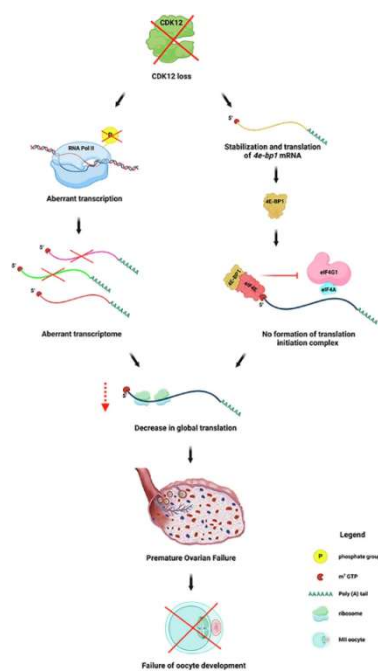


Figure 12: The absence of CDK12 in oocytes leads to complete female sterility. The fully developed oocytes capable of completing meiosis I are absent from the ovaries. Mechanistically, CDK12 regulates RNAPII activity in growing oocytes and ensures the maintenance of the physiological maternal transcriptome, which is essential for protein synthesis that drives further oocyte growth. Notably, CDK12-deficient growing oocytes exhibit a 71% reduction in transcriptional activity. Furthermore, impaired oocyte development disrupts folliculogenesis, leading to premature ovarian failure without terminal follicle maturation or ovulation. In conclusion, our findings identify CDK12 as a key master regulator of the oocyte transcriptional program and gene expression, indispensable for oocyte growth and female fertility, adapted from Appendix 13 [130].

The connection between the activity of CDK12 and the activity of 4E-BP1 was demonstrated by the Kathrine Jones group [2]. The CDK12 phosphorylates 4E-BP1 on Ser65 and Tyr70 and promotes translation of specific mRNA of factors involved in mitotic spindle regulation and chromosome segregation (Fig. 13). The same mechanism could be applicable for the regulation of translation in growing oocytes. In addition, CDK13 can also phosphorylate 4E-BP1 and promote protein synthesis of tumor progression-associated factors [122]. If the phosphorylation of Thr46 by CDK13 is a prerequisite to phosphorylation by CDK12, the absence of CDK13 potentiates a profound decrease in global translation in CDK12^{-/-} oocytes (Fig. 13). The dynamic changes in phosphorylation status of 4E-BP1 are well characterized during the transition between GV and MI, MII oocytes [133]. Therefore, the modulation of phosphorylation status of 4E-BP1 by CDK12 and CDK13 most likely works as a regulatory circuit in the growing oocytes to drive translation of developmentally unique mRNAs.

The connection of CDK12 and CDK13 with translation was recognized earlier, yet only recently have we started to appreciate their role in the control of translation of *bona fide* oncoproteins and their protein stability. In *Saccharomyces cerevisiae* the Rps2, a member of the small 40S ribosomal subunit, is phosphorylated by Ctk1, the yeast ortholog of CDK12 and CDK13 [6, 134]. Ctk1 thus participates in the initiation and elongation phases of translation. Previously we mentioned direct phosphorylation of Ser-65 and Thr-70 in negative translation factor 4E-BP1 by CDK12 converging in translation of many mRNAs which are target of mTOR pathway [2, 6]. This observation was further expanded by the synergistic effects of EGFR and CDK12/13 inhibitors, Gefitinib and THZ531, respectively, on inhibition of translation of oncogenic proteins [5].

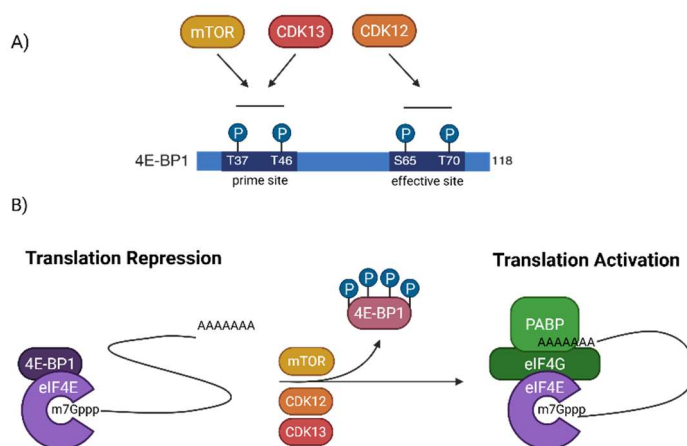


Figure 13: A schematic of the two-step phosphorylation model for 4E-BP1. The mTORC1 facilitates subsequent CDK13 phosphorylation of Thr-46 in 4E-BP1 followed by CDK12 phosphorylation at two consensus Ser-Pro sites S65 and T70. The coordinated phosphorylation of 4E-BP1 then drives translation of specific mRNAs and thus controls expressions of specific genes like oncoproteins and regulatory factors, adapted from [2, 122].

The effect was primarily mediated by reduced phosphorylation of 4E-BP1 by THZ531 and enhanced by Gefitinib. Since THZ531 can inhibit CDK12 and CDK13, it is also likely that phosphorylation of Thr-46 by CDK13 is contributing to the reported effect [122]. All this data supports a unique role of CDK12 and CDK13 in the regulation of translation-coupled oncoprotein stability and thus are a valuable target for cancer treatment. Indeed, dual inhibition of both

kinases led to the discovery of cancer-relevant genes in high-grade serous ovarian cancer presenting CDK12 and CDK13 as valuable therapeutic targets for tumor intervention [135].

5 SUMMARY AND FUTURE DIRECTIONS

Even though we have been learning a great deal of biology related to transcription-associated CDKs, there is still more to discover. It is apparent that CDKs are not connected only to the regulation of cell cycle or transcription, but atypical CDKs participate in many functionally diverse cellular processes, likely CDK12 and CDK13 as well. Both kinases phosphorylate the CTD of RNAPII and modulate the initiation of the elongation phase, splicing, alternative splicing, exon skipping, termination, and assembly of the export complex. Orchestrating the transcription of distinct sets of genes, they actively participate in DDR, replication competence, differentiation, immunity, viral infection, morphogenesis, and apoptosis. It was also demonstrated that CDK12 and CDK13 can phosphorylate additional substrates among them proteins of translation machinery.

The most intriguing and relevant to our future research directions, in my opinion, is discovered function of CDK12 and CDK13 in the regulation of translation mediated by phosphorylation of 4E-BP1. The concept of regulation of translation through the phosphorylation of 4E-BP1 is very exciting because it offers a very elegant way to synchronize several signaling pathways at once by activities of CDKs, situation similar to mTOR signaling pathway. The ability to restrict translation of distinctive classes of mRNA during physiological processes such as oocyte growth, or carcinogenesis by stabilization of oncoproteins mRNA makes them valuable candidates not only as experimental models to study diverse roles of CDK12 and CDK13 but also as valuable targets of patient mono- or combined therapy for medical interventions.

6 CITATIONS

- [1] CHIRACKAL MANAVALAN, Anil Paul, Kveta PILAROVA, Michael KLUGE, Koen BARTHOLOMEEUSEN, Michal RAJECKY, Jan OPPELT, Prashant KHIRSARIYA, Kamil PARUCH, Lumir KREJCI, Caroline C. FRIEDEL a Dalibor BLAZEK. CDK12 controls G1/S progression by regulating RNAPII processivity at core DNA replication genes. *EMBO reports* [online]. 2019, **20**(9), e47592. ISSN 1469-3178. Dostupné z: doi:10.15252/embr.201847592
- [2] CHOI, Seung H., Thomas F. MARTINEZ, Seongjae KIM, Cynthia DONALDSON, Maxim N. SHOKHIREV, Alan SAGHATELIAN a Katherine A. JONES. CDK12 phosphorylates 4E-BP1 to enable mTORC1-dependent translation and mitotic genome stability. *Genes & Development* [online]. 2019, **33**(7–8), 418–435. ISSN 1549-5477. Dostupné z: doi:10.1101/gad.322339.118
- [3] TIEN, Jerry F., Alborz MAZLOOMIAN, S.-W. Grace CHENG, Christopher S. HUGHES, Christalle C. T. CHOW, Leanna T. CANAPI, Arusha OLOUMI, Genny TRIGO-GONZALEZ, Ali BASHASHATI, James XU, Vicky C.-D. CHANG, Sohrab P. SHAH, Samuel APARICIO a Gregg B. MORIN. CDK12 regulates alternative last exon mRNA splicing and promotes breast cancer cell invasion. *Nucleic Acids Research* [online]. 2017, **45**(11), 6698–6716. ISSN 1362-4962. Dostupné z: doi:10.1093/nar/gkx187
- [4] MAGNUSON, Brian, Karan BEDI, Ishwarya Venkata NARAYANAN, Bartłomiej BARTKOWIAK, Hailey BLINKIEWICZ, Michelle T. PAULSEN, Arno GREENLEAF a Mats LJUNGMAN. CDK12 regulates co-transcriptional splicing and RNA turnover in human cells. *iScience* [online]. 2022, **25**(9), 105030. ISSN 2589-0042. Dostupné z: doi:10.1016/j.isci.2022.105030
- [5] ANG, Hazel X., Natalia SUTIMAN, Xinyue L. DENG, Annie LIU, Christian G. CERDA-SMITH, Haley M. HUTCHINSON, Holly KIM, Luke C. BARTELT, Qiang CHEN, Alejandro BARRERA, Jiaying LIN, Zhecheng SHENG, Ian C. MCDOWELL, Timothy E. REDDY, Christopher V. NICCHITTA a Kris C. WOOD. Cooperative regulation of coupled oncoprotein synthesis and stability in triple-negative breast cancer by EGFR and CDK12/13. *Proceedings of the National Academy of Sciences of the United States of America* [online]. 2023, **120**(38), e2221448120. ISSN 1091-6490. Dostupné z: doi:10.1073/pnas.2221448120
- [6] COORDES, Britta, Katharina M. BRÜNGER, Kaspar BURGER, Boumediene SOUFI, Juliane HORENK, Dirk EICK, Jesper V. OLSEN a Katja STRÄSSER. Ctk1 function is necessary for full translation initiation activity in *Saccharomyces cerevisiae*. *Eukaryotic Cell* [online]. 2015, **14**(1), 86–95. ISSN 1535-9786. Dostupné z: doi:10.1128/EC.00106-14
- [7] HOOK, R. Micrographia, or Some Physiological Descriptions of Minute Bodies Made by Magnifying Glasses, with Observations and Inquiries Thereupon. 1665.
- [8] SCHWANN, T. a H. SMITH. *Microscopical researches into the accordance in the structure and growth of animals and plants*. 1857.
- [9] MOLENAAR, J. C. [From the library of the Netherlands Journal of Medicine. Rudolf Virchow: Die Cellularpathologie in ihrer Begründung auf physiologische und pathologische Gewebelehre; 1858]. *Nederlands Tijdschrift Voor Geneeskunde*. 2003, **147**(45), 2236–2244. ISSN 0028-2162.
- [10] PAWELETZ, N. Walther Flemming: pioneer of mitosis research. *Nature Reviews. Molecular Cell Biology* [online]. 2001, **2**(1), 72–75. ISSN 1471-0072. Dostupné z: doi:10.1038/35048077

- [11] HOWARD, A. a S. R. PELC. Synthesis of nucleoprotein in bean root cells. *Nature* [online]. 1951, **167**(4250), 599–600. ISSN 0028-0836. Dostupné z: doi:10.1038/167599a0
- [12] HOWARD, A. a PELC, S. R. Synthesis of Deoxyribonucleic Acid in Normal and Irradiated Cells and Its Relation to Chromosome Breakage. 1953, (6), 261–273.
- [13] HARTWELL, L. H. *Saccharomyces cerevisiae* cell cycle. *Bacteriological Reviews* [online]. 1974, **38**(2), 164–198. ISSN 0005-3678. Dostupné z: doi:10.1128/br.38.2.164-198.1974
- [14] NURSE, P. A long twentieth century of the cell cycle and beyond. *Cell* [online]. 2000, **100**(1), 71–78. ISSN 0092-8674. Dostupné z: doi:10.1016/s0092-8674(00)81684-0
- [15] HARTWELL, L. H., R. K. MORTIMER, J. CULOTTI a M. CULOTTI. Genetic Control of the Cell Division Cycle in Yeast: V. Genetic Analysis of *cdc* Mutants. *Genetics* [online]. 1973, **74**(2), 267–286. ISSN 0016-6731. Dostupné z: doi:10.1093/genetics/74.2.267
- [16] LOHKA, M. J., M. K. HAYES a J. L. MALLER. Purification of maturation-promoting factor, an intracellular regulator of early mitotic events. *Proceedings of the National Academy of Sciences of the United States of America* [online]. 1988, **85**(9), 3009–3013. ISSN 0027-8424. Dostupné z: doi:10.1073/pnas.85.9.3009
- [17] HARTWELL, L. H., J. CULOTTI, J. R. PRINGLE a B. J. REID. Genetic control of the cell division cycle in yeast. *Science (New York, N.Y.)* [online]. 1974, **183**(4120), 46–51. ISSN 0036-8075. Dostupné z: doi:10.1126/science.183.4120.46
- [18] NURSE, P., P. THURIAUX a K. NASMYTH. Genetic control of the cell division cycle in the fission yeast *Schizosaccharomyces pombe*. *Molecular & general genetics: MGG* [online]. 1976, **146**(2), 167–178. ISSN 0026-8925. Dostupné z: doi:10.1007/BF00268085
- [19] BEACH, D., B. DURKACZ a P. NURSE. Functionally homologous cell cycle control genes in budding and fission yeast. *Nature* [online]. 1982, **300**(5894), 706–709. ISSN 0028-0836. Dostupné z: doi:10.1038/300706a0
- [20] LEE, M. G. a P. NURSE. Complementation used to clone a human homologue of the fission yeast cell cycle control gene *cdc2*. *Nature* [online]. 1987, **327**(6117), 31–35. ISSN 0028-0836. Dostupné z: doi:10.1038/327031a0
- [21] GAUTIER, J., C. NORBURY, M. LOHKA, P. NURSE a J. MALLER. Purified maturation-promoting factor contains the product of a *Xenopus* homolog of the fission yeast cell cycle control gene *cdc2+*. *Cell* [online]. 1988, **54**(3), 433–439. ISSN 0092-8674. Dostupné z: doi:10.1016/0092-8674(88)90206-1
- [22] EVANS, T., E. T. ROSENTHAL, J. YOUNGBLOM, D. DISTEL a T. HUNT. Cyclin: a protein specified by maternal mRNA in sea urchin eggs that is destroyed at each cleavage division. *Cell* [online]. 1983, **33**(2), 389–396. ISSN 0092-8674. Dostupné z: doi:10.1016/0092-8674(83)90420-8
- [23] NORBURY, Chris a Paul NURSE. ANIMAL CELL CYCLES AND THEIR CONTROL. *Annual Review of Biochemistry* [online]. 1992, **61**(Volume 61, 1992), 441–468. ISSN 0066-4154, 1545-4509. Dostupné z: doi:10.1146/annurev.bi.61.070192.002301
- [24] SHERR, C. J. a J. M. ROBERTS. CDK inhibitors: positive and negative regulators of G1-phase progression. *Genes & Development* [online]. 1999, **13**(12), 1501–1512. ISSN 0890-9369. Dostupné z: doi:10.1101/gad.13.12.1501

- [25] PELLARIN, Ilenia, Alessandra DALL'ACQUA, Andrea FAVERO, Ilenia SEGATTO, Valentina ROSSI, Nicole CRESTAN, Javad KARIMBAYLI, Barbara BELLETTI a Gustavo BALDASSARRE. Cyclin-dependent protein kinases and cell cycle regulation in biology and disease. *Signal Transduction and Targeted Therapy* [online]. 2025, **10**(1), 11. ISSN 2059-3635. Dostupné z: doi:10.1038/s41392-024-02080-z
- [26] MEYERSON, M., G. H. ENDERS, C. L. WU, L. K. SU, C. GORKA, C. NELSON, E. HARLOW a L. H. TSAI. A family of human cdc2-related protein kinases. *The EMBO journal* [online]. 1992, **11**(8), 2909–2917. ISSN 0261-4189. Dostupné z: doi:10.1002/j.1460-2075.1992.tb05360.x
- [27] HELLMICH, M. R., H. C. PANT, E. WADA a J. F. BATTEY. Neuronal cdc2-like kinase: a cdc2-related protein kinase with predominantly neuronal expression. *Proceedings of the National Academy of Sciences of the United States of America* [online]. 1992, **89**(22), 10867–10871. ISSN 0027-8424. Dostupné z: doi:10.1073/pnas.89.22.10867
- [28] SOLOMON, M. J., T. LEE a M. W. KIRSCHNER. Role of phosphorylation in p34cdc2 activation: identification of an activating kinase. *Molecular Biology of the Cell* [online]. 1992, **3**(1), 13–27. ISSN 1059-1524. Dostupné z: doi:10.1091/mbc.3.1.13
- [29] TASSAN, J. P., M. JAQUENOUD, P. LÉOPOLD, S. J. SCHULTZ a E. A. NIGG. Identification of human cyclin-dependent kinase 8, a putative protein kinase partner for cyclin C. *Proceedings of the National Academy of Sciences of the United States of America* [online]. 1995, **92**(19), 8871–8875. ISSN 0027-8424. Dostupné z: doi:10.1073/pnas.92.19.8871
- [30] GRAÑA, X., A. DE LUCA, N. SANG, Y. FU, P. P. CLAUDIO, J. ROSENBLATT, D. O. MORGAN a A. GIORDANO. PITALRE, a nuclear CDC2-related protein kinase that phosphorylates the retinoblastoma protein in vitro. *Proceedings of the National Academy of Sciences of the United States of America* [online]. 1994, **91**(9), 3834–3838. ISSN 0027-8424. Dostupné z: doi:10.1073/pnas.91.9.3834
- [31] KOHOUTEK, Jiri. P-TEFb- the final frontier. *Cell Division* [online]. 2009, **4**, 19. ISSN 1747-1028. Dostupné z: doi:10.1186/1747-1028-4-19
- [32] MALUMBRES, Marcos. Cyclin-dependent kinases. *Genome Biology* [online]. 2014, **15**(6), 122. ISSN 1474-760X. Dostupné z: doi:10.1186/gb4184
- [33] QUANDT, Eva, Mariana P. C. RIBEIRO a Josep CLOTET. Atypical cyclins: the extended family portrait. *Cellular and molecular life sciences: CMLS* [online]. 2020, **77**(2), 231–242. ISSN 1420-9071. Dostupné z: doi:10.1007/s00018-019-03262-7
- [34] LEW, J., K. BEAUDETTE, C. M. LITWIN a J. H. WANG. Purification and characterization of a novel proline-directed protein kinase from bovine brain. *The Journal of Biological Chemistry*. 1992, **267**(19), 13383–13390. ISSN 0021-9258.
- [35] PETERLIN, B. Matija a David H. PRICE. Controlling the Elongation Phase of Transcription with P-TEFb. *Molecular Cell* [online]. 2006, **23**(3), 297–305. ISSN 1097-2765. Dostupné z: doi:10.1016/j.molcel.2006.06.014
- [36] BUSHNELL, David A. a Roger D. KORNBERG. Complete, 12-subunit RNA polymerase II at 4.1-Å resolution: Implications for the initiation of transcription. *Proceedings of the National Academy of Sciences* [online]. 2003, **100**(12), 6969–6973. Dostupné z: doi:10.1073/pnas.1130601100

- [37] SUN, Rui a Robert P. FISHER. The CDK9-SPT5 Axis in Control of Transcription Elongation by RNAPII. *Journal of Molecular Biology* [online]. 2025, **437**(1), Controlling Transcription Elongation and Termination, 168746. ISSN 0022-2836. Dostupné z: doi:10.1016/j.jmb.2024.168746
- [38] HSIN, Jing-Ping a James L. MANLEY. The RNA polymerase II CTD coordinates transcription and RNA processing. *Genes & Development* [online]. 2012, **26**(19), 2119–2137. ISSN 1549-5477. Dostupné z: doi:10.1101/gad.200303.112
- [39] HARLEN, Kevin M. a L. Stirling CHURCHMAN. The code and beyond: transcription regulation by the RNA polymerase II carboxy-terminal domain. *Nature Reviews Molecular Cell Biology* [online]. 2017, **18**(4), 263–273. ISSN 1471-0080. Dostupné z: doi:10.1038/nrm.2017.10
- [40] FISHER, R. P. a D. O. MORGAN. A novel cyclin associates with MO15/CDK7 to form the CDK-activating kinase. *Cell* [online]. 1994, **78**(4), 713–724. ISSN 0092-8674. Dostupné z: doi:10.1016/0092-8674(94)90535-5
- [41] SHIEKHATTAR, R., F. MERMELSTEIN, R. P. FISHER, R. DRAPKIN, B. DYNLACHT, H. C. WESSLING, D. O. MORGAN a D. REINBERG. Cdk-activating kinase complex is a component of human transcription factor TFIIH. *Nature* [online]. 1995, **374**(6519), 283–287. ISSN 0028-0836. Dostupné z: doi:10.1038/374283a0
- [42] YU, David S., Runxiang ZHAO, Emory L. HSU, Jennifer CAYER, Fei YE, Yan GUO, Yu SHYR a David CORTEZ. Cyclin-dependent kinase 9-cyclin K functions in the replication stress response. *EMBO reports* [online]. 2010, **11**(11), 876–882. ISSN 1469-3178. Dostupné z: doi:10.1038/embor.2010.153
- [43] ANSHABO, Abel Tesfaye, Robert MILNE, Shudong WANG a Hugo ALBRECHT. CDK9: A Comprehensive Review of Its Biology, and Its Role as a Potential Target for Anti-Cancer Agents. *Frontiers in Oncology* [online]. 2021, **11** [vid. 2025-03-01]. ISSN 2234-943X. Dostupné z: doi:10.3389/fonc.2021.678559
- [44] FUJINAGA, Koh, Fang HUANG a B. Matija PETERLIN. P-TEFb: The master regulator of transcription elongation. *Molecular Cell* [online]. 2023, **83**(3), 393–403. ISSN 1097-2765. Dostupné z: doi:10.1016/j.molcel.2022.12.006
- [45] KOPCZYŃSKA, Magda, Upasana SAHA, Anastasiia ROMANENKO, Takayuki NOJIMA, Michał R. GDULA a Kinga KAMIENIARZ-GDULA. Defining gene ends: RNA polymerase II CTD threonine 4 phosphorylation marks transcription termination regions genome-wide. *Nucleic Acids Research* [online]. 2025, **53**(2), gkae1240. ISSN 1362-4962. Dostupné z: doi:10.1093/nar/gkae1240
- [46] SIMS, Robert J., Rimma BELOTSERKOVSKAYA a Danny REINBERG. Elongation by RNA polymerase II: the short and long of it. *Genes & Development* [online]. 2004, **18**(20), 2437–2468. ISSN 0890-9369. Dostupné z: doi:10.1101/gad.1235904
- [47] CORE, Leighton J., Joshua J. WATERFALL a John T. LIS. Nascent RNA sequencing reveals widespread pausing and divergent initiation at human promoters. *Science (New York, N.Y.)* [online]. 2008, **322**(5909), 1845–1848. ISSN 1095-9203. Dostupné z: doi:10.1126/science.1162228
- [48] MIN, Irene M., Joshua J. WATERFALL, Leighton J. CORE, Robert J. MUNROE, John SCHIMENTI a John T. LIS. Regulating RNA polymerase pausing and transcription elongation in embryonic stem cells. *Genes & Development* [online]. 2011, **25**(7), 742–754. ISSN 1549-5477. Dostupné z: doi:10.1101/gad.2005511

- [49] NGUYEN, V. T., T. KISS, A. A. MICHELS a O. BENSUAUDE. 7SK small nuclear RNA binds to and inhibits the activity of CDK9/cyclin T complexes. *Nature* [online]. 2001, **414**(6861), 322–325. ISSN 0028-0836. Dostupné z: doi:10.1038/35104581
- [50] YANG, Z., Q. ZHU, K. LUO a Q. ZHOU. The 7SK small nuclear RNA inhibits the CDK9/cyclin T1 kinase to control transcription. *Nature* [online]. 2001, **414**(6861), 317–322. ISSN 0028-0836. Dostupné z: doi:10.1038/35104575
- [51] KUSUHARA, Masatoshi, Koichi NAGASAKI, Kensuke KIMURA, Nicolai MAASS, Tomohiro MANABE, Shiro ISHIKAWA, Minoru AIKAWA, Koji MIYAZAKI a Ken YAMAGUCHI. Cloning of hexamethylene-bis-acetamide-inducible transcript, HEXIM1, in human vascular smooth muscle cells. *Biomedical Research* [online]. 1999, **20**(5), 273–279. ISSN 0388-6107. Dostupné z: doi:10.2220/biomedres.20.273
- [52] OUCHIDA, Rika, Masatoshi KUSUHARA, Noriaki SHIMIZU, Tetsuya HISADA, Yuichi MAKINO, Chikao MORIMOTO, Hiroshi HANDA, Fumitaka OHSUZU a Hirotohi TANAKA. Suppression of NF- κ B-dependent gene expression by a hexamethylene bisacetamide-inducible protein HEXIM1 in human vascular smooth muscle cells. *Genes to Cells* [online]. 2003, **8**(2), 95–107. ISSN 1365-2443. Dostupné z: doi:10.1046/j.1365-2443.2003.00618.x
- [53] MICHELS, Annemieke A., Van Trung NGUYEN, Alessandro FRALDI, Valérie LABAS, Mia EDWARDS, François BONNET, Luigi LANIA a Olivier BENSUAUDE. MAQ1 and 7SK RNA interact with CDK9/cyclin T complexes in a transcription-dependent manner. *Molecular and Cellular Biology* [online]. 2003, **23**(14), 4859–4869. ISSN 0270-7306. Dostupné z: doi:10.1128/MCB.23.14.4859-4869.2003
- [54] GHATPANDE, S., S. GOSWAMI, S. MATHEW, G. RONG, L. CAI, S. SHAFIQ a M. A. SIDDIQUI. Identification of a novel cardiac lineage-associated protein(cCLP-1): A candidate regulator of cardiogenesis. *Developmental Biology* [online]. 1999, **208**(1), 210–221. ISSN 0012-1606. Dostupné z: doi:10.1006/dbio.1998.9180
- [55] SIDDIQUI, M. A. Q., Michael WAGNER, Eduardo MASCARENO a Saiyid SHAFIQ. Signal Transduction in Myofibrillogenesis, Cell Growth, and Hypertrophy. In: Dipak K. DUBE, ed. *Myofibrillogenesis* [online]. Boston, MA: Birkhäuser, 2002 [vid. 2025-03-01], s. 143–152. ISBN 978-1-4612-0199-1. Dostupné z: doi:10.1007/978-1-4612-0199-1_9
- [56] WITTMANN, Bryan M., Nancy WANG a Monica M. MONTANO. Identification of a novel inhibitor of breast cell growth that is down-regulated by estrogens and decreased in breast tumors. *Cancer Research*. 2003, **63**(16), 5151–5158. ISSN 0008-5472.
- [57] BARBORIC, Matjaz, Jiri KOHOUTEK, Jason P. PRICE, Dalibor BLAZEK, David H. PRICE a B. Matija PETERLIN. Interplay between 7SK snRNA and oppositely charged regions in HEXIM1 direct the inhibition of P-TEFb. *The EMBO journal* [online]. 2005, **24**(24), 4291–4303. ISSN 0261-4189. Dostupné z: doi:10.1038/sj.emboj.7600883
- [58] BLAZEK, Dalibor, Matjaz BARBORIC, Jiri KOHOUTEK, Irena OVEN a B. Matija PETERLIN. Oligomerization of HEXIM1 via 7SK snRNA and coiled-coil region directs the inhibition of P-TEFb. *Nucleic Acids Research* [online]. 2005, **33**(22), 7000–7010. ISSN 1362-4962. Dostupné z: doi:10.1093/nar/gki997
- [59] KOHOUTEK, Jiri, Dalibor BLAZEK a B. Matija PETERLIN. Hexim1 sequesters positive transcription elongation factor b from the class II transactivator on MHC class II promoters. *Proceedings of*

- the National Academy of Sciences* [online]. 2006, **103**(46), 17349–17354. Dostupné z: doi:10.1073/pnas.0603079103
- [60] LI, Qintong, Jason P. PRICE, Sarah A. BYERS, Dongmei CHENG, Junmin PENG a David H. PRICE. Analysis of the large inactive P-TEFb complex indicates that it contains one 7SK molecule, a dimer of HEXIM1 or HEXIM2, and two P-TEFb molecules containing Cdk9 phosphorylated at threonine 186. *The Journal of Biological Chemistry* [online]. 2005, **280**(31), 28819–28826. ISSN 0021-9258. Dostupné z: doi:10.1074/jbc.M502712200
- [61] CHEN, Ruichuan, Zhiyuan YANG a Qiang ZHOU. Phosphorylated positive transcription elongation factor b (P-TEFb) is tagged for inhibition through association with 7SK snRNA. *The Journal of Biological Chemistry* [online]. 2004, **279**(6), 4153–4160. ISSN 0021-9258. Dostupné z: doi:10.1074/jbc.M310044200
- [62] CONTRERAS, Xavier, Matjaz BARBORIC, Tina LENASI a B. Matija PETERLIN. HMBA releases P-TEFb from HEXIM1 and 7SK snRNA via PI3K/Akt and activates HIV transcription. *PLoS pathogens* [online]. 2007, **3**(10), 1459–1469. ISSN 1553-7374. Dostupné z: doi:10.1371/journal.ppat.0030146
- [63] KIM, Young Kyeung, Uri MBONYE, Joseph HOKELLO a Jonathan KARN. T-cell receptor signaling enhances transcriptional elongation from latent HIV proviruses by activating P-TEFb through an ERK-dependent pathway. *Journal of Molecular Biology* [online]. 2011, **410**(5), 896–916. ISSN 1089-8638. Dostupné z: doi:10.1016/j.jmb.2011.03.054
- [64] FUJINAGA, Koh, Matjaz BARBORIC, Qintong LI, Zeping LUO, David H. PRICE a B. Matija PETERLIN. PKC phosphorylates HEXIM1 and regulates P-TEFb activity. *Nucleic Acids Research* [online]. 2012, **40**(18), 9160–9170. ISSN 1362-4962. Dostupné z: doi:10.1093/nar/gks682
- [65] MBONYE, Uri, Konstantin LESKOV, Meenakshi SHUKLA, Saba VALADKHAN a Jonathan KARN. Biogenesis of P-TEFb in CD4+ T cells to reverse HIV latency is mediated by protein kinase C (PKC)-independent signaling pathways. *PLoS pathogens* [online]. 2021, **17**(9), e1009581. ISSN 1553-7374. Dostupné z: doi:10.1371/journal.ppat.1009581
- [66] ESPINOZA-DEROUT, Jorge, Michael WAGNER, Katayoun SHAHMIRI, Eduardo MASCARENO, Brahim CHAQOUR a M. a. Q. SIDDIQUI. Pivotal role of cardiac lineage protein-1 (CLP-1) in transcriptional elongation factor P-TEFb complex formation in cardiac hypertrophy. *Cardiovascular Research* [online]. 2007, **75**(1), 129–138. ISSN 0008-6363. Dostupné z: doi:10.1016/j.cardiores.2007.03.019
- [67] CHEN, Ruichuan, Min LIU, Huan LI, Yuhua XUE, Wanichaya N. RAMEY, Nanhai HE, Nanping AI, Haohong LUO, Ying ZHU, Nan ZHOU a Qiang ZHOU. PP2B and PP1alpha cooperatively disrupt 7SK snRNP to release P-TEFb for transcription in response to Ca²⁺ signaling. *Genes & Development* [online]. 2008, **22**(10), 1356–1368. ISSN 0890-9369. Dostupné z: doi:10.1101/gad.1636008
- [68] WANG, Yan, Eugene C. DOW, Yao-Yun LIANG, Rajesh RAMAKRISHNAN, Hongbing LIU, Tzu-Ling SUNG, Xia LIN a Andrew P. RICE. Phosphatase PPM1A regulates phosphorylation of Thr-186 in the Cdk9 T-loop. *The Journal of Biological Chemistry* [online]. 2008, **283**(48), 33578–33584. ISSN 0021-9258. Dostupné z: doi:10.1074/jbc.M807495200
- [69] JERONIMO, Célia, Diane FORGET, Annie BOUCHARD, Qintong LI, Gordon CHUA, Christian POITRAS, Cynthia THÉRIEN, Dominique BERGERON, Sylvie BOURASSA, Jack GREENBLATT, Benoit CHABOT, Guy G. POIRIER, Timothy R. HUGHES, Mathieu BLANCHETTE, David H. PRICE a Benoit

- COULOMBE. Systematic analysis of the protein interaction network for the human transcription machinery reveals the identity of the 7SK capping enzyme. *Molecular Cell* [online]. 2007, **27**(2), 262–274. ISSN 1097-2765. Dostupné z: doi:10.1016/j.molcel.2007.06.027
- [70] KRUEGER, Brian J., Célia JERONIMO, Bibhuti Bhusan ROY, Annie BOUCHARD, Charlotte BARRANDON, Sarah A. BYERS, Courtney E. SEARCEY, Jeffrey J. COOPER, Olivier BENSAUDE, Eric A. COHEN, Benoit COULOMBE a David H. PRICE. LARP7 is a stable component of the 7SK snRNP while P-TEFb, HEXIM1 and hnRNP A1 are reversibly associated. *Nucleic Acids Research* [online]. 2008, **36**(7), 2219–2229. ISSN 1362-4962. Dostupné z: doi:10.1093/nar/gkn061
- [71] BACON, Curtis W. a Iván D'ORSO. CDK9: a signaling hub for transcriptional control. *Transcription* [online]. 2019, **10**(2), 57–75. ISSN 2154-1272. Dostupné z: doi:10.1080/21541264.2018.1523668
- [72] MBONYE, Uri R., Giridharan GOKULRANGAN, Manish DATT, Curtis DOBROWOLSKI, Maxwell COOPER, Mark R. CHANCE a Jonathan KARN. Phosphorylation of CDK9 at Ser175 enhances HIV transcription and is a marker of activated P-TEFb in CD4(+) T lymphocytes. *PLoS pathogens* [online]. 2013, **9**(5), e1003338. ISSN 1553-7374. Dostupné z: doi:10.1371/journal.ppat.1003338
- [73] MBONYE, Uri, Benlian WANG, Giridharan GOKULRANGAN, Wuxian SHI, Sichun YANG a Jonathan KARN. Cyclin-dependent kinase 7 (CDK7)-mediated phosphorylation of the CDK9 activation loop promotes P-TEFb assembly with Tat and proviral HIV reactivation. *The Journal of Biological Chemistry* [online]. 2018, **293**(26), 10009–10025. ISSN 1083-351X. Dostupné z: doi:10.1074/jbc.RA117.001347
- [74] LLOYD, Sarah M., Daniel B. LEON, Mari O. BRADY, Deborah RODRIGUEZ, Madison P. MCREYNOLDS, Junghun KWEON, Amy E. NEELY, Laura A. BLUMENSAADT, Patric J. HO a Xiaomin BAO. CDK9 activity switch associated with AFF1 and HEXIM1 controls differentiation initiation from epidermal progenitors. *Nature Communications* [online]. 2022, **13**(1), 4408. ISSN 2041-1723. Dostupné z: doi:10.1038/s41467-022-32098-2
- [75] HARGREAVES, Diana C., Tiffany HORNG a Ruslan MEDZHITOV. Control of inducible gene expression by signal-dependent transcriptional elongation. *Cell* [online]. 2009, **138**(1), 129–145. ISSN 1097-4172. Dostupné z: doi:10.1016/j.cell.2009.05.047
- [76] BARTKOWIAK, Bartłomiej, Pengda LIU, Hemali P. PHATNANI, Nicholas J. FUDA, Jeffrey J. COOPER, David H. PRICE, Karen ADELMAN, John T. LIS a Arno L. GREENLEAF. CDK12 is a transcription elongation-associated CTD kinase, the metazoan ortholog of yeast Ctk1. *Genes & Development* [online]. 2010, **24**(20), 2303–2316. ISSN 1549-5477. Dostupné z: doi:10.1101/gad.1968210
- [77] BLAZEK, Dalibor, Jiri KOHOUTEK, Koen BARTHOLOMEEUSEN, Eric JOHANSEN, Petra HULINKOVA, Zeping LUO, Peter CIMERMANCIC, Jernej ULE a B. Matija PETERLIN. The Cyclin K/Cdk12 complex maintains genomic stability via regulation of expression of DNA damage response genes. *Genes & Development* [online]. 2011, **25**(20), 2158–2172. ISSN 1549-5477. Dostupné z: doi:10.1101/gad.16962311
- [78] KOHOUTEK, Jiri a Dalibor BLAZEK. Cyclin K goes with Cdk12 and Cdk13. *Cell Division* [online]. 2012, **7**, 12. ISSN 1747-1028. Dostupné z: doi:10.1186/1747-1028-7-12
- [79] DENG, Chu-Xia. BRCA1: cell cycle checkpoint, genetic instability, DNA damage response and cancer evolution. *Nucleic Acids Research* [online]. 2006, **34**(5), 1416–1426. ISSN 1362-4962. Dostupné z: doi:10.1093/nar/gkl010

- [80] JIANG, Qinqin a Roger A. GREENBERG. Deciphering the BRCA1 Tumor Suppressor Network. *The Journal of Biological Chemistry* [online]. 2015, **290**(29), 17724–17732. ISSN 1083-351X. Dostupné z: doi:10.1074/jbc.R115.667931
- [81] BAJRAMI, Ilirjana, Jessica R. FRANKUM, Asha KONDE, Rowan E. MILLER, Farah L. REHMAN, Rachel BROUGH, James CAMPBELL, David SIMS, Rumana RAFIQ, Sean HOOPER, Lina CHEN, Iwanka KOZAREWA, Ioannis ASSIOTIS, Kerry FENWICK, Rachael NATRAJAN, Christopher J. LORD a Alan ASHWORTH. Genome-wide profiling of genetic synthetic lethality identifies CDK12 as a novel determinant of PARP1/2 inhibitor sensitivity. *Cancer Research* [online]. 2014, **74**(1), 287–297. ISSN 1538-7445. Dostupné z: doi:10.1158/0008-5472.CAN-13-2541
- [82] LORD, Christopher J. a Alan ASHWORTH. PARP inhibitors: Synthetic lethality in the clinic. *Science (New York, N.Y.)* [online]. 2017, **355**(6330), 1152–1158. ISSN 1095-9203. Dostupné z: doi:10.1126/science.aam7344
- [83] LI, Shuangying, Liangliang WANG, Yuanyuan WANG, Changyi ZHANG, Zhenya HONG a Zhiqiang HAN. The synthetic lethality of targeting cell cycle checkpoints and PARPs in cancer treatment. *Journal of Hematology & Oncology* [online]. 2022, **15**(1), 147. ISSN 1756-8722. Dostupné z: doi:10.1186/s13045-022-01360-x
- [84] MCNEELY, S., R. BECKMANN a A. K. BENCE LIN. CHEK again: revisiting the development of CHK1 inhibitors for cancer therapy. *Pharmacology & Therapeutics* [online]. 2014, **142**(1), 1–10. ISSN 1879-016X. Dostupné z: doi:10.1016/j.pharmthera.2013.10.005
- [85] BAHASSI, E. M., J. L. OVESEN, A. L. RIESENBERG, W. Z. BERNSTEIN, P. E. HASTY a P. J. STAMBROOK. The checkpoint kinases Chk1 and Chk2 regulate the functional associations between hBRCA2 and Rad51 in response to DNA damage. *Oncogene* [online]. 2008, **27**(28), 3977–3985. ISSN 1476-5594. Dostupné z: doi:10.1038/onc.2008.17
- [86] GAILLARD, Hélène, Tatiana GARCÍA-MUSE a Andrés AGUILERA. Replication stress and cancer. *Nature Reviews. Cancer* [online]. 2015, **15**(5), 276–289. ISSN 1474-1768. Dostupné z: doi:10.1038/nrc3916
- [87] PACULOVÁ, Hana, Juraj KRAMARA, Šárka ŠIMEČKOVÁ, Radek FEDR, Karel SOUČEK, Ondřej HYLSE, Kamil PARUCH, Marek SVOBODA, Martin MISTRÍK a Jiří KOHOUTEK. BRCA1 or CDK12 loss sensitizes cells to CHK1 inhibitors. *Tumour Biology: The Journal of the International Society for Oncodevelopmental Biology and Medicine* [online]. 2017, **39**(10), 1010428317727479. ISSN 1423-0380. Dostupné z: doi:10.1177/1010428317727479
- [88] KIM, Marianne K., Dong J. MIN, George WRIGHT, Ian GOLDLUST a Christina M. ANNUNZIATA. Loss of compensatory pro-survival and anti-apoptotic modulator, IKK ϵ , sensitizes ovarian cancer cells to CHEK1 loss through an increased level of p21. *Oncotarget* [online]. 2014, **5**(24), 12788–12802. ISSN 1949-2553. Dostupné z: doi:10.18632/oncotarget.2665
- [89] CANCER GENOME ATLAS NETWORK. Comprehensive molecular portraits of human breast tumours. *Nature* [online]. 2012, **490**(7418), 61–70. ISSN 1476-4687. Dostupné z: doi:10.1038/nature11412
- [90] PACULOVÁ, Hana a Jiří KOHOUTEK. The emerging roles of CDK12 in tumorigenesis. *Cell Division* [online]. 2017, **12**, 7. ISSN 1747-1028. Dostupné z: doi:10.1186/s13008-017-0033-x
- [91] PETROPOULOS, Michalis, Angeliki KARAMICHALI, Giacomo G. ROSSETTI, Alena FREUDENMANN, Luca G. IACOVINO, Vasilis S. DIONELLIS, Sotirios K. SOTIRIOU a Thanos D. HALAZONETIS.

- Transcription–replication conflicts underlie sensitivity to PARP inhibitors. *Nature* [online]. 2024, **628**(8007), 433–441. ISSN 1476-4687. Dostupné z: doi:10.1038/s41586-024-07217-2
- [92] KOLESNICHENKO, Marina a Claus SCHEIDEREIT. Synthetic lethality by PARP inhibitors: new mechanism uncovered based on unresolved transcription-replication conflicts. *Signal Transduction and Targeted Therapy* [online]. 2024, **9**(1), 179. ISSN 2059-3635. Dostupné z: doi:10.1038/s41392-024-01893-2
- [93] HELLEDAY, Thomas. The underlying mechanism for the PARP and BRCA synthetic lethality: clearing up the misunderstandings. *Molecular Oncology* [online]. 2011, **5**(4), 387–393. ISSN 1878-0261. Dostupné z: doi:10.1016/j.molonc.2011.07.001
- [94] CURTI, Laura, Sara ROHBAN, Nicola BIANCHI, Ottavio CROCI, Adrian ANDRONACHE, Sara BAROZZI, Michela MATTIOLI, Fernanda RICCI, Elena PASTORI, Silvia SBERNA, Simone BELLOTTI, Anna ACCIALINI, Roberto BALLARINO, Nicola CROSETTO, Mark WADE, Dario PARAZZOLI a Stefano CAMPANER. CDK12 controls transcription at damaged genes and prevents MYC-induced transcription-replication conflicts. *Nature Communications* [online]. 2024, **15**(1), 7100. ISSN 2041-1723. Dostupné z: doi:10.1038/s41467-024-51229-5
- [95] TIEN, Jean Ching-Yi, Jie LUO, Yu CHANG, Yuping ZHANG, Yunhui CHENG, Xiaoju WANG, Jianzhang YANG, Rahul MANNAN, Somnath MAHAPATRA, Palak SHAH, Xiao-Ming WANG, Abigail J. TODD, Sanjana EYUNNI, Caleb CHENG, Ryan J. REBERNICK, Lanbo XIAO, Yi BAO, James NEISWENDER, Rachel BROUGH, Stephen J. PETTITT, Xuhong CAO, Stephanie J. MINER, Licheng ZHOU, Yi-Mi WU, Estefania LABANCA, Yuzhuo WANG, Abhijit PAROLIA, Marcin CIESLIK, Dan R. ROBINSON, Zhen WANG, Felix Y. FENG, Jonathan CHOU, Christopher J. LORD, Ke DING a Arul M. CHINNAIYAN. CDK12 loss drives prostate cancer progression, transcription-replication conflicts, and synthetic lethality with paralog CDK13. *Cell Reports. Medicine* [online]. 2024, **5**(10), 101758. ISSN 2666-3791. Dostupné z: doi:10.1016/j.xcrm.2024.101758
- [96] TANG, Jun, Natasha E. WEISER, Guiping WANG, Sudhir CHOWDHRY, Ellis J. CURTIS, Yanding ZHAO, Ivy Tsz-Lo WONG, Georgi K. MARINOV, Rui LI, Philip HANOIAN, Edison TSE, Salvador Garcia MOJICA, Ryan HANSEN, Joshua PLUM, Auzon STEFFY, Snezana MILUTINOVIC, S. Todd MEYER, Jens LUEBECK, Yanbo WANG, Shu ZHANG, Nicolas ALTEMOSE, Christina CURTIS, William J. GREENLEAF, Vineet BAFNA, Stephen J. BENKOVIC, Anthony B. PINKERTON, Shailaja KASIBHATLA, Christian A. HASSIG, Paul S. MISCHER a Howard Y. CHANG. Enhancing transcription-replication conflict targets ecDNA-positive cancers. *Nature* [online]. 2024, **635**(8037), 210–218. ISSN 1476-4687. Dostupné z: doi:10.1038/s41586-024-07802-5
- [97] KOHOUTEK, Jiri, Qintong LI, Dalibor BLAZEK, Zeping LUO, Huimin JIANG a B. Matija PETERLIN. Cyclin T2 Is Essential for Mouse Embryogenesis. *Molecular and Cellular Biology* [online]. 2009, **29**(12), 3280–3285. ISSN null. Dostupné z: doi:10.1128/MCB.00172-09
- [98] DONG, Peng a Zhe LIU. Shaping development by stochasticity and dynamics in gene regulation. *Open Biology* [online]. 2017, **7**(5), 170030. ISSN 2046-2441. Dostupné z: doi:10.1098/rsob.170030
- [99] I, Oven, Brdicková N, Kohoutek J, Vaupotic T, Narat M a Peterlin BM. AIRE recruits P-TEFb for transcriptional elongation of target genes in medullary thymic epithelial cells. *Molecular and cellular biology* [online]. 2007, **27**(24) [vid. 2025-03-02]. ISSN 1098-5549. Dostupné z: doi:10.1128/MCB.01085-07
- [100] HEINO, M., P. PETERSON, J. KUDOH, K. NAGAMINE, A. LAGERSTEDT, V. OVOD, A. RANKI, I. RANTALA, M. NIEMINEN, J. TUUKKANEN, H. S. SCOTT, S. E. ANTONARAKIS, N. SHIMIZU a K.

- KROHN. Autoimmune regulator is expressed in the cells regulating immune tolerance in thymus medulla. *Biochemical and Biophysical Research Communications* [online]. 1999, **257**(3), 821–825. ISSN 0006-291X. Dostupné z: doi:10.1006/bbrc.1999.0308
- [101] NAGAMINE, K., P. PETERSON, H. S. SCOTT, J. KUDOH, S. MINOSHIMA, M. HEINO, K. J. KROHN, M. D. LALIOTI, P. E. MULLIS, S. E. ANTONARAKIS, K. KAWASAKI, S. ASAKAWA, F. ITO a N. SHIMIZU. Positional cloning of the APECED gene. *Nature Genetics* [online]. 1997, **17**(4), 393–398. ISSN 1061-4036. Dostupné z: doi:10.1038/ng1297-393
- [102] JUAN, H.-C., Y. LIN, H.-R. CHEN a M.-J. FANN. Cdk12 is essential for embryonic development and the maintenance of genomic stability. *Cell Death and Differentiation* [online]. 2016, **23**(6), 1038–1048. ISSN 1476-5403. Dostupné z: doi:10.1038/cdd.2015.157
- [103] NOVÁKOVÁ, Monika, Marek HAMPL, Dávid VRÁBEL, Jan PROCHÁZKA, Silvia PETREZSELYOVÁ, Michaela PROCHÁZKOVÁ, Radislav SEDLÁČEK, Michaela KAVKOVÁ, Tomáš ZIKMUND, Jozef KAISER, Hsien-Chia JUAN, Ming-Ji FANN, Marcela BUCHTOVÁ a Jiří KOHOUTEK. Mouse Model of Congenital Heart Defects, Dysmorphic Facial Features and Intellectual Developmental Disorders as a Result of Non-functional CDK13. *Frontiers in Cell and Developmental Biology* [online]. 2019, **7**, 155. ISSN 2296-634X. Dostupné z: doi:10.3389/fcell.2019.00155
- [104] WANG, Jianchu, Ying ZHANG, Libai LU, Yuan LU, Qianli TANG a Jian PU. Insight into the molecular mechanism of LINC00152/miR-215/CDK13 axis in hepatocellular carcinoma progression. *Journal of Cellular Biochemistry* [online]. 2019, **120**(11), 18816–18825. ISSN 1097-4644. Dostupné z: doi:10.1002/jcb.29197
- [105] WAHEED-ULLAH, Qazi, Anna WILSDON, Aseel ABBAD, Sophie ROCHETTE, Frances BU'LOCK, Asma Ali SAED, Marc-Phillip HITZ, J. David BROOK a Siobhan LOUGHNA. Cyclin-dependent kinase 13 is indispensable for normal mouse heart development. *Journal of Anatomy* [online]. 2024. ISSN 1469-7580. Dostupné z: doi:10.1111/joa.14175
- [106] NEUMÜLLER, Ralph A., Constance RICHTER, Anja FISCHER, Maria NOVATCHKOVA, Klaus G. NEUMÜLLER a Juergen A. KNOBLICH. Genome-wide analysis of self-renewal in Drosophila neural stem cells by transgenic RNAi. *Cell Stem Cell* [online]. 2011, **8**(5), 580–593. ISSN 1875-9777. Dostupné z: doi:10.1016/j.stem.2011.02.022
- [107] CHEN, Hong-Ru, Guan-Ting LIN, Chun-Kai HUANG a Ming-Ji FANN. Cdk12 and Cdk13 regulate axonal elongation through a common signaling pathway that modulates Cdk5 expression. *Experimental Neurology* [online]. 2014, **261**, 10–21. ISSN 1090-2430. Dostupné z: doi:10.1016/j.expneurol.2014.06.024
- [108] CHEN, Hong-Ru, Hsien-Chia JUAN, Yu-Hui WONG, Jin-Wu TSAI a Ming-Ji FANN. Cdk12 Regulates Neurogenesis and Late-Arising Neuronal Migration in the Developing Cerebral Cortex. *Cerebral Cortex (New York, N.Y.: 1991)* [online]. 2017, **27**(3), 2289–2302. ISSN 1460-2199. Dostupné z: doi:10.1093/cercor/bhw081
- [109] SIFRIM, Alejandro, Marc-Phillip HITZ, Anna WILSDON, Jeroen BRECKPOT, Saeed H. AI TURKI, Bernard THIENPONT, Jeremy MCRAE, Tomas W. FITZGERALD, Tarjinder SINGH, Ganesh Jawahar SWAMINATHAN, Elena PRIGMORE, Diana RAJAN, Hashim ABDUL-KHALIQ, Siddharth BANKA, Ulrike M. M. BAUER, Jamie BENTHAM, Felix BERGER, Shoumo BHATTACHARYA, Frances BU'LOCK, Natalie CANHAM, Irina-Gabriela COLGIU, Catherine COSGROVE, Helen COX, Ingo DAEHNERT, Allan DALY, John DANESH, Alan FRYER, Marc GEWILLIG, Emma HOBSON, Kirstin HOFF, Tessa HOMFRAY, INTERVAL STUDY, Anne-Karin KAHLERT, Ami KETLEY, Hans-Heiner KRAMER, Katherine LACHLAN, Anne Katrin LAMPE, Jacoba J. LOUW, Ashok Kumar MANICKARA,

Dorin MANASE, Karen P. MCCARTHY, Kay METCALFE, Carmel MOORE, Ruth NEWBURY-ECOB, Seham Osman OMER, Willem H. OUWEHAND, Soo-Mi PARK, Michael J. PARKER, Thomas PICKARDT, Martin O. POLLARD, Leema ROBERT, David J. ROBERTS, Jennifer SAMBROOK, Kerry SETCHFIELD, Brigitte STILLER, Chris THORNBOROUGH, Okan TOKA, Hugh WATKINS, Denise WILLIAMS, Michael WRIGHT, Seema MITAL, Piers E. F. DAUBENEY, Bernard KEAVNEY, Judith GOODSHIP, UK10K CONSORTIUM, Riyadh Mahdi ABU-SULAIMAN, Sabine KLAASSEN, Caroline F. WRIGHT, Helen V. FIRTH, Jeffrey C. BARRETT, Koenraad DEVRIENDT, David R. FITZPATRICK, J. David BROOK, DECIPHERING DEVELOPMENTAL DISORDERS STUDY a Matthew E. HURLES. Distinct genetic architectures for syndromic and nonsyndromic congenital heart defects identified by exome sequencing. *Nature Genetics* [online]. 2016, **48**(9), 1060–1065. ISSN 1546-1718. Dostupné z: doi:10.1038/ng.3627

- [110] BOSTWICK, Bret L., Scott MCLEAN, Jennifer E. POSEY, Haley E. STREFF, Karen W. GRIPP, Alyssa BLESSON, Nina POWELL-HAMILTON, Jessica TUSI, David A. STEVENSON, Elynn FARRELLY, Louanne HUDGINS, Yaping YANG, Fan XIA, Xia WANG, Pengfei LIU, Magdalena WALKIEWICZ, Marianne MCGUIRE, Dorothy K. GRANGE, Marisa V. ANDREWS, Marybeth HUMMEL, Suneeta MADAN-KHETARPAL, Elena INFANTE, Zeynep COBAN-AKDEMIR, Karol MISZALSKI-JAMKA, John L. JEFFERIES, MEMBERS OF THE UNDIAGNOSED DISEASES NETWORK, Jill A. ROSENFELD, Lisa EMRICK, Kimberly M. NUGENT, James R. LUPSKI, John W. BELMONT, Brendan LEE a Seema R. LALANI. Phenotypic and molecular characterisation of CDK13-related congenital heart defects, dysmorphic facial features and intellectual developmental disorders. *Genome Medicine* [online]. 2017, **9**(1), 73. ISSN 1756-994X. Dostupné z: doi:10.1186/s13073-017-0463-8
- [111] HAMILTON, Mark James a Mohnish SURI. CDK13-related disorder. *Advances in Genetics* [online]. 2019, **103**, 163–182. ISSN 0065-2660. Dostupné z: doi:10.1016/bs.adgen.2018.11.001
- [112] HAMPL, Marek, Nela JANDOVÁ, Denisa LUSKOVÁ, Monika NOVÁKOVÁ, Tereza SZOTKOWSKÁ, Štěpán ČADA, Jan PROCHÁZKA, Jiri KOHOUTEK a Marcela BUCHTOVÁ. Early embryogenesis in CHDFIDD mouse model reveals facial clefts and altered cranial neurogenesis. *Disease Models & Mechanisms* [online]. 2024, **17**(6), dmm050261. ISSN 1754-8411. Dostupné z: doi:10.1242/dmm.050261
- [113] HIGASHIYAMA, Hiroki a Shigeru KURATANI. On the maxillary nerve. *Journal of Morphology* [online]. 2014, **275**(1), 17–38. ISSN 1097-4687. Dostupné z: doi:10.1002/jmor.20193
- [114] LEVI, Giovanni, Stefano MANTERO, Ottavia BARBIERI, Daniela CANTATORE, Laura PALEARI, Annemiek BEVERDAM, Francesca GENOVA, Benoit ROBERT a Giorgio R. MERLO. Msx1 and Dlx5 act independently in development of craniofacial skeleton, but converge on the regulation of Bmp signaling in palate formation. *Mechanisms of Development* [online]. 2006, **123**(1), 3–16. ISSN 0925-4773. Dostupné z: doi:10.1016/j.mod.2005.10.007
- [115] MACHON, Ondrej, Jan MASEK, Olga MACHONOVA, Stefan KRAUSS a Zbynek KOZMIK. Meis2 is essential for cranial and cardiac neural crest development. *BMC developmental biology* [online]. 2015, **15**, 40. ISSN 1471-213X. Dostupné z: doi:10.1186/s12861-015-0093-6
- [116] JEONG, Juhee, Junhao MAO, Toyooki TENZEN, Andreas H. KOTTMANN a Andrew P. MCMAHON. Hedgehog signaling in the neural crest cells regulates the patterning and growth of facial primordia. *Genes & Development* [online]. 2004, **18**(8), 937–951. ISSN 0890-9369. Dostupné z: doi:10.1101/gad.1190304
- [117] VERZI, Michael P., Pooja AGARWAL, Courtney BROWN, David J. MCCULLEY, John J. SCHWARZ a Brian L. BLACK. The transcription factor MEF2C is required for craniofacial development.

- Developmental Cell* [online]. 2007, **12**(4), 645–652. ISSN 1534-5807. Dostupné z: doi:10.1016/j.devcel.2007.03.007
- [118] DAI, Qian, Tingjun LEI, Changhong ZHAO, Jianqiao ZHONG, Yi-zhi TANG, Bin CHEN, Jie YANG, Chenghua LI, Siyu WANG, Xu SONG, Li LI a Qintong LI. Cyclin K-containing kinase complexes maintain self-renewal in murine embryonic stem cells. *The Journal of Biological Chemistry* [online]. 2012, **287**(30), 25344–25352. ISSN 1083-351X. Dostupné z: doi:10.1074/jbc.M111.321760
- [119] XIANG, Xiaocong, Li DENG, Jingli ZHANG, Xudong ZHANG, Tingjun LEI, Guangxin LUAN, Chunlei YANG, Zhi-Xiong XIAO, Qian LI a Qintong LI. A distinct expression pattern of cyclin K in mammalian testes suggests a functional role in spermatogenesis. *PLoS One* [online]. 2014, **9**(7), e101539. ISSN 1932-6203. Dostupné z: doi:10.1371/journal.pone.0101539
- [120] GREIFENBERG, Ann Katrin, Dana HÖNIG, Kveta PILAROVA, Robert DÜSTER, Koen BARTHOLOMEEUSEN, Christian A. BÖSKEN, Kanchan ANAND, Dalibor BLAZEK a Matthias GEYER. Structural and Functional Analysis of the Cdk13/Cyclin K Complex. *Cell Reports* [online]. 2016, **14**(2), 320–331. ISSN 2211-1247. Dostupné z: doi:10.1016/j.celrep.2015.12.025
- [121] LIANG, Kaiwei, Xin GAO, Joshua M. GILMORE, Laurence FLORENS, Michael P. WASHBURN, Edwin SMITH a Ali SHILATIFARD. Characterization of human cyclin-dependent kinase 12 (CDK12) and CDK13 complexes in C-terminal domain phosphorylation, gene transcription, and RNA processing. *Molecular and Cellular Biology* [online]. 2015, **35**(6), 928–938. ISSN 1098-5549. Dostupné z: doi:10.1128/MCB.01426-14
- [122] WU, Chao, Ting XIE, Ying GUO, Donghai WANG, Min QIU, Ruyi HAN, Guoliang QING, Kaiwei LIANG a Hudan LIU. CDK13 phosphorylates the translation machinery and promotes tumorigenic protein synthesis. *Oncogene* [online]. 2023, **42**(16), 1321–1330. ISSN 1476-5594. Dostupné z: doi:10.1038/s41388-023-02653-2
- [123] CHAI, Qingqing, Sunan LI, Morgan K. COLLINS, Rongrong LI, Iqbal AHMAD, Silas F. JOHNSON, Dylan A. FRABUTT, Zhichang YANG, Xiaojing SHEN, Liangliang SUN, Jian HU, Judd F. HULTQUIST, B. Matija PETERLIN a Yong-Hui ZHENG. HIV-1 Nef interacts with the cyclin K/CDK13 complex to antagonize SERINC5 for optimal viral infectivity. *Cell Reports* [online]. 2021, **36**(6), 109514. ISSN 2211-1247. Dostupné z: doi:10.1016/j.celrep.2021.109514
- [124] STERNLICHT, A. L. a R. M. SCHULTZ. Biochemical studies of mammalian oogenesis: kinetics of accumulation of total and poly(A)-containing RNA during growth of the mouse oocyte. *The Journal of Experimental Zoology* [online]. 1981, **215**(2), 191–200. ISSN 0022-104X. Dostupné z: doi:10.1002/jez.1402150209
- [125] SHA, Qian-Qian, Ye-Zhang ZHU, Sen LI, Yu JIANG, Lu CHEN, Xiao-Hong SUN, Li SHEN, Xiang-Hong OU a Heng-Yu FAN. Characterization of zygotic genome activation-dependent maternal mRNA clearance in mouse. *Nucleic Acids Research* [online]. 2020, **48**(2), 879–894. ISSN 1362-4962. Dostupné z: doi:10.1093/nar/gkz1111
- [126] OQANI, Reza K., Jin Yu ZHANG, Min Gu LEE, Yun Fei DIAO a Dong-Il JIN. Phosphorylation Status of RNA Polymerase II Carboxyl-terminal Domain in Porcine Oocytes and Early Embryos. *Asian-Australasian Journal of Animal Sciences* [online]. 2012, **25**(6), 789–793. ISSN 1011-2367. Dostupné z: doi:10.5713/ajas.2011.11396
- [127] ABE, Ken-Ichiro, Azusa INOUE, Masataka G. SUZUKI a Fugaku AOKI. Global gene silencing is caused by the dissociation of RNA polymerase II from DNA in mouse oocytes. *The Journal of*

Reproduction and Development [online]. 2010, **56**(5), 502–507. ISSN 0916-8818. Dostupné z: doi:10.1262/jrd.10-068a

- [128] BELLIER, S., S. CHASTANT, P. ADENOT, M. VINCENT, J. P. RENARD a O. BENSUAUDE. Nuclear translocation and carboxyl-terminal domain phosphorylation of RNA polymerase II delineate the two phases of zygotic gene activation in mammalian embryos. *The EMBO journal* [online]. 1997, **16**(20), 6250–6262. ISSN 0261-4189. Dostupné z: doi:10.1093/emboj/16.20.6250
- [129] ABE, Kenichiro, Tamas SCHAUER a Maria-Elena TORRES-PADILLA. Distinct patterns of RNA polymerase II and transcriptional elongation characterize mammalian genome activation. *Cell Reports* [online]. 2022, **41**(13), 111865. ISSN 2211-1247. Dostupné z: doi:10.1016/j.celrep.2022.111865
- [130] JANSOVA, Denisa, Veronika SEDMIKOVA, Fatima J. BERRO, Daria ALESHKINA, Michal DVORAN, Michal KUBELKA, Jitka REZACOVA, Jana RUTAROVA, Jiri KOHOUTEK a Andrej SUSOR. Absence of CDK12 in oocyte leads to female infertility. *Cell Death & Disease* [online]. 2025, **16**(1), 213. ISSN 2041-4889. Dostupné z: doi:10.1038/s41419-025-07536-w
- [131] DUBBURY, Sara J., Paul L. BOUTZ a Phillip A. SHARP. CDK12 regulates DNA repair genes by suppressing intronic polyadenylation. *Nature* [online]. 2018, **564**(7734), 141–145. ISSN 1476-4687. Dostupné z: doi:10.1038/s41586-018-0758-y
- [132] KRAJEWSKA, Malgorzata, Ruben DRIES, Andrew V. GRASSETTI, Sofia DUST, Yang GAO, Hao HUANG, Bandana SHARMA, Daniel S. DAY, Nicholas KWIATKOWSKI, Monica POMAVILLE, Oliver DODD, Edmond CHIPUMURO, Tinghu ZHANG, Arno L. GREENLEAF, Guo-Cheng YUAN, Nathanael S. GRAY, Richard A. YOUNG, Matthias GEYER, Scott A. GERBER a Rani E. GEORGE. CDK12 loss in cancer cells affects DNA damage response genes through premature cleavage and polyadenylation. *Nature Communications* [online]. 2019, **10**(1), 1757. ISSN 2041-1723. Dostupné z: doi:10.1038/s41467-019-09703-y
- [133] JANSOVA, Denisa, Marketa KONCICKA, Anna TETKOVA, Renata CERNA, Radek MALIK, Edgar DEL LLANO, Michal KUBELKA a Andrej SUSOR. Regulation of 4E-BP1 activity in the mammalian oocyte. *Cell Cycle (Georgetown, Tex.)* [online]. 2017, **16**(10), 927–939. ISSN 1551-4005. Dostupné z: doi:10.1080/15384101.2017.1295178
- [134] RÖTHER, Susanne a Katja STRÄSSER. The RNA polymerase II CTD kinase Ctk1 functions in translation elongation. *Genes & Development* [online]. 2007, **21**(11), 1409–1421. ISSN 0890-9369. Dostupné z: doi:10.1101/gad.428407
- [135] CESARI, Eleonora, Alessandra CIUCCI, Marco PIERACCIOLI, Cinzia CAGGIANO, Camilla NERO, Davide BONVISSUTO, Francesca SILLANO, Marianna BUTTARELLI, Alessia PIERMATTEI, Matteo LOVERRO, Floriana CAMARDA, Viviana GRECO, Maria DE BONIS, Angelo MINUCCI, Daniela GALLO, Andrea URBANI, Giuseppe VIZZIELLI, Giovanni SCAMBIA a Claudio SETTE. Dual inhibition of CDK12 and CDK13 uncovers actionable vulnerabilities in patient-derived ovarian cancer organoids. *Journal of experimental & clinical cancer research: CR* [online]. 2023, **42**(1), 126. ISSN 1756-9966. Dostupné z: doi:10.1186/s13046-023-02682-5

7 APPENDICES

- 1) BARBORIC, Matjaz, **Jirí KOHOUTEK**, Jason P. PRICE, Dalibor BLAZEK, David H. PRICE a B. Matija PETERLIN. Interplay between 7SK snRNA and oppositely charged regions in HEXIM1 direct the inhibition of P-TEFb. *The EMBO journal*. 2005, 24(24), 4291–4303.
- 2) BLAZEK, Dalibor, Matjaz BARBORIC, **Jiri KOHOUTEK**, Irena OVEN a B. Matija PETERLIN. Oligomerization of HEXIM1 via 7SK snRNA and coiled-coil region directs the inhibition of P-TEFb. *Nucleic Acids Research*. 2005, 33(22), 7000–7010.
- 3) **KOHOUTEK, Jiri**, Dalibor BLAZEK a B. Matija PETERLIN. Hexim1 sequesters positive transcription elongation factor b from the class II transactivator on MHC class II promoters. *Proceedings of the National Academy of Sciences*. 2006, 103(46), 17349–17354.
- 4) **KOHOUTEK, Jiri**. P-TEFb- the final frontier. *Cell Division*. 2009, 4, 19
- 5) BLAZEK, Dalibor, **Jiri KOHOUTEK**, Koen BARTHOLOMEEUSEN, Eric JOHANSEN, Petra HULINKOVA, Zeping LUO, Peter CIMERMANCIC, Jernej ULE a B. Matija PETERLIN. The Cyclin K/Cdk12 complex maintains genomic stability via regulation of expression of DNA damage response genes. *Genes & Development*. 2011, 25(20), 2158–2172.
- 6) **KOHOUTEK, Jiri** a Dalibor BLAZEK. Cyclin K goes with Cdk12 and Cdk13. *Cell Division*. 2012, 7, 12.
- 7) PACULOVÁ, Hana, Juraj KRAMARA, Šárka ŠIMEČKOVÁ, Radek FEDR, Karel SOUČEK, Ondřej HYLSE, Kamil PARUCH, Marek SVOBODA, Martin MISTRÍK a **Jiří KOHOUTEK**. BRCA1 or CDK12 loss sensitizes cells to CHK1 inhibitors. *Tumour Biology: The Journal of the International Society for Oncodevelopmental Biology and Medicine*. 2017, 39(10), 1010428317727479.
- 8) PACULOVÁ, Hana a **Jiří KOHOUTEK**. The emerging roles of CDK12 in tumorigenesis. *Cell Division*. 2017, 12, 7.
- 9) **KOHOUTEK, Jiri**, Qintong LI, Dalibor BLAZEK, Zeping LUO, Huimin JIANG a B. Matija PETERLIN. Cyclin T2 Is Essential for Mouse Embryogenesis. *Molecular and Cellular Biology*. 2009, 29(12), 3280–3285.
- 10) OVEN Irena, BRDICKOVA Nada, **KOHOUTEK Jiri**, VAUPOTIC Tomas, NARAT M a Peterlin B. Matija. AIRE recruits P-TEFb for transcriptional elongation of target genes in medullary thymic epithelial cells. *Molecular and cellular biology*. 2007, 27(24).

- 11) NOVÁKOVÁ, Monika, Marek HAMPL, Dávid VRÁBEL, Jan PROCHÁZKA, Silvia PETREZSELYOVÁ, Michaela PROCHÁZKOVÁ, Radislav SEDLÁČEK, Michaela KAVKOVÁ, Tomáš ZIKMUND, Jozef KAISER, Hsien-Chia JUAN, Ming-Ji FANN, Marcela BUCHTOVÁ a **Jiří KOHOUTEK**. Mouse Model of Congenital Heart Defects, Dysmorphic Facial Features and Intellectual Developmental Disorders as a Result of Non-functional CDK13. *Frontiers in Cell and Developmental Biology*. 2019, 7, 155.
- 12) HAMPL, Marek, Nela JANDOVÁ, Denisa LUSKOVÁ, Monika NOVÁKOVÁ, Tereza SZOTKOWSKÁ, Štěpán ČADA, Jan PROCHÁZKA, **Jiri KOHOUTEK** a Marcela BUCHTOVÁ. Early embryogenesis in CHDFIDD mouse model reveals facial clefts and altered cranial neurogenesis. *Disease Models & Mechanisms*. 2024, 17(6), dmm050261.
- 13) JANSOVA, Denisa, Veronika SEDMIKOVA, Fatima J. BERRO, Daria ALESHKINA, Michal DVORAN, Michal KUBELKA, Jitka REZACOVA, Jana RUTAROVA, **Jiri KOHOUTEK** and Andrej SUSOR. Absence of CDK12 in oocyte leads to female infertility. *Cell Death & Disease*. 2025, **16**(1), 213. ISSN 2041-4889.

APPENDIX 1

BARBORIC, Matjaz, **Jirí KOHOUTEK**, Jason P. PRICE, Dalibor BLAZEK, David H. PRICE and B. Matija PETERLIN. Interplay between 7SK snRNA and oppositely charged regions in HEXIM1 direct the inhibition of P-TEFb. *The EMBO journal*. 2005, 24(24), 4291–4303.

Interplay between 7SK snRNA and oppositely charged regions in HEXIM1 direct the inhibition of P-TEFb

Matjaz Barboric¹, Jiří Kohoutek¹, Jason P Price², Dalibor Blazek¹, David H Price² and B Matija Peterlin^{1,*}

¹Departments of Medicine, Microbiology, and Immunology, Rosalind Russell Medical Research Center, University of California at San Francisco, San Francisco, CA, USA and ²Department of Biochemistry, University of Iowa, Iowa City, Iowa, USA

Transcription elongation of eukaryotic genes by RNA polymerase II depends on the positive transcription elongation factor b (P-TEFb). When sequestered into the large complex, P-TEFb kinase activity is inhibited by the coordinate actions of 7SK small nuclear RNA (7SK snRNA) and hexamethylene bisacetamide (HMBA)-induced protein 1 (HEXIM1). We found that the basic region in HEXIM1 directs its nuclear import via two monopartite and two bipartite nuclear localization sequences. Moreover, the arginine-rich motif within it is essential for its binding to 7SK snRNA, P-TEFb, and inhibition of transcription. Notably, the basic region interacts with the adjacent acidic regions in the absence of RNA. The removal of the positive or negative charges from these regions in HEXIM1 leads to its sequestration into the large complex and inhibition of transcription independently of the arginine-rich motif. Finally, the removal of the negative charges from HEXIM1 results in its subnuclear localization into nuclear speckles. We propose a model where the interplay between 7SK snRNA and oppositely charged regions in HEXIM1 direct its binding to P-TEFb and subcellular localization that culminates in the inhibition of transcription.

The EMBO Journal (2005) 24, 4291–4303. doi:10.1038/sj.emboj.7600883; Published online 15 December 2005

Subject Categories: chromatin & transcription; RNA

Keywords: HEXIM1; nuclear speckles; P-TEFb; transcription elongation; 7SK snRNA

Introduction

The transcription of eukaryotic genes by RNA polymerase II (RNAPII) is coordinated tightly at many levels, including those of transcription elongation (Sims *et al*, 2004). Shortly after promoter clearance, the negative transcription elongation factor (N-TEF) forms a paused complex with RNAPII. The transition to robust transcription elongation depends on the positive transcription elongation factor b (P-TEFb), which

is required for the expression of the human immunodeficiency virus (HIV) and most cellular protein-coding genes (Chao and Price, 2001; Barboric and Peterlin, 2005). It consists of heterodimers between a catalytic subunit, the cyclin-dependent kinase 9 (Cdk9), and one of the four C-type cyclin regulatory subunits, CycT1, CycT2a, CycT2b, or CycK. When recruited to paused transcription complexes, P-TEFb phosphorylates serines at position 2 in the C-terminal domain (CTD) of the Rpb1 subunit of RNAPII and subunits of N-TEF, resulting in the efficient elongation and cotranscriptional processing of nascent pre-mRNA molecules.

Besides the active, heterodimeric form, P-TEFb exists in a larger, catalytically inactive complex in cells in which the 7SK small nuclear RNA (7SK snRNA) was found initially (Nguyen *et al*, 2001; Yang *et al*, 2001). In addition to P-TEFb and 7SK snRNA, this large complex contains the hexamethylene bisacetamide (HMBA)-induced protein 1 (HEXIM1) (Michels *et al*, 2003; Yik *et al*, 2003) that has been identified previously as a protein whose expression is induced by HMBA in vascular smooth muscle cells (Kusuhara *et al*, 1999). Growing body of evidence suggests that the coordinated actions of 7SK snRNA and HEXIM1 result in the inhibition of P-TEFb (Yik *et al*, 2003; Michels *et al*, 2004). In a proposed model, 7SK snRNA binds the basic region in HEXIM1 (BR), which is the prerequisite for the interaction between the C-terminus of HEXIM1 and CycT1, culminating in the inactivation of P-TEFb (Michels *et al*, 2004; Li *et al*, 2005; Schulte *et al*, 2005). Notably, another HEXIM1-related protein, HEXIM2, binds and inhibits P-TEFb in the presence of 7SK snRNA (Byers *et al*, 2005; Yik *et al*, 2005). Moreover, the assembly of the large complex is facilitated due to the homo- and hetero-oligomerization of HEXIM1 and HEXIM2 (Dulac *et al*, 2005; Li *et al*, 2005; Yik *et al*, 2005). Finally, the ratio between active and inactive P-TEFb complexes controls cell growth. For example, several growth signals release P-TEFb from the inactive complex in cardiac hypertrophy in mice, a disease characterized by the enlargement of cardiac myocytes due to a global increase in mRNA and protein contents (Sano *et al*, 2002).

In addition to binding 7SK snRNA, the BR is required for the nuclear import of HEXIM1 (Ouchida *et al*, 2003). In principle, nucleocytoplasmic transport occurs through the nuclear pore complexes (NPCs) and is carried out by karyopherins, which include importins and exportins (Weis, 2003). Most karyopherins bind the topogenic sequences for protein transport directly. For example, importin β translocates the HIV-1 regulatory proteins Tat and Rev by binding their arginine-rich nuclear localization sequences (NLSs) directly (Truant and Cullen, 1999). In contrast, importin β can also bind the classical, lysine-rich, NLS-containing cargos via an adaptor protein, importin α . This latter mechanism constitutes the classical nuclear import pathway, in which importin α binds the NLS and importin β docks the ternary complex at

*Corresponding author. Box 0703, 3rd and Parnassus Aves, San Francisco, CA 94143-0703, USA. Tel.: +1 415 502 1902; Fax: +1 415 502 1901; E-mail: matija@itsa.ucsf.edu

Received: 21 February 2005; accepted: 2 November 2005; published online: 15 December 2005

the NPC. Classical NLSs are typified by either a single basic cluster (monopartite NLS) or two interdependent basic clusters separated by 10–12 amino-acid linker region (bipartite NLS). The proposed consensus sequences for monopartite NLS comprises KKxK, whereas the consensus sequence for the bipartite NLS is KR_X₁₀₋₁₂KRxK, in which the shorter basic cluster precedes the longer one (Weis, 2003).

At present, little is known about the detailed mechanisms that govern the nuclear import of HEXIM1. Moreover, the requirement for 7SK snRNA in turning HEXIM1 into a P-TEFb inhibitor is understood poorly. In this study, we present a comprehensive analysis of the central region in HEXIM1 that consists of oppositely charged BR and adjacent acidic region (AR). Based on our findings, we propose a scenario in which the interplay between 7SK snRNA and the oppositely charged regions dictate nuclear localization of HEXIM1 and binding to P-TEFb, leading to its inactivation and thus inhibition of transcription elongation.

Results

BR in HEXIM1 contains multiple predicted NLSs

Primary structure analysis of HEXIM1 showed that 14% of the protein consists of basic and 21% of acidic residues. In total, 54% of the former and 63% of the latter are clustered in several regions with high probability of low structural complexity, among which one is especially rich in basic and another in acidic residues, thus constituting BR and AR, respectively (Figure 1A). We first focused on the BR in HEXIM1 from positions 150 to 177, which includes BR1 and BR2, and determined that it is conserved among HEXIM proteins from different species (Figure 1B). Of note, the BR2 from positions 175 to 177 in HEXIM1 is conserved in the mouse ortholog but absent in other HEXIM proteins. Next, we analyzed the BR in detail and identified nearly perfect consensus sequences for two monopartite and two bipartite NLSs (Figure 1C).

Two monopartite and two bipartite NLSs in the BR of HEXIM1 direct its nuclear import

To understand the nuclear import of HEXIM1, we disrupted the predicted NLSs by constructing a series of FLAG epitope-tagged HEXIM1 (f.Hex1) proteins, in which the selected basic clusters (B1–6) were replaced with alanines individually or in combination (Figure 1D), and determined their subcellular localizations by using indirect immunofluorescence visualized by confocal microscopy in transiently transfected HeLa cells (Figure 2). In agreement with a previous report (Ouchida *et al*, 2003), we observed a nuclear localization for f.Hex1, which was converted into a cytoplasmic one upon the deletion of the BR (f.Hex1ΔBR; Figure 2A, compare images 2 and 3). Critically, only when we disrupted all four selected basic clusters at the same time (f.Hex1mB1256) did we observe a cytoplasmic localization, similar to the localization of the mutant f.Hex1ΔBR protein (Figure 2A, compare image 4 with images 2 and 3). Thus, four distinct NLSs in HEXIM1 direct its nuclear import.

To decode monopartite and bipartite NLSs, we next examined subcellular localizations of mutant f.Hex1 proteins with individual, double, or triple disruptions of the basic clusters. All of these proteins were nuclear (Figure 2A, images 5–7 and data not presented), except for the mutant f.Hex1mB256

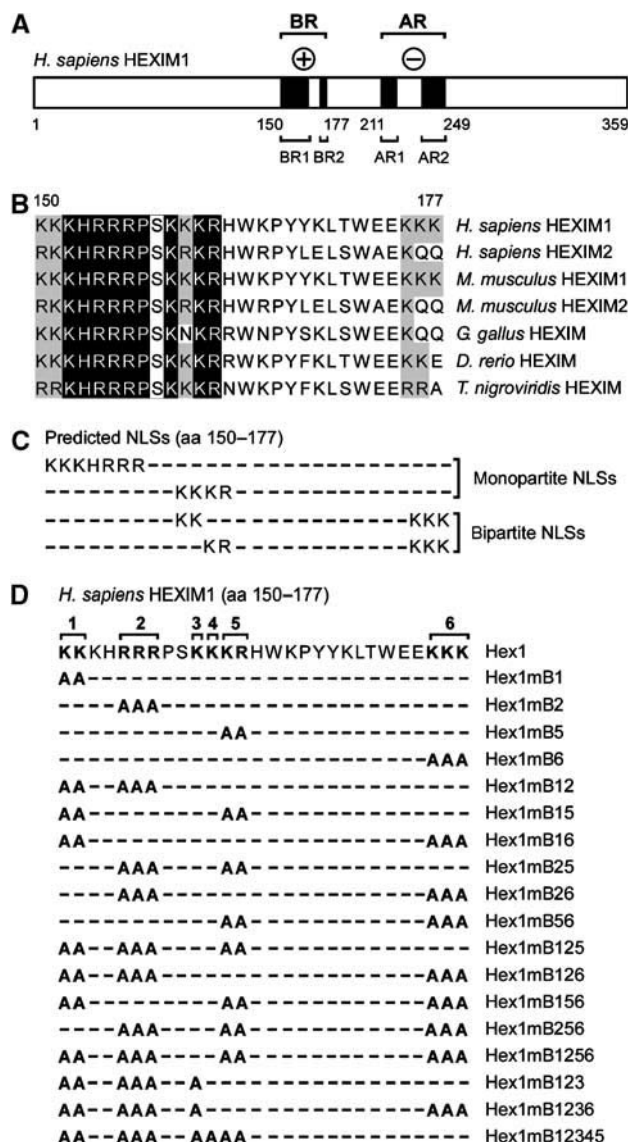


Figure 1 BR in HEXIM1 contains multiple predicted NLSs. (A) HEXIM1 protein is presented as a white rectangle. Black boxes represent two basic (BR; BR1 and BR2) and two acidic (AR; AR1 and AR2) regions and the encircled signs above them represent the charge of these regions. The sequence numberings correspond to the N-terminus, the boundaries of the BRs and ARs, and the C-terminus, respectively. (B) Alignment of the BRs of human, mouse, chicken, zebrafish, and fish HEXIM1 and HEXIM2 proteins. Reverse type indicates basic amino-acid identity whereas shaded boxes indicate basic amino-acid similarity. (C) Predicted monopartite and bipartite NLSs within the BR in HEXIM1 is presented. (D) HEXIM1 proteins used in the first part of the study. Hex1 represents the primary amino-acid sequence of the BR in HEXIM1, which was a subject to site-directed mutagenesis. Numbers above this sequence indicate a disruption of the corresponding basic cluster. The names of wild-type and mutant Hex1 proteins are presented on the right-hand side of the panel. A capital letter B symbolizes basic cluster, whereas small letter m symbolizes the replacement of corresponding basic clusters with alanines.

protein, whose nuclear localization was reduced modestly (Figure 2A, image 8). Thus, the mutant f.Hex1mB156 and f.Hex1mB126 proteins still contain functional first and second predicted monopartite NLSs, respectively, whereas in the mutant f.Hex1mB256 protein, the first predicted monopartite

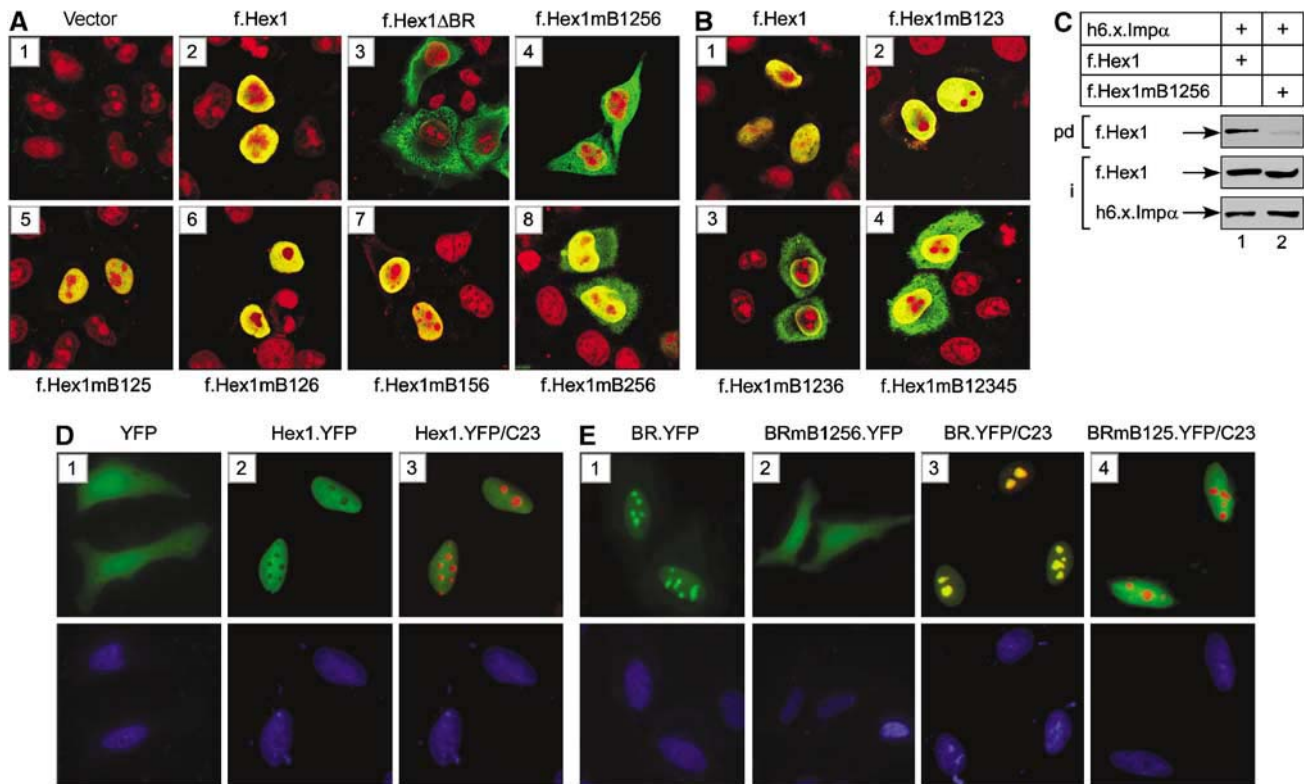


Figure 2 Four distinct NLSs direct nuclear import of HEXIM1. (A, B) f.Hex1 proteins (green) that were expressed in HeLa cells are indicated above and below the microscopic images. Cell nuclei were visualized by propidium iodide (PI; red). The images depict the merge of the f.Hex1 and PI images. (C) HeLa cell lysates, which expressed f.Hex1 or f.Hex1mB1256 from corresponding plasmid effectors (10 μg), were incubated with h6.x.Impα as indicated. Arrows to the left indicate bound f.Hex1 proteins (pd) and 10% inputs (i) of the proteins used in the assay, respectively. (D) YFP (image 1) and Hex1.YFP (images 2 and 3) proteins (green) were expressed in HeLa cells. The panel marked Hex1.YFP/C23 depict the merge of the Hex1.YFP (green) and C23 (red) images. (E) BR.YFP proteins (green) that were expressed in HeLa cells are indicated above the microscopic images. Where indicated, the images depict the merge of the respective BR.YFP (green) and C23 (red) images. Lower parts of the panels D and E indicate the cell nuclei of which the DNA was counterstained by DAPI (blue).

NLS was disrupted partially. Similarly, when contrasted to the nuclear localization of the mutant f.Hex1mB126 protein, the partially cytoplasmic localization of the mutant f.Hex1mB1236 protein (Figure 2A and B, compare images 6 and 3, respectively) confirms the presence of the second predicted monopartite NLS. Next, the nuclear localizations of the mutant f.Hex1mB125 protein and the cytoplasmic localization of the mutant f.Hex1mB1256 protein indicate the activity of the first predicted bipartite NLS, which comprises the basic clusters B34 and B6, separated by a spacer of 14 residues. To address further the importance of the basic cluster B6 and thus the existence of the second predicted bipartite NLS, we constructed another series of mutant f.Hex1 proteins and determined their subcellular localizations (Figure 2B). Indeed, the nuclear localization of the mutant f.Hex1mB123 protein was affected greatly by the disruption of the basic cluster B6 (Figure 2B, compare images 2 and 3), suggesting the activity of the second predicted bipartite NLS. Finally, we observed a partial cytoplasmic localization of the mutant f.Hex1mB12345 protein (Figure 2B, image 4), demonstrating that the basic cluster B6 is not a monopartite NLS. We conclude that two monopartite and two bipartite NLSs in HEXIM1 direct its nuclear import. Moreover, the basic clusters B1, B45, and B6 do not constitute fully functional monopartite NLSs. Rather, the former two are part of both monopartite NLSs whereas the latter form the second basic cluster of the two bipartite NLSs.

The first step in the classical nuclear import pathway is the interaction between importin α and the classical monopartite or bipartite NLSs (Weis, 2003). To examine if HEXIM1 binds importin α *in vitro* and whether this binding depends on its NLSs, we purified bacterially expressed importin α as a His₆-Xpress epitope-tagged protein (h6.x.Impα) and incubated it with HeLa cell lysates, which contained the f.Hex1 or mutant f.Hex1mB1256 proteins. The wild-type f.Hex1 protein bound h6.x.Impα efficiently whereas the mutant f.Hex1mB1256 protein did not (Figure 2C, compare lanes 1 and 2). Also, the inputs of f.Hex1 proteins and h6.x.Impα were comparable in the binding reactions (Figure 2C, lower panel). Thus, HEXIM1 binds importin α via its NLSs *in vitro*.

Two monopartite and two bipartite NLSs of HEXIM1 direct the nuclear import of the enhanced yellow fluorescent protein

To confirm the identification of the four distinct NLSs in HEXIM1, we used a heterologous system, in which we fused the cDNAs of HEXIM1 and a plethora of the wild-type or the mutated BRs described above to the N-terminus of the enhanced yellow fluorescent protein (YFP). Subcellular localizations of these chimeras were determined by using immunofluorescence microscopy of transiently transfected HeLa cells (Figure 2D and E). In these experiments, DAPI staining of the DNA was employed throughout to visualize the nuclei of the cells. As expected, the fusion between the

HEXIM1 and YFP proteins (Hex1.YFP) resulted in the nuclear localization of the Hex1.YFP chimera, whereas the YFP protein itself displayed a nuclear and cytoplasmic localization (Figure 2D, compare images 1 and 2). Notably, since it failed to colocalize with the nucleolar marker C23, the Hex1.YFP protein was excluded from nucleoli and was present exclusively in the nucleoplasm (Figure 2D, image 3).

Finally, we examined the subcellular localizations of the BR.YFP fusion proteins. Localizations of these chimeras correlated entirely with the ones in which the BR was part of the f.Hex1 proteins (Figure 2D and E and Supplementary Figure 1). As expected, only the wild-type BR.YFP but not the mutant BRmB1256.YFP chimera was imported into the nucleus efficiently (Figure 2E, images 1 and 2). Interestingly, the presence of the evolutionary conserved arginine-rich motif (ARM) (position 154–156 in HEXIM1; basic cluster B2) within the BR.YFP protein caused a predominantly nucleolar localization whereas its disruption led to a nucleoplasmic localization (Figure 2E, images 3 and 4 and

Supplementary Figure 1). Thus, the four distinct NLSs function fully when fused to the heterologous protein. Taken together, we conclude that two monopartite and two bipartite NLSs within the evolutionary conserved BR direct the nuclear import of HEXIM. Moreover, when present in the BR.YFP chimera, an intact ARM constitutes a nucleolar localization sequence (NoLS) that was not observed functional within the Hex1.YFP chimeric protein, which was localized in the nucleoplasm.

ARM in the BR1 is essential for the binding of HEXIM1 to 7SK snRNA

The binding between 7SK snRNA and the BR in HEXIM1 is a prerequisite for its ability to inhibit P-TEFb (Michels *et al*, 2004; Yik *et al*, 2004). To map the surfaces on HEXIM1 critical for binding 7SK snRNA, we took advantage of the mutant HEXIM1 proteins with disrupted basic clusters (B1, 2, 5, 6; see Figure 1D) and performed electrophoretic mobility shift assays (EMSA; Figure 3A). For these experiments, we pur-

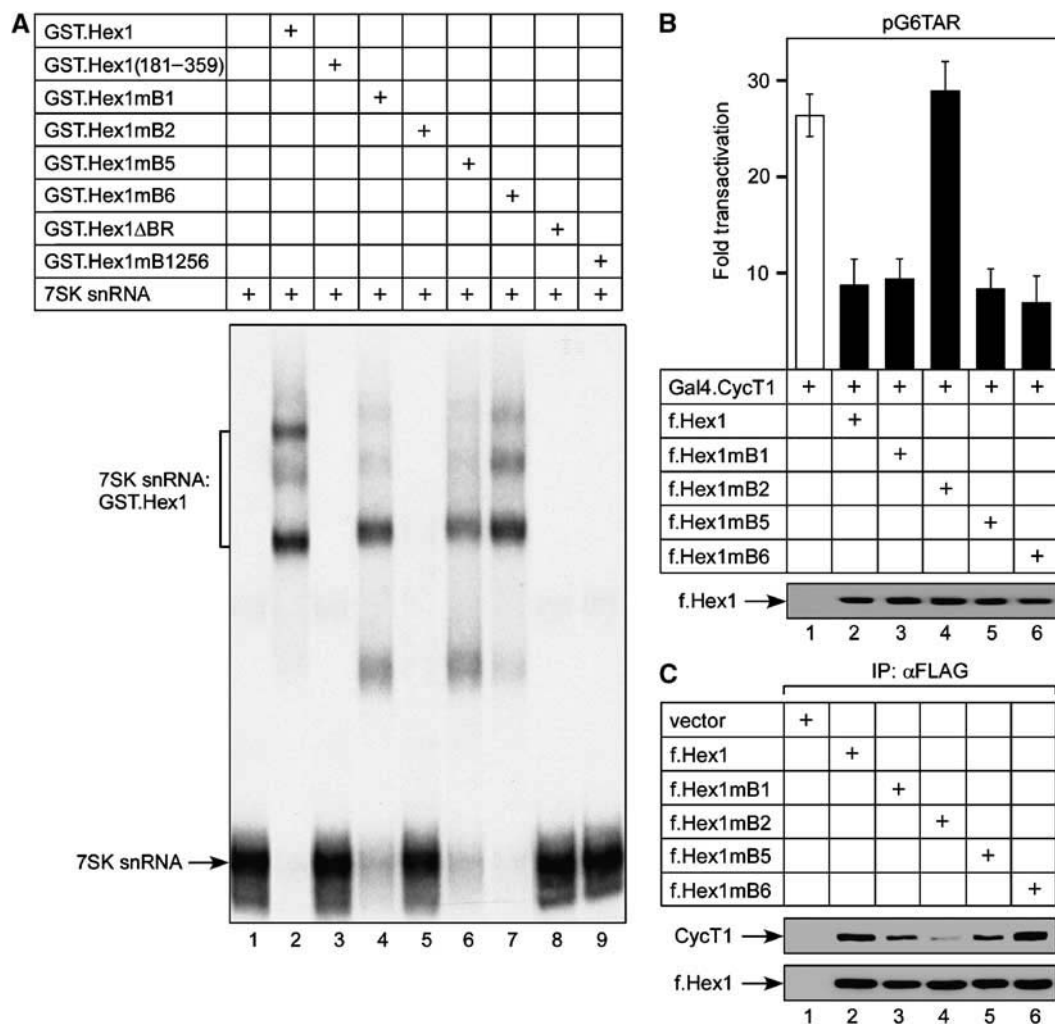


Figure 3 The disruption of the ARM in HEXIM1 disables its binding to 7SK snRNA *in vitro* and inhibition of transcription and binding to P-TEFb *in vivo*. (A) Chimeric GST.Hex1 proteins are indicated above the autoradiograph. α -³²P-labeled 7SK snRNA was present in all reactions. Arrow to the left indicates the free 7SK snRNA probe and the presence of 7SK snRNA:GST.Hex1 RNA–protein complexes is bracketed. (B) HeLa cells expressed plasmid reporter pG6TAR (0.4 μ g; bars 1–6). Proteins that were coexpressed from corresponding plasmid effectors (Gal4.CycT1, 0.6 μ g; f.Hex1, 0.8 μ g) with the plasmid reporter are presented below CAT data. The lower panels present the expression of f.Hex1 proteins as indicated by the arrow. (C) f.Hex1 proteins that were expressed in HeLa cells from corresponding plasmid effectors (10 μ g; lanes 2–6) and immunoprecipitated by anti-FLAG M2 beads are indicated above the Western blots. Arrows to the left indicate the bound P-TEFb and the amounts of immunoprecipitated f.Hex1 proteins, respectively.

ified bacterially expressed chimeric GST.HEXIM1 (GST.Hex1) proteins and incubated them with the *in vitro* transcribed and α -³²P-labeled 7SK snRNA. As expected, the wild-type GST.Hex1 chimera bound 7SK snRNA efficiently and the N-terminal deletion mutant of GST.Hex1 (GST.Hex1 (181–359)) or the GST.Hex1 Δ BR fusion proteins did not, confirming the requirement of the BR for this binding (Figure 3A, compare lane 2 with lanes 3 and 8). Importantly, the mutant GST.Hex1mB2 chimera, where the ARM was disrupted, failed to bind 7SK snRNA (Figure 3A, lane 5). In contrast, the bindings between 7SK snRNA and the mutant GST.Hex1mB1 and GST.Hex1mB5 chimeras, respectively, decreased slightly when compared to the wild-type GST.Hex1 fusion protein, whereas the mutant GST.Hex1mB6 chimera retained the ability to bind 7SK snRNA fully (Figure 3A, lanes 4, 6, and 7). Predictably, when all four basic clusters were disrupted, the mutant GST.Hex1mB1256 chimera did not bind 7SK snRNA (Figure 3A, lane 9). We conclude that the ARM in the BR1 is essential for its binding to 7SK snRNA and that the basic clusters B1 and B5 contribute to these protein–RNA interactions whereas the basic cluster B6 does not.

ARM in the BR1 is essential for HEXIM1 to inhibit transcription and bind to P-TEFb

To extend our *in vitro* binding studies presented in Figure 3A, we addressed the importance of the ARM for the ability of HEXIM1 to bind and inhibit P-TEFb in cells. We performed transcriptional assays followed by binding studies using transiently transfected HeLa cells (Figure 3B and C). To monitor the transcriptional activation by P-TEFb and the inhibitory effects of HEXIM1 proteins on this activation, we used the system, consisting of a plasmid reporter pG6TAR, which contains six Gal4 DNA-binding sites positioned upstream of the HIV-1 long terminal repeat (HIV LTR), followed by the CAT reporter gene, and the chimeric Gal4.CycT1 protein. Its recruitment to the pG6TAR promoter activates transcription that depends on the kinase activity of P-TEFb (Taube *et al*, 2002).

When we expressed Gal4.CycT1 chimera together with pG6TAR in HeLa cells, the levels of CAT activity increased 28-fold over the basal levels, whereas the coexpression of the wild-type f.Hex1 protein decreased this activity to nine-fold (Figure 3B, compare bars 1 and 2). Critically, the disruption of the ARM rendered the mutant f.Hex1mB2 protein largely inactive (Figure 3B, bar 3). Moreover, the disruptions of the basic clusters B1, B5, and B6 had no effect, since the corresponding mutant f.Hex1 proteins inhibited the activation of transcription by the Gal4.CycT1 chimera similarly to the wild-type f.Hex1 protein (Figure 3B, bars 3, 5, and 6). We observed the same results when we monitored effects of these mutant f.Hex1 proteins on Tat transactivation of the HIV LTR (data not presented). Also, levels of the f.Hex1 proteins were comparable (Figure 3B, lower panel). Thus, the ARM in the BR1 of HEXIM1 is critical for its inhibition of transcription in cells.

To address the requirements of the basic clusters for its binding to P-TEFb, we performed immunoprecipitation assays (Figures 3C). We again employed the wild-type or mutant f.Hex1 proteins tested in Figure 3B and found predictably that the wild-type f.Hex1 protein bound P-TEFb in cells (Figure 3C, lane 2). In contrast, the mutant

f.Hex1mB2 protein bound P-TEFb poorly, whereas the disruptions of basic clusters B1, B5, and B6 had only modest to no effects on the binding (Figure 3C, lanes 3–6). Also, levels of the f.Hex1 proteins in the immunoprecipitations were comparable (Figure 3C, lower panel). Overall, we conclude that the ability of HEXIM1 to inhibit transcription and bind P-TEFb depends on its ARM.

BR and AR mediate the interaction between the N- and C-terminal regions of HEXIM1 in the absence of RNA

Thus far, our findings suggested that the BR performs two functions, nuclear import and 7SK snRNA binding, which results in P-TEFb binding and inhibition of transcription. However, as presented in Figure 1A, the BR is followed by AR, consisting of AR1 and AR2. Owing to the close proximity of BR and AR, their high likelihood of low structural complexity and opposite charge, we hypothesized that they might interact with one another and thus lead to an autoinhibitory conformation of HEXIM1 that would be refractory to P-TEFb binding. Moreover, we postulated that this conformation could be changed by the interaction between the BR and 7SK snRNA, resulting in a conformation of HEXIM1 that would allow the binding and inhibition of P-TEFb.

To address this hypothesis, we examined if the N- and C-terminal regions of HEXIM1 interact *in vitro* and whether this interaction is mediated by the BR, AR, and the presence of RNA (Figure 4). For these binding experiments, we used the mutant HEXIM1 proteins that either contain or lack the BR and AR, respectively (Figure 4A). The two bacterially expressed C-terminal deletion mutant HEXIM1 proteins were purified as GST chimeras and the three N-terminal deletion mutant HEXIM1 proteins were expressed as His₆-Xpress epitope-tagged (h6.x.Hex1) chimeras *in vitro* using the rabbit reticulocyte lysate.

First, we asked whether the N- and C-terminal regions of HEXIM1 interact (Figure 4B). Indeed, the mutant GST.Hex1(1–180) and h6.x.Hex1(181–359) proteins bound each other in the presence of RNase A (Figure 4B, lanes 3 and 4). In contrast, the mutant GST.Hex1(1–150) chimera, which lacked the BR, failed to bind the mutant h6.x.Hex1(181–359) protein in the presence of RNase A (Figure 4B, lanes 1 and 2). Also, the inputs of the mutant h6.x.Hex1(181–359) protein were comparable in the binding reactions (data not presented). Thus, the interaction between the N- and C-terminal regions of HEXIM1 *in vitro* is mediated by the BR and occurs in the absence of RNA.

Moreover, we addressed the importance of the adjacent AR for the binding between the N- and C-terminal regions of HEXIM1 (Figure 4C). We performed the binding between the mutant GST.Hex1(1–180) chimera with the intact BR and the series of the N-terminal deletion mutant h6.x.Hex1 proteins as described above. Predictably, the mutant GST.Hex1(1–180) chimera bound the mutant h6.x.Hex1(181–359) protein in the presence of RNase A (Figure 4C, lanes 1 and 2). Critically, the mutant GST.Hex1(1–180) chimera failed to bind the mutant h6.x.Hex1(255–359) protein, which lacked the AR (Figure 4C, lanes 5 and 6). In contrast, the binding was not affected with the mutant h6.x.Hex1(206–359) protein, which still retained the AR (Figure 4C, lanes 3 and 4). Also, the inputs of the mutant h6.x.Hex1 proteins were comparable in the binding reactions (Figure 4C, lanes 7–9). Overall, we conclude that

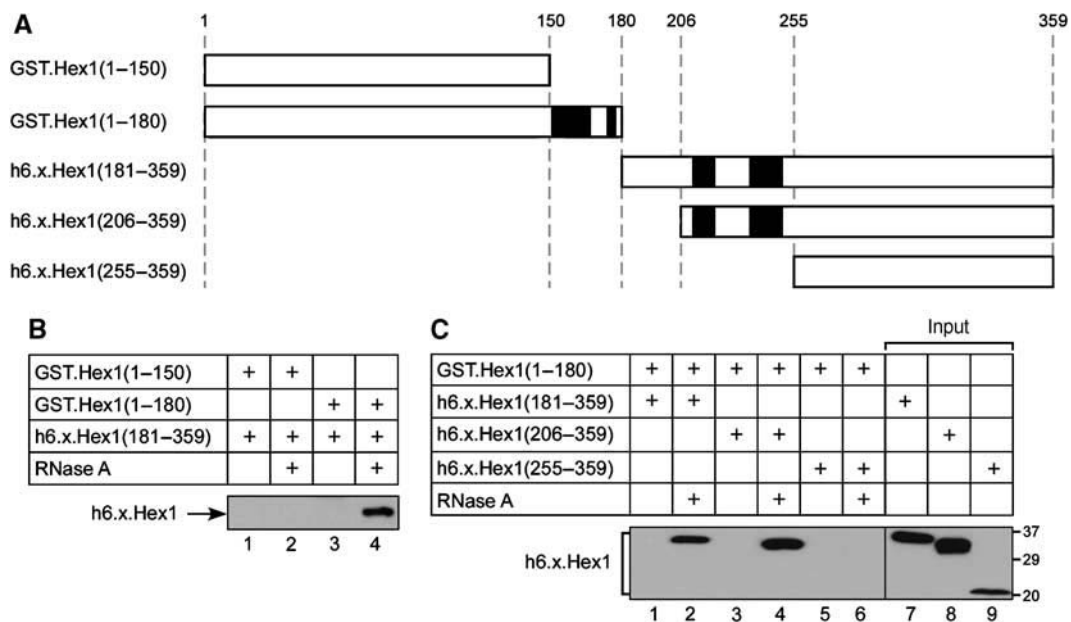


Figure 4 The interaction between the BR and AR within HEXIM1 *in vitro* is abolished in the presence of RNA. (A) The mutant GST.Hex1 and h6.x.Hex1 proteins are presented as white rectangles. Black boxes depict BR and AR as in Figure 1A. The numberings above the schematic correspond to the N- and/or C-terminal boundaries of the proteins. The names of the proteins are presented on the left-hand side of the panel. (B, C) Chimeric GST.Hex1 proteins were incubated with the mutant h6.x.Hex1 protein in the presence or absence of RNase A as indicated above the Western blot. Arrow to the left in panel B indicates the bound h6.x.Hex1 protein. In the panel C, the h6.x.Hex1 proteins are bracketed. Left part of the panel (lanes 1–6) represents the bound h6.x.Hex1 proteins, whereas the right part of the panel (lanes 7–9) represents the 20% inputs of the proteins used in the assay. Numbers to the right indicate relative molecular mass markers (in kDa).

the interaction between the N- and C-terminal regions of HEXIM1 *in vitro* depends on the BR and AR and that the presence of RNA prevents this binding.

Disruption of the BR in HEXIM1 renders the ARM dispensable for inhibition of transcription

To this end, we established that the BR and AR bind each other in the absence of RNA. These observations support our hypothetical model, where 7SK snRNA binds the ARM within the BR to alter a conformation of HEXIM1 that would lead to the binding and inhibition of P-TEFb. Thus, one could predict that the removal of either a positive charge from the BR or the negative charge from the AR would result in this changed conformation, thus mimicking artificially the requirement for 7SK snRNA for the inhibition of P-TEFb.

To test this prediction, we first took advantage of the mutant Hex1mB1256 protein, in which the majority of the positive charge within the BR was removed (Figure 1C) and asked whether it could bind and inhibit P-TEFb in cells (Figure 5). To do so, we used the same strategy as employed in Figure 4B. Since the mutant f.Hex1mB1256 protein localizes in the cytoplasm (Figure 2A, image 4), we fused the NLS of the SV-40 large T antigen to its N-terminus to create the mutant f.NLS.Hex1mB1256 chimera, which resulted in its nuclear localization (Figure 5B, compare images 1 and 2). Strikingly, the mutant f.NLS.Hex1mB1256 chimera inhibited the activation of transcription by the Gal4.CycT1 chimera equivalently to the wild-type f.Hex1 protein, whereas the mutant f.Hex1mB1256 protein had no effect, most likely due to its cytoplasmic localization (Figure 5A, compare bar 4 with bars 1–3). Levels of the mutant f.Hex1 proteins were comparable (Figure 5A, lower panel). Next, we performed immunoprecipitation assays as described in Figure 3C and

found that the mutant f.NLS.Hex1mB1256 chimera bound P-TEFb in cells (Figure 5C, lane 3). Notably, the mutant GST.Hex1mB1256 chimera did not bind 7SK snRNA *in vitro* (Figure 3A, lane 9).

Collectively, these results suggested that the mutant f.NLS.Hex1mB1256 chimera gets sequestered into the large complex independently of ARM and that the 7SK snRNA is not required for this event in cells. To test these notions, we performed a glycerol gradient sedimentation analysis to observe the small and large P-TEFb complexes in cells (Figure 5D). Indeed, we observed two distinct pools of endogenous P-TEFb and HEXIM1 complexes in HeLa cells (Figure 5D, panels a and b). As expected, the wild-type f.Hex1 protein was sequestered into the large complex efficiently whereas the mutant f.Hex1mB2 with a disrupted ARM was not (Figure 5D, panels c and d). Importantly, the additional removal of positive charge from the BR of the mutant f.Hex1mB2 rescued the sequestration into the large complex, since we detected the mutant f.NLS.Hex1mB1256 chimera in it (Figure 5D, panel e). Critically, the destruction of 7SK snRNA by RNase A did not result in a disappearance of the mutant f.NLS.Hex1mB1256 chimera from the large complex, which occurred in the case of the wild-type f.Hex1 protein (Figure 5D, panels f and g). Thus, the removal of positive charge from the BR in HEXIM1 alleviates the requirement for the ARM to bind and inhibit P-TEFb. The fact that the sequestration of the mutant f.NLS.Hex1mB1256 protein was insensitive to RNase A treatment suggests that this mutant HEXIM1 protein inhibits P-TEFb independently of 7SK snRNA. Overall, we conclude that the interaction between the 7SK snRNA and the BR in HEXIM1 via the ARM is critical for the HEXIM1 inhibitory function.

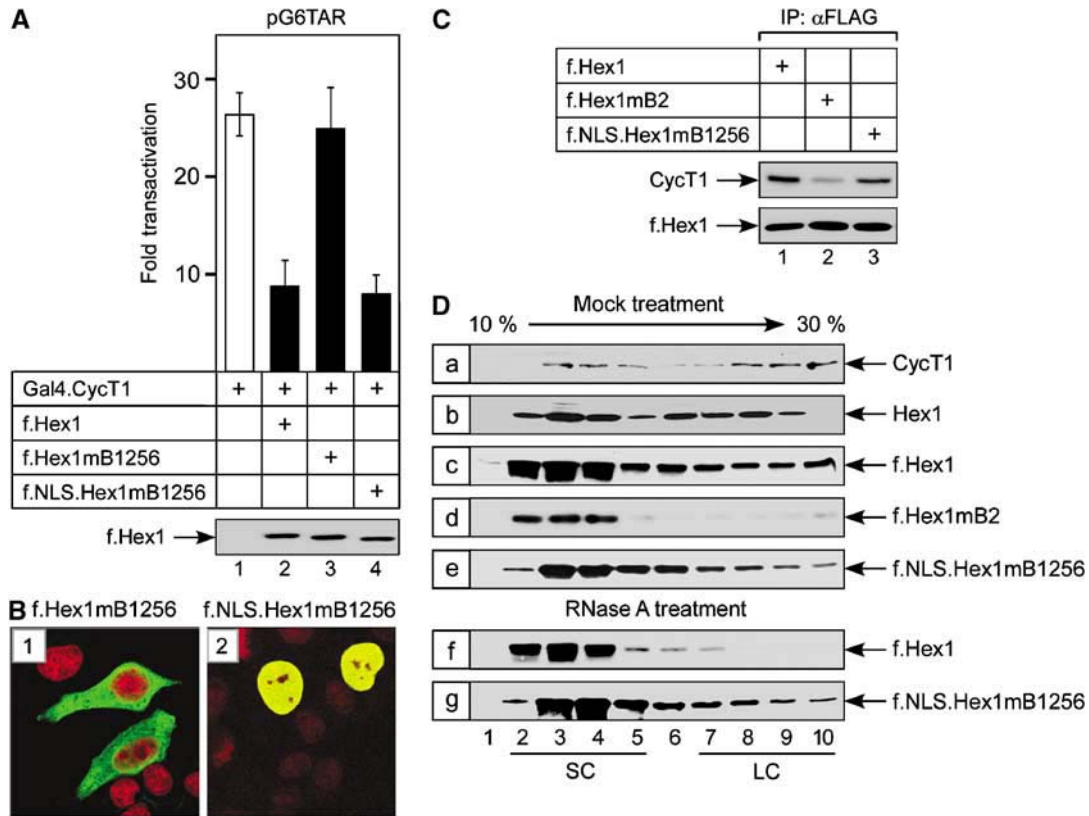


Figure 5 The disruption of the BR in HEXIM1 enables the ARM-independent inhibition of transcription and binding to P-TEFb *in vivo*. (A) HeLa cells expressed plasmid reporter pG6TAR (0.4 μ g; bars 1–6). Proteins that were coexpressed from corresponding plasmid effectors (Gal4.CycT1, 0.6 μ g; f.Hex1, 0.8 μ g) with the plasmid reporter are presented below CAT data. The lower panel presents the expression of f.Hex1 proteins as indicated by the arrow. (B) f.Hex1 proteins that were expressed in HeLa cells from corresponding plasmid effectors (1 μ g) are indicated above and below the microscopic images. f.Hex1 proteins (green) and nuclei (red) were visualized by laser confocal microscopy. (C) f.Hex1 proteins that were expressed in HeLa cells from corresponding plasmid effectors (10 μ g; lanes 1–3) and immunoprecipitated by anti-FLAG M2 beads are indicated above the Western blots. Arrows to the left indicate bound P-TEFb and the amounts of immunoprecipitated f.Hex1 proteins, respectively. (D) Total cell lysates of untransfected HeLa cells and those that expressed the indicated f.Hex1 proteins were subjected to glycerol gradient (10–30%) sedimentation analysis. The lysates were mock or RNase A treated as indicated above the Western blots. Arrows to the right indicate the presence of endogenous CycT1 and HEXIM1 (Hex1) proteins, and f.Hex1 proteins that were expressed from corresponding plasmid effectors (6 μ g). Numberings below the Western blots correspond to particular fractions obtained from the sedimentation analysis. SC and LC indicate fractions containing the small and large complexes, respectively.

Moreover, this dependency on the 7SK snRNA could be overcome by disrupting the BR, suggesting that the postulated autoinhibitory conformation of HEXIM1 is changed into the one that could bind and inhibit P-TEFb.

Disruption of the AR1 in HEXIM1 renders the ARM dispensable for inhibition of transcription

To substantiate this model further, we addressed the significance of the AR for the inhibition of P-TEFb in cells (Figure 6). We analyzed the AR in detail and determined that the AR1 from positions 211 to 219 is conserved among HEXIM1 and HEXIM2 proteins from different species, whereas the AR2 from positions 234 to 249 is absent from human and mouse HEXIM2 proteins (Figure 6A). Next, we designed a reciprocal experiment to the one presented in Figure 5 by constructing a series of mutant f.Hex1 proteins, in which the selected acidic clusters (A1–3) were disrupted by alanines individually or in combination (Figure 6A, lower panel) in the context of the wild-type f.Hex1 and the mutant f.Hex1mB2 proteins. We argued that the removal of the negative charge from the AR could alleviate the requirement for the ARM and thus 7SK snRNA binding, turning the

inactive mutant f.Hex1mB2 protein into a P-TEFb inhibitor. First, we tested the ability of these mutant f.Hex1 proteins to inhibit transcriptional activation by P-TEFb in cells using the same strategy as presented in Figures 3 and 5. Indeed, when we removed the negative charge from the AR1, the inhibitory activity of the mutant f.Hex1mB2 protein was restored (Figure 6B, bars 1–3). However, the individual disruptions of the acidic clusters A1 and A2 within the AR1 or the disruption of the entire AR2 had no effect (Figure 6B, bars 4–6). Importantly, the alanine mutagenesis of the AR1 and AR2 in the context of the wild-type f.Hex1 protein had no effect since both mutant proteins inhibited transcriptional activation by the Gal4.CycT1 chimera (Figure 6B, bars 7–9). Also, the levels of the f.Hex1 proteins were comparable (Figure 6B, lower panel). Thus, similar to the removal of positive charge, the absence of the negative charge in the evolutionary conserved AR1 alleviates the need for the ARM and turns the mutant f.Hex1mB2 protein into a transcriptional inhibitor.

To explore further the mechanism by which the mutant f.Hex1mB2A12 protein with a disrupted AR1 inhibited transcription, we tested whether the disruption of ARs would

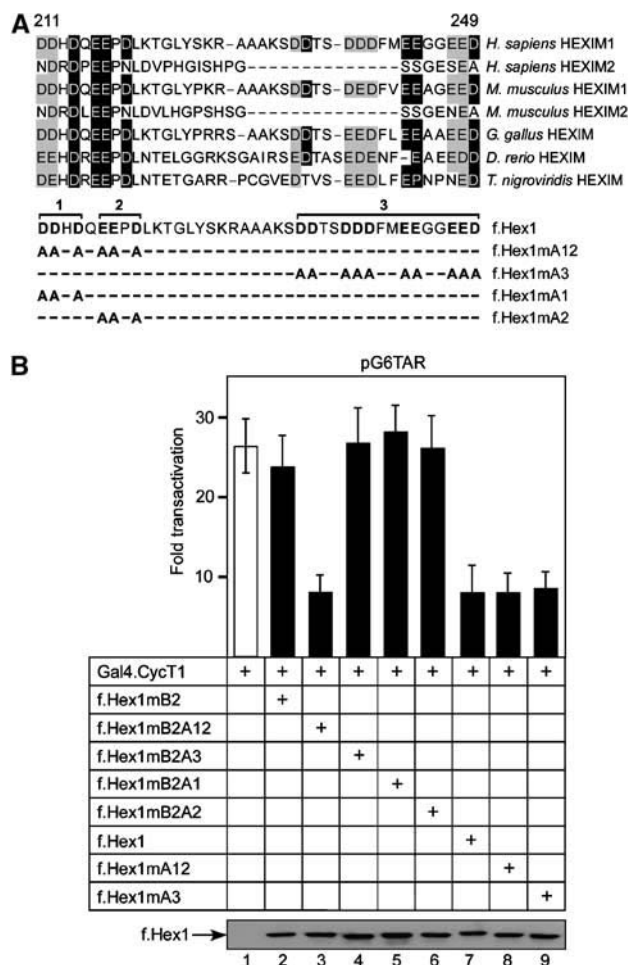


Figure 6 The disruption of the AR1 in HEXIM1 enables the ARM-independent inhibition of transcription. (A) Alignment of human, mouse, chicken, zebrafish, and fish HEXIM1 and HEXIM2 proteins and f.Hex1 proteins used in the study. The sequence numberings correspond to the boundaries of the ARs in HEXIM1. Reverse type indicates acidic amino-acid identity, whereas shaded boxes indicate acidic amino-acid similarity. The lower panel represents the primary amino-acid sequence of the AR in HEXIM1, which was a subject to site-directed mutagenesis. Numbers above this sequence indicate a disruption of the corresponding acidic cluster. The names of Hex1 proteins are presented on the right-hand side of the panel. A capital letter A symbolizes acidic cluster, whereas a small letter m symbolizes the replacement of corresponding acidic clusters with alanines. (B) HeLa cells expressed plasmid reporter pG6TAR (0.4 µg; bars 1–9). Proteins that were coexpressed from corresponding plasmid effectors (Gal4.CycT1, 0.6 µg; f.Hex1, 0.8 µg) with the plasmid reporter are presented below CAT data. The lower panel presents the expression of f.Hex1 proteins as indicated by the arrow.

affect 7SK snRNA binding (Figure 7A). We expressed and purified the wild-type and the mutant GST.Hex1 proteins from *Escherichia coli* and performed EMSAs as described in Figure 3A. Predictably, whereas all the mutant GST.Hex1 chimeras with intact ARM in HEXIM1 bound 7SK snRNA, those with the disrupted ARM failed to bind 7SK snRNA similarly (Figure 7A, lanes 1–7). Next, we asked whether the disrupted acidic clusters alleviate the requirement for the ARM in HEXIM1 to bind P-TEFb (Figure 7B). We performed a GST pull-down assay in which we took advantage of the GST.Hex1 chimeras and used them to pull down P-TEFb from a total cell lysate of HeLa cells that were treated with

actinomycin D to release P-TEFb from the 7SK snRNA-bound HEXIM1. Whereas the mutant GST.Hex1mB2 failed to bind P-TEFb efficiently, the mutant GST.Hex1 proteins with the disrupted AR1 and AR2 bound P-TEFb similarly to the wild-type GST.Hex1 chimera (Figure 7B, lanes 1–4). Also, the input levels of the GST.Hex1 and P-TEFb proteins in the binding reactions were comparable (Figure 7B, lower panel). Since the mutant f.Hex1mB2A12 protein bound P-TEFb and inhibited transcription in cells without the ability to bind 7SK snRNA *in vitro*, we asked whether it gets sequestered into the large complex in cells in the ARM- and 7SK snRNA-independent manner. We again employed the glycerol gradient sedimentation analysis (Figure 7C). Indeed, we found that the disruptions of both AR1 and AR2 restored the ability of the mutant f.Hex1mB2 protein to be sequestered into the large complex (Figure 7C, panels a and b). Importantly, this sequestration was not affected by the destruction of 7SK snRNA by RNase A (Figure 7C, panels c and d). Finally, we found that the disruptions of ARs within the mutant f.Hex1 and f.Hex1mB2 proteins did not affect their oligomerization properties (Supplementary Figure 2 and data not presented). Overall, we conclude that the removal of negative charges from the ARs renders the ARM in HEXIM1 dispensable for its incorporation into the large complex and the binding to P-TEFb. However, only the disruption of the AR1 leads to the inhibitory function of f.Hex1mB2.

Disruption of the AR1 in HEXIM1 leads to its localization into nuclear speckles

To address the latter phenomenon, we lastly turned our attention to subcellular localizations of the HEXIM1 proteins with the disrupted ARs (Figure 8). We fused the corresponding cDNAs to the N-terminus of the YFP protein and performed a subcellular localization analysis of these chimeric proteins as described in Figure 2. As expected, the localization of the mutant Hex1mB2.YFP chimeric protein that has the disrupted ARM was nucleoplasmic (Figure 8A, image 1). Surprisingly, the disruption of the AR1 led to the speckled nuclear localization of the mutant Hex1mB2A12.YFP protein, whereas the disruption of the AR2 had no effect (Figure 8A, images 2 and 3). In addition, the same phenotype was observed when we disrupted the ARs in the context of the wild-type Hex1.YFP chimeras (data not presented). Thus, these findings correlate nicely with the inhibitory properties of the mutant f.Hex1mB2 proteins that have disrupted AR1 and AR2 and suggest that subnuclear localization influences their function.

To disclose the identity of the Hex1mB2A12.YFP speckled localization, we next attempted to colocalize it with several markers of distinct subnuclear structures (Figure 8B). Speckled localization was highly reminiscent of a subnuclear structure called nuclear speckles (Lamond and Spector, 2003), which is enriched in pre-mRNA processing components and could be identified by the SC-35 antibody. Indeed, Hex1mB2A12.YFP colocalized extensively with the nuclear speckles (Figure 8B, images 1–3). In contrast, it failed to colocalize with two other subnuclear structures, promyelocytic leukemia (PML) nuclear bodies and nucleoli (Figure 8B, images 4–9), which were identified by antibodies directed against the PML and C23 proteins, respectively.

Notably, the C-terminal deletion mutant protein of the Hex1mB2A12.YFP chimera, which lacked the P-TEFb-binding domain (Hex1(1-286)mB2A12.YFP) retained its localization in nuclear speckles (Figure 8C, images 1-3). However, the presence of this C-terminal deletion mutant protein in nuclear speckles *per se* was not sufficient for inhibiting transcription (Figure 8D). Similar to the mutant f.Hex1 protein which failed to bind and inhibit P-TEFb in cells (f.Hex1(1-286); Schulte *et al*, 2005), the mutant f.Hex1mA12 and f.Hex1mB2A12

proteins did not inhibit the activation of transcription by the Gal4.CycT1 chimera (Figure 8D, bars 1-5). Levels of these f.Hex1 chimeras were comparable (Figure 8D, lower panel). Overall, we conclude that AR does not only bind the BR to constitute an inhibitory conformation in HEXIM1. It also mediates HEXIM1 subnuclear localization, since the disruption of AR1 leads to its localization into nuclear speckles, which is a necessary prerequisite for inhibiting transcription.

Discussion

By targeting P-TEFb, HEXIM1 inhibits the transcription by RNAPII. In this study, we conducted a comprehensive analysis of the BR and AR in HEXIM1 and provide evidence that these charged regions regulate its function. First, we found that the two monopartite and two bipartite NLSs within the BR in HEXIM1 direct its nuclear import. Second, the evolutionary conserved ARM within the BR1 was essential for the binding between HEXIM1 and 7SK snRNA *in vitro* and for the binding to P-TEFb and inhibition of transcription in cells. Third, BR and AR mediated the interactions between the N- and C-terminal regions of HEXIM1 in the absence of RNA. In addition, the removal of positive or negative charges from these regions alleviated the requirement for the ARM for sequestration of these mutant HEXIM1 proteins into the large complex and their inhibition of transcription. Finally, by removing the negative charges from the AR1 in HEXIM1, its subnuclear localization changed into nuclear speckles. Thus, the interplay between 7SK snRNA and oppositely charged regions in HEXIM1 direct its binding to P-TEFb, subcellular localization, and inhibition of transcription.

Detailed analysis of the BR in HEXIM1, which encompasses only 28 residues, led us to identify four functionally independent NLSs. Since HEXIM1 bound importin α *in vitro* and the monopartite and bipartite NLSs are of the classical type, the HEXIM1 protein is likely to be translocated into the nucleus via the importin α -dependent pathway. However, the presence of ARM within the first monopartite NLS could constitute an arginine-rich NLS, which would bind importin β directly. Such a high number of NLSs in HEXIM1 could ensure its nuclear import in various tissues and organs, since the expression levels of various isoforms of importin α vary in different tissues. Alternatively, various importins may occupy different NLSs at once, leading to a more efficient

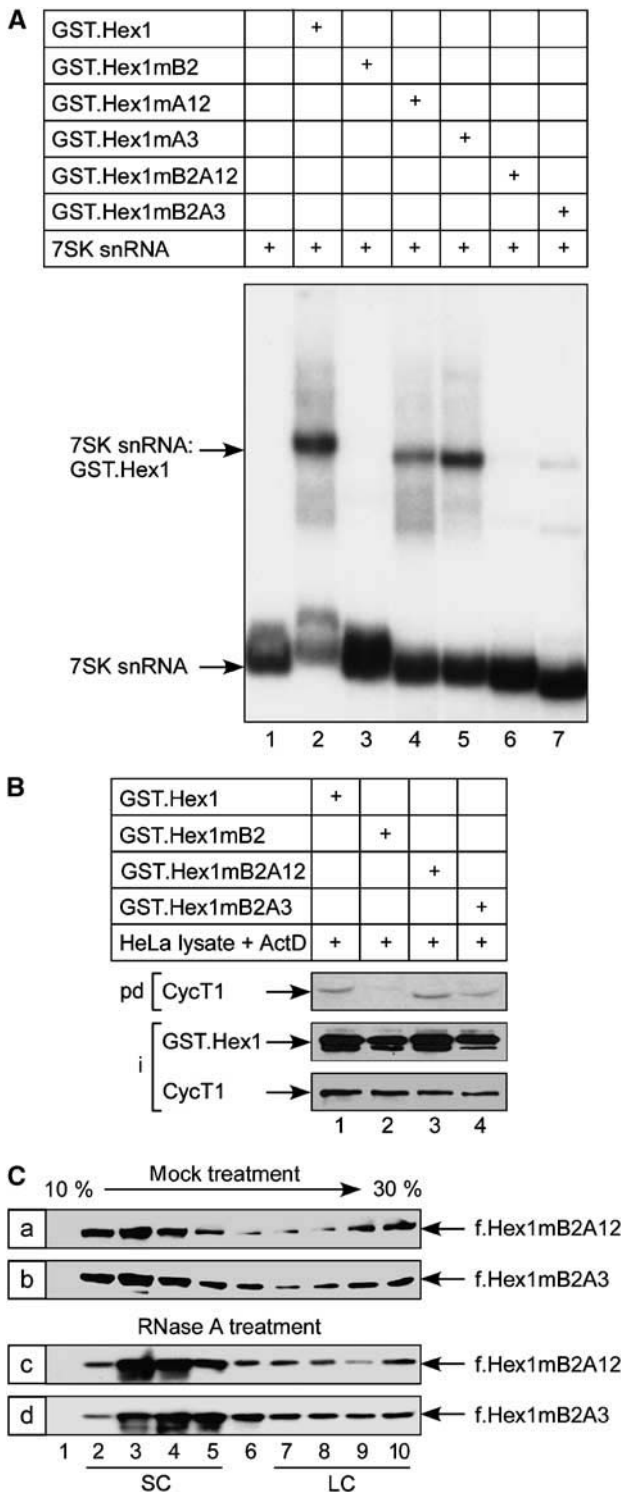


Figure 7 The disruption of the AR in HEXIM1 enables the ARM-independent binding to P-TEFb. (A) Chimeric GST.Hex1 proteins that were used in EMSAs are indicated above the autoradiograph. α - 32 P-labeled 7SK snRNA was present in all reactions. Arrows to the left indicate the free 7SK snRNA probe and the presence of 7SK snRNA:GST.Hex1 RNA-protein complexes. (B) HeLa cell lysates, which were treated with ActD, were incubated with the chimeric GST.Hex1 proteins as indicated. Arrows to the left indicate bound GST.Hex1 proteins (pd) and 20% inputs (i) of the proteins used in the assay, respectively. (C) Total cell lysates of HeLa cells that expressed the indicated f.Hex1 proteins were subjected to glycerol gradient (10-30%) sedimentation analysis. The lysates were mock or RNase A treated as indicated above the Western blots. Arrows to the right indicate the presence of f.Hex1 proteins that were expressed from corresponding plasmid effectors (6 μ g). Numberings below the Western blots correspond to particular fractions obtained from the sedimentation analysis. SC and LC indicate fractions containing the small and large complexes, respectively.

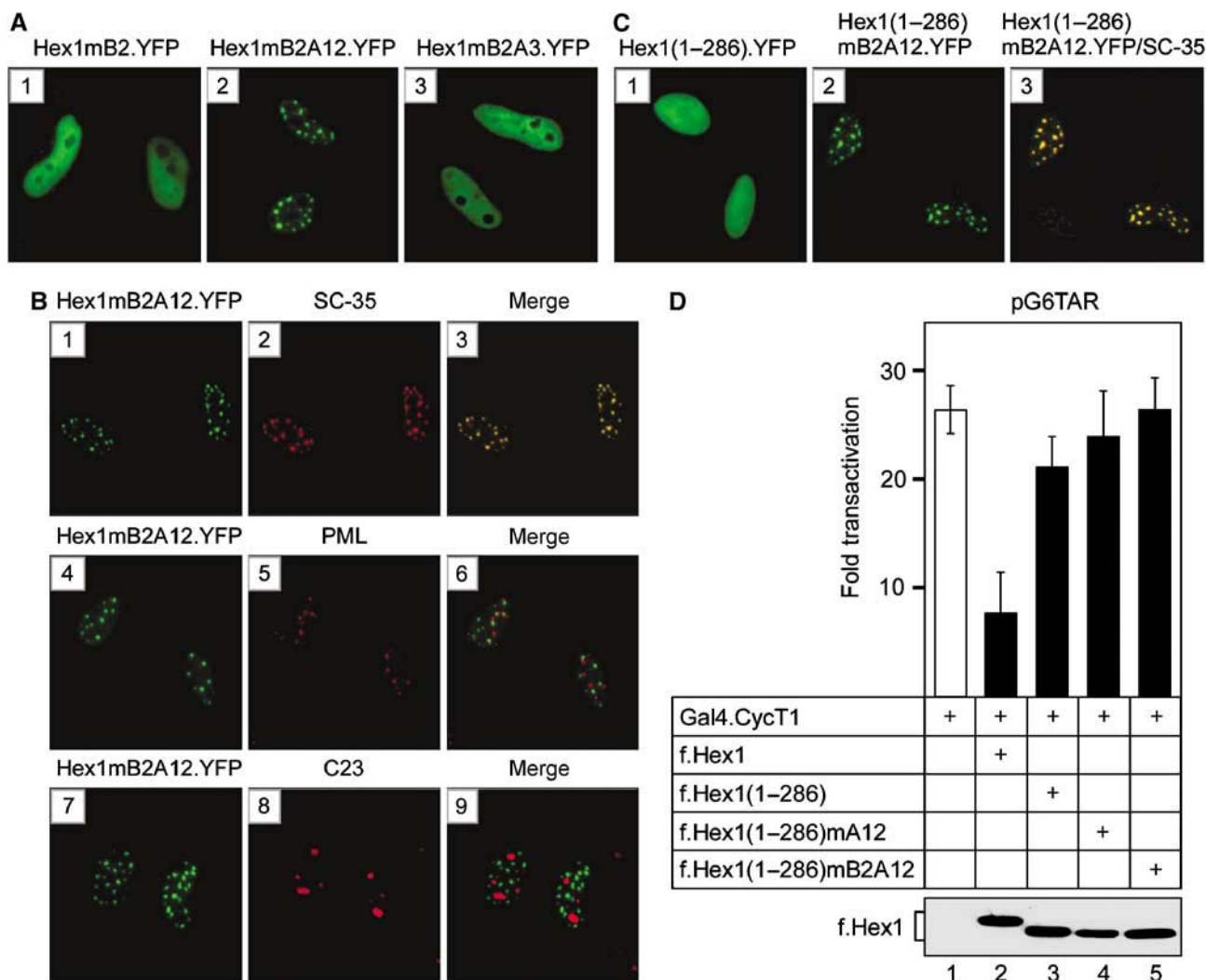


Figure 8 The disruption of the AR1 in HEXIM1 leads to its localization into nuclear speckles. (A) Hex1.YFP proteins that were expressed in HeLa cells are indicated above the microscopic images. (B) HeLa cells expressed Hex1mB2A12.YFP (green) (images 1–9). The panels marked with SC-35, PML, and C23 (red) represent the images of nuclear speckles, PML nuclear bodies, and nucleoli, whereas the panels marked with merge depict the merge of the Hex1mB2A12.YFP and SC-35, PML, and C23 images, respectively. (C) Hex1.YFP proteins (green) that were expressed in HeLa cells are indicated above the microscopic images. The panel marked Hex1(1-286)mB2A12.YFP/C23 depicts the merge of the Hex1(1-286)mB2A12.YFP (green) and C23 (red) images. (D) HeLa cells expressed plasmid reporter pG6TAR (0.4 μ g; bars 1–5). Proteins that were coexpressed from corresponding plasmid effectors (Gal4.CycT1, 0.6 μ g; f.Hex1, 0.8 μ g) with the plasmid reporter are presented below CAT data. The lower panel presents the expression of f.Hex1 proteins as indicated by the bracket.

nuclear import. Interestingly, when part of the BR.YFP chimera, the ARM constitutes a NoLS. Since nucleoli are dynamic structures with which proteins can associate transiently and under specific metabolic conditions, this finding raises the possibility that the wild-type HEXIM1 protein that resides in the nucleoplasm of HeLa cells under steady-state conditions could be translocated into the nucleolus as well. This is a rather attractive scenario due to the fact that the nucleoli are also sites of RNA modifications (Carmo-Fonseca, 2002), which if operating could regulate its binding to 7SK snRNA.

Recent work demonstrated the critical role for the KHRR motif within the BR in HEXIM1 for its interaction with 7SK snRNA and binding to P-TEFb (Michels *et al*, 2004). Likewise, our EMSAs indicate that the evolutionary conserved ARM is essential for the binding between HEXIM1 and 7SK snRNA

in vitro. Moreover, the intact ARM is also required for the inhibition of transcription and binding to P-TEFb. On the other hand, we found that the 7SK snRNA interacting surface overlaps with the NLSs and possibly NoLS. This observation is reminiscent of the situation in certain viral RNA-binding proteins. For example, the ARMs in the Tat and Rev proteins of HIV-1, as well as in the Rex protein from the human T-cell leukemia virus type 1, function as effective NLSs and NoLSs (Palmeri and Malim, 1999; Truant and Cullen 1999). Rather than dedicating two separate locations within the protein sequences, HEXIM1 and the viral proteins evolved the same region for these distinct biological functions. Since the bindings to corresponding RNA molecules and importins operate in different locations within cells, namely, in the nucleus and cytoplasm, respectively, these functions are not mutually exclusive. This notion is supported by the mirror image

from the studies investigating the hepatitis delta virus (HDV) antigen (HDAg). One of the biological functions of HDAg is to translocate the HDV RNA genome from the cytoplasm to the nucleus. Beautifully, since both the binding to HDV RNA and importins occur in the cytoplasm, the ARMs and the NLS of the HDAg protein evolved in two separate locations (Chou *et al*, 1998).

How does 7SK snRNA turn HEXIM1 into a P-TEFb inhibitor? Recent reports suggested that 7SK snRNA binds the BR in HEXIM1 to relieve its N-terminal autoinhibitory domain, thus enabling P-TEFb binding (Michels *et al*, 2004; Li *et al*, 2005). Our findings led us to propose a model in which the BR does not only direct the nuclear import of HEXIM1 and its 7SK snRNA binding but could also be involved in establishing an autoinhibitory conformation within the central region of HEXIM1 via its electrostatic interactions with the adjacent AR. According to this scenario, such conformation would be unable to bind P-TEFb unless the 7SK snRNA engaged the BR. Collectively, both models are not mutually exclusive and could therefore operate in concert. For example, we envision a situation where 7SK snRNA would disrupt initially the autoinhibitory conformation in HEXIM1 governed by the centrally located BR and AR, followed by a further conformational change which would reposition the N-terminal autoinhibitory domain and unmask the P-TEFb-binding site. Importantly, both models are consistent by suggesting that the 7SK snRNA releases an autoinhibition of HEXIM1 and that it plays a structural role for the assembly of the inactive complex, rather than contributing directly to P-TEFb inhibition. Notably, by binding the BR, 7SK snRNA facilitates oligomerization of HEXIM1 (Blazek *et al*, 2005). Thus, it is tempting to speculate that this RNA-protein interaction represents a rate-limiting step that could be regulated by at present unknown mechanism and might signify an important checkpoint in determining levels of active and inactive P-TEFb complexes *in vivo*.

Additionally, our study provides exciting observations about the subnuclear localization of HEXIM1 protein. Besides the above-mentioned role of AR in binding the BR and thus disfavoring P-TEFb binding in the absence of 7SK snRNA, we found that the disruption of AR1 within the mutant Hex1.YFPmB2 did not only restore its inhibitory properties by sequestering it into the large complex but also caused its relocalization into nuclear speckles. Consequently, this finding suggests that inhibition of P-TEFb takes place in these subnuclear structures. In support of this conclusion, active transcription does not seem to be associated with nuclear speckles (Cmarko *et al*, 1999). Moreover, a considerable overlap between nuclear speckles and P-TEFb has been documented (Herrmann and Mancini, 2001). Thus, the determination of the subnuclear localization of endogenous components of the complex between 7SK snRNA, HEXIM1, and P-TEFb would be of great interest. Possible perturbations of these localizations, which could result after exposing the cells to various stress-related agents or physiological signals, would provide us further clues about the regulation of this inhibitory complex.

In summary, our study highlights how a plethora of mutually dependent mechanisms meet in a centrally located region in HEXIM1, which in concert with 7SK snRNA directs the sequestration of P-TEFb into the large complex and consequently its catalytic inactivation. In addition, it indi-

cates the importance of intricate subcellular and subnuclear localizations of HEXIM1 that are necessary determinants for exerting its function. Future functional and structural studies will clarify our understanding of HEXIM proteins and uncover the physiological significance of their negative regulation of transcription elongation.

Materials and methods

Cell culture

HeLa cells were grown at 37°C with 5% CO₂ in Dulbecco's modified Eagle's medium (DMEM) containing 10% fetal calf serum, 100 mM L-glutamine, and 50 µg each of penicillin and streptomycin per ml.

Plasmid DNAs

Plasmid reporter pG6TAR and a plasmid coding for the Gal4.CycT1 chimera were described (Taube *et al*, 2002). Plasmids coding for the f.Hex1, f.Hex1(181–359), f.Hex1ΔBR, GST.Hex1, GST.Hex1(1–180), and h6.x.Impα proteins were gifts from Dr Zhou, Dr Tanaka, and Dr Weis, respectively. Plasmid coding for 7SK snRNA was described (Michels *et al*, 2004). Plasmids coding for the wild-type and mutant f.Hex1, h6.x.Hex1, GST.Hex1, Hex1.YFP, and BR.YFP proteins were generated as described in detail in Supplementary data 3.

Immunoreagents and chemicals

The anti-C23 (nucleolin) (Cat. No. sc-8031, sc-17826), anti-CycT1 (Cat. No. sc-8127), and anti-PML (Cat. No. sc-5621) antibodies were obtained from Santa Cruz Biotechnology (Santa Cruz, CA). The anti-FLAG M2 (Cat. No. F3165), anti-splicing factor SC-35 (Cat. No. S4045) antibodies, and the anti-FLAG M2 beads (Cat. No. FLAGIPT-1) were purchased from Sigma-Aldrich Corp. (St Louis, MO). The anti-Xpress antibody (Cat. No. R910-25) was purchased from Invitrogen (Carlsbad, CA). The secondary anti-mouse or anti-rabbit antibodies conjugated with Alexa fluor 568 or Alexa-fluor 488, respectively, were purchased from Invitrogen (Cat. No. A-11019, A-11008; Molecular probes, Carlsbad, CA). The rabbit anti-HEXIM1 antibody was generated against HEXIM1 epitope LHRQGER-APLSKFGD and obtained from Antibody Solutions (Mountain View, CA). Actinomycin D (Cat. No. A 1410) was purchased from Sigma-Aldrich Corp (St Louis, MO).

Transient transfection and CAT reporter gene assay

HeLa cells were seeded into six-well plates or 100-mm-diameter petri dishes approximately 12 h prior to transfection and transfected with FuENE6 reagent (Cat. No. 1 815 091; Roche Applied Science, Indianapolis, IN). CAT enzymatic assays were performed as described (Taube *et al*, 2002). Fold transactivation represents the ratio between the Gal4.CycT1-activated transcription and the activity of the reporter plasmid alone. Error bars give standard errors of the mean.

Immunoprecipitation assay and Western blotting

HeLa cells were lysed in 0.8 ml of lysis buffer A (10 mM Tris-HCl (pH 7.4), 150 mM NaCl, 2 mM EDTA, 1% NP-40, 0.1% protease inhibitor) for 1 h at 4°C 36 h post-transfection. The lysates were immunoprecipitated with the anti-FLAG M2 beads and the bound proteins were separated on SDS-PAGE electrophoresis. Western blotting was performed according to the standard protocols.

Glycerol gradient sedimentation analysis

HeLa cells were lysed in 0.6 ml of lysis buffer B (20 mM HEPES (pH 7.9), 0.3 M KCl, 0.2 mM EDTA, 0.1% NP-40, 0.1% protease inhibitor) containing either 0.5% RNase inhibitor or RNase A (100 µg/ml) for 1 h at 4°C 36 h post-transfection. The lysates were subjected to ultracentrifugation in a SW41 Ti rotor (Beckman) at 38 000 r.p.m. for 16 h in a 10 ml glycerol gradient solution (10–30%) containing buffer B. Fractions were collected and analyzed as described (Yik *et al*, 2005).

Protein purification

Chimeric h6.x.Impα and GST.Hex1 proteins were expressed in the BL21(DE3)pLysS strain of *E. coli* (Novagen, Madison, WI) after a 4 h induction with 1 mM IPTG and purified from total cell lysates by

using Ni-NTA agarose (Qiagen, Chatsworth, CA) and glutathione-Sepharose beads (Amersham Biosciences Corp., Piscataway, NJ), respectively. For EMSAs, purified GST.Hex1 proteins were eluted from the beads by using 20 mM glutathione and 150 mM NaCl in 50 mM Tris-HCl (pH 8.0) and subjected to dialysis against a HGKEDP buffer containing 20 mM HEPES (pH 7.6), 15% glycerol, 50 mM KCl, 0.1 mM EDTA, 1 mM DTT, and 0.1% protease inhibitor. The purity of eluted proteins was determined by silver staining.

In vitro binding assays

For the binding assay between the f.Hex1 proteins and h6.x.Imp α , HeLa cells expressed indicated proteins and were lysed in 0.5 ml of lysis buffer A for 1 h at 4°C. Total cell lysates were incubated with equal amounts of the h6.x.Imp α protein, coupled to the Ni-NTA agarose beads for 2 h at 4°C. For the GST-pull down assay between GST.Hex1 and h6.x.Hex1 chimeras, the GST.Hex1 proteins were expressed and purified as described above and the mutant h6.x.Hex1 proteins were transcribed and translated *in vitro* using the TNT-T7 Coupled Reticulocyte Lysate System (Cat. No. L4610; Promega Corp., Madison, WI). Each binding reaction was performed in 250 μ l of the binding buffer C (20 mM HEPES (pH 7.9), 150 mM KCl, 0.7% β -mercaptoethanol, 0.2% BSA, 0.5% Igepal CA-630 (Cat. No. I-3021; Sigma-Aldrich Corp, St Louis, MO), 1% Triton X-100, 0.1% protease inhibitor) containing either 0.5% RNase inhibitor or RNase A (100 μ g/ml) for 2 h at 4°C. For the GST-pull down assay between GST.Hex1 chimeras and P-TEFb, the GST.Hex1 proteins were expressed and purified as described above and P-TEFb was obtained from total HeLa cell lysates which were prepared by treating the HeLa cells with actinomycin D (ActD; 1 μ g/ml) for 1.5 h prior to lysis in the lysis buffer D (10 mM HEPES (pH 7.9), 1.5 mM MgCl₂, 10 mM KCl, 200 mM NaCl, 0.2 mM EDTA, 0.5% NP-40). Each binding reaction was performed in 300 μ l of the buffer D.

EMSA

Reactions (12 μ l final) were carried out in 25 mM HEPES (pH 7.6), 15% glycerol, 60 mM KCl, 0.1 mM EDTA, 0.01% NP-40, and 1 μ g

BSA, and contained 500 pg α -³²P-labeled 7SK snRNA and 1 μ g poly(I)-poly(C) as a nonspecific competitor RNA. The assay was performed as described (Michels *et al*, 2004).

Immunofluorescence and confocal microscopy

HeLa cells were seeded on cover slips into six-well plates approximately 12 h prior to transfection and transfected with 1 μ g of corresponding plasmids as described above. At 24 h after transfection, the cells were fixed with 4% paraformaldehyde and permeabilized in 0.2% Triton X-100 in PBS according to the standard protocols. These steps were followed by incubation with the indicated primary antibodies over night at 4°C. After washing in PBA (PBS + BSA (1 mg/ml)), the cells were incubated for 1 h with the appropriate secondary antibody. Finally, the cells were washed with PBA, incubated with 0.01% PI where indicated in PBS for 10 min, and washed with PBA. Alternatively, the cells were mounted by the ProLong Gold antifade reagent with DAPI (Cat. No. P36935; Molecular Probes, Invitrogen detection technologies, Carlsbad, CA). Confocal microscopy was performed on Zeiss inverted microscope ZW510. Fluorescence of the images containing YFP chimeras was monitored with a Nikon Eclipse E800 microscope using \times 40 objective.

Supplementary data

Supplementary data are available at *The EMBO Journal* Online.

Acknowledgements

We thank Q Zhou, JH Yik, H Tanaka, and K Weis for sharing their plasmid reagents, and B Kobe, M Geyer, G Drozina, I Oven, T Vaupotic, and other members of the Peterlin laboratory for help and insightful discussions. This work was supported by a grant from the NIH (PO1 AI058708 from the NIH). MB was supported in part by Grant Number 106584-36-RFNT from the American Foundation for AIDS Research (amfAR).

References

- Barboric M, Peterlin BM (2005) A new paradigm in eukaryotic biology: HIV Tat and the control of transcriptional elongation. *PLoS Biol* **3**: e76
- Blazek D, Barboric M, Kohoutek J, Oven I, Peterlin BM (2005) Oligomerization of HEXIMI via 7SK snRNA and coiled-coil region directs the inhibition of P-TEFb. *Nucleic Acids Res* (in press)
- Byers SA, Price JP, Cooper JJ, Li Q, Price DH (2005) HEXIM2, a HEXIM1 related protein, regulates P-TEFb through association with 7SK. *J Biol Chem* **280**: 16360–16367
- Carmo-Fonseca M (2002) The contribution of nuclear compartmentalization to gene regulation. *Cell* **108**: 513–521
- Chao SH, Price DH (2001) Flavopiridol inactivates P-TEFb and blocks most RNA polymerase II transcription *in vivo*. *J Biol Chem* **276**: 31793–31799
- Chou HC, Hsieh TY, Sheu GT, Lai MM (1998) Hepatitis delta antigen mediates the nuclear import of hepatitis delta virus RNA. *J Virol* **72**: 3684–3690
- Cmarko D, Verschure PJ, Martin TE, Dahmus ME, Krause S, Fu XD, van Driel R, Fakan S (1999) Ultrastructural analysis of transcription and splicing in the cell nucleus after bromo-UTP microinjection. *Mol Biol Cell* **10**: 211–223
- Dulac C, Michels AA, Fraldi A, Bonnet F, Nguyen VT, Napolitano G, Lania L, Bensaude O (2005) Transcription-dependent association of multiple positive transcription elongation factor units to a HEXIM multimer. *J Biol Chem* **280**: 30619–30629
- Herrmann CH, Mancini MA (2001) The Cdk9 and cyclin T subunits of TAK/P-TEFb localize to splicing factor-rich nuclear speckle regions. *J Cell Sci* **114**: 1491–1503
- Kusuhara M, Nagasaki K, Kimura K, Maass N, Manabe T, Ishikawa S, Aikawa M, Miyazaki K, Yamaguchi K (1999) Cloning of hexamethylene-bis-acetamide-inducible transcript, HEXIM1, in human vascular smooth muscle cells. *Biomed Res* **20**: 273–279
- Lamond AI, Spector DL (2003) Nuclear speckles: a model for nuclear organelles. *Nat Rev Mol Cell Biol* **4**: 605–612
- Li Q, Price JP, Byers SA, Cheng D, Peng J, Price DH (2005) Analysis of the large inactive P-TEFb complex indicates that it contains one 7SK molecule, a dimer of HEXIM1 or HEXIM2, and two P-TEFb molecules containing Cdk9 phosphorylated at threonine 186. *J Biol Chem* **280**: 28819–28826
- Michels AA, Fraldi A, Li Q, Adamson TE, Bonnet F, Nguyen VT, Sedore SC, Price JP, Price DH, Lania L, Bensaude O (2004) Binding of the 7SK snRNA turns the HEXIM1 protein into a P-TEFb (CDK9/cyclin T) inhibitor. *EMBO J* **23**: 2608–2619
- Michels AA, Nguyen VT, Fraldi A, Labas V, Edwards M, Bonnet F, Lania L, Bensaude O (2003) MAQ1 and 7SK RNA interact with CDK9/cyclin T complexes in a transcription-dependent manner. *Mol Cell Biol* **23**: 4859–4869
- Nguyen VT, Kiss T, Michels AA, Bensaude O (2001) 7SK small nuclear RNA binds to and inhibits the activity of CDK9/cyclin T complexes. *Nature* **414**: 322–325
- Ouchida R, Kusuhara M, Shimizu N, Hisada T, Makino Y, Morimoto C, Handa H, Ohsuzu F, Tanaka H (2003) Suppression of NF- κ B-dependent gene expression by a hexamethylene bisacetamide-inducible protein HEXIM1 in human vascular smooth muscle cells. *Genes Cells* **8**: 95–107
- Palmeri D, Malim MH (1999) Importin beta can mediate the nuclear import of an arginine-rich nuclear localization signal in the absence of importin alpha. *Mol Cell Biol* **19**: 1218–1225
- Sano M, Abdellatif M, Oh H, Xie M, Bagella L, Giordano A, Michael LH, DeMayo FJ, Schneider MD (2002) Activation and function of cyclin T-Cdk9 (positive transcription elongation factor-b) in cardiac muscle-cell hypertrophy. *Nat Med* **8**: 1310–1317
- Schulte A, Czudnochowski N, Barboric M, Schonichen A, Blazek D, Peterlin BM, Geyer M (2005) Identification of a cyclin T-binding domain in Hexim1 and biochemical analysis of its binding competition with HIV-1 Tat. *J Biol Chem* **280**: 24968–24977
- Sims III RJ, Belotserkovskaya R, Reinberg D (2004) Elongation by RNA polymerase II: the short and long of it. *Genes Dev* **18**: 2437–2468

- Taube R, Lin X, Irwin D, Fujinaga K, Peterlin BM (2002) Interaction between P-TEFb and the C-terminal domain of RNA polymerase II activates transcriptional elongation from sites upstream or downstream of target genes. *Mol Cell Biol* **22**: 321–331
- Truant R, Cullen BR (1999) The arginine-rich domains present in human immunodeficiency virus type 1 Tat and Rev function as direct importin beta-dependent nuclear localization signals. *Mol Cell Biol* **19**: 1210–1217
- Weis K (2003) Regulating access to the genome: nucleocytoplasmic transport throughout the cell cycle. *Cell* **112**: 441–451
- Yang Z, Zhu Q, Luo K, Zhou Q (2001) The 7SK small nuclear RNA inhibits the CDK9/cyclin T1 kinase to control transcription. *Nature* **414**: 317–322
- Yik JH, Chen R, Nishimura R, Jennings JL, Link AJ, Zhou Q (2003) Inhibition of P-TEFb (CDK9/Cyclin T) kinase and RNA polymerase II transcription by the coordinated actions of HEXIM1 and 7SK snRNA. *Mol Cell* **12**: 971–982
- Yik JH, Chen R, Pezda AC, Samford CS, Zhou Q (2004) A human immunodeficiency virus type 1 Tat-like arginine-rich RNA-binding domain is essential for HEXIM1 to inhibit RNA polymerase II transcription through 7SK snRNA-mediated inactivation of P-TEFb. *Mol Cell Biol* **24**: 5094–5105
- Yik JH, Chen R, Pezda AC, Zhou Q (2005) Compensatory contributions of HEXIM1 and HEXIM2 in maintaining the balance of active and inactive P-TEFb complexes for control of transcription. *J Biol Chem* **280**: 16368–16376

APPENDIX 2

BLAZEK, Dalibor, Matjaz BARBORIC, **Jiri KOHOUTEK**, Irena OVEN and B. Matija PETERLIN. Oligomerization of HEXIM1 via 7SK snRNA and coiled-coil region directs the inhibition of P-TEFb. *Nucleic Acids Research*. 2005, 33(22), 7000–7010.

Oligomerization of HEXIM1 via 7SK snRNA and coiled-coil region directs the inhibition of P-TEFb

Dalibor Blazek¹, Matjaz Barboric¹, Jiri Kohoutek¹, Irena Oven^{1,2} and B. Matija Peterlin^{1,*}

¹Departments of Medicine, Microbiology and Immunology, Rosalind Russell Medical Research Center, University of California at San Francisco, San Francisco, CA 94143-0703, USA and ²Biochemical Faculty, Department of Animal Science, University of Ljubljana, Groblje 3, SI-1230 Domzale, Slovenia

Received October 13, 2005; Revised and Accepted November 16, 2005

ABSTRACT

Transcriptional elongation of most eukaryotic genes by RNA polymerase II requires the kinase activity of the positive transcription elongation factor b (P-TEFb). The catalytically active P-TEFb complex becomes inactive when sequestered into the large complex by the cooperative actions of 7SK snRNA and HEXIM1. In this study, we report that HEXIM1 forms oligomers in cells. This oligomerization is mediated by its predicted coiled-coil region in the C-terminal domain and 7SK snRNA that binds a basic region within the central part of HEXIM1. Alanine-mutagenesis of evolutionary conserved leucines in the coiled-coil region and the digestion of 7SK snRNA by RNase A treatment prevent this oligomerization. Importantly, mutations of the N-terminal part of the coiled-coil region abrogate the ability of HEXIM1 to bind and inhibit P-TEFb. Finally, the formation of HEXIM1 oligomers via the C-terminal part of the coiled-coil or basic regions is critical for the inhibition of transcription. Our results suggest that two independent regions in HEXIM1 form oligomers to incorporate P-TEFb into the large complex and determine the inhibition of transcriptional elongation.

INTRODUCTION

Transcription of eukaryotic protein-coding genes by RNA polymerase II (RNAPII) is tightly regulated at numerous levels, which include the assembly of preinitiation complexes, transcription initiation, promoter clearance, pausing, elongation and termination (1). Studies of the regulation of the

human immunodeficiency virus (HIV) gene expression have uncovered primarily the mechanisms that govern transcription pausing and elongation (2). The transition to productive elongation requires the positive transcription elongation factor b (P-TEFb), which consists of heterodimers between a catalytic subunit, the cyclin-dependent kinase 9 (Cdk9) and one of the four C-type cyclin regulatory subunits, CycT1, CycT2a, CycT2b or CycK (3). Upon its recruitment to the paused RNAPII, P-TEFb phosphorylates serines at position 2 in the C-terminal domain of the Rpb1 subunit of RNAPII, and components of the negative transcription elongation factor (N-TEF), which inactivates N-TEF and facilitates pre-mRNA processing (1–4). P-TEFb is critical not only for productive HIV gene expression, but is a general transcription factor that is recruited to several cellular promoters and is required for proper gene expression of most protein-coding genes in human cells (5,6).

Recently, important aspects of the regulation of P-TEFb have been revealed (2). Notably, P-TEFb exists in two major forms in cells. The small complex (SC) is a heterodimeric complex and is catalytically active. In contrast, the large complex (LC) is inactive and contains 7SK small nuclear RNA (snRNA) and HEXIM1 or HEXIM2 (7–13). The inhibition of P-TEFb is achieved by the cooperative actions of 7SK snRNA and HEXIM1 or HEXIM2 (8,13). The binding between the first 175 nt of 7SK snRNA and the evolutionary conserved basic region (BR) in HEXIM1 via its KHRR motif leads to the interaction between the C- and N-terminal regions of HEXIM1 and CycT1 or CycT2, respectively, resulting in the inactivation of P-TEFb (8,9). The assembly of P-TEFb into the LC can be prevented by disrupting the conserved PYNT motif in HEXIM1 and HEXIM2 (7,8). On the other hand, several stress-inducing agents and cardiac hypertrophic signals disassemble the LC in cells (10,11,14,15). Interestingly, diminution of HEXIM1 in HeLa cells results in the incorporation of an otherwise free form of HEXIM2 into

*To whom correspondence should be addressed. Tel: +1 415 502 1902; Fax: +1 415 502 1901; Email: matija@itsa.ucsf.edu

the large complex, demonstrating the dynamic and tightly regulated nature of the assembly and disassembly of the large complex (7,12).

Although several studies revealed aspects of the complex assembly of the LC (7–9,12,13), and we presented data on HEXIM1 homodimers and binding between the C-terminus in HEXIM1 and CycT1 *in vitro* (16), no comprehensive analysis of these RNA–protein and protein–protein interactions or their functional correlates *in vivo* has been presented. To these ends, we embarked on an extensive mutagenesis of HEXIM1, defined surfaces that form oligomers in the presence and absence of 7SK snRNA as well as those that bind CycT1 and assemble the LC in cells. In addition, functional studies of these mutant HEXIM1 proteins were performed on a plasmid target that depends uniquely on active P-TEFb complexes (17). A model of the assembly of the LC is presented.

MATERIALS AND METHODS

Cell culture and cell lines

HeLa cells were grown in DMEM containing 10% fetal calf serum at 37°C with 5% CO₂.

Plasmids

The plasmid reporter pG6TAR and plasmid encoding Gal.CycT1 protein were described (17). Plasmids coding for f.Hex1, f.Hex1(1–278), f.Hex1(1–314) were a gift from Dr H. Tanaka (18) and Q. Zhou (13). Plasmid f.Hex1mBR (as well as other Hexim1 mutants carrying mBR) contains the sequence of the SV-40 NLS at its N-terminus and was described previously (19). To construct plasmids encoding the mutant f.Hex1 proteins, the pFLAG-CMV2HEXIM1 plasmids were subjected to site-directed mutagenesis with the QuickChange II XL Site-Directed Mutagenesis Kit (Stratagene, La Jolla, CA). The plasmid encoding f.Hex1mBR(1–315) was prepared according to the procedure described previously (20). The plasmid coding for x.Hex1 was made by cloning the cDNA of HEXIM1 into KpnI and ApaI restriction sites of vector pcDNA3.1HisB (Invitrogen, Carlsbad, CA). Hex1.CFP and Hex1.YFP constructs were created by cloning of the wild-type HEXIM1 into pECFP-N1 and pEYFP-N1 expression vectors (Clontech). To prepare plasmids encoding the mutant Hex1.CFP and Hex1.YFP proteins, the Hex1.CFP and Hex1.YFP constructs were subjected to site-directed mutagenesis with the QuickChange II XL Site-Directed Mutagenesis Kit (Stratagene). All plasmids coding for Hex1.CFP and Hex1.YFP and carrying mB2 mutation contain the sequence of the SV-40 NLS at its N-terminus and were prepared as described previously (20).

Immunoprecipitation assay and western blot analysis

HeLa cells were grown on 100 mm plates. A total of 12 µg of plasmids were co-transfected by the FuGENE6 reagent (Roche Applied Science, Indianapolis, IN). After 40 h, HeLa cells were harvested and lysed in 0.75 ml of lysis buffer [1% NP-40, 10 mM Tris–HCl, pH 7.4, 150 mM NaCl, 2 mM EDTA, 0.1% protease inhibitor and either 0.5% RNase inhibitor (Roche, Indianapolis, IN) or RNase A (100 µg/ml final concentration) (Qiagen, Hilden, Germany)] for 1 h at 4°C. The

lysates were immunoprecipitated with anti-FLAG M2 beads for 2–4 h at 4°C and bound proteins were separated by SDS–PAGE electrophoresis and analyzed by immunoblotting with appropriate antibodies.

Transient transfection and CAT assay

HeLa cells were grown on 60 mm plates. Subsequently 0.3 µg of the pG6TAR reporter plasmid, 1 µg of Gal.CycT1 and 2.7 µg of appropriate f.Hex1 plasmid were co-transfected by the FuGENE6 reagent. A CAT assay was performed as described previously (17). In all transfections, the amount of DNA was equilibrated with an empty vector. Fold transactivation represents the ratio between the Gal.CycT1 activated transcription and the activity of the empty reporter plasmid alone, which was given as one.

Immunoreagents

The mouse monoclonal anti-FLAG M2 antibody was obtained from Sigma–Aldrich Corp. (St Louis, MO), the mouse monoclonal anti-Xpress antibody from Invitrogen and the goat polyclonal anti-CycT1 antibody (sc-8127) from Santa Cruz Biotechnology (Santa Cruz, CA).

The rabbit anti-HEXIM1 antibody was generated against HEXIM1 epitope LHRQQERAPLSKFGD and obtained from Antibody Solutions (Mountain View, CA).

Coiled-coil prediction

The prediction of coiled-coil was performed on programs available at the following addresses http://www.ch.embnet.org/software/COILS_form.html and <http://2zip.molgen.mpg.de/cgi-bin/2zip.pl> (21).

Fluorescence resonance energy transfer (FRET) microscopy

HeLa cells were plated onto culture dishes containing a 25 mm coverglass, transfected with the indicated expression plasmid DNAs and subjected to fluorescence microscopy 24 h post transfections as described previously (22). Briefly, the fluorescence images were acquired using an inverted IX-70 Olympus microscope using an Olympus ×40 Plan Apochromat objective lens (Olympus Corp., Lake Success, NY). For each cell, three fluorescence channels were collected. The donor channel consisted of CFP excited with 431–440 nm light and CFP fluorescence collected at 455–485 nm, the acceptor channel consisted of YFP excited with 496–505 nm light and YFP fluorescence collected at 520–550 nm, and the FRET channel consisted of CFP excited with 431–440 nm light and YFP fluorescence collected at 520–550 nm. Image collection and data analyses were conducted with MetaMorph imaging software (Universal Imaging Corp.).

Glycerol gradient centrifugation

Glycerol gradients (10–30%) were established by pipetting 2 ml of each of the glycerol fractions (10, 15, 20, 25 and 30% v/v) in buffer A (20 mM HEPES, pH 7.9, 0.3 M KCl, 0.2 mM EDTA, 0.1% NP-40) into centrifugation tubes (Beckman, Palo Alto, CA), catalog number 331372. Gradients were formed by standing for 6 h at 4°C. HeLa cells either transfected with the corresponding plasmids or not transfected were lysed in 0.5 ml of buffer A containing 0.1% protease inhibitor and either 0.5%

RNase inhibitor or RNase A (100 µg/ml final concentration) for 30 min at 4°C. The lysates were centrifuged at 10000 *g* for 10 min and the supernatants were loaded into tubes with the preformed glycerol gradients. Protein complexes were then fractionated by centrifugation in an SW 41Ti rotor (Beckman) at 38 000 r.p.m. for 21 h. Ten fractions (1 ml) were collected, precipitated with trichloroacetic acid and finally analyzed by immunoblotting with the appropriate antibodies (12).

RESULTS

Prediction of an evolutionary conserved CR in the C-terminal domain of HEXIM1

To obtain further insight into the function of HEXIM1, we first performed multiple sequence alignments between human HEXIM1 and HEXIM1 and HEXIM2 proteins from different species. While the N-termini of HEXIM1 and HEXIM2 proteins differ, the conserved regions include the centrally located basic region (BR; positions 150 to 177 in the human HEXIM1 protein) and the C-terminal domain of the protein (Figure 1A). We further analyzed C-terminal region in greater detail and found that it contains several conserved clusters of amino acids from position 279 to 339 in the human HEXIM1 protein (Figure 1B). Among these, the consensus sequence indicated a high number of conserved leucines. Notably, the leucines are assembled in heptad repeats, which is the hallmark of coiled-coil and oligomer-forming regions (23). Indeed, a prediction program suggested a high probability for a coiled-coil in the C-terminal domain of HEXIM1 from positions 279 to 352 (Figure 1C). Moreover, this analysis further indicated that this CR could be composed of two parts. Its N-terminal part from positions 279 to 315 could form a leucine zipper and its C-terminal part from positions 319 to 352 could constitute a coiled-coil. The highly conserved nature of the C-terminus of HEXIM1 suggests its functional importance. Finally, since it contains a predicted CR, we hypothesized that HEXIM1 could form oligomers.

HEXIM1 forms oligomers in living cells

To test this hypothesis, we first examined whether HEXIM1 proteins can interact with each other in living cells (Figure 2). For these experiments, we used FRET microscopy. The effective energy transfer between cyan (CFP) and yellow fluorescent protein (YFP) fluorophores requires the two proteins to be 1–5 nM apart which typically corresponds to direct interaction of proteins tagged with YFP and CFP. Thus, FRET imaging provides the ability to monitor protein–protein interactions in living cells and has also been recently used to detect protein oligomerization (24–26). We fused the YFP and CFP to the C-termini of different human HEXIM1 proteins, which resulted in the construction of the hybrid Hex1.YFP and Hex1.CFP proteins. Next, we expressed these chimeras individually or in combination in HeLa cells and performed FRET microscopy. When we co-expressed both chimeras, energy transfer resulted in an increased FRET signal at the expense of the donor emission (FRET/donor) relative to the cells expressing the donor alone (Figure 2A, compare image i with c and f). Residual signal in the FRET channel of the images c and f represents

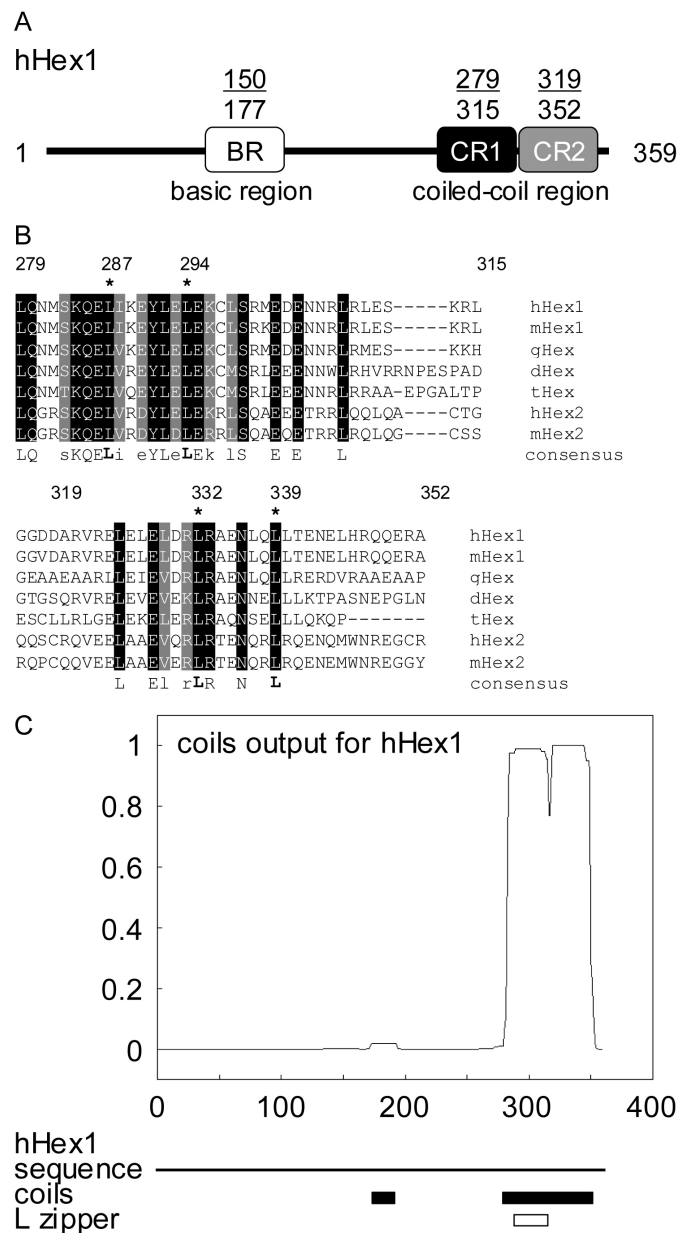


Figure 1. Prediction of CR1 and CR2 in the C-terminal domain of HEXIM1. (A) Schematic depiction of human HEXIM1 protein (hHex1). White box represents the BR. CR1 and CR2 are represented by black and gray boxes, respectively. The numbering above the boxes defines the boundaries of the regions. (B) Alignment of human (hHex1), mouse (mHex1), chicken (gHex1), zebrafish (dHex1), fish (tHex1) HEXIM1 and human (hHex2) and mouse (mHex2) HEXIM2 proteins. Black boxes indicate amino acid identity while shaded boxes the amino acid similarity. The numbering above the alignment corresponds to the boundaries of the predicted CR1 and CR2. Also, the numbered leucines, which are marked by an asterisk, were mutated to alanines. The consensus sequence is indicated below the alignment. (C) The graph indicates the probability of coiled-coil for the human HEXIM1 protein as predicted by the coils prediction program. The line below the graph corresponds to the sequence of hHex1 and the boxes indicate regions with high probability of coiled-coil (black box) and leucine zipper (white box) as predicted by the coils software.

bleedthrough of the donor and acceptor channels to the FRET channel, respectively. Similarly, when we plotted the FRET/donor against the acceptor/donor ratios, we observed an increase in the FRET signal with increasing amounts of

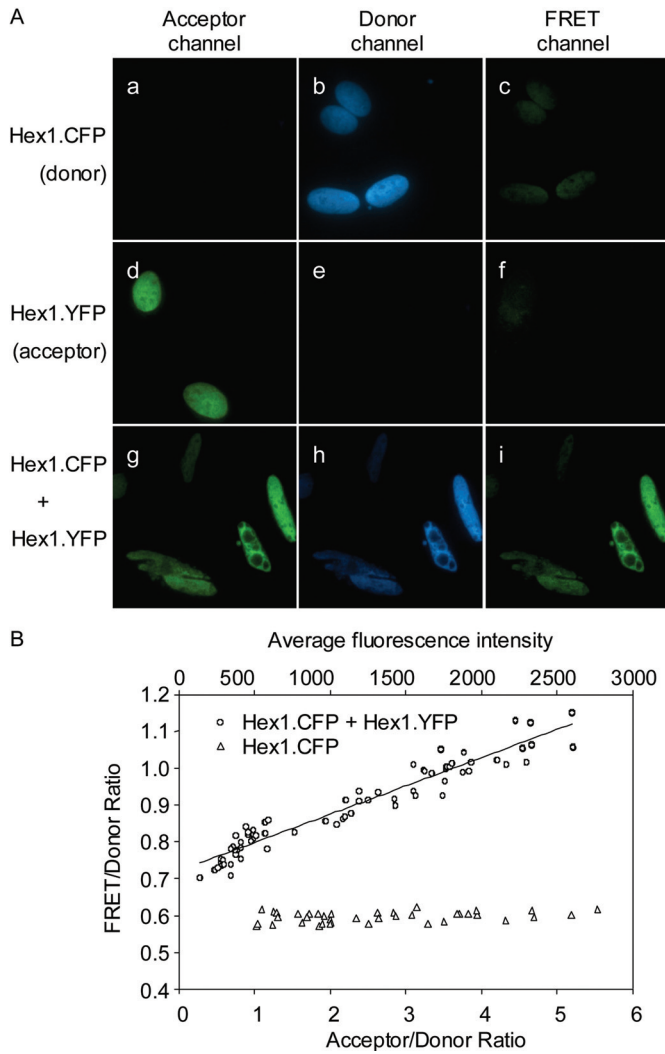


Figure 2. HEXIM1 oligomerizes in the nucleus of cells. (A) Representative images of Hex1.YFP and Hex1.CFP chimeras, which were expressed alone or together in cells. Amounts of nuclear fluorescence were quantified in the yellow, cyan and FRET channels. Energy transfer resulted in an increased FRET at the expense of donor emissions (FRET/donor) in the co-expressing cells relative to the cells containing the donors alone. (B) FRET/donor ratio increased proportionally with the amount of the acceptor relative to the donor in cells co-expressing Hex1.YFP and Hex1.CFP chimeras. The slope of the graph represents the extent of FRET at normalized acceptor/donor levels. There was no FRET between Hex1.CFP proteins expressed alone.

acceptor relative to donor, whereas no FRET signal was observed in cells that expressed the donor alone (Figure 2B). Also, the levels of Hex1.YFP and Hex1.CFP proteins were comparable and these fusion proteins inhibited P-TEFb similarly to the wild-type HEXIM1 protein (data not shown). As a negative control we used an irrelevant protein, the class II transactivator (CIITA), fused to CFP and Hex1.YFP. Co-expression of both chimeras resulted in no FRET signal and no increase in the FRET signal when we plotted the FRET/donor against the acceptor/donor ratios (data not shown). Thus, HEXIM1 proteins interact with each other in living cells and consequently can form oligomers.

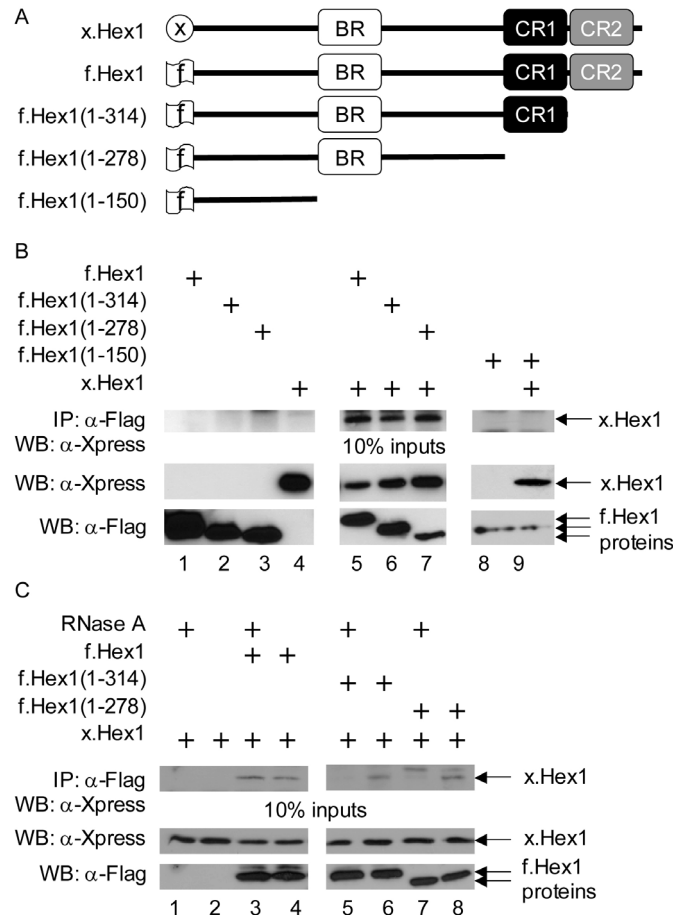


Figure 3. The C-terminal domain and 7SK snRNA mediate the oligomerization of HEXIM1. (A) Schematic diagram of Hex1 proteins used. The signs at their N-termini depict the respective tags. (B) HEXIM1 forms oligomers. The x.Hex1 and f.Hex1 proteins were either expressed alone (lanes 4 and 1, 2, 3, 8, respectively) or f.Hex1 was co-expressed with x.Hex1 in HeLa cells (lanes 5–7 and 9) as indicated. Lysates were co-immunoprecipitated with anti-FLAG agarose beads and immunoprecipitates of x.Hex1 were identified as presented on the upper western blot (WB). The middle and lower WB contain 10% of input proteins for immunoprecipitations (IP). Wild-type and mutant HEXIM1 proteins are identified by arrows. (C) 7SK snRNA and the C-terminal domain of HEXIM1 mediate the oligomerization of HEXIM1. x.Hex1 was expressed alone (lanes 1 and 2) or with the indicated f.Hex1 proteins (lanes 3–8). IP were performed as in (B) and were treated with RNase A where indicated.

The C-terminal domain of HEXIM1 and the 7SK snRNA-bound BR direct HEXIM1 oligomerization

To define the regions that might form oligomers, we performed immunoprecipitation assays (Figure 3). For these studies, we constructed a series of FLAG epitope-tagged HEXIM1 (f.Hex1) proteins, in which their C-termini were shortened progressively (Figure 3A). While the mutant f.Hex1(1–314) protein lacked the CR2, the mutant f.Hex1(1–278) and f.Hex1(1–150) proteins lacked the entire CR. Also, except for the mutant f.Hex1(1–150) protein, the rest of the proteins contained the BR. Finally, we constructed an Xpress epitope-tagged HEXIM1 (x.Hex1) protein. Next, we expressed the f.Hex1 and x.Hex1 proteins in HeLa cells, immunoprecipitated them from the total cell lysates using anti-FLAG agarose beads and followed their binding by western blotting with antibodies directed against the Xpress epitope. Consistent

with the results obtained in Figure 2, the wild-type f.Hex1 protein bound x.Hex1 protein in cells (Figure 3B, lane 5). The same result was obtained with the mutant f.Hex1(1–314) protein (Figure 3B, lane 6). Surprisingly, the mutant f.Hex1(1–278) protein retained the ability to bind x.Hex1 whereas the mutant f.Hex1(1–150) protein did not (Figure 3B, lanes 7 and 9). Since the wild-type x.Hex1 protein was not present in the anti-FLAG immunoprecipitations in the absence of f.Hex1 protein (Figure 3B, lane 4) the binding results were specific. These results suggest that in the absence of the C-terminal domain of HEXIM1, BR is critical for the formation of oligomers in HEXIM1. Furthermore, since 7SK snRNA binds the BR in HEXIM1, we predicted that the BR could mediate the oligomerization via 7SK snRNA.

To address this prediction directly and to assess the requirements of the C-terminal domain for HEXIM1 oligomerization, we repeated the experiments described in Figure 3B and additionally performed parallel experiments in which we digested 7SK snRNA by treatment of the total cell lysates with RNase A (Figure 3C). The wild-type f.Hex1 protein bound x.Hex1 protein in the presence of RNase A (Figure 3C, lanes 3 and 4). This result corresponds with the recent findings that the full-length HEXIM1 protein association does not change significantly upon RNase A treatment (12). In contrast, RNase A treatment disrupted the ability of the mutant f.Hex1(1–314) and f.Hex1(1–278) proteins to bind x.Hex1 (Figure 3C, lanes 5–8). Also, levels of the f.Hex1 and x.Hex1 proteins in cell lysates were comparable (Figure 3C, lower panel). Thus, the oligomerization of HEXIM1 depends on the intact C-terminal domain and the 7SK snRNA-bound BR.

Combined disruptions of the CR and 7SK snRNA abolish HEXIM1 oligomerization

Next, we wanted to elucidate the importance of the predicted CR in mediating HEXIM1 oligomerization (Figure 4). Since the leucines within the heptad coiled-coil repeats are critical for the coiled-coil structure and for the formation of oligomers (21,23), we mutated a series of conserved leucines to alanines. Alanine-mutagenesis was employed since non-polar alanines maintain an α -helical structure of the region but prevent its oligomerization capacity, which is mediated by the hydrophobic side chain methyl groups of the leucines. We mutated the leucine doublets at positions 287 and 294 within the CR1 and at positions 332 and 339 within the CR2 in the C-terminus of HEXIM1 individually or in combination (Figure 4A). In this way, we constructed the mutant proteins f.Hex1mCR1, f.Hex1mCR2 and f.Hex1mCR12, respectively. Next, we tested the ability of the wild-type and these mutant f.Hex1 proteins to oligomerize with the x.Hex1 protein by immunoprecipitation in the presence or absence of RNase A as described above. The wild-type and the mutant f.Hex1 proteins bound x.Hex1 in the absence of RNase A (Figure 4B, lanes 6, 8, 10 and 12). In contrast, the mutant f.Hex1mCR12 protein, in which both parts of the predicted CR were disrupted, failed to bind x.Hex1 in the presence of RNase A (Figure 4B, lane 7). However, the mutant f.Hex1 proteins with individually disrupted coiled-coil parts bound x.Hex1 under the same conditions (Figure 4B, lanes 9 and 11). Also, levels of the f.Hex1 and x.Hex1 proteins in cell lysates

were comparable (Figure 4B, lower panel). Thus, these results indicate that the predicted CR directs HEXIM1 oligomerization. Since the CR1 and CR2 mediate the formation of the HEXIM1 oligomers by themselves in the context of the entire C-terminus of HEXIM1, these two sequences could in principle serve different functions.

To confirm the results observed in immunoprecipitation experiments, we decided to analyze oligomerization properties of HEXIM1 mutants in living cells by FRET microscopy. We constructed mutants of Hex1.YFP and Hex1.CFP with disrupted oligomerization regions in the BR and in the C-terminal domain of the protein. Mutants in the BR, where arginines 154–156 were mutated to alanines, were designated mB2 and represent the situation, where 7SK snRNA does not bind to HEXIM1 (19). We prepared mutant Hex1mB2, Hex1.mB2CR1 and Hex1.mB2CR12 as YFP and CFP fusion proteins, where the 7SK snRNA binding site was disrupted alone or in combination with disrupted CR1 and CR12, respectively. Furthermore, we constructed Hex1.CR12 YFP and CFP fusion proteins with disrupted CR but intact BR. Next, we examined the ability of these mutant Hex1.CFP/YFP proteins to interact with each other in living cells by analyzing the FRET signal. Combined co-expression of YFP and CFP fusion mutants, which carried at least one intact oligomerization region resulted in a FRET signal (Figure 4C, images c, f and i). In contrast, mutant Hex1.mB2CR12YFP/CFP proteins with no functional oligomerization region showed no FRET signal (Figure 4C, image l). Also, when we plotted the FRET/donor against the acceptor/donor ratios we observed an increase in the FRET signal with increasing amounts of acceptor relative to donor with mutant proteins with at least one functional oligomerization region, but not with mutant proteins where all oligomerization regions were disrupted (data not shown). We conclude that combined disruptions of the CR and the 7SK snRNA binding site abolish completely HEXIM1 oligomerization and that at least one functional oligomerization domain is sufficient to mediate the formation of HEXIM1 oligomers in cells.

CR1 in HEXIM1 is required for its binding to P-TEFb and inhibition of transcription

To explore the possibility that the CR1 and CR2 could be functionally separable, we asked whether their individual disruptions could affect the binding to P-TEFb and thus inhibit transcription differently (Figure 5). To accomplish this goal, we first expressed the wild-type f.Hex1 and the mutant f.Hex1mCR1 and f.Hex1mCR2 proteins in HeLa cells and performed immunoprecipitation assays as described above. The presence of P-TEFb in the immunoprecipitations was followed by western blotting with antibodies directed against the endogenous CycT1 subunit of P-TEFb. As expected, the wild-type f.Hex1 protein bound P-TEFb (Figure 5A, lane 1) and the same was true for the mutant f.Hex1mCR2 protein (Figure 5A, lane 3). In contrast, the mutant f.Hex1mCR1 protein decreased considerably its ability to bind P-TEFb (Figure 5A, lane 2). Also, levels of f.Hex1 proteins were comparable (Figure 5A, lower panel). We conclude that CR1 in HEXIM1 is critical for binding to P-TEFb.

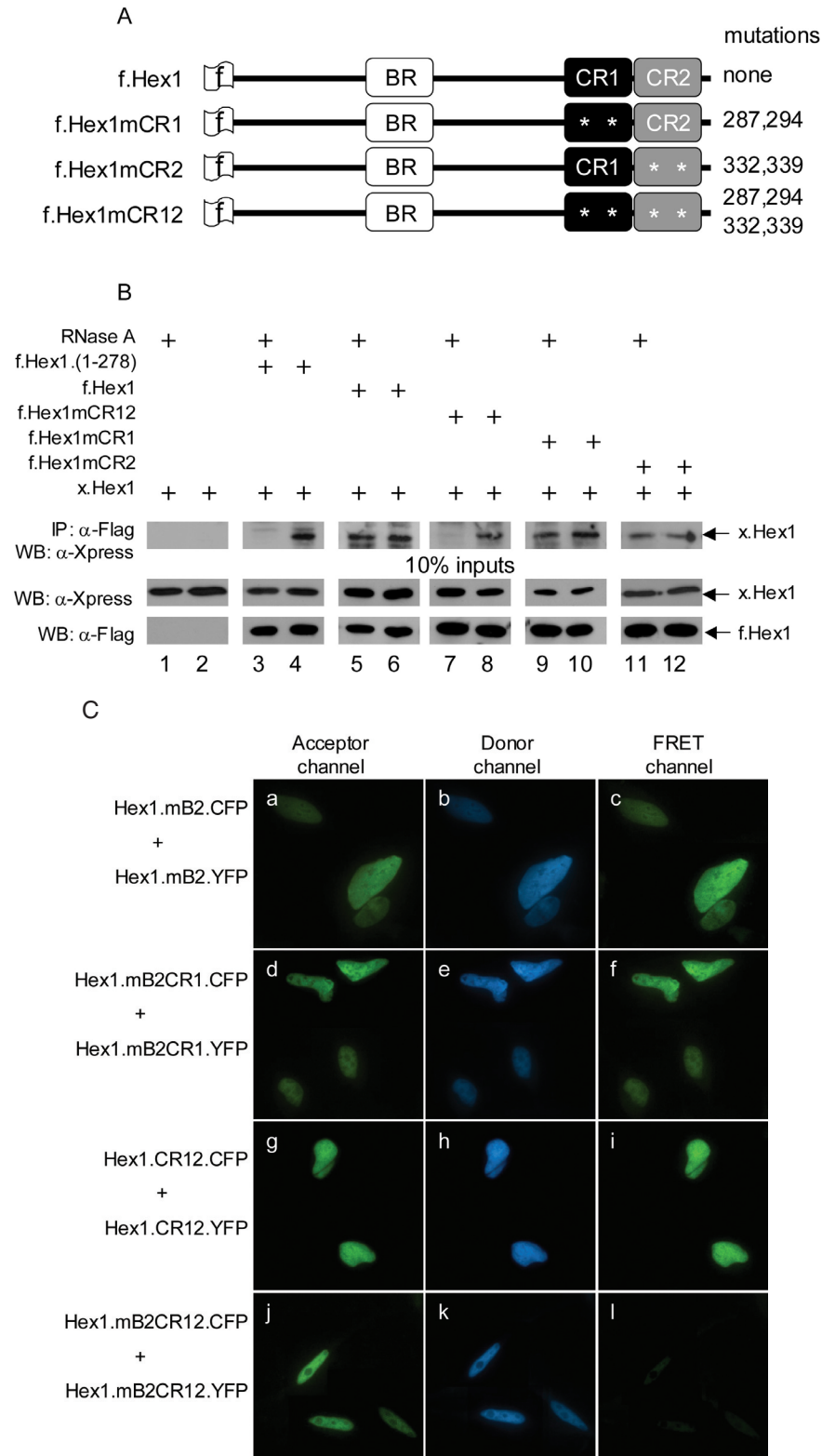


Figure 4. Combined disruptions of the CR and BR abolish HEXIM1 oligomerization. (A) Schematic diagram of Hex1 proteins used. The sign at their N-termini depicts the FLAG tag. The asterisks within the CR1 and CR2 indicate the mutations of leucines to alanines. The numbering indicates the positions of the mutated leucines in f.Hex1 proteins. (B) HEXIM1 with the disrupted CR does not oligomerize in the absence of 7SK snRNA. Proteins with the disrupted CR1 or CR2 (lanes 9–12) or CR (lanes 7 and 8) were co-expressed with x.Hex1 in HeLa cells. The lysates were treated with RNase A where indicated, immunoprecipitated with anti-FLAG agarose beads and immunoprecipitates were subjected to SDS-PAGE and WB (upper panel). Lower panels represent 10% input of proteins. (C) Combined disruptions of the CR and the 7SK snRNA binding site abolish completely HEXIM1 oligomerization in cells. FRET analysis was performed as in Figure 2. Representative images of the nuclei in which Hex1.YFP and Hex1.CFP mutant proteins were co-expressed are presented. The amounts of nuclear fluorescence were quantified in the yellow, cyan and FRET channels.

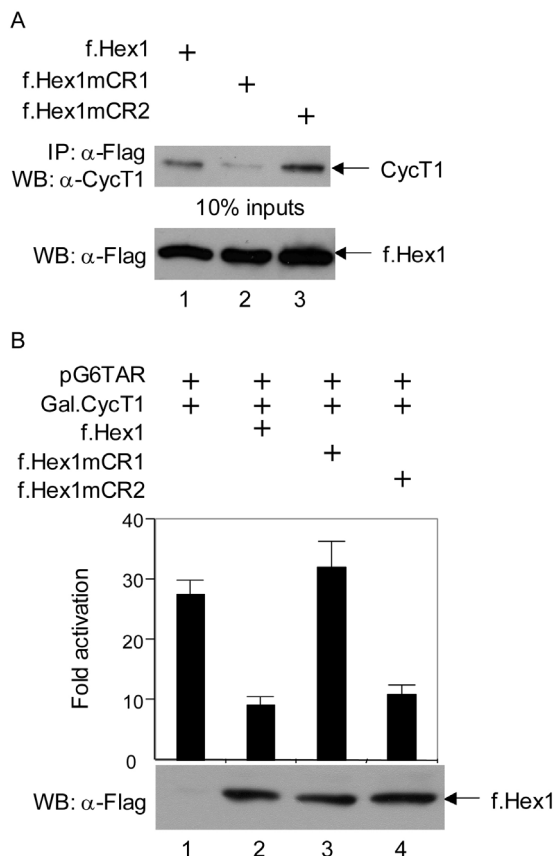


Figure 5. CR1 in HEXIM1 is required for its binding to P-TEFb and inhibition of transcription. (A) Disruption of the CR1 abrogates P-TEFb binding. f.Hex1 proteins were expressed in HeLa cells (6 μ g, lanes 1–3) and immunoprecipitated with anti-FLAG agarose beads. Amounts of bound endogenous CycT1 is presented by WB (upper panel). The amounts of f.Hex1 proteins are indicated in WB below (lower panel). (B) f.Hex1mCR1 does not inhibit transcription. HeLa cells expressed pG6TAR (0.3 μ g), Gal.CycT1 (1 μ g) and f.Hex1 (2.7 μ g) as depicted. Bars correspond to CAT values and the lower panel presents expression (WB) of f.Hex1 as indicated by the arrow.

To extend our binding studies, we assessed the ability of these f.Hex1 proteins to inhibit P-TEFb in a transcriptional assay in HeLa cells (Figure 5B). We employed a system consisting of a plasmid reporter pG6TAR, which contained six Gal4 DNA-binding sites positioned upstream of the HIV long terminal repeat, followed by the CAT reporter gene, and a plasmid effector coding for the chimeric Gal.CycT1 protein. Its recruitment to pG6TAR promoter activates transcription and can be measured by the CAT reporter assay (17). When we co-expressed the Gal.CycT1 chimera with pG6TAR, levels of CAT activity increased 27-fold over basal levels whereas co-expression of the wild-type f.Hex1 protein decreased this activity to 9-fold (Figure 5B, compare bars 1 and 2). Strikingly, when we co-expressed the mutant f.Hex1mCR1 protein, this inhibitory function was lost (Figure 5B, bar 3). In contrast, the mutant f.Hex1mCR2 protein inhibited P-TEFb similarly to the wild-type f.Hex1 protein (Figure 5B, bar 4). Levels of f.Hex1 proteins were comparable (Figure 5B, lower panel). Also, the subcellular localization of both f.Hex1 mutants was the same as the wt f.Hex1 protein (data not shown). Thus, it can be concluded that CR1 and CR2 are functionally separable and only the CR1 in HEXIM1 is

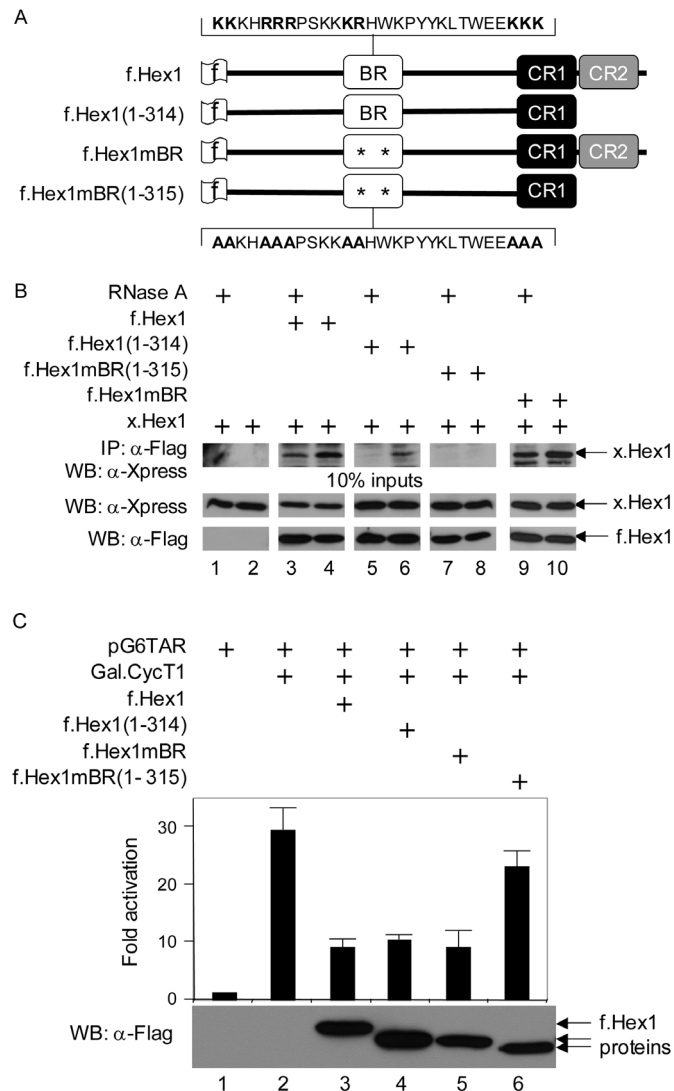


Figure 6. Oligomerization of HEXIM1 via its BR or CR2 is required for the inhibition of transcription. (A) Schematic diagram of Hex1 proteins used. The BR, CR1 and CR2 regions participating in the oligomerization are depicted. The wild-type and the mutated residues of the BR are depicted above and below the diagram, respectively. The mutated BR is indicated by asterisk. The schematic picture represents the f.Hex1 and mutant f.Hex1(1–314), f.Hex1mBR and f.Hex1mBR(1–315) proteins used. (B) HEXIM1 without the BR and the CR2 does not oligomerize. The x.Hex1 and f.Hex1 proteins were co-expressed as depicted. Lysates were treated with RNase A where noted and IP was performed as described. Upper panel represents WB with the immunoprecipitated x.Hex1 proteins, whereas the middle and lower panels show 10% input of proteins used for IP. (C) HEXIM1 without the BR and the CR2 does not inhibit P-TEFb. Bars represent CAT data obtained by co-transfection of HeLa cells with pG6TAR (0.3 μ g), Gal.CycT1 (1 μ g) and indicated f.Hex1 plasmids (2.7 μ g). The lower panel presents the expression of f.Hex1 proteins.

required for the binding to P-TEFb, resulting in the inhibition of its transcriptional activity.

Oligomerization of HEXIM1 via BR or CR2 is required for the inhibition of transcription

To examine the functional importance of HEXIM1 oligomers, we asked whether the ability of HEXIM1 to inhibit P-TEFb depends on its oligomerization (Figure 6). We used the series of f.Hex1 proteins presented in Figure 6A. The mutant

f.Hex1(1–314) and the wild-type f.Hex1 proteins, which possess one or two regions that form oligomers, respectively, were described above. Two additional mutant f.Hex1 proteins were constructed. The mutant f.Hex1mBR protein, in which most of the basic residues in the BR were mutated to alanines, contains a disrupted BR. It does not bind 7SK snRNA *in vitro*, but inhibits P-TEFb in transcriptional assays (19). Finally, the mutant f.Hex1mBR(1–315) has a disrupted BR and CR2. Both of these mutant proteins also contain the SV-40 NLS, which enables their nuclear localization. To examine the oligomerization of these f.Hex1 proteins, we performed immunoprecipitation assays in the presence or absence of RNase A (Figure 6B). As already presented in Figure 3 and in the recent report (12), the RNase A treatment did not change considerably the binding between the wild-type f.Hex1 and x.Hex1 proteins (Figure 6B, lanes 3 and 4) but it prevented the binding with the mutant f.Hex1(1–314) protein (Figure 6B, lanes 5 and 6). Predictably, the mutant f.Hex1mBR protein with the intact CR bound x.Hex1 independently of RNase A treatment (Figure 6B, lanes 9 and 10). In contrast, the mutant f.Hex1mBR(1–315), which lacks the CR2 and the BR, failed to bind x.Hex1 in the presence or absence of RNase A (Figure 6B, lanes 7 and 8). Levels of f.Hex1 and x.Hex1 proteins in cell lysates were comparable (Figure 6B, lower panel). The result in Figure 6B, lane 5, may seem to contradict the result obtained with the immunoprecipitation of mutant f.Hex1mCR2 under RNase A treatment where oligomers were observed (Figure 4B, lane 11). However, it is important to note that in the mutant f.Hex1mCR2 protein just two C-terminally located leucines were mutated in comparison with the deletion of the entire CR2 in the f.Hex1(1–314).

Finally, to determine whether the oligomerization of HEXIM1 correlates with its inhibitory function, we assessed the abilities of these f.Hex1 proteins to inhibit P-TEFb by using transcriptional assays in HeLa cells (Figure 6C). We employed the same system as described in Figure 5. The wild-type f.Hex1 protein decreased the activity of the Gal.-CycT1 chimeric protein from 29- to 9-fold over the basal levels (Figure 6C, compare bars 1–3). Similarly, the mutant f.Hex1(1–314) and f.Hex1mBR proteins inhibited P-TEFb equivalently to the wild-type f.Hex1 protein (Figure 6C, bars 4 and 5). Critically, the mutant f.Hex1mBR(1–314) protein, which could not form oligomers, failed to inhibit P-TEFb (Figure 6C, bar 6). Thus, the separate disruption of two oligomerization domains does not affect the abilities of these mutant HEXIM1 proteins to inhibit P-TEFb. Rather, the combined disruption of the BR and the CR2 prevents not only the formation of oligomers, but also the inhibition of transcriptional activity of P-TEFb. We conclude that the ability of HEXIM1 to inhibit P-TEFb requires its oligomerization.

Oligomerization of HEXIM1 via BR or CR2 is required for the incorporation of HEXIM1 into the LC

To confirm these results, we correlated the inhibitory function of f.Hex1 proteins with their ability to bind P-TEFb and to incorporate into the LC (Figure 7). We hypothesized that mutant f.Hex1 proteins, which do not inhibit P-TEFb, also do not bind it. For this purpose, we expressed our mutant f.Hex1 proteins and performed immunoprecipitation assays as described (Figure 7A). The presence of P-TEFb in the

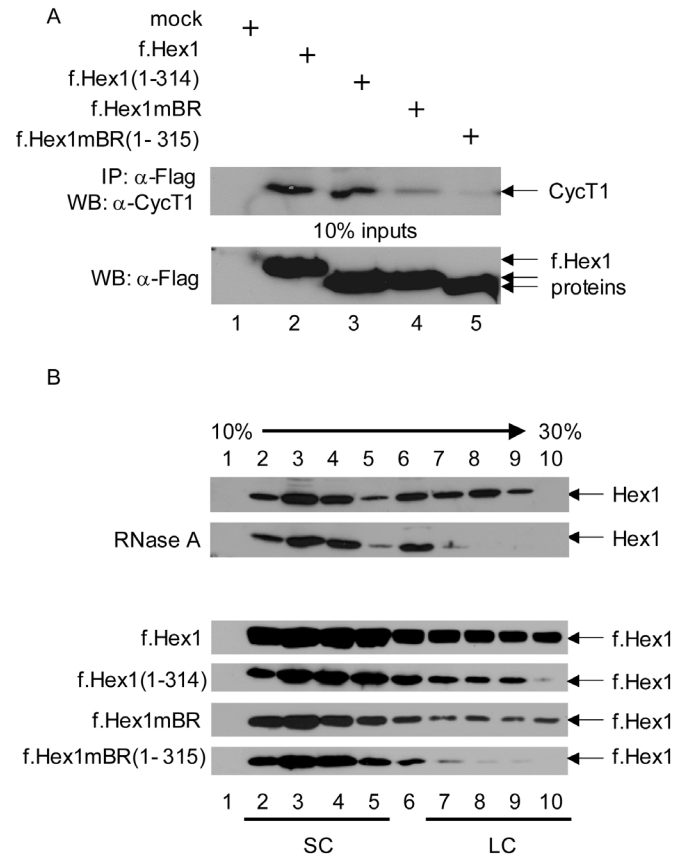


Figure 7. Oligomerization of HEXIM1 via BR or CR2 is required for the incorporation of HEXIM1 into the LC of P-TEFb. (A) HEXIM1 with disrupted BR and CR2 does not bind P-TEFb. HeLa cells were either mock transfected (lane 1) or transfected with f.Hex1 plasmids (6 μ g, lanes 2–5). The f.Hex1 proteins were immunoprecipitated with anti-FLAG agarose beads. Amounts of bound endogenous CycT1 is presented by WB (upper panel). The amounts of f.Hex1 proteins are indicated in WB below (lower panel). (B) HEXIM1 with disrupted BR and CR2 does not incorporate into the LC. Lysates from either mock or f.Hex1 plasmids transfected cells were divided into ten fractions by glycerol gradient centrifugation. Amounts of endogenous HEXIM1 proteins in each fraction were analyzed by immunoblotting as shown on the panels. The numbers below and above panels depict the glycerol fractions and arrow indicates increasing glycerol gradient (from 10 to 30%). SC and LC stand for small complex and large complex of the P-TEFb, respectively.

immunoprecipitations was followed by western blotting with antibodies directed against the endogenous CycT1 subunit of P-TEFb. The wild-type f.Hex1 protein bound P-TEFb (Figure 7A, lane 2) and the lysate from the mock transfected cell did not (Figure 7A, lane 1). As predicted, the mutant f.Hex1(1–314) and f.Hex1mBR proteins with only one disrupted oligomerization region, which inhibited P-TEFb, also bound P-TEFb (Figure 7A, lanes 3 and 4), although f.Hex1mBR shown reduced binding in comparison with f.Hex1. In contrast, the mutant protein f.Hex1mBR(1–315) did not interact with P-TEFb at all, which corresponds well with its abrogated inhibitory function (Figure 7A, lane 5). The levels of f.Hex1 proteins were comparable (Figure 7A, lower panel). Thus, the loss of the inhibitory function of the mutant Hex1 protein with the combined disruption of BR and CR2 is due to its inability to bind P-TEFb.

Part of the P-TEFb in HeLa cells is incorporated into functionally inactive LC. The rest of P-TEFb is catalytically active

and forms SC (8,9,13,27). On the basis that HEXIM1 with the combined disruption of BR and CR2 neither inhibits nor binds P-TEFb, we hypothesized that these two regions are critical for the incorporation of HEXIM1 into the LC. To prove this assumption, we employed glycerol gradient centrifugation of lysates from HeLa cells that expressed different mutant f.Hex1 proteins and analyzed the ability of these mutants to form LC with endogenous P-TEFb (Figure 7B). As a control, we observed endogenous HEXIM1 proteins in SC and LC in lysates of the mock transfected cells (Figure 7B, upper two panels). Upon treatment with RNase A, HEXIM1 was released from the LC and was found only in the free form. Subsequently, we expressed wild-type and mutant f.Hex1 proteins with either separately disrupted BR and CR2 or in combination. As expected, the wild-type f.Hex1 and mutant f.Hex(1–314) and f.Hex1mBR proteins, which oligomerize and inhibit P-TEFb, were also incorporated into the LC. In contrast, the mutant f.Hex1mBR(1–315) protein existed only in the free form and failed to be incorporated into the LC (Figure 7B, compare four lower panels), which is consistent with its inability to inhibit P-TEFb. Thus, we conclude that the BR and CR2 regions are required for oligomerization and incorporation of HEXIM1 into the LC to direct the inhibition of P-TEFb.

DISCUSSION

In this study, we investigated mechanisms dictating the assembly of the 7SK snRNA:HEXIM1:P-TEFb complex that inhibits transcriptional elongation. First, a predicted CR was found in the C-terminus of HEXIM1. Second, HEXIM1 forms oligomers via this CR and BR that binds 7SK snRNA in cells. Third, in the presence of 7SK snRNA, the CR1 binds P-TEFb whereas the CR2 mediates HEXIM1 oligomerization. Finally, we determined that the oligomerization of HEXIM1 is a prerequisite for its incorporation into the LC and thus binding and inhibition of P-TEFb in cells.

This work extends our earlier observations that the C-terminus of HEXIM1 forms homodimers and also binds CycT1 *in vitro* (16). However, in that study, HEXIM1 dimers were not stable in the presence of CycT1, most likely because 7SK snRNA and its binding site on HEXIM1 were not provided. Notably, these findings are consistent with previous reports on the C-terminus of HEXIM1, in which the N-terminal 274 amino acids of HEXIM1 did not interact with P-TEFb in the yeast two-hybrid assay, but the inclusion of additional 26 residues to position 300 partly restored this binding (8,9). However, the precise mapping of the surfaces involved in these protein–protein interactions and the role of 7SK snRNA in this process had not been addressed. For these reasons, we elected to move all our experiments into the physiological setting of the cell, where we could examine our mutations for binding and function in the same context and correlate them to what has been surmised largely from biochemical analyses. Importantly, our study provided further details on surfaces involved in these interactions and presented a kinetic picture of how the LC could be assembled. Namely, it demonstrated the critical contribution of 7SK snRNA to the formation of the stable LC. Combining deletions and clustered point mutations also defined these surfaces precisely, so that we could distinguish between the oligomerization of HEXIM1

via CR2 and its binding to CycT1 and thus P-TEFb via CR1. Since HEXIM1 oligomers do not bind P-TEFb in the absence of 7SK snRNA, it is possible that the entire CR dictates their self-association. In this scenario, the presence of 7SK snRNA then provides the decisive oligomerization function, which exposes CR1 for binding to CycT1, thus leading to the assembly of the LC and P-TEFb inhibition. Importantly, our binding studies were complemented with functional data, where we examined wild-type and mutant HEXIM1 proteins for their ability to block transcription directed by P-TEFb. First, we used a plasmid target that depends uniquely on P-TEFb and then we targeted P-TEFb to the promoter via a heterologous DNA-tethering of CycT1 (17). Previously, we demonstrated that this reporter and target are blocked by dominant negative Cdk9 protein as well DRB or flavopiridol, which are two ATP analogs that inhibit the kinase activity of P-TEFb (17). Thus, the assay depends critically on the catalytically active Cdk9 protein. In this way, we could distinguish directly between HEXIM1 proteins that can and cannot inhibit P-TEFb and correlate the formation of the LC with its functional consequences *in vivo*.

A recent report demonstrated the formation of homo- and hetero-oligomers between HEXIM1 and HEXIM2 proteins, which were thought to be independent of 7SK snRNA (12). Notably, our findings suggest that 7SK snRNA is pivotal in directing the incorporation of HEXIM1 and HEXIM2 proteins into the LC. These LCs with the homo- or hetero-oligomers of HEXIM1/2 could subserve different physiological functions, which would reflect different expression levels of these proteins in various tissues and cells (7,12). This situation would be reminiscent of transcription factors with basic region-leucine zippers (b/ZIP), where homo- and hetero-dimerizations via coiled-coil regions modulate their transcriptional properties (28,29). Although we refer to HEXIM1 oligomers throughout, *in vitro* data (16) and glycerol gradient sedimentation analyses (10) favor strongly the notion of HEXIM1 dimers. In addition, the BR in HEXIM1 that resembles the arginine-rich motif in Tat (27) could bind the top of the first stem loop in 7SK snRNA that resembles the transactivation response (TAR) region in HIV-1. In TAR, Tat and CycT1 bind the 5' bulge and central loop as a heterodimer (30). Analogously, Tat from the equine infectious anemia virus (EIAV) and equine CycT1 bind the central loop in TAR from EIAV as a heterodimer (31). Moreover, the coat protein of bacteriophage MS2/R17 binds the central loop of the operator as a homodimer, which gives it greater affinity and specificity (32,33). From these considerations, we propose that HEXIM1 also forms homodimers on 7SK snRNA. These conclusions are supported by the calculated molecular mass of the LC, which is ~500 kDa (10). This size would encompass one molecule of 7SK snRNA, two HEXIM1, two CycT1 and two Cdk9 proteins, for a final ratio of these subunits of 1:2:2:2.

When this manuscript was in preparation, two papers describing HEXIM1 oligomerization were published (34,35). In agreement with our conclusions, the oligomeric (most probably dimeric) nature of HEXIM1 was reported for free and 7SK snRNA-bound HEXIM1 *in vitro* and *in vivo*. Furthermore, the mutations of leucines at positions 287 and 294 were found to be sufficient for the disruption of HEXIM1 dimerization using native gel electrophoresis in the absence of 7SK snRNA *in vitro* (35). This discrepancy with our data

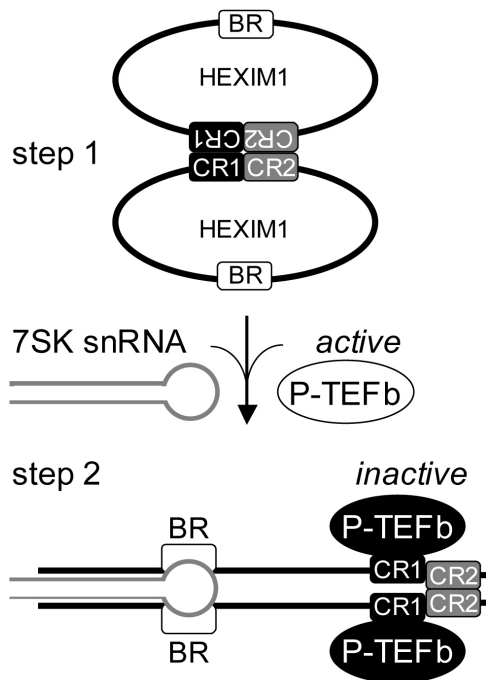


Figure 8. A model how the oligomerization of HEXIM1 via 7SK snRNA and CR directs the incorporation of P-TEFb into the LC. In the absence of 7SK snRNA, free HEXIM1 proteins are oligomers (two ovals, step 1). This oligomerization is mediated solely by the CR1 and CR2 (black and gray rectangles, respectively) in the C-terminal domain of HEXIM1. The BR is depicted as a white rectangle. The small complex of P-TEFb (white oval) is active. In contrast, when 7SK snRNA (hairpin) binds the BRs in HEXIM1, it facilitates the second oligomerization event. Subsequently, P-TEFb is incorporated into the LC, leading to its inactivation (black ovals, step 2). In this complex, the CR1 in HEXIM1 mediates the binding to P-TEFb, whereas the CR2 facilitates HEXIM1 oligomerization.

could be explained by the usage of different leucine mutants in our studies. Their mutations of leucines to positively charged arginines could have more severe effects on dimer stability than our mutations of leucines to non-polar alanines. Interestingly, although their *in vitro* kinase assay revealed only minor decreases in the inhibitory function of the mutant HEXIM1 L287, 294R protein, their analysis of this mutant protein in SC and LC by glycerol gradient centrifugation clearly indicated its absence from the LC *in vivo* (35). This finding corresponds better to the decreased binding of our mutant f.Hex1mCR1 protein to CycT1 and disruption of its inhibitory function in our *in vivo* experiments.

Finally, our study suggests a very dynamic picture for the assembly and disassembly of the LC that dictates the overall transcription in the cell (7–13). Moreover, the balance between the LC and SC is important to the organism as evidenced by the genetic inactivation of HEXIM1 in the mouse that leads to embryonic lethality due to cardiac hypertrophy (36). Additionally, levels of HEXIM1 and P-TEFb are likely to play important roles in cellular activation, proliferation and differentiation. These conclusions are revealed also by the drug hexamethylene-bis-acetamide (HMBA), which is one of the most potent differentiation agents, possibly due to its effects on increased expression of HEXIM1 (12,18,37). Moreover, P-TEFb and HEXIM1 have now been implicated in several cancers and their metastatic potential (38–41).

However, more studies are needed to define the precise roles of these RNA–protein and protein–protein interactions in these diseases. Thus, it is of great importance to determine not only how LC and SC form but their dynamic interplay in cells. To these ends, our study revealed the complex steps in the assembly of the LC, which require 7SK snRNA to coordinate the oligomerization of HEXIM1 proteins and the correct alignment of their C-termini so that they can bind P-TEFb, resulting in its inhibition (Figure 8). Finer details of these structures and the mechanism of P-TEFb inhibition will come from NMR or crystallographic approaches. At the same time, future studies will reveal the post-translational modifications of the respective components that affect the transition between the LC and SC.

ACKNOWLEDGEMENTS

The authors wish to thank Q. Zhou, J.H. Yik and H. Tanaka for sharing their plasmid reagents, F. Schaufele for his help with FRET microscopy and all the members of Peterlin's laboratory for their insightful discussions and help. This work was supported by a grant from NIH (RO1 AI49104 from NIH) to B.M.P. D.B. was supported by an NIH training grant. M.B. was supported in part by a fellowship (106584-36-RFNT) from the American Foundation for AIDS Research (amfAR). Funding to pay the Open Access publication charges for this article was provided by a grant from the NIH (P01 AI058708).

Conflict of interest statement. None declared.

REFERENCES

- Sims,R.J.,III, Belotserkovskaya,R. and Reinberg,D. (2004) Elongation by RNA polymerase II: the short and long of it. *Genes Dev.*, **18**, 2437–2468.
- Barboric,M. and Peterlin,B.M. (2005) A new paradigm in eukaryotic biology: HIV Tat and the control of transcriptional elongation. *PLoS Biol.*, **3**, e76.
- Price,D.H. (2000) P-TEFb, a cyclin-dependent kinase controlling elongation by RNA polymerase II. *Mol. Cell. Biol.*, **20**, 2629–2634.
- Shim,E.Y., Walker,A.K., Shi,Y. and Blackwell,T.K. (2002) CDK-9/cyclin T (P-TEFb) is required in two postinitiation pathways for transcription in the *C.elegans* embryo. *Genes Dev.*, **16**, 2135–2146.
- Chao,S.H. and Price,D.H. (2001) Flavopiridol inactivates P-TEFb and blocks most RNA polymerase II transcription *in vivo*. *J. Biol. Chem.*, **276**, 31793–31799.
- Garriga,J. and Grana,X. (2004) Cellular control of gene expression by T-type cyclin/CDK9 complexes. *Gene*, **337**, 15–23.
- Byers,S.A., Price,J.P., Cooper,J.J., Li,Q. and Price,D.H. (2005) HEXIM2, a HEXIM1 related protein, regulates P-TEFb through association with 7SK. *J. Biol. Chem.*, **280**, 16360–16367.
- Michels,A.A., Fraldi,A., Li,Q., Adamson,T.E., Bonnet,F., Nguyen,V.T., Sedore,S.C., Price,J.P., Price,D.H., Lania,L. and Bensaude,O. (2004) Binding of the 7SK snRNA turns the HEXIM1 protein into a P-TEFb (CDK9/cyclin T) inhibitor. *EMBO J.*, **23**, 2608–2619.
- Michels,A.A., Nguyen,V.T., Fraldi,A., Labas,V., Edwards,M., Bonnet,F., Lania,L. and Bensaude,O. (2003) MAQ1 and 7SK RNA interact with CDK9/cyclin T complexes in a transcription-dependent manner. *Mol. Cell. Biol.*, **23**, 4859–4869.
- Nguyen,V.T., Kiss,T., Michels,A.A. and Bensaude,O. (2001) 7SK small nuclear RNA binds to and inhibits the activity of CDK9/cyclin T complexes. *Nature*, **414**, 322–325.
- Yang,Z., Zhu,Q., Luo,K. and Zhou,Q. (2001) The 7SK small nuclear RNA inhibits the CDK9/cyclin T1 kinase to control transcription. *Nature*, **414**, 317–322.
- Yik,J.H., Chen,R., Pezda,A.C. and Zhou,Q. (2005) Compensatory contributions of HEXIM1 and HEXIM2 in maintaining the balance of

- active and inactive P-TEFb complexes for control of transcription. *J. Biol. Chem.*, **280**, 16368–16376.
13. Yik, J.H., Chen, R., Nishimura, R., Jennings, J.L., Link, A.J. and Zhou, Q. (2003) Inhibition of P-TEFb (CDK9/Cyclin T) kinase and RNA polymerase II transcription by the coordinated actions of HEXIM1 and 7SK snRNA. *Mol. Cell*, **12**, 971–982.
 14. Kulkarni, P.A., Sano, M. and Schneider, M.D. (2004) Phosphorylation of RNA polymerase II in cardiac hypertrophy: cell enlargement signals converge on cyclinT/Cdk9. *Recent Prog. Horm. Res.*, **59**, 125–139.
 15. Sano, M., Abdellatif, M., Oh, H., Xie, M., Bagella, L., Giordano, A., Michael, L.H., DeMayo, F.J. and Schneider, M.D. (2002) Activation and function of cyclin T-Cdk9 (positive transcription elongation factor-b) in cardiac muscle-cell hypertrophy. *Nature Med.*, **8**, 1310–1317.
 16. Schulte, A., Czudnochowski, N., Barboric, M., Schonichen, A., Blazek, D., Peterlin, B.M. and Geyer, M. (2005) Identification of a dimeric Cyclin T-binding domain in HEXIM1 and biochemical analysis of its binding competition with HIV-1 Tat. *J. Biol. Chem.*, **280**, 24968–24977.
 17. Taube, R., Lin, X., Irwin, D., Fujinaga, K. and Peterlin, B.M. (2002) Interaction between P-TEFb and the C-terminal domain of RNA polymerase II activates transcriptional elongation from sites upstream or downstream of target genes. *Mol. Cell. Biol.*, **22**, 321–331.
 18. Ouchida, R., Kusuhashi, M., Shimizu, N., Hisada, T., Makino, Y., Morimoto, C., Handa, H., Ohsuzu, F. and Tanaka, H. (2003) Suppression of NF-kappaB-dependent gene expression by a hexamethylene bisacetamide-inducible protein HEXIM1 in human vascular smooth muscle cells. *Genes Cells*, **8**, 95–107.
 19. Barboric, M., Kohoutek, J., Price, J.P., Blazek, D., Price, D.H. and Peterlin, B.M. (2005) Interplay between 7SK sn RNA and oppositely charged regions in HEXIM1 direct the inhibition of P-TEFb. *EMBO J.*, doi: 10.1038/sj.emboj.7600883.
 20. Makarova, O., Kamberov, E. and Margolis, B. (2000) Generation of deletion and point mutations with one primer in a single cloning step. *Biotechniques*, **29**, 970–972.
 21. Bornberg-Bauer, E., Rivals, E. and Vingron, M. (1998) Computational approaches to identify leucine zippers. *Nucleic Acids Res.*, **26**, 2740–2746.
 22. Ross, S.E., Radomska, H.S., Wu, B., Zhang, P., Winnay, J.N., Bajnok, L., Wright, W.S., Schaufele, F., Tenen, D.G. and MacDougald, O.A. (2004) Phosphorylation of C/EBPalpha inhibits granulopoiesis. *Mol. Cell. Biol.*, **24**, 675–686.
 23. Vinson, C., Myakishev, M., Acharya, A., Mi, A.A., Moll, J.R. and Bonovich, M. (2002) Classification of human B-ZIP proteins based on dimerization properties. *Mol. Cell. Biol.*, **22**, 6321–6335.
 24. Sorkina, T., Doolen, S., Galperin, E., Zahniser, N.R. and Sorkin, A. (2003) Oligomerization of dopamine transporters visualized in living cells by fluorescence resonance energy transfer microscopy. *J. Biol. Chem.*, **278**, 28274–28283.
 25. van Kuppeveld, F.J.M., Melchers, W.J.G., Willems, P.H.G.M. and Gadella, T.W.J., Jr (2002) Homomultimerization of the Coxsackievirus 2B protein in living cells visualized by fluorescence resonance energy transfer microscopy. *J. Virol.*, **76**, 9446–9456.
 26. Zacharias, D.A., Violin, J.D., Newton, A.C. and Tsien, R.Y. (2002) Partitioning of lipid-modified monomeric GFPs into membrane microdomains of live cells. *Science*, **296**, 913–916.
 27. Yik, J.H.N., Chen, R.C., Pezda, A.C., Samford, C.S. and Zhou, Q. (2004) A human immunodeficiency virus type 1 tat-like arginine-rich RNA-binding domain is essential for HEXIM1 to inhibit RNA polymerase II transcription through 7SK snRNA-mediated inactivation of P-TEFb. *Mol. Cell. Biol.*, **24**, 5094–5105.
 28. Burkhard, P., Stetefeld, J. and Strelkov, S.V. (2001) Coiled coils: a highly versatile protein folding motif. *Trends Cell Biol.*, **11**, 82–88.
 29. Klemm, J.D., Schreiber, S.L. and Crabtree, G.R. (1998) Dimerization as a regulatory mechanism in signal transduction. *Annu. Rev. Immunol.*, **16**, 569–592.
 30. Wei, P., Garber, M.E., Fang, S.-M., Fischer, W.H. and Jones, K.A. (1998) A novel CDK9-associated C-type cyclin interacts directly with HIV-1 Tat and mediates its high-affinity, loop specific binding to TAR RNA. *Cell*, **92**, 451–462.
 31. Taube, R., Fujinaga, K., Irwin, D., Wimmer, J., Geyer, M. and Peterlin, B.M. (2000) Interactions between equine cyclin T1, Tat and TAR are disrupted by a leucine-to-valine substitution found in human cyclin T1. *J. Virol.*, **74**, 892–898.
 32. Horn, W.T., Convery, M.A., Stonehouse, N.J., Adams, C.J., Liljas, L., Phillips, S.E.V. and Stockley, P.G. (2004) The crystal structure of a high affinity RNA stem-loop complexes with the bacteriophage MS2 capsid: Further challenges in the modeling of ligand-RNA interactions. *RNA*, **10**, 1776–1782.
 33. Peabody, D.S. (1997) Role of the coat protein-RNA interaction the life cycle of bacteriophage MS2. *Mol. Gen. Genet.*, **254**, 358–364.
 34. Dulac, C., Michels, A.A., Fraldi, A., Bonnet, F., Nguyen, V.T., Napolitano, G., Lania, L. and Bensaude, O. (2005) Transcription-dependent association of multiple P-TEFb units to HEXIM1 multimer. *J. Biol. Chem.*, **280**, 30619–30629.
 35. Li, Q., Price, J.P., Byers, S.A., Cheng, D., Peng, J. and Price, D.H. (2005) Analysis of the large inactive P-TEFb complex indicates that it contains one 7SK molecule, a dimer of HEXIM1 or HEXIM2, and two P-TEFb molecules containing Cdk9 phosphorylated at threonine 186. *J. Biol. Chem.*, **280**, 28819–28826.
 36. Huang, F., Wagner, M. and Siddiqui, M.A. (2004) Ablation of the CLP1 gene leads to down-regulation of the HAND1 gene and abnormality of the left ventricle of the heart and fetal death. *Mech. Dev.*, **121**, 559–572.
 37. Kusuhashi, M., Nagasaki, K., Kimura, K., Maass, N., Manabe, T., Ishikawa, S., Aikawa, M., Miyazaki, K. and Yamaguchi, K. (1999) Cloning of hexamethylene-bis-acetamide-inducible transcript, HEXIM1, in human vascular smooth muscle cells. *Biomed. Res.*, **20**, 273–279.
 38. Shan, B., Zhou, Y., Chin, D., Morris, C.A., Morris, G.F. and Lasky, J.A. (2005) Cyclin-dependent kinase 9 is required for tumor necrosis factor-alpha-stimulated matrix metalloproteinase-9 expression in human lung adenocarcinoma cells. *J. Biol. Chem.*, **280**, 1103–1111.
 39. Stone, B., Schummer, M., Paley, P.J., Thompson, L., Stewart, J., Ford, M., Crawford, M., Urban, N., O'Brian, K. and Nelson, B.H. (2003) Serologic analysis of ovarian tumor antigens reveals a bias toward antigens encoded on 17q. *Int. J. Cancer*, **104**, 73–84.
 40. Wittmann, B.M., Fujinaga, K., Deng, H., Ogburn, N. and Montano, M.M. (2005) The breast cell growth inhibitor, estrogen down regulated gene 1, modulates a novel functional interaction between estrogen receptor alpha and transcriptional elongation factor cyclin T1. *Oncogene*, **36**, 5576–5588.
 41. Wittmann, B.M., Wang, N. and Montano, M.M. (2003) Identification of a novel inhibitor of breast cell growth that is down-regulated by estrogens and decreased in breast tumors. *Cancer Res.*, **63**, 5151–5158.

APPENDIX 3

KOHOUTEK, Jiri, Dalibor BLAZEK and B. Matija PETERLIN. Hexim1 sequesters positive transcription elongation factor b from the class II transactivator on MHC class II promoters. *Proceedings of the National Academy of Sciences*. 2006, 103(46), 17349–17354.



Hexim1 sequesters positive transcription elongation factor b from the class II transactivator on MHC class II promoters

Jiri Kohoutek, Dalibor Blazek, and B. Matija Peterlin*

Departments of Medicine, Microbiology, and Immunology, Rosalind Russell Medical Research Center, University of California, San Francisco, CA 94143-0703

Edited by Laurie H. Glimcher, Harvard Medical School, Boston, MA, and approved September 28, 2006 (received for review April 14, 2006)

The class II transactivator (CIITA) is the master integrator of expression of MHC class II genes. It interacts with variety of basal transcription factors to initiate and elongate transcription of these genes. Among others, it recruits positive transcription elongation factor b (P-TEFb) to MHC class II promoters. In cells, P-TEFb is found in small active or large inactive complexes. The large complex is composed of P-TEFb, 7SK small nuclear RNA, and hexamethylene bisacetamide-inducible protein 1 (Hexim1). The present study identifies Hexim1 as a potent inhibitor of CIITA-mediated transcription. Not only the exogenously expressed but also IFN- γ -induced CIITA was inhibited by Hexim1. This inhibition did not result from an association between Hexim1 and CIITA but depended on the intact Cyclin T1-binding domain in Hexim1. Importantly, Hexim1 sequestered P-TEFb from CIITA, as documented by binding competition and ChIP assays. Conversely, the depletion of Hexim1 from cells by siRNA increased CIITA-mediated transcription. Thus, modulating ratios between active and inactive P-TEFb complexes is an additional mechanism of regulating transcriptional activators such as CIITA.

7SK small nuclear RNA

MHC class II are glycoproteins presenting exogenous antigens to helper T lymphocytes to initiate adaptive immune responses. Constitutive expression of MHC class II genes is restricted to professional antigen-presenting cells, macrophages, dendritic cells, B cells, medullary thymic epithelial cells, and activated T cells (1). Other somatic cells types lack MHC class II molecules, but their expression can be induced by the exposure to certain cytokines, e.g., IFN- γ (2, 3).

The class II transactivator (CIITA) is the coactivator orchestrating the transcription of MHC class II genes (4). Three different isoforms of CIITA are expressed from three different promoters in certain cell types (5). Whereas the CIITA isoform 1 (CIITA.IF1) is expressed in dendritic cells and macrophages, the CIITA isoform 3 (CIITA.IF3) is present constitutively in B cells but can also be induced by IFN- γ in melanomas, glioblastomas (6–8) and HeLa cells (9). CIITA isoform 4 (CIITA.IF4) is the primary IFN- γ -inducible isoform in nonhematopoietic cells (10).

Promoters of all MHC class II genes contain a specific DNA element, which contains the S, X1/2, and Y boxes. This sequence is first recognized and occupied by RFX and NFY proteins and subsequently by CIITA. CIITA recruits general transcription factors, histone acetyl transferases (p300, CBP, and PCAF), and chromatin remodeling complexes (BRG1) leading to the initiation phase of transcription (11). Early after initiation, RNA polymerase II (RNAPII) is paused by the action of negative transcription elongation factors (NTEF), such as the negative elongation factor and 5,6-dichloro-1- β -D-ribofuranosylbenzimidazole (DRB)-sensitivity-inducing factor (12). To overcome this block, CIITA recruits the positive transcription elongation factor b (P-TEFb) to MHC class II promoters. P-TEFb then phosphor-

ylates the C-terminal domain of RNAPII and NTEF, allowing RNAPII to elongate and generate mature mRNA species.

P-TEFb is a heterodimer composed of the cyclin-dependent kinase 9 and one C type cyclin, cyclin T1 (CycT1), cyclin T2, or cyclin K. In cells, P-TEFb is found in two distinct molecular complexes (13, 14). Catalytically active P-TEFb forms a small complex. However, P-TEFb is inactive in a large complex (LC), where it associates with the 7SK small nuclear RNA (7SK snRNA) and hexamethylene bisacetamide (HMBA) inducible protein 1 (Hexim1) (15, 16). In the current view, the binding of 7SK snRNA to the basic region (BR; amino acids 150–177) in Hexim1 leads to the exposure of the CycT1-binding domain (TBD) in its C terminus (17–19). This change allows for the binding between CycT1 and Hexim1 and results in the formation of the LC.

In addition to its role in the inactivation of P-TEFb, Hexim1 can also inhibit the transcriptional activity of a variety of activators, such as the p65 subunit of NF- κ B, glucocorticoid receptor and estrogen receptor α (ER α) (20–22). In these cases, Hexim1 binds these activators by its BR and interferes with their function. Moreover, even when Hexim1 binds ER α , this interaction is not sufficient to inhibit completely its activity in cells. Rather, the competition between ER α and Hexim1 for the binding to CycT1 is responsible for decreased ER α -mediated transcription (22).

In this study, we demonstrated that the ability of CIITA to activate transcription of MHC class II genes is inhibited by Hexim1. Indeed, Hexim1 blocked the activity of CIITA by its CycT1-binding domain, even in the absence of its BR. Also, data from *in vitro* binding experiments and ChIP analyses demonstrated that Hexim1 competes with CIITA for the binding to CycT1. In support of this notion, the depletion of Hexim1 from cells led to the increased activity of CIITA and the induction of CIITA-dependent genes.

Results

Hexim1 Decreases the Transcriptional Activity of CIITA on the HLA-DRA Promoter. To test the hypothesis that increased levels of Hexim1 lead to the inhibition of CIITA, HeLa cells expressed

Author contributions: J.K. and B.M.P. designed research; J.K. and D.B. performed research; D.B. contributed new reagents/analytic tools; J.K., D.B., and B.M.P. analyzed data; and J.K. and B.M.P. wrote the paper.

The authors declare no conflict of interest.

This article is a PNAS direct submission.

Abbreviations: CIITA, class II transactivator; HMBA, hexamethylene bisacetamide; Hexim1, HMBA inducible protein 1; P-TEFb, positive transcription elongation factor b; BR, basic region; TBD, cyclin T1-binding domain; RNAPII, RNA polymerase II; CycT1, cyclin T1; ER α , estrogen receptor α ; f:Hex1, Flag epitope-tagged Hexim1; f:CIITA.IF1, Flag epitope-tagged CIITA isoform I; hIFN- γ , human IFN- γ ; x:Hex1, Xpress epitope-tagged Hexim1; siRNA.Hex1, siRNA against Hexim1; siRNA.mock, mock siRNA; CAT, chloramphenicol acetyltransferase; Q-PCR, quantitative real-time PCR.

*To whom correspondence should be addressed. E-mail: matija.peterlin@ucsf.edu.

© 2006 by The National Academy of Sciences of the USA

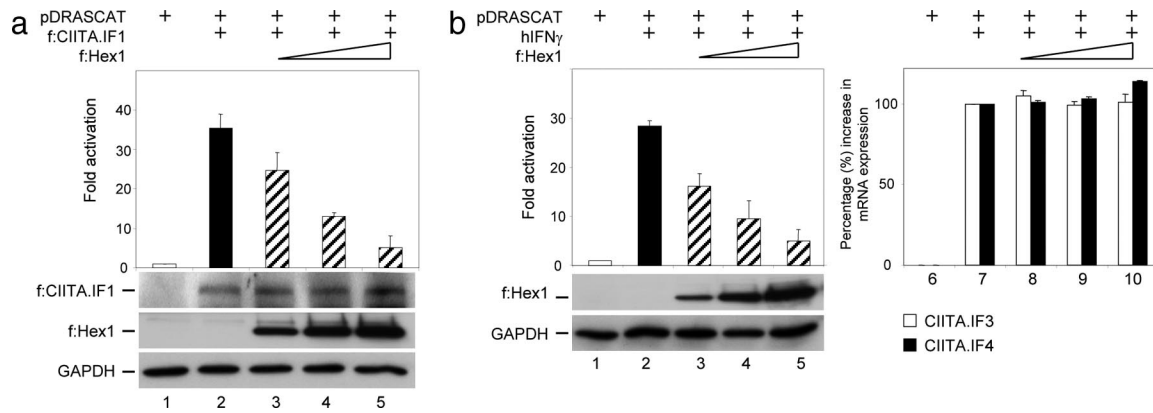


Fig. 1. Hexim1 decreases the transcriptional activity of CIITA isoforms on the *HLA-DRA* promoter. (a) Increased levels of Hexim1 block CIITA-mediated transcription on the *HLA-DRA* promoter. pDRASCAT reporter (0.5 μ g) and f:CIITA.IF1 (0.1 μ g) were coexpressed with increasing amounts of f:Hex1 (0.1, 0.5, and 1 μ g), and CAT assays were performed. CAT activity of the plasmid reporter alone was given as 1 (open bar). The filled bar represents fold activation by CIITA, and hatched bars depict fold activation of CIITA in the presence of increasing amounts of Hexim1. Total amounts of Flag epitope-tagged CIITA.IF1 (f:CIITA.IF1) and Hexim1 (f:Hex1) proteins were assessed by Western blotting (WB) (below the bar graph). Levels of endogenous GAPDH were determined by WB to validate input for each sample (Bottom). Results are representative of three independent CAT assays. Error bars give standard errors of the mean. (b) Hexim1 inhibits transcriptional activity of CIITA induced by hIFN- γ . Expression of CIITA.IF3 and CIITA.IF4 was induced by hIFN- γ (500 units/ml) in HeLa cells expressing pDRASCAT and increasing amounts of f:Hex1 (0.1, 0.5, and 1 μ g). CAT assays were done as in a. Protein levels for f:Hex1 and GAPDH were determined by WB (Bottom). Endogenous mRNA for CIITA.IF3 (open bars) and CIITA.IF4 (filled bars) were measured by Q-PCR (Right). Samples were normalized to GAPDH mRNA, and values obtained from samples treated only with hIFN- γ were set at 100%. Results are representative of three independent experiments, and error bars give standard errors of the mean.

transiently the target *HLA-DRA* promoter linked to the chloramphenicol acetyltransferase (CAT) reporter gene (pDRASCAT) and the Flag epitope-tagged CIITA isoform I (f:CIITA.IF1) alone or with increasing amounts of the Flag epitope-tagged Hexim1 (f:Hex1). When CIITA was expressed alone, the CAT activity increased 35-fold (Fig. 1a; compare lanes 1 and 2). However, when the same amount of f:Hex1 was coexpressed, CAT activity decreased to 25-fold (Fig. 1a, lane 3). With increasing amounts of f:Hex1 to CIITA (ratios of 1:5 to 1:10), the activity of CIITA decreased progressively to 5-fold (Fig. 1a, lanes 4 and 5). To exclude the possibility that f:Hex1 led to decreased expression of CIITA, levels of f:CIITA.IF1 and f:Hex1 were assessed by Western blotting (Fig. 1a Top and Middle below the bar graph). As a control, the input levels of GAPDH were also determined by Western blotting (Fig. 1a Bottom). Because the expression of f:Hex1 did not change considerably the expression of f:CIITA.IF1, the decrease in CAT activity was not because of changes in f:CIITA.IF1 levels.

To determine whether other isoforms of CIITA are also sensitive to Hexim1, the expression of CIITA.IF3 and CIITA.IF4 was induced by human IFN- γ (hIFN- γ) in HeLa cells (9, 23). HeLa cells coexpressed pDRASCAT and increasing amounts of f:Hex1 at the same ratios as in Fig. 1a. Twelve hours later, hIFN- γ was added to the medium (500 units/ml) for another 36 h. hIFN- γ alone increased CAT activity 28-fold (Fig. 1b on the left, compare lanes 1 and 2). However, when increasing amounts of f:Hex1 were coexpressed, CAT activities decreased dramatically to 5-fold (Fig. 1b, compare lanes 3, 4, and 5). Western blotting under the bar graph depicts total amounts of f:Hex1 and GAPDH in HeLa cells (Fig. 1b, below the bar graph). To assure that the expression of f:Hex1 did not interfere with the induction of mRNA levels for CIITA isoforms after IFN- γ treatment, quantitative real-time PCR (Q-PCR) was performed with primers specific for these two isoforms of CIITA (Fig. 1b, on the right). Indeed, levels of mRNA for CIITA.IF3 upon hIFN- γ did not change considerably in the presence of increasing amounts of f:Hex1 and varied from 100% to 105% (Fig. 1b, open bars; compare lane 7 to lanes 8–10). Interestingly, levels of mRNA for CIITA.IF4 went up from 100% to 114% in the presence of the same amounts of f:Hex1 (Fig. 1b, filled bars, lanes 7–10).

Relative amounts of these isoforms of CIITA were normalized to the level of GAPDH transcript in each sample. In conclusion, Hexim1 suppresses transcriptional activities of all studied isoforms of CIITA, and this block is downstream of CIITA-mediated transcription.

Hexim1 Lacking BR Blocks the Transcriptional Activity of CIITA. To address the possibility that the binding between the BR of Hexim1 and CIITA is responsible for the inhibition of CIITA, several deletion mutant Flag epitope-tagged Hexim1 proteins were prepared (Fig. 2a). First, the localization of all truncated forms of f:Hex1 was determined by immunocytochemistry performed with α Flag antibodies, and all truncated forms of f:Hex1 demonstrated a nuclear localization as f:Hex1 (Fig. 6 and Supporting Text, which are published as supporting information on the PNAS web site). Then, CAT assays with mutant f:Hex1 proteins were carried out as in Fig. 1a. The mutant f:Hex1(1–200) protein with the BR but no TBD had no effect on CIITA-mediated transcription (Fig. 2b; compare lane 2 with lanes 3–5). In contrast, the mutant f:Hex1(150–359) protein with BR and TBD inhibited CIITA (Fig. 2b, lanes 6–8). Surprisingly, the mutant f:NLS.Hex1(181–359) protein without the BR but containing the TBD inhibited CIITA equivalently (Fig. 2b, lanes 9–11). Levels of f:CIITA.IF1, truncated f:Hex1 proteins, and GAPDH were assessed by Western blotting (Fig. 2b, below the bar graph). Contrary to previous reports, these data suggest an additional mechanism of how Hexim1 modulates transcriptional activity of CIITA, which does not depend on the BR in Hexim1. Indeed, in control experiments where RelA, a subunit of NF- κ B, was coexpressed with its target plasmid reporter and increasing amounts of Hexim1 proteins, RelA activity was considerably less inhibited by the mutant f:NLS.Hex1 (181–359) protein than CIITA (Fig. 7 and Supporting Text, which are published as supporting information on the PNAS web site). Thus, the BR of Hexim1 is not necessary for the inhibition of transcriptional activity of CIITA; rather, the intact TBD in Hexim1 is sufficient for this inhibition.

Hexim1 Competes with CIITA for the Binding to Cyt1 *in Vitro*. To examine whether Hexim1, instead of binding to CIITA, removes

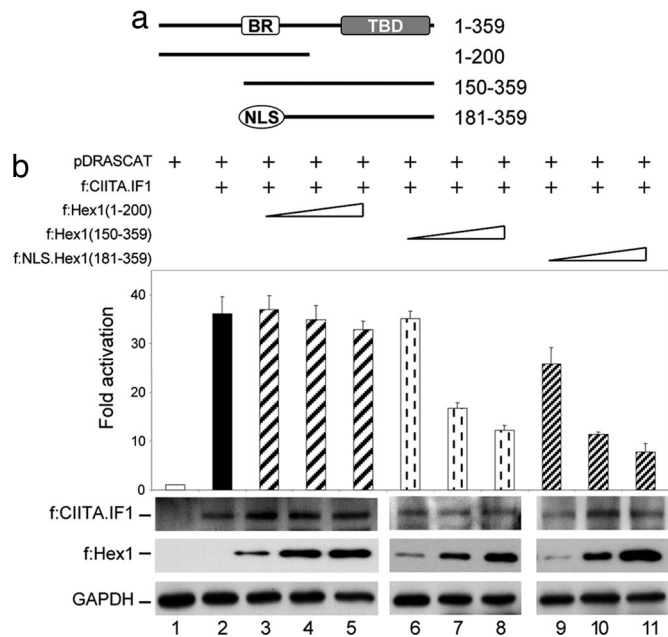


Fig. 2. The CycT1-binding domain, but not BR, in Hexim1 inhibits CIITA-mediated transcription. (a) Deletion mutant Hexim1 proteins used in CAT assays. Numbers to the right mark boundaries of wild-type and mutant Hexim1 proteins. The white box represents the BR, the gray box marks the TBD, and the white oval depicts the nuclear localization signal (NLS). (b) Hexim1 with the intact TBD represses the activity of CIITA. Experiments were performed as in Fig. 1a, with the same amounts of pDRASCAT (lane 1), f:CIITA.IF1 (lane 2), and deletion mutant Hexim1 proteins. f:Hex1(1-200) (lanes 3-5), f:Hex1(150-359) (lanes 6-8), and f:NLS.Hex1(181-359) (lanes 9-11). Images below the bar graph represent expression of f:CIITA.IF1, truncated Hexim1 proteins, and GAPDH as determined by Western blotting.

P-TEFb from CIITA to inactivate its activity, we performed *in vitro* competition assays. The chimera between GST and CycT1 (GST.CycT1) was expressed in *Escherichia coli* and purified by GST affinity chromatography. f:Hex1 and f:CIITA.IF1 proteins were transcribed and translated by using the rabbit reticulocyte lysate *in vitro*, and their expressions were determined by Western blotting by using α Flag antibodies. Then, ratios between these proteins were calculated based on densitometric measurements. The GST.CycT1 chimera was incubated with f:CIITA.IF1 and f:Hex1 alone or in combination. f:CIITA.IF1 and f:Hex1 bound the GST.CycT1 chimera protein (Fig. 3, lanes 1 and 2). However, when f:CIITA.IF1 was incubated with a 7-fold excess of f:Hex1, the binding of f:CIITA.IF1 to the GST.CycT1 chimera disappeared almost completely (Fig. 3, lane 3). Lanes 4 and 5 represent input of f:CIITA.IF1 and f:Hex1 for each lane (Fig. 3,

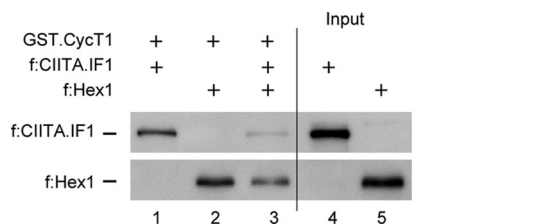


Fig. 3. Hexim1 competes with the CIITA for the binding to CycT1 *in vitro*. The GST.CycT1 chimera was expressed in *E. coli* and purified from the lysate. f:CIITA.IF1 together with f:Hex1 were synthesized as described in *Materials and Methods*. f:CIITA.IF1 and f:Hex1 were incubated alone with GST.CycT1 chimera (lanes 1 and 2) or in combination, with a 7-fold excess of f:Hex1 (lane 3). Lanes 4 and 5 represent input for f:CIITA.IF1 and f:Hex1 used in competition assays.

lanes 4 and 5). Additionally, f:CIITA.IF1 and f:Hex1 did not bind GST-agarose beads alone (data not presented). Thus, Hexim1 and CIITA compete for the binding to CycT1.

Hexim1 Sequesters P-TEFb from CIITA on Endogenous MHC Class II Promoters. Thus far, our data indicated clearly that the block in CIITA-mediated transcription was not because of binding of Hexim1 to CIITA but rather the association between CycT1 and Hexim1. To evaluate whether P-TEFb is really removed from CIITA by Hexim1, ChIP assays on an endogenous MHC class II (*HLA-DRA*) promoter were carried out. First, the f:CIITA.IF1 protein was expressed alone or with the Xpress epitope-tagged Hexim1 (x:Hex1) (ratio 1:1) in HeLa cells. Expression patterns of these proteins were analyzed by Western blotting with α CIITA and α Xpress antibodies (Fig. 4a *Top* and *Middle*). Also, to ensure that equivalent amounts of lysates were loaded for each sample, levels of GAPDH were determined with α GAPDH antibodies (Fig. 4a *Bottom*).

Next, these proteins were immunoprecipitated with appropriate antibodies, and PCR analyses with primers spanning S-X1/2-Y box of the *HLA-DRA* promoter and the *GAPDH* promoter were performed. With α CIITA antibodies, sequences specific for the *HLA-DRA* promoter were enriched in cells expressing f:CIITA.IF1 alone or in combination with x:Hex1 (Fig. 4b, lanes 2 and 3). In the absence of CIITA.IF1, no CIITA was associated with the *DRA* promoter (Fig. 4b, lane 1). Importantly, there was no signal detected for the *GAPDH* promoter with α CIITA antibodies indicating that the association with *HLA-DRA* promoter is specific. Critically, when antibodies against Cyclin T1 (α CycT1) were used, the *HLA-DRA* promoter sequence was enriched only in cells expressing f:CIITA.IF1 (Fig. 4b, lane 2). Importantly, no signal for *HLA-DRA* promoter was observed when f:CIITA.IF1 was co-expressed with x:Hex1 (Fig. 4b, lane 3). Contrary to this observation, *GAPDH* promoter sequence was occupied by CycT1 irrespective of the expression of f:CIITA.IF1 and x:Hex1 (Fig. 4b, lanes 4-6). Additionally, there was considerably more RNAPII associated with the *HLA-DRA* promoter when f:CIITA.IF1 was expressed (Fig. 4b, compare lanes 1 and 2). Again, there was no difference in the occupancy of the *GAPDH* promoter by RNAPII under any condition (Fig. 4b, lanes 4-6). To demonstrate that amplifications were performed in the linear range, PCR with different cycles are presented for immunoprecipitations carried out with α CIITA and α CycT1 antibodies (Fig. 4c *Left* and *Right*). We conclude that Hexim1 sequesters P-TEFb away from CIITA on endogenous MHC class II promoters *in vivo*.

Depletion of Endogenous Hexim1 in HeLa Cells Increases the Activity of CIITA. Because the transcriptional activity of CIITA depends mainly on active P-TEFb, the depletion of Hexim1 from cells should increase its activity. To address this hypothesis, the expression of endogenous Hexim1 was decreased by siRNA against Hexim1 (siRNA.Hex1), and CAT assays were performed as in Fig. 1b. The mock siRNA (siRNA.mock) (Fig. 5a, lanes 1 and 2) or specific siRNA.Hex1 (Fig. 5a, lane 3) were coexpressed with pDRASCAT in HeLa cells and after 12 h, IFN- γ was administered for an additional 24 h. When siRNA.mock was used, CIITA activity induced by IFN- γ increased 16-fold (Fig. 5a, compare lanes 1 and 2). Critically, when levels of Hexim1 were reduced extensively by siRNA.Hex1 (Fig. 5a *Top*), CIITA activity was increased by 60% in comparison to siRNA.mock (Fig. 5a, compare lanes 2 and 3). Western blotting with α Hexim1 antibodies revealed that Hexim1 was almost completely abolished when siRNA.Hex1 was used (Fig. 5a *Top*, lane 3), but there was no effect of siRNA.mock on the expression of Hexim1 (Fig. 5a, compare lanes 1 and 2). To exclude the possibility that the actual increase in CAT activity after IFN- γ administration was

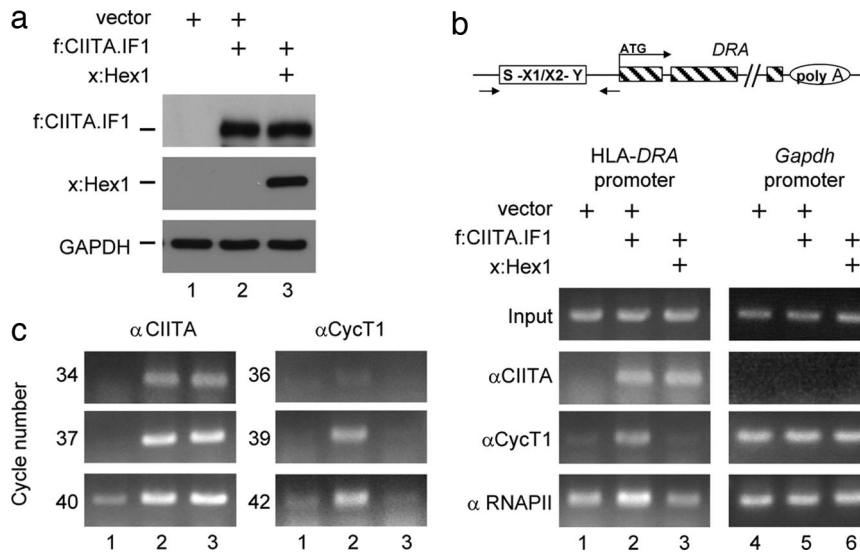


Fig. 4. Hexim1 sequesters P-TEFb from CIITA on the endogenous *HLA-DRA* promoter. (a) Levels of f:CIITA.IF1 and x:Hex1 proteins in HeLa cells. f:CIITA.IF1 (1 μ g) was expressed alone or with x:Hex1 (1 μ g) in HeLa cells. The expression of these proteins was determined by Western blotting with α CIITA and α Xpress antibodies (Top and Middle). Levels of GAPDH were used to assess inputs of proteins for immunoblotting (Bottom). (b) ChIP assays were carried out with α CIITA, α CycT1, and α RNAPII antibodies. Sequences corresponding to the endogenous *HLA-DRA* promoter were detected by PCR. Additionally, the promoter for *GAPDH* gene was used as the negative control. Presented above the analyses is a diagrammatic representation of the *HLA-DRA* promoter and gene. Arrows below the diagram define positions of primers used in ChIP assays. Antibodies used in ChIP analyses are named next to the gels. (c) All results for PCR analyses were in the linear range of PCR. Amplifications with different numbers of cycles were carried out with α CycT1 and α CIITA immunoprecipitates. Numbers to the left depict actual number of cycles used in PCR.

because of the enhanced expression of mRNA for CIITA.IF3 and CIITA.IF4, Q-PCR was performed as in Fig. 1b. Surprisingly, transcripts for CIITA.IF3 and CIITA.IF4 decreased to 95% and 87% in siRNA.Hex1-treated cells compared with

siRNA.mock-treated cells (Fig. 5b, open and filled bars; compare lanes 2 and 3). Additionally, the abundance of endogenous MHC class II transcripts (*HLA-DRA*) was measured by Q-PCR. Reduced levels of endogenous Hexim1 in HeLa cells resulted in consistently greater expression of MHC class II genes, in average \approx 58% (Fig. 5b, hatched bars; compare lanes 2 and 3), which nicely correlates with observed 60% activation on the artificial reporter plasmid (Fig. 5a). These data confirmed our premise that P-TEFb liberated from Hexim1 can be more efficiently recruited and consequently used by CIITA to promote MHC class II transcription in cells.

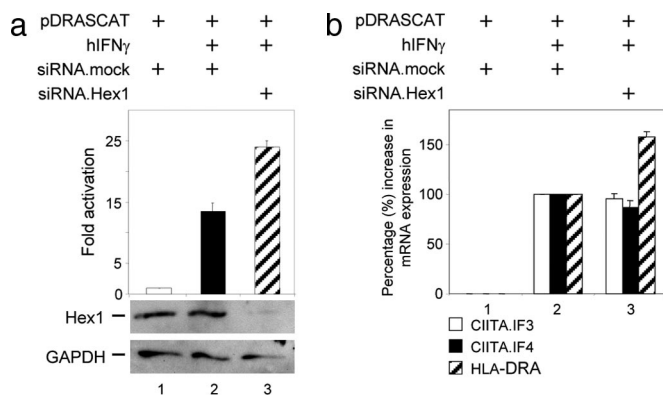


Fig. 5. Depletion of endogenous Hexim1 increases the activity of CIITA and transcription of its dependent gene after IFN- γ stimulation. (a) Decreased levels of endogenous Hexim1 elevate transcription from a CIITA-dependent plasmid reporter. HeLa cells were transfected with either siRNA.mock (lanes 1 and 2) or siRNA.Hex1 (lane 3) and pDRASCAT. The next day, hIFN- γ (500 units/ml) was added to the medium (lanes 2 and 3). After an additional 24 h, CAT assays were performed as in Fig. 1b. Amounts of endogenous Hex1 and GAPDH after siRNA treatment were assessed by immunoblotting with α Hexim1 and α GAPDH antibodies (below the bar graph). (b) Decreased levels of the endogenous Hexim1 protein augment transcription of CIITA-dependent genes in HeLa cells. HeLa cells were transfected with either siRNA.mock (lanes 1 and 2) or siRNA.Hex1 (lane 3). Subsequently, total RNA was isolated, and endogenous mRNA species for CIITA.IF3 (open bars), CIITA.IF4 (filled bars), and *HLA-DRA* (hatched bars) were measured by Q-PCR. Samples were normalized to *GAPDH* mRNA, and the value obtained from the sample treated only with hIFN- γ was set to 100%. Results are representative of three independent experiments, and error bars give standard errors of the mean.

Discussion

In this study, we demonstrated that Hexim1 is a potent inhibitor of CIITA-mediated transcription. Surprisingly, the TBD but not the BR in Hexim1 was sufficient for this inhibition. Additionally, Hexim1 sequestered P-TEFb away from CIITA bound to the *HLA-DRA* promoter. Finally, the depletion of Hexim1 by siRNA led to the increased activity of CIITA and consequently higher expression of MHC class II genes. We are proposing an additional mechanism of how Hexim1 can block certain activators. Instead of binding to the activator via its BR, Hexim1 sequesters P-TEFb away and inhibits its function.

To elucidate whether Hexim1 can also inhibit the activity of CIITA, which requires P-TEFb for its function, we examined first transcription from the *HLA-DRA* promoter in the absence or presence of Hexim1. Indeed, Hexim1 blocked not only the exogenously expressed CIITA.IF1 but also IFN- γ -induced CIITA.IF3 and CIITA.IF4 (Fig. 1). Because Spilianakis *et al.* (9) also detected CIITA.IF3 in HeLa cells treated with IFN- γ , our induction of CIITA.IF3 does not contradict previously published data on CIITA.IF3 in melanomas and glioblastomas (6–8). Thus, results in Fig. 1 illustrate clearly that Hexim1 possesses the ability to block the activity of all CIITA isoforms.

Next, we wanted to identify the mechanism of Hexim1-mediated repression. Because BR in Hexim1 is necessary for the inhibition of p65, ER α , and glucocorticoid receptors, we were

interested in whether the same is true for CIITA (20–22). Surprisingly, the mutant f:NLS.Hex1(181–359) protein lacking the BR still inhibited the activity of CIITA to the same extent as the mutant f:Hex1 (150–359) protein. To validate that the inhibition of CIITA was not because of its binding to the mutant f:NLS.Hex1 (181–359) protein, we also performed binding assays *in vitro*. Indeed, the mutant GST.Hex1(180–359) chimera was not able to bind CIITA.IF1 but could still bind CycT1 (data not shown). These findings suggested that Hexim1 represses transcription by a mechanism, which is independent of its association with the activator. Indeed, we were able to dissect the capacity of Hexim1 to sequester P-TEFb from CIITA *in vitro* and *in vivo* (Figs. 3 and 4).

Our data can be extrapolated to the control of MHC class II transcription during development. Hexim1 not only inhibits MHC class II transcription but also is important for the differentiation of neural and hematopoietic cells (24–26). Because HMBA induces Hexim1 (20, 27), it also differentiates a variety of cells (28, 29). Importantly, HMBA differentiates Raji cells and decreases their expression of the *HLA-DRA* gene (30). Additionally, Hexim1 could also influence later stages of differentiation of mature B cells to plasma cells. During this transition, MHC class II expression is extinguished, in part, by the B lymphocyte-induced maturation protein I (BLIMP-1) (31). In this scenario, Hexim1 might enhance this inhibition. Indeed, Hexim1 inhibited the induction of MHC class II by IFN- γ in HeLa cells. However, no differences were observed for MHC class I expression in these cells (data not shown). Thus, HMBA or Hexim1 could be used to decrease antigen processing and presentation in a variety of diseases where MHC class II determinants are expressed inappropriately.

The inhibition of activators by the sequestration of active P-TEFb into the inactive complex with Hexim1 and 7SK small nuclear RNA is an attractive global mechanism of transcriptional repression. Principally, any changes between inactive and active form of P-TEFb should impact cellular homeostasis. In fact, when P-TEFb is released from Hexim1 in cardiac myocytes, it results in cardiac hypertrophy (32–34). The liberation of P-TEFb most likely affects a certain cluster of genes that depend on P-TEFb for their transcription (Fig. 5*b*). Indeed, we observed increased CIITA-mediated transcription when Hexim1 was depleted with siRNA (Fig. 5). This finding reflects different sensitivities for effects of Hexim1 on regulated and housekeeping genes.

Our observation extends already established mechanisms of repression by Hexim1, where its BR binds transcriptional activators and blocks their activity (20–22). In addition, our data reveal that Hexim1 can inhibit transcriptional activators in trans, by decoying P-TEFb away from them, which presents a conceptually previously undescribed mechanism for the inhibition of transcription by Hexim1. Nevertheless, more studies are needed to understand pathways orchestrating the transition between active and inactive P-TEFb complexes in a physiological context.

Materials and Methods

Plasmid Construction. Plasmid reporter pDRASCAT bearing *HLA-DRA* promoter in front of CAT reporter gene was described (35). Plasmid coding for Flag epitope-tagged CIITA.IF1 (f:CIITA.IF1) was described (36). f:Hex1 and f:Hex1 (1–200) were generously provided by H. Tanaka (20). Plasmids coding for f:Hex1 (150–359) and f:NLS.Hex1 (181–359) were prepared by the QuikChange II XL Site-Directed Mutagenesis Kit (Stratagene, La Jolla, CA) (37). In the case of f:NLS.Hex1 (181–359), cDNA coding for the SV-40 NLS was then inserted into HindIII-EcoRI sites of the pFLAG-CMV-2 vector. The Xpress epitope-tagged Hexim1 (x:Hex1) is described in ref. 18. The Flag epitope-tagged Hexim1 (f:Hex1) protein, which was used in *in vitro* competition studies, was generated by mutating the Xpress

epitope-tag to the Flag epitope-tag in x:Hex1. The plasmid encoding the fusion protein between GST and Cyclin T1 (GST-CycT1) was described (38).

Cell Culture. HeLa cells (purchased from American Type Culture Collection, Manassas, VA) were grown at 37°C with 5% atmosphere of CO₂ in DMEM containing 10% FCS, 100 mM L-glutamine, and 50 μ g each of penicillin and streptomycin per milliliter.

Transient Transfections and CAT Assays. HeLa cells were seeded into 60-mm dishes \approx 24 h before transfection. The next day, cells were cotransfected with pDRASCAT (0.5 μ g) and different plasmid effectors with FuGENE6 reagent (Roche Applied Science, Indianapolis, IN). The ratios of plasmids encoding activators (f:CIITA.IF1) vs. repressors (f:Hex1) were 1:1; 1:5, and 1:10, respectively. Amounts of DNA used for transfections were balanced to the total 1.6 μ g with appropriate empty vectors. At 36 h after transfection, cells were harvested, and CAT enzymatic assays were performed as described (39). The activity of reporter plasmid alone was set to 1. Fold transactivation represents the ratio between the CIITA-activated transcription and the activity of the reporter plasmid alone. Error bars give standard errors of the mean. Three independent transfections were performed for each experiment.

For induction of CIITA isoforms by hIFN- γ , HeLa cells were cotransfected with pDRASCAT (0.5 μ g) and f:Hex1 (0.1, 0.5, and 1 μ g) plasmids with FuGENE6 reagent. At 12 h after the transfection, new medium with hIFN- γ (500 units/ml; Roche Applied Science) was administered, cells were grown under standard conditions for 36 h, and then CAT enzymatic assays were performed.

Q-PCR. Total RNA was prepared with TRIzol reagent (Invitrogen, Carlsbad, CA). Synthesis of cDNA from RNA was performed with M-MLV reverse transcriptase (Invitrogen). Q-PCR was done with the Mx3005P QPCR System (Stratagene). PCR conditions for all reactions included an initial 10-min denaturation step at 95°C, followed by 42 cycles of 30 sec at 95°C, 30 sec at 61°C, and 30 sec at 72°C. Primers for different isoforms of CIITA and *HLA-DRA* can be obtained upon request. The sequences of primers for the *GAPDH* gene have been described (9). Presented values from Q-PCR were calculated on the basis of standard curves generated for each gene. Samples were normalized by dividing the number of copies of *CIITA.IF3*, *CIITA.IF4*, and MHC class II mRNA by the number of copies of *GAPDH* mRNA.

Western Blotting. To determine the expression of proteins used in CAT assays, one-fourth of lysates used for CAT assay were mixed with double-strength Laemmli sample buffer and boiled for 5 min. Samples were then subjected to 10% SDS/PAGE, electrotransferred onto Hybond-P membrane (Amersham Biosciences, Piscataway, NJ), immunodetected by using mouse monoclonal α Flag M2 antibodies (F3165; Sigma-Aldrich, St. Louis, MO), and rabbit polyclonal α CIITA amino acid 1–333 (Rockland, Gilbertsville, PA), followed by incubation with the appropriate secondary antibody, and visualized by Western Lightning chemiluminescence Reagent Plus (Perkin-Elmer Life Sciences, Boston, MA). To determine the amounts of expressed proteins used for immunoprecipitation in ChIP assays, mouse monoclonal α CIITA (sc-13556; Santa Cruz Biotechnology, Santa Cruz, CA), and mouse monoclonal α Xpress antibodies (Invitrogen) were used. When endogenous Hexim1 was depleted by specific siRNA, its level was determined by usage of rabbit polyclonal α Hexim1 antibody generated against Hexim1 epitope LHRQQ-ERAPLSKFGD (Antibody Solutions, Mountain View, CA).

Mouse monoclonal α GAPDH antibodies (Ambion, Austin, TX) were used to detect total protein in each sample.

In Vitro Competition Assays. The GST.CycT1 fusion protein was produced and purified as described (38). Proteins f:Hex1 and f:CIITA.IF1 were transcribed and translated *in vitro* by using the TNT-T7 Coupled Reticulocyte Lysate System (Promega, Madison, WI). Each binding reaction was performed in 250 μ l of binding buffer [20 mM Hepes (pH 7.9)/0.5% Igepal CA-630/1% Triton X-100/0.7% 2-mercaptoethanol/0.2% BSA/150 mM KCl] for 2 h at 4°C. After binding, GST-agarose beads with bound proteins were extensively washed with binding buffer at 4°C. Samples were then mixed with double-strength Laemmli sample buffer, boiled for 5 min, and finally subjected to SDS/PAGE, followed by Western blotting with mouse monoclonal α Flag M2 antibody.

ChIP Assay. HeLa cells (5×10^6) were used for each ChIP assay. They were cotransfected with 1 μ g of f:CIITA.IF1 alone or in combination with 1 μ g of x:Hex1. Chromatin was prepared, and protein-DNA complexes were immunoprecipitated with the following antibodies: rabbit polyclonal α CIITA amino acid 1–333 (Rockland) and goat polyclonal α CycT1 and polyclonal rabbit α RNAPII (sc-8127, sc-899; Santa Cruz Biotechnology) antibodies at 4°C overnight (40). Elution of immunocomplexes from beads, reverse cross-linking, phenol-chloroform protein extraction, and DNA precipitation by ethanol were done as in ref. 40. Finally, 2 μ l of DNA was used with appropriate primer

sets, and PCR products, taken at various cycle numbers, were separated on 1.2% agarose gel and visualized with ethidium bromide. All PCRs were carried out at cycles where amplification was in the linear range. Sequences of primers used for PCRs: *HLA-DR* promoter: DRAsense, 5'-GCCAAATT-CAGACAATCTCCATGGC-3'; DRAntisense, 5'-CCCAAT-TACTCTTTGGCCAATCAGAAAAATATTTTG-3'. Primers for GAPDH promoter were used from ref. 9.

Knockdown of Hexim1 Using siRNA and CAT Reporter Assays. Freshly grown HeLa cells, at 60% confluence in a six-well plate, were transfected with a 0.5 μ M concentration of either siRNA.Hex1 or siRNA.mock per well by using 5 μ l of Lipofectamine 2000 (Invitrogen), according to the manufacturer's instructions. After 4 h, the medium was removed, and cells were washed with PBS and transfected with pDRASCAT plasmid reporter (0.5 μ g) with FuGENE6 (Roche Applied Sciences). After 2 h, the medium was removed, cells were washed with PBS, and fresh DMEM with 10% FBS was supplied. At 12 h after the transfection, medium with hIFN- γ (500 units/ml) was supplied, and cells were cultured under standard conditions for 24 h. RNA oligonucleotides, based on publication (41), can be obtained upon request.

We thank Marek Gajdusek for expert secretarial assistance, members of the Peterlin laboratory for discussion and helpful comments on the manuscript, and Dr. Tanaka (University of Tokyo, Tokyo, Japan) for reagents. This work was supported by grants from the National Institutes of Health.

- Ting JP, Trowsdale J (2002) *Cell* 109 (Suppl):S21–S33.
- Harton JA, Ting JP (2000) *Mol Cell Biol* 20:6185–6194.
- Pattenden SG, Klose R, Karaskov E, Bremner R (2002) *EMBO J* 21:1978–1986.
- Reith W, Mach B (2001) *Annu Rev Immunol* 19:331–373.
- Muhlethaler-Mottet A, Otten LA, Steimle V, Mach B (1997) *EMBO J* 16:2851–2860.
- Deffrennes V, Vedrenne J, Stolzenberg MC, Piskurich J, Barbieri G, Ting JP, Charron D, Alcaide-Loridan C (2001) *J Immunol* 167:98–106.
- Goodwin BL, Xi H, Tejiram R, Eason DD, Ghosh N, Wright KL, Nagarajan U, Boss JM, Blanck G (2001) *Cell Growth Differ* 12:327–335.
- Piskurich JF, Linhoff MW, Wang Y, Ting JP (1999) *Mol Cell Biol* 19:431–440.
- Spilianakis C, Kretsovali A, Agalioi T, Makatounakis T, Thanos D, Papamathakis J (2003) *EMBO J* 22:5125–5136.
- Waldburger JM, Suter T, Fontana A, Acha-Orbea H, Reith W (2001) *J Exp Med* 194:393–406.
- Drozina G, Kohoutek J, Jabrane-Ferrat N, Peterlin BM (2005) *Curr Top Microbiol Immunol* 290:147–170.
- Sims RJ, III, Belotserkovskaya R, Reinberg D (2004) *Genes Dev* 18:2437–2468.
- Nguyen VT, Kiss T, Michels AA, Bensaude O (2001) *Nature* 414:322–325.
- Yang Z, Zhu Q, Luo K, Zhou Q (2001) *Nature* 414:317–322.
- Michels AA, Nguyen VT, Fraldi A, Labas V, Edwards M, Bonnet F, Lania L, Bensaude O (2003) *Mol Cell Biol* 23:4859–4869.
- Yik JH, Chen R, Nishimura R, Jennings JL, Link AJ, Zhou Q (2003) *Mol Cell* 12:971–982.
- Barboric M, Kohoutek J, Price JP, Blazek D, Price DH, Peterlin BM (2005) *EMBO J* 24:4291–4303.
- Blazek D, Barboric M, Kohoutek J, Oven I, Peterlin BM (2005) *Nucleic Acids Res* 33:7000–7010.
- Schulte A, Czudnochowski N, Barboric M, Schonichen A, Blazek D, Peterlin BM, Geyer M (2005) *J Biol Chem* 280:24968–24977.
- Ouchida R, Kusahara M, Shimizu N, Hisada T, Makino Y, Morimoto C, Handa H, Ohsuzu F, Tanaka H (2003) *Genes Cells* 8:95–107.
- Shimizu N, Ouchida R, Yoshikawa N, Hisada T, Watanabe H, Okamoto K, Kusahara M, Handa H, Morimoto C, Tanaka H (2005) *Proc Natl Acad Sci USA* 102:8555–8560.
- Wittmann BM, Fujinaga K, Deng H, Ogba N, Montano MM (2005) *Oncogene* 24:5576–5588.
- Greer SF, Zika E, Conti B, Zhu XS, Ting JP (2003) *Nat Immunol* 4:1074–1082.
- De Falco G, Bellan C, D'Amuri A, Angeloni G, Leucci E, Giordano A, Leoncini L (2005) *Cancer Biol Ther* 4:277–281.
- Liou LY, Haaland RE, Herrmann CH, Rice AP (2006) *J Leukocyte Biol* 79:388–396.
- Marshall RM, Salerno D, Garriga J, Grana X (2005) *J Immunol* 175:6402–6411.
- Yik JH, Chen R, Pezda AC, Zhou Q (2005) *J Biol Chem* 280:16368–16376.
- Richon VM, Webb Y, Merger R, Sheppard T, Jursic B, Ngo L, Civoli F, Breslow R, Rifkind RA, Marks PA (1996) *Proc Natl Acad Sci USA* 93:5705–5708.
- Turano M, Napolitano G, Dulac C, Majello B, Bensaude O, Lania L (2006) *J Cell Physiol* 206:603–610.
- Semmel M, Hanania N, Huet S, Pavloff N, Gay F, Biquard JM (1988) *Mol Biol Rep* 13:151–157.
- Piskurich JF, Lin KI, Lin Y, Wang Y, Ting JP, Calame K (2000) *Nat Immunol* 1:526–532.
- Huang F, Wagner M, Siddiqui MA (2004) *Mech Dev* 121:559–572.
- Sano M, Abdellatif M, Oh H, Xie M, Bagella L, Giordano A, Michael LH, DeMayo FJ, Schneider MD (2002) *Nat Med* 8:1310–1317.
- Sano M, Wang SC, Shirai M, Scaglia F, Xie M, Sakai S, Tanaka T, Kulkarni PA, Barger PM, Youker KA, et al. (2004) *EMBO J* 23:3559–3569.
- Fontes JD, Jabrane-Ferrat N, Toth CR, Peterlin BM (1996) *J Exp Med* 183:2517–2521.
- Nickerson K, Sisk TJ, Inohara N, Yee CS, Kennell J, Cho MC, Yannie PJ, II, Nunez G, Chang CH (2001) *J Biol Chem* 276:19089–19093.
- Makarova O, Kamberov E, Margolis B (2000) *BioTechniques* 29:970–972.
- Kanazawa S, Okamoto T, Peterlin BM (2000) *Immunity* 12:61–70.
- Taube R, Lin X, Irwin D, Fujinaga K, Peterlin BM (2002) *Mol Cell Biol* 22:321–331.
- Jiang H, Zhang F, Kurosu T, Peterlin BM (2005) *Mol Cell Biol* 25:10675–10683.
- Byers SA, Price JP, Cooper JJ, Li Q, Price DH (2005) *J Biol Chem* 280:16360–16367.

APPENDIX 4

KOHOUTEK, Jiri. P-TEFb- the final frontier. *Cell Division*. 2009, 4, 19

Review

Open Access

P-TEFb- the final frontier

Jiri Kohoutek

Address: Veterinary Research Institute, Hudcova 70, 621 00 Brno, Czech Republic

Email: Jiri Kohoutek - Kohoutek@vri.cz

Published: 2 September 2009

Received: 11 August 2009

Cell Division 2009, 4:19 doi:10.1186/1747-1028-4-19

Accepted: 2 September 2009

This article is available from: <http://www.celldiv.com/content/4/1/19>

© 2009 Kohoutek; licensee BioMed Central Ltd.

This is an Open Access article distributed under the terms of the Creative Commons Attribution License (<http://creativecommons.org/licenses/by/2.0>), which permits unrestricted use, distribution, and reproduction in any medium, provided the original work is properly cited.

Abstract

Regulation of gene expression is essential to all aspects of physiological processes in single-cell as well as multicellular organisms. It gives ultimately cells the ability to efficiently respond to extra- and intracellular stimuli participating in cell cycle, growth, differentiation and survival. Regulation of gene expression is executed primarily at the level of transcription of specific mRNAs by RNA polymerase II (RNAPII), typically in several distinct phases. Among them, transcription elongation is positively regulated by the positive transcription elongation factor b (P-TEFb), consisting of CDK9 and cyclin T1, T2 or K. P-TEFb enables transition from abortive to productive transcription elongation by phosphorylating carboxyl-terminal domain (CTD) in RNAPII and negative transcription elongation factors. Over the years, we have learned a great deal about molecular composition of P-TEFb complexes, their assembly and their role in transcription of specific genes, but function of P-TEFb in other physiological processes was not apparent until just recently. In light of emerging discoveries connecting P-TEFb to regulation of cell cycle, development and several diseases, I would like to discuss these observations as well as future perspectives.

Introduction

Gene expression is a highly organized and tightly controlled process involved in a broad spectrum of biological processes, ultimately giving cells the ability to take control of their growth, cell division, differentiation and apoptosis. Regulation of gene expression is executed primarily at the level of transcription of specific mRNAs by RNA polymerase II (RNAPII), typically in several distinct phases: preinitiation, initiation, promoter clearance, elongation, RNA processing, and termination [1-3]. RNAPII is characteristic by the presence of an extended carboxyl-terminal domain (CTD), consisting of 52 tandem hepta-peptide repeats of canonical sequence, YSPTSPS [4]. Coincidentally, CTD is subjected to numerous modifications, which control its ability to associate with transcription factors involved in RNA processing, elongation and termination [5]. Therefore, it seems that modification sta-

tus of CTD is important for control of a particular phase of transcription [6].

Importantly, RNAPII can not initiate transcription alone. General transcription factors assist RNAPII to form a preinitiation complex (PIC) at the promoter of protein-coding genes. To initiate transcription, activity of TFIIF (CDK7/cyclin H) factor is required to begin promoter clearance and synthesis of short nascent RNA by RNAPII. TFIIF also phosphorylates Ser 5 at the CTD evoking its conformational changes that allow binding of capping complex and co-transcriptional capping of nascent RNA. After synthesizing around 50 ribonucleotides, RNAPII is recognized by negative elongation factor (NELF) and DRB-sensitivity inducing factor (DSIF) causing its promoter-proximal pausing. To overcome inhibitory effect of NELF/DSIF factors and to initiate productive elongation,

the positive transcription elongation factor b (P-TEFb) is subsequently recruited to the paused/poised RNAPII. After phosphorylation of RNA recognition motif-containing protein RD (a NELF-E component) and Spt5 (a subunit of human DSIF) by P-TEFb, NELF leaves RNAPII; however, DSIF stays there and becomes a positive elongation factor [7-9]. Most importantly, P-TEFb phosphorylates Ser 2 of CTD, increasing its affinity towards components of splicing and polyadenylation machineries [3,10,11].

Much of what we know about regulation of elongation phase has come from studies using ATP analog 5,6-dichloro-1-b-D-ribofuranosylbenzimidazole (DRB). Treatment of cells with DRB caused dramatic reduction in mRNA synthesis characteristic by production of short capped RNA transcripts, suggestive of block in the elongation phase [12,13]. DRB blocked CTD phosphorylation as well [14]. Importantly, inhibition of RNAPII elongation by Flavopiridol, a selective P-TEFb inhibitor, resulted in abortive transcription of most protein coding genes [15].

It has been thought for years that formation of a preinitiation complex and subsequent recruitment of RNAPII to the promoter is a rate-limiting step in transcription regulation [16]. However, transcription of several genes, such as *c-myc*, *HSP70*, *JunB*, did not fit the general concept [17-20]. Over the years, it became increasingly clear that a block of the elongation phase is a critical control mechanism of transcription [21,22].

We have learned a great deal of P-TEFb genetics, biochemistry and molecular function from studying its function in HIV replication in cells. Nevertheless, function of P-TEFb in other physiological processes, such as cell differentiation, cell cycle, development and diseases, has not been pursued efficiently until just recently. The next parts of this review are dedicated to shed a light on new discoveries in these processes with future perspectives.

P-TEFb - history and presence

P-TEFb is a heterodimer consisting of cyclin-dependent kinase 9 and one of the C-type cyclins T1, T2a, T2b or K [4,23-27]. CDK9 was first discovered by the Giordano lab as a cell division cycle 2 - related kinase with PITALRE motif [24]. It consists of 372 amino acids with a relative molecular mass around 42 kDa. It was believed that CDK9 42 kDa form (CDK9 or CDK9₄₂) is the only functional form in cells. But such a presumption was challenged by a rather puzzling observation made by several laboratories. When commercially available antibodies specific for C-terminus or other domains of human CDK9₄₂ were used in western blotting, an extra band migrating around 55 kDa was always detected [28,29]. Indeed, an additional form of CDK9 was identified in

2003 by the Price lab [29]. Transcription of this CDK9 form starts from an alternative TATA box upstream of previously described housekeeping-type promoter for the CDK9₄₂ gene. Newly described form of CDK9 contains an entire amino acid sequence of CDK9₄₂ and additional 117 amino acids extension bearing proline-rich region and glycine-rich region in its N-terminus [29,30]. The expression of both isoforms varies across different mouse tissues [30]. The CDK9₄₂ is predominantly expressed in spleen, thymus and testes, whereas CDK9₅₅ is highly abundant in brain, lung, spleen and thymus [30]. In many other cell types, the relative abundance of both isoforms depends on the original tissue, developmental stage, and cell commitment. For instance, CDK9₄₂ isoform is highly expressed in human cervical carcinoma cells (HeLa) and mouse fibroblasts (NIH 3T3)[29]. An opposite picture is seen in primary hepatocytes, cultured macrophages or primary lymphocytes- in these cells, CDK9₅₅ form is prevalent at steady state [29,30]. Yet, in hepatocyte cultures, in activated macrophages by lipopolysaccharide or lymphocytes by PMA/PHA CDK9₄₂ is induced, while the level of CDK9₅₅ remained relatively constant or decreases upon activation [29-31]. Interestingly enough, the CDK9₅₅ form is almost undetectable in primary human monocytes or primary satellite cells, but its expression is robustly induced upon their differentiation, simply implying an essential function for CDK9₅₅ in cell commitment and differentiation [31,32].

It is possible to speculate at the moment that the presence of an extra N-terminus in CDK9₅₅ will play - at least in part - a key role in the final outcome of its function. Therefore, both forms of CDK9 might control transcription of diverse sets of genes and consequently be expressed in developmental or cell fate specific manner. For example, both CDK9 forms associate with MyoD, a factor involved in muscle differentiation, but CDK9₅₅ seems to be more important for satellite differentiation during injury [32].

Four years later after discovery of CDK9₄₂, a new type of cyclins, called C-type cyclins, was identified to associate with CDK9₄₂ [26,27]. Cyclin T1 (CycT1) and two splicing isoforms of cyclin T2a and T2b (CycT2a and CycT2b) constitute the family of C-type cyclins. All cyclins associate with both forms of CDK9 with kinase activity towards CTD in RNAPII. They bear two prototypical cyclin boxes at the N-terminus, histidine-rich region, providing binding to CTD of RNAPII, and proline-serine rich C-terminus. CycT1, in contrast to CycT2a/b, contains TAR recognition motif (TRM) next to cyclin boxes, which is important for the formation of ternary complex between Tat/TAR/P-TEFb and initiation of HIV transcription [27,33]. Vice-versa, CycT2 bears a leucine-rich stretch next to its cyclin boxes capable of binding to CTD, thus providing an extra domain capable of targeting RNAPII [26,34]. Even though

CycT1 seems to be the most abundant partner of CDK9 in cultured cell lines, the expression of both CycT2 isoforms is found in other cells and tissues as well [35,36]. Expression of CycT1/2 is regulated not just at the transcription level, but also at the level of RNA stability, translation and ubiquitination [37,38]. Several years after identification of CycT1 and CycT2, an additional cyclin was identified to associate with CDK9 by two hybrid screens of lymphocyte cDNA library [23]. This new member of C-type cyclins was called cyclin K and in contrast to CycT1 and CycT2, its whole C-terminus (normally found in other C-type cyclins) was missing. Three labs have shown that CycK can support phosphorylation of CTD by CDK9 *in vitro*, activation of P-TEFb-dependent genes when artificially tethered to RNA but not DNA, supporting its function in transcriptional elongation [23,25,39]. Moreover, expression of CycK is transcriptionally activated by p53, thus CycK could participate in control of cell cycle or apoptosis, but these observations were not followed in greater details [40].

Another milestone in P-TEFb biology was reached when two labs independently demonstrated that 7SK small nuclear RNA (7SK snRNA) is bound to P-TEFb and inhibits its kinase activity [41,42]. When RNase treatment or extracellular stress signals were used, active P-TEFb was released from association with 7SK snRNA, and transcription of long transcripts was restored. Surprisingly, later in 2003, the same laboratories discovered a protein which was able to cooperate with 7SK snRNA to inactivate P-TEFb in the 7SK small nuclear ribonucleic acid particle (7SK snRNP) or simply 'large' complex [43,44]. The protein was named hexamethylene bisacetamide inducible protein 1 (Hexim1), since Hexim1 was originally discovered as a protein induced in vascular smooth muscle cell after exposure to hexamethylene bisacetamide (HMBA) [45]. Later the same year, Hexim2 was discovered as an additional member of the Hexim protein family. It is highly homologous to Hexim1 and was shown to substitute function of Hexim1 *in vivo* and *in vitro* [46,47]. Importantly, Hexim1 and Hexim2 can form homo- or heterodimers to incorporate P-TEFb into the large complex. The oligomerization is mediated through the basic region within the central part, with bound 7SK snRNA, and its coiled-coil region in the C-terminal domain [48,49]. The binding of 7SK snRNA to the basic region in the Hexim oligomer induces exposure of the CycT1-binding domain in its C-terminus and formation of large complex [43,44,46-50]. Hexim1 and Hexim2 do not represent bona fide cyclin-dependent kinase inhibitors (CKI). The most surprising feature of both is the fact that they associate with 7SK snRNA first in order to inhibit P-TEFb; therefore, they exhibit a completely new group of CKIs, since none of the so-far studied CKIs utilize RNA as a partner to inhibit kinase activity of CDK/cyclin complex.

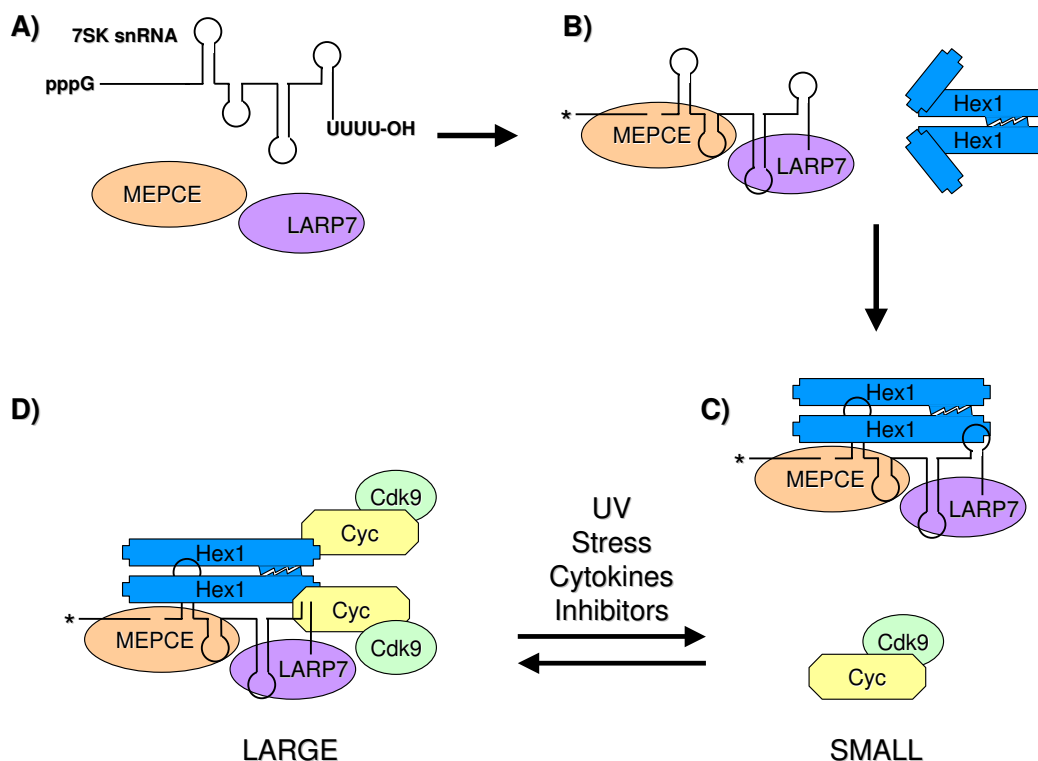
Critically, the exploration of P-TEFb associating partners in the large P-TEFb complex has not been finished yet. Two additional proteins participating in the formation of large P-TEFb complex were identified during the last two years. MEPCE (7SK snRNA methylphosphate capping enzyme) was identified as a specific 7SK snRNA methyltransferase causing methylation of the gamma-phosphate of its first 5' nucleotide [51]. LARP7 (La-related protein 7) stabilizes 7SK snRNA by binding to its 3'-UUUU-OH tail protecting it from degradation by exonucleases [52-54]. Both proteins are stably associated with 7SK snRNA after release of P-TEFb caused by stress or cellular signals in contrast to Hexim1, which are displaced from 7SK snRNA right after disruption of large complex [52-56].

Importantly, studies of biology of active complex led to identification of bromodomain protein 4 (Brd4), a major binding partner of P-TEFb when 7SK snRNA along with Hexim1/2 are displaced from P-TEFb [57,58]. Brd4 binds to acetylated histones and might be therefore targeting P-TEFb to actively transcribed genes if there is no specific factor recruiting P-TEFb to these genes [59]. Therefore, P-TEFb is typically present in two distinct complexes in most cell types. Heterodimer of CDK9/cyclin represents active P-TEFb and is here referred to as a 'small' complex of P-TEFb, irrespective of Brd4 binding (Figure 1). Whereas, cooperative binding of P-TEFb/cyclin/7SK snRNA/Hexim1 or 2/MEPCE/LARP7 identifies an inactive P-TEFb form, also recognized as 'large' complex of P-TEFb (Figure 1). Application of stress stimuli, UV radiation, cytokine treatment, chemical compounds, etc. on cells leads to dissociation of P-TEFb from Hexim1/2 and 7SK snRNA/MEPCE/LARP7 (Figure 1).

Posttranslational modifications of P-TEFb components

Besides inhibition of P-TEFb by recruitment to the large complex, its activation or inhibition depends primarily on posttranslational modifications of CDK9 and its associated cyclin. We would like to discuss relevance of these modifications in respect to their putative functions in development. During many developmental processes, such as gastrulation, left-right patterning, organogenesis and many others, the morphogens are literally a moving force navigating development forward. Morphogens can make appropriate impact only if there is a proper receptor on cell surface, which can pass message through various cellular signaling pathways to particular transcription activators or repressors. Thus, it is highly possible that the same signaling circuits involved in signal transmission could target and consequently modify activity of P-TEFb either in a positive or negative way.

Among so-far documented posttranslational modifications of P-TEFb, phosphorylation of cyclin and especially

**Figure 1**

Composition and assembly of P-TEFb complexes. **A)** 7SK snRNA contains 5'- and 3'- ends with pppG (triphosphate guanosine) and UUUU-OH (oligouridylate tail), respectively. 7SKsnRNA is recognized by MEPCE (7SK snRNA methylphosphate capping enzyme) and LARP7 (La-related protein 7). **B)** MEPCE methylates gamma-phosphate of its first 5'ribonucleotide, depicted by an asterisk, and LARP7 stabilizes 7SK snRNA by binding to its oligouridylate tail. HeximI (Hex1) homodimerizes (or heterodimerizes with Hexim2) via its coiled-coil domain in the C-terminus, but N-terminus adopts conformation which does not allow binding to P-TEFb (CDK9/Cyc). **C)** Binding of 7SK snRNA from 7SK snRNA/MEPCE/LARP7 complex to basic region in central part of HeximI triggers conformational changes of hexim dimer leading to exposition of CycT1-binding domain at the C-terminus of Hex1 and consequent binding of P-TEFb ('SMALL' complex). **D)** The 'LARGE' complex is formed and is stabilized due to multiple protein-protein and protein-RNA contacts within the complex. Activity of P-TEFb is inhibited in the large complex. Several stimuli have been reported to disrupt the large complex, such as UV radiation, diverse stress signals (mechanical, hypertrophic), cytokines (TNF- α , IL-6) and inhibitors (Actinomycin D, DRB).

of CDK9 is a key feature of its regulation *in vivo*. Several serines and threonines residues (Ser347, 354 and 357; Thr350 and 354) at its C-terminus must be phosphorylated for P-TEFb activity first [60,61]. Nevertheless, full activation of P-TEFb is completed after conserved Thr186 in the T-loop is phosphorylated, an event triggering major conformational changes in CDK9/CycT1 heterodimer leading to exposition of ATP binding pocket together with substrate site [49,62,63]. Recently, phosphorylation of Thr29 in CDK9₄₂ within the HIV elongation complex was able to block transcription of viral RNAs [64]. To complete list of CDK9/cyclin phosphorylation status, several other residues, not previously described, were identified by global mass spectrometric technology to be phosphorylated *in vivo* [65,66]. Of course, functional consequences of these modifications have not been investigated yet, but

they might serve as a first clue for further studies to identify appropriate kinases.

Phosphorylation of Thr186 is also a prerequisite for the assembly of the large complex [49,62]. The reason why large complex bears principally active P-TEFb is most likely to allow cells, in time of need, an efficient and fast release of stored P-TEFb to support transcription of genes involved in given cellular responses. Indeed, certain stress or pathological conditions induces liberation of P-TEFb from the large complex. Two years ago, PI3K/Akt signaling pathway was reported to disrupt large complex, by phosphorylating Hexim1 on two serines and two threonines in the CycT-binding domain, after HMBA treatment [67]. In addition, the Zhou lab demonstrated that UV and HMBA, agents known to activate P-TEFb, disrupt P-TEFb from the

large complex by cooperative action of calcium ion (Ca²⁺)-calmodulin-protein phosphatase 2B (PP2B) and protein phosphatase 1 (PP1 α) [68]. In detail, activated PP2B provokes conformational changes in 7SK snRNP first, allowing PP1 α to liberate P-TEFb by dephosphorylating Thr186. Alternatively, PPM1A and PPM1B (protein phosphatases, magnesium-dependent) were found to mediate dephosphorylation of Thr186 in cells under non-stress conditions, pointing towards several alternative mechanisms used by cells to accommodate different stress or non-stress (physiological) stimuli [69]. Nevertheless, inactive P-TEFb (dephosphorylated on Thr186) is subsequently recruited to the transcription initiation complex by Brd4. These finding correlates with *in vitro* studies demonstrating that Thr186 is kept unphosphorylated by action of TFIIH in the HIV preinitiation complex [70]. Interestingly, phosphorylation of Thr29 in CDK9 mediated by Brd4 was detected in HIV transcription initiation complex just recently [64]. Upon dissociation of TFIIH and Brd4 during elongation transcription induced by Tat, P-TEFb is fully activated by *de novo* phosphorylation of Thr186 and dephosphorylation of Thr29 [64,70]. Given importance of protein phosphatase-2A (PP2A) in the augmentation of basal activity of the HIV-1, it is tempting to speculate that PP2A is a phosphatase acting on Thr29 [71].

Even though phosphorylation might seem to be most essential for P-TEFb activity, ubiquitination and acetylation participate in regulation of P-TEFb activity as well. Ubiquitination of CycT1 and CDK9 by Skp2 controls its protein turnover and interaction with Tat/TAR, respectively [72,73]. Also, human double minute-2 protein (HDM2), a p53-specific E3 ubiquitin ligase, ubiquitinates Hexim1 in the basic region [74]. Ubiquitination of Hexim1 is not involved in Hexim1 proteasome-mediated protein degradation but rather interferes with inhibition of P-TEFb [74]. Further, acetylation of CDK9 on Lys44 located in the ATP binding domain by p300/CBP increases its kinase activity towards CTD of RNAPII [75]. In contrast, acetylation of two lysines at positions 44 and 48 in CDK9 by P/CAF and GCN5 complexes exhibited inhibition of its kinase activity and relocalization to insoluble nuclear matrix [76]. Importantly, acetylation of cyclin T1 triggers dissociation of P-TEFb from the large complex and its activation [77]. Given the importance of p300/CBP in the acetylation of Tat and activation of HIV transcription, it is not surprising that the HIV virus utilizes the same acetyl transferase complex to acetylate Tat in order to stabilize formation of Tat-P-TEFb-TAR complex to initiate viral transcription [78]. Therefore, one could assume that the virus intentionally subverts natural cellular cofactors of P-TEFb to support its own replication cycle.

Together documented posttranslational modifications are of great interest in respect to their possible function in regulation of P-TEFb activity in diverse cellular responses, (stress, cytokines, cell communication), disease and development. One could predict that simple recruitment of P-TEFb to the promoter of given genes does not guarantee transcriptional initiation *per se*. Rather, current pattern of posttranslational modifications (phosphorylation, acetylation, ubiquitination) of subunits of P-TEFb will decide if transcription is turned on or off. For example, two P-TEFb complexes located at two different promoters might differ in transcriptional response to given signals, because of the Thr29 phosphorylation or Lys44 and 48 acetylation of CDK9 within one of the P-TEFb complexes.

Function of P-TEFb in cell cycle

Each phase or intercalating transitions of cell cycle are controlled by spatio-temporal expression of CDKs and appropriate cyclins, but in the case of CDK9 and C-type cyclins, neither levels nor associating CDK9 kinase activity were changed or dramatically fluctuated during this process [24]. Such an observation does not necessary rule out CDK9 function in the control of cell cycle, since protein level or associated kinase activity of other CKDs and cyclins are not changing during cell cycle as well [79]. Nevertheless, recent identification of Brd4 can provide the missing link to the function of P-TEFb in cell cycle control, since Brd4 is implicated in transition of epigenetic memory through binding to acetylated histones [57-59,80]. The Zhou lab was able to demonstrate a dramatic increase in P-TEFb-Brd4 interaction from late mitosis to early G1 phases of cell cycle and active recruitment of P-TEFb to the chromosomes, followed by initiation of transcription of key genes for G1 progression. Importantly, depletion of Brd4 abrogated the whole process by reducing transcription of essential G1 genes, leading to G1 cell cycle arrest and apoptosis [80]. Therefore, it is very tempting to speculate that Brd4-mediated recruitment of P-TEFb to G1 genes is fundamental for successful G1/S transition and could serve as a hallmark of transcriptional memory across cell division [59,80]. However, other functional aspect/s of Brd4-P-TEFb interaction in respect to cell cycle must be explored first. For instance, how is the association of Brd4 with P-TEFb and consequent recruitment to specific genes regulated in cell cycle-dependent manner in the first place? From recent studies, we have learned that Brd4 recruits P-TEFb to inflammatory and Hox genes by interaction with acetylated NF- κ B on Lys-310 or acetylated histone 4 on Lys-5, 8 and 12, respectively [81,82]. Also, acetylation of histone 3 at promoter-proximal regions in CD80 genes was critical for Brd4-dependent P-TEFb recruitment and transcription initiation [83]. If the same mechanisms/principles apply for Brd4/P-TEFb recruitment to chromosomes at G1 phase remains to be explored in the future.

Moreover - is simple recruitment of P-TEFb to Brd4 enough or are posttranslational modifications involved too? If the answer is yes, then what residues are involved, and most importantly, what is their nature (phosphorylation, acetylation, etc)? Such a scenario would imply an existence of specific complexes able to carry these modifications. What are these factors? It will be of great interest to explore in more detail if CDKs participating in M or G1 phases are engaged in these events, but involvement of other protein kinases must be taken in account, too.

Additional function of P-TEFb in cell cycle could be in connection to the retinoblastoma protein (pRB). CDK9 was first identified as a cell division cycle-2 related kinase, with strong kinase activity towards pRB, but not histone 1, suggesting its role in G1/S transition [84]. Indeed, silencing of CDK9 in cells by RNA interference approach led to the enrichment of cells in G1 phase of cell cycle supporting function of P-TEFb in the G1/S transition [85]. Interestingly, CDK9/CycT2 but not CDK9/CycT1 complex binds pRB suggesting diverse function of C-type cyclins in cell cycle regulation [86].

Last but not least, CDK9 phosphorylates p53 on multiple Ser residues (Ser33, 315 and 392). Phosphorylation of Ser 33 and 315 was implicated in the association with propyl isomerase Pin1. Phosphorylation-dependent Pin1/p53 interaction induces conformational changes in p53 leading to elevated DNA binding and transactivation capacity [87]. Phosphorylation of 392 resulted in stabilization of p53 tetramer and enhancement of target gene expression [88,89]. Interestingly, Cdk9 gene was also activated by binding of p53 to its promoter, suggesting a positive role of p53 in the regulation of its basal transcription [88]. Since Ser392 phosphorylation is not required for p53-mediated cell cycle arrest, it is possible to speculate that there is a positive regulatory loop between expression of CDK9 and p53 transactivation mediated by Ser392. Nevertheless, two major questions need to be elucidated. First, why does CDK9 phosphorylate p53: is it to strengthen DNA repair machinery or is to support apoptosis mediated by p53? Second, why does p53 need to control expression of CDK9, is it required for its function or is it to ensure optimal expression of other genes involved in adequate p53 response?

Function of P-TEFb in development

In the past decade, we have learned a great deal about genetic, biochemical and molecular properties of P-TEFb, mostly due to its indispensable role in HIV replication, cytokine responses, cell differentiation, etc. Just very recently we have started to appreciate physiological role/s of P-TEFb in development. Individual genetic depletion of CycT1 or CycT2 in *Caenorabditis elegans* had no dramatic impact on its development. In contrast, genetic inactivation

of both cyclins simultaneously resulted in early embryonic lethality, similarly to genetic inactivation of RNAPII [90].

To test whether P-TEFb is essential for *Drosophila* development, CDK9 was down-regulated by RNA interference (RNAi) approach. CDK9 knock-down flies died during metamorphosis, suggesting fundamental role of P-TEFb in *Drosophila* early development [91]. Relatively later lethality in flies in comparison to *C. elegans* could reflect major differences between these two species. First, timing and efficiency of CDK9 knock-down could differ and most importantly, stored maternal mRNA or protein might compensate for the loss of *de novo* expression of CDK9 for some time [91].

The role of CDK9 in zebra fish development was investigated by usage of specific morpholinos (MO), which mediate degradation of CDK9 messenger RNA and consequent down-regulation of CDK9 protein. Injection of specific Cdk9-morpholinos had a severe effect on definitive erythropoiesis manifested by significant reduction of runx1 signal in the dorsal aorta precursor population [92,93]. Taking into account ubiquitous expression of CDK9 in the whole developing embryo, it is surprising that only an effect on hematopoietic system was observed. It was probably due to insufficient depletion of CDK9 from other cells; therefore, these cells have enough CDK9 for their proper function. In the case of hematopoietic cells, the level of CDK9 did not reach critical threshold necessary for terminal differentiation of hematopoietic precursors. Supporting evidence to this threshold scenario comes from studies of HIV replication in cells, too. RNA mediated knock-down of P-TEFb in HeLa cells did not cause cellular death but inhibited Tat transactivation and HIV-1 transcription instead [94].

To investigate final consequences of nonfunctional P-TEFb in mice, we tried to generate knock-out mice for CycT1 and CycT2 using the β -geo gene trap technology [95]. Regretfully, our attempts to generate a complete knock-out mouse for CycT1 were not successful, and only a hypomorphic mouse with residual expression of CycT1 in the whole body was generated. These hypomorphic mice exhibited only modest immunological defects, such as, altered class switch recombination (not published data) and moderate appearance of autoimmunity due to impaired negative selection of autoreactive T cells in thymus [96]. In the case of CycT2, after conducting numerous matings of heterozygous mice, we were not able to detect any newborn mice bearing nonfunctional allele of *CcnT2* gene. When developing embryos and fetuses at different developmental stages were genotyped, still no null animal for *CcnT2* gene was found, suggesting a developmental block even before mid gestational period. Indeed,

embryonic lethality preceding even blastocyst implantation was observed. This early lethality could be attributed to impaired zygotic gene activation taking place in two-four cell embryos or to decreased expression of critical genes, which were revealed by siRNAs against *CycT2* in embryonic stem cells [36,97].

So far, only examples of developmental consequences of P-TEFb loss of function were described, but ectopic activation of P-TEFb exhibits dramatic consequences for normal development as well. Genetic ablation of *Clp-1*, the mouse homologue of human *Hexim1*, resulted in embryonic death at E16.5 due to cardiac hypertrophy [98]. Down-regulation of *LARP7* orthologue in zebra fish caused embryonic death due to aberrant splicing, suggesting a fundamental role for P-TEFb in coupling transcription elongation with alternative splicing [52].

To finalize developmental properties of P-TEFb, we would like to describe a situation where inhibition of P-TEFb is necessary indeed for normal development of germ-line blastomeres (*C. elegans*) or polar cells (*D. melanogaster*), specialized cell types similar to primordial germ cells in mammals. These cells are kept in undifferentiated stage by repressed mRNA transcription due to absence of Ser2 phosphorylation in CTD of the RNAPII. *PIE-1* in *C. elegans* and *pgc* (polar granule component) in *D. melanogaster* block Ser2 phosphorylation by binding to P-TEFb and preventing its recruitment to CTD [99-101]. Predictably, the next step should be to elucidate if the inhibition of P-TEFb is a common mechanism for germ line specification in other species as well. Similarly to *PIE-1* and *Pgc*, *Runx1*, a repressor of *CD4* expression in double negative thymocytes, disables transcription of *CD4* gene by decoying P-TEFb from the already engaged RNAPII [102].

Collectively, we have learned a key role of P-TEFb in early development from nematodes to mammals, but still we do not know what the target genes are within developmental programs. The first clue pointing to the right direction/s could come from our siRNA experiments in ES cells [36]. RNAi approach was used to down-regulate *CycT1* or *CycT2* and check for changes, by microarrays, in the expression of genes influenced by depletion of either cyclin. Reduction in *CycT2* affected mostly expression of genes participating in the TGF β and Wnt signaling pathways, as well as autophagy. The most affected genes were *Lefty 1* and *Lefty 2*, members of the TGF β superfamily, which are highly expressed in the inner cell mass and trophoctoderm during embryogenesis [103]. Moreover, genes involved in ubiquitin-proteasomal system and autophagy, which are indispensable for rapid degradation of maternal protein during the transition from oocytes to embryos, were also lessened. Of note, autophagy-defec-

tive oocytes fail to develop beyond the four- and eight-cell stage [104]. In contrast, *CycT1* knock-down decreased expression of genes involved in fatty acid and glucose metabolism, cell communication and cell cycle [36]. Critically, although glucose metabolism was affected in both cases, targeted genes were different.

From these or similar microarray data, we can indeed pinpoint target genes of different P-TEFb complexes, yet fundamental questions remain to be solved.

- 1) *How does P-TEFb achieve its broad binding capacity towards myriad transcription factors?*
- 2) *What are principal transcription factors driving normal development, cell fate commitment or terminal differentiation through interaction with P-TEFb?*
- 3) *Why is only a specific subset of P-TEFb-dependent genes transcribed in response to given intra- and extracellular stimuli?*

Ad 1) Usually, when we think of P-TEFb, two functional states are considered: active (small complex, typically CDK9₄₂/*CycT1*) and inactive (large complex, CDK9₄₂/*CycT1*/7SK snRNA/*Hexim1*/*LARP7*/*MEPCE*). One must actually revise our rather simplified view on P-TEF complexes, as proposed in several publications [36,105]. Active P-TEFb consists of CDK9 and C-type cyclin, but two forms of CDK9 exist (CDK9₄₂ and CDK9₅₅) and at least four isoforms of C-type cyclins (*CycT1*, *CycT2a*, *CycT2b* and *CycK*). By simple combinatorial math, it leaves us with 8 different complexes of active P-TEFb (Figure 2A). Taking in account the existence of *Hexim1*, *Hexim2*, 7SK snRNA, *LARP7* and *MEPCE*, we will come to number 16 for inactive P-TEFb complexes (Figure 2B). All together there are 24 P-TEFb complexes with unique molecular surface composition. One might argue that binding of P-TEFb strictly depends on recognition capacity of cyclin boxes, histidine-rich and leucine rich regions in cyclins and substrate binding site in CDK9, but other possibilities should be considered, too. CDK9/cyclin adopts more open conformation different from CDK2/*CycA* providing extra molecular surfaces available for new interactions [63]. Also, other components of small or large complexes can mediate interaction with various factors. Indeed, nucleophosmin and NF κ B associate with basic region of *Hexim1* [45,106]. Also, estrogen and glucocorticoid receptors bind *Hexim1* through its basic region [107,108]. Examples of these associations have served only to demonstrate hidden reserves of P-TEFb to interact with distinct factors.

Ad 2) We found that *Lefty1* and *Lefty2* proteins were less expressed in ES cells with down-regulated *CycT2* but not

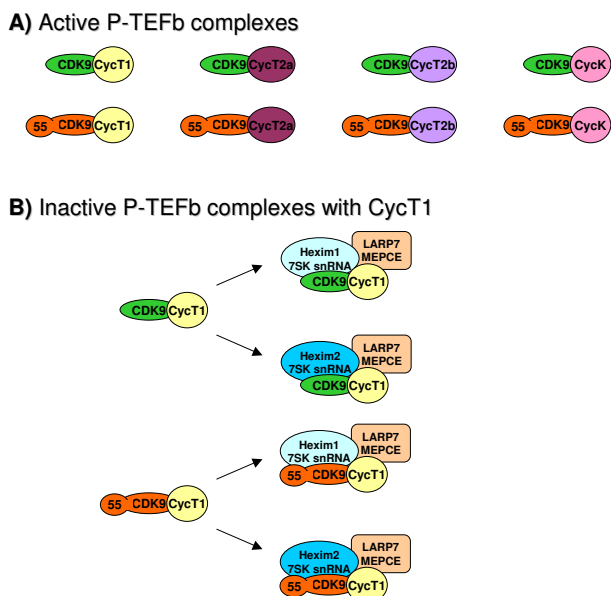


Figure 2
Active and inactive P-TEFb complexes. A) Active P-TEFb complexes. CDK9₄₂ (green oval) and CDK9₅₅ (orange oval) can separately bind to individual CycT1 (yellow circle), CycT2a (violet oval), CycT2b (lavender oval) and CycK (pink oval). **B)** Inactive P-TEFb complexes with CycT1. Only large complexes with CycT1 are presented for illustration, but the same would apply for CycT2a, CycT2b and CycK too. Complexes of 42- and CDK9₅₅ with CycT1 are presented at the left side. 'Large' complexes consisting of CDK9/CycT1 are at the right side. Hexim1/7SK snRNA (light blue oval), Hexim2/7SK snRNA (turquoise blue oval), MEPCE/LARP7 (light orange oval).

CycT1. Oct4, Sox2, key transcriptional factors guarding self-renewal property of ES, were shown to bind to the promoter of Lefty1 gene and activate it [109]. Thus, it is possible that CycT2 binds specifically Oct4 and Sox2 but CycT1 does not. Along with this line, CycT2 together with CDK9₄₂ is required for myogenesis *in vitro* by activating MyoD-dependent transcription [110]. On the contrary, MEF-2 related to MyoD, associates with CycT1 [111]. Recently, function of P-TEFb complex composed of CDK9₅₅ and CycT2 was demonstrated to play a fundamental role in muscle regeneration by governing myoblast differentiation from satellite cells *in vivo* [32]. These examples demonstrate clearly that one developmental program (myogenic differentiation) can employ three distinct P-TEFb complexes to regulate a particular part of differentiation process. Of note, two repressors of MyoD family, I-mfa (inhibitor of MyoD family) and HIC (human I-mfa-domain-containing) employ P-TEFb for their function in myogenic differentiation too [112]. In addition, PPAR γ (peroxisome proliferator-activated recep-

tor γ), a master regulator of adipogenesis, utilizes CDK9₅₅ for its function [113]. Importantly, CycT2 was identified by two-hybrid screen as a Mix.3/mixer, a Pax-like homeo-domain protein, essential for endoderm formation [114]. On the other hand, association of CycT1 with GATA-1, a transcription factor involved in differentiation of numerous hematopoietic lineages, is indispensable for efficient megakaryopoiesis [115]. Last but not least, CDK9 participates in haematopoiesis in zebra fish through regulation of Ldb1 (LIM domain binding protein), which controls transcription of Hox genes [93]. Thus, specific transcription factors operating in certain developmental process utilize different P-TEFb complexes for their developmental tasks.

Ad 3) We believe that two equally important mechanisms help P-TEFb to decide if certain gene/s will be turned on or off. A) One layer of control is provided by functional interaction with specific cofactors (chromatin remodeling complexes, mediators) bound at transcription sites. B) The other one is the result of co-operative effect of signaling pathways regulating P-TEFb activity.

- **A)** Once P-TEFb is recruited to the promoter, it is exposed to interactions with other multiprotein complexes and to their catalytic activities resulting in post-translational modifications triggering activation or inhibition of P-TEFb activity (Figure 3B). Indeed, representatives of histone acetyltransferases p300/CBP and GCN5 with P/CAF can acetylate CDK9 to either activate or repress its kinase activity [75,76]. BRG1, a component of mammalian homologous of the SWI/SNF chromatin remodeling complexes, binds CDK9; together they activate STAT3-mediated transcription in response to cytokine receptor stimulation [116]. Moreover, co-repressor of thyroid hormone receptors (TR) and retinoic acid receptors (RAR) - N-CoR - associates with Hexim1 affecting ability of CDK9 to phosphorylate CTD of RNAPII [75].

- **B)** Signaling pathways serve, most likely, two primary functions in P-TEFb biology: first to trigger release of P-TEFb from the large complex; second to target and modify components of P-TEFb complexes (Figure 3A and 3C). At present, we know what stimuli/signals dissociate P-TEFb from the large complex, but we have just begun to explore signaling pathways responsible for it (see also posttranslational modification). Regrettably, we have almost no basic knowledge about signaling pathways operating and targeting P-TEFb activity during development, except for few examples. The PKN α , a fatty acid- and Rho-activated serine/threonine protein kinase, which was shown to bind CycT2a and consequently enhanced CycT2a mediated expression of myogenic differentiation markers during starvation, induced differentiation [117]. Further, the

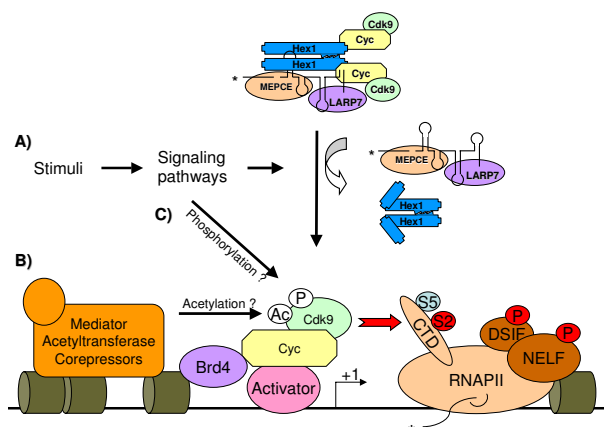


Figure 3
Regulation of P-TEFb activity during transcription.

A) P-TEFb is inactivated in the large complex. After given stimuli (UV radiation, cytokines, hypertrophic signals), active P-TEFb is released from the large complex by activity of signaling pathways downstream of these stimuli. Then, P-TEFb is recruited to the responsive promoter/s either by a specific activator (pink oval) such as MyoD or a co-activator, such as Brd4 (violet oval). P-TEFb is engaged at the promoters with poised RNAPII phosphorylated on Ser5 (light blue oval with letter S5) in CTD mediated by TFIIF. P-TEFb initiates transcription elongation by phosphorylating Ser2 of CTD in RNAPII (red oval with letter S2), DSIF or NELF (red ovals with letter P). Still, activity of P-TEFb can be controlled by two additional mechanisms. **B)** If there is a co-factor (acetyltransferase, mediator, corepressor) associating with P-TEFb at the promoter, then the activity of P-TEFb will depend on particular posttranslational modifications mediated by these co-factors, for example acetylation of Lys44 and 48 in CDK9 (white oval with letters Ac). **C)** Also, signaling pathways activated by given stimuli can modify components of the small complex, for example phosphorylation of CDK9 on Thr28 and Thr186 (white oval with letter P), and additionally modulate final activity of P-TEFb. Khaki barrels represent nucleosomes, and +1 depicts transcription start site.

MEK1-extracellular signal-regulated kinase (ERK) signaling pathway promotes CDK9/CycT1 dimer formation and induction of immediate early genes (like *c-fos*) in neuroendocrine cells [118]. From our microarray data we know that transcription of *Lefty1* is CycT2-dependent [36]. *Lefty1* contributes to the establishment of left-right symmetry during vertebrate development. Bone morphogenetic protein (BMP) type I receptor was demonstrated to positively regulate *Lefty1* expression in the chimeric embryo [119]. Therefore, one could hypothesize that BMP signaling could be involved in P-TEFb (CycT2) activation. Even if we identify pathways modulating P-TEFb activity, it is still critical to determine what component/s of P-TEFb complexes they target and what the nature of particular modification is. In summary, it is realistic to assume that

recruitment of particular P-TEFb complex in combination with transcriptional co-factors to unique set of genes can control various aspects of transcriptional programs in normal development.

Except already introduced transcriptional factors, a plethora of diverse transcriptional factors/enhancers were found during the past decade to utilize P-TEFb for various cellular pathways and physiological processes: 1) cytokine signaling - p65 subunit of NFκB, STAT3 [45,116,120,121]; 2) hormone nuclear receptors - estrogen, glucocorticoid and androgen receptors [107,122,123]; xenobiotic sensing - arylhydrocarbon receptor [124]; immunity - class II transactivator, AIRE [96,125,126] and cell proliferation/differentiation - c-myc [127]. P-TEFb plays a special function in HIV infection by initiating its transcription through binding to Tat, a specific viral transcriptional transactivator [27].

Promoter-proximal pausing of RNAPII

At last, we would like to dedicate a special part of this review to a very intriguing function of P-TEFb in developmental control through activation of stalled RNAPII. Historically, initiation of transcription was viewed as a rate-limiting step in the expression of majority of genes [16]. Interestingly, early studies indicated that specific genes, such as *c-myc*, *junB* and *HSP70*, surpass this concept, and their expression is subjected to elongation control through poised polymerase [17,18,20]. In principal, RNAPII initiates transcription but is immediately poised after synthesizing short RNA by action of negative elongation factors at the promoter-proximal region [21]. Nevertheless, a growing body of evidence demonstrates that RNAPII pausing is a novel mode of transcription control rather than exception from the rule [128-130]. Recent studies in *Drosophila* and mammalian system validated RNAPII distribution across the whole genome and clearly demonstrated that a significant number of genes was regulated at an early step of transcription elongation [129,130]. Among them, genes involved in development, cellular response to stimuli, cell communication, cell adhesion and differentiation demonstrated promoter-proximal RNAPII stalling. Importantly, down-regulation of NELF by RNAi resulted in loss of stalled RNAPII mark and re-expression of most of these genes [129]. To extend the concept of stalled polymerase to developmental perspective, transcription of *Hox* genes, governing anterior-posterior patterning in metazoan embryos, was found to be regulated at the level of elongation. Intact CDK9 activity was necessary to alleviate stalled RNAPII at the promoter of two *hox* genes in *Drosophila* (*Ultrabithorax* and *Abdominal-B*) [131]. Authors also suggested that Cdk9 could be involved in the regulation of Notch-, EGF-, and Dpp-signaling genes, again pointing towards connection of P-TEFb and regulation of developmental genes [131].

During preparation of this manuscript, new publication had appeared focusing on biological function of stalled RNAPII in the signal-dependent gene expression [81]. To study genes fitting to this criterion, authors employed LPS-inducible inflammatory gene expression in macrophages to demonstrate: 1) that genes induced in the primary response (LPS) have stalled RNAPII at the promoter-proximal region, 2) their induction is regulated by signal-dependent P-TEFb, 3) which is recruited via Brd4 binding to Histone 4 acetylated on Lys 5, 8 and 12. Moreover, transcription of these genes is repressed before stimulation by cooperative function of repressors [81]. Interestingly, developmentally regulated genes share the same characteristics as the LPS-inducible genes. It is stalled RNAPII and hierarchical expression of activators/repressors along with their co-factors.

These are very important observations in respect to possible role of P-TEFb in development. Since P-TEFb induces a transition from abortive to productive transcription elongation by phosphorylation of NELF and DSIF, it is logical to envision that P-TEFb might be a primary sensor to various developmental demands. In theory, P-TEFb could work as a platform capable of accommodating diverse stimuli and respond to them by switching on and off appropriate set of genes, along with cooperative function of developmental activators and repressors. Considering all available facts, it is now becoming clear that elongation block, by means of stalled RNAPII, represents a highly specific control module in transcription regulation.

P-TEFb and disease

Cardiac hypertrophy

Cardiac hypertrophy is probably the best illustrative example how deregulation of p-TEFb activity manifests in pathological phenotype, a disease. Cardiac hypertrophy (heart growth) is characterized by enlargement of cardiac myocytes in response to diverse signals, such as biomechanical stress, sarcomeric and cytoskeletal protein mutations, G protein-coupled receptors for ligands, etc. At the molecular level, cardiac hypertrophy is characterized by an increase in cell size and protein synthesis and reactivation of the fetal gene program [132]. In turn, increased synthesis of mRNA species results in elevated activity of RNAPII phosphorylated at Ser2 within CTD [133]. Ser2 is a target of P-TEFb, thus it is not surprising that P-TEFb was identified to be the limiting factor for pathological manifestation *in vitro* and *in vivo* [98,134]. Briefly, ectopic activation of P-TEFb either by ablation of cardiac lineage protein 1 (Clp-1), the mouse homologue of Hexim1, or overexpression of CycT1 in adult heart led to fetal lethality or heart growth due to cardiac hypertrophy, respectively [98,132].

Striking characteristic of cardiac hypertrophy is the fact that all hypertrophic stimuli led to release and activation of P-TEFb [132]. Since most of the signaling pathways downstream of these signals are well characterized, it will be critical to determine their role in the activation of P-TEFb. Truly enough, Jak/STAT signal transduction pathway is involved in the release of P-TEFb from large complexes [135]. Yet, it is not clear at the moment if Jak/STAT pathway targets and modifies any component of the large complex directly or indirectly. Moreover, from developmental perspectives of P-TEFb, it is highly probable that the signaling pathways governing pathological activation of P-TEFb will be, in part, the same signaling circuits driving growth of heart earlier during normal heart development [135]. Therefore, it will be of great interest to explore and characterize what the major differences in signaling pathways diverging to either adaptive or pathological P-TEFb activation are. In particular, what are these pathways by nature? Do they 'just' disrupt large complex or do they modify components of large/small P-TEFb complexes? Finally, how can we use this acquired knowledge to modulate de-repressed activity of P-TEFb in various diseases?

Cancer

Historically, the first recognition of P-TEFb in malignant processes came from a study focused on identification of novel tumor antigens associated with serous ovarian cancer [136]. By employing SEREX immunoscreening, the authors identified 9 immunogenic antigens, among them Hexim1, to be potential targets for immunotherapy. Relevance of P-TEFb in progression of ovarian cancer was not recognized at the time, since connection between Hexim1 and P-TEFb had not been established yet.

Another piece of the P-TEFb puzzle in cancer came from studies of mixed-lineage leukemia (MLL) fusion proteins in leukemic transformation. The gene for the histone methyltransferase MLL often participates in chromosomal translocations that eventually create MLL-fusion proteins associated with very aggressive forms of childhood acute leukemia [137,138]. Two proteins, Eleven Nineteen Leukemia (ENL) and AF4 proteins, common associating partners of MLL in childhood acute leukemia, were found to bind and utilize P-TEFb for their transformation properties [139,140]. These studies provided compelling evidence for direct role of AF4 and ENL in the regulation of transcription elongation and chromatin modification. This could also suggest that therapies targeting P-TEFb activity in leukemia might be a direction to pursue. Indeed, Flavopiridol, a specific inhibitor of CDK9, was able to induce apoptosis in chronic lymphocytic leukemia cells by suppressing transcription of short-lived antiapoptotic proteins, such as Mcl-1 [141].

Connection of Hexim1 in malignant processes through its binding to estrogen receptor was recently provided [108]. Estrogen receptors (ERs) are found in significant numbers of breast cancer, and targeted therapy against ERs has been used intensively [142]. Hexim1 binds ER α through its basic region and blocks ER α mediated gene expression [123]. Critically, overexpression of Hexim suppressed proliferation of breast cells. In accordance with this finding, expression of Hexim1 was down-regulated in samples from invasive breast cancer patients in comparison to Hexim1 level in normal breast tissue [108].

Certainly, the most illustrative example of P-TEFb dysfunction in malignant conversion has been demonstrated by the Zhou lab [53]. They identify PIP7S, also known as La-related protein 7 (LARP7), to associate and stabilize 7SK snRNP formation. LARP7 contains 3 RNA binding motifs, La binding motif in its N-terminus, a RNA recognition motif (RRM) 1 and RRM3, which are all needed for the stabilization of 7SK snRNA and formation of large complex [52-54]. Interestingly, its C-terminus is often deleted in human tumors suggesting that activation of P-TEFb mediated by LARP7 destabilization of large complex is important for proliferation and tumorigenicity of cancer cells. Indeed, RNAi mediated down-regulation of LARP7 blocking mammary epithelial cell differentiation [53]. In the same line, genetic inactivation of MXC, the Drosophila homologue of LARP7, resulted in overgrowth of lymph glands and hematocyte overproliferation [143]. Moreover, down-regulation of LARP7 was reported to be a suitable prognostic marker to predict the presence of lymph node metastasis in early stage of squamous cell cervical cancer before treatment [144]. In conclusion, it is likely that ectopic activation of P-TEFb in cancer cells serves to support transcription of key tumor-progressing genes, unchecked proliferation ultimately converging in tumorigenesis.

Frontiers

What is the future of P-TEFb in development? We know that targeted inactivation of cyclin T2 in mouse caused embryonic lethality even prior implantation [36]. To be able to follow function of CycT2 in other developmental processes, conditional mouse for CycT2 must be generated first. In these animals, expression of CycT2 can be switch off at a precise developmental stage; then, impact of CycT2 ablation on particular developmental program can be examined. Not only the aspect of CycT2 in early development can be addressed, but function of CycT2 in cell differentiation, regeneration and cell cycle can be revealed, too. Similarly, generation of conditional transgenic mice for other components of P-TEFb complexes will be instrumental to understand their function in various developmental processes.

By utilizing those conditional animals, other important question rendering function of P-TEFb can be revealed. For example, how is P-TEFb recruited to developmental genes? Is recruitment of P-TEFb by a specific activator sufficient or are additional co-factors needed? If so, are these co-factors components of histone-remodeling machinery, mediator complexes? And finally, is P-TEFb released from the large complex and then recruited to the promoter or is large complex bound to promoter/enhancer structures and active P-TEFb is released locally then? Thus, future studies are necessary to gain more light on these and other P-TEFb challenges.

If one thinks of function of P-TEFb in cancer, two aspects of involvement just come to mind. In the literature, one can find examples of indirect or direct involvement of dysregulated activity of P-TEFb in cancer. Down-regulation of Hexim1 and/or LARP7 in breast and cervical cancer most likely leads to increase of free-pool P-TEFb and consequent activation of cancer-related genes. Nevertheless, is simple increase in P-TEFb activity enough to promote malignant transformation or is it part of multi-step tumorigenic process? Yes, activation of P-TEFb in breast cancer cells seemed to be sufficient to promote malignant transformation [53]. Yet, in case of acute childhood leukemia,

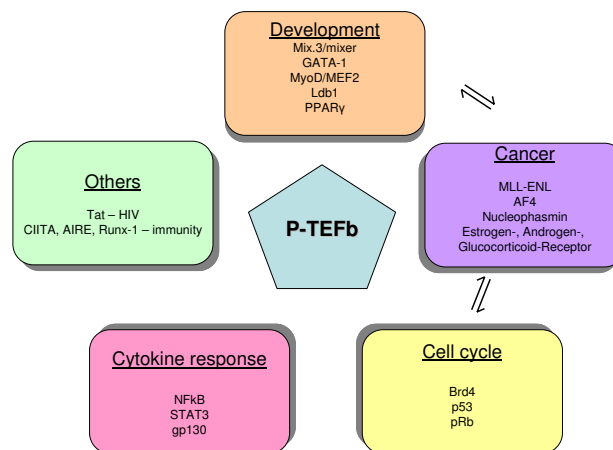


Figure 4
Role of P-TEFb in a broad spectrum of biological processes. P-TEFb (blue pentagon) participates in many different biological processes, such as development (light orange oval), cancer (violet oval), cell cycle (yellow oval), cytokine response (pink oval) and others (green oval). Abbreviations in each oval represent particular transcription factors which have been found to employ P-TEFb in given biological phenomena (more information in the text). Importantly, dysregulation of P-TEFb-dependent transcription factors involved in development or cell cycle could also significantly contribute to malignant transformation of normal cells, as depicted by arrows in this figure.

simple activation has no effect on induction of tumorigenesis but rather misplaced recruitment of P-TEFb through oncogenic chimeric proteins (MLL-ENL) is the driving force [140]. Also, ectopic expression of cyclin T1 in heart did not lead to tumor formation, implying existence of buffering mechanism in cells to deal with elevated P-TEFb activity. On the other hand, ectopic expression of CycT1 in other cellular systems might have deleterious consequences, because of no existing compensatory mechanisms. Again, generation of conditional mouse model might be helpful in this regard to ultimately dissect this conundrum.

It is becoming increasingly clear that P-TEFb participates in broad spectrum of biological processes (Figure 4). It is feasible to assume that the same transcription factors, different co-factors and signaling pathways co-operating with P-TEFb in cell cycle and development will be involved in pathophysiological effects of P-TEFb in various diseases, too. Therefore, the final task will be to identify what differences in these regulatory circuits are. What is the nature of these changes and if there is a way, to revert de-repressed P-TEFb activity back to normal "physiological state".

Competing interests

The author declares that they have no competing interests.

Acknowledgements

I would like to thank Sabina Sevcikova and Dalibor Blazek for helpful comments during manuscript preparation. For research carried out over several years, the author has been supported by Czech Science Foundation grant 301/09/1832 and Czech Ministry of Agriculture MZE0002716202.

References

- Margaritis T, Holstege FC: **Poised RNA polymerase II gives pause for thought.** *Cell* 2008, **133**:581-584.
- Saunders A, Core LJ, Lis JT: **Breaking barriers to transcription elongation.** *Nat Rev Mol Cell Biol* 2006, **7**:557-567.
- Sims RJ 3rd, Mandal SS, Reinberg D: **Recent highlights of RNA-polymerase-II-mediated transcription.** *Curr Opin Cell Biol* 2004, **16**:263-271.
- Peterlin BM, Price DH: **Controlling the elongation phase of transcription with P-TEFb.** *Mol Cell* 2006, **23**:297-305.
- Hirose Y, Ohkuma Y: **Phosphorylation of the C-terminal domain of RNA polymerase II plays central roles in the integrated events of eucaryotic gene expression.** *J Biochem* 2007, **141**:601-608.
- Bres V, Yoh SM, Jones KA: **The multi-tasking P-TEFb complex.** *Curr Opin Cell Biol* 2008, **20**:334-340.
- Fujinaga K, Irwin D, Huang Y, Taube R, Kurosu T, Peterlin BM: **Dynamics of human immunodeficiency virus transcription: P-TEFb phosphorylates RD and dissociates negative effectors from the transactivation response element.** *Mol Cell Biol* 2004, **24**:787-795.
- Kim JB, Sharp PA: **Positive transcription elongation factor B phosphorylates hSPT5 and RNA polymerase II carboxyl-terminal domain independently of cyclin-dependent kinase-activating kinase.** *J Biol Chem* 2001, **276**:12317-12323.
- Ping YH, Rana TM: **DSIF and NELF interact with RNA polymerase II elongation complex and HIV-1 Tat stimulates P-TEFb-mediated phosphorylation of RNA polymerase II and DSIF during transcription elongation.** *J Biol Chem* 2001, **276**:12951-12958.
- Fabrega C, Shen V, Shuman S, Lima CD: **Structure of an mRNA capping enzyme bound to the phosphorylated carboxy-terminal domain of RNA polymerase II.** *Mol Cell* 2003, **11**:1549-1561.
- Marshall NF, Peng J, Xie Z, Price DH: **Control of RNA polymerase II elongation potential by a novel carboxyl-terminal domain kinase.** *J Biol Chem* 1996, **271**:27176-27183.
- Marshall NF, Price DH: **Control of formation of two distinct classes of RNA polymerase II elongation complexes.** *Mol Cell Biol* 1992, **12**:2078-2090.
- Sehgal PB, Darnell JE Jr, Tamm I: **The inhibition by DRB (5,6-dichloro-1-beta-D-ribofuranosylbenzimidazole) of hnRNA and mRNA production in HeLa cells.** *Cell* 1976, **9**:473-480.
- Dubois MF, Bellier S, Seo SJ, Bensaude O: **Phosphorylation of the RNA polymerase II largest subunit during heat shock and inhibition of transcription in HeLa cells.** *J Cell Physiol* 1994, **158**:417-426.
- Chao SH, Price DH: **Flavopiridol inactivates P-TEFb and blocks most RNA polymerase II transcription in vivo.** *J Biol Chem* 2001, **276**:31793-31799.
- Hochheimer A, Tjian R: **Diversified transcription initiation complexes expand promoter selectivity and tissue-specific gene expression.** *Genes Dev* 2003, **17**:1309-1320.
- Aida M, Chen Y, Nakajima K, Yamaguchi Y, Wada T, Handa H: **Transcriptional pausing caused by NELF plays a dual role in regulating immediate-early expression of the junB gene.** *Mol Cell Biol* 2006, **26**:6094-6104.
- Bentley DL, Groudine M: **A block to elongation is largely responsible for decreased transcription of c-myc in differentiated HL60 cells.** *Nature* 1986, **321**:702-706.
- Krumm A, Meulia T, Brunvand M, Groudine M: **The block to transcriptional elongation within the human c-myc gene is determined in the promoter-proximal region.** *Genes Dev* 1992, **6**:2201-2213.
- Rougvie AE, Lis JT: **The RNA polymerase II molecule at the 5' end of the uninduced hsp70 gene of D. melanogaster is transcriptionally engaged.** *Cell* 1988, **54**:795-804.
- Nechaev S, Adelman K: **Promoter-proximal Pol II: when stalling speeds things up.** *Cell Cycle* 2008, **7**:1539-1544.
- Price DH: **Poised polymerases: on your market setgo!** *Mol Cell* 2008, **30**:7-10.
- Edwards MC, Wong C, Elledge SJ: **Human cyclin K, a novel RNA polymerase II-associated cyclin possessing both carboxy-terminal domain kinase and Cdk-activating kinase activity.** *Mol Cell Biol* 1998, **18**:4291-4300.
- Grana X, De Luca A, Sang N, Fu Y, Claudio PP, Rosenblatt J, Morgan DO, Giordano A: **PITALRE, a nuclear CDC2-related protein kinase that phosphorylates the retinoblastoma protein in vitro.** *Proc Natl Acad Sci USA* 1994, **91**:3834-3838.
- Lin X, Taube R, Fujinaga K, Peterlin BM: **P-TEFb containing cyclin K and Cdk9 can activate transcription via RNA.** *J Biol Chem* 2002, **277**:16873-16878.
- Peng J, Zhu Y, Milton JT, Price DH: **Identification of multiple cyclin subunits of human P-TEFb.** *Genes Dev* 1998, **12**:755-762.
- Wei P, Garber ME, Fang SM, Fischer WH, Jones KA: **A novel CDK9-associated C-type cyclin interacts directly with HIV-1 Tat and mediates its high-affinity, loop-specific binding to TAR RNA.** *Cell* 1998, **92**:451-462.
- Liu H, Rice AP: **Genomic organization and characterization of promoter function of the human CDK9 gene.** *Gene* 2000, **252**:51-59.
- Shore SM, Byers SA, Maury W, Price DH: **Identification of a novel isoform of Cdk9.** *Gene* 2003, **307**:175-182.
- Shore SM, Byers SA, Dent P, Price DH: **Characterization of Cdk9(55) and differential regulation of two Cdk9 isoforms.** *Gene* 2005, **350**:51-58.
- Liu H, Herrmann CH: **Differential localization and expression of the Cdk9 42k and 55k isoforms.** *J Cell Physiol* 2005, **203**:251-260.
- Giacinti C, Musaro A, De Falco G, Jourdan I, Molinaro M, Bagella L, Simone C, Giordano A: **Cdk9-55: a new player in muscle regeneration.** *J Cell Physiol* 2008, **216**:576-582.
- Wimmer J, Fujinaga K, Taube R, Cujec TP, Zhu Y, Peng J, Price DH, Peterlin BM: **Interactions between Tat and TAR and human immunodeficiency virus replication are facilitated by human**

- cyclin T1 but not cyclins T2a or T2b.** *Virology* 1999, **255**:182-189.
34. Kurosu T, Zhang F, Peterlin BM: **Transcriptional activity and substrate recognition of cyclin T2 from P-TEFb.** *Gene* 2004, **343**:173-179.
 35. De Luca A, De Falco M, Baldi A, Paggi MG: **Cyclin T: three forms for different roles in physiological and pathological functions.** *J Cell Physiol* 2003, **194**:101-107.
 36. Kohoutek J, Li Q, Blazek D, Luo Z, Jiang H, Peterlin BM: **Cyclin T2 is essential for mouse embryogenesis.** *Mol Cell Biol* 2009, **29**:3280-3285.
 37. Liou LY, Haaland RE, Herrmann CH, Rice AP: **Cyclin T1 but not cyclin T2a is induced by a post-transcriptional mechanism in PAMP-activated monocyte-derived macrophages.** *J Leukoc Biol* 2006, **79**:388-396.
 38. Marshall RM, Salerno D, Garriga J, Grana X: **Cyclin T1 expression is regulated by multiple signaling pathways and mechanisms during activation of human peripheral blood lymphocytes.** *J Immunol* 2005, **175**:6402-6411.
 39. Fu TJ, Peng J, Lee G, Price DH, Flores O: **Cyclin K functions as a CDK9 regulatory subunit and participates in RNA polymerase II transcription.** *J Biol Chem* 1999, **274**:34527-34530.
 40. Mori T, Anazawa Y, Matsui K, Fukuda S, Nakamura Y, Arakawa H: **Cyclin K as a direct transcriptional target of the p53 tumor suppressor.** *Neoplasia* 2002, **4**:268-274.
 41. Nguyen VT, Kiss T, Michels AA, Bensaude O: **7SK small nuclear RNA binds to and inhibits the activity of CDK9/cyclin T complexes.** *Nature* 2001, **414**:322-325.
 42. Yang Z, Zhu Q, Luo K, Zhou Q: **The 7SK small nuclear RNA inhibits the CDK9/cyclin T1 kinase to control transcription.** *Nature* 2001, **414**:317-322.
 43. Michels AA, Nguyen VT, Fraldi A, Labas V, Edwards M, Bonnet F, Lania L, Bensaude O: **MAQ1 and 7SK RNA interact with CDK9/cyclin T complexes in a transcription-dependent manner.** *Mol Cell Biol* 2003, **23**:4859-4869.
 44. Yik JH, Chen R, Nishimura R, Jennings JL, Link AJ, Zhou Q: **Inhibition of P-TEFb (CDK9/Cyclin T) kinase and RNA polymerase II transcription by the coordinated actions of HEXIMI1 and 7SK snRNA.** *Mol Cell* 2003, **12**:971-982.
 45. Ouchida R, Kusuhara M, Shimizu N, Hisada T, Makino Y, Morimoto C, Handa H, Ohsuzu F, Tanaka H: **Suppression of NF-kappaB-dependent gene expression by a hexamethylene bisacetamide-inducible protein HEXIMI1 in human vascular smooth muscle cells.** *Genes Cells* 2003, **8**:95-107.
 46. Byers SA, Price JP, Cooper JJ, Li Q, Price DH: **HEXIM2, a HEXIMI1-related protein, regulates positive transcription elongation factor b through association with 7SK.** *J Biol Chem* 2005, **280**:16360-16367.
 47. Yik JH, Chen R, Pezda AC, Zhou Q: **Compensatory contributions of HEXIMI1 and HEXIM2 in maintaining the balance of active and inactive positive transcription elongation factor b complexes for control of transcription.** *J Biol Chem* 2005, **280**:16368-16376.
 48. Blazek D, Barboric M, Kohoutek J, Oven I, Peterlin BM: **Oligomerization of HEXIMI1 via 7SK snRNA and coiled-coil region directs the inhibition of P-TEFb.** *Nucleic Acids Res* 2005, **33**:7000-7010.
 49. Li Q, Price JP, Byers SA, Cheng D, Peng J, Price DH: **Analysis of the large inactive P-TEFb complex indicates that it contains one 7SK molecule, a dimer of HEXIMI1 or HEXIM2, and two P-TEFb molecules containing Cdk9 phosphorylated at threonine 186.** *J Biol Chem* 2005, **280**:28819-28826.
 50. Barboric M, Kohoutek J, Price JP, Blazek D, Price DH, Peterlin BM: **Interplay between 7SK snRNA and oppositely charged regions in HEXIMI1 direct the inhibition of P-TEFb.** *EMBO J* 2005, **24**:4291-4303.
 51. Jeronimo C, Forget D, Bouchard A, Li Q, Chua G, Poitras C, Therien C, Bergeron D, Bourassa S, Greenblatt J, Chabot B, Poirier GG, Hughes TR, Blanchette M, Price DH, Coulombe B: **Systematic analysis of the protein interaction network for the human transcription machinery reveals the identity of the 7SK capping enzyme.** *Mol Cell* 2007, **27**:262-274.
 52. Barboric M, Lenasi T, Chen H, Johansen EB, Guo S, Peterlin BM: **7SK snRNP/P-TEFb couples transcription elongation with alternative splicing and is essential for vertebrate development.** *Proc Natl Acad Sci USA* 2009, **106**:7798-7803.
 53. He N, Jahchan NS, Hong E, Li Q, Bayfield MA, Maraia RJ, Luo K, Zhou Q: **A La-related protein modulates 7SK snRNP integrity to suppress P-TEFb-dependent transcriptional elongation and tumorigenesis.** *Mol Cell* 2008, **29**:588-599.
 54. Krueger BJ, Jeronimo C, Roy BB, Bouchard A, Barrandon C, Byers SA, Searcey CE, Cooper JJ, Bensaude O, Cohen EA, Coulombe B, Price DH: **LARP7 is a stable component of the 7SK snRNP while P-TEFb, HEXIMI1 and hnRNP A1 are reversibly associated.** *Nucleic Acids Res* 2008, **36**:2219-2229.
 55. Diribarne G, Bensaude O: **7SK RNA, a non-coding RNA regulating P-TEFb, a general transcription factor.** *RNA Biol* 2009, **6**:122-128.
 56. Markert A, Grimm M, Martinez J, Wiesner J, Meyerhans A, Meyuhos O, Sickmann A, Fischer U: **The La-related protein LARP7 is a component of the 7SK ribonucleoprotein and affects transcription of cellular and viral polymerase II genes.** *EMBO Rep* 2008, **9**:569-575.
 57. Jang MK, Mochizuki K, Zhou M, Jeong HS, Brady JN, Ozato K: **The bromodomain protein Brd4 is a positive regulatory component of P-TEFb and stimulates RNA polymerase II-dependent transcription.** *Mol Cell* 2005, **19**:523-534.
 58. Yang Z, Yik JH, Chen R, He N, Jang MK, Ozato K, Zhou Q: **Recruitment of P-TEFb for stimulation of transcriptional elongation by the bromodomain protein Brd4.** *Mol Cell* 2005, **19**:535-545.
 59. Mochizuki K, Nishiyama A, Jang MK, Dey A, Ghosh A, Tamura T, Natsume H, Yao H, Ozato K: **The bromodomain protein Brd4 stimulates G1 gene transcription and promotes progression to S phase.** *J Biol Chem* 2008, **283**:9040-9048.
 60. Fong YW, Zhou Q: **Relief of two built-in autoinhibitory mechanisms in P-TEFb is required for assembly of a multicomponent transcription elongation complex at the human immunodeficiency virus type I promoter.** *Mol Cell Biol* 2000, **20**:5897-5907.
 61. Garber ME, Mayall TP, Suess EM, Meisenhelder J, Thompson NE, Jones KA: **CDK9 autophosphorylation regulates high-affinity binding of the human immunodeficiency virus type I tat-P-TEFb complex to TAR RNA.** *Mol Cell Biol* 2000, **20**:6958-6969.
 62. Chen R, Yang Z, Zhou Q: **Phosphorylated positive transcription elongation factor b (P-TEFb) is tagged for inhibition through association with 7SK snRNA.** *J Biol Chem* 2004, **279**:4153-4160.
 63. Baumli S, Lolli G, Lowe ED, Troiani S, Rusconi L, Bullock AN, Debreczeni JE, Knapp S, Johnson LN: **The structure of P-TEFb (CDK9/cyclin T1), its complex with flavopiridol and regulation by phosphorylation.** *EMBO J* 2008, **27**:1907-1918.
 64. Zhou M, Huang K, Jung KJ, Cho WK, Klase Z, Kashanchi F, Pise-Masison CA, Brady JN: **Bromodomain protein Brd4 regulates human immunodeficiency virus transcription through phosphorylation of CDK9 at threonine 29.** *J Virol* 2009, **83**:1036-1044.
 65. Gnad F, Ren S, Cox J, Olsen JV, Macek B, Oroshi M, Mann M: **PHOSIDA (phosphorylation site database): management, structural and evolutionary investigation, and prediction of phosphosites.** *Genome Biol* 2007, **8**:R250.
 66. Olsen JV, Blagoev B, Gnad F, Macek B, Kumar C, Mortensen P, Mann M: **Global, in vivo, and site-specific phosphorylation dynamics in signaling networks.** *Cell* 2006, **127**:635-648.
 67. Contreras X, Barboric M, Lenasi T, Peterlin BM: **HMBA releases P-TEFb from HEXIMI1 and 7SK snRNA via PI3K/Akt and activates HIV transcription.** *PLoS Pathog* 2007, **3**:1459-1469.
 68. Chen R, Liu M, Li H, Xue Y, Ramey WN, He N, Ai N, Luo H, Zhu Y, Zhou N, Zhou Q: **PP2B and PPIalpha cooperatively disrupt 7SK snRNP to release P-TEFb for transcription in response to Ca2+ signaling.** *Genes Dev* 2008, **22**:1356-1368.
 69. Wang Y, Dow EC, Liang YY, Ramakrishnan R, Liu H, Sung TL, Lin X, Rice AP: **Phosphatase PPM1A regulates phosphorylation of Thr-186 in the Cdk9 T-loop.** *J Biol Chem* 2008, **283**:33578-33584.
 70. Zhou M, Nekhai S, Bharucha DC, Kumar A, Ge H, Price DH, Egly JM, Brady JN: **TFIIH inhibits CDK9 phosphorylation during human immunodeficiency virus type I transcription.** *J Biol Chem* 2001, **276**:44633-44640.
 71. Faulkner NE, Lane BR, Bock PJ, Markovitz DM: **Protein phosphatase 2A enhances activation of human immunodeficiency virus type I by phorbol myristate acetate.** *J Virol* 2003, **77**:2276-2281.

72. Barboric M, Zhang F, Besenica M, Plemenitas A, Peterlin BM: **Ubiquitination of Cdk9 by Skp2 facilitates optimal Tat transactivation.** *J Virol* 2005, **79**:11135-11141.
73. Kiernan RE, Emiliani S, Nakayama K, Castro A, Labbe JC, Lorca T, Nakayama K, Benkirane M: **Interaction between cyclin T1 and SCF(SKP2) targets CDK9 for ubiquitination and degradation by the proteasome.** *Mol Cell Biol* 2001, **21**:7956-7970.
74. Lau J, Lew QJ, Diribarne G, Michels AA, Dey A, Bensaude O, Lane DP, Chao SH: **Ubiquitination of HEXIM1 by HDM2.** *Cell Cycle* 2009, **8**:2247-2254.
75. Fu J, Yoon HG, Qin J, Wong J: **Regulation of P-TEFb elongation complex activity by CDK9 acetylation.** *Mol Cell Biol* 2007, **27**:4641-4651.
76. Sabo A, Lusic M, Cereseto A, Giacca M: **Acetylation of conserved lysines in the catalytic core of cyclin-dependent kinase 9 inhibits kinase activity and regulates transcription.** *Mol Cell Biol* 2008, **28**:2201-2212.
77. Cho S, Schroeder S, Kaehle K, Kwon HS, Pedal A, Herker E, Schnoelzer M, Ott M: **Acetylation of cyclin T1 regulates the equilibrium between active and inactive P-TEFb in cells.** *EMBO J* 2009, **28**:1407-1417.
78. Ott M, Schnoelzer M, Garnica J, Fischle W, Emiliani S, Rackwitz HR, Verdin E: **Acetylation of the HIV-1 Tat protein by p300 is important for its transcriptional activity.** *Curr Biol* 1999, **9**:1489-1492.
79. Tyers M, Tokiwa G, Futcher B: **Comparison of the Saccharomyces cerevisiae G1 cyclins: Cln3 may be an upstream activator of Cln1, Cln2 and other cyclins.** *EMBO J* 1993, **12**:1955-1968.
80. Yang Z, He N, Zhou Q: **Brd4 recruits P-TEFb to chromosomes at late mitosis to promote G1 gene expression and cell cycle progression.** *Mol Cell Biol* 2008, **28**:967-976.
81. Hargreaves DC, Horng T, Medzhitov R: **Control of inducible gene expression by signal-dependent transcriptional elongation.** *Cell* 2009, **138**:129-145.
82. Huang B, Yang XD, Zhou MM, Ozato K, Chen LF: **Brd4 coactivates transcriptional activation of NF-kappaB via specific binding to acetylated RelA.** *Mol Cell Biol* 2009, **29**:1375-1387.
83. Sharma M, George AA, Singh BN, Sahoo NC, Rao KV: **Regulation of transcript elongation through cooperative and ordered recruitment of cofactors.** *J Biol Chem* 2007, **282**:20887-20896.
84. De Luca A, Esposito V, Baldi A, Claudio PP, Fu Y, Caputi M, Pisano MM, Baldi F, Giordano A: **CDC2-related kinase PITALRE phosphorylates pRb exclusively on serine and is widely expressed in human tissues.** *J Cell Physiol* 1997, **172**:265-273.
85. Bettencourt-Dias M, Giet R, Sinka R, Mazumdar A, Lock WG, Balloux F, Zafiroopoulos PJ, Yamaguchi S, Winter S, Carthew RW, Cooper M, Jones D, Frenz L, Glover DM: **Genome-wide survey of protein kinases required for cell cycle progression.** *Nature* 2004, **432**:980-987.
86. Simone C, Bagella L, Bellan C, Giordano A: **Physical interaction between pRb and cdk9/cyclinT2 complex.** *Oncogene* 2002, **21**:4158-4165.
87. Radhakrishnan SK, Gartel AL: **CDK9 phosphorylates p53 on serine residues 33, 315 and 392.** *Cell Cycle* 2006, **5**:519-521.
88. Claudio PP, Cui J, Ghafouri M, Mariano C, White MK, Safak M, Sheffield JB, Giordano A, Khalili K, Amini S, Sawaya BE: **Cdk9 phosphorylates p53 on serine 392 independently of CKII.** *J Cell Physiol* 2006, **208**:602-612.
89. Kim YY, Park BJ, Kim DJ, Kim WH, Kim S, Oh KS, Lim JY, Kim J, Park C, Park SI: **Modification of serine 392 is a critical event in the regulation of p53 nuclear export and stability.** *FEBS Lett* 2004, **572**:92-98.
90. Shim EY, Walker AK, Shi Y, Blackwell TK: **CDK-9/cyclin T (P-TEFb) is required in two postinitiation pathways for transcription in the C. elegans embryo.** *Genes Dev* 2002, **16**:2135-2146.
91. Eissenberg JC, Shilatifard A, Dorokhov N, Michener DE: **Cdk9 is an essential kinase in Drosophila that is required for heat shock gene expression, histone methylation and elongation factor recruitment.** *Mol Genet Genomics* 2007, **277**:101-114.
92. Grosveld F, Rodriguez P, Meier N, Krpic S, Pourfarzad F, Papadopoulos P, Kolodziej K, Patrinos GP, Hostert A, Strouboulis J: **Isolation and characterization of hematopoietic transcription factor complexes by in vivo biotinylation tagging and mass spectrometry.** *Ann N Y Acad Sci* 2005, **1054**:55-67.
93. Meier N, Krpic S, Rodriguez P, Strouboulis J, Monti M, Krijgsvelde J, Gering M, Patient R, Hostert A, Grosveld F: **Novel binding partners of Ldb1 are required for haematopoietic development.** *Development* 2006, **133**:4913-4923.
94. Chiu YL, Cao H, Jacque JM, Stevenson M, Rana TM: **Inhibition of human immunodeficiency virus type 1 replication by RNA interference directed against human transcription elongation factor P-TEFb (CDK9/CyclinT1).** *J Virol* 2004, **78**:2517-2529.
95. Schnutgen F, De-Zolt S, Van Sloun P, Hollatz M, Floss T, Hansen J, Altschmied J, Seisenberger C, Ghyselincx NB, Ruiz P, Chambon P, Wurst W, von Melchner H: **Genomewide production of multipurpose alleles for the functional analysis of the mouse genome.** *Proc Natl Acad Sci USA* 2005, **102**:7221-7226.
96. Oven I, Brdicovka N, Kohoutek J, Vaupotic T, Narat M, Peterlin BM: **AIRE recruits P-TEFb for transcriptional elongation of target genes in medullary thymic epithelial cells.** *Mol Cell Biol* 2007, **27**:8815-8823.
97. Bellier S, Chastant S, Adenot P, Vincent M, Renard JP, Bensaude O: **Nuclear translocation and carboxyl-terminal domain phosphorylation of RNA polymerase II delineate the two phases of zygotic gene activation in mammalian embryos.** *EMBO J* 1997, **16**:6250-6262.
98. Huang F, Wagner M, Siddiqui MA: **Ablation of the CLP-1 gene leads to down-regulation of the HAND1 gene and abnormality of the left ventricle of the heart and fetal death.** *Mech Dev* 2004, **121**:559-572.
99. Batchelder C, Dunn MA, Choy B, Suh Y, Cassie C, Shim EY, Shin TH, Mello C, Seydoux G, Blackwell TK: **Transcriptional repression by the Caenorhabditis elegans germ-line protein PIE-1.** *Genes Dev* 1999, **13**:202-212.
100. Hanyu-Nakamura K, Sonobe-Nojima H, Tanigawa A, Lasko P, Nakamura A: **Drosophila Pgc protein inhibits P-TEFb recruitment to chromatin in primordial germ cells.** *Nature* 2008, **451**:730-733.
101. Zhang F, Barboric M, Blackwell TK, Peterlin BM: **A model of repression: CTD analogs and PIE-1 inhibit transcriptional elongation by P-TEFb.** *Genes Dev* 2003, **17**:748-758.
102. Jiang H, Peterlin BM: **Differential chromatin looping regulates CD4 expression in immature thymocytes.** *Mol Cell Biol* 2008, **28**:907-912.
103. Adjaye J, Huntriss J, Herwig R, BenKahla A, Brink TC, Wierling C, Hultschig C, Groth D, Yaspo ML, Picton HM, Gosden RG, Lehrach H: **Primary differentiation in the human blastocyst: comparative molecular portraits of inner cell mass and trophectoderm cells.** *Stem Cells* 2005, **23**:1514-1525.
104. Tsukamoto S, Kuma A, Murakami M, Kishi C, Yamamoto A, Mizushima N: **Autophagy is essential for preimplantation development of mouse embryos.** *Science* 2008, **321**:117-120.
105. Yu W, Ramakrishnan R, Wang Y, Chiang K, Sung TL, Rice AP: **Cyclin T1-dependent genes in activated CD4 T and macrophage cell lines appear enriched in HIV-1 co-factors.** *PLoS ONE* 2008, **3**:e3146.
106. Gurumurthy M, Tan CH, Ng R, Zeiger L, Lau J, Lee J, Dey A, Philp R, Li Q, Lim TM, Price DH, Lane DP, Chao SH: **Nucleophosmin interacts with HEXIM1 and regulates RNA polymerase II transcription.** *J Mol Biol* 2008, **378**:302-317.
107. Shimizu N, Ouchida R, Yoshikawa N, Hisada T, Watanabe H, Okamoto K, Kusuhara M, Handa H, Morimoto C, Tanaka H: **HEXIM1 forms a transcriptionally abortive complex with glucocorticoid receptor without involving 7SK RNA and positive transcription elongation factor b.** *Proc Natl Acad Sci USA* 2005, **102**:8555-8560.
108. Wittmann BM, Wang N, Montano MM: **Identification of a novel inhibitor of breast cell growth that is down-regulated by estrogens and decreased in breast tumors.** *Cancer Res* 2003, **63**:5151-5158.
109. Nakatake Y, Fukui N, Iwamoto Y, Masui S, Takahashi K, Yagi R, Yagi K, Miyazaki J, Matoba R, Ko MS, Niwa H: **Klf4 cooperates with Oct3/4 and Sox2 to activate the Lefty1 core promoter in embryonic stem cells.** *Mol Cell Biol* 2006, **26**:7772-7782.
110. Simone C, Stiegler P, Bagella L, Pucci B, Bellan C, De Falco G, De Luca A, Guanti G, Puri PL, Giordano A: **Activation of MyoD-dependent transcription by cdk9/cyclin T2.** *Oncogene* 2002, **21**:4137-4148.

111. Nojima M, Huang Y, Tyagi M, Kao HY, Fujinaga K: **The positive transcription elongation factor b is an essential cofactor for the activation of transcription by myocyte enhancer factor 2.** *J Mol Biol* 2008, **382**:275-287.
112. Wang Q, Young TM, Mathews MB, Pe'ery T: **Developmental regulators containing the I-mfa domain interact with T cyclins and Tat and modulate transcription.** *J Mol Biol* 2007, **367**:630-646.
113. Iankova I, Petersen RK, Annicotte JS, Chavey C, Hansen JB, Kratchmarova I, Sarruf D, Benkirane M, Kristiansen K, Fajas L: **Peroxisome proliferator-activated receptor gamma recruits the positive transcription elongation factor b complex to activate transcription and promote adipogenesis.** *Mol Endocrinol* 2006, **20**:1494-1505.
114. Zhu H, Doherty JR, Kuliyeve E, Mead PE: **CDK9/cyclin complexes modulate endoderm induction by direct interaction with Mix.3/mixer.** *Dev Dyn* 2009, **238**:1346-1357.
115. Elagib KE, Mihaylov IS, Delehanty LL, Bullock GC, Ouma KD, Caronia JF, Gonias SL, Goldfarb AN: **Cross-talk of GATA-1 and P-TEFb in megakaryocyte differentiation.** *Blood* 2008, **112**:4884-4894.
116. Giraud S, Hurlstone A, Avril S, Coqueret O: **Implication of BRG1 and cdk9 in the STAT3-mediated activation of the p21 waf1 gene.** *Oncogene* 2004, **23**:7391-7398.
117. Cottone G, Baldi A, Palescandolo E, Manente L, Penta R, Paggi MG, De Luca A: **Pkn is a novel partner of cyclin T2a in muscle differentiation.** *J Cell Physiol* 2006, **207**:232-237.
118. Fujita T, Ryser S, Piuz I, Schlegel W: **Up-regulation of P-TEFb by the MEK1-extracellular signal-regulated kinase signaling pathway contributes to stimulated transcription elongation of immediate early genes in neuroendocrine cells.** *Mol Cell Biol* 2008, **28**:1630-1643.
119. Kishigami S, Yoshikawa S, Castranio T, Okazaki K, Furuta Y, Mishina Y: **BMP signaling through ACVRI is required for left-right patterning in the early mouse embryo.** *Dev Biol* 2004, **276**:185-193.
120. Barboric M, Nissen RM, Kanazawa S, Jabrane-Ferrat N, Peterlin BM: **NF-kappaB binds P-TEFb to stimulate transcriptional elongation by RNA polymerase II.** *Mol Cell* 2001, **8**:327-337.
121. Hou T, Ray S, Brasier AR: **The functional role of an interleukin 6-inducible CDK9. STAT3 complex in human gamma-fibrinogen gene expression.** *J Biol Chem* 2007, **282**:37091-37102.
122. Lee DK, Duan HO, Chang C: **Androgen receptor interacts with the positive elongation factor P-TEFb and enhances the efficiency of transcriptional elongation.** *J Biol Chem* 2001, **276**:9978-9984.
123. Wittmann BM, Fujinaga K, Deng H, Ogba N, Montano MM: **The breast cell growth inhibitor, estrogen down regulated gene 1, modulates a novel functional interaction between estrogen receptor alpha and transcriptional elongation factor cyclin T1.** *Oncogene* 2005, **24**:5576-5588.
124. Tian Y, Ke S, Chen M, Sheng T: **Interactions between the aryl hydrocarbon receptor and P-TEFb. Sequential recruitment of transcription factors and differential phosphorylation of C-terminal domain of RNA polymerase II at cyplal promoter.** *J Biol Chem* 2003, **278**:44041-44048.
125. Kanazawa S, Okamoto T, Peterlin BM: **Tat competes with CIITA for the binding to P-TEFb and blocks the expression of MHC class II genes in HIV infection.** *Immunity* 2000, **12**:61-70.
126. Kohoutek J, Blazek D, Peterlin BM: **Hexim1 sequesters positive transcription elongation factor b from the class II transactivator on MHC class II promoters.** *Proc Natl Acad Sci USA* 2006, **103**:17349-17354.
127. Kanazawa S, Soucek L, Evan G, Okamoto T, Peterlin BM: **c-Myc recruits P-TEFb for transcription, cellular proliferation and apoptosis.** *Oncogene* 2003, **22**:5707-5711.
128. Guenther MG, Levine SS, Boyer LA, Jaenisch R, Young RA: **A chromatin landmark and transcription initiation at most promoters in human cells.** *Cell* 2007, **130**:77-88.
129. Muse GV, Gilchrist DA, Nechaev S, Shah R, Parker JS, Grissom SF, Zeitlinger J, Adelman K: **RNA polymerase is poised for activation across the genome.** *Nat Genet* 2007, **39**:1507-1511.
130. Zeitlinger J, Stark A, Kellis M, Hong JW, Nechaev S, Adelman K, Levine M, Young RA: **RNA polymerase stalling at developmental control genes in the Drosophila melanogaster embryo.** *Nat Genet* 2007, **39**:1512-1516.
131. Chopra VS, Hong JW, Levine M: **Regulation of Hox gene activity by transcriptional elongation in Drosophila.** *Curr Biol* 2009, **19**:688-693.
132. Sano M, Schneider MD: **Cyclin-dependent kinase-9: an RNAPII kinase at the nexus of cardiac growth and death cascades.** *Circ Res* 2004, **95**:867-876.
133. Kulkarni PA, Sano M, Schneider MD: **Phosphorylation of RNA polymerase II in cardiac hypertrophy: cell enlargement signals converge on cyclin T/Cdk9.** *Recent Prog Horm Res* 2004, **59**:125-139.
134. Sano M, Abdellatif M, Oh H, Xie M, Bagella L, Giordano A, Michael LH, DeMayo FJ, Schneider MD: **Activation and function of cyclin T-Cdk9 (positive transcription elongation factor-b) in cardiac muscle-cell hypertrophy.** *Nat Med* 2002, **8**:1310-1317.
135. Espinoza-Derout J, Wagner M, Shahmiri K, Mascareno E, Chaqour B, Siddiqui MA: **Pivotal role of cardiac lineage protein-1 (CLP-1) in transcriptional elongation factor P-TEFb complex formation in cardiac hypertrophy.** *Cardiovasc Res* 2007, **75**:129-138.
136. Stone B, Schummer M, Paley PJ, Thompson L, Stewart J, Ford M, Crawford M, Urban N, O'Brian K, Nelson BH: **Serologic analysis of ovarian tumor antigens reveals a bias toward antigens encoded on 17q.** *Int J Cancer* 2003, **104**:73-84.
137. Hess JL: **MLL: a histone methyltransferase disrupted in leukemia.** *Trends Mol Med* 2004, **10**:500-507.
138. Slany RK: **When epigenetics kills: MLL fusion proteins in leukemia.** *Hematol Oncol* 2005, **23**:1-9.
139. Bitoun E, Oliver PL, Davies KE: **The mixed-lineage leukemia fusion partner AF4 stimulates RNA polymerase II transcriptional elongation and mediates coordinated chromatin remodeling.** *Hum Mol Genet* 2007, **16**:92-106.
140. Mueller D, Bach C, Zeisig D, Garcia-Cuellar MP, Monroe S, Sreekumar A, Zhou R, Nesvizhskii A, Chinnaiyan A, Hess JL, Slany RK: **A role for the MLL fusion partner ENL in transcriptional elongation and chromatin modification.** *Blood* 2007, **110**:4445-4454.
141. Chen R, Keating MJ, Gandhi V, Plunkett W: **Transcription inhibition by flavopiridol: mechanism of chronic lymphocytic leukemia cell death.** *Blood* 2005, **106**:2513-2519.
142. Dey A, Chao SH, Lane DP: **HEXIM1 and the control of transcription elongation: from cancer and inflammation to AIDS and cardiac hypertrophy.** *Cell Cycle* 2007, **6**:1856-1863.
143. Remillieux-Leschelle N, Santamaria P, Randsholt NB: **Regulation of larval hematopoiesis in Drosophila melanogaster: a role for the multi sex combs gene.** *Genetics* 2002, **162**:1259-1274.
144. Biewenga P, Buist MR, Moerland PD, Ver Loren van Themaat E, van Kampen AH, ten Kate FJ, Baas F: **Gene expression in early stage cervical cancer.** *Gynecol Oncol* 2008, **108**:520-526.

Publish with **BioMed Central** and every scientist can read your work free of charge

"BioMed Central will be the most significant development for disseminating the results of biomedical research in our lifetime."

Sir Paul Nurse, Cancer Research UK

Your research papers will be:

- available free of charge to the entire biomedical community
- peer reviewed and published immediately upon acceptance
- cited in PubMed and archived on PubMed Central
- yours — you keep the copyright

Submit your manuscript here:
http://www.biomedcentral.com/info/publishing_adv.asp



APPENDIX 5

BLAZEK, Dalibor, **Jiri KOHOUTEK**, Koen BARTHOLOMEEUSEN, Eric JOHANSEN, Petra HULINKOVA, Zeping LUO, Peter CIMERMANCIC, Jernej ULE and B. Matija PETERLIN. The Cyclin K/Cdk12 complex maintains genomic stability via regulation of expression of DNA damage response genes. *Genes & Development*. 2011, 25(20), 2158–2172.

The Cyclin K/Cdk12 complex maintains genomic stability via regulation of expression of DNA damage response genes

Dalibor Blazek,^{1,2,9,10} Jiri Kohoutek,^{3,9} Koen Bartholomeeusen,¹ Eric Johansen,⁴ Petra Hulinkova,³ Zeping Luo,¹ Peter Cimermanic,^{5,6,7} Jernej Ule,⁸ and B. Matija Peterlin^{1,9}

¹Department of Medicine, Microbiology, and Immunology, Rosalind Russell Medical Research Center, University of California at San Francisco (UCSF), San Francisco, California 94143, USA; ²Central European Institute of Technology, Masaryk University, 62500 Brno, Czech Republic; ³Department of Toxicology, Pharmacology, and Immunotherapy, Veterinary Research Institute, 62100 Brno, Czech Republic; ⁴UCSF Sandler-Moore Mass Spectrometry Core Facility, UCSF Helen Diller Family Comprehensive Cancer Center, University of California at San Francisco (UCSF), San Francisco, California 94143, USA; ⁵Department of Bioengineering and Therapeutic Sciences, University of California at San Francisco, San Francisco, California 94158, USA; ⁶Department of Pharmaceutical Chemistry, University of California at San Francisco, San Francisco, California 94158, USA; ⁷California Institute for Quantitative Biosciences, University of California at San Francisco, San Francisco, California 94158, USA; ⁸MRC, Laboratory of Molecular Biology, Cambridge CB20QH, United Kingdom

Various cyclin-dependent kinase (Cdk) complexes have been implicated in the regulation of transcription. In this study, we identified a 70-kDa Cyclin K (CycK) that binds Cdk12 and Cdk13 to form two different complexes (CycK/Cdk12 or CycK/Cdk13) in human cells. The CycK/Cdk12 complex regulates phosphorylation of Ser2 in the C-terminal domain of RNA polymerase II and expression of a small subset of human genes, as revealed in expression microarrays. Depletion of CycK/Cdk12 results in decreased expression of predominantly long genes with high numbers of exons. The most prominent group of down-regulated genes are the DNA damage response genes, including the critical regulators of genomic stability: BRCA1 (breast and ovarian cancer type 1 susceptibility protein 1), ATR (ataxia telangiectasia and Rad3-related), FANCI, and FANCD2. We show that CycK/Cdk12, rather than CycK/Cdk13, is necessary for their expression. Nuclear run-on assays and chromatin immunoprecipitations with RNA polymerase II on the *BRCA1* and *FANCI* genes suggest a transcriptional defect in the absence of CycK/Cdk12. Consistent with these findings, cells without CycK/Cdk12 induce spontaneous DNA damage and are sensitive to a variety of DNA damage agents. We conclude that through regulation of expression of DNA damage response genes, CycK/Cdk12 protects cells from genomic instability. The essential role of CycK for organisms in vivo is further supported by the result that genetic inactivation of *CycK* in mice causes early embryonic lethality.

[*Keywords:* P-TEFb; CTD kinase; Cdk9; camptothecin; mitomycin C; γ -H2AX]

Supplemental material is available for this article.

Received May 5, 2011; revised version accepted September 12, 2011.

Eukaryotic transcription can be divided into several stages, including preinitiation complex formation and productive elongation (Sims et al. 2004; Fuda et al. 2009). For the regulation of transcription, the phosphorylation status of the C-terminal domain (CTD) of RNA polymerase II (RNAPII) is essential (Buratowski 2009; Fuda et al. 2009; Munoz et al. 2010). In humans, the CTD consists of 52 repeats of a heptapeptide, YSPTSPS, in which individual serine residues can be differentially phosphorylated (Phatnani and Greenleaf 2006; Egloff and Murphy 2008).

Phosphorylation of serine at position 2 (Ser2) is thought to be responsible for productive transcriptional elongation and synthesis of full-length mature mRNA (Peterlin and Price 2006; Bres et al. 2008). Cyclin-dependent kinase 9 (Cdk9), a subunit of positive transcription elongation factor b (P-TEFb) is considered to be the main Ser2 kinase (Chao et al. 2000); however, recent studies suggest that other Ser2 kinases exist in cells (Gomes et al. 2006; Bartkowiak et al. 2010).

Human Cyclin K (CycK), a 40-kDa and 357-amino-acid protein, was considered to be the cyclin subunit of Cdk9, together with CyclinT1 (CycT1) and CycT2 (Fu et al. 1999; Peterlin and Price 2006). It was found to be associated with RNAPII and potent CTD kinase activity (Edwards et al. 1998), and, in functional studies, it acti-

⁹These authors contributed equally to this work.

¹⁰Corresponding author.

E-mail dblazek@med.muni.cz.

Article is online at <http://www.genesdev.org/cgi/doi/10.1101/gad.16962311>.

vated transcriptional elongation (Lin et al. 2002). Cdk12 and Cdk13 are 1490- and 1512-amino-acid-long proteins, respectively, with a conserved CTD kinase domain (Ko et al. 2001; Even et al. 2006). A recent study suggested that Cdk12 in *Drosophila*, with Cdk12 and Cdk13 in mammals, is a homolog of Ctk1 in yeast (Bartkowiak et al. 2010). It also showed that *Drosophila* Cdk12 and human Cdk12 have a Ser2 kinase activity, and found *Drosophila* Cdk12 associated with CycK (Bartkowiak et al. 2010). However, many basic facts about these Cdks and their cyclin partners remain unknown or poorly understood.

DNA damage response (DDR) is an evolutionarily conserved mechanism that detects and signals the presence of DNA lesions and mediates their repair (Harper and Elledge 2007; Jackson and Bartek 2009; Ciccina and Elledge 2010). Impaired DDR leads to the accumulation of DNA lesions, which results in genomic instability and can be followed by the malignant transformation of a cell (Motoyama and Naka 2004). DNA double-stranded breaks (DSBs) and DNA interstrand cross-links (ICLs) are among the most severe DNA lesions (Harper and Elledge 2007; Bonner et al. 2008; Jackson and Bartek 2009; Moldovan and D'Andrea 2009). DDR operates through a large network of proteins; however, some proteins lie at the core of DDR mechanisms and regulate responses to several types of lesions (Matsuoka et al. 2007; Jackson and Bartek 2009; Ciccina and Elledge 2010). For example, ataxia telangiectasia and Rad3-related (ATR) kinase phosphorylates hundreds of targets and signals for DNA replication and repair (Matsuoka et al. 2007). Similarly, breast and ovarian cancer type 1 susceptibility protein 1 (BRCA1) acts on several types of DNA lesions, and its pivotal task is the maintenance of genomic stability (Huen et al. 2010). The FANCD2 and recently discovered FANCI proteins are the central players in the Fanconi anemia (FA) pathway, which repairs ICLs and protects against genomic instability (Smogorzewska et al. 2007; Moldovan and D'Andrea 2009).

In this study, we report the identification of a 70-kDa CycK that associates with Cdk12 and Cdk13 in two separate, functionally distinct complexes. We show that the CycK/Cdk12 complex protects cells from genomic instability via the regulation of expression of DDR genes.

Results

Human CycK is a 70-kDa protein with a C-terminal proline-rich region and does not associate with Cdk9

We were initially interested in potential differences among three Cdk9 complexes formed by different cyclin subunits: CycT1, CycT2, or CycK. Our attention was brought to a single band of 70-kDa protein identified by Western blotting, with an antibody directed against the N-terminal cyclin box of CycK (Fig. 1A). Although the molecular mass of the originally identified CycK protein was ~40 kDa (Edwards et al. 1998), we did not find any protein of such size in cell lysates from various cell lines tested with different CycK antibodies (Fig. 1A; data not

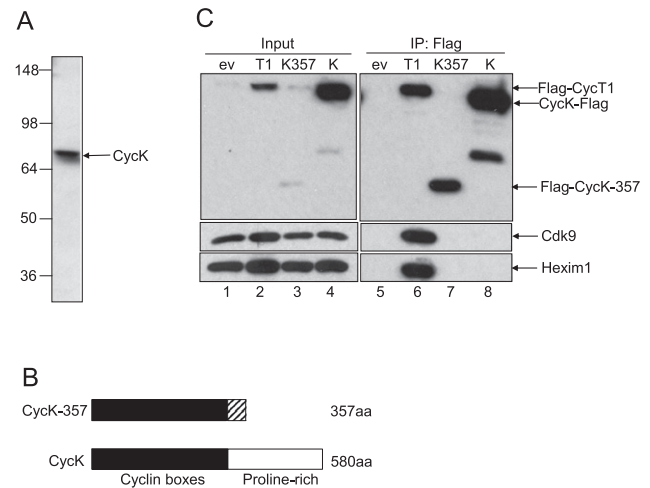


Figure 1. Identification of CycK as 70-kDa protein in cells. (A) Detection of the 70-kDa form of CycK in cell lysates from 293 cells with an antibody directed against the N-terminal cyclin box of CycK (Sigma, HPA000645). (B) Schematic representation of 40-kDa CycK-357 (Edwards et al. 1998) and the 70-kDa forms of CycK. (C) CycK and CycK-357 do not bind Cdk9. Flag-CycT1, CycK-Flag, Flag-CycK-357, and Flag-ev were immunoprecipitated from 293 cells and probed with antibodies to Cdk9 (*right middle panel*) and Hexim1 (*right bottom panel*) by Western blotting. (*Left panels*) Expression of the Cdk9, Hexim1, and Flag epitope-tagged proteins was measured with appropriate antibodies and represents 5% input of cell lysates.

shown). Interestingly, next to the published 40-kDa and 357-amino-acid human CycK protein (CycK-357) (Edwards et al. 1998), the Ensembl database (<http://www.ensembl.org>) provides information on a 580-amino-acid human CycK protein with a predicted size of ~70 kDa. This form of CycK differs from the original one in the C-terminal proline-rich region (Fig. 1B).

Next, we generated stable cell lines expressing the Flag epitope-tagged CycK (CycK-Flag), CycT1 (Flag-CycT1), 357-amino-acid form of CycK (Flag-CycK-357), and empty plasmid vector (Flag-ev) in 293 cells. Western blotting of the cell lysates probed with an antibody against CycK revealed two proteins next to each other—one belonging to the endogenous CycK, and another belonging to CycK-Flag—confirming that this form of CycK is expressed in cells (Fig. 2A, bottom panel, lane 2; data not shown). To determine whether CycK interacts with Cdk9, we immunoprecipitated CycK-Flag from cells, but there was no detectable association of CycK with Cdk9 (Fig. 1C, lane 8). Also, we could not observe any association of the Flag-CycK-357 with Cdk9 or Hexim1 (another P-TEFb-associated protein) (Fig. 1C, lane 7), while the interaction of Flag-CycT1 with Cdk9 and Hexim1 was observed (see Fig. 1C, lane 6).

To investigate which kinases are associated with CycK, we immunoprecipitated CycK-Flag stably expressed in 293 cells and identified associated proteins by high-performance liquid chromatography (HPLC) electrospray ionization mass spectrometry (ESI-MS) and tandem MS (MS/MS) techniques. This experiment provided several

Blazek et al.

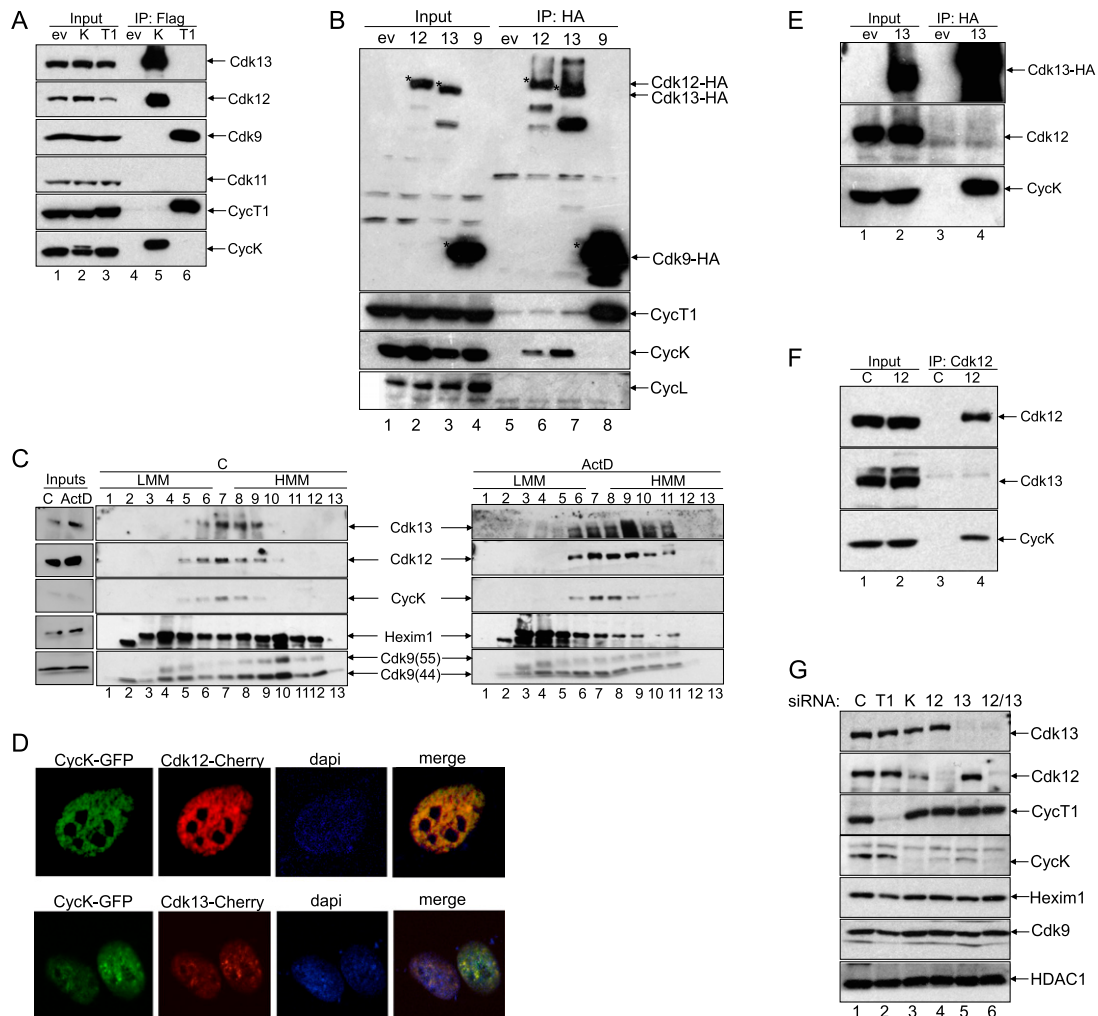


Figure 2. CycK binds Cdk12 and Cdk13 in two separate complexes. (A) CycK interacts with Cdk12 and Cdk13, but not with Cdk9. (Lanes 4–6) Flag epitope-tagged proteins or empty plasmid vector (ev) were immunoprecipitated from lysates of 293 cells, immunoprecipitations were resolved by Western blotting, and bound proteins were identified with antibodies indicated on the right. Lanes 1–3 represent 5% input of cell lysates. (B) Cdk12 and Cdk13 interact with CycK, rather than with CycL. (Lanes 5–8) HA epitope-tagged proteins or empty plasmid vector (ev) were immunoprecipitated from lysates of 293 cells, immunoprecipitations were resolved by SDS-PAGE, and bound proteins were identified with antibodies indicated on the right by Western blotting. Lanes 1–4 represent 5% input of the cell lysates to the immunoprecipitation. Stars indicate the positions of HA epitope-tagged proteins. (C) CycK, Cdk12, and Cdk13 comigrate in glycerol gradient. Lysates of 293 cells from control (left panel) or actinomycin D-treated (right panel) cells were divided into 13 fractions by a glycerol gradient centrifugation. Amounts of endogenous proteins were assessed with antibodies indicated on the inner sides of both panels by Western blotting. Numbers above and below the panels refer to the glycerol gradient fraction. (LMM) Low molecular mass; (HMM) high molecular mass; (ActD) actinomycin D; (C) control. Five percent input of lysates in glycerol gradients is presented in the panel on the left. (D) CycK colocalizes with Cdk12 and Cdk13. Expression of GFP- and Cherry-tagged proteins in HeLa cells was visualized by confocal microscopy either alone or merged as indicated above the pictures. DAPI depicts for the staining of the nucleus. (E) The CycK/Cdk13 complex is free of Cdk12. (Lanes 3,4) Cdk13-HA or HA-ev were immunoprecipitated from the lysate of 293 cells and immunoprecipitations were resolved by SDS-PAGE followed by Western blotting, where bound proteins were identified with antibodies indicated on the right. Lanes 1 and 2 represent 5% input of cell lysate. (F) The CycK/Cdk12 complex is free of Cdk13. Endogenous Cdk12 or control (C) immunoprecipitation without antibody was carried out as in E. (Lanes 3,4) Proteins identified by Western blotting are indicated on the right. Lanes 1 and 2 represent 5% input of cell lysate. (G) CycK stabilizes CycK/Cdk12 and CycK/Cdk13 complexes. Proteins were knocked down in HCT116 cells by the indicated siRNAs and lysates were separated by SDS-PAGE followed by Western blotting with the antibodies indicated on the side of the panels.

peptides corresponding to Cdk12 and Cdk13 (Supplemental Table S1A). To confirm that Cdk12 and Cdk13 interact with CycK, immunoprecipitations of endogenous Cdk12 and HA epitope-tagged Cdk13 (Cdk13-HA) proteins from 293 cells were carried out. The Coomassie blue-stained

gel provided a band of 70-kDa protein in both immunoprecipitations (data not shown). The HPLC ESI-MS and MS/MS procedure identified that peptides isolated from the 70-kDa bands represented the sequences of CycK (Supplemental Fig. S1A). For the detailed list of peptides

of CycK found in Cdk12 or Cdk13 immunoprecipitations, see Supplemental Table S1B. Notably, CycK is evolutionarily conserved, mainly in its N-terminal cyclin box and also in the newly identified C-terminal proline-rich region, suggesting an important function of this protein in the organisms (see Supplemental Fig. S1B). These experiments established the existence of the 70-kDa CycK, which is the CycK form referred to throughout the present study. In addition, we did not find any evidence for the existence of CycK-357 at the protein level even though our antibody should, in principle, recognize both forms of the protein.

CycK associates with Cdk12 and Cdk13 to form two separate complexes: CycK/Cdk12 and CycK/Cdk13

To confirm that Cdk12 and Cdk13 indeed bind CycK, we used 293 cells stably expressing CycK-Flag, Flag-CycT1, and Flag-ev. We immunoprecipitated these Flag epitope-tagged proteins and followed the binding of Cdks by Western blotting (Fig. 2A). As expected, CycK-Flag bound the endogenous Cdk12 and Cdk13 proteins but not Cdk9 and Cdk11 (Fig. 2A, lane 5), and Flag-CycT1 immunoprecipitated only endogenous Cdk9 protein, rather than Cdk11, Cdk12, or Cdk13 (Fig. 2A, lane 6). Also, the Flag epitope-tagged proteins were properly immunoprecipitated (Fig. 2A, two bottom panels, lanes 5,6).

To further examine the association of kinases with cyclins, we used 293 cells stably expressing Cdk13-HA, Cdk12-HA, and Cdk9-HA proteins and empty plasmid vector. HA epitope-tagged kinases were immunoprecipitated, and Western blots were reprobed with antibodies against CycK and CycT1 (Fig. 2B). Cdk9 associated only with CycT1 rather than with CycK (Fig. 2B, lane 8); in contrast, Cdk12 and Cdk13 associated only with CycK (Fig. 2B, lanes 6,7). Also, all HA epitope-tagged proteins were efficiently immunoprecipitated (Fig. 2B, top panel, lanes 6–8). As overexpressed CycL was also shown to be an interacting partner of Cdk12 and Cdk13 (Chen et al. 2006, 2007), we reprobed our Western blot with anti-CycL antibody. However, none of the tested kinases interacted with endogenous CycL (Fig. 2B, lanes 5–8). Coincidentally, with a recently published study (Bartkowiak et al. 2010), we also did not recover any CycL peptides in Cdk12 and Cdk13 immunoprecipitations subjected to LC-MS/MS.

To elucidate further the biochemical and functional characteristics of these new CycK kinases, cell lysates were fractionated on a 10%–30% glycerol gradient (Fig. 2C). As predicted, antibodies to CycK, Cdk12, and Cdk13 revealed significant overlap among these proteins in fractions 5–9, while Cdk9 and Hexim1 proteins were found in fractions 2–13 (Fig. 2C, left panel). Fractionation of lysates from cells treated with actinomycin D, which disrupts the large inactive complex of P-TEFb (Li et al. 2005; Yang et al. 2005), revealed almost no shift of the CycK/Cdk12 and CycK/Cdk13 complexes; in contrast, Hexim1 and Cdk9 shifted to a lower molecular mass fraction, as expected (Fig. 2C, right panel). These experiments further confirm that CycK/Cdk12 and CycK/Cdk13 form different complexes from P-TEFb in

cells. Moreover, fluorescence microscopy experiments analyzing GFP-fused CycK and Cherry-fused Cdk12 and Cdk13 proteins also support our data that CycK is a bona fide partner of these kinases, as CycK-GFP colocalized with Cdk12-Cherry and Cdk13-Cherry (Fig. 2D).

Furthermore, we were interested in determining whether CycK exists in mutually exclusive complexes with Cdk12 or Cdk13. We immunoprecipitated either Cdk13-HA or endogenous Cdk12 from 293 cells and followed the Cdk12 or Cdk13 binding, respectively, by Western blotting (Fig. 2E,F). While Cdk13 did not coimmunoprecipitate with Cdk12, CycK was efficiently recovered (Fig. 2E, lane 4). Similarly, while the endogenous Cdk12 did not immunoprecipitate Cdk13, its interaction with CycK was detected (Fig. 2F, lane 4). This experiment indicates that CycK forms two separate complexes with Cdk12 and Cdk13. Interestingly, fluorescence microscopy analysis of Cdk12-GFP and Cdk13-Cherry demonstrated colocalization between most of these two proteins; however, in certain regions, Cdk12 and Cdk13 seem to exist independently of each other (Supplemental Fig. S2A).

Taking into account that cyclin and Cdk subunits usually stabilize each other in the heterodimer complex, we explored this possibility with CycK/Cdk12 and CycK/Cdk13 (Fig. 2G). We knocked down CycT1 in cells and observed no significant change in Cdk12 and Cdk13 levels, while Cdk9 and Hexim1 levels decreased (although not completely, due to the stabilization effect of CycT2 on Cdk9) (Fig. 2G, lane 2). Knockdown of CycK led to a significant decrease of levels of Cdk12 and a slight decrease of levels of Cdk13 (Fig. 2G, lane 3). The loss of Cdk12 resulted in a significant decrease in the amount of CycK (Fig. 2G, lane 4). A similar situation occurred after Cdk13 was depleted from cells (Fig. 2G, lane 5). The knockdown of Cdk12 and Cdk13 together led to the complete loss of CycK (Fig. 2G, lane 6). Complementing these results, individual overexpression of Cdk12 or Cdk13 led to their inefficient expression; however, when coexpressed with CycK, their protein levels increased significantly, as these Cyc/Cdk complexes were stabilized (Supplemental Fig. S2B, cf. lanes 1,4 and 2,3,5,6, respectively). These experiments defined the existence of two separate complexes: CycK/Cdk12 and CycK/Cdk13.

CycK/Cdk12 can activate transcription and phosphorylate Ser2 in the CTD of RNAPII

Since Cdk12 has a kinase domain similar to Cdk9 (Malumbres et al. 2009), and work on CycK-357 indicated its role in transcription (Edwards et al. 1998; Fu et al. 1999; Lin et al. 2002), we were interested in whether the CycK/Cdk12 can also regulate transcription (Fig. 3). To begin to answer this question, we used an RNA-tethering assay (Fig. 3A) that measures transcriptional activity (Fig. 3B). Indeed, when we coexpressed the Rev-Cdk9 chimera with the SLIIB-CAT reporter plasmid, the levels of chloramphenicol acetyltransferase (CAT) activity increased >20-fold compared with when the reporter was coexpressed with the empty plasmid vector (Fig. 3B, cf. lanes 2 and 1). This increase was not detected when the kinase-

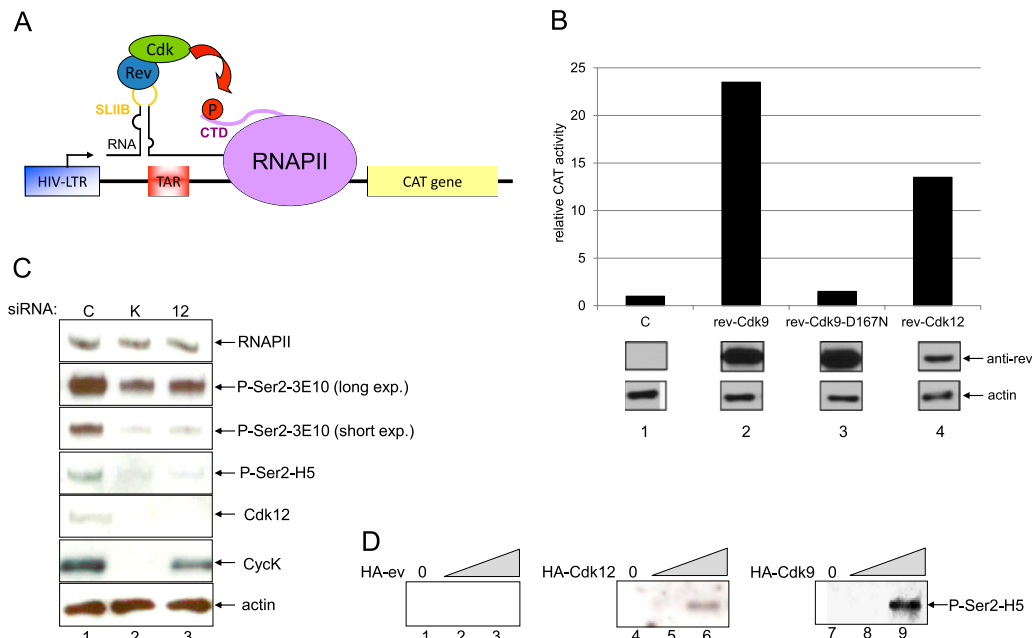


Figure 3. CycK/Cdk12 regulates transcription and phosphorylates Ser2 in the CTD of RNAPII. (A) Schematic depiction of heterologous RNA tethering assay. Plasmid reporter used to test transcription contains modified HIV-LTR promoter (blue square) followed by TAR (transactivation response RNA) (red square) with inserted stem-loop IIB (SLIIB) (yellow line in RNA) from the HIV Rev response element (RRE). Nascent RNA (black dashed line) synthesized by RNAPII (violet oval) forms a dsRNA loop with the SLIIB element. Rev-cdk fusion proteins tethered via SLIIB to paused RNAPII can release RNAPII when phosphorylate Ser2 (P) (red circle) in its CTD (violet line), which results in the transcription of CAT reporter gene (yellow square). (B) Rev-Cdk12 activates transcription from the SLIIB-CAT plasmid. The activity of the CAT reporter SLIIB-CAT coexpressed with empty plasmid vector (C) was set as 1, and bars represent relative CAT activity obtained by the cotransfection of the reporter with indicated plasmids in HeLa cells. Western blotting shows expression of Rev fusion proteins and actin. (C) Knockdown of CycK/Cdk12 decreases the global phosphorylation of Ser2 in the CTD of RNAPII. HCT116 cell were transfected with the indicated siRNAs, and the levels of proteins were followed with the indicated antibodies by Western blotting. (D) CycK/Cdk12 phosphorylates Ser2 in the GST-CTD *in vitro*. Ten nanograms of GST-CTD was incubated with increasing amounts (indicated by the triangle) of purified HA-ev, Cdk12-HA, and Cdk9-HA. The amounts of phosphorylated Ser2 (P-Ser2) were monitored by Western blotting with the indicated anti-Ser2 phospho-specific antibody.

inactive mutant of Cdk9, Rev-Cdk9D167N, was coexpressed (Fig. 3B, cf. lanes 1 and 3), confirming that an increase in CAT activity, and thus transcription, is the result of the kinase activity of Cdk9. Rev-Cdk9 and Rev-Cdk9D167N expressed equally (Fig. 3B, cf. lanes 2 and 3). Coexpression of Rev-Cdk12 with SLIIB-CAT resulted in >10-fold increase in transcriptional activity (Fig. 3B, cf. lanes 1 and 4), indicating that Cdk12 could also direct transcription. Of note, expression levels of Rev-Cdk12 were lower than Rev-Cdk9 (Fig. 3B, cf. lanes 2 and 4). Thus, CycK/Cdk12 can affect transcription.

As phosphorylation of Ser2 in the CTD of RNAPII is thought to be critical to overcome an early elongation block and for subsequent processivity of transcribing polymerases (Peterlin and Price 2006; Egloff and Murphy 2008; Buratowski 2009), we examined whether the absence of CycK complexes affects its global levels (Fig. 3C). We used 3E10 and H5 antibodies, both of which recognize phosphorylated Ser2. While 3E10 predominantly recognizes heptapeptides phosphorylated solely on the Ser2, H5 is more specific for the phosphorylated Ser2 in the context of phosphorylated neighboring Ser5 residues (Chapman et al. 2007). Indeed, CycK knockdown resulted in a significant decrease of phosphorylation of Ser2 when

evaluated by both antibodies (Fig. 3C, cf. lanes 1 and 2), and depletion of Cdk12 provided the same result (Fig. 3C, cf. lanes 1 and 3). Knockdown of Cdk13 did not change the levels of phosphorylation of Ser2 significantly (Bartkowiak et al. 2010; data not shown).

To determine whether Cdk12 is able to directly phosphorylate Ser2 in the CTD of RNAPII, we performed an *in vitro* kinase assay (Fig. 3D). For this purpose, we purified HA-ev, Cdk12-HA, and Cdk9-HA proteins and incubated them with the recombinant GST-CTD fusion protein. As predicted, addition of increasing amounts of purified Cdk12 and Cdk9 led to dose-dependent phosphorylation of GST-CTD (Fig. 3D, lanes 5,6 and 8,9 respectively). We conclude that the CycK/Cdk12 complex can phosphorylate Ser2 in the CTD domain of RNAPII and control transcription in human cells.

Depletion of CycK/Cdk12 changes the expression of a small subset of genes

Since the depletion of CycK and Cdk12 had an effect on levels of phosphorylation of Ser2 (Fig. 3C), we explored the role of the CycK/Cdk12 complex in the regulation of eukaryotic gene expression (Fig. 4). For this purpose, we

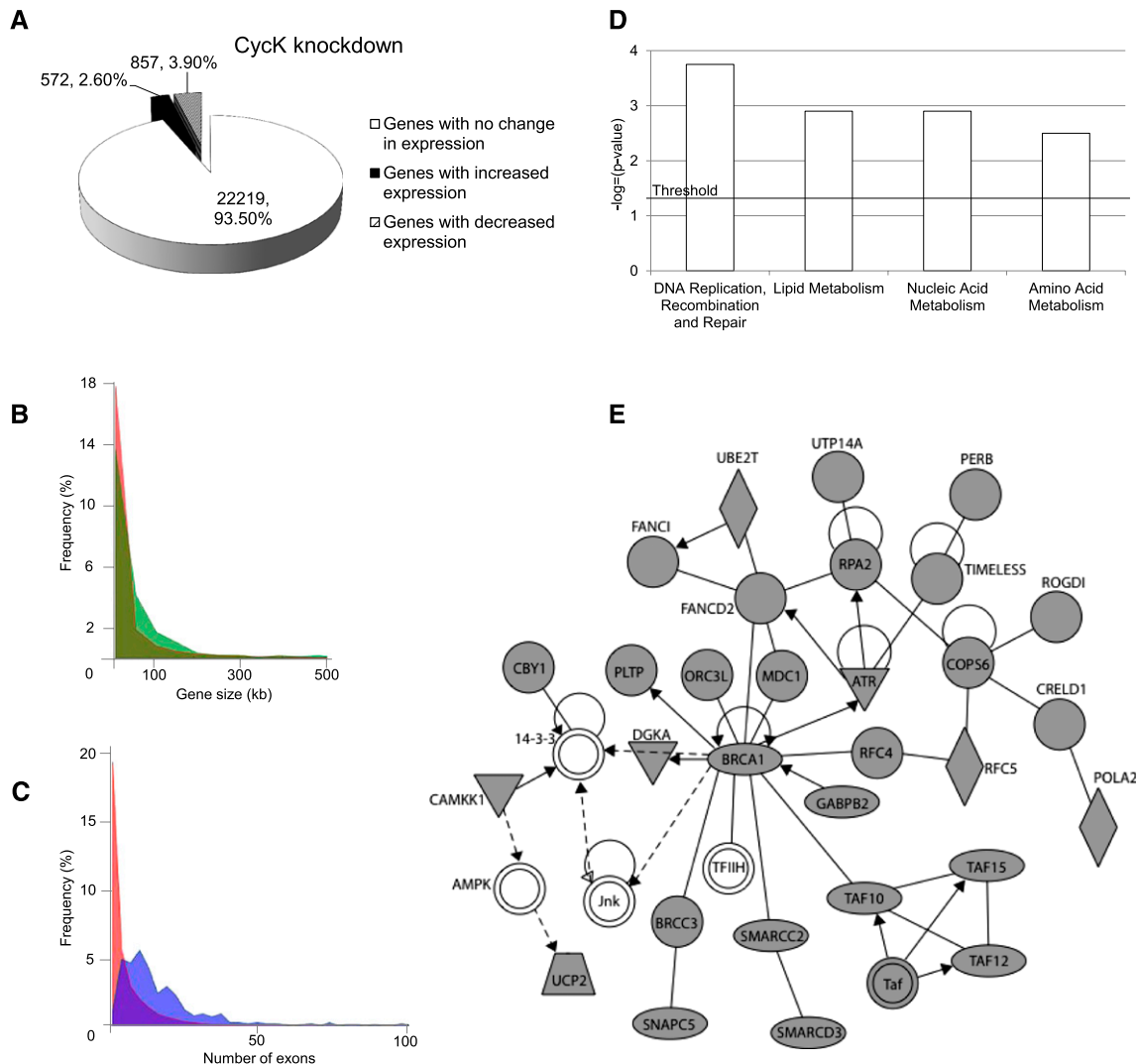


Figure 4. CycK/Cdk12 knockdown changes expression of a small subset of human genes. (A) Distribution of genes either differentially expressed or with no change of expression after CycK knockdown in HeLa cells. (B) The graph presents the distributions of the length of all human genes (red) and genes down-regulated in expression microarray in Cdk12-depleted cells (green). Human gene length data were obtained from the University of California at Santa Cruz (UCSC) Genome Browser. (C) The graph presents the distributions of the number of exons in all human genes (red) and genes down-regulated in expression microarray in Cdk12-depleted cells (blue). Data about the number of exons were obtained from the UCSC browser. (D) The classification of genes with reduced expression after CycK knockdown is based on their enrichment relative to total numbers in their specific category. Significance is expressed as $-\log(P\text{-value})$ with a threshold value of $1.3 = -\log(P = 0.05)$, and was calculated by the Ingenuity program using right-tailed Fischer's exact test. (E) Depiction of the BRCA1 network. The network was generated by the Ingenuity program from genes down-regulated after CycK knockdown. (Gray shapes) Genes down-regulated in the microarray; (white shapes) genes not found down-regulated in the microarray; (oval) transcriptional regulator; (diamond) enzyme; (triangle) kinase; (trapezoid) transporter. A solid line represents direct interaction, a dashed line indicates indirect interaction, a line without arrows indicates binding, and an arrow from protein A to protein B means that protein A acts on protein B.

employed expression microarrays in cells depleted of CycK. The data revealed that 3.9% of the genes were down-regulated, 2.6% were up-regulated, and 93.5% were unaffected (Fig. 4A). The RT-qPCR with selected genes confirmed the validity of the microarray data, as ~85% of the RT-qPCR data mirrored the microarray results (for examples of validated genes, see Supplemental Fig. S3A). Furthermore, expression microarrays in Cdk12-depleted cells showed that 2.14% of the genes were down-regulated,

0.53% were up-regulated, and 97.33% were not affected (Supplemental Fig. S3B). A high Pearson correlation coefficient ($r = 0.64$) among the genes affected in both microarrays further supports the hypothesis that CycK/Cdk12 acts as a complex (Supplemental Fig. S3C). For the numbers of commonly affected genes in both microarrays, see Supplemental Table S2. We were interested in the regulation of expression by the CycK/Cdk12 complex and focused our attention on the group of down-regulated genes.

We compared gene length-based distributions of all human genes with the down-regulated genes in Cdk12-depleted cells (Fig. 4B). The group of down-regulated genes showed higher frequencies of long genes in comparison with their representation among all human genes (Fig. 4B, cf. both distributions). Analysis of the down-regulated genes from the CycK microarray provided a similar result (Supplemental Fig. S3D). For the comparison of the representation of genes longer than 10 kb and 50 kb among all human genes and the down-regulated genes in the CycK and Cdk12 microarrays, see Supplemental Table S3. The genes with reduced expression after Cdk12 or CycK knockdowns have higher numbers of exons in comparison with all human genes (Fig. 4C; Supplemental Fig. S3E, respectively). These analyses suggest that CycK/Cdk12 directs expression of predominantly long and complex genes. The identified down-regulated genes in the CycK microarray were further classified into gene ontology groups (Fig. 4D; for information about the pathways enriched in the up-regulated genes, see Supplemental Fig. S3F). In the classification according to molecular and cellular function, DNA replication, recombination, and repair scored the highest. Network modeling using the Ingenuity Program identified as the top network the BRCA1 module. This centers the BRCA1 protein in functional connection with the key regulators of the FA pathway—proteins FANCI and FANCD2, DNA damage sensor kinase ATR, and a subunit of the SWI/SNF remodeling complex, SMARCC2—participating in the regulation of the DDR (Fig. 4E). These proteins are the key components of several DDR pathways (Motoyama and Naka 2004; Harper and Elledge 2007; Jackson and Bartek 2009; Huen et al. 2010). The complete list of DDR genes down-regulated in the microarray after depletion of CycK is in Supplemental Table S4. Most of these DDR genes were also down-regulated in the microarray from Cdk12-depleted cells (Supplemental Table S4, the Cdk12 column). These data demonstrated that depletion of CycK/Cdk12 from cells resulted in disrupted expression of a small subset of genes and in the down-regulation of predominantly long, complex genes and a group of DDR genes.

CycK/Cdk12 directs transcription of key DDR genes

Given the importance of genes from the BRCA1 module for the DDR, we focused our attention on elucidating the mechanism by which CycK/Cdk12 contributes to their expression (Fig. 5). To confirm the microarray data for these genes, we knocked down CycK, Cdk12, and Cdk13 in cells and measured mRNA levels of *BRCA1*, *ATR*, *FANCI*, *FANCD2*, and *SMARCC2* genes by RT-qPCR (Fig. 5A). Cells with depleted CycK had significantly lower levels of mRNA for all five genes in comparison with cells with control siRNA (Fig. 5A, cf. bars for control and CycK siRNAs). Depletion of Cdk12 provided the same result except for the *ATR* gene (Fig. 5A, cf. bars for control and Cdk12 siRNAs), while knockdown of Cdk13 resulted in no significant change in mRNA levels for all five genes (Fig. 5A, cf. bars for control and Cdk13 siRNA).

To determine whether knockdown of CycK, Cdk12, and Cdk13 alters the protein levels of BRCA1, ATR, FANCI, and FANCD2, we performed Western blotting (Fig. 5B). Indeed, knockdown of CycK and also of Cdk12 resulted in significantly lower levels of these proteins (Fig. 5B, lanes 2,3), in contrast to when Cdk13 was depleted (Fig. 5B, lane 4). These results suggest that CycK/Cdk12 rather than CycK/Cdk13 regulates expression of these genes and show that the CycK/Cdk12 and CycK/Cdk13 complexes have different functions in cells.

P-TEFb is considered to be the major Ser2 kinase and was implicated in the regulation of transcriptional elongation of most, if not all, protein-coding genes (Chao et al. 2000; Nechaev and Adelman 2008; Rahl et al. 2010). To determine how depletion of P-TEFb and the CycK/Cdk12 complex affects BRCA1 protein levels and global phosphorylation of Ser2, we knocked down both cyclin subunits of P-TEFb and the CycK/Cdk12 complex (Fig. 5C). As expected, loss of CycK/Cdk12 but not of P-TEFb resulted in lowered BRCA1 levels (Fig. 5C, cf. lanes 1,2 and 3,4). Although depletion of CycK/Cdk12 and P-TEFb had a similar effect on the levels of phosphorylation of Ser2 when measured by the 3E10 antibody (Fig. 5C, cf. lanes 1–3 and 4), the phosphorylation of Ser2 detected by the H5 antibody was reproducibly less affected by the loss of P-TEFb than the CycK/Cdk12 complex (Fig. 5C, cf. lanes 1,2 and 3). It can be concluded that BRCA1 expression is not sensitive to P-TEFb depletion.

To address the discrepancy between the significant drop of global phosphorylation of Ser2 (Figs. 3C, 5C) and few detected changes of gene expression (Fig. 4A; Supplemental Fig. S3B), we performed global nascent RNA analysis experiments (Lin et al. 2008) to determine whether CycK/Cdk12 affects global transcription (Fig. 5D,E). To measure nascent transcripts, cells were labeled with ³H-uridine and total RNA (processed and unprocessed) was precipitated with trichloroacetic acid. The rate of global transcription was correlated in the amount of ³H-uridine labeling of newly synthesized RNA. Knockdown of CycK/Cdk12 did not reduce the global rate of transcription in comparison with control siRNA, while treatment with the transcriptional inhibitor actinomycin D resulted in its significant decrease (Fig. 5D). Similarly, the amounts of ³H-uridine-labeled polyadenylated nascent mRNA purified with oligodT sepharose from CycK/Cdk12-depleted cells did not exhibit any decrease within the total polyadenylated RNA pool in comparison with control siRNA (Fig. 5E), suggesting that RNAPII transcription was not globally impaired in cells without CycK/Cdk12.

To examine whether the defect in the expression of DDR genes (Fig. 5A,B) after CycK/Cdk12 depletion is transcriptional, we performed nuclear run-on assays and measured the levels of nascent RNA of *BRCA1* and *FANCI* genes by RT-qPCR (Fig. 5F). As a control, we measured the levels of nascent RNA of the *TNSK1BP1* gene that was not differentially expressed in microarrays after CycK/Cdk12 knockdown. Levels of nascent RNA of *BRCA1* and *FANCI* genes were significantly reduced when CycK or Cdk12 were silenced, but not when Cdk13 or control siRNA were transfected. Importantly, treatment with actinomycin D

CycK/Cdk12 maintains genomic stability

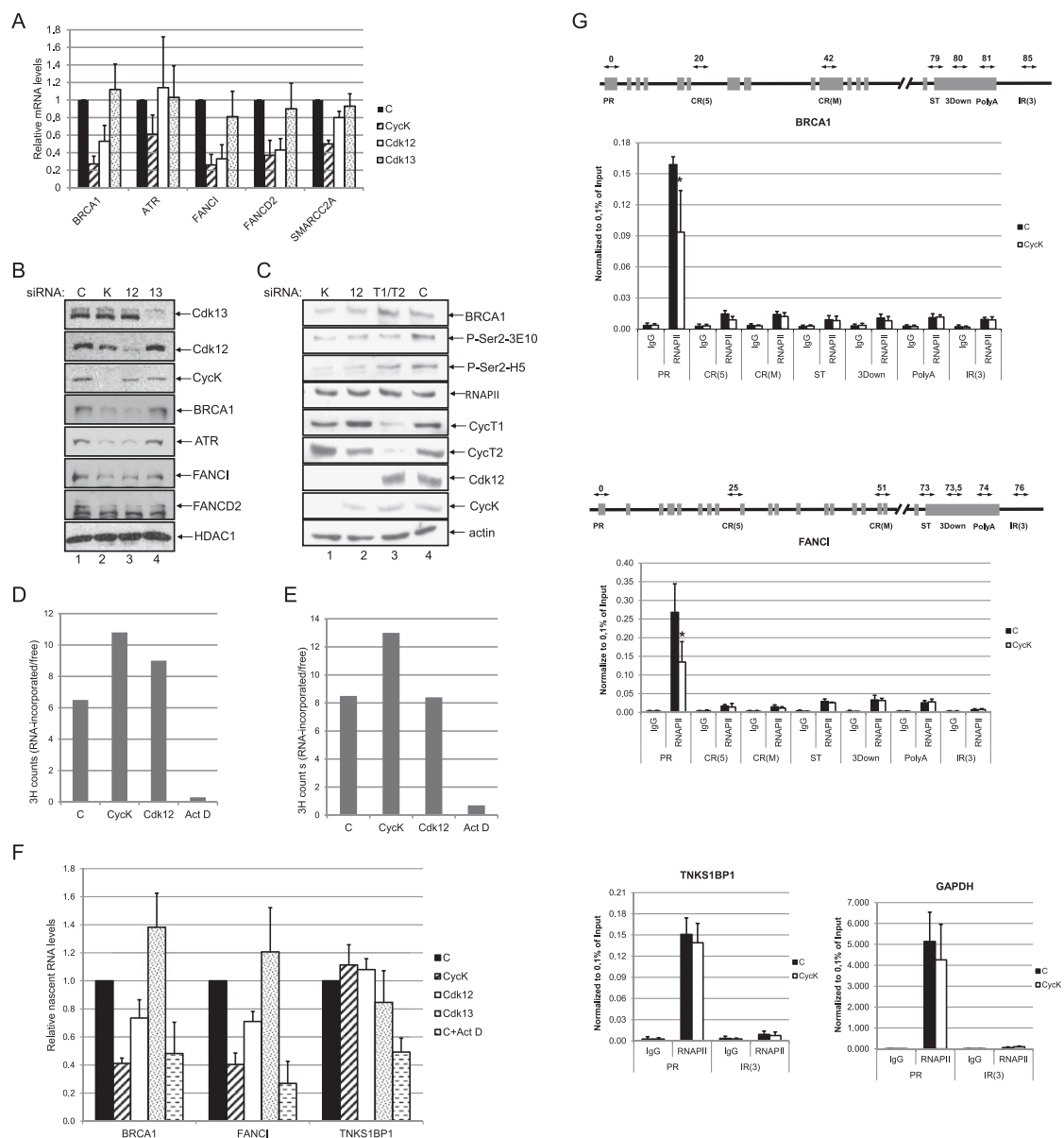


Figure 5. CycK/Cdk12 regulates transcription of key DDR genes. (A) Knockdown of CycK/Cdk12 results in decreased mRNA levels of key DDR genes in HCT116 cells. Graphs present levels of mRNA of described genes in cells transfected with control (C), CycK, Cdk12, or Cdk13 siRNA. RT-qPCR results are normalized to the mRNA of GAPDH. (B) Knockdown of CycK/Cdk12, rather than CycK/Cdk13, depletes protein levels of the DDR genes. HCT116 cells were transfected with indicated siRNAs, and protein levels were measured with indicated antibodies by Western blotting. (C) Knockdown of P-TEFb does not decrease expression of the BRCA1 gene. HCT116 cells were transfected with the depicted siRNAs, and protein levels were measured by Western blotting with the indicated antibodies. (D,E) Depletion of CycK/Cdk12 in cells does not affect the global transcription rate in nascent RNA analysis. HeLa cells were transfected with indicated siRNA for 48 h or treated with actinomycin D for 1 h. The graphs present the ratio of RNA-incorporated ^3H -uridine in precipitated nascent RNA (D) or in polyadenylated nascent mRNA (E) to free ^3H -uridine as a measure of the amount of cells. Representative experiments are shown. (F) Reduction of nascent transcript of BRCA1 and FANCI in nuclear run-on from CycK/Cdk12-depleted cells. HCT116 cells were transfected with indicated siRNA or treated with actinomycin D. Graphs show relative abundance of nascent RNA transcripts for indicated genes in nuclear run-on measured by RT-qPCR. RT-qPCR results are normalized to the nascent mRNA of GAPDH, and error bars indicate the standard deviation from three independent transfections. (G) Depletion of the CycK leads to lower levels of the RNAPII on the promoters of *BRCA1* and *FANCI* genes. ChIP analysis for the occupation of RNAPII on the regions of indicated genes after transfection with mock or CycK siRNAs. Schemes depicting *BRCA1* and *FANCI* genes show the position of ChIP primers. Their location is marked by the arrows, and the number indicates their approximate distance in kilobases from the transcription start site. (PR) Promotor; [CR(5)] 5' prime of the coding region; [CR(M)] coding region; (ST) stop codon; (3Down) region down of the stop codon; (PolyA) polyadenylation signal; [IR(3)] intergenic region. IgG corresponds to the empty beads control. Experiments are the results of four (*BRCA1* and *FANCI*) or three (*TNSK1BP1* and *GAPDH*) independent transfections of HCT116 cells, and qPCR was performed in triplicate for each transfection. Statistical significance of each pairwise comparison is depicted with a star; (*) $P < 0.05$.

decreased the abundance of nascent transcripts for both genes (Fig. 5F, cf. bars for *BRCA1* and *FANCI* genes). In contrast, the amount of nascent RNA transcript for the *TNKS1BP1* gene was not affected in CycK/Cdk12-depleted cells (Fig. 5F, cf. bars for *TNKS1BP1* gene).

To further address the transcriptional defect on these genes, we performed chromatin immunoprecipitation (ChIP) with RNAPII on *BRCA1* and *FANCI* genes (Fig. 5G). ChIPs were performed in cells transfected with mock or CycK siRNA using an antibody that recognizes RNAPII and primers covering several regions of both genes. In cells where CycK was depleted, we observed significantly less RNAPII on the promoter of *FANCI* and *BRCA1* compared with mock-transfected cells, while its levels on the other regions did not change significantly (Fig. 5G, cf. bars). Likewise, RNAPII occupancy on the ATR promoter was also reduced significantly in the absence of CycK (data not shown). In contrast, amounts of RNAPII on the promoters of CycK/Cdk12-independent genes *TNKS1BP1* and *glyceraldehyde 3-phosphate dehydrogenase (GAPDH)* were not affected significantly (Fig. 5G). These experiments established that the depletion of CycK/Cdk12 does not affect global transcriptional rates, but CycK/Cdk12 is the limiting factor that affects the transcription of a small subset of genes, including some key DDR genes.

CycK/Cdk12 is required for the maintenance of genomic stability

Since the CycK/Cdk12 complex regulates the expression of several important DDR genes, we hypothesized that it should play a broad role in the cellular response to DNA damage and in the maintenance of genomic stability (Fig. 6). We knocked down CycK in HeLa cells and measured their sensitivity to various DNA-damaging agents in survival assays (Smogorzewska et al. 2007; O'Connell et al. 2010). As a positive and negative control, we used *BRCA1* and ATR siRNAs and scrambled siRNA, respectively (Fig. 6A). Loss of CycK resulted in a strong and dose-dependent sensitivity of cells to DSB inducers etoposide and camptothecin, an effect comparable with cells with depleted *BRCA1* and ATR proteins (Fig. 6A). Knockdown of CycK also led to moderate sensitivity to mitomycin C, an agent causing DNA ICLs, indicating that CycK may play a more general role in cellular response to DNA damage (Fig. 6A). Consistent with this finding, CycK-depleted cells show increased levels of mitomycin C-induced chromosome instability (data not shown). As expected, knockdown of *Cdk12* rather than of *Cdk13* caused sensitivity of cells to etoposide, camptothecin, and mitomycin C (Supplemental Fig. S4), confirming the essential function of the CycK/Cdk12 but not the

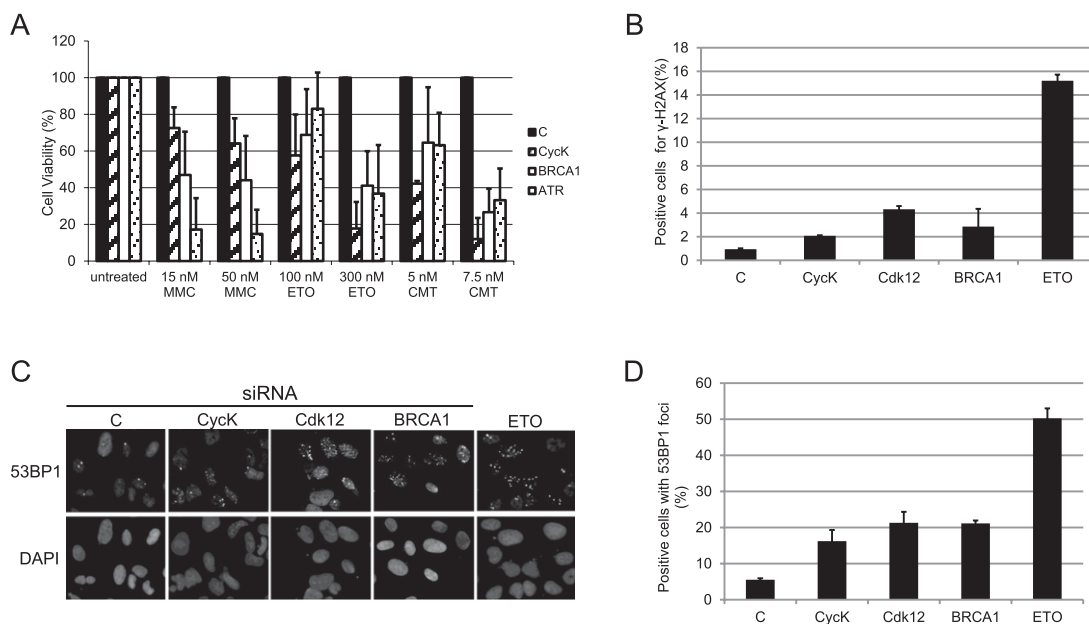


Figure 6. CycK/Cdk12 is required for the maintenance of genomic stability. (A) CycK-depleted cells are sensitive to a variety of DNA damage agents. The graphs represent the results of survival assays of HeLa cells transfected with siRNA directed to the shown targets and treated with either mitomycin C (MMC), etoposide (ETO), or camptothecin (CMT), or left untreated. Mean and standard deviation values represent the result of at least three independent transfections. Cell viability was normalized to relative growth of cells transfected with specific siRNA. (B) Depletion of CycK/Cdk12 induces DNA damage signaling. The graph shows percentage of positive cells \times median fluorescence intensity of HeLa cells transfected with indicated siRNAs or treated with etoposide (ETO), labeled with γ -H2AX antibody, and analyzed by fluorescence-activated cell counting. The results represent the values of four independent experiments. (C,D) Knockdown of the CycK/Cdk12 complex causes spontaneous DNA damage. (C) U2OS cells transfected with the indicated siRNAs or treated with etoposide (ETO) were labeled with 53BP1 antibody or DAPI, and images showing 53BP1 foci were visualized by indirect immunofluorescence. (D) Graph represents the quantification of cells positive for 53BP1 foci from three independent experiments. Cells with at least five foci were considered positive, and a minimum of 300 cells were analyzed for each condition in each experiment.

CycK/Cdk13 complex in the cellular response to exogenous DNA damage.

To address the role of the CycK/Cdk12 complex in the maintenance of genomic stability in the absence of exogenous DNA damage, we measured the levels of γ -H2AX (Fig. 6B) and the number of 53BP1 foci (Fig. 6C,D) in cells depleted with either CycK or Cdk12. Knockdown of CycK or Cdk12 in HeLa cells caused an increase in the amount of γ -H2AX protein. This increase was similar to the situation in which BRCA1 was depleted from cells and indicated that the loss of the CycK/Cdk12 complex in the absence of the exogenous DNA damage induces DNA damage signaling (Fig. 6B). Since 53BP1 accumulates at the γ -H2AX foci, it can be used as another marker of DSBs in cells (Bonner et al. 2008); we observed the formation and counted the number of 53BP1 foci in U2OS cells without CycK and Cdk12 using immunofluorescence microscopy (Fig. 6C,D). Silencing of CycK or Cdk12 resulted in the formation of strong 53BP1 foci (five or more foci per cell) in ~20% of cells, in comparison with cells treated with control siRNA, where only ~5% of cells developed the foci. BRCA1-depleted and etoposide-treated cells scored the strong foci in 20% and 50% of cells, respectively (Fig. 6C,D). Cell cycle analysis of CycK and Cdk12-depleted cells showed in-

creased numbers of accumulated cells in G2-M phase (Supplemental Fig. S5), indicating the activation of this DNA damage cell cycle checkpoint (Lobrich and Jeggo 2007) and supporting the role of CycK/Cdk12 in the maintenance of genomic stability. These data show that CycK/Cdk12 regulates resistance of cells to the exogenous DNA-damaging agents and is essential for the maintenance of genomic stability.

CycK is required for early embryonic development

To define the function of CycK in an organism, we generated a CycK knockout mouse (Fig. 7). Mouse embryonic stem cells with β -geo gene trap insertion (plasmid) within intron 1 of the *CycK* gene were obtained from the German Gene Trap Consortium and were used to generate chimeric mice (Fig. 7A). Indeed, the trap could be detected using primers to intron 1 (WTf and WTr) and β -Geo (TRf and TRr) sequences (Fig. 7B). Since translation of CycK mRNA is initiated from the second exon, the insertion of the trap vector within the first intron resulted in the loss-of-function allele of the *CycK* gene. Although our wild-type and heterozygous *CycK*^{+/-} mice were healthy, appeared normal, and reproduced well, their mating did not generate any homozygous *CycK*^{-/-} off-

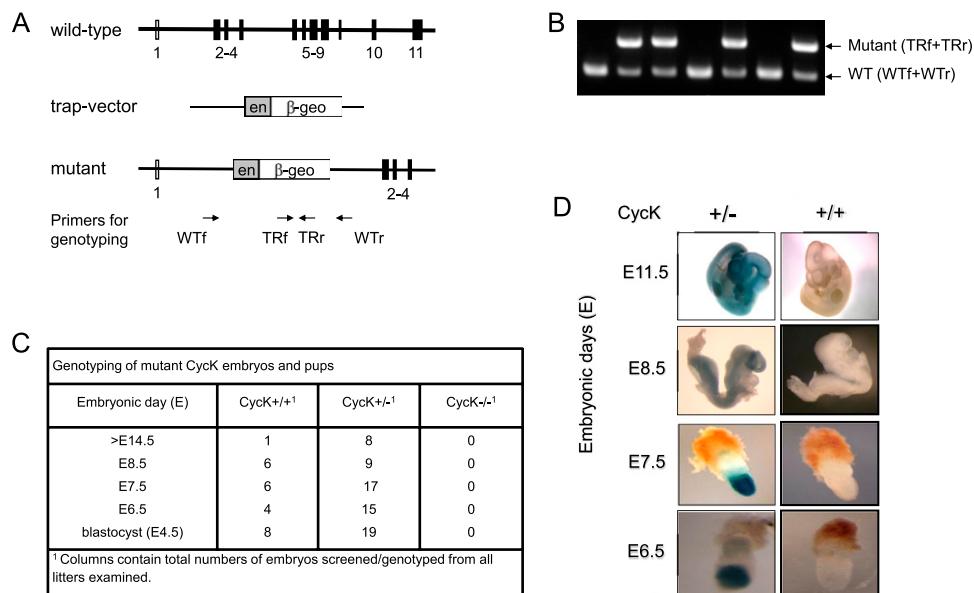


Figure 7. Genetic inactivation of *CycK* leads to early embryonic lethality. (A) Schematic representation of wild-type (WT) and trapped (TR) (*CycK*. β -geo) alleles. Wild-type and trapped loci contain one to 11 and one to four exons, respectively. The integration of the gene trap vector into intron 1 of the *CycK* gene. The insertion also led to an in-frame fusion of *CycK* with the β -geo (encoding β -galactosidase and neomycin phosphotransferase) reporter gene. Arrows below the scheme represent primer sets for wild-type (WT) (WTf and WTr) and trapped (TR) (TRf and TRr) alleles used in B. (B) Representative result of PCR genotyping. PCR genotyping of genomic DNA from the adult mouse was performed with two sets of primers—WTf+WTr and TRf+TRr (shown in A, below the mutant allele of the *CycK* gene)—to detect wild-type (lower band) and trapped (upper band) alleles of the *CycK* gene. Genomic DNA was isolated from 3-wk-old mice. For the primers used, see the Supplemental Material. (C) The table presents the results of genotyping of specified *CycK* embryos at indicated embryonic days. (D) Expression of CycK during mouse mid-gestation and early embryogenesis. LacZ staining of heterozygous embryos was used to visualize spatiotemporal expression of CycK. β -geo, which reflects transcription from the endogenous *CycK* promoter. Wild-type (+/+) and heterozygous (+/-) embryos were isolated at the given embryonic day and stained with X-Gal. CycK was expressed in forming tissues and organs in E8.5 and E11.5 embryos. Importantly, the expression of CycK was localized to the embryonic region and ectoderm in E6.5 and E7.5 embryos.

spring. To examine further the function of CycK during mouse development, embryos at embryonic day 4.5 (E4.5) (blastocyst), E6.5, E7.5, E8.5, and E14.5 were genotyped (Fig. 7C). Importantly, no CycK^{-/-} embryos were detected at any given time period, suggesting that CycK might play an important role during early mouse development (Fig. 7C).

To further explore the spatiotemporal expression of CycK in developing mouse embryos, LacZ staining was monitored in E6.5, E7.5, E8.5, and E11.5 embryos. Since its transcription is driven by the endogenous *CycK* promoter, the expression of the hybrid CycK- β -Geo protein reflects the expression of CycK (Fig. 7D). The β -Galactosidase activity, monitored by blue staining, was detected in the embryonic region (E6.5), embryonic ectoderm (E7.5), and throughout the forming embryonic tissues and organs (E8.5 and E11.5) (Fig. 7D).

Discussion

In this study, we report the identification of a 70-kDa form of the human CycK and found Cdk12 and Cdk13 as its bona fide partners. We show that depletion of the CycK/Cdk12 complex affects expression of a small subset of genes, predominantly relatively longer and complex ones. The most prominent group of genes down-regulated in the absence of CycK/Cdk12 belongs to the group of DDR genes such as *BRCA1*, *ATR*, *FANCI*, and *FANCD2*. Consistent with this finding, CycK/Cdk12-depleted cells are sensitive to a variety of DNA damage agents and develop spontaneous DNA damage signaling. We propose that the CycK/Cdk12 complex maintains genome stability via regulation of expression of DDR genes.

We were unable to identify the previously described 40-kDa CycK-357 at the level of mRNA (data not shown) or protein (Fig. 1A), and could not confirm any association of CycK (both 40-kDa or 70-kDa forms) with Cdk9 (Fig. 1C; Fu et al. 1999; Lin et al. 2002). However, it is still possible that CycK-357 exists in other cells or during certain developmental stages of an organism to play alternative functions to CycK; for example, as a splicing variant. Silencing of CycK or Cdk12 resulted in an at least 50% decrease of phosphorylation of bulk Ser2 (Figs. 3C, 5C). Of note, the yeast homolog of Cdk12, Ctk1, is considered to be the major Ser2 kinase, and Bur1 (homolog of P-TEFb) partially contributes to bulk Ser2 phosphorylation (Cho et al. 2001; Qiu et al. 2009). Since elongating RNAPII is primarily phosphorylated at Ser2, it is surprising that CycK/Cdk12 silenced cells did not show global transcription defect (Figs. 4A, 5D). We can speculate that absence of CycK/Cdk12 can transform the cell into a different pattern of CTD phosphorylation compatible with the productive transcription on most of the genes. Alternatively, modifications of neighboring residues of phosphorylated Ser2 in the CTD can render phosphorylated Ser2 undetectable by the phospho-Ser2-specific antibodies. Of note, yeast deficient of Ctk1 or phosphorylated Ser2 do not exhibit transcription defects (Cho et al. 2001; Ahn et al. 2004; Kim et al. 2010).

Data from the microarray demonstrate that a subset of genes have reduced expression in the absence of CycK.

Interestingly, these genes were the ones associated with the primary functions of the cell, such as DNA replication/repair or lipid/nucleic acid metabolism (Fig. 4D). We present evidence that CycK/Cdk12 is crucial for the expression of many DDR genes, and for at least *BRCA1*, *FANCI*, and *ATR*, the defect is transcriptional. The knock-down of CycK resulted in lower amounts of RNAPII on the promoters of *BRCA1*, *FANCI*, and *ATR* genes (Fig. 5G; data not shown), and amounts of their nascent mRNA was reduced (Fig. 5F; data not shown). Since a common feature of these and other CycK/Cdk12-regulated DDR genes is their length (tens of kilobases) and high complexity (presence of many exons), it is attractive to speculate that phosphorylation of Ser2 by Cdk12 throughout the whole transcription unit might be the major "bottleneck" for not only their efficient transcription, but also proper splicing. However ChIP experiments with phospho-Ser2-specific antibodies did not give any signal on the body of the *BRCA1* or *FANCI* genes (data not shown). We did not observe accumulation of RNAPII on the body of these genes in the absence of CycK (Fig. 5G) that would be indicative of aberrant transcriptional processing or polyadenylation (Ahn et al. 2004; Kim et al. 2010). Of note, splicing-sensitive microarrays in the absence of CycK or Cdk12 did not show any splicing defect for *BRCA1*, *FANCI*, *ATR*, *FANCD2*, and *SMARCC2* (data not shown). As long genes are expressed at low levels (Castillo-Davis et al. 2002), it might be that it is technically unfeasible to detect existing changes in the density/modification of RNAPII on the body of these genes, as their levels there are very low (Fig. 5G). Cdk12 was localized on several genes in *Drosophila* and its amounts culminated in the middle and end of transcription units, indicating that Cdk12 might indeed be responsible for the phosphorylation of Ser2 in the middle and at the 3' end of some genes (Bartkowiak et al. 2010). What might cause the drop of RNAPII levels at the promoters of these predominantly long and complex genes? Several features of the TATA-box core promoter elements were correlated to the gene length, the number and size of exons, and the strength of gene expression (Moshonov et al. 2008). The mechanistic link of these correlations is unknown, but could explain the less efficient loading of the RNAPII on the promoters of these long and complex CycK/Cdk12-dependent genes.

Transcriptional regulation of *BRCA1* and FA proteins is significant in the development and progression of cancer; however, the mechanism is largely unknown. Lower expression of *BRCA1* was identified in sporadic breast cancer patients and was correlated with poor prognosis (Thompson et al. 1995; Wilson et al. 1999). Reduced expression of *FANCD2* protein was also reported in ovarian cancer samples that showed genomic instability when exposed to mitomycin C (Pejovic et al. 2006). CycK was identified in a genome-wide shRNA screen as one of the major proteins responsible for the resistance to the DNA damage-inducing drug camptothecin (O'Connell et al. 2010). The strength of the CycK phenotype is comparable with the effect of known regulators of camptothecin resistance *ATR* and *BRCA1*, and also with newly identified protein *MMS22L*. This study also demonstrates that

MMS22L is required for the resistance to mitomycin C and the maintenance of genomic stability (O'Connell et al. 2010). Notably, we found decreased expression of MMS22L in our microarrays when CycK or Cdk12 was depleted (Supplemental Table S4). These data support our finding that CycK/Cdk12 directs DDR and maintenance of genomic stability via regulation of expression of key DDR genes.

The role of CycK/Cdk9 in the pathways that maintain genomic stability in response to replication stress has been suggested recently (Yu et al. 2010; Yu and Cortez 2011). This work found that knockdown of CycK/Cdk9 causes impaired cell cycle recovery after challenge with hydroxyurea and induction of γ -H2AX in the absence of exogenous DNA damage. However, expression defects of DDR genes were excluded as a causative mechanism, since depletion of Cdk9 did not show any changes in expression of DDR genes in their transcriptional genome-wide microarray. Consistently, transcriptional changes of DDR genes were also not observed for the kinase-dead mutant of Bur1 (yeast homolog of Cdk9) (Clausing et al. 2010). Our data show the down-regulation of many key DDR genes in expression microarrays after knockdown of CycK or Cdk12 (Supplemental Table S4). Supported by the biochemical and mechanistic characterization of CycK complexes, we suggest that CycK/Cdk12 is a master regulator of expression of DDR genes and an important player in cellular response to DNA damage. Since a recent study found Cdk12 among significantly mutated genes in ovarian cancer, evidence pointing to its significant clinical relevance is also accumulating (Bell et al. 2011).

We also analyzed mice with genetic inactivation of CycK. We observed the lethal phenotype during early mouse development. This implies that CycK/Cdk12 and/or CycK/Cdk13 kinases play a major role during embryo development, perhaps by the modulation of phosphorylation of the CTD of RNAPII during expression of the genes regulating the development. Similarly, genetic inactivation of CycT2 led to embryonic lethality during the preimplantation period (Kohoutek et al. 2009). These results emphasize the importance of CTD kinases for the regulation of early stages of development. Also, given that CycK regulates expression of DDR genes and other genes participating in the primary processes of the cell (Fig. 4D), it is not surprising that the mouse knockout has an early embryonic-lethal phenotype. Notably, BRCA1 and ATR knockout mice also have embryonically lethal phenotypes (Hakem et al. 1996; de Klein et al. 2000).

In summary, this study identifies new players in the emerging field of CTD kinases. It establishes CycK/Cdk12-directed transcription as a critical regulatory step in DDR and maintenance of genomic stability. These findings should provide a foundation for future research and potential medical therapeutic applications.

Materials and methods

Antibodies

Cdk11 and CycL antibodies were generous gifts of Dr. J. Lahti (Loyer et al. 2008); BRCA1 antibody was a generous gift from Dr.

K. Gardner (De Siervi et al. 2010). For more information on antibodies, see the Supplemental Material.

Immunoprecipitation

Cells were lysed in buffer with 150 mM NaCl, 2 mM EDTA, 1% NP-40, 10 mM Tris-HCl (pH 7.4), and protease (Sigma, P8340) and phosphatase (Sigma, P00044) inhibitor. Lysate was pre-cleared with G-Sepharose (GE Healthcare) for 1 h and then incubated with either HA- or Flag-conjugated agarose (Sigma) or a relevant antibody, followed by 1 h of incubation with the G-Sepharose. Immunoprecipitates were washed three times with 0.5 mL of the lysis buffer, eluted from the beads with SDS sample buffer, and boiled for 3 min. Immunoprecipitates were then resolved on SDS-PAGE gel followed by Western blotting.

Constructs

For cloning purposes, the cDNA sequence for Cdk12 was PCR-amplified from a eukaryotic expression vector kindly provided by Dr. J. Pines (Ko et al. 2001). The Cdk13 cDNA was PCR-amplified for subsequent cloning from a eukaryotic expression plasmid kindly provided by Dr. A.-M. Genevière (Even et al. 2006). The Rev fusion assay reporter plasmid encoding CAT and pSLIIB-CAT, and plasmids encoding Rev-Cdk9 and Rev-Cdk9D167N were described previously (Lin et al. 2002).

A CycK expression plasmid encoding the human 580-amino-acid CycK with a C-terminal Flag tag was purchased from Origene (pCMVentryCCNK, RC202024, cloned into SgfII and MluI restriction sites), here termed pCycK-Flag. Eukaryotic expression plasmids encoding C-terminally HA-tagged fusion proteins were produced by ligating Cdk12 and Cdk13 PCR-amplified cDNA into NheI and AflII restriction sites in the pcDNA3.1 HA plasmid (Invitrogen), rendering pCdk12-HA and pCdk13-HA, respectively. Expression plasmids encoding C-terminally Flag-tagged Cdk12 and Cdk13 fusion proteins were produced by oligo ligation of a 3xFlag tag sequence into the pCdk12-HA and pCdk13-HA plasmids using restriction sites AflII-XbaI and AflII-XhoI, respectively, while removing the HA tag, rendering pCdk12-Flag and pCdk13-Flag. An expression plasmid encoding a C-terminal eGFP fusion of CycK was produced by ligating PCR-amplified eGFP cDNA into the MluI and XhoI sites of pCycK-Flag, rendering pCycK-GFP. An expression plasmid encoding untagged CycK was produced by restriction linearization, fill-in, and religation of the pCycK-Flag plasmid, removing the Flag tag, rendering pCycK. Expression plasmids encoding a C-terminal mCherry fusion of Cdk12 and Cdk13 were produced by ligation of mCherry cDNA into the pCdk12-HA and pCdk13-HA plasmids using restriction sites AflII-XbaI and AflII-XhoI, respectively, rendering pCdk12-mCherry and pCdk13-mCherry. An expression plasmid encoding a C-terminal eGFP fusion of Cdk12 was produced by ligating PCR-amplified eGFP cDNA into the AflII and XbaI sites of pCdk12-HA, rendering pCdk12-GFP. Rev fusion expression plasmid for Cdk12 was produced by inserting PCR-amplified cDNA for Cdk12 into the pRev expression plasmid at restriction sites NheI and SalI, rendering pRev-Cdk12. The integrity of the DNA sequence of the expression plasmids was verified by DNA sequencing, and a 123-base-pair (bp) deletion in the N-terminal region of the Cdk13 CDS was noted in plasmids encoding HA-tagged and mCherry-tagged Cdk13. This in-frame deletion from base pair 417 to 540 removes a 44-amino-acid region that is outside the kinase domain and does not remove any known functional protein region. To prepare the eukaryotic expression plasmid expressing the N-terminally Flag-tagged short form of CycK-357, the corresponding DNA sequence was cloned into the BamHI

Blazek et al.

and XhoI restriction sites, resulting in the vector, here rendering pFlag-CycK-357. The cDNA of the human cycT1 was inserted into the pcDNA3.1Flag vector (Invitrogen) by the PCR site-directed insertion, resulting in N-terminally Flag-tagged CycT1, here rendering pFlag-CycT1.

Stable cell lines

293 cells were transfected with appropriate plasmids using Eugene6 (Roche) and were selected with either G418 (Flag-ev, Flag-CycT1, Flag-CycK-357, CycK-Flag, and HA-ev) or hygromycin (Cdk9-HA, Cdk12-HA, and Cdk13-HA). The cell lines carrying the stably integrated plasmid were expanded from the single colony.

Rev fusion assay

HeLa cells were plated in 96-well format at 10,000 cells per well. A total of 300 ng of plasmid was transfected using Eugene6 (Roche) according to the manufacturer's protocol (30 ng of pSLIB-CAT and 270 ng of Rev fusion or empty control plasmid as indicated in the text). After 48 h, CAT activity in the cell lysate was measured by a scintillation counter. The protein content of whole-cell lysate for normalization was determined using the BCA protein determination kit (Pierce).

In vitro kinase assay

HA-tagged proteins were immunoprecipitated from the established stable cell lines using HA agarose as described. Immunoprecipitations were extensively washed, and bound HA-tagged proteins were eluted with 1.5 μ g of HA peptide (Sigma, I2149). The kinase reaction was performed in the volume of 30 μ L containing 20 mM HEPES (pH 7.8), 400 μ M ATP, 1.5 μ g of BSA, phosphatase inhibitor (1:1000; Sigma), and 10 ng of GST-CTD (Proteinone, P4016-02), and with 0 μ L, 1 μ L, or 3 μ L of eluted immunoprecipitation. The kinase reaction was carried out for 30 min at 30°C and the reaction was stopped with 30 μ L of 2 \times SDS sample buffer. Reactions were resolved on SDS-PAGE gel and the amount of phosphorylation of Ser2 was measured by Western blotting with Ser2 phospho-specific antibody (Covance, H5).

Fluorescence-activated cell counting

Fluorescence cell counting after antibody staining was performed as described previously (Krutzik et al. 2011). Phosphorylated H2AX was detected using rabbit anti-phospho-H2AX (20E3, Cell Signaling) as the primary antibody and Alexa594-labeled donkey anti-rabbit (Molecular Probes Invitrogen) as the secondary antibody. Cell counting was performed using a BD-FACSAria II (Becton-Dickinson) installed with the BD-FACSDiva software, and data were subsequently analyzed using FlowJo software.

Survival assay

HeLa cells were transfected with indicated siRNAs as described in the Supplemental Material. The next day, the cells were counted and equal numbers of cells were seeded, followed by incubation with DNA-damaging agents mitomycin C, camptothecin, or etoposide for 6 d. The ratio of cells transfected with specific siRNA and control siRNA in untreated cells was used to normalize for the relative cell growth. The relative survival of control siRNA-transfected cells after treatment with a DNA damage agent was set to 100% as described previously (Smogorzewska et al. 2007; O'Connell et al. 2010).

RT-qPCR

HeLa cells were transfected with control or CycK siRNA as described in the Supplemental Material. After 72 h, cells were harvested and total RNA was isolated by the miRNeasy minikit. A total of 0.5 μ g of RNA was used for reverse transcription with the M-MLV reverse transcriptase system and random primers (Invitrogen, 28025-013 and 48190-011). Then, an equal amount of cDNA was mixed with the LightCycler 480 probes master mix (Roche Diagnostic, 4707494001). The amplifications of the samples were carried out in a final volume of 20 μ L in a reaction mixture containing 5 μ L of probes Master (Roche Diagnostics), 6 μ L of H₂O, 0.2 μ L of forward primer, 0.2 μ L of reverse primer, 0.2 μ L of probe, and 3 μ L of cDNA. The final concentration of each primer was 1.0 μ M, and the final concentration of the probe was 1 μ M. The amplifications were run on the LightCycler480II (Roche Diagnostics) using the following conditions: initial activation step for 5 min at 95°C, followed by 40–45 cycles of 15 sec at 95°C, and 35 cycles of 60 sec at 60°C and 1 sec 72°C. Changes in gene expression were calculated using the comparative threshold cycle method with GAPDH. All primers were synthesized at VBC-Biotech, and probes were used from the universal probe library (Roche Diagnostics).

Glycerol gradients

Glycerol gradients were performed as described previously (Blazek et al. 2005). The cells were treated with 1 μ g/mL actinomycin D (Sigma) for 1 h.

Expression microarray

HeLa cells were transfected with control, CycK, or Cdk12 siRNA and left for 72 h. The total RNA from cells was purified using miRNeasy minikit (Qiagen). A total of six samples were used: three from the siRNA control and three from knockdown. The high-resolution AltSplice expression microarrays were produced by Affymetrix, and the cDNA samples were prepared using GeneChip WT cDNA Synthesis and Amplification kit (Affymetrix 900673), followed by GeneChip Hybridization, Wash, and Stain kit (Affymetrix 900720) using the Affymetrix Gene Chip Fluidics Station 450, and were scanned on an Affymetrix GeneChip Scanner 3000 7G. The resulting .CEL files were first analyzed with version 3 of ASPIRE software (Konig et al. 2010). The dTrank threshold, which combines fold transcript level change (dT) and Student's *t*-test, was calculated by ASPIRE software and was applied to rank the genes. The genes were considered to be differentially expressed when dTrank was >1. To validate the changes in the expression of the genes predicted by the microarray, RT-qPCR was performed with selected down-regulated or up-regulated genes. Ingenuity program was used for the gene ontology term and network modeling.

Correlation analysis

Correlation analysis was performed with all genes with dTrank of >1 in CycK and Cdk12 microarrays (total of 1713 genes). The Pearson correlation coefficient (*r*) was calculated among their dT values in both data sets.

More Materials and Methods and a list of all primers are available in the Supplemental Material.

Acknowledgments

We thank the members of Peterlin's laboratory for their helpful discussions. We also thank Kevin Gardner, Ann-Marie Genevieve,

Jill Lahti, and Jonathon Pines for generously providing the reagents; Melis Kayikci for analyzing the microarray data; Hana Paculova for help with experiments; Audrey Low for helping with the preparation of the figures; and Matjaz Barboric, Tomas Brdicka, Jim Cleaver, Wendy Fantl, Tina Lenasi, and Yien-Ming Kuo for their comments on the manuscript. The work was supported by the following grants: from the NIH (IP50 GM082250, R01 AI049104, and R01 AI49104 ARRA supplement) to B.M.P.; from the Czech Science Foundation (P305/11/1564), SoMoPro (SRGA454), and the Ministry of Education, Youth, and Sports (ME09047) to D.B.; and from the Czech Ministry of Agriculture (MZE0002716202) and the Czech Science Foundation (301/09/1832) to J.K..

References

- Ahn SH, Kim M, Buratowski S. 2004. Phosphorylation of serine 2 within the RNA polymerase II C-terminal domain couples transcription and 3' end processing. *Mol Cell* **13**: 67–76.
- Bartkowiak B, Liu P, Phatnani HP, Fuda NJ, Cooper JJ, Price DH, Adelman K, Lis JT, Greenleaf AL. 2010. CDK12 is a transcription elongation-associated CTD kinase, the metazoan ortholog of yeast Ctk1. *Genes Dev* **24**: 2303–2316.
- Bell D, Berchuck A, Birrer M, Chien J, Cramer DW, Dao F, Dhir R, DiSaia P, Gabra H, Glenn P, et al. 2011. Integrated genomic analyses of ovarian carcinoma. *Nature* **474**: 609–615.
- Blazek D, Barboric M, Kohoutek J, Oven I, Peterlin BM. 2005. Oligomerization of HEXIM1 via 7SK snRNA and coiled-coil region directs the inhibition of P-TEFb. *Nucleic Acids Res* **33**: 7000–7010.
- Bonner WM, Redon CE, Dickey JS, Nakamura AJ, Sedelnikova OA, Solier S, Pommier Y. 2008. γ H2AX and cancer. *Nat Rev Cancer* **8**: 957–967.
- Bres V, Yoh SM, Jones KA. 2008. The multi-tasking P-TEFb complex. *Curr Opin Cell Biol* **20**: 334–340.
- Buratowski S. 2009. Progression through the RNA polymerase II CTD cycle. *Mol Cell* **36**: 541–546.
- Castillo-Davis CI, Mekhedov SL, Hartl DL, Koonin EV, Kondrashov FA. 2002. Selection for short introns in highly expressed genes. *Nat Genet* **31**: 415–418.
- Chao SH, Fujinaga K, Marion JE, Taube R, Sausville EA, Senderowicz AM, Peterlin BM, Price DH. 2000. Flavopiridol inhibits P-TEFb and blocks HIV-1 replication. *J Biol Chem* **275**: 28345–28348.
- Chapman RD, Heidemann M, Albert TK, Mailhammer R, Flatley A, Meisterernst M, Kremmer E, Eick D. 2007. Transcribing RNA polymerase II is phosphorylated at CTD residue serine-7. *Science* **318**: 1780–1782.
- Chen HH, Wang YC, Fann MJ. 2006. Identification and characterization of the CDK12/cyclin L1 complex involved in alternative splicing regulation. *Mol Cell Biol* **26**: 2736–2745.
- Chen HH, Wong YH, Genevriere AM, Fann MJ. 2007. CDK13/CDC2L5 interacts with L-type cyclins and regulates alternative splicing. *Biochem Biophys Res Commun* **354**: 735–740.
- Cho EJ, Kobar MS, Kim M, Greenblatt J, Buratowski S. 2001. Opposing effects of Ctk1 kinase and Fcp1 phosphatase at Ser 2 of the RNA polymerase II C-terminal domain. *Genes Dev* **15**: 3319–3329.
- Ciccio A, Elledge SJ. 2010. The DNA damage response: making it safe to play with knives. *Mol Cell* **40**: 179–204.
- Clausing E, Mayer A, Chanarat S, Muller B, Germann SM, Cramer P, Lisby M, Strasser K. 2010. The transcription elongation factor Bur1–Bur2 interacts with replication protein A and maintains genome stability during replication stress. *J Biol Chem* **285**: 41665–41674.
- de Klein A, Muijtjens M, van Os R, Verhoeven Y, Smit B, Carr AM, Lehmann AR, Hoeijmakers JH. 2000. Targeted disruption of the cell-cycle checkpoint gene ATR leads to early embryonic lethality in mice. *Curr Biol* **10**: 479–482.
- De Siervi A, De Luca P, Byun JS, Di LJ, Fufa T, Haggerty CM, Vazquez E, Moiola C, Longo DL, Gardner K. 2010. Transcriptional autoregulation by BRCA1. *Cancer Res* **70**: 532–542.
- Edwards MC, Wong C, Elledge SJ. 1998. Human cyclin K, a novel RNA polymerase II-associated cyclin possessing both carboxy-terminal domain kinase and Cdk-activating kinase activity. *Mol Cell Biol* **18**: 4291–4300.
- Egloff S, Murphy S. 2008. Cracking the RNA polymerase II CTD code. *Trends Genet* **24**: 280–288.
- Even Y, Durieux S, Escande ML, Lozano JC, Peaucellier G, Weil D, Genevriere AM. 2006. CDC2L5, a Cdk-like kinase with RS domain, interacts with the ASF/SF2-associated protein p32 and affects splicing in vivo. *J Cell Biochem* **99**: 890–904.
- Fu TJ, Peng J, Lee G, Price DH, Flores O. 1999. Cyclin K functions as a CDK9 regulatory subunit and participates in RNA polymerase II transcription. *J Biol Chem* **274**: 34527–34530.
- Fuda NJ, Ardehali MB, Lis JT. 2009. Defining mechanisms that regulate RNA polymerase II transcription in vivo. *Nature* **461**: 186–192.
- Gomes NP, Bjerke G, Llorente B, Szostek SA, Emerson BM, Espinosa JM. 2006. Gene-specific requirement for P-TEFb activity and RNA polymerase II phosphorylation within the p53 transcriptional program. *Genes Dev* **20**: 601–612.
- Hakem R, de la Pompa JL, Sirard C, Mo R, Woo M, Hakem A, Wakeham A, Potter J, Reitmair A, Billia F, et al. 1996. The tumor suppressor gene Brcal is required for embryonic cellular proliferation in the mouse. *Cell* **85**: 1009–1023.
- Harper JW, Elledge SJ. 2007. The DNA damage response: ten years after. *Mol Cell* **28**: 739–745.
- Huen MS, Sy SM, Chen J. 2010. BRCA1 and its toolbox for the maintenance of genome integrity. *Nat Rev Mol Cell Biol* **11**: 138–148.
- Jackson SP, Bartek J. 2009. The DNA-damage response in human biology and disease. *Nature* **461**: 1071–1078.
- Kim H, Erickson B, Luo W, Seward D, Graber JH, Pollock DD, Megee PC, Bentley DL. 2010. Gene-specific RNA polymerase II phosphorylation and the CTD code. *Nat Struct Mol Biol* **17**: 1279–1286.
- Ko TK, Kelly E, Pines J. 2001. CrkRS: a novel conserved Cdc2-related protein kinase that colocalises with SC35 speckles. *J Cell Sci* **114**: 2591–2603.
- Kohoutek J, Li Q, Blazek D, Luo Z, Jiang H, Peterlin BM. 2009. Cyclin T2 is essential for mouse embryogenesis. *Mol Cell Biol* **29**: 3280–3285.
- Konig J, Zarnack K, Rot G, Curk T, Kayikci M, Zupan B, Turner DJ, Luscombe NM, Ule J. 2010. iCLIP reveals the function of hnRNP particles in splicing at individual nucleotide resolution. *Nat Struct Mol Biol* **17**: 909–915.
- Krutzik PO, Trejo A, Schulz KR, Nolan GP. 2011. Phospho flow cytometry methods for the analysis of kinase signaling in cell lines and primary human blood samples. *Methods Mol Biol* **699**: 179–202.
- Li Q, Price JP, Byers SA, Cheng D, Peng J, Price DH. 2005. Analysis of the large inactive P-TEFb complex indicates that it contains one 7SK molecule, a dimer of HEXIM1 or HEXIM2, and two P-TEFb molecules containing Cdk9 phosphorylated at threonine 186. *J Biol Chem* **280**: 28819–28826.
- Lin X, Taube R, Fujinaga K, Peterlin BM. 2002. P-TEFb containing cyclin K and Cdk9 can activate transcription via RNA. *J Biol Chem* **277**: 16873–16878.

Blazek et al.

- Lin S, Coutinho-Mansfield G, Wang D, Pandit S, Fu XD. 2008. The splicing factor SC35 has an active role in transcriptional elongation. *Nat Struct Mol Biol* **15**: 819–826.
- Lobrich M, Jeggo PA. 2007. The impact of a negligent G2/M checkpoint on genomic instability and cancer induction. *Nat Rev Cancer* **7**: 861–869.
- Loyer P, Trembley JH, Grenet JA, Busson A, Corlu A, Zhao W, Kocak M, Kidd VJ, Lahti JM. 2008. Characterization of cyclin L1 and L2 interactions with CDK11 and splicing factors: influence of cyclin L isoforms on splice site selection. *J Biol Chem* **283**: 7721–7732.
- Malumbres M, Harlow E, Hunt T, Hunter T, Lahti JM, Manning G, Morgan DO, Tsai LH, Wolgemuth DJ. 2009. Cyclin-dependent kinases: a family portrait. *Nat Cell Biol* **11**: 1275–1276.
- Matsuoka S, Ballif BA, Smogorzewska A, McDonald ER III, Hurov KE, Luo J, Bakalarski CE, Zhao Z, Solimini N, Lerenthal Y, et al. 2007. ATM and ATR substrate analysis reveals extensive protein networks responsive to DNA damage. *Science* **316**: 1160–1166.
- Moldovan GL, D'Andrea AD. 2009. How the Fanconi anemia pathway guards the genome. *Annu Rev Genet* **43**: 223–249.
- Moshonov S, Elfakess R, Golan-Mashiach M, Sinvani H, Dikstein R. 2008. Links between core promoter and basic gene features influence gene expression. *BMC Genomics* **9**: 92. doi: 10.1186/1471-2164-9-92.
- Motoyama N, Naka K. 2004. DNA damage tumor suppressor genes and genomic instability. *Curr Opin Genet Dev* **14**: 11–16.
- Munoz MJ, de la Mata M, Kornblihtt AR. 2010. The carboxy terminal domain of RNA polymerase II and alternative splicing. *Trends Biochem Sci* **35**: 497–504.
- Nechaev S, Adelman K. 2008. Promoter-proximal Pol II: when stalling speeds things up. *Cell Cycle* **7**: 1539–1544.
- O'Connell BC, Adamson B, Lydeard JR, Sowa ME, Ciccia A, Bredemeyer AL, Schlabach M, Gygi SP, Elledge SJ, Harper JW. 2010. A genome-wide camptothecin sensitivity screen identifies a mammalian MMS22L–NFKBIL2 complex required for genomic stability. *Mol Cell* **40**: 645–657.
- Pejovic T, Yates JE, Liu HY, Hays LE, Akkari Y, Torimaru Y, Keeble W, Rathbun RK, Rodgers WH, Bale AE, et al. 2006. Cytogenetic instability in ovarian epithelial cells from women at risk of ovarian cancer. *Cancer Res* **66**: 9017–9025.
- Peterlin BM, Price DH. 2006. Controlling the elongation phase of transcription with P-TEFb. *Mol Cell* **23**: 297–305.
- Phatnani HP, Greenleaf AL. 2006. Phosphorylation and functions of the RNA polymerase II CTD. *Genes Dev* **20**: 2922–2936.
- Qiu H, Hu C, Hinnebusch AG. 2009. Phosphorylation of the Pol II CTD by KIN28 enhances BUR1/BUR2 recruitment and Ser2 CTD phosphorylation near promoters. *Mol Cell* **33**: 752–762.
- Rahl PB, Lin CY, Seila AC, Flynn RA, McCuine S, Burge CB, Sharp PA, Young RA. 2010. c-Myc regulates transcriptional pause release. *Cell* **141**: 432–445.
- Sims RJ III, Belotserkovskaya R, Reinberg D. 2004. Elongation by RNA polymerase II: the short and long of it. *Genes Dev* **18**: 2437–2468.
- Smogorzewska A, Matsuoka S, Vinciguerra P, McDonald ER III, Hurov KE, Luo J, Ballif BA, Gygi SP, Hofmann K, D'Andrea AD, et al. 2007. Identification of the FANCI protein, a mono-ubiquitinated FANCD2 paralog required for DNA repair. *Cell* **129**: 289–301.
- Thompson ME, Jensen RA, Obermiller PS, Page DL, Holt JT. 1995. Decreased expression of BRCA1 accelerates growth and is often present during sporadic breast cancer progression. *Nat Genet* **9**: 444–450.
- Wilson CA, Ramos L, Villasenor MR, Anders KH, Press MF, Clarke K, Karlan B, Chen JJ, Scully R, Livingston D, et al. 1999. Localization of human BRCA1 and its loss in high-grade, non-inherited breast carcinomas. *Nat Genet* **21**: 236–240.
- Yang Z, Yik JH, Chen R, He N, Jang MK, Ozato K, Zhou Q. 2005. Recruitment of P-TEFb for stimulation of transcriptional elongation by the bromodomain protein Brd4. *Mol Cell* **19**: 535–545.
- Yu DS, Cortez D. 2011. A role for cdk9-cyclin k in maintaining genome integrity. *Cell Cycle* **10**: 28–32.
- Yu DS, Zhao R, Hsu EL, Cayer J, Ye F, Guo Y, Shyr Y, Cortez D. 2010. Cyclin-dependent kinase 9-cyclin K functions in the replication stress response. *EMBO Rep* **11**: 876–882.



The Cyclin K/Cdk12 complex maintains genomic stability via regulation of expression of DNA damage response genes

Dalibor Blazek, Jiri Kohoutek, Koen Bartholomeeusen, et al.

Genes Dev. 2011, **25**:

Access the most recent version at doi:[10.1101/gad.16962311](https://doi.org/10.1101/gad.16962311)

Supplemental Material

<https://genesdev.cshlp.org/content/suppl/2011/10/19/25.20.2158.DC1>

References

This article cites 57 articles, 19 of which can be accessed free at:
<https://genesdev.cshlp.org/content/25/20/2158.full.html#ref-list-1>

License

Email Alerting Service

Receive free email alerts when new articles cite this article - sign up in the box at the top right corner of the article or [click here](#).



APPENDIX 6

KOHOUTEK, Jiri and Dalibor BLAZEK. Cyclin K goes with Cdk12 and Cdk13. *Cell Division*. 2012, 7, 12.

REVIEW

Open Access

Cyclin K goes with Cdk12 and Cdk13

Jiri Kohoutek¹ and Dalibor Blazek^{2*}

Abstract

The cyclin-dependent kinases (Cdks) regulate many cellular processes, including the cell cycle, neuronal development, transcription, and posttranscriptional processing. To perform their functions, Cdks bind to specific cyclin subunits to form a functional and active cyclin/Cdk complex. This review is focused on Cyclin K, which was originally considered an alternative subunit of Cdk9, and on its newly identified partners, Cdk12 and Cdk13. We briefly summarize research devoted to each of these proteins. We also discuss the proteins' functions in the regulation of gene expression via the phosphorylation of serine 2 in the C-terminal domain of RNA polymerase II, contributions to the maintenance of genome stability, and roles in the onset of human disease and embryo development.

Keywords: Transcription, Posttranscriptional processing, DNA damage, P-TEFb, Cyclin L, CTD code, CTD kinase, Phosphorylation of serine 2, BRCA1, ATR, FANCI, FANCD2

Introduction

The family of cyclin-dependent kinases (Cdks) consists of 21 proteins whose activities usually require association with a specific cyclin subunit [1]. The first Cdks to be described were regulators of the cell cycle, such as Cdk1, Cdk2, Cdk4, and Cdk6. Their corresponding cyclins are also the most well characterized [2,3]. Another group of cyclin/Cdk complexes, including cyclin H/Cdk7 and cyclin T/Cdk9, have cell cycle-independent activities. These complexes are engaged in the regulation of transcription and posttranscriptional mRNA processing via the phosphorylation of the C-terminal domain (CTD) of RNA polymerase II (RNAPII) and other transcriptional regulators, such as DRB (5,6-dichloro-1-β-D-ribofuranosylbenzimidazole) sensitivity inducing factor (DSIF) or negative elongation factor (NELF) [4]. Recent work led to the characterization of new transcription cycle-related Cdk complexes: cyclin K/cyclin-dependent kinase 12 (CycK/Cdk12) and CycK/Cdk13 [5,6]. In addition, it has been shown that CycK/Cdk12 maintains genome stability by regulating the expression of several important DNA damage response (DDR) genes [5,7]. These findings were fueled by recent developments in the field of RNAPII-mediated transcription that led to: 1) increased interest in the

elucidation of the CTD code [4,8]; 2) the finding that promoter-paused RNAPII and elongation represent important regulatory steps in gene expression [9,10]; 3) the conclusion that phosphorylation of the CTD couples transcription to other cellular processes [11-13]; and 4) clarification of the relationship between what was considered to be the only human serine 2 (Ser2) CTD kinase, Cdk9, and its two putative yeast homologs, Bur1 and Ctk1 [6,14].

A brief history of CycK, Cdk12, and Cdk13

CycK

Human CycK was first identified as a protein that can rescue the lethality caused by deletion of the G1 cyclin genes *CLN1*, *CLN2*, and *CLN3* in *Saccharomyces cerevisiae* [15]. It was discovered as a 40-kDa and 357-amino acid protein whose mRNA is ubiquitously expressed in all tested human and mouse tissues, and most abundantly in testis and ovaries [15]. Although at the time its relevant Cdk was not known, its association with RNAPII and potent *in vitro* and *in vivo* kinase activity on the CTD of RNAPII was well documented [15]. This activity was later associated with Cdk9, which was identified as a CycK interacting partner in a yeast two-hybrid assay [16]. Since then, CycK has long been considered to be an alternative cyclin subunit of Cdk9, together with CyclinT1 (CycT1) and two forms of CyclinT2, CycT2a and CycT2b [17,18]. At that time, it was also well-established that Cdk9 [in complex with

* Correspondence: dblazek@med.muni.cz

²Central European Institute of Technology (CEITEC), Masaryk University, 62500 Brno, Czech Republic

Full list of author information is available at the end of the article

cyclin subunits, also called positive transcription elongation factor b (P-TEFb)], is a crucial regulator of transcriptional elongation via phosphorylation of Ser2 in the CTD of RNAPII [19,20]. The lack of interest in further characterizing the CycK/Cdk9 complex probably stemmed from the discovery that CycT1/Cdk9 is the only Cdk9 complex able to bind HIV Tat protein and support HIV transcription [21]. This finding led the large majority of Cdk9 research to focus on the CycT1/Cdk9 complex, while CycK (and also CycT2) was only marginally studied. The only major functional difference between CycK and the CycT1/T2 subunits was noted by the Peterlin lab: when these cyclins are artificially tethered to a promoter, CycK activated transcription only via RNA recruitment, while CycT1 and CycT2 by both, RNA and DNA recruitment [22]. The first hints that CycK might not be associated with Cdk9 came from several mass spectrometry studies that failed to identify CycK associated with human Cdk9 complexes [23,24]. This was followed by the discovery that *Drosophila* Cdk12 interacts with CycK and the notion that metazoan CycK protein sequences are most similar to Ctk2, a cyclin partner of Ctk1 kinase, a yeast ortholog of Cdk12 [6]. Finally, a recent study revealed that human CycK is a 70-kDa and 580-amino acid protein with a C-terminal proline-rich region [5]. It associates with Cdk12 and Cdk13 in two separate complexes, but not with its previously identified partner, Cdk9 [5].

Cdk12 and Cdk13

Cdk12 and Cdk13 were identified in cDNA screens for cell cycle regulators. Because their cyclin partners were not yet known, they were initially named CRKRS [25] and CDC2L5 [26], respectively. They were found to be 1490- and 1512-amino acid proteins, respectively, with a conserved central CTD kinase domain and degenerate RS domains identified in their N- and C-terminal regions [25-27]. Cdk12 was shown to phosphorylate CTD of RNAPII, *in vitro* [25]. Based on the interaction of Cdk12 and Cdk13 with overexpressed Cyclin L (CycL), CycL was reported to be their regulatory subunit, and the same studies suggested a role in the regulation of alternative splicing [28,29]. However, recent studies have reported that the endogenous *Drosophila* Cdk12 and human Cdk12 and Cdk13 do not associate with CycL, but rather with CycK [5,6]. In humans (and likely in other higher organisms), CycK binds Cdk12 and Cdk13 in two separate complexes [5], while in *Drosophila*, the related paralog of Cdk13 is missing and there is only a CycK/Cdk12 complex [6,30,31].

Drosophila and human Cdk12 phosphorylate Ser2 in the CTD of RNAPII, *in vitro* and *in vivo* [5,6], and Cdk13 phosphorylates the CTD of RNAPII, *in vitro* [6]. The functional link between CycK and Cdk12 is strongly

supported by the overlapping set of genes affected by the absence of CycK or Cdk12, and their common phenotypes leading to genomic instability [5,7]. The exact function of the CycK/Cdk13 is not known.

A study by Bartkowiak et al. also showed that yeast Ctk2/Ctk1 are homologs of CycK/Cdk12 (and Cdk13 in mammals) and that yeast Bur2/Bur1 are homologs of CycT/Cdk9 [6]. Since it was assumed for many years that Cdk9 is a major Ser2 kinase in metazoan cells [20] and that its Ser2 kinase activity is split in yeast between its two homologs, Ctk1 and Bur1 [14], these findings represent an important milestone in our knowledge of Ser2 kinases and their relevant cyclin subunits. Table 1 provides a summary of information on the transcription cycle-related Cdk9s, their cyclin partners, yeast homologs, and kinase activity on the CTD of RNAPII. Of note, we could not identify the previously described 40-kDa form of CycK [15] at the level of mRNA or protein and were unable to confirm any association of the 40- or 70-kDa forms of CycK with Cdk9 in several cell lines [5]. Although we cannot completely exclude the possibility that CycK interacts with Cdk9 at certain developmental stages or under certain physiological conditions, the conclusions of several publications that consider CycK a bona fide partner of Cdk9 should be evaluated cautiously.

Domain composition of CycK, Cdk12, and Cdk13

CycK has two N-terminal cyclin boxes and a C-terminal proline-rich region (Figure 1A). The N-terminal structure of CycK resembles the classical cyclin composition, with two cyclin boxes consisting of fifteen helices that mediate binding to a Cdk partner [42]. The newly described proline-rich region [5] consists of several proline-rich motifs (PRMs; Figure 1A). Proteins with PRMs are recognized for their function in transcriptional regulation, RNA processing, and alternative splicing [43].

The domain composition of Cdk12 is comparable to Cdk13 (Figure 1B). In both proteins, CTD kinase domain is localized in the center (Figure 1B), consists of about 300 amino acids, and their sequences are highly similar (> 93%). They contain a PITAIRES motif at the conserved position of the PSTAIRES motif found in yeast *cdc2* and related kinases [25,26]. Like the *cdc2* ATP-binding region, Cdk12 and Cdk13 also have characteristic threonine and tyrosine residues at the beginning of the ATP-binding region, implicating these residues in the regulation of the kinase activity. Both kinases also have a threonine in the activation 'T-loop' that is typically phosphorylated by a Cdk-activating kinase [25] and reviewed in [44,45].

There are 20 and 17 arginine/serine rich (RS) motifs in the N-terminus of Cdk12 and Cdk13, respectively (Figure 1B). RS domains serve as docking sites for the

Table 1 Transcription-cycle related Cdks and their cyclin partners, yeast homologs, and kinase substrates

Cdk	Other nomenclature	Yeast homolog	Cyclin	Kinase activity on the CTD of RNAPII
Cdk7	CAK	Kin28	CycH [32]	Ser5 [33,34]
	CAK1			Ser7 [34,35]
	STK1			
	MO15			
Cdk8		Srb10	CycC [36]	CTD [37]
Cdk9-42 kDa	PITALRE	Bur1 [6]	CycT1 [17,18] CycT2a/b [17,18]	Ser2 [20]
Cdk9-55 kDa			CycT1 [38]	
Cdk11-46 kDa			CycL1 [39]	
			CycL2 [39]	
Cdk11-58 kDa			CycL1 [39]	
			CycL2 [39]	
			CycD3 [40]	
Cdk11-110 kDa	PITSLRE	Ste20	CycL1 [39,41]	CTD [41]
	CDC2L2		CycL2 [39,41]	
Cdk12	CRKRS CRKS	Ctk1 [6]	CycK [5,6]	Ser2 [5,6]
	CRK7			
	PITAIRE			
Cdk13	CDC2L5	Ctk1 [6]	CycK [5]	CTD [6]
	PITAIRE			

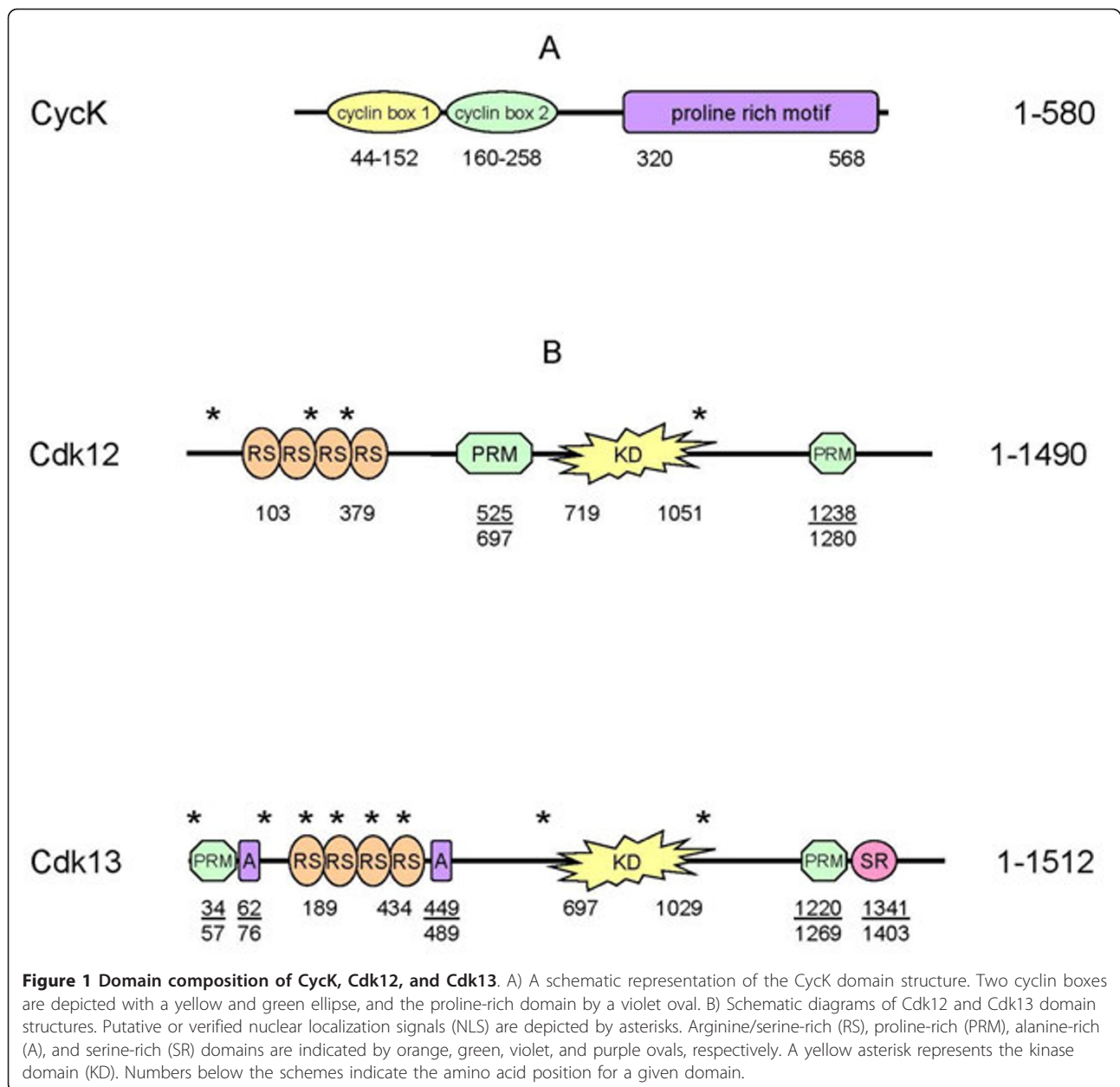
assembly of protein complexes and are found in splicing factors and regulators of splicing [46,47]. Cdk12, Cdk13, and CycK are localized in nuclear speckles, subnuclear structures enriched in mRNA splicing factors [5,25,28]. The common presence of the RS and CTD kinase domains in these Cdks makes them ideal candidates for coupling CTD phosphorylation with transcription and splicing [48-50]. Modulation of the level of Cdk12 and Cdk13 protein in cells affects the alternative splicing of certain splicing reporter constructs [27-29], and Cdk13 is suggested to be involved in the phosphorylation of ASF/SF2 and in the alternative splicing of HIV [51]. However, these studies involved the overexpression of Cdk12 and Cdk13, without their relevant cyclin partner, and thus, their direct roles in alternative splicing is still a matter of future research. Notably, using splicing-sensitive microarrays, we did not observe any significant splicing defects in several genes that are differentially expressed upon CycK or Cdk12 depletion [5].

Similar to CycK, PRMs are also present in the C-terminal region of both Cdks. In addition, Cdk12 carries one more PRM motif in its central region and Cdk13 has one in its N-terminus (Figure 1B). These PRMs may serve as binding sites for SH3, WW, or profilin domain containing proteins (reviewed in [52]). In contrast to Cdk12, the N-terminus of Cdk13 contains an alanine-rich motif with an unknown function. In addition, several putative or verified bipartite and non-bipartite

nuclear localization signals have been described for both kinases [25,28].

The CycK/Cdk12 complex phosphorylates Ser2 in the CTD of RNAPII

RNAPII directs the transcription of protein coding genes. The transcription process consists of several stages, including preinitiation complex formation, promoter clearance, pausing, productive elongation, and termination [53,54]. This transcription cycle is tightly linked to the co-transcriptional maturation of nascent transcripts, including pre-mRNA splicing and polyadenylation [13,55]. RNAPII contains an unstructured CTD with repeats of the evolutionarily conserved heptapeptide, Y₁S₂P₃T₄S₅P₆S₇, where individual serines (Ser2, 5, and 7), threonine, and tyrosine can be phosphorylated [20,56-59]. Several Cdks and phosphatases regulate the phosphorylation status of the CTD and subsequent binding of transcription and pre-mRNA processing factors [4]. Patterns of phosphorylation (and other posttranslational modifications) of the CTD form the so-called "CTD code", which defines the action of RNAPII during the transcription cycle and directs the posttranscriptional processing of nascent transcripts [8]. Our knowledge of phosphorylation events on the CTD is based mostly on data obtained with phospho-specific antibodies. However, the reactivities of the antibodies are often affected by modifications on neighboring residues and the concentration used. In



addition, they do not distinguish modifications among individual repeats [57,60,61] (*Saccharomyces cerevisiae* has 26, *Drosophila* has 44, and humans have 52 heptapeptide repeats [62]). Although these caveats should be taken into account (discussed below), some aspects of the CTD code and its role in the transcription cycle are relatively well established. Unphosphorylated RNA-Pol II is recruited to the promoter for preinitiation complex assembly. Phosphorylation of Ser5 is a hallmark of paused RNA-Pol II and is mediated by Cdk7 during initiation and promoter clearance. To release the paused RNA-Pol II and allow productive elongation, Ser2 is phosphorylated by Cdk9. In early elongation, Ser5 residues

are dephosphorylated, and the phosphorylation of Ser2 steadily accumulates to saturation while elongating on the transcription unit. Termination results in dephosphorylation of the CTD, which makes the RNA-Pol II ready for another round of re-initiation (reviewed in [4,20,56,63]). How do the CycK/Cdk12 and CycK/Cdk13 affect phosphorylation of the CTD and regulate gene expression? For a long time, Cdk9 was considered to be the major elongation-associated Ser2 kinase in mammalian cells [20]. However, recent studies have found that Cdk12 phosphorylates Ser2, *in vitro*, and depletion of Cdk12 results in at least a fifty percent decrease in Ser2 levels in human cells [5,6].

Consistently, the requirement of Cdk12 for the bulk of Ser2 phosphorylation has also been documented in *Drosophila*, where Cdk12 also localized on several active genes, *in vivo*, predominantly in the middle and at the end of the transcriptional units [6]. In contrast, knockdown of Cdk13 did not produce any observable change in the levels of phosphorylated Ser2 [5,6]; however, subtle changes in the CTD phosphorylation were observed [6]. Although Ser2 phosphorylation is thought to be an important marker for the elongation of transcripts of most protein-coding genes [64-66], depletion of CycK and Cdk12 results in the downregulation of only a small subset of genes (predominantly long and complex ones) and in no change in the rate of global transcription [5]. However, the downregulated genes, including *breast cancer type 1 (BRCA1)*, *Fanconi anemia complementation group I (FANCI)*, and *ataxia telangiectasia and rad3-related (ATR)* had less RNAPII on their promoters and reduced amounts of nascent transcripts, which is indicative of a transcriptional defect [5]. Whether the diminished expression of a subset of genes is due to aberrant co-transcriptional processing, as suggested by the length and complexity of CycK/Cdk12-dependent genes, is not currently known. Notably, no global polyadenylation defects or splicing defects in most of the down-regulated genes were detected in the absence of CycK/Cdk12 [5].

A recent finding that Cdk12/13 and Cdk9 are homologs of yeast Ctk1 and Bur1, respectively, provided further insight into the possible role of Cdk12/13 and Cdk9 kinases in metazoans [6]. In yeast, Ctk1 is responsible for most of the Ser2 phosphorylation in promoter-distal regions and most of the Ser2 phosphorylation in bulk [67-69], while Bur1 contributes to the phospho-Ser2 marks at the 5' end of genes and the residual Ser2 phosphorylation [68,69]. Conspicuously, yeast deficient in Ctk1 or phosphorylated Ser2 do not have transcriptional defects [67,70,71], a finding consistent with results in mammalian cells depleted of CycK and Cdk12 [5]. These findings are surprising considering the well-recognized role of phosphorylated Ser2 in the regulation of transcriptional elongation [64-66]. However, there are alternative explanations. For example, upon depletion of Ctk1 or Cdk12, phospho-Ser2-specific antibody does not recognize phosphorylated Ser2 due to modification(s) of neighboring residues in the CTD repeats. In a different scenario, the absence of Ctk1 or Cdk12 results in different patterns of CTD phosphorylation, compatible with productive elongation. Alternatively, the functional outcome of phosphorylated Ser2 depends on which individual CTD repeat it is positioned on and by what kinase; phospho-Ser2 marks at certain CTD repeats deposited by the P-TEFb would direct transcription, while the ones at different CTD repeats deposited by the CycK/

Cdk12 would be irrelevant for the efficiency of transcription of most genes.

It was also shown that Ser2 is phosphorylated during elongation by Ctk1, but Ctk1 is not required for association of elongation factors with transcribing RNAPII [70]. A study by Kim et al. shows that depletion of Ctk1 leads to the accumulation of RNAPII at the poly(A) sites of genes with good consensus poly(A) sites [71], while the distribution of RNAPII on other genes is unaffected [70,71]. This finding corresponds to the suggested role of Ser2 phosphorylation in 3' end RNA processing [70].

More insight into the function of phosphorylated Ser2, Cdk12, and Cdk9 was provided through the use of two phospho-Ser2-specific antibodies, H5 and 3E10. Whereas H5 predominantly recognizes phosphorylated Ser2 in the context of the phosphorylated neighboring Ser5 mark, 3E10 is more specific to CTD phosphorylated solely at Ser2 [60]. Loss of CycK/Cdk12 diminished the bulk levels of phosphorylated Ser2 to a similar extent when measured by both antibodies. The result was distinct from what was seen with depletion of Cdk9, where a smaller decline in Ser2 phosphorylation was observed when measured by the H5 antibody compared to the 3E10 antibody [5]. Interestingly, experiments in yeast suggest that there are two forms of Ser2 marks, one recognized by H5, which is dephosphorylated prior to termination, and another recognized by 3E10, which is dephosphorylated just after termination [72].

Because Ser2 phosphorylation is a marker of elongating RNAPII and is thought to be crucial for coupling transcription with mRNA-processing and other cellular processes, future studies untangling the physiological role of Cdk12 in these mechanisms promises to bring exciting findings.

CycK/Cdk12 in the maintenance of genome stability

Genome stability is crucial for the viability of the cell and prevention of diseases, such as cancer, and is mediated by the DDR pathways [73,74]. Genome stability is maintained through the cooperation of hundreds of DDR proteins that detect lesions and mediate their repair [75,76]. Reparation of each type of DNA lesion requires the action of a specific group of DDR proteins. BRCA1, ATR, ataxia telangiectasia mutated (ATM), and Fanconi anemia proteins are at the core of several DDR pathways and are crucial for the maintenance of genome stability [77-79]. Many new players and cellular processes essential for the maintenance of genome stability have been identified from recent genome-wide screens [80]. Pathways and factors with little explored connection to DDR, including those involved in transcription and mRNA processing, were identified in several screens [75,76,81]. Notably, transcriptional cyclin-dependent

kinases and phosphorylation of the CTD of RNAPII were functionally linked to the DDR and the maintenance of genome stability via regulation of transcription and mRNA processing [82,83].

Our work showed that the expression of several DDR genes, including some core players involved in the maintenance of genome stability, is CycK/Cdk12-dependent [5,7]. At least in the case of BRCA1, ATR, and FANCI, the regulation is at the transcriptional level [5,7]. In accordance with the observed down-regulation of many DDR genes, cells without CycK/Cdk12 induce spontaneous DNA damage signaling, as indicated by the accumulation of 53BP1 and γ -H2AX foci and an increased number of cells in the G2-M phase [5]. Cells depleted of CycK/Cdk12 are sensitive to various DNA damaging agents, including camptothecin, mitomycin C, and etoposide. These compounds cause various types of DNA lesions, and this sensitivity of CycK/Cdk12-depleted cells to various types of DNA damage is consistent with the proposed broad role of this complex in the DDR and maintenance of genome stability [5,7]. CycK was also independently identified in a genome-wide screen for proteins mediating resistance to the DNA damage-inducing compound, camptothecin [81].

A recent study by Yu et al. suggests a direct role for CycK in replication stress response [84]. Cells depleted of CycK show impaired cell cycle recovery after challenge with hydroxyurea and amphidicolin [84]. However, this result can also be explained by the indirect effect of decreased expression of ATR, the replication stress response regulator, in CycK-depleted cells [5]. The conclusion of this study is also complicated by the fact that CycK was studied as a cyclin subunit of Cdk9 [84]. Although a weak interaction of CycK with ATR was detected [84], the possibility of a direct role for CycK/Cdk12 in the replication stress response requires more research. Another line of evidence supporting a role for CycK in the DDR comes from the p53-dependent expression of CycK in response to treatment with adriamycin, ultraviolet, or gamma irradiation [85].

Supported by biochemical, functional, and the evolutionary characterization of the CycK/Cdk12 and CycT/Cdk9 complexes [5,6], it is conceivable that both contribute to the maintenance of genome stability, but through different mechanisms. The CycK/Cdk12 complex maintains genome stability through the regulation of DDR gene expression [5,7]. Consistently, its yeast homolog, Ctk2/Ctk1, is also implicated in the expression of several DDR genes, and a mutation in the Ctk1 kinase domain renders cells sensitive to DNA damage [83]. In contrast, the function of Cdk9 and its yeast homolog, Bur1, in the maintenance of genome integrity appears to be direct and independent of the modulation of DDR gene expression, as judged by results from genome-wide expression

arrays [84,86]. Cdk9 was found in complex with replication stress response proteins ATR, ataxia telangiectasia and Rad3-related interacting protein (ATRIP), and claspin, and, upon replication stress, it localizes to chromatin to eliminate the collapse of stalled replication forks [84]. The kinase activity of Cdk9 seems to be essential for cell cycle recovery after replication stress, but whether the CTD of RNAPII or other Cdk9-associated proteins are substrates mediating this function is unknown [84]. Notably, the 55-kDa, but not the 42-kDa isoform, of Cdk9 was shown to associate with Ku70, a protein directly involved in DNA repair by non-homologous end-joining [87]. In yeast, Bur1 binds the Rfa1 protein that protects ssDNA and maintains genome stability during DNA replications stress [86]. Deletion of the Rfa1-binding domain in Bur1 renders cells sensitive to hydroxyurea and methanesulfonate [86].

Cdk12 and Cdk13 in disease

Considering that Cdk12 regulates the expression of several cancer-related genes, such as *BRCA1* [5,7], it comes as no surprise that the dysregulation of Cdk12 has been identified in several cancers. A comprehensive genomic approach identified *Cdk12* to be one of the most frequently somatically mutated genes in high-grade serous ovarian cancer, the most fatal form of the disease [88]. Next to the nonsense and indel mutations that lead to the loss of protein function, several point mutations in the kinase domain have also been identified [88]. This finding points to the critical importance of the kinase activity of Cdk12 for the development/progression of this disease. Since about half of the ovarian cancer samples were defective in homologous recombination (HR) [88], we can speculate that the aberrant CTD kinase activity of Cdk12 results in the down-regulation of several HR regulators [5,7], and defective HR can lead to the development of the disease [7].

Several pieces of evidence also point to an important role for Cdk12 in the development of breast cancer. Notably, Cdk12 is located on chromosome 17, within the 17q21 locus that contains several candidate genes for breast cancer susceptibility [89,90], and it is co-amplified with the tyrosine kinase receptor ERBB2, a protein amplified and overexpressed in about 20% of breast tumors [91,92]. Gene fusion between *Cdk12* and *ERBB2* was also detected in gastric cancer [93]. Cdk12 is also implicated in the modification of tamoxifen sensitivity in estrogen-positive breast cancer via the modulation of the mitogen-activated protein kinase pathway [94]. Interestingly, decreased expression of BRCA1 was linked to the occurrence of sporadic breast cancer and is correlated with a poor prognosis for patients [95,96]; however, the mechanism of this aberrant expression is poorly understood.

Currently, less evidence exists for the clinical significance of Cdk13. Increased levels of Cdk13 were found in patients with refractory anemia with ringed sideroblasts, associated with marked thrombocytosis, a disease caused by ineffective hematopoiesis [97]. Another report demonstrates that Cdk13 is necessary for megakaryocyte development [98]. It has been suggested that Cdk13 affects the splicing of HIV and might act as its restriction factor [51] and that CycK inhibits HIV expression by interfering with CycT1/Cdk9 complex formation in a Nef-dependent manner [99].

Evidence is accumulating that the aberrant phosphorylation of CTD correlates with the onset and progression of many diseases (for example, cardiac hypertrophy [100], leukemia [101-103], and HIV [20,104,105]). Thus, the identification of Cdk12, along with Cdk9, as the major Ser2 kinases, makes these attractive candidate targets for the development of small chemical inhibitors as therapeutic agents. At present, approximately 30 compounds are known to inhibit Ser2 phosphorylation in the CTD [106]. Among them, DRB and flavopiridol are mostly used in research studies to inhibit Cdk9. It will be of great interest to validate the ability of these compounds to inhibit the Ser2 kinase activity of Cdk12 and to compare their effects with the inhibition of Cdk9. So far, it has been suggested that flavopiridol, the most specific inhibitor of Cdk9 [64,107], does not inhibit Cdk12 and Cdk13 in concentrations sufficient for the inhibition of Cdk9 [63].

CycK in development

CycK complexes play a crucial role in embryo development, as genetic inactivation of *CycK* in mice leads to a lethal phenotype at the stage of the morula-blastocyst transition [5]. However, currently we can only speculate about the specific function of the CycK complexes in embryo development. It is possible that CycK complexes, through regulating phosphorylation of the CTD of RNAPII, direct the expression of genes important for the transition of individual developmental stages. Although, no aberrant expression of genes known to be involved directly in development was detected when CycK or Cdk12 were depleted in human cell lines [5], more physiologically relevant experiments in CycK knock-out mouse embryonic stem cells could better address this question. Genetic inactivation of other cyclin/Cdk complexes involved in CTD phosphorylation results in an embryonic lethal phenotype. For example, inactivation of *CycT2* leads to the death of embryos at 4-cell stage and depletion of *CycT2* in mouse embryonic stem cells affects the expression of *Lefty1* and *Lefty2*, important regulators of early development [108]. Cdk8 was shown to be essential for preimplantation mouse development, perhaps by affecting the transcriptional repression of genes critical for an early cell fate

determination [109]. Dysregulated expression of genes responsible for DDR and the regulation of basic processes in the cell could be another reason for the embryonic lethal phenotype of the CycK knock out mice [5]. In support of this hypothesis, knock out of some members of the DDR pathways, such as *ATR* [110,111] and *BRCA1* [112], also lead to early embryonic lethality in mice. The monitoring of CycK expression in embryos by the activity of the *beta-galactosidase* gene under the control of an endogenous *CycK* promoter revealed that CycK is globally expressed in embryos at different embryonic stages [5]. This observation correlates with the proposed function of CycK in early embryo development. Interestingly, the most distinct signal was observed in the formation of neural tube and brain structures at embryonic day 8.5 [5], suggesting an important role for CycK in the process of neurogenesis. In agreement with this observation, CycK was identified as one of the factors necessary for the development of nervous system in *Drosophila* [113]. A study performed in *Xenopus laevis* showed that recruitment of CycK and CycT2 has different effects on the endoderm-inducing activity of the homeodomain protein, Mix.3 [114].

Perspective

Although research of CycK, Cdk12, and Cdk13 is at an early stage, recent studies have already uncovered several pieces of evidence of these proteins' significant medical relevance. In the next few years, we should learn more about these proteins' roles in regulation of transcription, posttranscriptional mRNA processing, and other CTD RNAPII-regulated cellular functions. These studies should reveal more about the function of these proteins in cellular processes, human disease, and embryonic development.

Acknowledgements

We wish to thank Koen Bartholomeeusen and Tomas Brdicka for their helpful comments on the manuscript. D.B. is supported by the following grants from the Czech Science Foundation (P305/11/1564), SoMoPro (SRGA454), the Ministry of Education, Youth, and Sports (ME09047) and by the project "CEITEC - Central European Institute of Technology" (CZ.1.05/1.1.00/02.0068) and J.K. by the grant from Ministry of Agriculture (MZE0002716202).

Author details

¹Department of Toxicology, Pharmacology and Immunotherapy, Veterinary Research Institute, Hudcova 70, 62100 Brno, Czech Republic. ²Central European Institute of Technology (CEITEC), Masaryk University, 62500 Brno, Czech Republic.

Authors' contributions

Both J.K. and D.B. contributed to writing this article. Both authors read and approved the final manuscript.

Competing interests

The authors declare that they have no competing interests.

Received: 25 March 2012 Accepted: 18 April 2012

Published: 18 April 2012

References

- Malumbres M, Harlow E, Hunt T, Hunter T, Lahti JM, Manning G, Morgan DO, Tsai LH, Wolgemuth DJ: **Cyclin-dependent kinases: a family portrait.** *Nat Cell Biol* 2009, **11**(11):1275-1276.
- Satyanarayana A, Kaldis P: **Mammalian cell-cycle regulation: several Cdks, numerous cyclins and diverse compensatory mechanisms.** *Oncogene* 2009, **28**(33):2925-2939.
- Malumbres M, Barbacid M: **Cell cycle, CDKs and cancer: a changing paradigm.** *Nat Rev Cancer* 2009, **9**(3):153-166.
- Buratowski S: **Progression through the RNA polymerase II CTD cycle.** *Mol Cell* 2009, **36**(4):541-546.
- Blazek D, Kohoutek J, Bartholomeeusen K, Johansen E, Hulinkova P, Luo Z, Cimermancic P, Ule J, Peterlin BM: **The Cyclin K/Cdk12 complex maintains genomic stability via regulation of expression of DNA damage response genes.** *Genes Dev* 2011, **25**(20):2158-2172.
- Bartkowiak B, Liu P, Phatnani HP, Fuda NJ, Cooper JJ, Price DH, Adelman K, Lis JT, Greenleaf AL: **CDK12 is a transcription elongation-associated CTD kinase, the metazoan ortholog of yeast Ctk1.** *Genes Dev* 2010, **24**(20):2303-2316.
- Blazek D: **The cyclin K/Cdk12 complex: An emerging new player in the maintenance of genome stability.** *Cell Cycle* 2012, **11**(6):1049-1050.
- Buratowski S: **The CTD code.** *Nat Struct Biol* 2003, **10**(9):679-680.
- Zeitlinger J, Stark A, Kellis M, Hong JW, Nechaev S, Adelman K, Levine M, Young RA: **RNA polymerase stalling at developmental control genes in the *Drosophila melanogaster* embryo.** *Nat Genet* 2007, **39**(12):1512-1516.
- Muse GW, Gilchrist DA, Nechaev S, Shah R, Parker JS, Grissom SF, Zeitlinger J, Adelman K: **RNA polymerase is poised for activation across the genome.** *Nat Genet* 2007, **39**(12):1507-1511.
- Pandit S, Wang D, Fu XD: **Functional integration of transcriptional and RNA processing machineries.** *Curr Opin Cell Biol* 2008, **20**(3):260-265.
- Perales R, Bentley D: **"Cotranscriptionality": the transcription elongation complex as a nexus for nuclear transactions.** *Mol Cell* 2009, **36**(2):178-191.
- Moore MJ, Proudfoot NJ: **Pre-mRNA processing reaches back to transcription and ahead to translation.** *Cell* 2009, **136**(4):688-700.
- Wood A, Shilatifard A: **Bur1/Bur2 and the Ctk complex in yeast: the split personality of mammalian P-TEFb.** *Cell Cycle* 2006, **5**(10):1066-1068.
- Edwards MC, Wong C, Elledge SJ: **Human cyclin K, a novel RNA polymerase II-associated cyclin possessing both carboxy-terminal domain kinase and Cdk-activating kinase activity.** *Mol Cell Biol* 1998, **18**(7):4291-4300.
- Fu TJ, Peng J, Lee G, Price DH, Flores O: **Cyclin K functions as a CDK9 regulatory subunit and participates in RNA polymerase II transcription.** *J Biol Chem* 1999, **274**(49):34527-34530.
- Peng J, Zhu Y, Milton JT, Price DH: **Identification of multiple cyclin subunits of human P-TEFb.** *Genes Dev* 1998, **12**(5):755-762.
- Wei P, Garber ME, Fang SM, Fischer WH, Jones KA: **A novel CDK9-associated C-type cyclin interacts directly with HIV-1 Tat and mediates its high-affinity, loop-specific binding to TAR RNA.** *Cell* 1998, **92**(4):451-462.
- Price DH: **P-TEFb, a cyclin-dependent kinase controlling elongation by RNA polymerase II.** *Mol Cell Biol* 2000, **20**(8):2629-2634.
- Peterlin BM, Price DH: **Controlling the elongation phase of transcription with P-TEFb.** *Mol Cell* 2006, **23**(3):297-305.
- Garber ME, Wei P, KewalRamani VN, Mayall TP, Herrmann CH, Rice AP, Littman DR, Jones KA: **The interaction between HIV-1 Tat and human cyclin T1 requires zinc and a critical cysteine residue that is not conserved in the murine Cyt1 protein.** *Genes Dev* 1998, **12**(22):3512-3527.
- Lin X, Taube R, Fujinaga K, Peterlin BM: **P-TEFb containing cyclin K and Cdk9 can activate transcription via RNA.** *J Biol Chem* 2002, **277**(19):16873-16878.
- Barboric M, Lenasi T, Chen H, Johansen EB, Guo S, Peterlin BM: **7SK snRNP/P-TEFb couples transcription elongation with alternative splicing and is essential for vertebrate development.** *Proc Natl Acad Sci USA* 2009, **106**(19):7798-7803.
- Bezstarosti K, Ghamari A, Grosveld FG, Demmers JA: **Differential proteomics based on 18O labeling to determine the cyclin dependent kinase 9 interactome.** *J Proteome Res* 2010, **9**(9):4464-4475.
- Ko TK, Kelly E, Pines J: **CrkRS: a novel conserved Cdc2-related protein kinase that colocalises with SC35 speckles.** *J Cell Sci* 2001, **114**(Pt 14):2591-2603.
- Marques F, Moreau JL, Peaucellier G, Lozano JC, Schatt P, Picard A, Callebaut I, Perret E, Genevieve AM: **A new subfamily of high molecular mass CDC2-related kinases with PITAI/VRE motifs.** *Biochem Biophys Res Commun* 2000, **279**(3):832-837.
- Even Y, Durieux S, Escande ML, Lozano JC, Peaucellier G, Weil D, Genevieve AM: **CDC2L5, a Cdk-like kinase with RS domain, interacts with the ASF/SF2-associated protein p32 and affects splicing in vivo.** *J Cell Biochem* 2006, **99**(3):890-904.
- Chen HH, Wang YC, Fann MJ: **Identification and characterization of the CDK12/cyclin L1 complex involved in alternative splicing regulation.** *Mol Cell Biol* 2006, **26**(7):2736-2745.
- Chen HH, Wong YH, Genevieve AM, Fann MJ: **CDK13/CDC2L5 interacts with L-type cyclins and regulates alternative splicing.** *Biochem Biophys Res Commun* 2007, **354**(3):735-740.
- Liu J, Kipreos ET: **Evolution of cyclin-dependent kinases (CDKs) and CDK-activating kinases (CAKs): differential conservation of CAKs in yeast and metazoa.** *Mol Biol Evol* 2000, **17**(7):1061-1074.
- Guo Z, Stiller JW: **Comparative genomics of cyclin-dependent kinases suggest co-evolution of the RNAP II C-terminal domain and CTD-directed CDKs.** *BMC Genomics* 2004, **5**:69.
- Morgan DO, De Bondt HL: **Protein kinase regulation: insights from crystal structure analysis.** *Curr Opin Cell Biol* 1994, **6**(2):239-246.
- Komarnitsky P, Cho EJ, Buratowski S: **Different phosphorylated forms of RNA polymerase II and associated mRNA processing factors during transcription.** *Genes Dev* 2000, **14**(19):2452-2460.
- Akhtar MS, Heidemann M, Tietjen JR, Zhang DW, Chapman RD, Eick D, Ansari AZ: **TFIIH kinase places bivalent marks on the carboxy-terminal domain of RNA polymerase II.** *Mol Cell* 2009, **34**(3):387-393.
- Glover-Cutter K, Larochelle S, Erickson B, Zhang C, Shokat K, Fisher RP, Bentley DL: **TFIIH-associated Cdk7 kinase functions in phosphorylation of C-terminal domain Ser7 residues, promoter-proximal pausing, and termination by RNA polymerase II.** *Mol Cell Biol* 2009, **29**(20):5455-5464.
- Tassan JP, Jaquenoud M, Leopold P, Schultz SJ, Nigg EA: **Identification of human cyclin-dependent kinase 8, a putative protein kinase partner for cyclin C.** *Proc Natl Acad Sci USA* 1995, **92**(19):8871-8875.
- Rickert P, Seghezzi W, Shanahan F, Cho H, Lees E: **Cyclin C/CDK8 is a novel CTD kinase associated with RNA polymerase II.** *Oncogene* 1996, **12**(12):2631-2640.
- Shore SM, Byers SA, Maury W, Price DH: **Identification of a novel isoform of Cdk9.** *Gene* 2003, **307**:175-182.
- Loyer P, Trembley JH, Grenet JA, Busson A, Corlu A, Zhao W, Kocak M, Kidd VJ, Lahti JM: **Characterization of cyclin L1 and L2 interactions with CDK11 and splicing factors: influence of cyclin L isoforms on splice site selection.** *J Biol Chem* 2008, **283**(12):7721-7732.
- Ji Y, Xiao F, Sun L, Qin J, Shi S, Yang J, Liu Y, Zhou D, Zhao J, Shen A: **Increased expression of CDK11p58 and cyclin D3 following spinal cord injury in rats.** *Mol Cell Biochem* 2008, **309**(1-2):49-60.
- Dickinson LA, Edgar AJ, Ehley J, Gottesfeld JM: **Cyclin L is an RS domain protein involved in pre-mRNA splicing.** *J Biol Chem* 2002, **277**(28):25465-25473.
- Baek K, Brown RS, Birrane G, Ladias JA: **Crystal structure of human cyclin K, a positive regulator of cyclin-dependent kinase 9.** *J Mol Biol* 2007, **366**(2):563-573.
- Sudol M, Sliwa K, Russo T: **Functions of WW domains in the nucleus.** *FEBS Lett* 2001, **490**(3):190-195.
- Fisher RP: **Secrets of a double agent: CDK7 in cell-cycle control and transcription.** *J Cell Sci* 2005, **118**(Pt 22):5171-5180.
- Morgan DO: **Principles of CDK regulation.** *Nature* 1995, **374**(6518):131-134.
- Hertel KJ, Graveley BR: **RS domains contact the pre-mRNA throughout spliceosome assembly.** *Trends Biochem Sci* 2005, **30**(3):115-118.
- Long JC, Caceres JF: **The SR protein family of splicing factors: master regulators of gene expression.** *Biochem J* 2009, **417**(1):15-27.
- Mortillaro MJ, Blencowe BJ, Wei X, Nakayasu H, Du L, Warren SL, Sharp PA, Berezney R: **A hyperphosphorylated form of the large subunit of RNA polymerase II is associated with splicing complexes and the nuclear matrix.** *Proc Natl Acad Sci USA* 1996, **93**(16):8253-8257.
- de la Mata M, Alonso CR, Kadener S, Fededa JP, Blaustein M, Pelisch F, Cramer P, Bentley D, Kornblihtt AR: **A slow RNA polymerase II affects alternative splicing in vivo.** *Mol Cell* 2003, **12**(2):525-532.

50. de la Mata M, Kornblihtt AR: RNA polymerase II C-terminal domain mediates regulation of alternative splicing by SRp20. *Nat Struct Mol Biol* 2006, **13**(11):973-980.
51. Berro R, Pedati C, Kehn-Hall K, Wu W, Klase Z, Even Y, Geneviere AM, Ammosova T, Nekhai S, Kashanchi F: CDK13, a new potential human immunodeficiency virus type 1 inhibitory factor regulating viral mRNA splicing. *J Virol* 2008, **82**(14):7155-7166.
52. Ball LJ, Kuhne R, Schneider-Mergener J, Oschkinat H: Recognition of proline-rich motifs by protein-protein-interaction domains. *Angew Chem Int Ed Engl* 2005, **44**(19):2852-2869.
53. Sims RJ III, Belotserkovskaya R, Reinberg D: Elongation by RNA polymerase II: the short and long of it. *Genes Dev* 2004, **18**(20):2437-2468.
54. Fuda NJ, Ardehali MB, Lis JT: Defining mechanisms that regulate RNA polymerase II transcription in vivo. *Nature* 2009, **461**(7261):186-192.
55. Lenasi T, Barboric M: P-TEFb stimulates transcription elongation and pre-mRNA splicing through multilateral mechanisms. *RNA Biol* 2010, **7**(2):145-150.
56. Egloff S, Murphy S: Cracking the RNA polymerase II CTD code. *Trends Genet* 2008, **24**(6):280-288.
57. Phatnani HP, Greenleaf AL: Phosphorylation and functions of the RNA polymerase II CTD. *Genes Dev* 2006, **20**(21):2922-2936.
58. Hsin JP, Sheth A, Manley JL: RNAP II CTD phosphorylated on threonine-4 is required for histone mRNA 3' end processing. *Science* 2011, **334**(6056):683-686.
59. Palancade B, Bensaude O: Investigating RNA polymerase II carboxyl-terminal domain (CTD) phosphorylation. *Eur J Biochem* 2003, **270**(19):3859-3870.
60. Chapman RD, Heidemann M, Albert TK, Mailhammer R, Flatley A, Meisterernst M, Kremmer E, Eick D: Transcribing RNA polymerase II is phosphorylated at CTD residue serine-7. *Science* 2007, **318**(5857):1780-1782.
61. Jones JC, Phatnani HP, Haystead TA, MacDonald JA, Alam SM, Greenleaf AL: C-terminal repeat domain kinase I phosphorylates Ser2 and Ser5 of RNA polymerase II C-terminal domain repeats. *J Biol Chem* 2004, **279**(24):24957-24964.
62. Allison LA, Wong JK, Fitzpatrick VD, Moyle M, Ingles CJ: The C-terminal domain of the largest subunit of RNA polymerase II of *Saccharomyces cerevisiae*, *Drosophila melanogaster*, and mammals: a conserved structure with an essential function. *Mol Cell Biol* 1988, **8**(1):321-329.
63. Bartkowiak B, Greenleaf AL: Phosphorylation of RNAPII: To P-TEFb or not to P-TEFb? *Transcription* 2011, **2**(3):115-119.
64. Chao SH, Price DH: Flavopiridol inactivates P-TEFb and blocks most RNA polymerase II transcription in vivo. *J Biol Chem* 2001, **276**(34):31793-31799.
65. Nechaev S, Adelman K: Promoter-proximal Pol II: when stalling speeds things up. *Cell Cycle* 2008, **7**(11):1539-1544.
66. Rahl PB, Lin CY, Seila AC, Flynn RA, McGuire S, Burge CB, Sharp PA, Young RA: c-Myc regulates transcriptional pause release. *Cell* 2010, **141**(3):432-445.
67. Cho EJ, Kobor MS, Kim M, Greenblatt J, Buratowski S: Opposing effects of Ctk1 kinase and Fcp1 phosphatase at Ser 2 of the RNA polymerase II C-terminal domain. *Genes Dev* 2001, **15**(24):3319-3329.
68. Liu Y, Warfield L, Zhang C, Luo J, Allen J, Lang WH, Ranish J, Shokat KM, Hahn S: Phosphorylation of the transcription elongation factor Spt5 by yeast Bur1 kinase stimulates recruitment of the PAF complex. *Mol Cell Biol* 2009, **29**(17):4852-4863.
69. Qiu H, Hu C, Hinnebusch AG: Phosphorylation of the Pol II CTD by KIN28 enhances BUR1/BUR2 recruitment and Ser2 CTD phosphorylation near promoters. *Mol Cell* 2009, **33**(6):752-762.
70. Ahn SH, Kim M, Buratowski S: Phosphorylation of serine 2 within the RNA polymerase II C-terminal domain couples transcription and 3' end processing. *Mol Cell* 2004, **13**(1):67-76.
71. Kim H, Erickson B, Luo W, Seward D, Graber JH, Pollock DD, Megee PC, Bentley DL: Gene-specific RNA polymerase II phosphorylation and the CTD code. *Nat Struct Mol Biol* 2010, **17**(10):1279-1286.
72. Bataille AR, Jeronimo C, Jacques PE, Laramée L, Fortin ME, Forest A, Bergeron M, Hanes SD, Robert F: A Universal RNA Polymerase II CTD Cycle Is Orchestrated by Complex Interplays between Kinase, Phosphatase, and Isomerase Enzymes along Genes. *Mol Cell* 2012, **45**(2):158-170.
73. Jackson SP, Bartek J: The DNA-damage response in human biology and disease. *Nature* 2009, **461**(7267):1071-1078.
74. Ciccio A, Elledge SJ: The DNA damage response: making it safe to play with knives. *Mol Cell* 2010, **40**(2):179-204.
75. Matsuoka S, Ballif BA, Smogorzewska A, McDonald ER III, Hurov KE, Luo J, Bakalarski CE, Zhao Z, Solimini N, Lerenthal Y, et al: ATM and ATR substrate analysis reveals extensive protein networks responsive to DNA damage. *Science* 2007, **316**(5828):1160-1166.
76. Paulsen RD, Soni DV, Wollman R, Hahn AT, Yee MC, Guan A, Hesley JA, Miller SC, Cromwell EF, Solow-Cordero DE, et al: A genome-wide siRNA screen reveals diverse cellular processes and pathways that mediate genome stability. *Mol Cell* 2009, **35**(2):228-239.
77. Cimprich KA, Cortez D: ATR: an essential regulator of genome integrity. *Nat Rev Mol Cell Biol* 2008, **9**(8):616-627.
78. Smogorzewska A, Matsuoka S, Vinciguerra P, McDonald ER III, Hurov KE, Luo J, Ballif BA, Gygi SP, Hofmann K, D'Andrea AD, et al: Identification of the FANCI protein, a monoubiquitinated FANCD2 paralog required for DNA repair. *Cell* 2007, **129**(2):289-301.
79. Moldovan GL, D'Andrea AD: How the fanconi anemia pathway guards the genome. *Annu Rev Genet* 2009, **43**:223-249.
80. Harper JW, Elledge SJ: The DNA damage response: ten years after. *Mol Cell* 2007, **28**(5):739-745.
81. O'Connell BC, Adamson B, Lydeard JR, Sowa ME, Ciccio A, Bredemeyer AL, Schlabach M, Gygi SP, Elledge SJ, Harper JW: A Genome-wide Campothecin Sensitivity Screen Identifies a Mammalian MMS22L-NFKBIL2 Complex Required for Genomic Stability. *Mol Cell* 2010, **40**(4):645-657.
82. Munoz MJ, de la Mata M, Kornblihtt AR: The carboxy terminal domain of RNA polymerase II and alternative splicing. *Trends Biochem Sci* 2010, **35**(9):497-504.
83. Ostapenko D, Solomon MJ: Budding yeast CTDK-I is required for DNA damage-induced transcription. *Eukaryot Cell* 2003, **2**(2):274-283.
84. Yu DS, Zhao R, Hsu EL, Cayer J, Ye F, Guo Y, Shyr Y, Cortez D: Cyclin-dependent kinase 9-cyclin K functions in the replication stress response. *EMBO Rep* 2010, **11**(11):876-882.
85. Mori T, Anazawa Y, Matsui K, Fukuda S, Nakamura Y, Arakawa H: Cyclin K as a direct transcriptional target of the p53 tumor suppressor. *Neoplasia* 2002, **4**(3):268-274.
86. Clausing E, Mayer A, Chanarat S, Muller B, Germann SM, Cramer P, Lisby M, Strasser K: The transcription elongation factor Bur1-Bur2 interacts with replication protein A and maintains genome stability during replication stress. *J Biol Chem* 2010, **285**(53):41665-41674.
87. Liu H, Herrmann CH, Chiang K, Sung TL, Moon SH, Donehower LA, Rice AP: 55K isoform of CDK9 associates with Ku70 and is involved in DNA repair. *Biochem Biophys Res Commun* 2010, **397**(2):245-250.
88. The Cancer Research Atlas Genome Network: Integrated genomic analyses of ovarian carcinoma. *Nature* 2011, **474**(7353):609-615.
89. Kauraniemi P, Barlund M, Monni O, Kallioniemi A: New amplified and highly expressed genes discovered in the ERBB2 amplicon in breast cancer by cDNA microarrays. *Cancer Res* 2001, **61**(22):8235-8240.
90. Kauraniemi P, Kuukasjarvi T, Sauter G, Kallioniemi A: Amplification of a 280-kilobase core region at the ERBB2 locus leads to activation of two hypothetical proteins in breast cancer. *Am J Pathol* 2003, **163**(5):1979-1984.
91. Benusiglio PR, Pharoah PD, Smith PL, Lesueur F, Conroy D, Luben RN, Dew G, Jordan C, Dunning A, Easton DF, et al: HapMap-based study of the 17q21 ERBB2 amplicon in susceptibility to breast cancer. *Br J Cancer* 2006, **95**(12):1689-1695.
92. Sircoulomb F, Bekhouche I, Finetti P, Adelaide J, Ben Hamida A, Bonansea J, Raynaud S, Innocenti C, Charafe-Jauffret E, Tarpin C, et al: Genome profiling of ERBB2-amplified breast cancers. *BMC Cancer* 2010, **10**:539.
93. Zang ZJ, Ong CK, Cutcutache I, Yu W, Zhang SL, Huang D, Ler LD, Dykema K, Gan A, Tao J, et al: Genetic and structural variation in the gastric cancer kinome revealed through targeted deep sequencing. *Cancer Res* 2011, **71**(1):29-39.
94. Iorns E, Martens-de Kemp SR, Lord CJ, Ashworth A: CRK7 modifies the MAPK pathway and influences the response to endocrine therapy. *Carcinogenesis* 2009, **30**(10):1696-1701.
95. Wilson CA, Ramos L, Villasenor MR, Anders KH, Press MF, Clarke K, Karlan B, Chen JJ, Scully R, Livingston D, et al: Localization of human BRCA1 and its loss in high-grade, non-inherited breast carcinomas. *Nat Genet* 1999, **21**(2):236-240.

96. Thompson ME, Jensen RA, Obermiller PS, Page DL, Holt JT: **Decreased expression of BRCA1 accelerates growth and is often present during sporadic breast cancer progression.** *Nat Genet* 1995, **9**(4):444-450.
97. Malcovati L, Della Porta MG, Pietra D, Boveri E, Pellagatti A, Galli A, Travaglino E, Brisci A, Rumi E, Passamonti F, et al: **Molecular and clinical features of refractory anemia with ringed sideroblasts associated with marked thrombocytosis.** *Blood* 2009, **114**(17):3538-3545.
98. Lapidot-Lifson Y, Patinkin D, Prody CA, Ehrlich G, Seidman S, Ben-Aziz R, Benseler F, Eckstein F, Zakut H, Soreq H: **Cloning and antisense oligodeoxynucleotide inhibition of a human homolog of cdc2 required in hematopoiesis.** *Proc Natl Acad Sci USA* 1992, **89**(2):579-583.
99. Khan SZ, Mitra D: **Cyclin K inhibits HIV-1 gene expression and replication by interfering with cyclin-dependent kinase 9 (CDK9)-cyclin T1 interaction in Nef-dependent manner.** *J Biol Chem* 2011, **286**(26):22943-22954.
100. Kulkarni PA, Sano M, Schneider MD: **Phosphorylation of RNA polymerase II in cardiac hypertrophy: cell enlargement signals converge on cyclin T/ Cdk9.** *Recent Prog Horm Res* 2004, **59**:125-139.
101. Lin C, Smith ER, Takahashi H, Lai KC, Martin-Brown S, Florens L, Washburn MP, Conaway JW, Conaway RC, Shilatifard A: **AFF4, a component of the ELL/P-TEFb elongation complex and a shared subunit of MLL chimeras, can link transcription elongation to leukemia.** *Mol Cell* 2010, **37**(3):429-437.
102. Mueller D, Bach C, Zeisig D, Garcia-Cuellar MP, Monroe S, Sreekumar A, Zhou R, Nesvizhskii A, Chinnaiyan A, Hess JL, et al: **A role for the MLL fusion partner ENL in transcriptional elongation and chromatin modification.** *Blood* 2007, **110**(13):4445-4454.
103. Bitoun E, Oliver PL, Davies KE: **The mixed-lineage leukemia fusion partner AF4 stimulates RNA polymerase II transcriptional elongation and mediates coordinated chromatin remodeling.** *Hum Mol Genet* 2007, **16**(1):92-106.
104. He N, Liu M, Hsu J, Xue Y, Chou S, Burlingame A, Krogan NJ, Alber T, Zhou Q: **HIV-1 Tat and host AFF4 recruit two transcription elongation factors into a bifunctional complex for coordinated activation of HIV-1 transcription.** *Mol Cell* 2010, **38**(3):428-438.
105. Sobhian B, Laguet N, Yatim A, Nakamura M, Levy Y, Kiernan R, Benkirane M: **HIV-1 Tat assembles a multifunctional transcription elongation complex and stably associates with the 7SK snRNP.** *Mol Cell* 2010, **38**(3):439-451.
106. Krystof V, Chamrad I, Jorda R, Kohoutek J: **Pharmacological targeting of CDK9 in cardiac hypertrophy.** *Med Res Rev* 2010, **30**(4):646-666.
107. Chao SH, Fujinaga K, Marion JE, Taube R, Sausville EA, Senderowicz AM, Peterlin BM, Price DH: **Flavopiridol inhibits P-TEFb and blocks HIV-1 replication.** *J Biol Chem* 2000, **275**(37):28345-28348.
108. Kohoutek J, Li Q, Blazek D, Luo Z, Jiang H, Peterlin BM: **Cyclin T2 is essential for mouse embryogenesis.** *Mol Cell Biol* 2009, **29**(12):3280-3285.
109. Westerling T, Kuuluvainen E, Makela TP: **Cdk8 is essential for preimplantation mouse development.** *Mol Cell Biol* 2007, **27**(17):6177-6182.
110. Brown EJ, Baltimore D: **ATR disruption leads to chromosomal fragmentation and early embryonic lethality.** *Genes Dev* 2000, **14**(4):397-402.
111. de Klein A, Muijtjens M, van Os R, Verhoeven Y, Smit B, Carr AM, Lehmann AR, Hoesjmakers JH: **Targeted disruption of the cell-cycle checkpoint gene ATR leads to early embryonic lethality in mice.** *Curr Biol* 2000, **10**(8):479-482.
112. Hakem R, de la Pompa JL, Sirard C, Mo R, Woo M, Hakem A, Wakeham A, Potter J, Reitmair A, Billia F, et al: **The tumor suppressor gene Brca1 is required for embryonic cellular proliferation in the mouse.** *Cell* 1996, **85**(7):1009-1023.
113. Neumuller RA, Richter C, Fischer A, Novatchkova M, Neumuller KG, Knoblich JA: **Genome-wide analysis of self-renewal in Drosophila neural stem cells by transgenic RNAi.** *Cell Stem Cell* 2011, **8**(5):580-593.
114. Zhu H, Doherty JR, Kuliyev E, Mead PE: **CDK9/cyclin complexes modulate endoderm induction by direct interaction with Mix.3/mixer.** *Dev Dyn* 2009, **238**(6):1346-1357.

doi:10.1186/1747-1028-7-12

Cite this article as: Kohoutek and Blazek: Cyclin K goes with Cdk12 and Cdk13. *Cell Division* 2012 **7**:12.

Submit your next manuscript to BioMed Central and take full advantage of:

- Convenient online submission
- Thorough peer review
- No space constraints or color figure charges
- Immediate publication on acceptance
- Inclusion in PubMed, CAS, Scopus and Google Scholar
- Research which is freely available for redistribution

Submit your manuscript at
www.biomedcentral.com/submit



APPENDIX 7

PACULOVÁ, Hana, Juraj KRAMARA, Šárka ŠIMEČKOVÁ, Radek FEDR, Karel SOUČEK, Ondřej HYLSE, Kamil PARUCH, Marek SVOBODA, Martin MISTRÍK and Jiří KOHOUTEK. BRCA1 or CDK12 loss sensitizes cells to CHK1 inhibitors. *Tumour Biology: The Journal of the International Society for Oncodevelopmental Biology and Medicine*. 2017, 39(10), 1010428317727479.

BRCA1 or CDK12 loss sensitizes cells to CHK1 inhibitors

Tumor Biology
October 2017: 1–11
© The Author(s) 2017
Reprints and permissions:
sagepub.co.uk/journalsPermissions.nav
DOI: 10.1177/1010428317727479
journals.sagepub.com/home/tub



Hana Paculová¹, Juraj Kramara², Šárka Šimečková^{3,4},
Radek Fedr^{3,5}, Karel Souček^{3,4,5}, Ondřej Hylse^{5,6}, Kamil Paruch^{5,6},
Marek Svoboda⁷, Martin Mistrík² and Jiří Kohoutek¹

Abstract

A broad spectrum of tumors develop resistance to classic chemotherapy, necessitating the discovery of new therapies. One successful strategy exploits the synthetic lethality between poly(ADP-ribose) polymerase 1/2 proteins and DNA damage response genes, including BRCA1, a factor involved in homologous recombination-mediated DNA repair, and CDK12, a transcriptional kinase known to regulate the expression of DDR genes. CHK1 inhibitors have been shown to enhance the anti-cancer effect of DNA-damaging compounds. Since loss of BRCA1 increases replication stress and leads to DNA damage, we tested a hypothesis that CDK12- or BRCA1-depleted cells rely extensively on S-phase-related CHK1 functions for survival. The silencing of BRCA1 or CDK12 sensitized tumor cells to CHK1 inhibitors *in vitro* and *in vivo*. BRCA1 downregulation combined with CHK1 inhibition induced excessive amounts of DNA damage, resulting in an inability to complete the S-phase. Therefore, we suggest CHK1 inhibition as a strategy for targeting BRCA1- or CDK12-deficient tumors.

Keywords

DNA damage response, BRCA1, CDK12, CHK1 inhibitor, transcription

Date received: 22 April 2017; accepted: 29 July 2017

Introduction

A shared feature of various malignancies is the dysregulation of DNA damage response (DDR), which leads to genomic instability.¹ The checkpoint kinase 1 (CHK1) represents a cellular factor that could be used to target the viability of tumor cells with genomic instability.^{2–4} This is because CHK1 is involved in numerous essential cellular processes. For example, a cell responds to DNA damage by activating CHK1 through ATR-promoted phosphorylation, which effectively blocks cell cycle progression. Once activated, CHK1 regulates the G2/M checkpoint by inactivating the CDC25 phosphatases that would otherwise remove the inhibitory phosphates of cyclin-dependent kinases (CDK), which are responsible for the G2/M transition.³ CHK1 also participates in the DNA damage repair mechanism by phosphorylating, and thus activating, the repair factors BRCA2 and RAD51.⁵ In addition, CHK1 is integral to the prevention of replication stress, as it stabilizes replication forks and regulates origin firing.³

Various CHK1 inhibitors have been tested as anti-tumor agents in combination with DNA-damaging agents, such as hydroxyurea, cisplatin, and topoisomerase inhibitors

¹Department of Chemistry and Toxicology, Veterinary Research Institute, Brno, Czech Republic

²Institute of Molecular and Translational Medicine, Faculty of Medicine and Dentistry, Palacky University, Olomouc, Czech Republic

³Institute of Biophysics of the Czech Academy of Sciences, Brno, Czech Republic

⁴Department of Experimental Biology, Faculty of Science, Masaryk University, Brno, Czech Republic

⁵International Clinical Research Center, St. Anne's University Hospital, Brno, Czech Republic

⁶Department of Chemistry, CZ Openscreen, Faculty of Science, Masaryk University, Brno, Czech Republic

⁷Department of Comprehensive Cancer Care, Masaryk Memorial Cancer Institute, Brno, Czech Republic

Corresponding author:

Jiří Kohoutek, Department of Chemistry and Toxicology, Veterinary Research Institute, Hudcova 296/70, 621 00 Brno, Czech Republic.
Email: kohoutek@vri.cz



(topotecan, irinotecan), and antimetabolites, such as gemcitabine.^{6–10} Several studies have reported that the anti-tumor effect of CHK1 inhibitors is determined by p53 status, with p53-deficient cells more responsive to CHK1 inhibitor treatment.^{2,11} However, other authors have reported that CHK1 inhibitors decrease cellular viability irrespective of p53 suppressor status,⁶ showing that CHK1 inhibitors strongly potentiate the effects of DNA-damaging agents in p53^{-/-} cells. These results suggest that patients with p53-mutated tumors could benefit from treatment approaches that include CHK1 inhibition.^{11,12} The identification of cellular factors that, when combined with CHK1 inhibitors, confer synthetic lethality could strengthen the portfolio of combinatory treatments with CHK1 inhibitors or potentially lead to the discovery of monotherapy approaches for tumors with relevant mutations. Certain scenarios have been described recently; for example, cells deficient in Fanconi anemia genes are hypersensitive to CHK1 inhibition, and a novel essential interplay between CHK1 and I-kappa-B kinase epsilon was observed in ovarian cells.^{13,14}

The CDK12 regulates the elongation phase of transcription by phosphorylating the C-terminal domain of RPB1, a subunit of RNA polymerase II (RNAPII).^{15–18} We previously identified CDK12 as a cellular factor that orchestrates the expression of several key DDR genes, for example, BRCA1, ATR, ATM, FANCI, and FANCD2.¹⁶ By regulating DDR genes, CDK12 consequently affects homologous recombination (HR)-mediated DNA repair. A downregulation of CDK12 leads to increased endogenous DNA damage, DDR activation, and pronounced sensitivity to DNA-damaging agents.^{16,19} Cancer-associated CDK12 mutations are predominantly located within the kinase domain and result in a catalytically inactive protein.²⁰ Based on these observations, CDK12 has been suggested to be a tumor suppressor candidate.^{19–21}

The breast cancer-associated gene 1 (BRCA1) tumor suppressor protein is a central component of several distinct protein complexes that are vital to HR-mediated DNA damage repair, cell cycle checkpoints, and transcriptional regulation.^{22,23} BRCA1 is inheritably mutated in about 9% and 13% of unselected women with newly diagnosed triple-negative breast cancer and ovarian cancer (respectively). If metastatic, these patients have generally very unfavorable prognosis and currently are candidates for targeted drug therapy, such as poly(ADP-ribose) polymerase (PARP) inhibitors.^{24–26} The loss of BRCA1, caused by homozygous mutations, reduces the ability of cells to carry out HR-mediated DNA repair, resulting in cellular genomic instability.²⁴ Interestingly, BRCA1 mutations are mutually exclusive with CDK12 mutations, which suggests that CDK12 belongs to the same HR-mediated DNA damage repair pathway as BRCA1.²¹

HR deficiency presents an opportunity for cancer treatment. Tumors exhibiting HR deficiency, especially those

with loss of BRCA1 or 2, are sensitive to inhibitors of PARP1/2, a protein involved in DNA repair. As with the loss of BRCA1/2, the loss or inhibition of CDK12 sensitizes cells to PARP inhibitors, which have recently been approved for the treatment of ovarian cancer.^{21,41} Nevertheless, research has reported that certain tumors have become resistant to PARP inhibitors as a result of restored HR capacity, altered non-homologous end-joining (NHEJ) capacity, decreased levels or activity of PARP1, and/or decreased intracellular availability of PARP inhibitors.²⁵ Thus, novel alternatives to PARP1 inhibitors are necessary for further patient treatment.

Although the genomic instability that results from DDR deficiency often drives tumor development, it also provides a great opportunity for cancer treatment.²⁶ The loss of BRCA1 and CDK12 function most likely potentiates the anti-tumor effects of PARP1/2 inhibitors by crippling HR-mediated DNA repair, with this mechanism a perfect example of the concept of synthetic lethality. Since the loss of BRCA1 compromises DDR and leads to replication stress and DNA damage,²⁷ we hypothesized that BRCA1- or CDK12-deficient cells will extensively rely on the S-phase-related kinase activity of CHK1 for survival. In this study, we demonstrate that silencing BRCA1 or CDK12 indeed sensitizes cancer cells to CHK1 inhibitors.

Materials and methods

Synthesis of CHK1 inhibitors

The racemic CHK1 inhibitor SCH900776 (Merck, Darmstadt, Germany) was prepared in-house through a previously published route.^{28,29} The enantiomers were separated by high-performance liquid chromatography (HPLC) with a chiral stationary phase (Chiralcel[®] OJ[™] column (Daicel Corporation, Tokyo, Japan), diameter 21 mm, length 250 mm; mobile phase: *n*-hexane/ethanol 80:20 + 0.5% diethylamine, flow: 20 mL/min). The desired active R-enantiomer of SCH900776 eluted faster (retention time: 10:04 min) than the inactive S-enantiomer (retention time: 13:07 min). LY2603618 was purchased from Selleckchem (Houston, TX, USA; cat. no. S2626).

Cell culture

HCT116 p53^{+/+} and p53^{-/-} cells were a kind gift from B. Vogelstein.³⁰ The cells were cultivated in Dulbecco's Modified Eagle's Medium (DMEM; Sigma-Aldrich, D6429, Darmstadt, Germany) medium supplemented with 5% fetal bovine serum (FBS; Sigma-Aldrich, F0804) at 37°C. MDA-MB-231 cells were obtained from the American Type Culture Collection (ATCC, Rockville, MD, USA) and were cultivated in DMEM medium supplemented with 10% FBS at 37°C with 5% CO₂.

Proliferation assays

HCT116 cells were transfected with the following small interfering RNAs (siRNAs; Santa Cruz Biotechnology, Dallas, TX, USA): CTRLA (sc-37007), BRCA1 (sc-29219), CDK12 (sc-44531), CDK13 (sc-72836), and CDK12_2 (Sigma-Aldrich, SIHK0490) using Lipofectamine RNAi MAX (Invitrogen, 13778150, Carlsbad, CA, USA). Viable cells were counted after 24 h and equal cell concentrations were seeded into 96-well plates. After an additional 24 h, cells were treated with a CHK1 inhibitor, either SCH900776 or LY2603618, in dimethyl sulfoxide (DMSO) for 6 days. The medium was exchanged after 48 and 96 h, and fresh inhibitors were added to the medium at these time points. For each siRNA, the cell viability was assessed with the CyQuant NF Cell Proliferation Assay Kit (Invitrogen) and normalized to the relative growth of cells treated with DMSO. All experiments were performed three times in triplicates.

MDA-MB-231 cells were seeded at equal concentrations into six-well plates. After 24 h, they were exposed to DMSO, along with either 0.3 or 1 μ M SCH900776. After 72 h, the cells were trypsinized and counted with a hemocytometer. Cell viability was normalized to relative growth of cells treated with DMSO for each short hairpin RNA (shRNA). The experiments were performed three times in duplicates.

Western blot

Cells were lysed in lysis buffer (100 mM Tris, pH 7.4, 1% sodium dodecyl sulfate (SDS), 10% glycerol), sonicated, and protein concentrations were assessed by the bicinchoninic acid (BCA) assay. Laemmli buffer (3 \times) was then added, and lysates were boiled for 5 min at 100°C. Cell lysates were separated with electrophoresis employing 8%–15% gels and then wet blotted to a nitrocellulose membrane (GE Healthcare, Amersham, #10600008, Little Chalfont, UK). Individual proteins were detected with specific antibodies: BRCA1 (Santa Cruz, sc-6954), CDK12 (Cell Signaling, #11973, Danvers, MA, USA), CDK13 (rabbit serum produced in-house), Cyclin K (Santa Cruz, sc-376371), p53 Pantropic Ab-6 (Millipore, OP43, Billerica, MA, USA), Cyclin T1 (Santa Cruz, sc-8127), CHK1 (Cell Signaling, #2360), CHK1-pSer296 (Cell Signaling, #2349), PARP (Cell Signaling, #9542), γ H2AX pSer 139 (Biolegend, 613402, San Diego, CA, USA), p21 (Santa Cruz, sc-397), p27 (Santa Cruz, sc-528), pRb (Cell Signaling, #9309), and pRb-pSer780 (Cell Signaling, #8180). Anti-rabbit and anti-mouse secondary horseradish peroxidase (HRP)-linked antibodies were obtained from GE Healthcare (NA934V, NA931V), and anti-goat antibody was obtained from Sigma-Aldrich (A5420). The immunoreactive bands were visualized using the Western blot Luminol reagent (Santa Cruz Biotechnology, SC-2048).

Reverse transcription–polymerase chain reaction

HCT116 cells were transfected with control or specific siRNAs using lipofectamine RNAiMAX (Invitrogen, 13778150). After 72 h, cells were harvested, and total RNA was isolated with RNAzol (Molecular Research Centre, RN190, Cincinnati, OH, USA). Reverse transcription (RT) and quantitative polymerase chain reaction (qPCR) were performed according to the method described by Blazek et al.¹⁶ Changes in gene expression were calculated using the comparative threshold cycle method with Hypoxanthine Phosphoribosyltransferase 1 (HPRT) to normalize for variations in RNA input. The following primers were used for PCR: *CDKN1A*—forward: CTGGAGACTCTCAGGGT CGAAA and reverse: GATTAGGGCTTCCTCTTG and HPRT—forward: 5'-CCAGACAAGTTTGTGTAGG ATATGCCCTTGAC-3' and reverse: 5'-ACTCCAGATG TTCCAAACTCAACTTGA ACTCTC-3'.

Plasmids

The pLKO.1 shBRCA1-2 and pLKO.1 shBRCA1-4 plasmids, which were used to generate stable BRCA1 knockdown cell lines, were part of the MISSION library (Sigma-Aldrich; construct numbers TRCN0000244985 and TRCN0000244987). The lentiviral packaging plasmids pMD2.G and psPAX2 were purchased from Addgene (Cambridge, MA, USA; Plasmids numbers 12259 and 12260).

Generation of MDA-MB-231 shBRCA1 cell lines

Lentiviral transduction was used to generate MDA-MB-231 cell lines that harbor a stable shRNA knockdown of BRCA1. Lentivirus production and transduction was performed according to the method described by Tiscornia et al.³¹ Briefly, lentiviruses were generated by co-transfecting 293T cells with 4 μ g of pMD2.G, 7 μ g of psPAX2, and 9 μ g of a lentiviral plasmid of interest using the CaPO4 precipitation method. Next, 6–8 h post-transfection, cells were washed with pre-warmed phosphate-buffered saline (PBS) and the medium was changed. Supernatant containing lentiviruses was collected 48 h later and supplemented with 4 μ g/mL polybrene (Sigma-Aldrich, 107689). Target cells were transduced at multiplicities of infection (MOIs) of 1–10. The medium was changed 24 h post-transduction, and the cells were selected with 1 μ g/mL puromycin. Resistant colonies were evaluated for expression of shRNA and the consequent reduction in BRCA1 protein levels.

Clonogenic assay

MDA-MB-231 cells were seeded at equal concentrations into six-well plates (150 cells/well) and, after 24 h, treated

with 0, 0.3, or 1 μM SCH900776 for 14 days. Medium was exchanged and fresh inhibitors were added every 3 days. After 2 weeks of treatment, the cells were fixed with 4% paraformaldehyde and stained with Gram I Solution (PENTAs.r.o., cat. no. 14600-11000, Prague, Czech Republic).

Cell cycle analysis

HCT116 or MDA-MB-231 cells were trypsinized, washed in PBS, and fixed with ice-cold 70% ethanol overnight. Cells were then washed in PBS and stained with Vindelov solution (1M TrisHCl, pH 8.0; 0.1% Triton-X100; 10 mM NaCl; propidium iodide, 50 $\mu\text{g}/\text{mL}$; RNase A 50 Kunitz U/mL) for 30 min at 37°C.

Xenograft model

All animal procedures were performed in strict accordance with the Guide for the Care and Use of Laboratory Animals and approved by the Institutional Animal Care and Use Committee. Tumor xenografts were generated by injecting 2×10^6 MDA-MB-231 parental or shBRCA #4 breast cancer cells, in PBS with a final volume of 100 μL , into the left mammary fat pads of Ctrl: SHO-*Prkdc*^{SCID} *Hr*^{tr} mice (Charles River Laboratories, Wilmington, MA, USA). In total, 12 mice were injected with MDA-MB-231 parental or shBRCA #4 cells and half of them (six mice) from particular transplantation was treated with the vehicle or CHK1 inhibitor SCH900776. Drug treatment began once a tumor had reached 0.03 cm^3 . The CHK1 inhibitor SCH900776 was dissolved in 20% Kolliphor ELP (Sigma-Aldrich, 30906) and administered intraperitoneally at a final concentration of 25 mg/kg for 5 days. This dose was selected based on a previously published study that investigated the same CHK1 inhibitor.⁶ Two-dimensional calipers were used to measure tumor volumes during and after the treatment period, and volume was calculated based on the equation: $\pi/6 \times \text{length} \times \text{width}^2$.⁹ Data were normalized to the starting tumor volume of 0.03 cm^3 . The whole experiment was carried out in two independent replicates. Increase in tumor volume after the treatment was statistically analyzed by Student's *t*-test.

Statistical analysis

All data were statistically analyzed and visualized using Prism5 (GraphPad Software, Inc., La Jolla, USA). Results were expressed as mean with standard error of the mean (SEM). Viability assays data were fitted to sigmoidal dose response curve and were analyzed with analysis of variance (ANOVA) test, and data from other experiments were analyzed by Student's *t*-test. Symbols used to express statistical significance are as follows: * $p \leq 0.05$; ** $p \leq 0.01$; and *** $p \leq 0.001$.

Results

CDK12 and BRCA1 downregulation sensitizes HCT116 cells to CHK1 inhibition irrespective of p53 status

CDK12 regulates BRCA1 expression, and a loss of BRCA1 results in increased DNA damage and replication stress.^{16,27} Thus, we hypothesized that cells with depleted BRCA1 or CDK12 should be extensively dependent on the S-phase-related function of CHK1. We tested how the CHK1 inhibitors SCH900776 and LY2603618 affect the proliferation of BRCA1- and CDK12-silenced tumor cells. Whether the functional status of p53 influences the anti-proliferative effect of CHK1 inhibitors remains an open question, so we employed a pair of HCT116 cell lines with p53 null and p53 WT status.³² In addition to CDK12 we validated the effects of CHK1 inhibitors on cells with silenced CDK13, another kinase binding Cyclin K that can phosphorylate RNAPII,³³ but that has no impact on BRCA1 levels.

We performed 6-day proliferation assays to assess the relationship between CDK12 or BRCA1 deficiency and CHK1 inhibition (Figure 1). The siRNA-transfected cells were treated with different concentrations of CHK1 inhibitor SCH900776. We used two distinct siRNAs against CDK12, a pool of three siRNAs (CDK12), and a single sequence different from the other three (CDK12_2). CDK12 and BRCA1 silencing significantly sensitized both p53+/+ and p53-/- cell lines to the CHK1 inhibitor SCH900776. In contrast, CDK13 silencing had no effect on sensitivity to SCH900776 (Figure 1(a) and (b)). To avoid the risk that the effect of SCH900776 on cell proliferation is compound-specific (i.e. that it employs unknown off-target effects), we tested the effect of another CHK1 inhibitor, LY2603618, which has a different chemical structure,³⁴ using the same setup as in Figure 1(a) and (b). This experiment provided similar results as those obtained when SCH900776 was used (Figure 1(c) and (d)). It is important to note that sensitivity to both tested CHK1 inhibitors was independent of the p53 status. In order to demonstrate that effect of CHK1 inhibitor is not limited only to the colorectal cell line HCT116, the same type of experiment as in Figure 1(a) was performed with an ovarian cancer cell line OVSAHO, which bears p53 mutation and wild-type BRCA1.³⁵ Sensitization to CHK1 inhibitor after BRCA1 and CDK12 silencing was observed similar to HCT116 cell line (Supplementary Figure S1).

The effective downregulation of CDK12, CDK13, cyclin K (associating partner of CDK12 and CDK13), and BRCA1 in the cells was verified by Western blot analysis (Figure 1(e)). As expected, the protein levels of cyclin K and BRCA1 decreased after CDK12 downregulation, which corresponds to our previous observations.^{16,20} Cyclin T1, an associating partner of CDK9 kinase involved in transcription elongation, was used as a loading control.

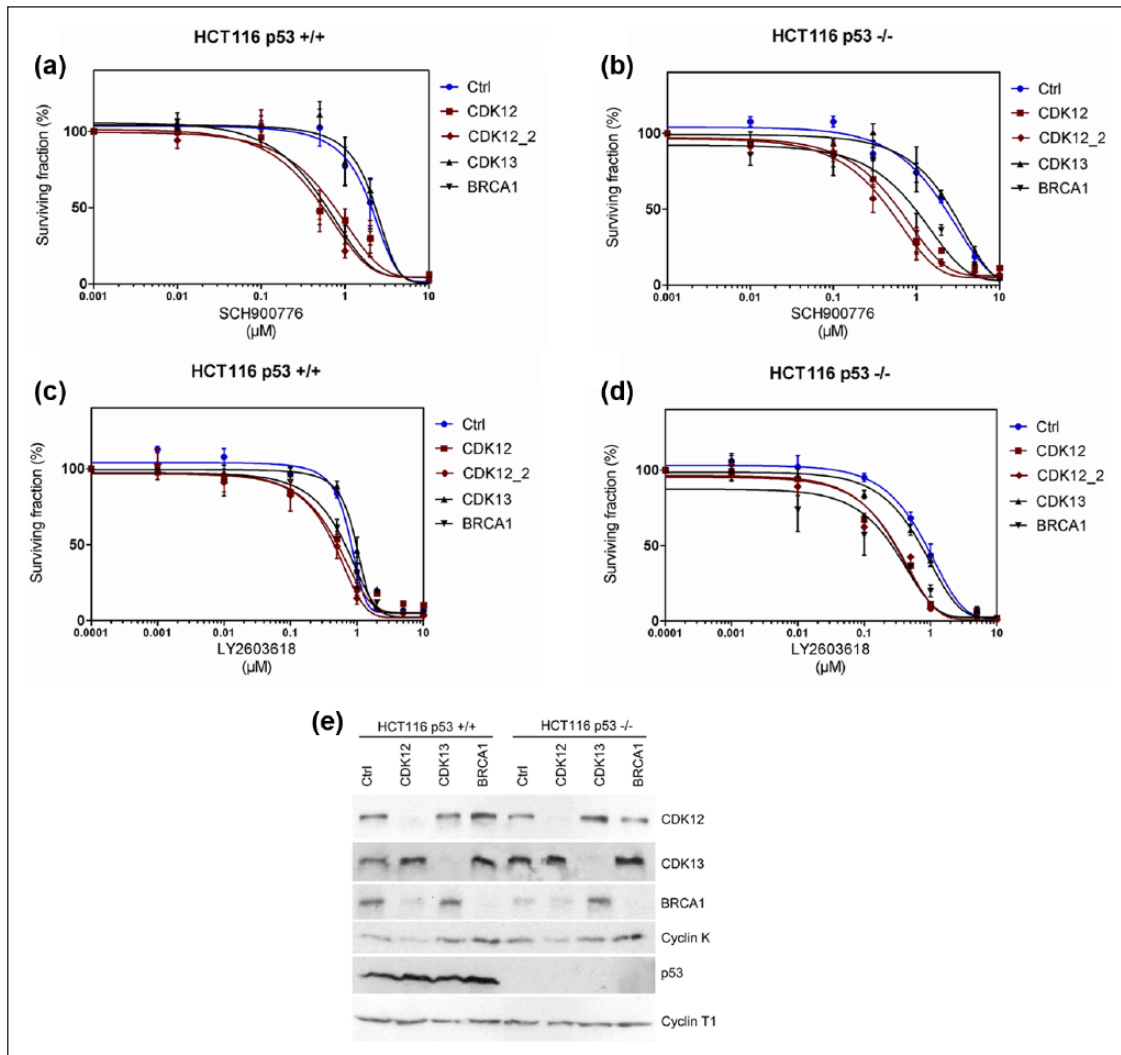


Figure 1. Downregulation of CDK12 or BRCA1 sensitizes HCT116 cells to CHK1 inhibitors. Six-day survival curves of (a, c) HCT116 p53+/+ or (b, d) HCT116 p53-/- cells transfected with various siRNAs (CTRL, CDK12, CDK13, and BRCA1) and treated with either the CHK1 inhibitor (a, b) SCH900776 or (c, d) LY2603618. Cell viability for each siRNA-treated cell line was assessed by the CyQuant NF kit and normalized to the relative growth of cells treated with DMSO. Error bars represent SEM for three independent experiments. CDK12- and BRCA1-silenced cells are sensitive to CHK1 inhibitors ($p < 0.001$, ANOVA). (e) The effective knockdown of indicated proteins after siRNA transfections was examined by Western blot analysis. HCT116 p53+/+ and HCT116 p53-/- cells were transfected with various siRNAs and protein levels were assessed by Western blot analysis after 72 h. The protein level of Cyclin T1 was used as a loading control.

BRCA1 or CDK12 depletion coupled with CHK1 inhibition induces p21-dependent proliferation block

We also investigated endogenous DNA damage, apoptosis, autophagy, and cell cycle status to gain more insight into the molecular mechanisms responsible for the enhanced cytostatic effect of CDK12 or BRCA1 downregulation coupled with CHK1 inhibition. HCT116 cells were depleted of CDK12, CDK13, or BRCA1 by siRNAs and were then, 24h post-transfection, exposed to a CHK1 inhibitor (SCH900776) for an additional 96h. Samples were collected and assessed for the DNA damage marker

γ H2AX³⁶ and CHK1 autophosphorylation at serine 296, an indication of activated CHK1 kinase.¹⁴

BRCA1 and Cyclin K levels once again decreased following CDK12 knockdown (Figure 2(a)). As expected, treatment with CHK1 inhibitor SCH900776 led to a noticeable decrease in the detected p-S296 CHK1 signal at all tested conditions (Figure 2(a)), and also induced CHK1 degradation in a dose-dependent manner, which is consistent with published research.¹⁴ Importantly, the γ H2AX signal, which reflects the amount of endogenous DNA damage, significantly increased after SCH900776 treatment. This effect was exacerbated in CDK12- and BRCA1-depleted cells, but not in CDK13 cells (Figure 2(a)).

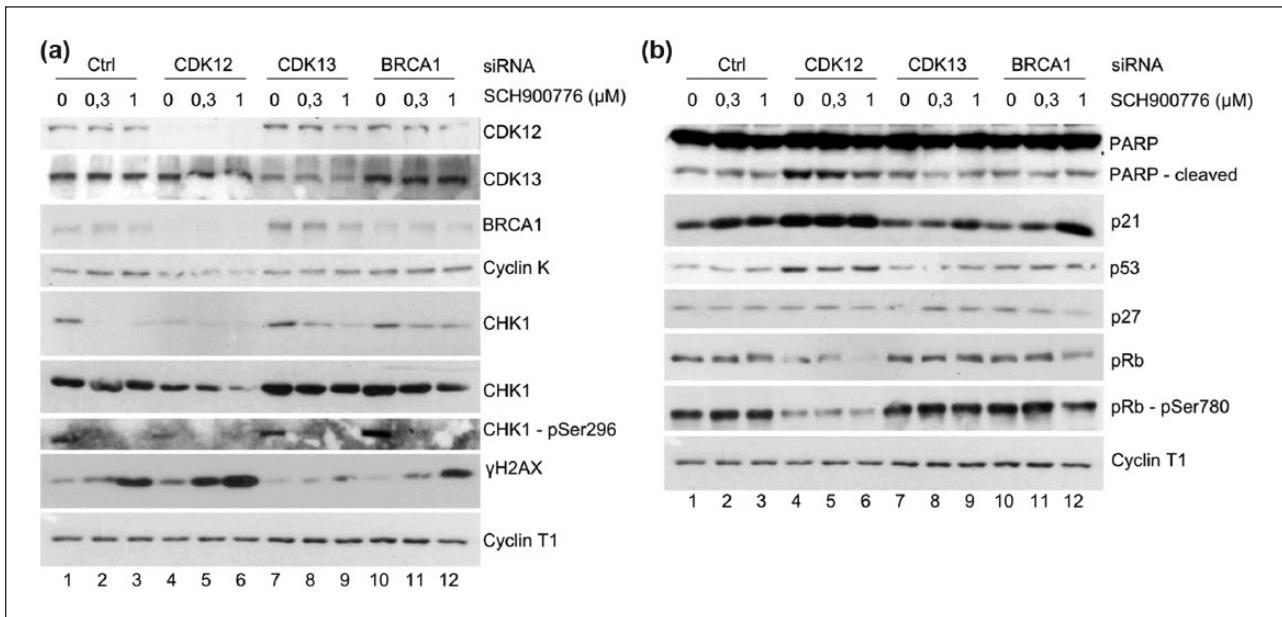


Figure 2. Impact of CDK12 and BRCA1 downregulation on DDR, apoptosis and cell cycle. (a) The effective knockdown of various proteins after siRNA transfection, CHK1 inhibition and DNA damage induction was assessed by Western blot analysis. HCT116 p53^{+/+} cells were transfected with control or specific siRNAs (CTRL, CDK12, CDK13, and BRCA1) and 2 days post-transfection cells were treated with 0, 0.3, or 1 μM CHK1 inhibitor SCH900776 for an additional 96 h. The protein levels of the studied proteins were elucidated by Western blot with indicated antibodies. The protein level of Cyclin T1 was used as a loading control. (b) Status of cellular factors participating in regulation of apoptosis and cell cycle. The protein levels of PARP, a marker of late apoptosis, tumor suppressor p53, and the cell-cycle regulating proteins p21, p27, pRb, and pRb-pSer780 were elucidated by Western blot with indicated antibodies. The protein level of Cyclin T1 was used as a loading control.

Together, these results verified that our experimental setting was successfully able to inhibit CHK1 and confirmed our hypothesis that CHK1 is necessary for the effective repair of endogenous DNA damage, especially in cells lacking functional components of DDR such as CDK12 or BRCA1.

Next we focused on induction of apoptosis, which was examined by the presence of cleaved PARP and Caspase 3, a commonly used markers of apoptosis. Surprisingly, SCH900776 treatment of CDK12-depleted cells only moderately increased PARP-1 cleavage (Figure 2(b)). In addition, no cleaved Caspase 3 was detected after transfection with any siRNAs or after administration of CHK1 inhibitor (Supplementary Figure S2). Furthermore, we were interested whether other types of cell death that might play a role in viability of CDK12-silenced cells, therefore the protein levels of specific autophagy markers were evaluated. As depicted in Supplementary Figure S2, no significant change in the protein level of Beclin, factor associated with vesicle-trafficking during autophagy, after CHK1 inhibitor administration in combination with any of the tested siRNAs was identified. Also, no detectable change in protein level of the cleaved product of LC3B protein was detected in any tested conditions.

Because decreased cell viability cannot be entirely explained by apoptosis or autophagy, we elucidated cell cycle progression. To corroborate this further, we checked

the status of the p21 (Cip1/Waf1), a protein that is a prominent inhibitor of CDKs, can induce cell cycle blockade, and is known to respond to CHK1 inhibition.¹⁴ Indeed, p21 protein levels increased proportionally to CHK1 inhibition under all tested conditions, with BRCA1-depleted cells showing the strongest induction (HCT116 p53^{+/+}) (Figure 2(b), lanes 3 and 12). Interestingly, a robust induction of p21 was also observed upon CDK12 downregulation, even without CHK1 inhibitor treatment (Figure 2(b), lanes 4–6). The p21 induction was detected in HCT116 p53^{-/-} cells as well (Supplementary Figure S3). On the contrary, the expression levels of a related cellular inhibitor of CDKs, the p27 protein, did not change following CHK1 inhibitor treatment, implying a specific induction of p21 in response to CDK12 downregulation (Figure 2(b)).

In addition to regulating G1/S progression through CDK inhibition, p21 also induces the degradation of another cell cycle regulator, the Retinoblastoma protein (pRb).³⁷ Therefore, we evaluated the levels and phosphorylation status of pRb. Silencing of CDK12 led to degradation of pRb regardless of CHK1 inhibition, and a moderate effect was also observed in BRCA1 depleted cells after treatment with 1 μM of SCH900776 (Figure 2(b)). In addition, the cell cycle status was examined by propidium iodide staining followed by flow cytometry. Depletion of CDK12 together with administration of CHK1 inhibitor led to significant prolonged G1 phase and shortened S phase of the cell cycle

in comparison to CTRL-, CDK13-, or BRCA1-silenced cells (Supplementary Figure S4).

Based on these data, we conclude that the enhanced cytostatic effect of CHK1 inhibition in CDK12- or BRCA1-depleted HCT116 p53^{+/+} cells is a result of increased DNA damage, which leads to a robust induction of p21 and delayed cell cycle progression.

BRCA1 depletion sensitizes MDA-MB-231 cells to CHK1 inhibition

Next we tested whether BRCA1 deficiency can sensitize other cancer models to the chemical inhibition of CHK1 kinase. Since BRCA1 deregulation or loss-of-function mutations are common characteristics of ovarian and breast cancers,^{38,39} we chose to manipulate MDA-MB-231 breast cancer cells, which have mutated form of p53 and normal BRCA1 status, prior to the administration of a CHK1 inhibitor. The therapeutic potential of CHK1 inhibitors has been already tested in triple-negative breast cancer (TNBC) cell lines and pre-clinical mouse models, but the status of BRCA1 has not been modified.¹¹

First, we generated two MDA-MB-231 cell lines with stable expression of BRCA1 shRNA (MDA-MB-231 shBRCA1 #2 and #4). Successful BRCA1 depletion at the protein and mRNA level was confirmed by Western blot and RT-PCR, respectively (Figure 3(a)). The effect of BRCA1 downregulation and CHK1 inhibition on cellular viability was assessed by a survival assay that employed the same setup as for HCT116 cells (Figure 3(b)). Treatment with 1 μ M of SCH900776 led to a severe reduction in cell viability, decreasing the cell counts of both depleted cell lines by 70% when compared to the parental non-transfected cells (Figure 3(b)). We examined the effect of CHK1 inhibition on cell viability in MDA-MB-231 (shBRCA1 #2 and #4) cell lines further by performing a clonogenic survival assay, which better reflects the effects of long-term exposure (Figure 3(c)). After 14 days of cultivation, we noticed that the colonies of both untreated shBRCA1 cell lines were larger than those of the parental cell line, suggesting faster cell cycle progression and higher mitotic potential. This is in line with the observation that BRCA1 loss accelerates the growth of cancer cells.⁴⁰ However, treatment with a CHK1 inhibitor (1 μ M) noticeably reduced colony size in both shBRCA1 cell lines and also led to dramatic decrease in cell counts (Figure 3(c)).

Moreover, the 3-day inhibition of CHK1 had no apparent effect on cell cycle in the parental MDA-MB-231 cell line, whereas the shBRCA1 clones experienced a prominent increase in the S-phase cells, suggesting major proliferation arrest (Figure 3(d)).

We then tested how BRCA1 downregulation enhances endogenous DNA instability. A rather moderate, yet

reproducible, increase in γ H2AX levels was observed in both shBRCA1 cell lines in comparison to the parental cells (Figure 3(e), lanes 1, 4, and 7). Interestingly, CHK1 inhibition led to a dramatic increase in the γ H2AX signal in both shBRCA1 cell lines, while the parental cells only demonstrated a moderate dose-dependent γ H2AX response (Figure 3(e)). As was earlier observed in the HCT116 cells, CHK1 inhibition led to a reduction in CHK1 levels and a dose-dependent decrease in total and phosphorylated pRb levels (Figure 3(e)).

In summary, BRCA1 downregulation also sensitizes MDA-MB-231 breast cancer cells to CHK1 inhibitors. As in HCT116 cells, treatment with a CHK1 inhibitor induced excessive DNA damage followed by arrest in the S-phase.

Xenograft mouse model

Based on our in vitro results, we decided to assess the in vivo therapeutic effects of CHK1 inhibitors by employing a mouse orthotopic xenograft model of the MDA-MB-231 parental and shBRCA1 #4 human breast carcinoma cells in the fat pads of SHO-*Prkdc*^{SCID} *Hr*^{Hr} mice. Mice were continuously monitored for the development of a primary xenograft tumor and sacrificed when tumors reached 10% of body weight. Besides the observation that animals transplanted with either parental or shBRCA1 #4 MDA-MB-231 cells all formed tumors (100% tumor growth), mice injected with shBRCA1 cells showed a slightly higher proportion of tumor volume, reflecting faster growth of shBRCA1 cells (Figure 3(c)). Furthermore, the growth rate and final size of the tumors differed distinctly between populations after CHK1 inhibitor treatment. The parental MDA-MB-231 control cells formed significant tumors over the course of 44 days, but treatment with a CHK1 inhibitor did not significantly affect the size of the tumors when compared to control animals (Figure 4(a)). In contrast, the animals injected with shBRCA1 MDA-MB-231 cells developed significantly larger tumors than the control group, and treatment with a CHK1 inhibitor significantly decreased tumor size (Figure 4(b)).

Discussion

CHK1 inhibitors represent a promising cancer therapy approach.³ Since the anti-cancer effect of CHK1 inhibitors is potentiated by DNA damaging drugs, we hypothesized that impaired DDR will have a similar synergistic effect. In our previous study, we demonstrated that CDK12 regulates the transcription of certain DDR genes, particularly HR genes (including BRCA1), and is necessary for maintaining genomic stability.¹⁶ In line with this observation, the loss of either BRCA1 or CDK12 is a prerequisite for sensitizing cancer cells to PARP1/2 inhibitors.^{21,41} In this study, we demonstrate that the loss of BRCA1 or CDK12 also potentiates the anti-proliferative effect of CHK1 inhibitors.

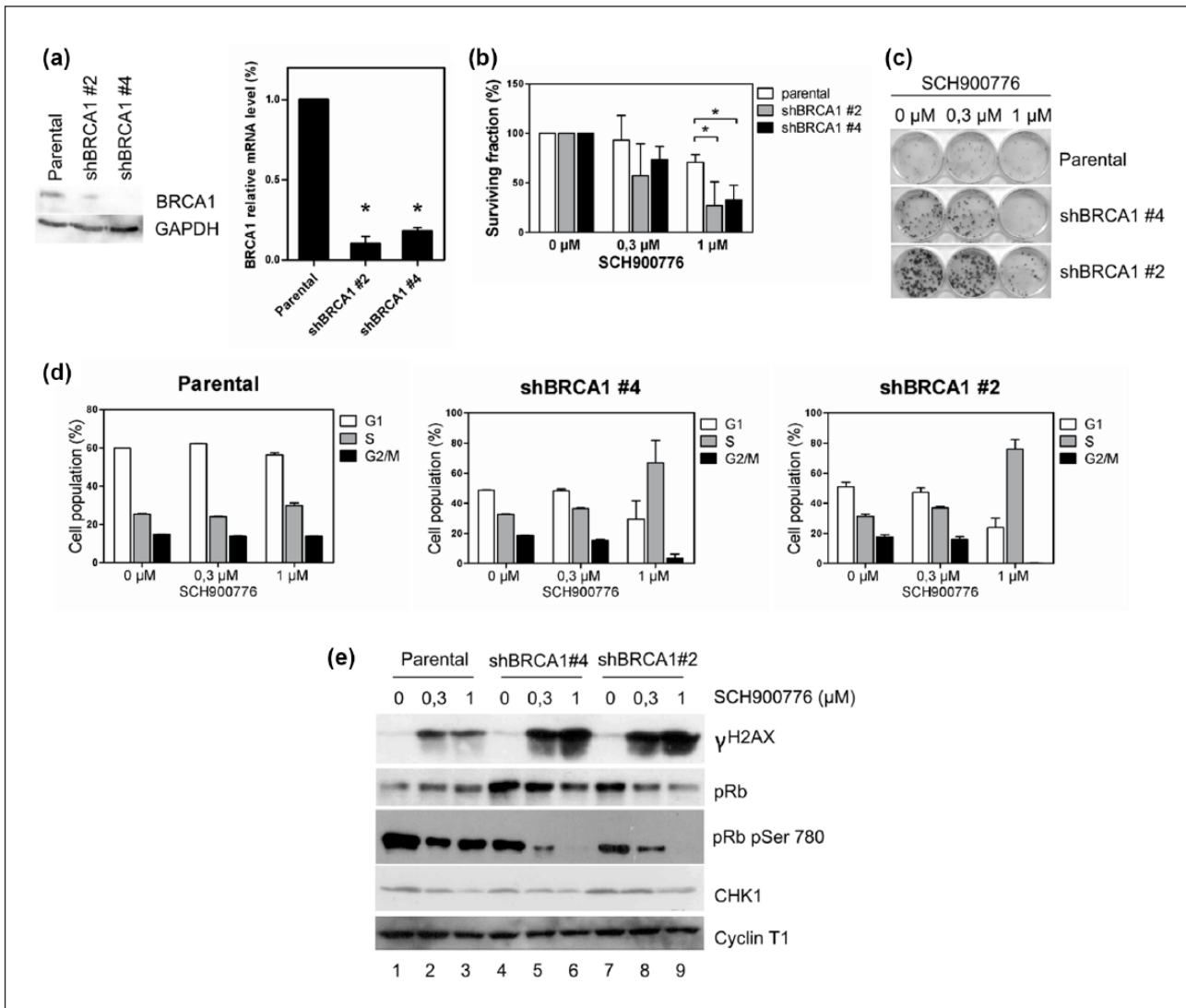


Figure 3. Downregulation of BRCA1 sensitizes MDA-MB-231 cells to CHK1 inhibitor. (a) BRCA1 protein levels were evaluated in shBRCA1 #2 and shBRCA1 #4 MDA-MB-231 cell lines by Western blot analysis. GAPDH was used as a loading control. The mRNA levels of BRCA1 in these cell lines were measured by RT-qPCR ($p < 0.05$, Student's *t*-test). These experiments confirmed effective BRCA1 downregulation by shRNAs in these cell lines. (b) CHK1 inhibition reduced the viability of MDA-MB-231 cells expressing shRNAs against BRCA1. The graphs show the results of survival assays of parental, shBRCA1 #2 and shBRCA1 #4 MDA-MB-231 cells treated with 0, 0.3, or 1 μ M CHK1 inhibitor SCH900776 for 3 days. For each cell line, the cell numbers were normalized to the relative growth of cells treated with DMSO. Error bars represent SEM for three independent experiments ($p < 0.05$, Student's *t*-test). (c) A 14-day clonogenic assay showed that the combination of BRCA1 silencing and CHK1 inhibition reduces cell viability. MDA-MB-231 cell lines were seeded and treated with the indicated SCH900776 concentrations. The experiment was performed three times in duplicates. BRCA1 silencing combined with CHK1 inhibition reduces cell viability. (d) CHK1 inhibition strongly affected the cell cycle progression of BRCA1-silenced MDA-MB-231 cell lines. Cells were cultivated and treated as described in (b). Cell cycle progression was evaluated by the incorporation of propidium iodide followed by flow cytometry. Error bars represent SEM for three experiments. (e) The combination of BRCA1 silencing and CHK1 inhibition induces a stronger activation of DDR. Cells were prepared and treated as described in (b). The activation of DDR and inhibition of CHK1 by SCH900776 were validated by Western blot with antibodies against γ H2AX pSer139 and CHK1, respectively. The dose-dependent degradation of total pRb and pRb phosphorylated on serine 780 following CHK1 inhibition was examined by Western blot. Cyclin T1 was used as a loading control.

Our results show that the anti-proliferative effect of CHK1 inhibitor treatment combined with BRCA1 or CDK12 deficiency is comparable in both cell lines regardless of p53 status. Previous reports have shown that CHK1 inhibition leads to increased DNA damage by measuring

the induction of γ H2AX pSer139 in HCT116 cells.^{6,14} The strongest effect was obtained when CHK1 inhibition was combined with CDK12 silencing. Interestingly, in contrast to the results obtained in HeLa cells,¹⁶ we did not observe increased γ H2AX Ser139 phosphorylation upon CDK12

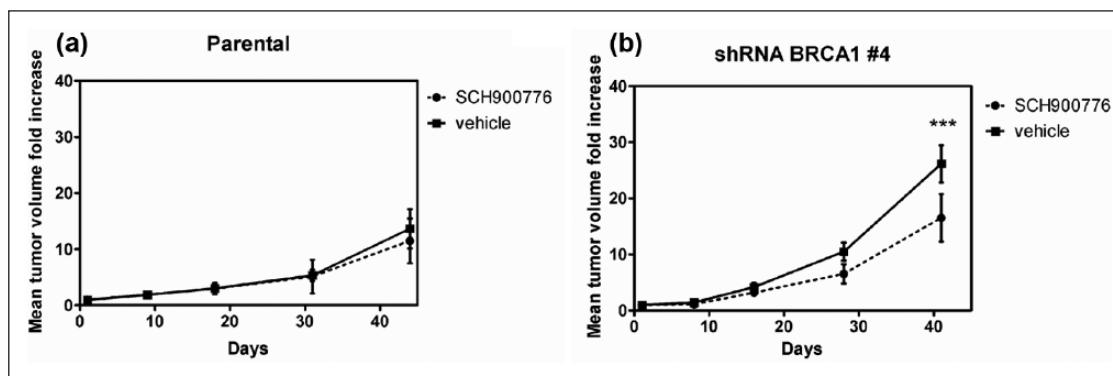


Figure 4. Inhibition of CHK1 prevents tumor growth in vivo. The CHK1 inhibitor SCH900776 decreased tumor growth. The (a) parental and (b) shBRCA1 MDA-MB-231 cells were transplanted into the mammary pads of SCID mice. When tumor mass reached a volume of 0.03 cm³, mice were treated with either a vehicle solution of 20% Kolliphor ELP or SCH900776 25 mg/kg/day dissolved in the same 20% Kolliphor solution, every day for 5 days. The growth of tumor mass was then monitored over set time periods. Each data point represents the mean increase in tumor volume after the beginning of treatment and error bars represent SEM, where *n* for each cohort was six animals ($p < 0.001$, Student's *t*-test for shBRCA1 SCH900776 vs shBRCA1 vehicle).

depletion in HCT116 cells. This may be partially due to differences between these cell lines. However, we observed robust γ H2AX pSer139 induction in the MDA-MB-231 BRCA-silenced cells after CHK1 inhibition. CHK1 inhibition was previously reported to induce the cell cycle regulator p21.¹⁴ We observed a particularly robust p21 increase in BRCA1-silenced cells. CDK12 silencing (regardless of CHK1 inhibition) resulted in increased apoptosis, which was consistent with result obtained from CDK12 inhibition.⁴² Based on the data obtained from MDA-MB-231 cells, one could speculate that CHK1 inhibitors trigger increased DNA damage and replication stress during the S-phase of the cell cycle, which is incompatible with cell proliferation or survival. Moreover, the potential of CHK1 inhibitors to weaken tumor growth has been reported by several groups, but, as of yet, the synergy between impaired CDK12 function and CHK1 inhibition to counteract tumor progression has not been investigated.^{6,9,11}

It has been demonstrated that CDK12 regulates the expression of DDR genes including CHK1.²⁰ Importantly, high-grade serous ovarian tumors bearing CDK12 mutations have reduced CHK1 expression.²⁰ Therefore, we speculate that viability of CDK12-depleted cells rely extensively on the residual activity of CHK1 making these cells sensitive to lower doses of CHK1 inhibitors.

Several studies have demonstrated that CDK12 regulates the expression of DDR genes (BRCA1, FANCI, FANCD2, and ATM).^{16,20,42} Nevertheless, the precise mechanism of this regulation has not yet been described. CDK12 loss might downregulate DDR genes directly through the role of CDK12 in the transcription of these genes, as has been suggested by numerous studies.^{16,19,20,42,43}

In addition, a recent publication reported that genomic instability in ovarian tumors with a loss of CDK12 has a specific pattern of defective HR caused by BRCA1/2

deficiency suggesting that CDK12 functions in additional parts of the DNA repair machinery.⁴⁴ From the clinical point of view, about 9% and 13% of unselected women with newly diagnosed triple-negative breast cancer and ovarian cancer (respectively) have an inheritable BRCA1 mutation. If metastatic, these patients have generally very unfavorable prognosis and currently are candidates for targeted drug therapy, such as PARP inhibitors.^{24–26} We confirmed the additive effect of BRCA1 loss-of-function and CHK1 on cell proliferation in vitro and in vivo. A xenograft model was employed to evaluate whether CHK1 inhibition confers an anti-proliferative effect on tumor growth in vivo. CHK1 inhibitor administration had no substantial impact on the parental MDA-MB-231 cells, which was in sharp contrast to significant decrease in tumor mass observed in BRCA1-silenced cells receiving CHK1 inhibitors (Figure 4). Recent studies have clearly shown that patients can develop a resistance to PARP1/2 inhibitors over the course of PARP inhibitor therapy.⁴⁵ Since many factors, such as HR and NHEJ status, as well as the level, activity, or intracellular concentration of PARP proteins, can influence the efficacy of PARP inhibitors, it is vital to identify different conditions that can either re-sensitize tumor cells to PARP inhibitors or enable the use of additional strategies that target the systems necessary for cell survival to treat resistant tumors. The anti-proliferative effect of CHK1 inhibitors in BRCA1-deficient (HR compromised) tumor cells differs from that of PARP1 inhibitors; hence, it seems rational to investigate how using CHK1 inhibitors as a second round of therapy will affect patients who have tumors resistant to PARP inhibitors due to the restoration of HR.

In summary, we have found that CHK1 inhibition is a promising strategy for targeting BRCA1- or CDK12-deficient cells. We propose that BRCA1 and CDK12 deficiency should be considered a CHK1 sensitivity biomarker candidate. The

cell cycle arrest triggered by recently developed specific CDK12 inhibitors is in line with our presented observations.⁴² Moreover, combination therapy with PARP1/2 inhibitors and a CDK12 inhibitor conferred a strong anti-proliferative effect in breast cancer cells.⁴¹ Our results provide promising evidence for the combinatory effect of CDK12 and CHK1 inhibitors in treating cancer patients.^{41–43}

Acknowledgements

The authors certify that they have NO affiliations with, or involvement in, any organization or entity with any financial or non-financial interest (such as personal or professional relationships, affiliations, knowledge or beliefs) in the subject matter or materials discussed in this manuscript. The authors would like to thank Dr Sabina Sevcikova and members of the J. Kohoutek laboratory for critical discussion and their suggestions during the preparation of this manuscript, Dr Jiri Jarkovsky for statistical analyses, Prof. Jiri Bartek for helpful discussion, D. Blazek for providing us with OVSAHO cells and Dr Miroslav Machala for the sharing antibodies that were used in the Western blot analyses.

Declaration of conflicting interests

The author(s) declared no potential conflicts of interest with respect to the research, authorship, and/or publication of this article.

Funding

The author(s) disclosed receipt of the following financial support for the research, authorship, and/or publication of this article: This study was supported by the Internal Grant Agency of the Ministry of Health of the Czech Republic, grant NT14599-3/2013 (M.S. and J.K.); the Ministry of Health of the Czech Republic, grant 16-34152A (J.K.); the Ministry of Agriculture, grant RO0517; the European Regional Development Fund, project no. LQ1605 from the National Program of Sustainability II (MEYS CR) (K.S., K.P., and O.H.); the Ministry of Health of the Czech Republic, grant 15-33999A (M.S., K.P., and K.S.); CZ-OPENSUREEN: National Infrastructure for Chemical Biology, LM2015063 (K.P.); the Czech National Program of Sustainability, LO1304 (J.K. and M.M.); and the Norwegian Financial Mechanism 2009-2014 Project, Contract 7F14061 (J.K.).

Supplementary material

Supplementary material is available for this article online

References

- Hanahan D and Weinberg RA. Hallmarks of cancer: the next generation. *Cell* 2011; 144: 646–674.
- Ma CX, Janetka JW and Piwnicka-Worms H. Death by releasing the breaks: CHK1 inhibitors as cancer therapeutics. *Trends Mol Med* 2011; 17: 88–96.
- McNeely S, Beckmann R and Bence Lin AK. CHEK again: revisiting the development of CHK 1 inhibitors for cancer therapy. *Pharmacol Ther* 2014; 142: 1–10.
- Thompson R and Eastman A. The cancer therapeutic potential of chk1 inhibitors: how mechanistic studies impact on clinical trial design. *Br J Clin Pharmacol* 2013; 76: 358–369.
- Bahassi EM, Ovesen JL, Riesenberg AL, et al. The checkpoint kinases Chk1 and Chk2 regulate the functional associations between hBRCA2 and Rad51 in response to DNA damage. *Oncogene* 2008; 27: 3977–3985.
- Guzi TJ, Paruch K, Dwyer MP, et al. Targeting the replication checkpoint using SCH 900776, a potent and functionally selective CHK1 inhibitor identified via high content screening. *Mol Cancer Ther* 2011; 10: 591–602.
- Kim MK, James J and Annunziata CM. Topotecan synergizes with CHEK1 (CHK1) inhibitor to induce apoptosis in ovarian cancer cells. *BMC Cancer* 2015; 15: 196.
- Ma CX, Ellis MJ, Petroni GR, et al. A phase II study of UCN-01 in combination with irinotecan in patients with metastatic triple negative breast cancer. *Breast Cancer Res Treat* 2013; 137: 483–492.
- Montano R, Thompson R, Chung I, et al. Sensitization of human cancer cells to gemcitabine by the Chk1 inhibitor MK-8776: cell cycle perturbation and impact of administration schedule in vitro and in vivo. *BMC Cancer* 2013; 13: 604.
- Perez RP, Lewis LD, Beelen AP, et al. Modulation of cell cycle progression in human tumors: a pharmacokinetic and tumor molecular pharmacodynamic study of cisplatin plus the Chk1 inhibitor UCN-01 (NSC 638850). *Clin Cancer Res* 2006; 12: 7079–7085.
- Ma CX, Cai S, Li S, et al. Targeting Chk1 in p53-deficient triple-negative breast cancer is therapeutically beneficial in human-in-mouse tumor models. *J Clin Invest* 2012; 122: 1541–1552.
- Chen Z, Xiao Z, Gu WZ, et al. Selective Chk1 inhibitors differentially sensitize p53-deficient cancer cells to cancer therapeutics. *Int J Cancer* 2006; 119: 2784–2794.
- Chen CC, Kennedy RD, Sidi S, et al. CHK1 inhibition as a strategy for targeting Fanconi Anemia (FA) DNA repair pathway deficient tumors. *Mol Cancer* 2009; 8: 24.
- Kim MK, Min DJ, Wright G, et al. Loss of compensatory pro-survival and anti-apoptotic modulator, ikkepsilon, sensitizes ovarian cancer cells to CHEK1 loss through an increased level of p21. *Oncotarget* 2014; 5: 12788–12802.
- Bartkowiak B, Liu P, Phatnani HP, et al. CDK12 is a transcription elongation-associated ctd kinase, the metazoan ortholog of yeast Ctk1. *Genes Dev* 2010; 24: 2303–2316.
- Blazek D, Kohoutek J, Bartholomeeusen K, et al. The cyclin K/Cdk12 complex maintains genomic stability via regulation of expression of DNA damage response genes. *Genes Dev* 2011; 25: 2158–2172.
- Cheng SW, Kuzyk MA, Moradian A, et al. Interaction of cyclin-dependent kinase 12/CRKRS with cyclin K1 is required for the phosphorylation of the C-terminal domain of RNA polymerase II. *Mol Cell Biol* 2012; 32: 4691–4704.
- Kohoutek J and Blazek D. Cyclin K goes with Cdk12 and Cdk13. *Cell Div* 2012; 7: 12.
- Joshi PM, Sutor SL, Huntoon CJ, et al. Ovarian cancer-associated mutations disable catalytic activity of CDK12, a kinase that promotes homologous recombination repair and resistance to cisplatin and poly(ADP-ribose) polymerase inhibitors. *J Biol Chem* 2014; 289: 9247–9253.
- Ekumi KM, Paculova H, Lenasi T, et al. Ovarian carcinoma CDK12 mutations misregulate expression of DNA repair genes via deficient formation and function of the Cdk12/CycK complex. *Nucleic Acids Res* 2015; 43: 2575–2589.

21. Bajrami I, Frankum JR, Konde A, et al. Genome-wide profiling of genetic synthetic lethality identifies CDK12 as a novel determinant of PARP1/2 inhibitor sensitivity. *Cancer Res* 2014; 74: 287–297.
22. Deng CX. BRCA1: cell cycle checkpoint, genetic instability, DNA damage response and cancer evolution. *Nucleic Acids Res* 2006; 34: 1416–1426.
23. Jiang Q and Greenberg RA. Deciphering the BRCA1 tumor suppressor network. *J Biol Chem* 2015; 290: 17724–17732.
24. Helleday T. Homologous recombination in cancer development, treatment and development of drug resistance. *Carcinogenesis* 2010; 31: 955–960.
25. Konecny GE and Kristeleit RS. PARP inhibitors for BRCA1/2-mutated and sporadic ovarian cancer: current practice and future directions. *Br J Cancer* 2016; 115: 1157–1173.
26. Bartek J, Mistrik M and Bartkova J. Thresholds of replication stress signaling in cancer development and treatment. *Nat Struct Mol Biol* 2012; 19: 5–7.
27. Gaillard H, Garcia-Muse T and Aguilera A. Replication stress and cancer. *Nat Rev Cancer* 2015; 15: 276–289.
28. Dwyer MP, Paruch K, Labroli M, et al. Discovery of pyrazolo[1,5-a]pyrimidine-based CHK1 inhibitors: a template-based approach—part 1. *Bioorg Med Chem Lett* 2011; 21: 467–470.
29. Labroli M, Paruch K, Dwyer MP, et al. Discovery of pyrazolo[1,5-a]pyrimidine-based CHK1 inhibitors: a template-based approach—part 2. *Bioorg Med Chem Lett* 2011; 21: 471–474.
30. Bunz F, Dutriaux A, Lengauer C, et al. Requirement for p53 and p21 to sustain G2 arrest after DNA damage. *Science* 1998; 282: 1497–1501.
31. Tiscornia G, Singer O and Verma IM. Production and purification of lentiviral vectors. *Nat Protoc* 2006; 1: 241–245.
32. Dai Y, Chen S, Kmiecik M, et al. The novel Chk1 inhibitor MK-8776 sensitizes human leukemia cells to HDAC inhibitors by targeting the intra-S checkpoint and DNA replication and repair. *Mol Cancer Ther* 2013; 12: 878–889.
33. Greifenberg AK, Honig D, Pilarova K, et al. Structural and functional analysis of the CDK13/Cyclin K complex. *Cell Rep* 2016; 14: 320–331.
34. Wang FZ, Fei HR, Cui YJ, et al. The checkpoint 1 kinase inhibitor LY2603618 induces cell cycle arrest, DNA damage response and autophagy in cancer cells. *Apoptosis* 2014; 19: 1389–1398.
35. Domcke S, Sinha R, Levine DA, et al. Evaluating cell lines as tumour models by comparison of genomic profiles. *Nat Commun* 2013; 4: 2126.
36. Sedelnikova OA, Rogakou EP, Panyutin IG, et al. Quantitative detection of (125)IdU-induced DNA double-strand breaks with gamma-H2AX antibody. *Radiat Res* 2002; 158: 486–492.
37. Broude EV, Swift ME, Vivo C, et al. P21(Waf1/Cip1/Sdi1) mediates retinoblastoma protein degradation. *Oncogene* 2007; 26: 6954–6958.
38. Cancer Genome Atlas Network. Comprehensive molecular portraits of human breast tumours. *Nature* 2012; 490: 61–70.
39. Cancer Genome Atlas Research Network. Integrated genomic analyses of ovarian carcinoma. *Nature* 2011; 474: 609–615.
40. Mullan PB, Quinn JE and Harkin DP. The role of BRCA1 in transcriptional regulation and cell cycle control. *Oncogene* 2006; 25: 5854–5863.
41. Johnson SF, Cruz C, Greifenberg AK, et al. CDK12 inhibition reverses de novo and acquired PARP inhibitor resistance in BRCA wild-type and mutated models of triple-negative breast cancer. *Cell Rep* 2016; 17: 2367–2381.
42. Zhang TH, Kwiatkowski N, Olson CM, et al. Covalent targeting of remote cysteine residues to develop CDK12 and CDK13 inhibitors. *Nat Chem Biol* 2016; 12: 876.
43. Blazek D. Transcriptional kinases caught by a sticky drug. *Nat Chem Biol* 2016; 12: 765–766.
44. Popova T, Manie E, Boeva V, et al. Ovarian cancers harboring inactivating mutations in CDK12 display a distinct genomic instability pattern characterized by large tandem duplications. *Cancer Res* 2016; 76(7): 1882–1891.
45. Ricks TK, Chiu HJ, Ison G, et al. Successes and challenges of parp inhibitors in cancer therapy. *Front Oncol* 2015; 5: 222.

APPENDIX 8

PACULOVÁ, Hana a Jiří KOHOUTEK. The emerging roles of CDK12 in tumorigenesis. *Cell Division*. 2017, 12, 7.

REVIEW

Open Access



The emerging roles of CDK12 in tumorigenesis

Hana Paculová and Jiří Kohoutek*

Abstract

Cyclin-dependent kinases (CDKs) are key regulators of both cell cycle progression and transcription. Since dysregulation of CDKs is a frequently occurring event driving tumorigenesis, CDKs have been tested extensively as targets for cancer therapy. Cyclin-dependent kinase 12 (CDK12) is a transcription-associated kinase which participates in various cellular processes, including DNA damage response, development and cellular differentiation, as well as splicing and pre-mRNA processing. CDK12 mutations and amplification have been recently reported in different types of malignancies, including loss-of-function mutations in high-grade serous ovarian carcinomas, and that has led to assumption that CDK12 is a tumor suppressor. On the contrary, CDK12 overexpression in other tumors suggests the possibility that CDK12 has oncogenic properties, similarly to other transcription-associated kinases. In this review, we discuss current knowledge concerning the role of CDK12 in ovarian and breast tumorigenesis and the potential for chemical inhibitors of CDK12 in future cancer treatment.

Keywords: CDK12, RNA pol II, Suppressor, Oncogene, Dinaciclib, THZ531

Background

Cyclin-dependent kinases (CDKs) are principal regulators of various cellular processes. They are divided into two subfamilies: cell cycle-associated CDKs (CDK1, 2, 4, 6), which directly regulate progression through individual cell cycle phases, and transcription-associated CDKs (CDK7, 8, 9, 11, 12, 13), which regulate gene transcription. These kinases phosphorylate the C-terminal domain (CTD) of Rbp1, the largest subunit of RNA polymerase II (RNA pol II) as well as various transcription regulatory factors. Since CDKs are frequently dysregulated in tumor cells, therefore they are attractive therapeutic targets for a broad spectrum of tumors [1, 2].

Eukaryotic transcription is very complex and tightly regulated. Essential cellular processes, including differentiation and response to extracellular stimuli, depend on regulation at the transcriptional level [3]. In addition, precise coordination of transcription with other events, such as mRNA processing, splicing, chromatin remodeling, and modification of histones is crucial for normal

cellular physiology. Consequently, deregulation of these processes drives cancer onset and progression [4].

Transcription factors are frequently mutated in cancer cells and represent typical oncogenes and tumor suppressors. These mutations lead to alterations in the gene expression programs and might create dependency on certain transcriptional regulators making cancer cells addicted to their activities [5]. Such a phenomenon is called “Transcriptional Addiction”, and it provides opportunities for novel therapeutic interventions in cancer [5].

CDK12 is a transcription-associated CDK that phosphorylates the CTD of RNA pol II and it is essential for DNA damage response (DDR), splicing, and differentiation [6]. CDK12 mutations as well as overexpression have been reported in various malignancies. Subsequently, two CDK12 inhibitors were developed independently. They will be instrumental for studying physiological function of CDK12 and could be tested as anti-cancer drugs [7, 8]. In this review, we summarize current knowledge concerning CDK12 role in tumorigenesis and its therapeutic potential.

*Correspondence: kohoutek@vri.cz

Department of Chemistry and Toxicology, Veterinary Research Institute, Hudcova 296/70, Brno 621 00, Czech Republic

CDKs in transcription regulation

Transcription is a complex process coordinated by numerous factors. Posttranslational modifications (particularly phosphorylation) of RNA pol II CTD constitute one of the crucial mechanisms of transcription regulation [3, 4]. RNA pol II is a multi-subunit complex responsible for RNA synthesis of eukaryotic genes coding most proteins and small RNAs. Modifications of CTD, which consists of repeated YSPTSPS heptapeptides, form patterns that enable specific binding of various factors coordinating transcription as well as co-transcriptional pre-mRNA processing [3, 4]. Phosphorylation of serines, threonine and tyrosine, among other post-translational modifications, is essential for the transition between individual phases of transcription, such as initiation, elongation, termination, and individual steps of pre-mRNA processing. The majority of kinases phosphorylating CTD of RNA pol II belong to the group of transcription-related CDKs. CDK7 is a part of transcription initiation factor TFIIF. CDK9, responsible for the activity of P-TEFb, is associated with early elongation [3, 4].

CDK12 structure, homologs and associating cyclin

In 2001, a new transcription-related kinase was discovered. It was described as a Cdc2-related kinase with an arginine/serine-rich (RS) domain (CrkRS). The CrkRS consists of 1490 amino acids and has a kinase domain, proline-rich regions and a serine-rich domain, which is typical for splicing factors from the SR protein family [9].

Later on, cyclins L1 and L2 were described as CDK12-associating cyclins and the CrkRS was renamed to CDK12 [10]. Nevertheless, the cloning of *Drosophila* CDK12 led to identification of cyclin K as a *bona fide* CDK12-associating cyclin. The cyclin K/CDK12 complex was demonstrated to phosphorylate the CTD of RNA pol II in vitro, and CDK12 was established as a CTD kinase [11]. The association between cyclin K and CDK12 was further confirmed by mass spectrometry and immunoprecipitation in mammalian cells [12, 13]. Additionally, the ability of CDK12 to phosphorylate the CTD of RNA pol II was clearly demonstrated [12]. Analogically to CDK9, CDK12 is expected to phosphorylate additional substrates other than CTD, such as transcription or splicing factors, which may be critical for CDK12 role in regulation of transcription and related processes. Additional CDK12 phosphorylation targets and related biological functions remain to be determined. The crystal structure of CDK12 was later described, opening new possibilities to study its function and its potential as a drug target and to develop specific CDK12 inhibitors [14]. The closest CDK12 human homologue is CDK13 (also known as CDC2L5, CHED). It contains a kinase domain which

displays high sequence identity to CDK12 kinase domain, but its sequence is unrelated on C- and N- terminus. CDK13 associates with Cyclin K and forms a separate complex [12]. Similarly to CDK12, CDK13 is capable of phosphorylating CTD [12]. Nevertheless, CDK13 is much less studied than CDK12 and its function is less clear. Due to the sequence similarity, one can expect a redundancy or overlap in functions of these two kinases.

In yeast (*S. cerevisiae*), there are two kinases capable of phosphorylating Ser2 of CTD, Ctk1 and Bur1. Before CDK12 and CDK13 were discovered, it was assumed that CDK9 is the only metazoan orthologue of Ctk1 and Bur1. Based on evolutionary and functional evidence Bartkowiak et al. identified *Drosophila* CDK12 and human CDK12 and CDK13 as an ortholog of yeast Ctk1, while Bur1 is CDK9 orthologue [11, 15]. Lsk1, less studied Ser2 CTD phosphorylating protein, is CDK12 ortholog in *S. pombe* [11].

CDK12 in transcription regulation

Similarly to CDK9, CDK12 is associated with transcription elongation and is able to phosphorylate the RNA pol II CTD serine at position 2 (Ser2) in *Drosophila* [11] and in human cells [12, 13]. However, downregulation of CDK12 activity does not affect the global transcription rate, and when CDK12 is depleted from cells, transcription of a unique subset of genes is altered (interestingly mainly the genes necessary for DDR). Depletion of CDK12 and Cyclin K results in decreased expression of long genes (> 10 kb) and genes with higher number of exons. Observations have led to the hypothesis that CDK12 is a kinase that promotes transcription of a set of specific genes [12]. Supporting this hypothesis, CDK12 was found to be necessary for the expression of Nrf2-dependent genes in *Drosophila* cells, where CDK12 does not affect the overall transcription but is rather involved in the transcriptional stress response [16].

Nevertheless, recent studies provide arguments against a hypothesis that CDK12 is a gene-specific CDK kinase. According to this concept, CDK12 is actively recruited to the body of transcribed genes by fully operated Pol II associated factor 1 (Paf1) right after paused RNA pol II is released into the productive elongation phase [17]. Also, when specific anti-CDK12 antibody was used in a ChIP-Seq experiment, it was found that CDK12 binds to promoters and bodies of protein-coding genes and to active transcription enhancers, with the ChIP-seq signal overlapping with the RNA pol II signal [8]. The same group developed a specific CDK12 inhibitor and identified CDK12-responsive genes in microarray experiments. Critically, a lower dose of the CDK12 inhibitor reduced transcription of core DDR genes (including BRCA1,

FANCF and ERCC4) and higher inhibitor dose decreased expression of super-enhancer-associated genes compared to genes associated with typical enhancers [8].

An additional aspect related to CDK12 function in transcription is the specificity of CDK12 in relation to the specific serine within CTD. In the classical view, CDK12 phosphorylates CTD Ser2 *in vivo* and *in vitro*. In contrast to CDK9, CDK12 is responsible for Ser2 phosphorylation on the 3' prime end of genes [8]. In an attempt to clarify CDK12 substrate preference, the Geyer group performed *in vitro* kinase assays and immunoprecipitation experiments. They described CDK12 ability to phosphorylate both CTD Ser2 and Ser5; however, it needs pre-phosphorylation of CTD on Ser7 for optimal activity [14]. Nonetheless, inhibition of CDK12 in HeLa cells led to a severe block of cell growth but global phosphorylation of individual CTD related serines was affected only moderately [18]. Finally, CDK12 inhibition leads to a reduction in global Ser2 but not Ser5 or Ser7 phosphorylation of the CTD [8]. To date, CTD substrate specificity studies have been dependent on antibodies against specific CTD modifications, such as H5, H14, and antibodies prepared by the Eick group [19]. The specificity of these antibodies seems to be affected by neighboring modifications [18], which could bias the results and make it challenging to draw conclusions. A cellular system suitable for mass spectroscopy analyses of CTD of RNA pol II modifications was recently developed. It provides a promising tool for elucidating the specificity of CDK12 and other CDKs in relation to individual CTD serines [20].

In addition to regulating the elongation phase of transcription, CDK12 participates in transcription termination. Polyadenylation-coupled phosphorylation of Ser2 at the 3' end of the *MYC* gene by CDK12 is necessary for recruitment of polyadenylation factor CstF77 and is therefore necessary for effective transcription termination [21]. Similarly, CDK12 depletion leads to reduced Ser2 phosphorylation and cleavage stimulation factor 64 (CstF64), thereby leading to impaired 3' end processing of the *c-FOS* gene after activation of EGF signaling [22]. These two studies clearly demonstrated how regulation of transcription is coupled to pre-mRNA processing by recruiting different factors to modified CTD.

It is evident that transcription elongation and termination serve as regulatory steps in gene expression. Dysregulation of these processes may alter levels of tumor suppressors or oncogenes and possibly result in tumorigenesis. Nevertheless, the exact role of CDK12 in transcription regulation is not fully understood. The fundamental question remains unanswered as to whether CDK12 affects transcription globally or if it is

kinase-specific for a unique set of genes, such as DDR or super-enhancer-associated genes? Similarly to CDK9, CDK12 could bind and phosphorylate also additional factors and thus regulate transcription employing CTD phosphorylation independent mechanisms.

CDK12 function in splicing

Since its discovery, it has been known that CDK12 co-localizes with SC35 (also known as SRSF2 or SFRS2), a spliceosome component, and contains the RS domain which is typical for RNA-interacting and splicing factors [9]. Supporting CDK12 involvement in RNA-splicing machinery, three studies independently identified several factors of the splicing apparatus and components of nuclear speckles to be putative CDK12-associating partners based on mass spectrometry analyses [18, 22, 23]. Nevertheless, most of these associations have not yet been confirmed by immunoprecipitation with endogenous CDK12. One example of CDK12 involvement in splicing is based on the observation that depletion of CDK12 leads to dysregulated alternative splicing of serine/arginine splicing factor1 (SRSF1). In addition to its association with splicing factors, CDK12 was demonstrated to co-immunoprecipitate proteins of exon junction complexes and RNA-binding proteins [22]. In addition, *Drosophila* CDK12 is involved in the alternative splicing of *neurexin IV* in coordination with mRNA-binding protein *HOW* during *Drosophila* nervous system development [24].

A recent study confirmed that CDK12 is involved in splicing. The authors described interaction of CDK12 with spliceosome components and splicing regulatory factors using immunoprecipitation followed by mass spectroscopy [25]. In RNA-seq experiments, Tien et al. described a new role of CDK12 in splicing: CDK12 regulates alternative last exon splicing, gene- and cell type-specific specialized type of alternative splicing. In breast cancer cells, depletion or overexpression of CDK12 leads to altered alternative last exon splicing of a subset of genes and may contribute to tumorigenesis [25].

Despite a growing body of evidence supporting CDK12 involvement in splicing, the precise role of CDK12 in this process as well as other co-transcriptional events is yet to be elucidated. Description of additional binding factors and new potential phosphorylation substrates may clarify the precise function of CDK12 in this process. CDK12 could form a functional link between transcription regulation and co-transcriptional pre-mRNA splicing. Alternative splicing affects a large number of transcripts in mammals and provides regulation for the majority of cellular processes. Aberrant splicing of various regulatory

factors also leads to tumorigenesis [26–28] providing one of the explanatory roles for CDK12 deficiency in tumorigenesis via splicing dysregulation.

CDK12 in development

Even though CDK12 is ubiquitously expressed, the CDK12 protein level differs in particular tissues. High human CDK12 levels can be found in testes, ovaries, leukocytes and adrenal gland, measured by mRNA levels [29]. High mouse CDK12 protein levels are in testes as well as in highly proliferative tissues and mouse embryonic stem cells [30]. This suggests that CDK12 could have tissue-specific roles in cellular commitment and differentiation. Several studies have pointed out CDK12 function in neuronal development and differentiation [31–33]. For instance, depletion of CDK12 (and CDK13) leads to reduced axonal outgrowth mediated probably by lowered CDK5 expression [32]. Ser2 phosphorylation in *C. elegans* germline depends on the activity of CDK12/cyclin K rather than on CDK9 [34].

As is evident from mouse studies, both CDK12 and its associating cyclin K are essential for early embryogenesis in mice. In vitro cultured CDK12 $-/-$ blastocysts fail to undergo inner cell mass outgrowth due to increased apoptosis and impaired repair of DNA damage [33].

CDK12 associating cyclin K is highly expressed in murine embryonic stem cells but not in their differentiated derivatives. The cyclin K protein level decreases with differentiation and correlates with levels of Oct4, Sox and Nanog proteins known to be necessary for maintaining stemness. These observations suggest that cyclin K/CDK12 and also cyclin K/CDK13 complexes take part in maintaining the self-renewal capacity of murine embryonic stem cells [35].

One of the features of various tumors is stemness and cell dedifferentiation. Since CDK12 maintains a dedifferentiated state in mouse embryonic stem cells, one could envision a scenario where CDK12 maintains the dedifferentiated state of cancer stem cells. High CDK12 activity would therefore accelerate tumor progression and therapy resistance, paradoxically to its proposed role as a tumor suppressor.

CDK12 role in DNA damage response

Even though the exact function of CDK12 is not fully understood, it is evident that it plays a significant role in DDR by affecting the expression of genes involved in homologous recombination (HR) promoted DNA damage repair and probably also other repair pathways [7, 12, 36]. Consequently, CDK12 silencing results in increased endogenous DNA damage [12]. Cells expressing catalytically inactive mutant forms of CDK12 exhibit

a compromised ability to effectively execute HR [36]. CDK12 $-/-$ cells derived from mouse blastocysts show decreased expression of DDR genes and increased levels of DNA damage [33]. Administration of CDK12 inhibitor THZ531 also reduces expression of DDR-associated genes [8].

However, a recent study pointed out that the DNA damage pattern in ovarian tumors with CDK12 loss is different than in the case of loss of HR-associated genes. Samples bearing inactive CDK12 have been shown to contain large tandem duplications rather than markers of impaired HR [37].

Cyclin K (in addition to BRCA1) was found in a global screen for genes sensitizing cells to the DNA-damaging drug camptothecin [38]. Furthermore, downregulation of CDK12 leads not only to spontaneous cell death but also to sensitization of cells to various DNA-damaging agents such as etoposide, mitomycin C and camptothecin [12]. Also, mutant, inactive forms of CDK12 sensitize cancer cells to cisplatin [39]. CDK12 deficiency sensitizes cells to inhibitors of PARP1/2, an important factor involved in DNA repair (discussed further in more detail) [7, 39, 40].

Despite the fact that CDK12 role in DDR is not yet fully understood, it is clear that CDK12 is necessary for maintaining genomic stability and functional DDR, particularly HR promoted DNA damage repair. Impaired DDR and accumulation of DNA damage is a typical hallmark of cancer [41], which directly links CDK12 deficiency to tumorigenesis.

Transcriptional CDKs and cancer

CDKs are principal regulators of the cell cycle and consequently participate in control of cell proliferation. Each CDK plays a distinct role in this process and is activated in coordination with multiple factors. Dysregulation of CDKs is a feature typical of a large number of tumor types. Hence, CDKs are attractive targets for cancer therapy and numerous CDK inhibitors have been synthesized and tested as anti-cancer drugs [1, 42]. In addition to cell cycle-associated CDKs, transcription-associated CDKs have emerged as prospective therapeutic targets, exploiting the so-called transcriptional addiction. According to this concept, cancer cells depend on dysregulated transcriptional programs maintained by principal transcriptional regulators, among them transcription-associated CDKs [5]. An increasing number of studies have pointed out the connection between individual transcriptional CDKs and cancerogenesis [5].

CDK9, a kinase responsible for the activity of positive transcription elongation factor (P-TEFb), regulates transition from the initiation to the productive elongation phase of transcription. Overexpression of oncogenic

transcription factor c-Myc leads to increased activity of CDK9 and enhances the current transcriptional program by stimulating RNA pol II elongation [43]. Consequently, CDK9 inhibitors have been shown to limit proliferation in Myc-overexpressing liver cancer cells [44] and B cell lymphoma [45]. CDK9 is activated in different types of leukemia. MLL, a histone methyltransferase, frequently fuses with components of the super-elongation complex to form oncogenic factors which activate P-TEFb and promote transcription. Inhibition of CDK9 subsequently limits proliferation of these cells [46].

After CDK13 amplification was described in hepatocellular cancer, CDK13 was consequently proposed to be an oncogene [47]. A high level of CDK11 in breast cancer correlates with clinicopathological parameters. CDK11 downregulation limits cell proliferation and migration in breast cancer cell lines. Targeting CDK11 has been proposed for breast cancer treatment [48].

In conclusion, overstimulation of transcription-associated CDKs promotes proliferation of various cancer types. Analogously, cancer cells may depend on CDK12 and thus it can serve as a therapeutic target. Importantly, CDK12 overexpression has been documented in breast tumors [49, 50].

CDK12 inhibitors

The anti-tumor potential of various CDK inhibitors has been tested in clinical trials. In addition to the pan-selective inhibitors such as flavopiridol and roscovitine, inhibitors showing specificity for individual CDKs have been developed targeting cell cycle- as well as transcription-linked CDKs [1]. Taking into account that CDK12 plays a critical role in multiple cellular processes and is mutated or overexpressed in various types of cancer, CDK12 inhibition emerges as a favorable strategy for cancer treatment. Two studies recently described CDK12 inhibitors with different chemical structure and specificity range.

Initially, dinaciclib (SCH 727965) was described as a potent inhibitor of CDK2, CDK5, CDK1 and CDK9 exhibiting an anti-proliferative effect in various cell lines [51]. Johnson et al. (2016) discovered that dinaciclib potentially inhibits also CDK12 with IC_{50} comparable to CDK9. Dinaciclib administration, similarly to CDK12 silencing, leads to reduced expression of HR genes and reduced RNA pol II CTD Ser2 phosphorylation, and the effects of dinaciclib are thus reminiscent of CDK12 inhibition. Moreover, BRCA1 wild-type cells treated with dinaciclib exhibit compromised HR, which conveys a sensitivity to PARP1 inhibitors. Importantly, combined treatment with PARP1/2 inhibitor veliparib and CDK12 inhibitor dinaciclib efficiently inhibited tumor growth in

a patient-derived xenograft model. These findings foresee a possibility to use a CDK12 inhibitor to sensitize or reverse PARP1/2 inhibitor resistance in tumors [7].

CDK7 inhibitor THZ1 has recently been shown to limit the transcription of factors dependent on super-enhancers, among them MYC proto-oncogenes, and it has been pre-clinically tested for treatment of lung carcinoma [43], T-cell acute lymphoblastic leukemia [44], and triple negative breast cancer [45]. THZ1 inhibits CDK12 at higher concentrations and its biological effect could be partly ascribed to CDK12 inhibition [52].

A selective and potent CDK12/13 inhibitor TZH531 was recently developed [8]. The attempt to synthesize a CDK12 inhibitor was based on THZ1, which covalently binds cysteine 312 located on an extension of the CDK7 kinase domain. CDK12 and CDK13 possess cysteines 1039/1017 in a similar extension close to the kinase domain. The authors exploited structural differences between CDK7 Cys312 and CDK12/13 Cys 1039/1017 and screened for an inhibitor specific solely for CDK12/13. THZ531 selectively inhibits CDK12/13 activity 50 times more efficiently than CDK7 or CDK9. In cells, THZ531 induced apoptosis, inhibited elongation of genes and led to reduced expression of DDR and super-enhancer dependent genes. THZ531 exhibited an antiproliferative effect in Jurkat T-cell acute lymphoblastic leukemia cells [8]. Yet, respective contributions of CDK12 and CDK13 to observed biological effects are not known [40].

In summary, CDK12 inhibitors show promise as anti-cancer drugs, either as a stand-alone treatment or in combination with other compounds such as PARP1/2 inhibitors.

CDK12 mutations in high-grade serous ovarian cancer (HGSOC)

Genomic instability is a typical feature of various malignancies. Mutations in DDR genes resulting in accumulation of DNA damage are often driving progressive events in cancerogenesis. Defective DNA repair machinery results in accumulation of mutations and accelerated cancer transformation and progression [41].

HR deficiency and genomic instability are characteristic for about 50% of HGSOC [53]. HR-associated genes such as BRCA1 or BRCA2 are mutated most frequently and represent typical tumor suppressors. In addition to p53, BRCA1 and BRCA2, CDK12 is one of only nine recurrently mutated genes; it is mutated in about 3% of HGSOC cases [53]. Additional studies have described these mutations in more detail. Mostly they are homozygous point mutations in the CDK12 kinase domain

leading to the loss of CDK12 function [36]. Mutant CDK12 forms have compromised ability to phosphorylate RNA pol II CTD, and cells display impairment in HR promoted DNA repair. This is caused predominantly by an inability to bind cyclin K [36, 39]. Furthermore, two studies have pointed out that in patients samples, BRCA1, BRCA2 and CDK12 mutations were mutually exclusive [40, 54]. This observation strongly suggests that BRCA1 and CDK12 participate in one regulatory pathway and supports the hypothesis that CDK12 controls expression of BRCA1 and other DDR genes. This suggestion can be further supported by the fact that more of the key DDR proteins were observed to be deregulated in patient tumor samples bearing CDK12 mutations [36]. Considering these observations, CDK12 was suggested to be a tumor suppressor.

CDK12 loss confers sensitivity to PARP1/2 inhibitors

Despite its contribution to tumor promotion, genomic instability also provides an opportunity for cancer therapy. Inhibitors of PARP1, a protein which participates in DDR, require defective HR for their anti-cancer activity. As defective HR is common in some tumors, PARP1 inhibition is becoming synthetically lethal to such cells [41]. Hence, loss-of-function mutations of HR regulators BRCA1 and BRCA2 are markers of application of PARP1/2 inhibitors-based therapy [55, 56]. Although PARP1/2 inhibitors have recently been translated into clinics, certain tumors develop resistance to PARP1/2 inhibitors, and new strategies for restoring PARP1/2 inhibitors sensitivity are needed [57].

A synthetic lethality screen determined *CDK12* to be one of the additional genes conferring sensitivity to the PARP1/2 inhibitor olaparib [40]. Ovarian cancer cell lines with lower expression of CDK12 are more sensitive to olaparib treatment, and downregulation of CDK12 leads to increased olaparib sensitivity. The therapeutic effect of olaparib on CDK12-silenced tumor cells was confirmed in vivo in xenograft experiments [40]. Increased sensitivity of CDK12-compromised cells to cisplatin, the alkylating agent melphalan, and the PARP1 inhibitor veliparib was observed in a CDK12-silenced ovarian cancer cell line [39]. In addition, Her2-positive breast cancer cells with downregulated CDK12 display sensitivity to PARP1/2 inhibitors [58]. Finally, the CDK12 inhibitor dinaciclib in combination with the PARP1/2 inhibitor veliparib resulted in inhibition of tumor growth in vitro, in vivo and in a patient-derived xenograft model [7].

Consistent with the fact that CDK12 is necessary for expression of HR genes, loss of CDK12 confers sensitivity

to PARP1/2 inhibitors. CDK12 loss in a tumor could serve as another marker for treatment with PARP1/2 inhibitors or additional inhibitors of DDR network, as well as with other DNA-damaging compounds.

CDK12 dysregulation in breast cancer

In addition to HGSOc, several studies have shown dysregulation of CDK12 in individual subtypes of breast cancer.

Triple-negative breast cancer (TNBC) samples contain mutational spectrum similar to ovarian cancer. These tumors do not amplify any characteristic receptor (ER, HER2, or PR) but display mutations in DDR genes that promote genomic instability. Recurrently mutated genes include p53 (80% of cases) and BRCA1 (30% of cases) [59]. CDK12 mutations were identified in 1.5% of TNBC cases [59, 60]. TNBC patients with defective HR (including loss-of-function mutated CDK12) may benefit from treatment using PARP1/2 inhibitors [59].

A large number of breast tumors are dependent on an overexpressed estrogen receptor (ER) and therefore its targeted inhibition is used for counteracting the tumor growth [61]. CDK12 silencing modifies the sensitivity of ER-positive cells to tamoxifen, a drug blocking ER signaling. CDK12 downregulation activates the mitogen-activated protein kinase (MAPK) pathway, which in turn leads to loss of ER dependency and causes resistance to tamoxifen [62].

Another subtype of breast cancer is characterized by amplification of oncogene HER2 (also known as ERBB2 or EGFR2), a tyrosine kinase receptor, which stimulates cell proliferation and inhibits apoptosis [59]. In breast cancer, HER2 is a part of the frequently amplified and overexpressed 17q12-q21 locus [63]. In addition to HER2, 17q12-q21 amplicon commonly contains several neighboring genes including *MED1*, *GRB7*, *MSL1*, *CASC3* and *TOP2A* [50, 59]. Interestingly, the HER2 amplicon also contains the *CDK12* gene in 71% of cases [50, 64].

HER2-amplified tumors may benefit from therapy based on usage of antibodies against HER2 receptor (trastuzumab, pertuzumab) or tyrosine-kinase inhibitors (lapatinib) [59]. In addition to HER2, overexpression of co-amplified genes might also have an impact on breast cancer development. Additional genes involved in the 17q12-q21 amplicon might therefore be oncogene candidates [63]. Moreover, amplification of additional genes in the 17q12-q21 locus might be responsible for resistance of certain tumors to HER2-targeted therapy. These oncogenic factors, including CDK12, represent potential druggable targets [64]. Mertins and colleagues analyzed the proteome of breast cancer samples and found

CDK12 amplification on mRNA and protein level as well as increased CDK12 phosphorylation in HER2-amplified tumors [50]. These observations indicate elevated CDK12 activity in these tumors, and CDK12 has been proposed as an additional druggable target in HER2-amplified breast tumors [50]. In parallel, the diFiore group performed a broad screen of serine/threonine kinases with altered expression in several human cancers, among them breast cancer. They found that CKD12 is upregulated in HER2-positive breast cancer samples and demonstrated a strong correlation between CDK12 level and high tumor grade. They also proposed that a high CDK12 level could serve as a prognostic marker [49].

In 13% of cases, rearrangements in 17q12-q21 amplicons lead to disruption of the CDK12 gene and resulted in CDK12 loss of function and PARP1/2 inhibitor sensitivity of these cells. This observation suggests that the subset of HER2-amplified patients with disrupted CDK12 could benefit from PARP1/2 inhibitor treatment [58]. Additionally, a fusion form of the likely nonfunctional CDK12 gene was also found in a micropapillary breast cancer sample [58].

An increasing number of studies describe loss of function or amplification of CDK12 in breast cancer samples. Loss of function in CDK12 may lead to genomic instability and be predictive of PARP1/2 inhibitor treatment. Tumors displaying CDK12 amplification, on the other hand, may be dependent on its overexpression and CDK12 may provide a new therapeutic target for breast malignancies.

Is CDK12 a tumor suppressor or does it have oncogenic properties?

Loss of tumor suppressors and addiction to oncogenes are mechanisms driving cancer onset and progression. A growing number of studies describe mutations or amplification of the *CDK12* gene in tumor samples. These data may seem contradictory, since CDK12 functions either as a tumor suppressor or it has features that resemble an oncogene.

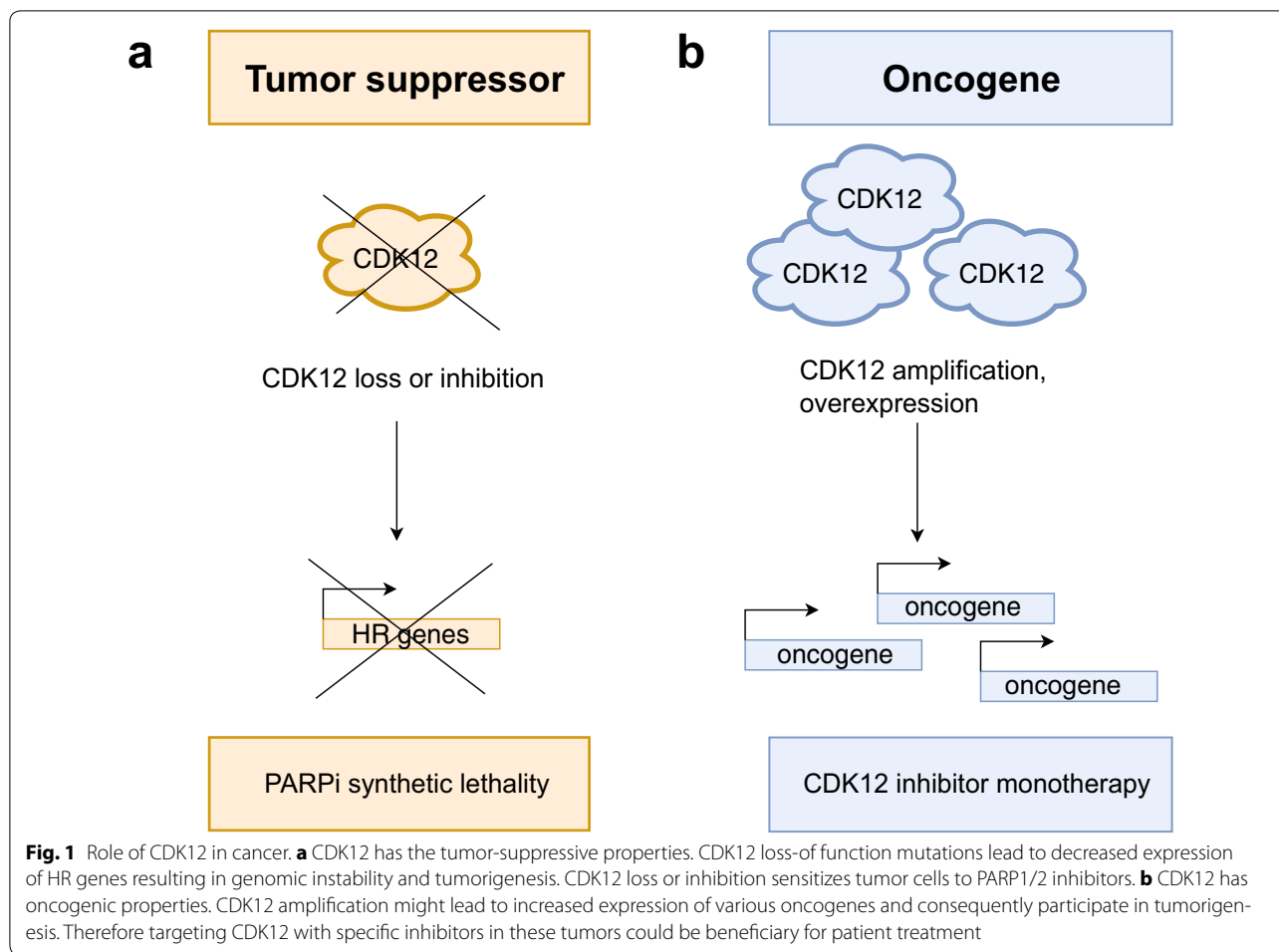
In HGSOC and TNBC, CDK12 is a tumor suppressor. CDK12 is necessary for expression of DDR genes and it is essential for HR mediated DNA repair [12, 50]. Consequently, CDK12 loss leads to increased genomic instability, which is a typical feature of these tumors and represents one of the hallmarks of cancer progression [65]. CDK12 loss-of-function mutations or inhibition confers sensitivity of cells to PARP1/2 inhibitors [7, 39, 40].

In a different context, CDK12 has properties that resemble oncogenes. CDK12 amplification, resulting in its overexpression, correlates with more aggressive tumor progression in HER2-positive breast cancers [49]. CDK12 is highly active in these tumors, and it has been proposed as a druggable target in HER2-amplified breast cancer [50]. This idea might be supported by the fact that CDK12 inhibition limits the growth of cancer cells [8, 66]. The concept of transcriptional addiction describes dependency of cancer cells on a certain transcriptional regulator, which maintains an altered transcriptional program [5]. In line with this concept, inhibitors of CDK12-related transcriptional kinases CDK7 and CDK9 reduce proliferation of cancer cells and are being tested as anti-tumor drugs. Similarly to CDK7, CDK12 inhibitors limit the expression of super-enhancer-associated oncogenic transcriptional factors [8, 67]. This suggests that certain tumors might be transcriptionally addicted to CDK12 and so CDK12 inhibition might be a promising anti-cancer strategy. A recent study described that CDK12 overexpression affects alternative last exon splicing. Therefore CDK12 overexpression can increase the invasiveness of a breast cancer cell line, by decreasing the expression of the long isoform of DNAJB6 [25].

Taken together, the dual role of CDK12 in cancerogenesis could be explained by the fact that CDK12 is essential for expression of both tumor suppressors and oncogenes, and it participates in multiple cellular processes. In different tissues and cell types, the process of tumorigenesis depends on amplification of particular oncogenes or loss of suppressors. Consequently, CDK12 can act as a tumor suppressor or its amplification can contribute to cancerogenesis depending on cellular context (Fig. 1).

Conclusions

CDK12 is a transcription-associated CDK essential for multiple cellular processes, including splicing, differentiation and DDR. Despite the fact that CDK12 has been extensively studied, our understanding of its functions remains limited. In vitro models will be instrumental to identify CDK12-associating factors and additional kinase targets and to elucidate whether it is a general transcriptional regulator or a specific factor for particular sets of genes. Mouse models recapitulating CDK12 loss or gain of function will be illustrative in studying particular aspects of diseases and development. Elucidation of CDK12 functions would lead to better assessment of its roles during tumorigenesis.



CDK12 mutations and amplification in tumors have been documented in an increasing number of studies. Recently developed CDK12 inhibitors constitute not only powerful research tools but also promising anti-cancer drugs. CDK12 inhibitor monotherapy could be useful for cancer patients tumors with overexpressed and activated CDK12. CDK12 inhibition increases sensitivity of cells to PARP1/2 inhibitors, thus presenting a potential strategy for targeting PARP1/2-resistant tumors.

Abbreviations

cdk: cyclin-dependent kinase; CTD: C-terminal domain; RNA pol II: RNA polymerase II; DDR: DNA damage response; CrkRS: Cdc2-related kinase with an arginine/serine-rich (RS) domain; HR: homologous recombination; P-TEFb: positive transcription elongation factor b; Paf1: pol II associated factor 1; Nrf: nuclear respiratory factor; CstF77: cleavage stimulation factor 77 kDa subunit; CstF64: cleavage stimulating 34 factor 64; SC35: SR splicing factor 2; SFRS1: serine/arginine splicing factor1; c-MYC: MYC proto-oncogene; HGSOC: high-grade serous ovarian cancer; PARP: poly (ADP-ribose) polymerase; TNBC: triple-negative breast cancer; ER: estrogen receptor; HER-2: human epidermal growth factor receptor 2.

Authors' contributions

HP and JK wrote the manuscript. Both authors read and approved the final manuscript.

Acknowledgements

The authors would like to thank prof. BM Peterlin, Dr. Sabina Sevcikova and members of the J. Kohoutek laboratory for critical discussion and their suggestions during the preparation of this review.

Competing interests

The authors certify that they have no affiliations with, or involvement in, any organization or entity with any financial or non-financial interest (such as personal or professional relationships, affiliations, knowledge or beliefs) in the subject matter or materials discussed in this manuscript.

Availability of data and materials

Not applicable.

Consent for publication

The authors agree with publishing this manuscript.

Ethics approval and consent to participate

Not applicable.

Funding

This study was supported by the Ministry of Health of the Czech Republic, Grant 16-34152A and by the Ministry of Agriculture, Grant RO0517 to J.K.

Publisher's Note

Springer Nature remains neutral with regard to jurisdictional claims in published maps and institutional affiliations.

Received: 10 July 2017 Accepted: 16 October 2017

Published online: 27 October 2017

References

- Asghar U, Witkiewicz AK, Turner NC, Knudsen ES. The history and future of targeting cyclin-dependent kinases in cancer therapy. *Nat Rev Drug Discov*. 2015;14:130–46.
- Bruyère C, Meijer L. Targeting cyclin-dependent kinases in anti-neoplastic therapy. *Curr Opin Cell Biol*. 2013;25:772–9.
- Eick D, Geyer M. The RNA polymerase II carboxy-terminal domain (CTD) code. *Chem Rev*. 2013;113:8456–90.
- Jeronimo C, Bataille AR, Robert F. The writers, readers, and functions of the RNA polymerase II C-terminal domain code. *Chem Rev*. 2013;113:8491–522.
- Bradner JE, Hnisz D, Young RA. Transcriptional addiction in cancer. *Cell*. 2017;168:629–43.
- Chilà R, Guffanti F, Damia G. Role and therapeutic potential of CDK12 in human cancers. *Cancer Treat Rev*. 2016;50:83–8.
- Johnson SF, Cruz C, Greifenberg AK, Dust S, Stover DG, Chi D, et al. CDK12 inhibition reverses de novo and acquired PARP inhibitor resistance in BRCA wild-type and mutated models of triple-negative breast cancer. *Cell Rep*. 2016;17:2367–81.
- Zhang T, Kwiatkowski N, Olson CM, Dixon-Clarke SE, Abraham BJ, Greifenberg AK, et al. Covalent targeting of remote cysteine residues to develop CDK12 and CDK13 inhibitors. *Nat Chem Biol*. 2016;12:876–84.
- Ko TK, Kelly E, Pines J. CrkRS: a novel conserved Cdc2-related protein kinase that colocalises with SC35 speckles. *J Cell Sci*. 2001;114:2591–603.
- Chen H-H, Wang Y-C, Fann M-J. Identification and characterization of the CDK12/cyclin L1 complex involved in alternative splicing regulation. *Mol Cell Biol*. 2006;26:2736–45.
- Bartkowiak B, Liu P, Phatnani HP, Fuda NJ, Cooper JJ, Price DH, et al. CDK12 is a transcription elongation-associated CTD kinase, the metazoan ortholog of yeast Ctk1. *Genes Dev*. 2010;24:2303–16.
- Blazek D, Kohoutek J, Bartholomeeusen K, Johansen E, Hulinkova P, Luo Z, et al. The cyclin K/Cdk12 complex maintains genomic stability via regulation of expression of DNA damage response genes. *Genes Dev*. 2011;25:2158–72.
- Cheng SWG, Kuzyk MA, Moradian A, Ichu TA, Chang VCD, Tien JF, et al. Interaction of cyclin-dependent kinase 12/CrkRS with cyclin K1 is required for the phosphorylation of the C-terminal domain of RNA polymerase II. *Mol Cell Biol*. 2012;32:4691–704.
- Bösken CA, Farnung L, Hintermair C, Merzel Schachter M, Vogel-Bachmayr K, Blazek D, et al. The structure and substrate specificity of human Cdk12/Cyclin K. *Nat Commun*. 2014;5:3505.
- Bartkowiak B, Greenleaf AL. Phosphorylation of RNAPII: to P-TEFb or not to P-TEFb? *Transcription*. 2011;2:115–9.
- Li X, Chatterjee N, Spirohn K, Boutros M, Bohmann D. Cdk12 is a gene-selective RNA polymerase II kinase that regulates a subset of the transcriptome, including Nrf2 target genes. *Sci Rep*. 2016;6:21455.
- Yu M, Yang W, Ni T, Tang Z, Nakadai T, Zhu J, et al. RNA polymerase II-associated factor 1 regulates the release and phosphorylation of paused RNA polymerase II. *Science*. 2015;350:1383–6.
- Bartkowiak B, Yan C, Greenleaf AL. Engineering an analog-sensitive CDK12 cell line using CRISPR/Cas. *Biochim Biophys Acta*. 2015;1849:1179–87.
- Hintermair C, Heidemann M, Koch F, Descostes N, Gut M, Gut I, et al. Threonine-4 of mammalian RNA polymerase II CTD is targeted by Polo-like kinase 3 and required for transcriptional elongation. *EMBO J*. 2012;31:2784–97.
- Schüller R, Forné I, Straub T, Schrieck A, Texier Y, Shah N, et al. Heptad-specific phosphorylation of RNA polymerase II CTD. *Mol Cell*. 2016;61:305–14.
- Davidson L, Muniz L, West S. 3' end formation of pre-mRNA and phosphorylation of Ser2 on the RNA polymerase II CTD are reciprocally coupled in human cells. *Genes Dev*. 2014;28:342–56.
- Eifler TT, Shao W, Bartholomeeusen K, Fujinaga K, Jäger S, Johnson JR, et al. Cyclin-dependent kinase 12 increases 3' end processing of growth factor-induced c-FOS transcripts. *Mol Cell Biol*. 2015;35:468–78.
- Liang K, Gao X, Gilmore JM, Florens L, Washburn MP, Smith E, et al. Characterization of human cyclin-dependent kinase 12 (CDK12) and CDK13 complexes in C-terminal domain phosphorylation, gene transcription, and RNA processing. *Mol Cell Biol*. 2015;35:928–38.
- Rodrigues F, Thuma L, Klämbt C. The regulation of glial-specific splicing of Neurexin IV requires HOW and Cdk12 activity. *Dev Camb Engl*. 2012;139:1765–76.
- Tien JF, Mazloomian A, Cheng S-WG, Hughes CS, Chow CCT, Canapi LT, et al. CDK12 regulates alternative last exon mRNA splicing and promotes breast cancer cell invasion. *Nucleic Acids Res*. 2017;45:6698–716.
- David CJ, Manley JL. Alternative pre-mRNA splicing regulation in cancer: pathways and programs unhinged. *Genes Dev*. 2010;24:2343–64.
- Oltean S, Bates DO. Hallmarks of alternative splicing in cancer. *Oncogene*. 2014;33:5311–8.
- Sveen A, Kilpinen S, Ruusulehto A, Lothe RA, Skotheim RI. Aberrant RNA splicing in cancer; expression changes and driver mutations of splicing factor genes. *Oncogene*. 2016;35:2413–27.
- Aken BL, Achuthan P, Akanni W, Amode MR, Bernsdrorf F, Bhai J, et al. Ensembl 2017. *Nucleic Acids Res*. 2017;45:D635–42.
- Xiang X, Deng L, Zhang J, Zhang X, Lei T, Luan G, et al. A distinct expression pattern of cyclin K in mammalian testes suggests a functional role in spermatogenesis. *PLoS ONE*. 2014;9:e101539.
- Chang TY, Cheng PL. Relay of cyclin-dependent kinases in the regulation of axonal growth. *Exp Neurol*. 2015;271:259–61.
- Chen HR, Juan HC, Wong YH, Tsai JW, Fann MJ. Cdk12 regulates neurogenesis and late-arising neuronal migration in the developing cerebral cortex. *Cereb Cortex*. 2017;27:2289–302.
- Juan H-C, Lin Y, Chen H-R, Fann M-J. Cdk12 is essential for embryonic development and the maintenance of genomic stability. *Cell Death Differ*. 2016;23:1038–48.
- Bowman EA, Kelly WG. RNA polymerase II transcription elongation and Pol II CTD Ser2 phosphorylation: a tail of two kinases. *Nucl Austin Tex*. 2014;5:224–36.
- Dai Q, Lei T, Zhao C, Zhong J, Tang Y, Chen B, et al. Cyclin K-containing kinase complexes maintain self-renewal in murine embryonic stem cells. *J Biol Chem*. 2012;287:25344–52.
- Ekumi KM, Paculova H, Lenasi T, Pospichalova V, Bösken CA, Rybarikova J, et al. Ovarian carcinoma CDK12 mutations misregulate expression of DNA repair genes via deficient formation and function of the Cdk12/CycK complex. *Nucleic Acids Res*. 2015;43:2575–89.
- Popova T, Manié E, Boeva V, Battistella A, Goundiam O, Smith NK, et al. Ovarian cancers harboring inactivating mutations in CDK12 display a distinct genomic instability pattern characterized by large tandem duplications. *Cancer Res*. 2016;76:1882–91.
- O'Connell BC, Adamson B, Lydeard JR, Sowa ME, Ciccio A, Bredemeyer AL, et al. A genome-wide camptothecin sensitivity screen identifies a mammalian MMS22L-NFKBIL2 complex required for genomic stability. *Mol Cell*. 2010;40:645–57.
- Joshi PM, Sutor SL, Huntoon CJ, Karnitz LM. Ovarian cancer-associated mutations disable catalytic activity of CDK12, a kinase that promotes homologous recombination repair and resistance to cisplatin and poly(ADP-ribose) polymerase inhibitors. *J Biol Chem*. 2014;289:9247–53.
- Bajrami I, Frankum JR, Konde A, Miller RE, Rehman FL, Brough R, et al. Genome-wide profiling of genetic synthetic lethality identifies CDK12 as a novel determinant of PARP1/2 inhibitor sensitivity. *Cancer Res*. 2014;74:287–97.
- Lord CJ, Ashworth A. The DNA damage response and cancer therapy. *Nature*. 2012;481:287–94.
- Lapenna S, Giordano A. Cell cycle kinases as therapeutic targets for cancer. *Nat Rev Drug Discov*. 2009;8:547–66.

43. Lin CY, Lovén J, Rahl PB, Paranal RM, Burge CB, Bradner JE, et al. Transcriptional amplification in tumor cells with elevated c-Myc. *Cell*. 2012;151:56–67.
44. Huang C-H, Lujambio A, Zuber J, Tschaharganeh DF, Doran MG, Evans MJ, et al. CDK9-mediated transcription elongation is required for MYC addiction in hepatocellular carcinoma. *Genes Dev*. 2014;28:1800–14.
45. Gregory GP, Hogg SJ, Kats LM, Vidacs E, Baker AJ, Gilan O, et al. CDK9 inhibition by dinaciclib potently suppresses Mcl-1 to induce durable apoptotic responses in aggressive MYC-driven B-cell lymphoma in vivo. *Leukemia*. 2015;29:1437–41.
46. Kryštof V, Baumli S, Fürst R. Perspective of cyclin-dependent kinase 9 (CDK9) as a drug target. *Curr Pharm Des*. 2012;18:2883–90.
47. Kim H-E, Kim D-G, Lee KJ, Son JG, Song M-Y, Park Y-M, et al. Frequent amplification of CENPF, GMN and CDK13 genes in hepatocellular carcinomas. *PLoS ONE*. 2012;7:e43223.
48. Zhou Y, Han C, Li D, Yu Z, Li F, Li F, et al. Cyclin-dependent kinase 11(p110) (CDK11(p110)) is crucial for human breast cancer cell proliferation and growth. *Sci Rep*. 2015;5:10433.
49. Capra M, Nuciforo PG, Confalonieri S, Quarto M, Bianchi M, Nebuloni M, et al. Frequent alterations in the expression of serine/threonine kinases in human cancers. *Cancer Res*. 2006;66:8147–54.
50. Mertins P, Mani DR, Ruggles KV, Gillette MA, Clauser KR, Wang P, et al. Proteogenomics connects somatic mutations to signalling in breast cancer. *Nature*. 2016;534:55–62.
51. Parry D, Guzi T, Shanahan F, Davis N, Prabhavalkar D, Wiswell D, et al. Dinaciclib (SCH 727965), a novel and potent cyclin-dependent kinase inhibitor. *Mol Cancer Ther*. 2010;9:2344–53.
52. Kwiatkowski N, Zhang T, Rahl PB, Abraham BJ, Reddy J, Ficarro SB, et al. Targeting transcription regulation in cancer with a covalent CDK7 inhibitor. *Nature*. 2014;511:616–20.
53. Cancer Genome Atlas Research Network. Integrated genomic analyses of ovarian carcinoma. *Nature*. 2011;474:609–15.
54. Carter SL, Cibulskis K, Heman E, McKenna A, Shen H, Zack T, et al. Absolute quantification of somatic DNA alterations in human cancer. *Nat Biotechnol*. 2012;30:413–21.
55. Bryant HE, Schultz N, Thomas HD, Parker KM, Flower D, Lopez E, et al. Specific killing of BRCA2-deficient tumours with inhibitors of poly(ADP-ribose) polymerase. *Nature*. 2005;434:913–7.
56. Farmer H, McCabe N, Lord CJ, Tutt ANJ, Johnson DA, Richardson TB, et al. Targeting the DNA repair defect in BRCA mutant cells as a therapeutic strategy. *Nature*. 2005;434:917–21.
57. Montoni A, Robu M, Pouliot É, Shah GM. Resistance to PARP-inhibitors in cancer therapy. *Front Pharmacol*. 2013;4:18.
58. Natrajan R, Wilkerson PM, Marchiò C, Piscuoglio S, Ng CKY, Wai P, et al. Characterization of the genomic features and expressed fusion genes in micropapillary carcinomas of the breast. *J Pathol*. 2014;232:553–65.
59. Network Cancer Genome Atlas. Comprehensive molecular portraits of human breast tumours. *Nature*. 2012;490:61–70.
60. Shah SP, Roth A, Goya R, Oloumi A, Ha G, Zhao Y, et al. The clonal and mutational evolution spectrum of primary triple-negative breast cancers. *Nature*. 2012;486:395–9.
61. Hart CD, Migliaccio I, Malorni L, Guarducci C, Biganzoli L, Di Leo A. Challenges in the management of advanced, ER-positive, HER2-negative breast cancer. *Nat Rev Clin Oncol*. 2015;12:541–52.
62. Iorns E, Martens-de Kemp SR, Lord CJ, Ashworth A. CRK7 modifies the MAPK pathway and influences the response to endocrine therapy. *Carcinogenesis*. 2009;30:1696–701.
63. Kauraniemi P, Kallioniemi A. Activation of multiple cancer-associated genes at the ERBB2 amplicon in breast cancer. *Endocr Relat Cancer*. 2006;13:39–49.
64. Sircoulomb F, Bekhouche I, Finetti P, Adélaïde J, Ben Hamida A, Bonansea J, et al. Genome profiling of ERBB2-amplified breast cancers. *BMC Cancer*. 2010;10:539.
65. Hanahan D, Weinberg RA. Hallmarks of cancer: the next generation. *Cell*. 2011;144:646–74.
66. Bartkowiak B, Greenleaf AL. Expression, purification, and identification of associated proteins of the full-length hCDK12/CyclinK complex. *J Biol Chem*. 2015;290:1786–95.
67. Wang Y, Zhang T, Kwiatkowski N, Abraham BJ, Lee TI, Xie S, et al. CDK7-dependent transcriptional addiction in triple-negative breast cancer. *Cell*. 2015;163:174–86.

Submit your next manuscript to BioMed Central and we will help you at every step:

- We accept pre-submission inquiries
- Our selector tool helps you to find the most relevant journal
- We provide round the clock customer support
- Convenient online submission
- Thorough peer review
- Inclusion in PubMed and all major indexing services
- Maximum visibility for your research

Submit your manuscript at
www.biomedcentral.com/submit



APPENDIX 9

KOHOUTEK, Jiri, Qintong LI, Dalibor BLAZEK, Zeping LUO, Huimin JIANG and B. Matija PETERLIN. Cyclin T2 Is Essential for Mouse Embryogenesis. *Molecular and Cellular Biology*. 2009, 29(12), 3280–3285.

Cyclin T2 Is Essential for Mouse Embryogenesis^{∇†}

Jiri Kohoutek,^{1*‡} Qintong Li,^{2‡} Dalibor Blazek,² Zeping Luo,² Huimin Jiang,² and B. Matija Peterlin²

Veterinary Research Institute, Hudcova 70, Brno, 621 00, Czech Republic,¹ and Departments of Medicine, Microbiology, and Immunology, Rosalind Russell Medical Research Center, University of California at San Francisco, San Francisco, California 94143-0703²

Received 5 February 2009/Returned for modification 7 March 2009/Accepted 29 March 2009

The positive transcription elongation factor b (P-TEFb) is essential for the elongation of transcription and cotranscriptional processing by RNA polymerase II. In mammals, it contains predominantly the C-type cyclin cyclin T1 (CycT1) or CycT2 and cyclin-dependent kinase 9 (Cdk9). To determine if these cyclins have redundant functions or affect distinct sets of genes, we genetically inactivated the CycT2 gene (*Ccnt2*) using the β -galactosidase–neomycin gene (β -geo) gene trap technology in the mouse. Visualizing β -galactosidase during mouse embryogenesis revealed that CycT2 is expressed abundantly during embryogenesis and throughout the organism in the adult. This finding was reflected in the expression of CycT2 in all adult tissues and organs. However, despite numerous matings of heterozygous mice, we observed no CycT2^{-/-} embryos, pups, or adult mice. This early lethality could have resulted from decreased expression of critical genes, which were revealed by short interfering RNAs against CycT2 in embryonic stem cells. Thus, CycT1 and CycT2 are not redundant, and these different P-TEFb complexes regulate subsets of distinct genes that are important for embryonic development.

Eukaryotic transcription by RNA polymerase II (RNAPII) is regulated at several distinct steps, which include initiation, promoter clearance, elongation, and cotranscriptional processing of primary transcripts (19, 25, 27). Of these, elongation is regulated by the positive transcription elongation factor b (P-TEFb), which contains predominantly the C-type cyclin cyclin T1 (CycT1) or CycT2 and cyclin-dependent kinase 9 (Cdk9). All these different P-TEFb complexes phosphorylate serines at position 2 (S2) in the C-terminal domain (CTD) of RNAPII, as well as components of the negative transcription elongation factor, which contains minimally the DRB (5,6-dichloro-1- β -D-ribofuranosylbenzimidazole) sensitivity-inducing factor (DSIF) and the negative elongation factor. These posttranslational modifications exchange basal transcription factors for splicing and polyadenylation machineries on RNAPII, as well as modify DSIF for productive elongation (25).

Although these P-TEFb complexes can phosphorylate the CTD and lead to transcriptional elongation when recruited to RNAPII via heterologous nucleic acid-tethering systems, it is not clear whether they have redundant or unique functions in cells (18, 33). Thus far, CycT1, which is the most abundant of these cyclins, has been implicated as the coactivator of the transcriptional transactivator Tat from human immunodeficiency virus, RelA from NF- κ B, class II transactivator, the protooncogene *c-myc*, several members of the steroid hormone receptor family, and the autoimmune regulator AIRE (3, 8, 14–16, 24, 29, 36). Moreover, Runx1, which is the active repressor of CD4 expression in double-negative thymocytes, decoys CycT1 away from the CD4 promoter, thus keeping the

engaged RNAPII from elongating on this gene (13). On the other hand, CycT2 has been implicated as the coactivator of MyoD, pRb, and ENL (23, 31, 32). However, except for Tat, it has not been ruled out formally that these two cyclins cannot substitute for one another.

Besides these specific interactions, little is known about the roles of different P-TEFb complexes during development and in the adult organism. Thus far, only the genetic inactivation of CycT1 has been reported, but with CycT1^{-/-} mice still expressing small amounts of the wild-type (WT) protein, only minor immunological defects were observed (24). Moreover, in *Caenorhabditis elegans*, the genetic inactivation of CycT1 or CycT2 alone had no effect, whereas inhibiting both cyclins led to the same severe phenotype as the genetic inactivation of RNAPII itself (28). Given these findings, we wanted to determine if these different P-TEFb complexes played redundant or unique roles in mammals. To this end, we genetically inactivated CycT2, which led to an embryonic-lethal phenotype. In this report, we present our findings with our CycT2^{-/-} mice and stem cells.

MATERIALS AND METHODS

Generation of CycT2^{+/-} mice. Embryonic stem (ES) cells (clone W048F02-04304) bearing a β -galactosidase–neomycin (β -geo) trap in the CycT2 gene (CycT2. β -geo), were obtained from the German Gene Trap Consortium (30). Morula-ES cell aggregations were carried out by the Mouse Genetics Core at the University of California at San Francisco (UCSF). They were injected into superovulated C57BL/6 morulas, and chimeric mice were generated. Chimeric males were then bred with C57BL/6 females, and heterozygous animals were identified by PCR genotyping. Staging of embryos for LacZ staining was also performed. After the breeding was set up, females were examined for vaginal plugs, and this developmental stage was set as embryonic day 0.5 (E0.5). Mid-gestation and preimplantation embryos at various stages were obtained by dissecting the uterine horn or the oviducts. The mice were maintained in accordance with UCSF regulations for the humane use of animals in research.

Genotyping. To distinguish WT and trapped (TR) CycT2. β -geo genes, one common forward primer (Wf, 5'-CCAAGTGATCGCCTCCAAGTTATCAG G-3') and two specific reverse primers (TRr, 5'-ATGCCAGCCAAAATCTT TCTGGCCTC-3', and WTr, 5'-GGATGGTAGTAGGAATCTCTACCAGGT-3') were designed. Direct sequencing revealed the expected sequences of these

* Corresponding author. Mailing address: Veterinary Research Institute, Hudcova 70, 621 00, Brno, Czech Republic. Phone: 420-533-331-802. Fax: 420-541-211-229. E-mail: kohoutek@vri.cz.

† Supplemental material for this article may be found at <http://mcb.asm.org/>.

‡ J.K. and Q.L. contributed equally.

∇ Published ahead of print on 13 April 2009.

PCR amplicons. They also validated the integration site of β -geo within intron 7 of the *CycT2* gene. Genomic DNA was isolated from mouse tails with the REDEExtract-N-Amp tissue PCR kit (Sigma, St. Louis, MO).

Western blotting. For detection of the fusion protein between the N terminus of *CycT2* and the β -Geo protein in donor ES cells (W048F02-04304) or for the detection of decreased expression of *CycT1* and *CycT2* after RNA interference, ES cells were collected in lysis buffer (10 mM Tris-HCl, pH 8.0, 25 mM EDTA, 1% sodium dodecyl sulfate), sonicated, and cleared by centrifugation at $10,000 \times g$ for 10 min at 4°C. Concentrations of total proteins were determined with the TMB Substrate Kit (Pierce, Rockford, IL). Lysates were diluted to the same concentration, mixed with Laemmli sample buffer, and boiled for 5 min. Western blotting was performed with anti- β -galactosidase (Z378A; Promega, Madison, WI) or anti-*CycT1*, -*CycT2*, and -*Cdk9* (sc-10750, sc-12421, and sc-484; Santa Cruz Biotechnology, Santa Cruz, CA).

For the assessment of protein levels of subunits of P-TEFb in diverse mouse organs, the heart, brain, lung, skeletal muscle, spleen, kidney, thymus, liver, testis, and pancreas were isolated from WT mice, lysed on ice in lysis buffer, sonicated, and cleared by centrifugation at $10,000 \times g$ for 10 min at 4°C. Concentrations of total proteins were determined with the TMB Substrate Kit (Pierce). Lysates were diluted to the same concentration, mixed with Laemmli sample buffer, and boiled for 5 min. Western blotting analyses were carried out with anti-*CycT1*, -*CycT2*, and -*Cdk9* antibodies (sc-10750, sc-12421, and sc-484; Santa Cruz Biotechnology).

LacZ staining. Embryos at a given developmental stage were removed from the uteruses of pregnant heterozygous female mice, after which supporting and extraembryonic tissues were dissected. Whole embryos were washed in cold phosphate-buffered saline and immediately transferred to 0.2% glutaraldehyde in phosphate buffer (23 mM NaH₂PO₄ · H₂O, 72 mM Na₂HPO₄, 5 mM EGTA, and 2 mM MgCl₂) for 15 min on ice. The embryos were then washed three times with washing buffer (23 mM NaH₂PO₄ · H₂O, 72 mM Na₂HPO₄, 2 mM MgCl₂, 0.01% deoxycholate, and 0.02% NP-40) for 15 min on ice. Finally, the embryos were transferred to staining solution [washing buffer supplemented with 5 mM K₄Fe(CN)₆ · 3H₂O, 5 mM K₃Fe(CN)₆, and 1 mg/ml X-Gal (5-bromo-4-chloro-3-indolyl- β -D-galactopyranoside)] and incubated at 30°C overnight.

Knockdown of *CycT1* and *CycT2* and microarray analyses. Feeder-free mouse E14 ES cells were maintained in the presence of LIF (Millipore). Cells in 6-cm plates were transfected with 200 pmol of individual short interfering RNAs (siRNAs) in duplicate with Lipofectamine 2000 (Invitrogen, Carlsbad, CA) following the manufacturer's instructions. Control siRNA contained an RNA duplex that did not match any sequence from the mouse genome (Integrated DNA Technologies, San Diego, CA). The siRNA duplex against *CycT1* contained 5'-UUCCGAAUACGUUUCAGCCUGCUUGGA-3' (sense) and 5'-AAGGC UUAUGCAAAGUCGGACGAAC-3' (antisense) sequences. Three siRNAs from Santa Cruz Biotechnology targeted different regions of mouse *CycT2* mRNA. Forty-eight hours after the transfection, the cells were harvested. Half of the cells were lysed with protein-loading buffer. We determined the concentrations of cell lysates with the bicinchoninic acid protein assay kit (Pierce). Equal amounts of protein were loaded for Western blotting. Total RNA was also extracted from the remaining cells with Trizol (Invitrogen), followed by RNeasy column purification (Qiagen). The concentration and quality of RNA were determined with an Agilent 2100 bioanalyzer, and all the purified RNA samples had scores of more than 9.80. Total RNA from each siRNA knockdown was amplified with an Illumina TotalPrep RNA Amplification kit (Ambion). The amplified RNA was examined with an Agilent 2100 bioanalyzer before microarray analysis to ensure that similar amplification efficiencies were achieved. Microarray analysis with MouseWG-6 v2.0 chips (Illumina) was carried out with the help of the UCSF Microarray Core. Data were extracted with the BeadStudio Gene Expression Module (Illumina), and gene ontology analysis was carried out using DAVID (<http://david.abcc.ncifcrf.gov/>) and grouped based on the Kyoto Encyclopedia of Genes and Genomes pathway.

RESULTS

Generation and characterization of *CycT2*^{+/-} mice. To gain more insight into the physiological function of *CycT2*, we utilized mouse ES cells (W048F02-04304) with a β -geo gene trap insertion (pT1ATGbetageo) in intron 7 from the German Gene Trap Consortium (Fig. 1A) (30). After implantation into mouse blastocysts, we achieved stable germ line transmission of our transgene (Fig. 1B). Indeed, the trap could be detected easily using primers to intron 7 (WTf) and β -geo (TRr) se-

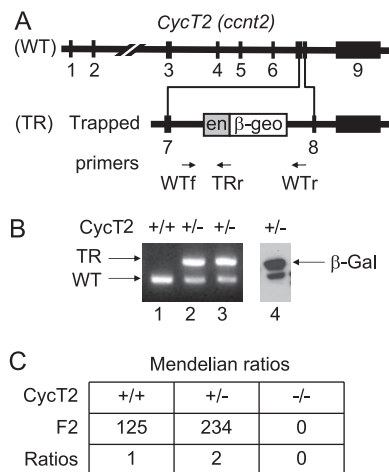


FIG. 1. Analysis of *CycT2*^{+/-} ES cells and mice. (A) Schematic representation of WT and TR (*CycT2*. β -geo) alleles. The integration of the gene trap vector containing part of intron 1 and exon 2 of the engrailed 2 (*en*) gene and β -galactosidase-neomycin gene (β -geo) into intron 7 inactivated the *CycT2* gene (*Ccnt2*). The arrows under the scheme represent DNA primers WTf, TRr, and WTr, which were used in panel B. (B) Representative result of PCR genotyping and protein expression. (Left) Genomic DNA was isolated from E12.5 embryos and genotyped with two sets of primers—WTf and WTr, and WTf and TRr—which distinguished WT from TR alleles of *CycT2*. (Right) The fusion protein between *CycT2* and β -Geo was detected in parental W048F02-04304 ES cells by Western blotting. The lower band represents a degradation product. β -Gal, β -galactosidase. (C) Ratios of genotypes from heterozygous breedings. A total of 125 WT (*CycT2*^{+/+}) and 234 heterozygous (*CycT2*^{+/-}) mice were obtained and genotyped. No homozygous (*CycT2*^{-/-}) mice were observed.

quences (Fig. 1A). This insertion created a fusion protein between the N terminus of *CycT2* and the β -Geo protein. We detected this fusion protein, which consisted of 235 and 1,323 residues from *CycT2* and β -Geo (170 kDa), respectively, with anti β -galactosidase antibodies by Western blotting (Fig. 1B, right). Of note, the fusion protein created a loss-of-function allele, which contained only the N terminus of *CycT2* but lacked the middle and C-terminal regions of the protein. Importantly, in the absence of complete cyclin boxes, this truncated *CycT2* protein neither binds nor exerts a dominant-negative phenotype on *Cdk9* (17). Indeed, we demonstrated previously that these missing sequences were essential for the function of this cyclin (17).

Although our WT and heterozygous *CycT2*^{+/-} mice were healthy, appeared normal, and reproduced well, their mating did not generate any homozygous *CycT2*^{-/-} mice (Fig. 1C). From analyzing 359 pups, we noted the Mendelian ratio of 1:2 for WT to *CycT2*^{+/-} mice, which indicates that the two strains have equal fitness. However, the predicted ratio (or 25%) of homozygous *CycT2*^{-/-} mice did not materialize. We conclude that our trapped allele does not encode a functional protein and that *CycT2* is essential for mouse development.

***CycT2* is expressed abundantly throughout mouse embryogenesis.** To define further the function of *CycT2* during mouse development, embryos at E7.5, E9.5, E10.5, and E14.5 or more from matings of heterozygous *CycT2*^{+/-} mice were genotyped (Table 1). Importantly, no *CycT2*^{-/-} embryos were detected in any given time period, suggesting that *CycT2* might play an

TABLE 1. Genotyping of mutant *CycT2* embryos and pups

Embryo stage	No. of embryos screened/genotyped ^a		
	<i>CycT2</i> ^{+/+}	<i>CycT2</i> ^{+/-}	<i>CycT2</i> ^{-/-}
>E15	4	11	0
E14.5	1	2	0
E10.5	7	9	0
E9.5	4	7	0
E7.5	11	14	0
Blastocyst (E3.5)	11	28	0
Morula	1	2	0
4-cell	2	4	0

^a Total numbers of embryos screened/genotyped from all litters examined.

important role even prior to implantation. To access this period of mouse development, E3.5 aggregates, which represent the blastocyst stage, were isolated from pregnant females. Again, no *CycT2*^{-/-} embryonic tissue was found, supporting an important role for *CycT2* in early mouse development (Table 1).

***CycT2* is expressed ubiquitously during mouse embryogenesis.** To elucidate the spatiotemporal expression of *CycT2* in developing mouse embryos, LacZ staining was monitored in E7.5, E8.5, E9.5, E11.5, and E14.5 embryos. Since the *CycT2* promoter directed the expression of the hybrid *CycT2*. β -Geo protein (Fig. 1A), this staining reflects the transcription of *CycT2* at any given developmental stage. As presented in Fig. 2, β -galactosidase was expressed in the embryonic region (E6.5) (data not presented), the embryonic ectoderm (E7.5), the forming brain and neural tube (E8.5/9.5), and throughout the forming tissues and organs (E11.5 and E14.5) (Fig. 2). This staining suggests further that this P-TEFb complex (*CycT2*-Cdk9) plays an important role throughout mouse embryogenesis.

***CycT2* is expressed in all tissues and organs of the adult mouse.** To extend these findings to the adult organism, we prepared lysates from various mouse tissues and organs. Western blotting was performed with anti-*CycT1*, -*CycT2*, and -Cdk9 antibodies (Fig. 3). Since previous studies had revealed that *CycT2* is the coactivator of MyoD (32), it was not surprising that we found high levels of expression in skeletal muscle (Fig. 3). Significant levels of *CycT2* were also found in the heart, brain, kidney, liver, testis, and pancreas, followed by lesser amounts in the lung, spleen, and thymus (Fig. 3, middle). Although *CycT2* is spliced differentially to produce *CycT2a* and *CycT2b*, our Western blots did not differentiate between them. In addition, levels of Cdk9 did not reflect those of *CycT2* (Fig. 3, bottom), which suggests that *CycT1* is the predominant cyclin in all P-TEFb complexes in the organism. Importantly, this pattern of expression parallels that found in a previous study (2). In contrast, since *CycT1* is found abundantly in hematopoietic cells, its highest levels were observed in the lung, spleen, and thymus (Fig. 3, top) (13, 20, 38). Interestingly, both cyclins were expressed abundantly in organs such as the testis, which contain many proliferating cells.

P-TEFb complexes containing *CycT1* and *CycT2* perform redundant and nonredundant functions in ES cells. Since the genetic inactivation of *CycT2* had such a dramatic effect on mouse development, we decided to study the functions of *CycT1* and *CycT2* in ES cells. These cells form the inner cell



FIG. 2. Expression of *CycT2* during mouse midgestation and early embryogenesis. LacZ staining of heterozygous embryos was used to visualize the spatiotemporal expression of *CycT2*. β -Geo, which reflects transcription from the *CycT2* promoter. WT (+/+) and heterozygous (+/-) mouse embryos were isolated at the indicated embryonic days after conception, fixed with glutaraldehyde, and stained with X-Gal. *CycT2* was expressed in all forming organs and supporting tissues in E10.5 to E14.5 embryos. Interestingly, the expression of *CycT2* was mostly localized to the embryonic ectoderm and the forming brain and neural tube in E7.5 and E8.5/E9.5 embryos, respectively.

mass of blastocysts and can differentiate into various cell types. We used specific siRNAs to decrease the levels of *CycT1* and *CycT2* (Fig. 4A). We analyzed RNA expression profiles after only 48 h so as to minimize secondary effects by transcription factors, whose expression depends on these different P-TEFb complexes. By densitometry, better than 90% reduction of both cyclins was achieved, and specific siRNAs for one cyclin did not affect the expression of the other (Fig. 4A, lanes 2 and

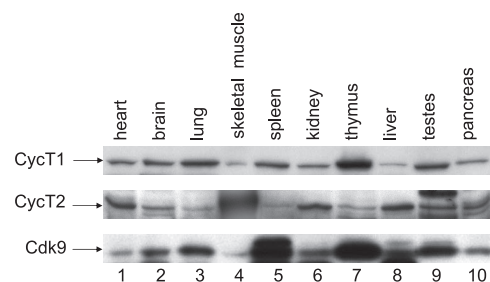


FIG. 3. *CycT2* is expressed in all tissues and organs in the adult mouse. Expression patterns of subunits of different P-TEFb complexes in tissues and organs from 3-month-old mice were probed with appropriate antibodies by Western blotting. Presented are data with anti-*CycT1*, -*CycT2*, and -Cdk9 antibodies.

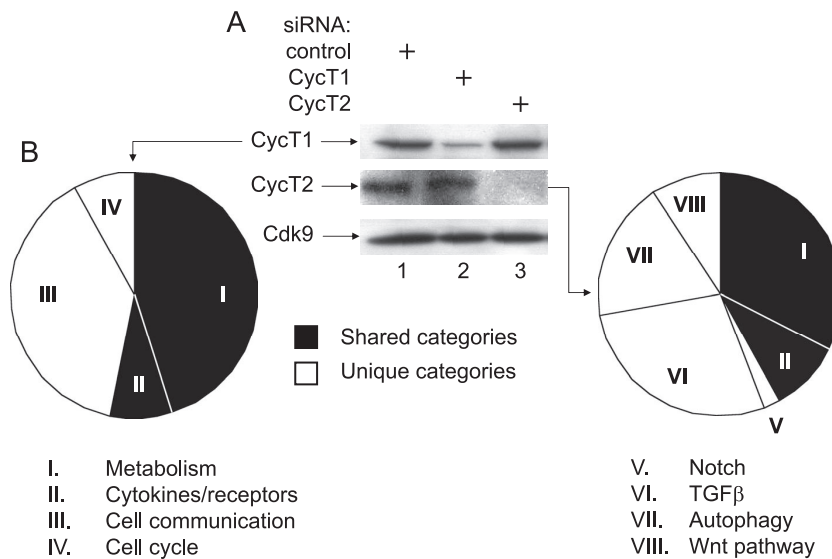


FIG. 4. Genes regulated by CycT1 and CycT2 in mouse ES cells. (A) Knockdown of CycT1 and CycT2 in ES cells. Specific siRNAs were used to decrease the expression of CycT1 and CycT2 in ES cells. Western blotting with antibodies against CycT1, CycT2, and Cdk9 detected the levels of these proteins. The arrows on the left point to specific proteins. (B) Mouse whole-genome RNA expression profiles between ES cells with siRNA species against CycT1 and CycT2. Forty-nine and 43 differentially expressed genes are depicted by pie charts for CycT1 and CycT2 knockdowns, respectively. Their expression differed more than 1.5-fold between control and CycT1 and CycT2 knockdown ES cells. Ontologic analyses were carried out using DAVID (<http://david.abcc.ncifcrf.gov/>) and grouped based on the Kyoto Encyclopedia of Genes and Genomes pathway. The black and white slices denote shared and unique categories of proteins, respectively. The supplemental material provides a list of genes that showed more than 1.5-fold reduction in their mRNA levels when CycT1 or CycT2 was knocked down in a descending order of reduction.

3). Levels of Cdk9 were reduced slightly, which reflects the almost equivalent levels of CycT1 and CycT2 in these cells. Similar downregulation of Cdk9 *in vivo* or in cultured cell lines was also reported by other researchers (24, 37).

Global gene expression profiles were examined with mouse whole-genome microarrays. If the functions of CycT1 and CycT2 were redundant, the expression of a majority of genes should not be altered. Out of ~8,600 genes expressed in ES cells (with signals twofold above background levels), only 59 or 76 genes demonstrated a 1.5-fold reduction in the amounts of mRNA when CycT1 or CycT2 was knocked down, respectively (see the supplemental material). Gene ontology analyses demonstrated that these knockdowns affected a distinct set of cellular genes and pathways (Fig. 4B; see the supplemental material). For CycT1 knockdown, 22 of 49 annotated genes were involved in fatty acid and glucose metabolism (45%). For CycT2 knockdowns, 14 out of 43 genes affected purine and glucose metabolism (32%) (see the supplemental material). Interestingly, although glucose metabolism was affected in both cases, the genes that were targeted were different. Knockdown of CycT1, but not CycT2, also affected genes involved in cell communication (39%), while knockdown of CycT2, but not CycT1, affected pathways important for early embryogenesis, including transforming growth factor β (TGF- β), Notch, Wnt signaling, and autophagy (58%) (Fig. 4B; see the supplemental material). From all these data, we conclude that different P-TEFb complexes are mostly redundant but that there is a set of genes that are specifically under the control of CycT1 or CycT2, some of which are also critical for the early development of the mouse embryo.

DISCUSSION

In this report, we analyzed the function of CycT2 for the organism. Since we found no *CycT2*^{-/-} embryos or blastocysts, its genetic inactivation must have led to preimplantation lethality. Nevertheless, the nature of the β -geo trap allowed us to follow the expression of CycT2 during embryogenesis. We found it expressed in all organs, which was confirmed with tissues from adult mice by Western blotting. Finally, we found that CycT1 and CycT2 are also required for the expression of distinct and important genes in ES cells. We conclude that different cyclins involved with P-TEFb serve many redundant and some nonredundant functions in the embryogenesis and early development of mammals.

Since these cyclins are redundant in *C. elegans*, it was surprising that genetic ablation of CycT2 led to embryonic lethality in mice. In *C. elegans*, genetic inactivation of CycT1 or CycT2 had no apparent phenotype (28). In contrast, their combined ablation had the same phenotype as the genetic inactivation of RNAPII, which resulted in early embryonic lethality. In addition, mice with greatly reduced levels of CycT1 are viable, albeit with several immunological defects (24). However, given their nonoverlapping critical target genes, as evidenced by our siRNA experiments (Fig. 4B), we expect that the complete genetic inactivation of CycT1 would also lead to an embryonic-lethal phenotype. Thus, both major P-TEFb complexes appear to be essential for the development and viability of mammals.

It is most likely that the lack of CycT2 directly caused this preimplantation lethality. When comprehensive analyses of expressed sequence tags were carried out in different develop-

mental stages of female gametogenesis, i.e., in oocytes prior to meiotic maturation, fully grown eggs, and two-cell embryos, an intriguing expression pattern of P-TEFb transcripts was revealed (11). Importantly, CycT1 and CycT2 mRNA species were found in the fully grown egg, but not in the two-cell embryo. Since, substantial amounts of stored RNA are destroyed shortly after fertilization (12, 26), it is likely that CycT1 and CycT2 transcripts are also lost at this stage. However, the expression of these cyclins must commence soon thereafter, as S2 in the CTD of RNAPII is heavily phosphorylated during zygotic gene activation, when transcription becomes a requirement for further development (4). However, with CycT2^{-/-} eggs, once maternal P-TEFb complexes are depleted and no new CycT2 is synthesized, this change in the transcriptional program could have lethal consequences. As a result, no blastocysts should be observed and all further embryonic development should stop.

Transcription of most genes by RNAPII requires P-TEFb (7). The best-characterized example is with human immunodeficiency virus, where the transcriptional transactivator Tat binds CycT1 (and not CycT2) on the transactivation response RNA stem-loop, which recruits and/or repositions Cdk9 to modify RNAPII for elongation and cotranscriptional processing of viral transcripts (35). Subsequent studies demonstrated that other activators also recruit P-TEFb via their interactions with CycT1 or CycT2 (3, 6, 10, 15–17). Among them, ENL binds CycT2 (23). Of note, attempts to inactivate the ENL gene also found no ENL^{-/-} embryos at E8.5 or earlier (9), which might provide another clue to the demise of our CycT2^{-/-} mice. Further candidates might have been revealed by our microarray data. We chose mouse ES cells, not only because of early embryonic lethality of our CycT2^{-/-} blastocysts, but because most developmental genes are expressed in these cells. Indeed, we found a subset of genes that were differentially regulated by P-TEFb complexes, which contained CycT1 or CycT2. Since the levels of transcripts encoding Oct-4, Nanog, and Sox2, which maintain stem cells, were unaltered, the observed effects with our siRNA species were not secondary to ES cell differentiation. In addition, our transfected cells appeared morphologically normal and stained positive for alkaline phosphatase. Since siRNA against CycT1 did not affect levels of CycT2, and vice versa, these effects were also cyclin specific. Importantly, levels of CycT1 and CycT2 were decreased substantially. We conclude that CycT1 and CycT2 serve redundant and nonredundant functions in mammals and that some of their target genes are essential for early embryonic development.

Which additional target genes could lead to this phenotype? Gene ontology analyses revealed that a reduction in CycT2 affected mostly TGF- β and Wnt signaling pathways, as well as autophagy. The most affected genes were those for Lefty 1 and Lefty 2, members of the TGF- β superfamily. Of note, the expression of Lefty is positively regulated by Wnt signaling in ES cells, which was also affected by siRNA against CycT2 (5). Importantly, both arms are critical components of early development and differentiation, as is autophagy. For example, Lefty proteins are highly expressed in the inner cell mass and trophoectoderm during embryogenesis (1). Whereas there are abnormalities in left-right axis formation in Lefty 1-deficient mice, excessive mesoderm is formed in Lefty 2-deficient mice

(21, 22). Moreover, during the transition from oocytes to embryos, maternal proteins are rapidly degraded and replaced by zygotic proteins. This process is mediated by the ubiquitin-proteasomal system and autophagy. Interestingly, autophagy-defective oocytes fail to develop beyond the four- and eight-cell stages, and its zygotic mRNA components can be detected as early as the two-cell stage (34). Thus, CycT2 and genes regulated by this form of P-TEFb are critically important for early developmental pathways in mice.

In summary, CycT2 is essential for mouse embryogenesis. Although most genes appear to be regulated by either or both cyclins, there are sets of genes that are specifically under the control of CycT1 or CycT2. Further studies will be needed to examine these direct targets of CycT2 during development. In addition, conditional knockouts will be instructive to further analyze their physiological functions in the adult organism.

ACKNOWLEDGMENTS

We thank Xin Lin, Nigel Killeen, and personnel from UCSF Mouse Transgenic and Histology Cores, as well as members of our laboratory, for help with experiments and comments on the manuscript.

This work was supported by grants from the NIH to B.M.P., from the Ministry of Education, Youth and Sports (ME09047) to D.B., and from the Czech Ministry of Agriculture (MZE0002716202) and the Czech Science Foundation (301/09/1832) to J.K.

REFERENCES

1. Adjaye, J., J. Huntriss, R. Herwig, A. BenKahla, T. C. Brink, C. Wierling, C. Hultschig, D. Groth, M. L. Yaspo, H. M. Picton, R. G. Gosden, and H. Lehrach. 2005. Primary differentiation in the human blastocyst: comparative molecular portraits of inner cell mass and trophectoderm cells. *Stem Cells* 23:1514–1525.
2. Bagella, L., T. K. MacLachlan, R. J. Buono, M. M. Pisano, A. Giordano, and A. De Luca. 1998. Cloning of murine CDK9/PITALRE and its tissue-specific expression in development. *J. Cell Physiol.* 177:206–213.
3. Barboric, M., R. M. Nissen, S. Kanazawa, N. Jabrane-Ferrat, and B. M. Peterlin. 2001. NF- κ B binds P-TEFb to stimulate transcriptional elongation by RNA polymerase II. *Mol. Cell* 8:327–337.
4. Bellier, S., S. Chastant, P. Adenot, M. Vincent, J. P. Renard, and O. Bensaud. 1997. Nuclear translocation and carboxyl-terminal domain phosphorylation of RNA polymerase II delineate the two phases of zygotic gene activation in mammalian embryos. *EMBO J.* 16:6250–6262.
5. Besser, D. 2004. Expression of nodal, lefty-A, and lefty-B in undifferentiated human embryonic stem cells requires activation of Smad2/3. *J. Biol. Chem.* 279:45076–45084.
6. Brasier, A. R. 2008. Expanding role of cyclin dependent kinases in cytokine inducible gene expression. *Cell Cycle* 7:2661–2666.
7. Chao, S. H., and D. H. Price. 2001. Flavopiridol inactivates P-TEFb and blocks most RNA polymerase II transcription in vivo. *J. Biol. Chem.* 276:31793–31799.
8. Cujec, T. P., H. Okamoto, K. Fujinaga, J. Meyer, H. Chamberlin, D. O. Morgan, and B. M. Peterlin. 1997. The HIV transactivator TAT binds to the CDK-activating kinase and activates the phosphorylation of the carboxy-terminal domain of RNA polymerase II. *Genes Dev.* 11:2645–2657.
9. Doty, R. T., G. J. Vanasse, C. M. Disteche, and D. M. Willerford. 2002. The leukemia-associated gene Mll1/ENL: characterization of a murine homolog and demonstration of an essential role in embryonic development. *Blood Cells Mol. Dis.* 28:407–417.
10. Elagib, K. E., I. S. Mihaylov, L. L. Delehanty, G. C. Bullock, K. D. Ouma, J. F. Caronia, S. L. Gonias, and A. N. Goldfarb. 2008. Cross-talk of GATA-1 and P-TEFb in megakaryocyte differentiation. *Blood* 112:4884–4894.
11. Evsikov, A. V., J. H. Graber, J. M. Brockman, A. Hampl, A. E. Holbrook, P. Singh, J. J. Eppig, D. Solter, and B. B. Knowles. 2006. Cracking the egg: molecular dynamics and evolutionary aspects of the transition from the fully grown oocyte to embryo. *Genes Dev.* 20:2713–2727.
12. Gosden, R. G. 2002. Oogenesis as a foundation for embryogenesis. *Mol. Cell Endocrinol.* 186:149–153.
13. Jiang, H., and B. M. Peterlin. 2008. Differential chromatin looping regulates CD4 expression in immature thymocytes. *Mol. Cell Biol.* 28:907–912.
14. Kanazawa, S., T. Okamoto, and B. M. Peterlin. 2000. Tat competes with CIITA for the binding to P-TEFb and blocks the expression of MHC class II genes in HIV infection. *Immunity* 12:61–70.
15. Kanazawa, S., L. Soucek, G. Evan, T. Okamoto, and B. M. Peterlin. 2003.

- c-Myc recruits P-TEFb for transcription, cellular proliferation and apoptosis. *Oncogene* **22**:5707–5711.
16. Kohoutek, J., D. Blazek, and B. M. Peterlin. 2006. Hexim1 sequesters positive transcription elongation factor b from the class II transactivator on MHC class II promoters. *Proc. Natl. Acad. Sci. USA* **103**:17349–17354.
 17. Kurosu, T., F. Zhang, and B. M. Peterlin. 2004. Transcriptional activity and substrate recognition of cyclin T2 from P-TEFb. *Gene* **343**:173–179.
 18. Lin, X., R. Taube, K. Fujinaga, and B. M. Peterlin. 2002. P-TEFb containing cyclin K and Cdk9 can activate transcription via RNA. *J. Biol. Chem.* **277**:16873–16878.
 19. Margaritis, T., and F. C. Holstege. 2008. Poised RNA polymerase II gives pause for thought. *Cell* **133**:581–584.
 20. Marshall, R. M., D. Salerno, J. Garriga, and X. Grana. 2005. Cyclin T1 expression is regulated by multiple signaling pathways and mechanisms during activation of human peripheral blood lymphocytes. *J. Immunol.* **175**:6402–6411.
 21. Meno, C., K. Gritsman, S. Ohishi, Y. Ohfuji, E. Heckscher, K. Mochida, A. Shimono, H. Kondoh, W. S. Talbot, E. J. Robertson, A. F. Schier, and H. Hamada. 1999. Mouse Lefty2 and zebrafish antivin are feedback inhibitors of nodal signaling during vertebrate gastrulation. *Mol. Cell* **4**:287–298.
 22. Meno, C., A. Shimono, Y. Saijoh, K. Yashiro, K. Mochida, S. Ohishi, S. Noji, H. Kondoh, and H. Hamada. 1998. lefty-1 is required for left-right determination as a regulator of lefty-2 and nodal. *Cell* **94**:287–297.
 23. Mueller, D., C. Bach, D. Zeisig, M. P. Garcia-Cuellar, S. Monroe, A. Sreekumar, R. Zhou, A. Nesvizhskii, A. Chinnaiyan, J. L. Hess, and R. K. Slany. 2007. A role for the MLL fusion partner ENL in transcriptional elongation and chromatin modification. *Blood* **110**:4445–4454.
 24. Oven, L., N. Brdickova, J. Kohoutek, T. Vaupotic, M. Narat, and B. M. Peterlin. 2007. AIRE recruits P-TEFb for transcriptional elongation of target genes in medullary thymic epithelial cells. *Mol. Cell. Biol.* **27**:8815–8823.
 25. Peterlin, B. M., and D. H. Price. 2006. Controlling the elongation phase of transcription with P-TEFb. *Mol. Cell* **23**:297–305.
 26. Pratt, H. P., V. N. Bolton, and K. A. Gudgeon. 1983. The legacy from the oocyte and its role in controlling early development of the mouse embryo. *Ciba Found Symp.* **98**:197–227.
 27. Saunders, A., L. J. Core, and J. T. Lis. 2006. Breaking barriers to transcription elongation. *Nat. Rev. Mol. Cell Biol.* **7**:557–567.
 28. Shim, E. Y., A. K. Walker, Y. Shi, and T. K. Blackwell. 2002. CDK-9/cyclin T (P-TEFb) is required in two postinitiation pathways for transcription in the *C. elegans* embryo. *Genes Dev.* **16**:2135–2146.
 29. Shimizu, N., R. Ouchida, N. Yoshikawa, T. Hisada, H. Watanabe, K. Okamoto, M. Kusuhara, H. Handa, C. Morimoto, and H. Tanaka. 2005. HEXIM1 forms a transcriptionally abortive complex with glucocorticoid receptor without involving 7SK RNA and positive transcription elongation factor b. *Proc. Natl. Acad. Sci. USA* **102**:8555–8560.
 30. Schnutgen, F., S. De-Zolt, P. Van Sloun, M. Hollatz, T. Floss, J. Hansen, J. Altschmied, C. Seisenberger, N. B. Ghyselinck, P. Ruiz, P. Chambon, W. Wurst, and H. von Melchner. 2005. Genomewide production of multipurpose alleles for the functional analysis of the mouse genome. *Proc. Natl. Acad. Sci. USA* **102**:7221–7226.
 31. Simone, C., L. Bagella, C. Bellan, and A. Giordano. 2002. Physical interaction between pRb and cdk9/cyclinT2 complex. *Oncogene* **21**:4158–4165.
 32. Simone, C., P. Stiegler, L. Bagella, B. Pucci, C. Bellan, G. De Falco, A. De Luca, G. Guanti, P. L. Puri, and A. Giordano. 2002. Activation of MyoD-dependent transcription by cdk9/cyclin T2. *Oncogene* **21**:4137–4148.
 33. Taube, R., X. Lin, D. Irwin, K. Fujinaga, and B. M. Peterlin. 2002. Interaction between P-TEFb and the C-terminal domain of RNA polymerase II activates transcriptional elongation from sites upstream or downstream of target genes. *Mol. Cell. Biol.* **22**:321–331.
 34. Tsukamoto, S., A. Kuma, M. Murakami, C. Kishi, A. Yamamoto, and N. Mizushima. 2008. Autophagy is essential for preimplantation development of mouse embryos. *Science* **321**:117–120.
 35. Wimmer, J., K. Fujinaga, R. Taube, T. P. Cujec, Y. Zhu, J. Peng, D. H. Price, and B. M. Peterlin. 1999. Interactions between Tat and TAR and human immunodeficiency virus replication are facilitated by human cyclin T1 but not cyclins T2a or T2b. *Virology* **255**:182–189.
 36. Wittmann, B. M., N. Wang, and M. M. Montano. 2003. Identification of a novel inhibitor of breast cell growth that is down-regulated by estrogens and decreased in breast tumors. *Cancer Res.* **63**:5151–5158.
 37. Yu, W., R. Ramakrishnan, Y. Wang, K. Chiang, T. L. Sung, and A. P. Rice. 2008. Cyclin T1-dependent genes in activated CD4 T and macrophage cell lines appear enriched in HIV-1 co-factors. *PLoS ONE* **3**:e3146.
 38. Yu, W., Y. Wang, C. A. Shaw, X. F. Qin, and A. P. Rice. 2006. Induction of the HIV-1 Tat co-factor cyclin T1 during monocyte differentiation is required for the regulated expression of a large portion of cellular mRNAs. *Retrovirology* **3**:32.

APPENDIX 10

OVEN Irena, BRDICKOVA Nada, **KOHOUTEK Jiri**, VAUPOTIC Tomas, NARAT M and Peterlin B. Matija. AIRE recruits P-TEFb for transcriptional elongation of target genes in medullary thymic epithelial cells. *Molecular and cellular biology*. 2007, 27(24).

AIRE Recruits P-TEFb for Transcriptional Elongation of Target Genes in Medullary Thymic Epithelial Cells^{∇†}

Irena Oven,^{1,2‡} Naděžda Brdičková,^{1‡} Jiri Kohoutek,^{1‡} Tomaz Vaupotic,³
Mojca Narat,² and B. Matija Peterlin^{1*}

Departments of Medicine, Microbiology and Immunology, Rosalind Russell Medical Research Center, University of California—San Francisco, San Francisco, California 94143-0703¹; Department of Animal Science, Biotechnical Faculty, University of Ljubljana, SI-1230 Domzale, Slovenia²; and Institute of Biochemistry, Faculty of Medicine, University of Ljubljana, SI-1000 Ljubljana, Slovenia³

Received 19 June 2007/Returned for modification 17 August 2007/Accepted 2 October 2007

AIRE is a transcriptional activator that directs the ectopic expression of many tissue-specific genes in medullary thymic epithelial cells, which plays an important role in the negative selection of autoreactive T cells. However, its mechanism of action remains poorly understood. In this study, we found that AIRE regulates the step of elongation rather than initiation of RNA polymerase II. For these effects, AIRE bound and recruited P-TEFb to target promoters in medullary thymic epithelial cells. In these cells, AIRE activated the ectopic transcription of insulin and salivary protein 1 genes. Indeed, by chromatin immunoprecipitation, we found that RNA polymerase II was already engaged on these promoters but was unable to elongate in the absence of AIRE. Moreover, the genetic inactivation of cyclin T1 from P-TEFb abolished the transcription of AIRE-responsive genes and led to lymphocytic infiltration of lacrimal and salivary glands in the *CycT1*^{-/-} mouse. Our findings reveal critical steps by which AIRE regulates the transcription of genes that control central tolerance in the thymus.

Among genetic factors implicated in autoimmunity, the autoimmune regulator (AIRE) is an important transcriptional activator that mediates central tolerance in the thymus. Loss-of-function mutations in the human *Aire* gene lead to the development of autoimmune polyendocrinopathy syndrome type 1 (APECED), which is manifested by the destruction of mostly endocrine glands (31). AIRE is expressed mainly in the thymus but is also present in low levels in lymph nodes, spleen, and fetal liver (16, 31). In the thymus, its expression is restricted to a subpopulation of medullary thymic epithelial cells (mTECs) (16). Indeed, mTECs express ectopically a number of tissue-restricted antigens (9, 19), which is abolished in *AIRE*^{-/-} mice (4). This absence leads to a defect in negative selection of autoreactive T cells in the thymus (3, 26) and autoimmunity in the periphery, which is manifested by the infiltration of autoreactive T cells in many tissues and the expression of autoantibodies in the periphery (4, 40).

AIRE is a 55-kDa nuclear protein. It has several functional domains, such as the N-terminal homogenously staining region, a functional bipartite nuclear localization signal, a putative DNA-binding SAND (*Sp100*, *AIRE*, *NucP41/75*, and *DEAF-1*) domain (5, 10), two plant homeodomain (PHD)-type Zn²⁺ fingers separated by a proline-rich region, and four LXXLL nuclear receptor motifs (1, 15). When fused to a heterologous DNA-binding domain, AIRE can activate tran-

scription in transient-expression assays (37). Because it binds preferentially to GG repeats and AT-rich sequences (24, 39), its interactions with DNA could be rather promiscuous (reviewed in references 28 and 36). The first PHD may also function as an E3 ubiquitin ligase (47). Finally, analyses of *AIRE*^{-/-} mice revealed that mouse insulin 2 (*Ins2*), salivary protein 1 (*Spt1*), casein α , and several hundred other genes are regulated by AIRE (4). Interestingly, some of these genes are localized in chromosomal clusters (9, 19).

Eukaryotic transcription starts with the recruitment of RNA polymerase II (RNAPII) to start sites of transcription. This process requires DNA-bound activators, general transcription factors, chromatin remodeling machinery, and RNAPII. This recruitment leads to the formation of the preinitiation complex (PIC) (reviewed in reference 30). At this stage, transcription is initiated but further elongation is blocked by the negative transcription elongation factor (N-TEF), which contains the DRB sensitivity-inducing factor and the negative elongation factor (reviewed in reference 35). To enable efficient elongation and cotranscriptional processing of primary transcripts, positive transcription elongation factor b (P-TEFb) must be recruited to the PIC. It counteracts N-TEF and prepares RNAPII for elongation. P-TEFb is a heterodimer of a C-type cyclin (*CycT1*, *CycT2*, or *CycK*) and cyclin-dependent kinase 9 (*Cdk9*). P-TEFb phosphorylates N-TEF and the C-terminal domain of RNAPII, and this change enables RNAPII to transition from abortive to productive elongation. In cells, P-TEFb is found in two molecular complexes. In the small complex, the catalytically active P-TEFb associates with activators and RNAPII. In the catalytically inactive large complex, P-TEFb binds 7SK snRNA and hexamethylene bis-acetamide inducible protein 1 (HEXIM1) (reviewed in reference 35). Thus, HEXIM1 is a specific inhibitor of P-TEFb.

* Corresponding author. Mailing address: Box 0703, 3rd and Parnassus Avenues, San Francisco, CA 94143-0703. Phone: (415) 502-1905. Fax: (415) 502-1901. E-mail: matija.peterlin@ucsf.edu.

‡ These authors contributed equally.

† Supplemental material for this article may be found at <http://mc.manuscriptcentral.com/mcb>.

[∇] Published ahead of print on 15 October 2007.

Transcriptional activators can be divided into three groups: type I (e.g., Sp1 and CTF), which stimulate initiation; type IIA (e.g., Tat from human immunodeficiency virus), which stimulate predominantly elongation; and type IIB (VP16, class II transactivator [CIITA], and NF- κ B, among others), which stimulate both initiation and elongation of transcription (6). Moreover, type I and type IIA activators can synergize with one another but not with type IIB activators. Synergy occurs from concerted actions of factors stimulating two different steps in transcription: initiation and elongation (6). In this study, we wanted to determine how AIRE regulates transcription in mTECs.

MATERIALS AND METHODS

Plasmids. Plasmid targets and effectors were described previously (34, 46). pMycAIRE, pFlagAIRE, and insulin reporters were generous gifts from P. Peterson (16) and M. German (33), respectively. We also moved AIRE cDNA into the retroviral expression vector pBABE-puro (pBABE.AIRE).

Chemicals and immunoreagents. Trichostatin A (TSA) and anti-Flag M2 (α Flag M2) agarose beads were from Sigma (St. Louis, MO). α Myc, α Cdk9, α AIRE, α CycT1, and α RNAPII were from Santa Cruz Biotechnology (Santa Cruz, CA); α GAPDH (GAPDH is glyceraldehyde-3-phosphate dehydrogenase) was from Ambion (Austin, TX); α HEXIM1 was from Antibody Solutions (Mountain View, CA); and α AIRE 6.1 was from J. Pitkänen.

Cell culture and transient-expression studies. HeLa-MAGI, 1C6, and Phoenix-ampho cells were grown and transfected as described in the supplemental material.

Activation of endogenous genes. 1C6 cells were grown, transfected, and analyzed as described in the supplemental material.

GST pulldowns, immunoprecipitations, and Western blotting. Glutathione S-transferase (GST) pulldowns and immunoprecipitations were performed essentially as described previously (20). In brief, 20 μ g of GST or GST fusion proteins was incubated with cell lysates, reacted with beads, and washed four times with lysis buffer. Bound proteins were eluted by being boiled in sodium dodecyl sulfate sample buffer, resolved by sodium dodecyl sulfate-polyacrylamide gel electrophoresis (SDS-PAGE) on a 12% gel, and analyzed by Western blotting using α AIRE 6.1 antibody. For immunoprecipitation, cells were lysed and immunoprecipitated with α Flag M2 agarose beads (Sigma) overnight. Bound proteins were eluted and separated by SDS-PAGE and analyzed by immunoblotting with α CycT1, α Cdk9, α Cdk7, and α Flag M2 antibodies.

Knockdown of HEXIM1 by use of siRNA and chloramphenicol acetyltransferase (CAT) reporter assays. In brief, 1C6 cells were transfected with specific or negative-control scrambled small interfering RNA (siRNA) (mock siRNA) by use of Lipofectamine 2000 (Invitrogen, Carlsbad, CA), analyzed for the expression of HEXIM1, and later transfected with plasmid effectors and targets. Further details are provided in the supplemental material.

ChIP. 1C6 and 1C6.AIRE cells were grown on 15-cm plates. They were subjected to chromatin immunoprecipitation (ChIP) by use of a ChIP assay kit (Upstate Biotechnology, Charlottesville, VA) according to the manufacturer's instructions. Lysates were sonicated at power 4 four times for 10 s each by use of a Sonic Dismembrator model 100 (Fisher Scientific, Pittsburgh, PA) to shear genomic DNA. The average size of sheared fragments was 300 to 500 bp. We used the following antibodies from Santa Cruz: α AIRE, α RNAPII, α CycT1, and α Cdk9. A portion (2 μ l) of the extracted DNA was amplified in 30- μ l reactions by use of ExTaq polymerase (Takara, Shiga, Japan) for 24 to 36 cycles, integrated over that range, and normalized to input DNA as described previously (51). Further details are provided in the supplemental material.

Generation of CycT1^{-/-} mice, histopathology, and clinical scoring. Details of the generation and characterization of CycT1^{-/-} mice are provided in the supplemental material.

RESULTS

AIRE is a type IIA activator and promotes transcriptional elongation. To investigate the mechanism of action of AIRE, we used a well-established assay for differentiating between transcriptional initiation and elongation (43). We chose three artificial plasmid targets, which differ by ability to recruit and

load RNAPII to the promoter and thus to initiate and/or elongate transcription. The plasmid target pG5CAT contains five Gal4 DNA-binding sites (upstream activation sequences [UASs]) placed in front of the E1b TATA promoter linked to the CAT reporter gene (Fig. 1A, pG5CAT) (43). pG5CAT recruits RNAPII inefficiently and thus cannot initiate or elongate transcription. The second plasmid target, pG6SpCAT, contains six UASs and three Sp1 binding sites placed in front of the E1b TATA promoter and the CAT gene (Fig. 1A, pG6SpCAT) (45). The third plasmid target, pG6TARCAT, contains six UASs positioned upstream of the κ B sites in the human immunodeficiency virus type 1 long terminal repeat, which also transcribes the transactivation response (TAR) RNA stem loop and the CAT gene (45). Three Sp1 sites load and position RNAPII on these two promoters, but they require an enhancer to recruit P-TEFb for the transition to the elongation phase of transcription and the expression of the CAT gene (45). We used these plasmid targets to determine whether AIRE stimulates the initiation and/or elongation of transcription.

To test whether AIRE can activate transcription in different cell types, we used the human epithelial HeLa-MAGI (49) and mouse 1C6 mTEC (22) cell lines, which do not express AIRE (47). Importantly, 1C6 cells were derived from primary mTECs and were never immortalized with the help of an oncogene or telomerase (22). As presented in Fig. 1A with pG5CAT, where no Sp1 sites are present, AIRE did not activate transcription (Fig. 1A, lanes 3 and 10). Indeed, neither AIRE nor the Gal4 DNA-binding domain protein from positions 1 to 147 (GalDBD) could activate transcription when coexpressed with this plasmid target alone (Fig. 1A, lanes 2, 3, 10, and 11). Of interest, GalDBD contains a weak activation domain (27), which behaves as a type I activator. In sharp contrast, when coexpressed with AIRE, GalDBD activated transcription 50-fold (Fig. 1A, lanes 4 and 12). Importantly, AIRE did not have to be tethered artificially to DNA for these effects. Therefore, our results suggest that AIRE promotes the elongation of transcription.

To confirm this observation, we used a cooperativity assay (43) with pG6SpCAT, where AIRE should synergize with Sp1. Indeed, in the presence of Sp1 sites, AIRE activated transcription 30- and 15-fold over background levels in HeLa-MAGI and 1C6 cells, respectively (Fig. 1A, lanes 5, 6, 13, and 14). AIRE also activated transcription of the pG6TARCAT reporter gene equivalently (Fig. 1A, lane 8). Thus, the presence of TAR did not alter the effects of AIRE on plasmid targets in cells. Importantly, the expression of GalDBD alone did not activate transcription of pG6SpCAT or pG6TARCAT reporter genes (data not presented). Furthermore, the exogenous expression of increasing amounts of AIRE resulted in a dose-dependent increase of transcriptional activation (Fig. 1B, lanes 2, 3, and 4). Thus, AIRE appears to function as a type IIA activator, which is unable to recruit RNAPII and assemble the PIC but can act synergistically with type I activators to stimulate transcriptional elongation.

To determine if AIRE affects the movement of RNAPII, we used an established assay for transcriptional elongation, which looks for promoter-proximal short transcripts (ST) and elongated long transcripts (LT) by use of quantitative reverse transcription-PCR (RT-qPCR) approaches (Fig. 1C) (21). Since AIRE behaved identically in 1C6 and HeLa-MAGI cells (Fig.

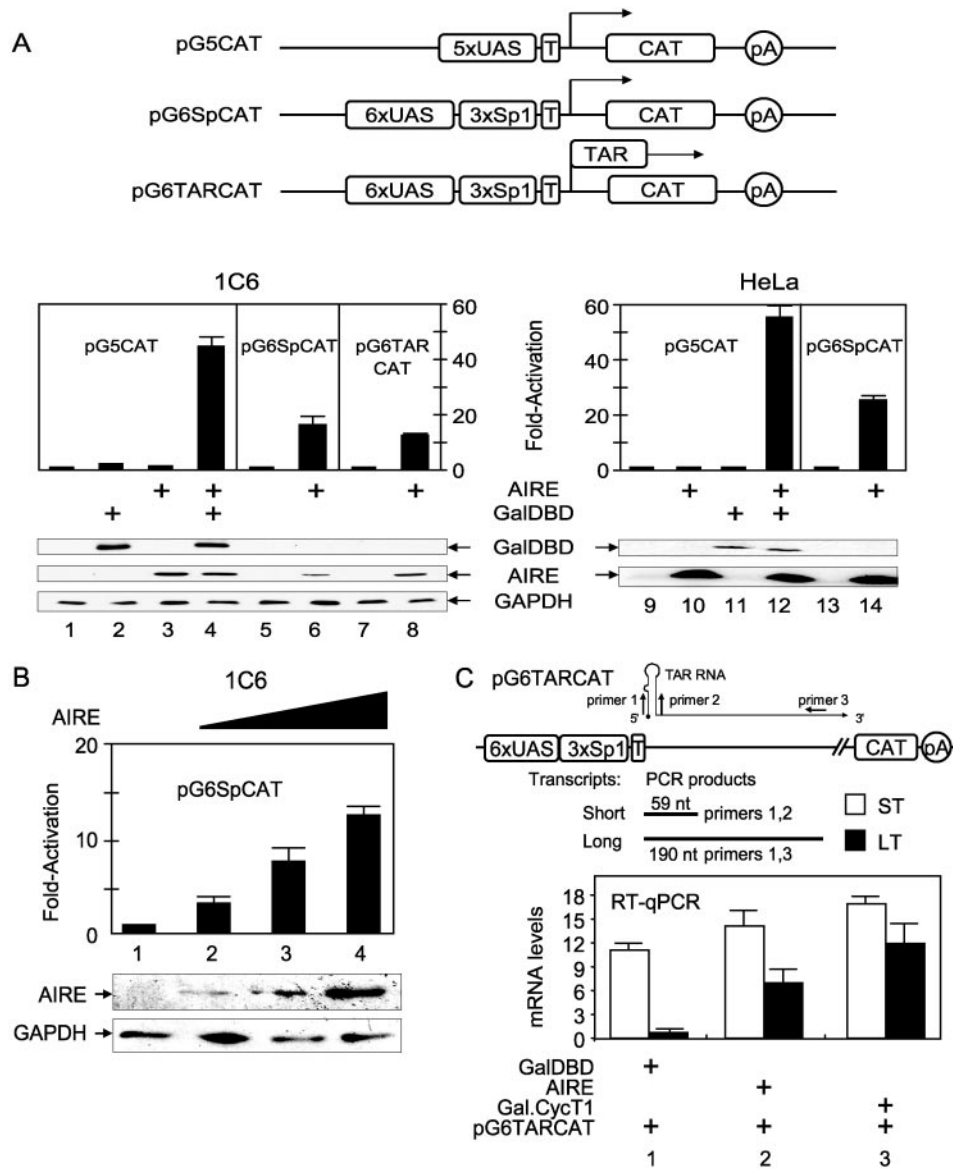


FIG. 1. AIRE cooperates with initiation factors to activate transcription. (A) (Top) Schematic representations of plasmid targets used in CAT assays. pG5CAT contains the CAT gene and five repeats of the GAL4 DNA-binding site (5xUAS) in front of the E1b TATA box (T). pG6SpCAT contains a complete promoter of three Sp1 sites (3xSp1) and the E1b TATA box in addition to six UASs and the CAT gene. pG6TARCAT contains a TAR RNA structure in addition to the elements present in pG6SpCAT. pA represents the polyadenylation signal. (Bottom) AIRE requires the presence of initiation factors to activate transcription in 1C6 and HeLa-MAGI cells. Cells expressed the indicated plasmid targets alone or with AIRE (lanes 3, 4, 6, 8, 10, 12, and 14) and GalDBD (lanes 2, 4, 11, and 12). Expression levels of AIRE and GalDBD, as determined by Western blotting, are presented below the CAT data. Levels of endogenous GAPDH were determined by Western blotting to validate input for each sample. Error bars denote standard errors of the means of three independent experiments. (B) AIRE activates transcription in a dose-dependent manner. 1C6 cells expressed pG6SpCAT and increasing amounts of AIRE (0.1, 0.25, and 0.8 μ g in lanes 2, 3, and 4, respectively). Expression levels of AIRE and GAPDH, as determined by Western blotting, are presented below the CAT data. Error bars denote standard errors of the means of three independent experiments. (C) AIRE induces the elongation of transcription. (Top) Primer combinations for the amplification of primary transcripts. Primers 1 and 2 amplify TAR and thus all transcripts (ST). Primers 1 and 3 amplify only the LT. nt, nucleotides. (Bottom) Total RNA was extracted from HeLa-MAGI cells coexpressing pG6TARCAT and AIRE or GalDBD and was analyzed by RT-qPCR. The Gal.CycT1 chimera was used as the positive control. Data are representative of three independent experiments.

1A), we used the latter cells for our studies. We analyzed RNA samples from cells coexpressing pG6TARCAT with AIRE, the Gal.CycT1 chimera, or GalDBD as positive or negative controls, respectively. The specificity of our primers and the ability to isolate ST or LT were demonstrated previously, where levels

of steady-state mRNA also correlated directly with RNase protection and nuclear run-on data (2). Only ST corresponding to TAR were observed when GalDBD was coexpressed with pG6TARCAT (Fig. 1C, lane 1). In sharp contrast, the Gal.CycT1 fusion protein, which served as the positive control

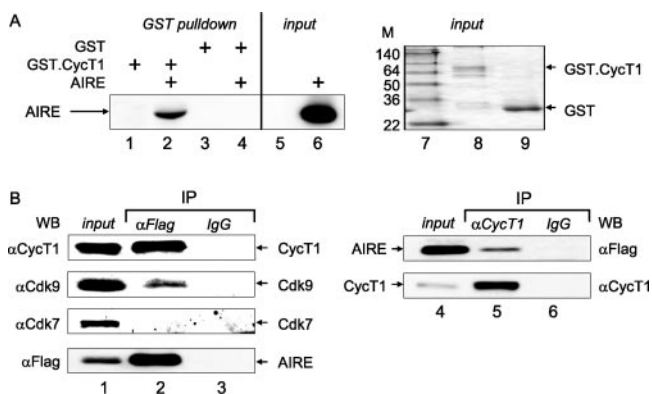


FIG. 2. AIRE binds CycT1 in vitro and in cells. (A) AIRE binds the GST.CycT1 chimera in vitro. Binding reactions were performed between GST and the GST.CycT1 chimera, which were expressed in *Escherichia coli*, and AIRE, which was expressed in HeLa-MAGI cells. (Left) Lanes 1 to 4 contain specific pull-downs, and lane 6 contains 10% of the input AIRE protein. (Right) Input of GST proteins, which were visualized by Coomassie blue staining of SDS-PAGE. Molecular size markers (in kilodaltons) are given in lane M. (B) AIRE interacts with the endogenous CycT1 and Cdk9 proteins in 1C6 cells. The Flag epitope-tagged AIRE protein (lanes 1 to 6) was expressed in 1C6 cells. Total cell lysates were immunoprecipitated (IP) with α Flag M2 agarose beads (lane 2), α CycT1 (lane 5), or mouse IgG (lanes 3 and 6) antibodies and examined for the presence of CycT1, Cdk9, Cdk7, and AIRE by Western blotting (WB) with α CycT1, α Cdk9, α Cdk7, and α Flag antibodies, respectively. Lanes 1 and 4 represent 10% of the input of indicated proteins.

(46), and AIRE promoted the elongation of ST to LT (Fig. 1C, lanes 2 and 3). These results demonstrate that AIRE enables RNAPII to elongate.

AIRE binds P-TEFb in vitro and in cells. As type IIA activators, including Tat, recruit P-TEFb to promote transcriptional elongation, we wanted to test whether AIRE also binds and recruits P-TEFb to the transcriptional machinery. First, we performed GST pull-down assays using the GST.CycT1 chimera or GST alone, which was incubated with lysates of HeLa-MAGI cells expressing AIRE. As shown in Fig. 2A, lane 2, AIRE bound the GST.CycT1 chimera. Since no interaction between GST alone and AIRE was detected, this binding was specific (Fig. 2A, lane 4). The inputs of AIRE, the GST.CycT1 chimera, and GST alone are also presented (Fig. 2A, lanes 6, 8, and 9, respectively).

Next, the endogenous CycT1 and Cdk9 proteins could be co-precipitated with AIRE from cells. We expressed the Flag epitope-tagged AIRE protein in 1C6 cells. Lysates were immunoprecipitated with α Flag M2 or normal mouse immunoglobulin G (IgG) antibodies as the negative control, and immunoprecipitation products were subjected to Western blotting with α CycT1 or α Cdk9 antibody. Whereas no CycT1 or Cdk9 was coimmunoprecipitated by mouse IgG antibodies (Fig. 2B, lane 3), both CycT1 and Cdk9 bound AIRE (Fig. 2B, lane 2). We further confirmed this interaction by immunoprecipitating CycT1 from cell lysates with α CycT1 antibodies and Western blotting for AIRE. Whereas no binding was observed with normal rabbit IgG antibodies (Fig. 2B, lane 6), AIRE bound CycT1 (Fig. 2B, lane 5). In contrast, Cdk7, which is not in the P-TEFb complex, did not bind AIRE (Fig. 2B, lane 2, Cdk7). In Fig. 2B, lanes 1 and 4 present inputs of the indicated proteins.

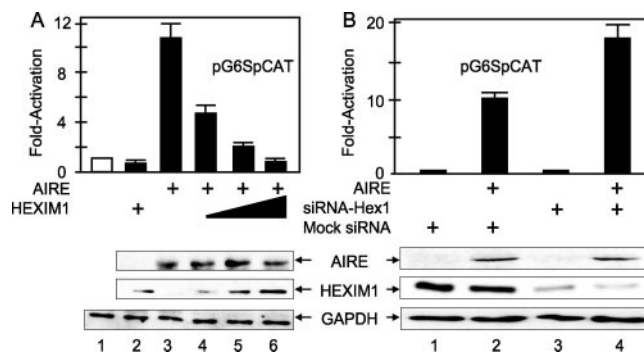


FIG. 3. HEXIM1 inhibits the transcriptional activity of AIRE. (A) Increased levels of HEXIM1 block AIRE-mediated transcription from pG6SpCAT. 1C6 cells coexpressed AIRE and increasing amounts of HEXIM1 (0.125, 0.25, and 0.5 μ g). CAT assays were performed 24 h after transfection. CAT activity of the plasmid target alone is given as 1 (white bar). Black bars represent activation (n -fold) by AIRE (lane 3). In the presence of increasing amounts of HEXIM1, the activity of AIRE decreases (lanes 4 to 6). Below the bar graphs are presented levels of AIRE, HEXIM1, and GAPDH as determined by Western blotting. Error bars denote standard errors of the means of three independent experiments. (B) Depletion of endogenous HEXIM1 protein increases the transcriptional activity of AIRE. 1C6 cells were transfected with mock siRNA (lanes 1 and 2) or siRNA-Hex1 (lanes 3 and 4). The next day, cells were cotransfected with pG6SpCAT and the plasmid encoding MycAIRE (lanes 2 and 4) or the empty plasmid vector as the control (lanes 1 and 3). After an additional 24 h, CAT assays were performed. Amounts of AIRE, endogenous HEXIM1, and GAPDH proteins after siRNA treatment were assessed by immunoblotting and are presented below the bar graph. Error bars denote standard errors of the means of three independent experiments.

To confirm that AIRE and CycT1 are expressed in the same subcellular compartments, we also performed colocalization studies of AIRE and CycT1. We expressed the Myc epitope-tagged AIRE protein in 1C6 cells grown on coverslips and performed double immunostaining with α Myc and α CycT1 antibodies. AIRE and CycT1 were expressed and colocalized in a speckled pattern in the nuclei of 1C6 cells (see Fig. S1 in the supplemental material, middle, colocalization). Although all AIRE colocalized with P-TEFb, since it was expressed at physiological levels, the majority of P-TEFb remained free (see Fig. S1 in the supplemental material, middle). We also observed the colocalization of AIRE with the splicing factor SC35, which localizes to sites of active transcription and was shown previously to colocalize with CycT1 (17 and data not presented). We conclude that AIRE binds and colocalizes with P-TEFb in cells.

HEXIM1 inhibits transcriptional activity of AIRE. A large fraction of P-TEFb is bound by HEXIM1 and 7SK snRNA in the inactive large complex (reviewed in reference 35). Thus, increased levels of HEXIM1 block the activity of P-TEFb and should therefore decrease the transcriptional activity of AIRE. To test this hypothesis, we coexpressed pG6SpCAT, AIRE, and increasing amounts of HEXIM1 in 1C6 cells. When AIRE was coexpressed with pG6SpCAT alone, the CAT activity increased 11-fold (Fig. 3A, lane 3). Importantly, the co-expression of increasing amounts of HEXIM1 (ratios between amounts of plasmids coding for AIRE and HEXIM1 increased from 8:1 to 4:1 and 2:1, respectively) resulted in a dose-dependent decrease of this activity (Fig. 3A, compare lanes 4, 5, and

6). Expression levels of AIRE and HEXIM1 are presented below the bar graph. Also, to ensure that equivalent amounts of lysates were loaded for each sample, levels of GAPDH were determined with α GAPDH antibodies (Fig. 3A, bottom).

Because transcriptional effects depend on the small complex (reviewed in reference 35), the depletion of endogenous HEXIM1 protein from cells increases this pool of active P-TEFb (23). As a result, the effects of AIRE should be increased. To address this hypothesis, levels of HEXIM1 were decreased by siRNA against HEXIM1 (siRNA-Hex1) and effects of AIRE measured in 1C6 cells. In these cells, negative-control scrambled siRNA (mock siRNA) (Fig. 3B, lanes 1 and 2) or specific siRNA-Hex1 (Fig. 3B, lanes 3 and 4) was coexpressed with AIRE and pG6SpCAT (Fig. 3B, lanes 2 and 4) or the empty plasmid vector as the control (Fig. 3B, lanes 1 and 3). The use of siRNA-Hex1 has been validated previously (23). CAT assays were performed after 36 h. When mock siRNA was used, AIRE activity increased 10-fold (Fig. 3B, compare lanes 1 and 2). Critically, when levels of HEXIM1 were reduced extensively by siRNA-Hex1, AIRE activity was increased by 60% in comparison to activity when mock siRNA was used (Fig. 3B, compare lanes 2 and 4). Western blotting with α HEXIM1 antibodies revealed that whereas amounts of HEXIM1 were reduced with siRNA-Hex1 (Fig. 3B, middle blot, lanes 3 and 4), the expression of AIRE and GAPDH remained unaffected (Fig. 3B, top and bottom blots, lanes 3 and 4). These data strengthen the connection between AIRE and P-TEFb for its transcriptional effects.

AIRE activates transcription from the human *Ins* promoter and induces expression of mouse *Ins2* and *Spt1* genes. In mTECs of AIRE^{-/-} mice, the expression of the mouse *Ins2* gene is decreased (4). To extend our findings to this relevant target in cells, we examined whether AIRE can activate transcription from the human *Ins* promoter. To this end, we coexpressed AIRE and this promoter from positions -339 to +50 linked to the firefly luciferase reporter gene (HIP339) (33) in 1C6 cells. *Renilla* luciferase readings were used to normalize the relative firefly luciferase activity of each sample. As presented in Fig. 4A, cells expressing the exogenous AIRE protein increased the luciferase activity 52-fold over background levels (Fig. 4A). Expression levels of AIRE and GAPDH are presented below the bar graph. These data demonstrate that AIRE also activates the transcription of the *Ins* gene.

To determine if AIRE activates the expression of its endogenous target genes in 1C6 cells, we performed semiquantitative RT-PCR analyses with fourfold serial dilutions of cDNA from 1C6 cells, which expressed AIRE or the empty plasmid vector. As presented in Fig. 4B, the two previously reported genes which are dependent on AIRE, those encoding *Ins2* and *Spt1*, were transcribed only in the presence of AIRE (Fig. 4B, *Ins2* and *Spt1*, compare lanes 1 to 4 and lanes 5 to 8). Importantly, the expression of c-reactive protein (CRP), a tissue-specific antigen which was reported previously to be independent of AIRE (4), and the expression of actin were independent of AIRE (Fig. 4B, CRP and actin, compare lanes 1 to 4 and lanes 5 to 8). Although we added TSA in our transient-expression assays, as suggested by others (8), TSA by itself had no effect on the expression of these genes (Fig. 4B, compare AIRE versus the vector control). Moreover, we created the AIRE.1C6 cell line, which expresses AIRE stably, and obtained identical results in the absence of TSA (Fig. 4B, lane 9).

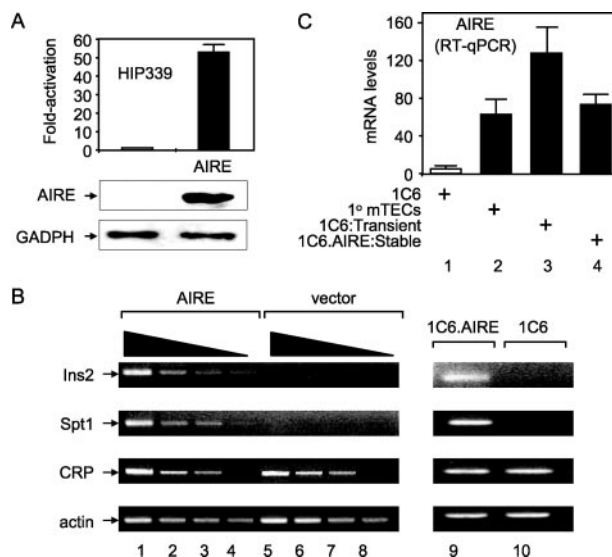


FIG. 4. AIRE activates the transcription of *Ins* and *Spt1* genes in mTECs. (A) AIRE activates transcription from the human *Ins* promoter. 1C6 cells coexpressed AIRE and the plasmid target containing the human *Ins* promoter linked to the firefly luciferase gene, and luciferase activity was measured. *Renilla* luciferase readings were used to normalize the firefly luciferase activity of each sample for all transfections. The expression of AIRE was confirmed by Western blotting and is presented below the bar graph. Error bars denote standard errors of the means of three independent transfections. (B) AIRE activates expression of *Ins2* and *Spt1* genes in mTECs. RNA was extracted from 1C6 cells transiently expressing AIRE (lanes 1 to 4) or the empty plasmid vector (lanes 5 to 8) and treated additionally with 100 mM TSA for 12 h or from AIRE.1C6 cells that stably expressed AIRE (lane 9). Semiquantitative RT-PCR (fourfold serial dilution) analyses of several tissue-specific genes were performed. PCR was carried out using gene-specific primers as indicated. (C) AIRE mRNA levels in mTECs. RNA was isolated from 1C6 cells (lane 1), primary (1°) mTECs (lane 2), and transiently (lane 3) or stably (lane 4) transfected 1C6 cells, and RT-qPCR was performed with primers specific for AIRE. mRNA levels were normalized to actin.

Importantly, mRNA levels of AIRE expression were comparable between AIRE.1C6 and primary mTECs (Fig. 4C, lanes 2, 3, and 4). This finding extends previously published results obtained with AIRE^{-/-} mice (4) and confirms that AIRE regulates the expression of *Ins2* and *Spt1* genes in mTECs.

AIRE recruits P-TEFb to *Ins2* and *Spt1* promoters and enables RNAPII to elongate. To determine if AIRE recruits P-TEFb to promoters of AIRE-responsive genes, we performed ChIP followed by quantitative PCR (ChIP/qPCR) assays (51) with 1C6 cells expressing AIRE or the empty plasmid vector. Formaldehyde-cross-linked chromatin extracts were prepared, and these extracts were immunoprecipitated with specific α AIRE, α RNAPII, α CycT1, and α Cdk9 antibodies. Immunoprecipitated DNA was amplified by PCR using primers specific for the promoters and coding regions of two AIRE-responsive genes, *Ins2* and *Spt1* (Fig. 5A and B), and two AIRE-independent genes, mouse major histocompatibility complex (MHC) class II (I-A α) and CD4 (Fig. 5C and D). We chose MHC class II because it is expressed in mTECs independently of AIRE. In contrast, CD4 is not expressed in mTECs, so no component of the transcriptional machinery

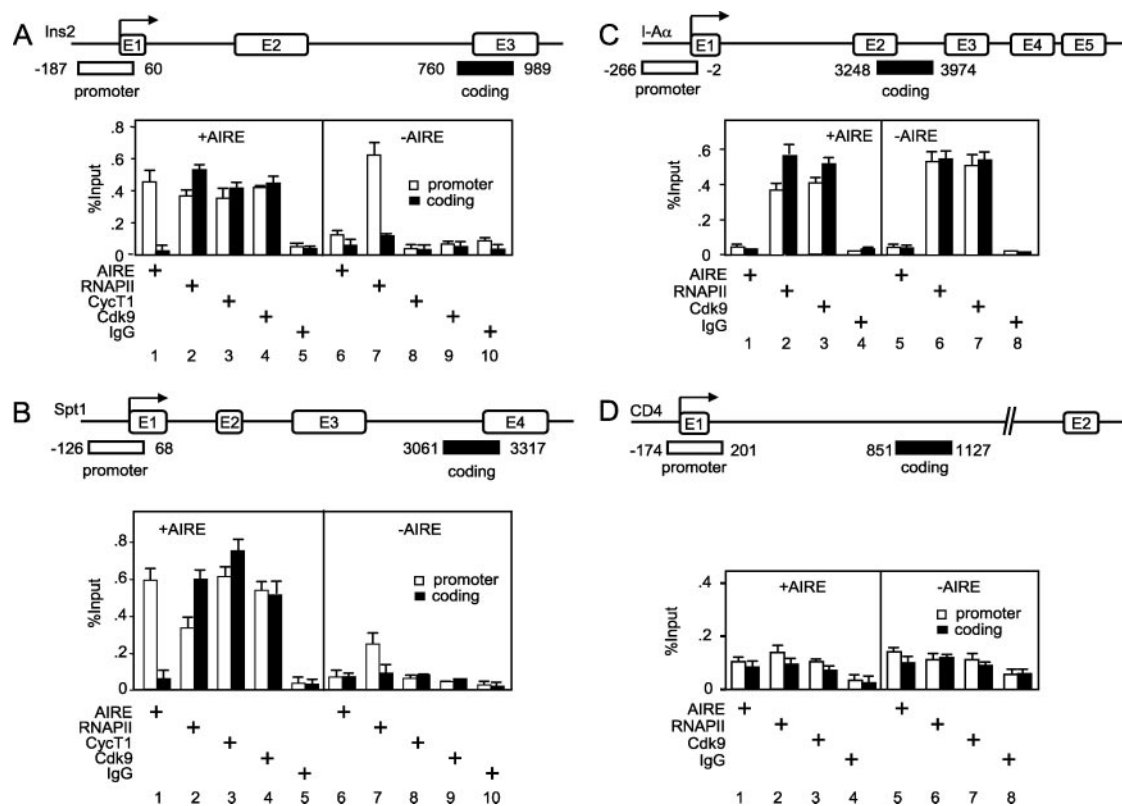


FIG. 5. AIRE recruits P-TEFb to *Ins2* and *Spt1* promoters and stimulates transcriptional elongation by RNAPII. 1C6 (–AIRE) and 1C6.AIRE (+AIRE) cells were analyzed. Formaldehyde-fixed and sonicated chromatin extracts were immunoprecipitated with the indicated antibodies. ChIP/qPCR was performed with the indicated primers to determine the amounts of DNA associated with immunoprecipitated proteins on promoters or coding sequences. The positions of primers are indicated in the diagrams above the graphs. We looked for the presence of AIRE, RNAPII, and subunits of P-TEFb on AIRE-responsive genes (A and B) and AIRE-nonresponsive genes (C and D). ChIP/qPCR with rabbit IgG antibodies was used as the negative control for specificity. All values are expressed relative to the control input DNA (% input) and represent experiments performed in triplicate, with errors indicated.

should be present on its promoter. Data were normalized to input DNA (Fig. 5).

First, we looked for the presence of AIRE and RNAPII on the indicated chromatin regions of the *Ins2* gene. Indeed, AIRE was recruited to the *Ins2* promoter and was absent from its coding region (Fig. 5A, compare bars in lanes 1 and 6). In sharp contrast, RNAPII was already engaged on the *Ins2* promoter whether or not AIRE was expressed (Fig. 5A, compare white bars in lanes 2 and 7). Although amounts of RNAPII on the *Ins2* promoter were comparable, RNAPII was present on the *Ins2* coding region only in the presence of AIRE (Fig. 5A, compare black bars in lanes 2 and 7). Thus, the presence of AIRE coincides with the elongation of RNAPII on this gene. Importantly, the same results were obtained when we analyzed the *Spt1* locus. Indeed, AIRE was present on the *Spt1* promoter (Fig. 5B, compare white bars in lanes 1 and 6) and RNAPII was present on the *Spt1* coding region only in the presence of AIRE (Fig. 5B, compare black bars in lanes 2 and 7). These data correlate the presence of AIRE with the elongation of RNAPII on two AIRE-responsive genes in cells.

Next, we wanted to determine if the elongation of RNAPII was due to the recruitment of P-TEFb, so we looked for the presence of components of P-TEFb on the indicated chromatin regions of the *Ins2* gene. We found that CycT1 and Cdk9

subunits of P-TEFb were found on the *Ins2* promoter (Fig. 5A, compare white bars in lanes 3, 4, 8, and 9) and on the coding region (Fig. 5A, compare black bars in lanes 3, 4, 8, and 9) only in the presence of AIRE. Identical results were observed for the *Spt1* gene (Fig. 5B, compare bars in lanes 3, 4, 8, and 9). Importantly, in the case of the *I-Aα* gene, whose expression is independent of AIRE but dependent on CIITA (reviewed in reference 41), RNAPII was present on the promoter and on the coding region whether or not AIRE was expressed (Fig. 5C, compare bars in lanes 2 and 6). It is known that CIITA also recruits P-TEFb to MHC class II promoters (20, 23). We observed that Cdk9 was also present on the *I-Aα* promoter and coding region independently of AIRE (Fig. 5C, compare bars in lanes 3 and 7). As an additional control, we analyzed the *CD4* locus. Since this gene is not expressed in mTECs, neither RNAPII nor Cdk9 was present on the *CD4* promoter or coding regions in 1C6 cells (Fig. 5D, compare bars in lanes 2, 3, 4, 6, 7, and 8). We conclude that the presence of AIRE correlates with the recruitment of P-TEFb and the elongation of RNAPII on two AIRE-responsive genes in cells.

AIRE-responsive genes are not expressed in the thymuses of *CycT1*^{-/-} mice. Next, we wanted to demonstrate that P-TEFb plays an important role in the transcription of AIRE-responsive genes in the organism. To this end, we generated mice with

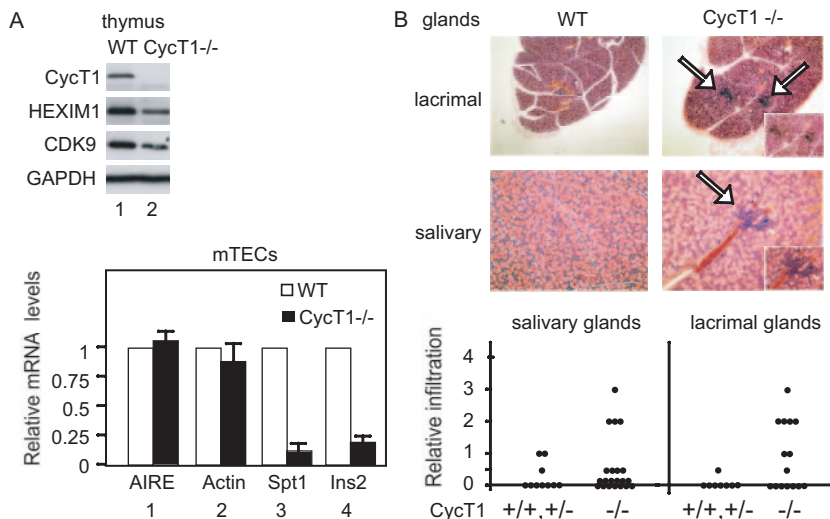


FIG. 6. CycT1^{-/-} mice do not express AIRE-responsive genes in the thymus and display lymphocytic infiltration of lacrimal and salivary glands. (A) Absent expression of CycT1 in the thymus (see Fig. S3 in the supplemental material) parallels the lack of Spt1 and Ins2 transcripts in CycT1^{-/-} mice. We assessed levels of CycT1, HEXIM1, Cdk9, and GAPDH in the thymuses from WT or CycT1^{-/-} mice by Western blotting (top). Next, primary mTECs were isolated from the thymuses of WT or CycT1^{-/-} mice, followed by isolation of total RNA and analyses by RT-qPCR with primers specific for AIRE, actin, Spt1, and Ins2 transcripts (bottom, 1 to 4). WT and CycT1^{-/-} denote parental CycT1^{+/+} and genetically inactivated CycT1^{-/-} mice, respectively. Amounts of RNA are expressed relative to those in WT mTECs, with standard errors from three independent measurements. (B) Lack of CycT1 in the mouse results in lymphocytic infiltration of lacrimal and salivary glands. Hematoxylin and eosin staining of formalin-fixed sections of lacrimal and salivary glands from 5- to 7-month-old WT and CycT1^{-/-} mice is presented. Arrows point to lymphocytic infiltrates in these organs. Photographs were obtained at $\times 40$ and $\times 100$ (insets) magnifications. Below histological sections are presented relative infiltrations of salivary and lacrimal glands of up to 10 CycT1^{+/+} and CycT1^{+/-} (WT) and 21 CycT1^{-/-} mice. Scoring was performed blindly, as described previously (18).

a severe depletion of CycT1 (see Fig. S2 in the supplemental material) in the thymus (Fig. 6A, top, lane 2) and other organs (see Fig. S3 in the supplemental material) by means of gene trap technology of embryonic stem cells (50). Interestingly, this ablation of CycT1 also resulted in decreased expression of HEXIM1 and Cdk9 (Fig. 6A, top, lane 2). Moreover, whereas levels of AIRE transcripts were not affected, those of Ins2 and Spt1 were decreased greatly in mTECs from CycT1^{-/-} mice (Fig. 6A, bottom, compare bars in lanes 1, 2, 3, and 4).

Since AIRE^{-/-} mice exhibited an autoimmune phenotype (4), which was manifested by lymphocytic infiltrates in many organs, we investigated if the same situation pertains to our CycT1^{-/-} mice. Paraffin sections from eye, lung, stomach, spleen, ovary, and lacrimal and salivary glands were prepared, stained with hematoxylin and eosin dyes, and examined for the presence of lymphocytic infiltrates. Importantly, we detected such infiltration in lacrimal and salivary glands in CycT1^{-/-} but not parental, wild-type (WT) mice (Fig. 6B, top right). Moreover, these infiltrations occurred in fewer than half of our CycT1^{-/-} mice and were relatively mild (Fig. 6B, bottom) (18). In contrast, their WT littermates had little to no infiltration of these organs (Fig. 6B, bottom). We conclude that the inactivation of the CycT1 gene in the mouse has a severe impact on the expression of AIRE-responsive genes in mTECs and leads to lymphocytic infiltration in endocrine organs, which resembles the autoimmune phenotype of AIRE^{-/-} mice.

DISCUSSION

In this study, we found that AIRE acts as a type IIA activator that regulates the elongation phase of transcription. First,

AIRE cooperated with initiation factors, such as Sp1, to elongate stalled transcripts. Second, AIRE bound CycT1 from P-TEFb. Third, the specificity of this interaction was confirmed by the inhibition of AIRE by HEXIM1. As a corollary, the depletion of HEXIM1 by siRNA led to the increased activity of AIRE. Fourth, AIRE activated the transcription of human and mouse Ins genes as well as the Spt1 gene in mTECs. Fifth, AIRE and P-TEFb were colocalized on Ins2 and Spt1 promoters and P-TEFb was found there only in the presence of AIRE, which was required for the elongation of RNAPII on these genes. Finally, the genetic inactivation of CycT1 led to loss of expression of AIRE-responsive genes and infiltration of lacrimal and salivary glands in the mouse. We conclude that by interacting with P-TEFb, AIRE stimulated transcriptional elongation of its target genes in mTECs.

Previously, AIRE was found to activate transcription via heterologous DNA tethering using the Gal.AIRE fusion proteins (14, 37, 38). In our study, we demonstrated that the free AIRE protein also acted synergistically with GalDBD or Sp1 to activate transcription. GalDBD has a weak activation domain (from positions 74 to 147), which can initiate but not elongate primary transcripts in higher eukaryotic cells (27). Sp1 interacts with general transcription and TATA binding protein-associated factors (reviewed in reference 30). This binding leads to the formation of the PIC at the start site of transcription and, in the presence of an activator, such as AIRE, to the elongation of transcription. Thus, AIRE is the first cellular type IIA activator besides the viral Tat protein, both of which promote transcriptional elongation.

In cells and synthesized in vitro, AIRE forms oligomers.

They migrate as a 670-kDa complex, which could contain up to 12 AIRE proteins (14). Monomers of AIRE neither bind DNA in vitro (24, 39) nor activate transcription in cells (14). Of interest, most mutations in patients disrupt this oligomerization of AIRE (14, 32). Moreover, the homogeneously staining region, SAND, and two PHD motifs are necessary for the formation of oligomers as well as the transcriptional activity of AIRE (5, 48). Thus, although discrete functional domains have not been defined, we were able to demonstrate that AIRE binds CycT1 and P-TEFb in vitro and in cells. AIRE and CycT1 also colocalized in cells. Furthermore, this interaction was confirmed functionally by its inhibition with HEXIM1, which is a specific inhibitor of P-TEFb (29). Of interest, both Tat and AIRE, two type IIA activators, proved to be exceedingly sensitive to the inhibition of P-TEFb. Finally, in chromatin, CycT1 and Cdk9 were present on promoters of AIRE-responsive genes only in the presence of AIRE.

We also demonstrated effects of AIRE on two known target genes in mTECs (4). Thus, the introduction of AIRE led to the expression of mouse *Ins2* and *Spt1* genes in 1C6 cells. By ChIP, this effect was on the elongation rather than the initiation of transcription of these genes and depended on the recruitment of P-TEFb. Our ChIP data also demonstrated that AIRE interacts with *cis*-acting sequences, and future studies will reveal further details of these DNA-protein interactions. Finally, the genetic inactivation of CycT1 led to the loss of expression of AIRE-responsive genes in the thymus and the lymphocytic infiltration of lacrimal and salivary glands. Since hematopoietic cells retained some expression of CycT1, these findings suggest that although central tolerance was compromised, inflammatory processes were preserved. Moreover, since only half of our CycT1^{-/-} mice developed these infiltrates of lacrimal and salivary glands, this finding argues against a global defect in T cells leading to this autoimmune phenotype. Consistent with this notion, our CycT1^{-/-} mice had normal numbers of B and T cells, with an appropriate ratio of CD4⁺ and CD8⁺ cells. These cells also lacked activation markers (data not presented). Thus, a combination of biochemical and genetic data indicate that P-TEFb is an important coactivator of AIRE.

In conclusion, we present a mechanism for the regulation of transcription by AIRE, which suggests that AIRE is a global activator that affects different target genes via the recruitment of P-TEFb. In prokaryotes, the mechanism of antitermination, i.e., the regulation of transcription at the stage of elongation, is well established and known to play a major role (13). However, such regulation in eukaryotic systems has been appreciated only recently. Indeed, RNAPII is engaged on many regulated but silent promoters in organisms from *Drosophila melanogaster* to humans (25). P-TEFb is also required for the transcription of many activated genes transcribed by RNAPII in cells (7). Of note, activators found on enhancers, such as CIITA, NF- κ B, steroid hormone receptors, and c-Myc, all bind and recruit P-TEFb to their transcription units (reviewed in reference 35). An important difference is that unlike these type IIB activators, AIRE cannot initiate transcription and its interactions with DNA appear more promiscuous (24, 39). Thus, it is able to interact with more targets but has a greater requirement for a preassembled PIC. These features are expected to give it greater and lesser flexibilities in pluripotent

and differentiated cells, where chromatin is relatively open and closed, respectively.

Some genes that are regulated by P-TEFb are likely to cluster. Indeed, DNA looping and interactions of distal enhancers and locus control regions with promoters are important for the expression of MHC class II and β -globin genes (12, 42), which are regulated at the level of transcriptional elongation. Moreover, one study found AIRE to be associated with such matrix attachment sites (44). Thus, global chromatin conformations are also likely to play a critical role in the regulation of genes by AIRE (9, 19). Different programs of gene expression would then depend only on the stage of differentiation of mTECs. To this end, it is interesting that populations of mTECs are highly heterogeneous in the thymus (11). They appear to emerge from pluripotent precursors and then differentiate so that individual populations express distinct sets of genes. In this scenario, AIRE can be viewed as a promiscuous activator that preys upon various differentiation profiles of mTECs to elicit central tolerance to as many tissue-restricted proteins as possible. However, further details of these effects of AIRE and P-TEFb in chromatin represent an important area for future study.

ACKNOWLEDGMENTS

We thank members of the Peterlin lab as well as M. Anderson, J. Gardner, and J. DeVoss for helpful discussions and critical reading of the manuscript. We thank M. German, M. Kasai, J. Pitkänen, and P. Peterson for reagents.

This work was supported by a grant from the Nora Eccles Treadwell Foundation. I. Oven was partially supported by the Slovenian Research Agency, Republic of Slovenia.

REFERENCES

1. Aasland, R., T. J. Gibson, and A. F. Stewart. 1995. The PHD finger: implications for chromatin-mediated transcriptional regulation. *Trends Biochem. Sci.* **20**:56–59.
2. Adams, M., L. Sharmeen, J. Kimpton, J. Romeo, J. Garcia, B. Peterlin, M. Groudine, and M. Emerman. 1994. Cellular latency in human immunodeficiency virus-infected individuals with high CD4 levels can be detected by the presence of promoter-proximal transcripts. *Proc. Natl. Acad. Sci. USA* **91**:3862–3866.
3. Anderson, M. S., E. S. Venanzi, Z. Chen, S. P. Berzins, C. Benoist, and D. Mathis. 2005. The cellular mechanism of Aire control of T cell tolerance. *Immunity* **23**:227–239.
4. Anderson, M. S., E. S. Venanzi, L. Klein, Z. Chen, S. P. Berzins, S. J. Turley, H. von Boehmer, R. Bronson, A. Dierich, C. Benoist, and D. Mathis. 2002. Projection of an immunological self shadow within the thymus by the aire protein. *Science* **298**:1395–1401.
5. Bjorses, P., M. Pelto-Huikko, J. Kaukonen, J. Aaltonen, L. Peltonen, and I. Ulmanen. 1999. Localization of the APECED protein in distinct nuclear structures. *Hum. Mol. Genet.* **8**:259–266.
6. Blau, J., H. Xiao, S. McCracken, P. O'Hare, J. Greenblatt, and D. Bentley. 1996. Three functional classes of transcriptional activation domain. *Mol. Cell. Biol.* **16**:2044–2055.
7. Chao, S.-H., K. Fujinaga, J. E. Marion, R. Taube, E. A. Sausville, A. M. Senderowicz, B. M. Peterlin, and D. H. Price. 2000. Flavopiridol inhibits P-TEFb and blocks HIV-1 replication. *J. Biol. Chem.* **275**:28345–28348.
8. Chin, R. K., J. C. Lo, O. Kim, S. E. Blink, P. A. Christiansen, P. Peterson, Y. Wang, C. Ware, and Y.-X. Fu. 2003. Lymphotoxin pathway directs thymic Aire expression. *Nat. Immunol.* **4**:1121–1127.
9. Derbinski, J., J. Gabler, B. Brors, S. Tierling, S. Jonnakuty, M. Hergenahn, L. Peltonen, J. Walter, and B. Kyewski. 2005. Promiscuous gene expression in thymic epithelial cells is regulated at multiple levels. *J. Exp. Med.* **202**:33–45.
10. Gibson, T. J., C. Ramu, C. Gemund, and R. Aasland. 1998. The APECED polyglandular autoimmune syndrome protein, AIRE-1, contains the SAND domain and is probably a transcription factor. *Trends Biochem. Sci.* **23**:242–244.
11. Gillard, G. O., and A. G. Farr. 2006. Features of medullary thymic epithelium implicate postnatal development in maintaining epithelial heterogeneity and tissue-restricted antigen expression. *J. Immunol.* **176**:5815–5824.

12. Gomez, J. A., P. Majumder, U. M. Nagarajan, and J. M. Boss. 2005. X box-like sequences in the MHC class II region maintain regulatory function. *J. Immunol.* **175**:1030–1040.
13. Greenblatt, J., J. R. Nodwell, and S. W. Mason. 1993. Transcriptional anti-termination. *Nature* **364**:401–406.
14. Halonen, M., H. Kangas, T. Ruppel, T. Ilmarinen, J. Ollila, M. Kolmer, M. Vihinen, J. Palvimo, J. Saarela, I. Ulmanen, and P. Eskelin. 2004. APECE D-causing mutations in AIRE reveal the functional domains of the protein. *Hum. Mutat.* **23**:245–257.
15. Heery, D. M., E. Kalkhoven, S. Hoare, and M. G. Parker. 1997. A signature motif in transcriptional co-activators mediates binding to nuclear receptors. *Nature* **387**:733–736.
16. Heino, M., P. Peterson, J. Kudoh, K. Nagamine, A. Lagerstedt, V. Ovod, A. Ranki, I. Rantala, M. Nieminen, J. Tuukkanen, H. S. Scott, S. E. Antonarakis, N. Shimizu, and K. Krohn. 1999. Autoimmune regulator is expressed in the cells regulating immune tolerance in thymus medulla. *Biochem. Biophys. Res. Commun.* **257**:821–825.
17. Herrmann, C. H., and M. A. Mancini. 2001. The Cdk9 and cyclin T subunits of TAK/P-TEFb localize to splicing factor-rich nuclear speckle regions. *J. Cell Sci.* **114**:1491–1503.
18. Jiang, W., M. S. Anderson, R. Bronson, D. Mathis, and C. Benoist. 2005. Modifier loci condition autoimmunity provoked by Aire deficiency. *J. Exp. Med.* **202**:805–815.
19. Johnnidis, J. B., E. S. Venanzi, D. J. Taxman, J. P.-Y. Ting, C. O. Benoist, and D. J. Mathis. 2005. Chromosomal clustering of genes controlled by the aire transcription factor. *Proc. Natl. Acad. Sci. USA* **102**:7233–7238.
20. Kanazawa, S., T. Okamoto, and B. M. Peterlin. 2000. Tat competes with CIITA for the binding to P-TEFb and blocks the expression of MHC class II genes in HIV infection. *Immunity* **12**:61–70.
21. Kao, S.-Y., A. F. Calman, P. A. Luciw, and B. M. Peterlin. 1987. Antitermination of transcription within the long terminal repeat of HIV-1 by tat gene product. *Nature* **330**:489–493.
22. Kasai, M., K. Hirokawa, K. Kajino, K. Ogasawara, M. Tatsumi, E. Hermel, J. J. Monaco, and T. Mizuochi. 1996. Difference in antigen presentation pathways between cortical and medullary thymic epithelial cells. *Eur. J. Immunol.* **26**:2101–2107.
23. Kohoutek, J., D. Blazek, and B. M. Peterlin. 2006. Hexim1 sequesters positive transcription elongation factor b from the class II transactivator on MHC class II promoters. *Proc. Natl. Acad. Sci. USA* **103**:17349–17354.
24. Kumar, P. G., M. Laloraya, C.-Y. Wang, Q.-G. Ruan, A. Davoodi-Semiromi, K.-J. Kao, and J.-X. She. 2001. The autoimmune regulator (AIRE) is a DNA-binding protein. *J. Biol. Chem.* **276**:41357–41364.
25. Lis, J. 1998. Promoter-associated pausing in promoter architecture and postinitiation transcriptional regulation. *Cold Spring Harbor Symp. Quant. Biol.* **63**:347–356.
26. Liston, A., S. Lesage, J. Wilson, L. Peltonen, and C. C. Goodnow. 2003. Aire regulates negative selection of organ-specific T cells. *Nat. Immunol.* **4**:350–354.
27. Ma, J., and M. Ptashne. 1987. Deletion analysis of GAL4 defines two transcriptional activating segments. *Cell* **48**:847–853.
28. Mathis, D., and C. Benoist. 2004. Back to central tolerance. *Immunity* **20**:509–516.
29. Michels, A. A., A. Fraldi, Q. Li, T. E. Adamson, F. Bonnet, V. T. Nguyen, S. C. Sedore, J. P. Price, D. H. Price, L. Lania, and O. Bensaude. 2004. Binding of the 7SK snRNA turns the HEXIM1 protein into a P-TEFb (CDK9/cyclin T) inhibitor. *EMBO J.* **23**:2608–2619.
30. Naar, A. M., B. D. Lemon, and R. Tjian. 2001. Transcriptional coactivator complexes. *Annu. Rev. Biochem.* **70**:475–501.
31. Nagamine, K., P. Peterson, H. S. Scott, J. Kudoh, S. Minoshima, M. Heino, K. J. Krohn, M. D. Lalioti, P. E. Mullis, S. E. Antonarakis, K. Kawasaki, S. Asakawa, F. Ito, and N. Shimizu. 1997. Positional cloning of the APECED gene. *Nat. Genet.* **17**:393–398.
32. Notarangelo, L. D., C. Mazza, C. Forino, E. Mazzolari, and F. Buzi. 2004. AIRE and immunological tolerance: insights from the study of autoimmune polyendocrinopathy candidiasis and ectodermal dystrophy. *Curr. Opin. Allergy Clin. Immunol.* **4**:491–496.
33. Ohneda, K., H. Ee, and M. German. 2000. Regulation of insulin gene transcription. *Semin. Cell Dev. Biol.* **11**:227–233.
34. Ouchida, R., M. Kusuhara, N. Shimizu, T. Hisada, Y. Makino, C. Morimoto, H. Handa, F. Ohsuzu, and H. Tanaka. 2003. Suppression of NF-kappaB-dependent gene expression by a hexamethylene bisacetamide-inducible protein HEXIM1 in human vascular smooth muscle cells. *Genes Cells* **8**:95–107.
35. Peterlin, B. M., and D. H. Price. 2006. Controlling the elongation phase of transcription with P-TEFb. *Mol. Cell* **23**:297–305.
36. Peterson, P., J. Pitkanen, N. Sillanpaa, and K. Krohn. 2004. Autoimmune polyendocrinopathy candidiasis ectodermal dystrophy (APECED): a model disease to study molecular aspects of endocrine autoimmunity. *Clin. Exp. Immunol.* **135**:348–357.
37. Pitkanen, J., V. Doucas, T. Sternsdorf, T. Nakajima, S. Aratani, K. Jensen, H. Will, P. Vahamurto, J. Ollila, M. Vihinen, H. S. Scott, S. E. Antonarakis, J. Kudoh, N. Shimizu, K. Krohn, and P. Peterson. 2000. The autoimmune regulator protein has transcriptional transactivating properties and interacts with the common coactivator CREB-binding protein. *J. Biol. Chem.* **275**:16802–16809.
38. Pitkanen, J., A. Rebane, J. Rowell, A. Murumagi, P. Strobel, K. Moll, M. Saare, J. Heikkila, V. Doucas, A. Marx, and P. Peterson. 2005. Cooperative activation of transcription by autoimmune regulator AIRE and CBP. *Biochem. Biophys. Res. Commun.* **333**:944–953.
39. Purohit, S., P. G. Kumar, M. Laloraya, and J. X. She. 2005. Mapping DNA-binding domains of the autoimmune regulator protein. *Biochem. Biophys. Res. Commun.* **327**:939–944.
40. Ramsey, C., O. Winqvist, L. Puhakka, M. Halonen, A. Moro, O. Kampe, P. Eskelin, M. Pelto-Huikko, and L. Peltonen. 2002. Aire deficient mice develop multiple features of APECED phenotype and show altered immune response. *Hum. Mol. Genet.* **11**:397–409.
41. Reith, W., and B. Mach. 2001. The bare lymphocyte syndrome and the regulation of MHC expression. *Annu. Rev. Immunol.* **19**:331–373.
42. Sawado, T., J. Halow, M. A. Bender, and M. Groudine. 2003. The beta-globin locus control region (LCR) functions primarily by enhancing the transition from transcription initiation to elongation. *Genes Dev.* **17**:1009–1018.
43. Southgate, C. D., and M. R. Green. 1991. The HIV-1 Tat protein activates transcription from an upstream DNA-binding site: implications for Tat function. *Genes Dev.* **5**:2496–2507.
44. Tao, Y., R. Kupfer, B. J. Stewart, C. Williams-Skipp, C. K. Crowell, D. D. Patel, S. Sain, and R. I. Scheinman. 2006. AIRE recruits multiple transcriptional components to specific genomic regions through tethering to nuclear matrix. *Mol. Immunol.* **43**:335–345.
45. Taube, R., K. Fujinaga, J. Wimmer, M. Barboric, and B. M. Peterlin. 1999. Tat transactivation: a model for the regulation of eukaryotic transcriptional elongation. *Virology* **264**:245–253.
46. Taube, R., X. Lin, D. Irwin, K. Fujinaga, and B. M. Peterlin. 2002. Interaction between P-TEFb and the C-terminal domain of RNA polymerase II activates transcriptional elongation from sites upstream or downstream of target genes. *Mol. Cell. Biol.* **22**:321–331.
47. Uchida, D., S. Hatakeyama, A. Matsushima, H. Han, S. Ishido, H. Hotta, J. Kudoh, N. Shimizu, V. Doucas, K. I. Nakayama, N. Kuroda, and M. Matsumoto. 2004. AIRE functions as an E3 ubiquitin ligase. *J. Exp. Med.* **199**:167–172.
48. Villasenor, J., C. Benoist, and D. Mathis. 2005. AIRE and APECED: molecular insights into an autoimmune disease. *Immunol. Rev.* **204**:156–164.
49. Vodicka, M. A., W. C. Goh, L. I. Wu, M. E. Rogel, S. R. Bartz, V. L. Schweickart, C. J. Raport, and M. Emerman. 1997. Indicator cell lines for detection of primary strains of human and simian immunodeficiency viruses. *Virology* **233**:193–198.
50. Wurst, W., J. Rossant, V. Prideaux, M. Kownacka, A. Joyner, D. P. Hill, F. Guillemot, S. Gasca, D. Cado, A. Auerbach, et al. 1995. A large-scale gene-trap screen for insertional mutations in developmentally regulated genes in mice. *Genetics* **139**:889–899.
51. Zhu, P., S. H. Baek, E. M. Bourk, K. A. Ohgi, I. Garcia-Bassets, H. Sanjo, S. Akira, P. F. Kotol, C. K. Glass, M. G. Rosenfeld, and D. W. Rose. 2006. Macrophage/cancer cell interactions mediate hormone resistance by a nuclear receptor derepression pathway. *Cell* **124**:615–629.

APPENDIX 11

NOVÁKOVÁ, Monika, Marek HAMPL, Dávid VRÁBEL, Jan PROCHÁZKA, Silvia PETREZSELYOVÁ, Michaela PROCHÁZKOVÁ, Radislav SEDLÁČEK, Michaela KAVKOVÁ, Tomáš ZIKMUND, Jozef KAISER, Hsien-Chia JUAN, Ming-Ji FANN, Marcela BUCHTOVÁ and **Jiří KOHOUTEK**. Mouse Model of Congenital Heart Defects, Dysmorphic Facial Features and Intellectual Developmental Disorders as a Result of Non-functional CDK13. *Frontiers in Cell and Developmental Biology*. 2019, 7, 155.



Mouse Model of Congenital Heart Defects, Dysmorphic Facial Features and Intellectual Developmental Disorders as a Result of Non-functional CDK13

Monika Nováková¹, Marek Hampel^{2,3}, Dávid Vrábel¹, Jan Procházka^{4,5},
Silvia Petrezselyová^{4,5}, Michaela Procházková^{4,5}, Radislav Sedláček^{4,5},
Michaela Kavková⁶, Tomáš Zikmund⁶, Jozef Kaiser⁶, Hsien-Chia Juan⁷, Ming-Ji Fann⁷,
Marcela Buchtová^{2,3*} and Jiří Kohoutek^{1*}

OPEN ACCESS

Edited by:

Eleonora Napoli,
University of California, Davis,
United States

Reviewed by:

Junichi Iwata,
University of Texas Health Science
Center at Houston, United States
Julie Siegenthaler,
University of Colorado Denver,
United States

*Correspondence:

Marcela Buchtová
buchtova@iach.cz
Jiří Kohoutek
kohoutek@vri.cz

Specialty section:

This article was submitted to
Cellular Biochemistry,
a section of the journal
Frontiers in Cell and Developmental
Biology

Received: 13 February 2019

Accepted: 23 July 2019

Published: 07 August 2019

Citation:

Nováková M, Hampel M, Vrábel D,
Procházka J, Petrezselyová S,
Procházková M, Sedláček R,
Kavková M, Zikmund T, Kaiser J,
Juan H-C, Fann M-J, Buchtová M
and Kohoutek J (2019) Mouse Model
of Congenital Heart Defects,
Dysmorphic Facial Features
and Intellectual Developmental
Disorders as a Result
of Non-functional CDK13.
Front. Cell Dev. Biol. 7:155.
doi: 10.3389/fcell.2019.00155

¹ Department of Chemistry and Toxicology, Veterinary Research Institute, Brno, Czechia, ² Laboratory of Molecular Morphogenesis, Institute of Animal Physiology and Genetics, Czech Academy of Sciences, Brno, Czechia, ³ Department of Experimental Biology, Faculty of Science, Masaryk University, Brno, Czechia, ⁴ Laboratory of Transgenic Models of Diseases, Institute of Molecular Genetics, Czech Academy of Sciences, Prague, Czechia, ⁵ Czech Centre for Phenogenomics, Institute of Molecular Genetics, Czech Academy of Sciences, Prague, Czechia, ⁶ Central European Institute of Technology, Brno University of Technology, Brno, Czechia, ⁷ Department of Life Sciences, Institute of Genome Sciences, National Yang-Ming University, Taipei, Taiwan

Congenital heart defects, dysmorphic facial features and intellectual developmental disorders (CHDFIDD) syndrome in humans was recently associated with mutation in *CDK13* gene. In order to assess the loss of function of *Cdk13* during mouse development, we employed gene trap knock-out (KO) allele in *Cdk13* gene. Embryonic lethality of *Cdk13*-deficient animals was observed by the embryonic day (E) 16.5, while live embryos were observed on E15.5. At this stage, improper development of multiple organs has been documented, partly resembling defects observed in patients with mutated *CDK13*. In particular, overall developmental delay, incomplete secondary palate formation with variability in severity among *Cdk13*-deficient animals or complete midline deficiency, kidney failure accompanied by congenital heart defects were detected. Based on further analyses, the lethality at this stage is a result of heart failure most likely due to multiple heart defects followed by insufficient blood circulation resulting in multiple organs dysfunctions. Thus, *Cdk13* KO mice might be a very useful model for further studies focused on delineating signaling circuits and molecular mechanisms underlying CHDFIDD caused by mutation in *CDK13* gene.

Keywords: cyclin-dependent kinase (CDK), cyclin, transcription regulation, development, mouse, cyclin-dependent kinase 13, cyclin K

INTRODUCTION

Recently, *de novo* missense variants in *Cyclin-dependent kinase 13 (CDK13)* gene have been identified as an emerging factor involved in the onset of congenital heart defects (CHD) in humans (Sifrim et al., 2016). Documented CHD cases were characterized by ventral and atrial septal defects accompanied by pulmonary valve abnormalities. CHD patients had syndromic facial gestalt, and two patients had agenesis of the corpus callosum. Additional mutations within the *CDK13* gene were recognized in humans resembling at clinical level many symptoms previously associated

with loss of function of *CDK13* or newly described symptoms, such as autism spectrum disorder, seizures, feeding difficulties and craniofacial dysmorphism including short upslanting palpebral fissures, hypertelorism or telecanthus, medial epicanthic folds, low-set, posteriorly rotated ears and small mouth with thin upper lip vermilion (Hamilton et al., 2018). In addition, genome wide search for *de novo* mutations responsible for developmental disorders in patients in Great Britain and Republic of Ireland led to identification of 14 genes that previously lacked compelling evidence of involvement in developmental disorders, among them the *CDK13* gene (Deciphering Developmental Disorders Study, 2017). However, heart defects do not seem to be the key feature of this disorder since patients with heterozygous constitutional mutation in *CDK13* lacking cardiac anomalies were reported by two groups (Carneiro et al., 2018; Uehara et al., 2018). Spectrum of clinical phenotypes of patients with *CDK13* mutations varies from mild to severe with the ubiquitous intellectual disability and developmental delay (ID/DD) (van den Akker et al., 2018). Based on these observations, congenital heart defects, dysmorphic facial features and intellectual development disorder (CHDFIDD) have been recognized as novel syndrome caused by *de novo* variants of *CDK13* gene (Sifrim et al., 2016; Bostwick et al., 2017; Carneiro et al., 2018; van den Akker et al., 2018).

Human CDK13 protein consists of 1512-amino acids with a conserved kinase domain surrounded by N- and C-terminal arms of undefined function (Kohoutek and Blazek, 2012). In order to be active, CDK13 binds cyclin K (CycK) and forms enzymatically active complex (Ko et al., 2001; Even et al., 2006; Bartkowiak et al., 2010; Blazek et al., 2011; Cheng et al., 2012; Dai et al., 2012; Kohoutek and Blazek, 2012; Liang et al., 2015). CDK13 belongs to the family of transcription-associated cyclin-dependent kinases phosphorylating the carboxyl-terminal domain (CTD) of RNA polymerase II (RNAPII). In particular, the CDK13 phosphorylates serine 2 (Ser2) and to a lesser extent also serine 5 (Ser5) within $Y^1S^2P^3T^4S^5P^6S^7$ heptapeptides within the CTD of RNAPII *in vitro* (Greifenberg et al., 2016). Nevertheless, downregulation of CDK13 in tumor derived cell lines had a very small, if any, effect on level of Ser2 within CTD of RNAPII (Blazek et al., 2011; Greifenberg et al., 2016). In parallel to CDK13, there is CDK12 in mammalian cells able to associate with CycK as well (Blazek et al., 2011; Dai et al., 2012; Liang et al., 2015). Even though CDK13 shares high amino acid similarity with CDK12, both kinases appear to function in mutually exclusive complexes in mammalian cells (Blazek et al., 2011; Kohoutek and Blazek, 2012; Greenleaf, 2018).

In comparison to CDK12, there is a limited number of papers envisioning the likely function of CDK13 in various biological processes. For instance, the CDK13 was proposed to be involved in oncogenesis; yet, its precise function is still under examination (Kim et al., 2012; Pan et al., 2012). Even though factors involved in RNA processing, RNA splicing, polyadenylation and RNA cleavage were demonstrated to bind CDK13 as a result of global protein-protein interactions, truly associating partners of this kinase are still unknown (Davidson et al., 2014; Bartkowiak and Greenleaf, 2015; Liang et al., 2015). In addition to involvement of CDK13 in diverse cellular processes, this protein participates

in regulation of alternative splicing of HIV-1 or influenza virus replication, thus suppressing viral production (Berro et al., 2008; Bakre et al., 2013). In developing mouse embryos and murine cells, CDK13 regulates hematopoiesis, stemness and axonal elongation, suggesting an important function in neuronal development (Pan et al., 2012; Chen et al., 2014).

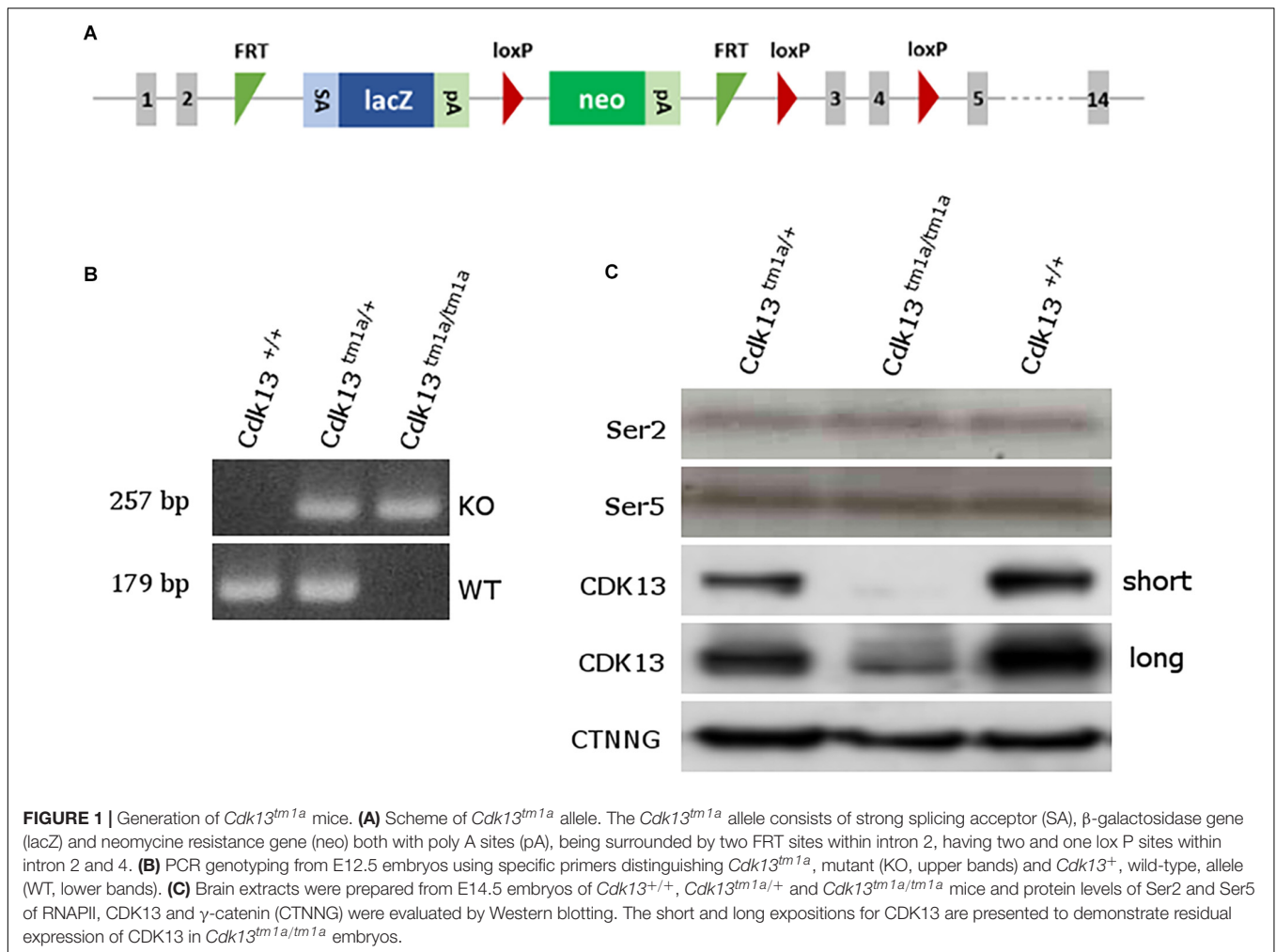
To this date, the impact of complete loss of *Cdk13* function during mammalian development has not been investigated. Therefore, we employed a *Cdk13* knock-out (KO) mouse model to explore a novel role of *Cdk13* during mouse embryonic development. We observed embryonic lethality of *Cdk13* KO animals at the embryonic day 16.5. At this stage, improper development of multiple organs has been observed (heart, brain, kidney, liver, and palate formation) resembling phenotype of human patients with *de novo* missense variants of *CDK13* gene. Therefore, our *Cdk13*-deficient mice may become an important model to study dysregulation of developmental processes occurring in human patients.

RESULTS

Disruption of Cdk13 Gene Leads to Embryonic Lethality in Mice

To examine the role of CDK13 during mouse development, the mice carrying *Cdk13^{tm1a}* allele were generated at the Transgenic and Archiving Module CCP (Institute of Molecular Genetics of the CAS, Prague). The *Cdk13^{tm1a}* allele of *Cdk13* gene enables cessation of transcription due to presence of two strong poly A sites leading to production of the aberrant transcript of *Cdk13* mRNA resulting in non-functional truncated form of CDK13 protein harboring only N-terminal part of this protein, without kinase domain and C-terminal part (**Figure 1A**). Heterozygous *Cdk13^{tm1a/+}* mice were intercrossed to obtain *Cdk13^{tm1a/tm1a}* offspring. Newborn mice were genotyped with specific sets of primers able to distinguish inserted cassette (257 bp PCR product, KO) and wild-type (179 bp PCR product, WT) alleles of *Cdk13* gene (**Figure 1B**). Although the offspring with *Cdk13* WT and heterozygous alleles was born at the expected Mendelian ratio, appeared normal and fertile, *Cdk13^{tm1a/tm1a}* mice were not born at all. This finding suggested that a homozygous deficiency in *Cdk13* gene leads to embryonic lethality in mice. To determine the precise stage, when the embryonic lethality occurs, mouse embryos were collected at various gestation time points (**Table 1**). There were no living *Cdk13^{tm1a/tm1a}* embryos after the embryonic stage 15.5 (E15.5) judging by the lack of their heart beating. Moreover, from E13.5 to E16.5, we observed increased number of absorbed embryos as a reflection of empty decidua (**Table 1**). Based on these finding, we concluded that the deficiency of *Cdk13* causes severe adverse developmental defects and consequent death from E14.5 resulting in total lethality before E16.5.

To confirm the loss of CDK13 protein in *Cdk13^{tm1a/tm1a}* mice, developing brain from WT and *Cdk13^{tm1a/tm1a}* homozygous embryos at E14.5 were collected and western blot analyses were carried out with specific antibodies recognizing CDK13 protein. As expected, the WT form of CDK13 was present in *Cdk13^{+/+}*



and *Cdk13^{tm1a/+}* mice, but surprisingly, corroborated residual expression of CDK13 protein was detected in the embryonic brain of *Cdk13^{tm1a/tm1a}* homozygous embryos (Figure 1C), suggesting that *Cdk13^{tm1a/tm1a}* mice represent a hypomorphic

mutant phenotype. Because the anti-Cdk13 antibody used in western blot recognizes its N-terminal part of CDK13, we were curious if the truncated form of CDK13, as a result of terminated transcription within intron 2, will be expressed in mice bearing the *Cdk13^{tm1a}* allele. Indeed, the truncated form of CDK13 was detected in *Cdk13^{tm1a/+}* and *Cdk13^{tm1a/tm1a}* animals (Supplementary Figure S1). Since CDK13 was demonstrated to phosphorylate CTD of RNAPII *in vitro*, we decided to evaluate phosphorylation status of CTD in hypomorphic mice. Thus, the effect of CDK13 downregulation on Ser2 was evaluated in the animal tissue. Even though expression of CDK13 was significantly lowered in *Cdk13^{tm1a/tm1a}* mice, no effect on either Ser2 or Ser5 phosphorylation within CTD of RNAPII was detected (Figure 1C). The Ser5 phosphorylation was checked in parallel since it is phosphorylated by other CDK kinase, CDK7 in particular (Kohoutek, 2009).

Cdk13 Loss Causes Growth Retardation, Developmental Delay and Its Failure

To examine deficiency of CDK13 protein in *Cdk13^{tm1a/tm1a}* mice, morphology at different embryonic stages compared to the WT animals was examined and various abnormalities were

TABLE 1 | Genotypes of offspring from *Cdk13^{tm1a/+}* intercross.

Stage	<i>Cdk13^{+/+}</i>	<i>Cdk13^{tm1a/+}</i>	<i>Cdk13^{tm1a/tm1a}</i>	Litters	Empty decidua
	(25%)	(50%)	(25%)		
E9.5	4 (21.1%)	12 (63.2%)	3 (15.8%)*	3	2
E10.5	4 (20%)	10 (50%)	6 (30%)*	2	0
E11.5	14 (31.8%)	23 (52.3%)	7 (15.9%)*	6	4
E12.5	31 (30.7%)	52 (51.5%)	18 (17.8%)*,#	15	13
E13.5	6 (16.2%)	18 (48.6%)	13 (35.1%)*	5	5
E14.5	48 (27.6%)	95 (54.6%)	31 (17.8%)*,#	26	9
E15.5	21 (27.5%)	34 (58%)	10 (14.5%)*	11	5
E16.5	8 (25%)	18 (56.3%)	6 (18.7%)*,#	4	0
P0	39 (33.1%)	79 (66.9%)	0	28	

*Growth retardation, #dead embryo.

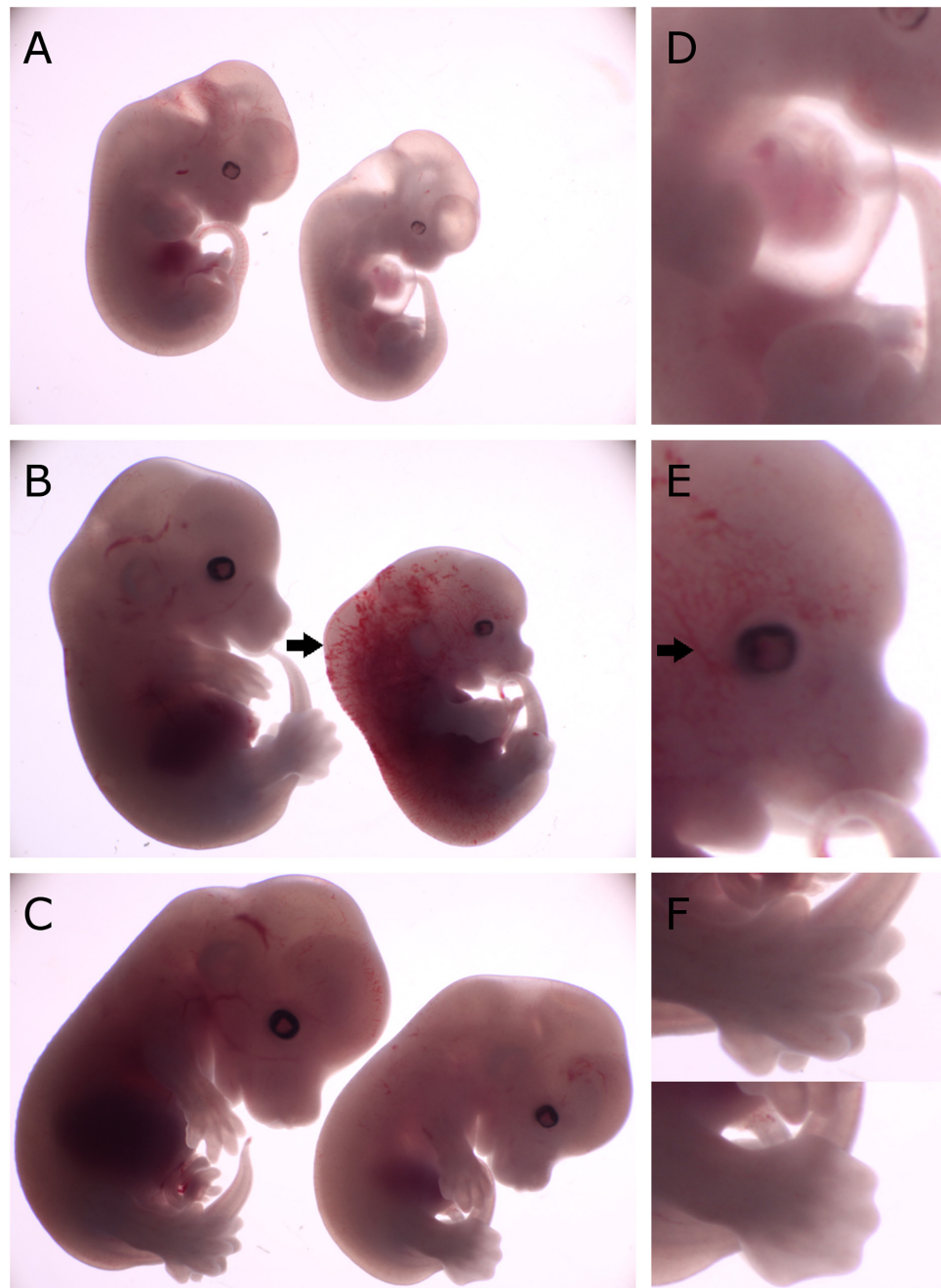


FIGURE 2 | Comparison of gross morphology of wild-type, *Cdk13^{tm1a/+}* and *Cdk13^{tm1a/tm1a}* embryos at various stages. *Cdk13^{tm1a/tm1a}* embryos display significant growth retardation compared to wild-type and heterozygous embryos. **(D–F)** Detailed images of *Cdk13^{tm1a/tm1a}* at relevant developmental stages. **(A)** Heterozygous and *Cdk13^{tm1a/tm1a}* embryos at E12.5. **(D)** Occasional chest wall deformities manifest as hypomorphs. **(B)** Wild-type and *Cdk13^{tm1a/tm1a}* embryos at E13.5. *Cdk13^{tm1a/tm1a}* embryo exhibits nuchal edema (black arrow). **(E)** Hypervascularization of the peripheral vessels capillaries (black arrow). **(C)** Wild-type and *Cdk13^{tm1a/tm1a}* embryos at E14.5. **(F, top)** Wild-type embryo demonstrates deep indentations between the developing fingers of embryos E14.5, although not yet separated. **(F, bottom)** In contrast, *Cdk13^{tm1a/tm1a}* embryo appears to be 1 day delayed in development as evidenced by the shallow indentation of the footpad, which is characteristic of embryos at E13.5.

observed in *Cdk13^{tm1a/tm1a}* embryos at each stage of gestation (**Supplementary Figure S2**). Observed growth retardation of *Cdk13*-deficient mice is presented in detail (**Figure 2**); however, the severity of the developmental delay was variable. On average,

the *Cdk13^{tm1a/tm1a}* embryos appeared to be one embryonic day behind in comparison to their littermate controls as evidenced by the shallow indentation of the footpad, which is characteristic of embryos at E13.5 (**Figure 2F, bottom**).

In contrast, *Cdk13*^{+/+} littermates exhibited deep indentations between the developing toes (not yet separated), what is characteristic of embryos at 14.5 (Figure 2F, top). In addition, the retarded embryo exhibited nuchal edema (black arrow, Figure 2B), which correlates with the presence of cardiovascular phenotypes. Occasionally, the pericardial effusion were detected in developing *Cdk13*^{tm1a/tm1a} embryos, most likely caused by dysfunction of the heart (Figure 2D). Summary of various developmental defects associated with hypomorphic *Cdk13*^{tm1a} allele is presented in Supplementary Table S1.

Cdk13 Is Indispensable for the Development of Several Organs

To narrow down possible cause of embryonic lethality, embryos at E14.5 were contrasted with Lugol's solution to visualize gross morphology of individual soft tissues by microCT (Figure 3). Indeed, several developmental abnormalities were detected within developing embryos. The heart wall of both ventricles in *Cdk13*^{tm1a/tm1a} embryos (Figures 3B,D) appeared thinner in comparison to *Cdk13*^{+/+} littermate controls (Figures 3A,C). In addition, lung, liver and kidney in *Cdk13*^{tm1a/tm1a} embryos were smaller and undeveloped (Figures 3D,F,H) in comparison to *Cdk13*^{+/+} littermates (Figures 3C,E,G). However, detailed 3D reconstruction of liver and kidney (Figures 3I–P) with movable display of E14.5 embryos of *Cdk13*^{tm1a/tm1a} and *Cdk13*^{+/+} genotypes (Supplementary Figures S3A,B) revealed no defect in general gross morphology of these organs.

To uncover possible discrepancies in developmental speed of individual organs, the volume analysis was performed with normalization to total body volume of given embryo. Liver size of *Cdk13*^{tm1a/tm1a} embryos represented only about 46% in comparison to *Cdk13*^{+/+} littermates (Figures 3, 11). Similarly, kidney size of *Cdk13*^{tm1a/tm1a} animals comprised only about 52% in comparison to *Cdk13*^{+/+}. In parallel, histological sections of selected organs were analyzed at stages between E14.5 and E16 (Figure 4). Decelerated development of kidneys was identified in *Cdk13*^{tm1a/tm1a} embryos at E14.5 and E16 (Figures 4D,F) including nephron differentiation as shown by altered proportional representation of individual nephron stages at E14.5 (Figure 4G). Moreover, statistically significant reduction in the number of S-shaped bodies and glomeruli was observed in *Cdk13*^{tm1a/tm1a} embryos (Figure 4H). At lethality stage E16.5, kidney tissue exhibited tissue abrogation with only few, much reduced tubules visible (data not shown), very likely caused by general pre-necrotic changes.

Brains of *Cdk13*^{tm1a/tm1a} embryos appeared developmentally delayed as demonstrated by reduced size as compared to littermate controls. Depicted in Figure 5 are E14.5 controls and *Cdk13*^{tm1a/tm1a} mutant samples from two separate litters. The two litters were developmentally at different stages, pre-palatal fusion in the control embryo depicted (Figures 5A,B) and post-palatal fusion in the control embryo depicted (Figures 5E,F). In order to assess the developmental delay in *Cdk13*^{tm1a/tm1a} embryos the cell proliferation was examined by Ki67 staining, a marker of proliferating cells (Figures 5A'–H', embryos A and C, as well as E and G are littermates, representative pictures of two

embryos are shown to display variability in mutant phenotype). As evident from performed quantification, there was decrease in number of proliferating cells in *Cdk13*^{tm1a/tm1a} embryos in comparison to *Cdk13*^{+/+} littermate controls, but this decrease was not statistically significant (Figure 5I).

The analysis of craniofacial area revealed also defective palatal shelves development in several *Cdk13*^{tm1a/tm1a} embryos resulting in their insufficient horizontal growth and the formation of the cleft palate at E15.5 (Figure 6) in *Cdk13*^{tm1a/tm1a} mouse. Incomplete secondary palate formation exhibited variability in severity among *Cdk13*-deficient animals. Observed penetrance of secondary cleft palate was 2/4 animals at E15.5. In addition, *Cdk13*^{tm1a/tm1a} mouse at E15.5 had smaller number of initiated nasal glands in comparison to the controls (Supplementary Figure S4, compare A–D and B–E).

Embryonic Lethality in *Cdk13*^{tm1a/tm1a} Mice Is Due to Heart Failure

The heart is the one of the first organs to form during mammalian development. During heart development, significant changes in organ morphology and cardiomyocyte differentiation and organization reflect the increasing needs of growing embryos for nutrition and oxygen supply. Any of these developmental steps are critical for further development of whole embryos. Therefore, we analyzed the microscopic structure of the heart and found that the heart wall of *Cdk13*^{tm1a/tm1a} mice embryos was less compact in comparison to the heart wall of *Cdk13*^{+/+} mice (Figures 7C,D). Further, apparent disruption of tissue architecture was detected in *Cdk13*^{tm1a/tm1a} embryos with the reduction of myocardium (Figure 7, compare C, E and G to D, F and H). The heart volume was slightly increased to 103% (organ ratio to total body volume) in *Cdk13*^{tm1a/tm1a} mice compared to *Cdk13*^{+/+} animals. However, the total volume of heart tissue to the organ volume was significantly lower in case of *Cdk13*^{tm1a/tm1a} embryos (62.5%) in comparison to WT littermates (80%) suggestive of the thinner heart wall at E15.5 in *Cdk13*^{tm1a/tm1a} embryos. Percent soft tissue volumes were measured by microCT using Bruker-microCT CT-analyzer, where the object volume representing soft tissues was divided by total VOI volume. The VOI area referring to the heart volume was selected from the dataset manually. Also, decreased expression of myosin was detected in ventricle myocardium of 14.5 hearts (Supplementary Figure S5, compare B and B' to E and E').

Since the heart mass of *Cdk13*^{tm1a/tm1a} E14.5 – E16 embryos is significantly reduced with hypomorphic muscular layers of myocardium compared with *Cdk13*^{+/+} mice (heart/body ratio), we presume that heart developmental defect is the cause of embryonic lethality. In order to evaluate cardiac circulatory physiology, we performed non-invasive ultrasound Doppler imaging to quantitatively assess the hemodynamic function in E14.5 and E15.5 embryos. Out of nine *Cdk13*^{tm1a/tm1a} embryos dissected at E14.5 stage, only one was found dead (Table 2). All the other *Cdk13*^{tm1a/tm1a} embryos at this stage exhibited comparable blood flow velocities and velocity-time integral (VTI) in dorsal aorta (Figures 8A,B). However, this situation changed

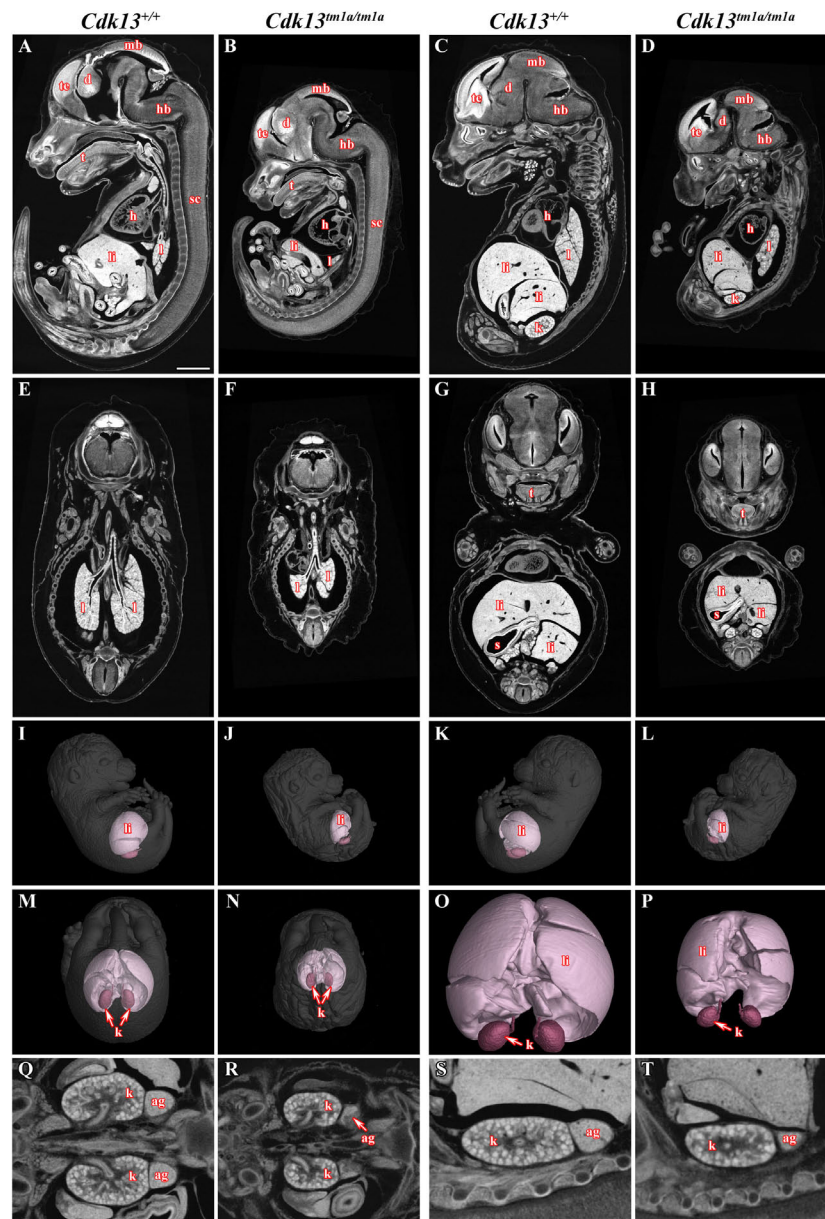
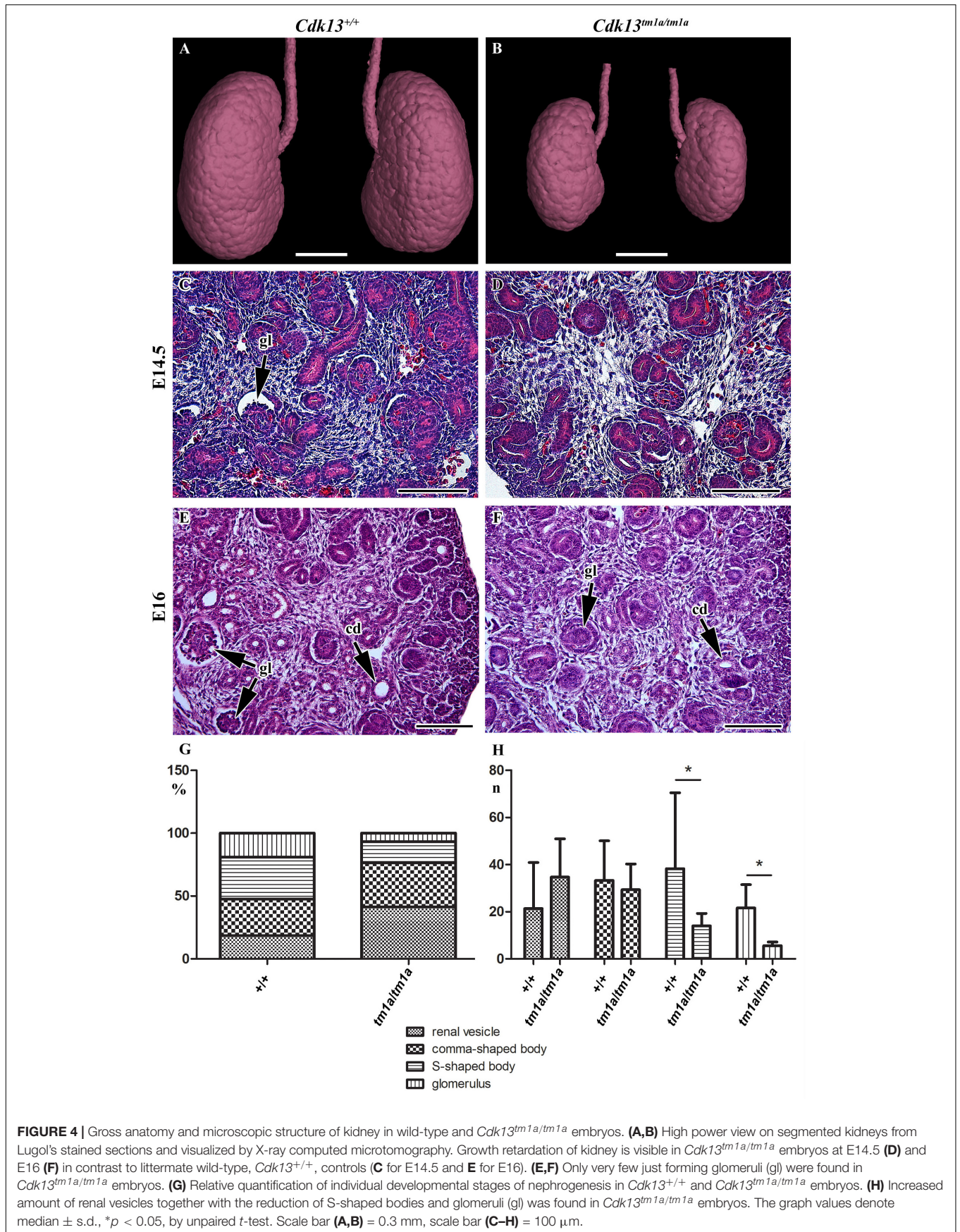


FIGURE 3 | MicroCT analysis of wild-type and *Cdk13^{tm1a/tm1a}* embryos. High-contrast differentiation resolution by X-ray computed microtomography, where Lugol's staining was used to visualize the soft tissues. Sagittal sections through body midline (**A,B**) and more lateral plane at E15.5 (**C,D**). Horizontal sections through lung (**E,F**) and liver (**G,H**). 3D reconstruction of kidney and liver in the right side view of embryo (**I,J**) and left side view (**K,L**) and caudal view (**M,N**) with embryo outlined in gray where segmentation of serial sections was used for the liver and kidney reconstruction. (**O,P**) High power of 3D imaging for liver and kidney. Horizontal view (**Q,R**) and sagittal detailed view (**S,T**) on kidney and suprarenal gland. Abbreviation used for individual organs: ag, adrenal gland; d, diencephalon; h, heart; hb, hindbrain; k, kidney; l, lung; li, liver; mb, midbrain; t, tongue; te, telencephalon; s, stomach; sc, spinal cord. Scale bar = 1 mm.

dramatically at embryonic stage E15.5 (**Figures 8C,D**), where only few *Cdk13^{tm1a/tm1a}* embryos retained normal blood flow parameters (5/16), while the rest of the embryos heart functions declined (standard measurements were not possible due to irregular or spare heart beating 11/16); moreover, an increased portion of embryos were already dead (**Table 2**).

The assessment of cardiac function in developmental interval E14.5 – E15.5 embryos showed dramatic failure

in heart function, probably corresponding to increasing needs of embryos at E15.5 for blood supply in growing organ systems, which is very challenging for the defective heart to achieve. The preserved blood flow in few *Cdk13^{tm1a/tm1a}* embryos was probably due to the observed variability of the embryo size. Our findings suggest that the heart failure appears in most cases during the transition from E14.5 to E15.5.



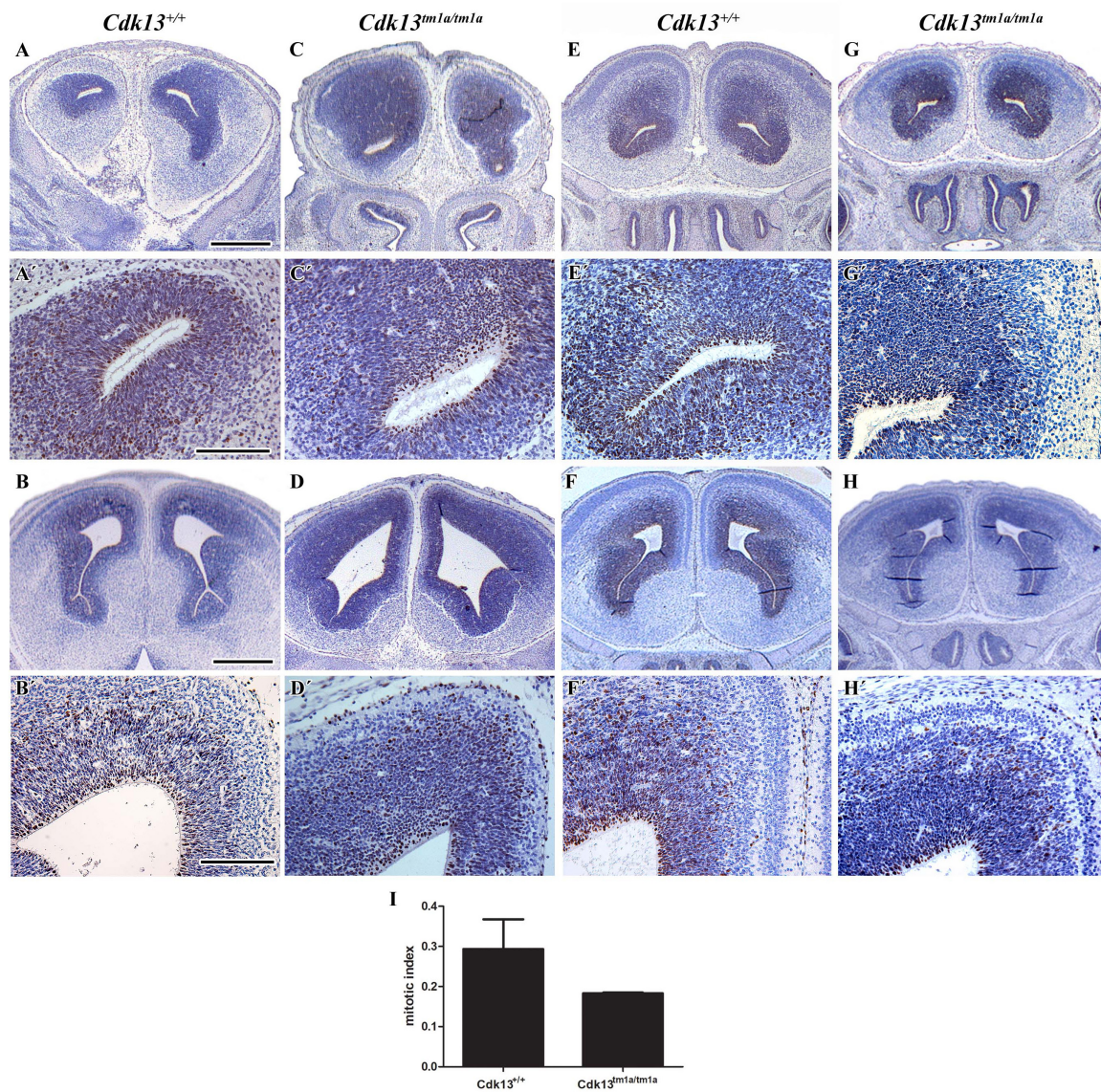


FIGURE 5 | Cell proliferation in brain area in wild-type and *Cdk13*^{tm1a/tm1a} embryos. (A,A',B,B') *Cdk13*^{+/+} and (C,C',D,D') *Cdk13*^{tm1a/tm1a} embryos before palatal shelves fusion. (E,E',F,F') *Cdk13*^{+/+} and (G,G',H,H') *Cdk13*^{tm1a/tm1a} embryos after palatal shelves fusion. Immunohistochemical nuclear labeling of Ki67-positive cells in the frontal head sections in the lower power view (A–H) and in detail (A'–H'). (I) Mitotic index was counted as the ratio between Ki67-positive cells and total amount of prosencephalon cells in three biological triplicates for each group. The graph values denote mean ± s.d, difference is not statistically significant according to unpaired *t*-test (*p*-value: 0.1047). Ki67-positive cells - brown nuclei, Ki67-negative cells - blue nuclei (hematoxylin). Scale bar (A–C) = 1 mm; scale bar (A'–C') = 100 μm.

Cdk13 Is Expressed in Affected Organs in the Prenatal and Also Postnatal Period

Currently, there is limited information about protein expression pattern of CDK13 either in developing or adult organs; therefore, we decided to evaluate expression of CDK13 protein in developing organs. First, the western blot of CDK13 protein was carried out in selected developing organs (Figure 9). As expected, expression of CDK13 was detected in organs with abnormal embryonic development. The highest protein level of CDK13 was detected in the brain, then lung, kidney and heart (Figure 9).

In case of detection of CDK13 in the developing heart, four times concentrated protein lysates had to be used to detect any reproducible signal.

To explore gene expression of *Cdk13* in adult tissues and organs, the particular organs were isolated and the expression of Cdk13 was examined by activity of β-galactosidase (Supplementary Figure S6). *Cdk13* was strongly expressed in the retina of the eye, testes, ovary, uterus, gall bladder (Supplementary Figures S6A,F–I). To a lesser extent, the *Cdk13* was detected in the urinary bladder (Supplementary Figure S6D). Interestingly, rather localized, yet strong expression

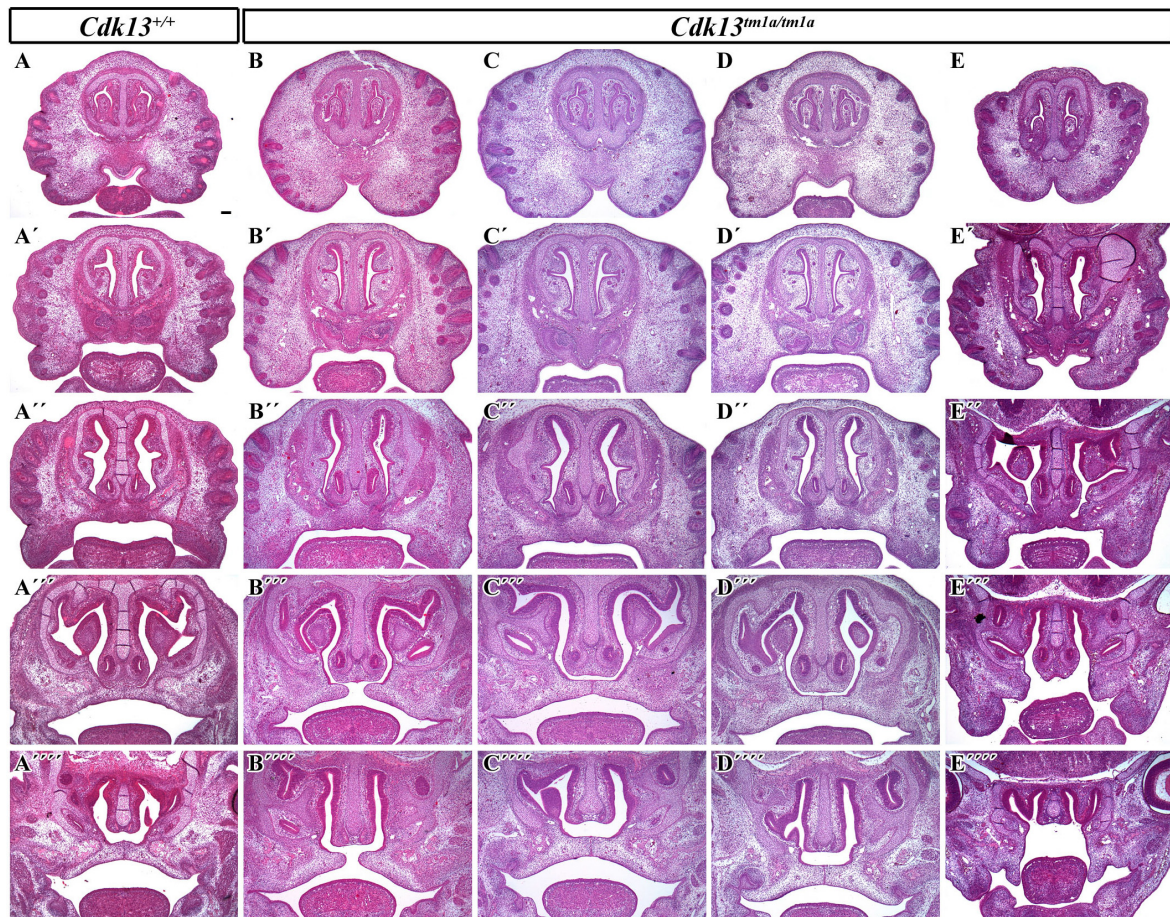


FIGURE 6 | Transversal sections of the head in control *Cdk13*^{+/+} and *Cdk13*^{tm1a/tm1a} embryos at E15.5. Rostro-caudal view in *Cdk13*^{+/+} animal (A) and four *Cdk13*^{tm1a/tm1a} mutant mice to show variability in the secondary palate morphology (B–E). Palatal shelves do not meet each other in the midline (B''', E''') and cleft of secondary palate is visible. Abnormal shape of palatal shelves was observed also caudally with cleft expanding into the soft palate area. (A'–A''', B'–B''', C'–C''', D'–D''', E'–E''') are transversal sections of head in individual embryos in rostrocaudal direction. Scale bar = 100 μm.

within organ structure was observed in renal pelvis in kidney, thyroid gland and heart atrium, with substantial expression in the heart ventricle (Supplementary Figures S6B,C,E).

Cdk13^{tm1d/tm1d} Mice Exhibits More Severe Phenotype and Earlier Lethality

As we observed residual expression of *Cdk13* in analyzed organs of hypomorphic *Cdk13*^{tm1a/tm1a} mice, we decided to cross *Cdk13*^{tm1a} mice with Flp-deleter mice and Cre-deleter (detailed description of the utilized transgenic strains is provided at the Section “Experimental Procedure”) mice to generate *Cdk13*^{tm1d} allele with deleted exons 3 and 4 (Figure 10A). As in case of *Cdk13*^{tm1a} mice, the expression of CDK13 protein was investigated in the *Cdk13*^{tm1d} mice. High expression of CDK13 was detected in the developing brain of WT *Cdk13*^{+/+} embryos (Figure 10B). Greatly downregulated expression of CDK13 was detected in heterozygous *Cdk13*^{tm1d/+} brain with undetectable expression of CDK13 protein in homozygous *Cdk13*^{tm1d/tm1d} brain (Figure 10B). As in the case of *Cdk13*^{tm1a} mice, no

significant reproducible downregulation of Ser2 phosphorylation was observed in *Cdk13*^{tm1d/tm1d} brain extract (Figure 10B). Interestingly, expected Mendelian ratios were reflected in the portion of *Cdk13*^{tm1d/tm1d} mice. High number of empty decidua at E12.5 were detected reflecting increased mortality before this stage (Table 3). Critically, only 19 litters out of 42 contained *Cdk13*^{tm1d/tm1d} embryos suggesting homozygous mice carrying *Cdk13*^{tm1d} alleles exhibited more severe defects in phenotype than *Cdk13*^{tm1a/tm1a} mice, especially in craniofacial area with midline facial cleft (Figure 10C). The prevalence of the midline orofacial deficiency and pericardial effusion was 60.5% in *Cdk13*^{tm1d} homozygous mice at E12.5–E14.5. Out of 94 cases, only two cases of *Cdk13*^{tm1a/tm1a} mice had externally visible orofacial clefting (Supplementary Table S1). The prevalence of the pericardial effusion (PE) in *Cdk13*^{tm1a/tm1a} embryos at E12.5–E14.5 was less than 20% in comparison to high occurrence in *Cdk13*^{tm1d/tm1d} embryos (Supplementary Table S1). No PE or orofacial cleft was recorded in any WT, though 6 embryos from 262 heterozygotes exhibited PE.

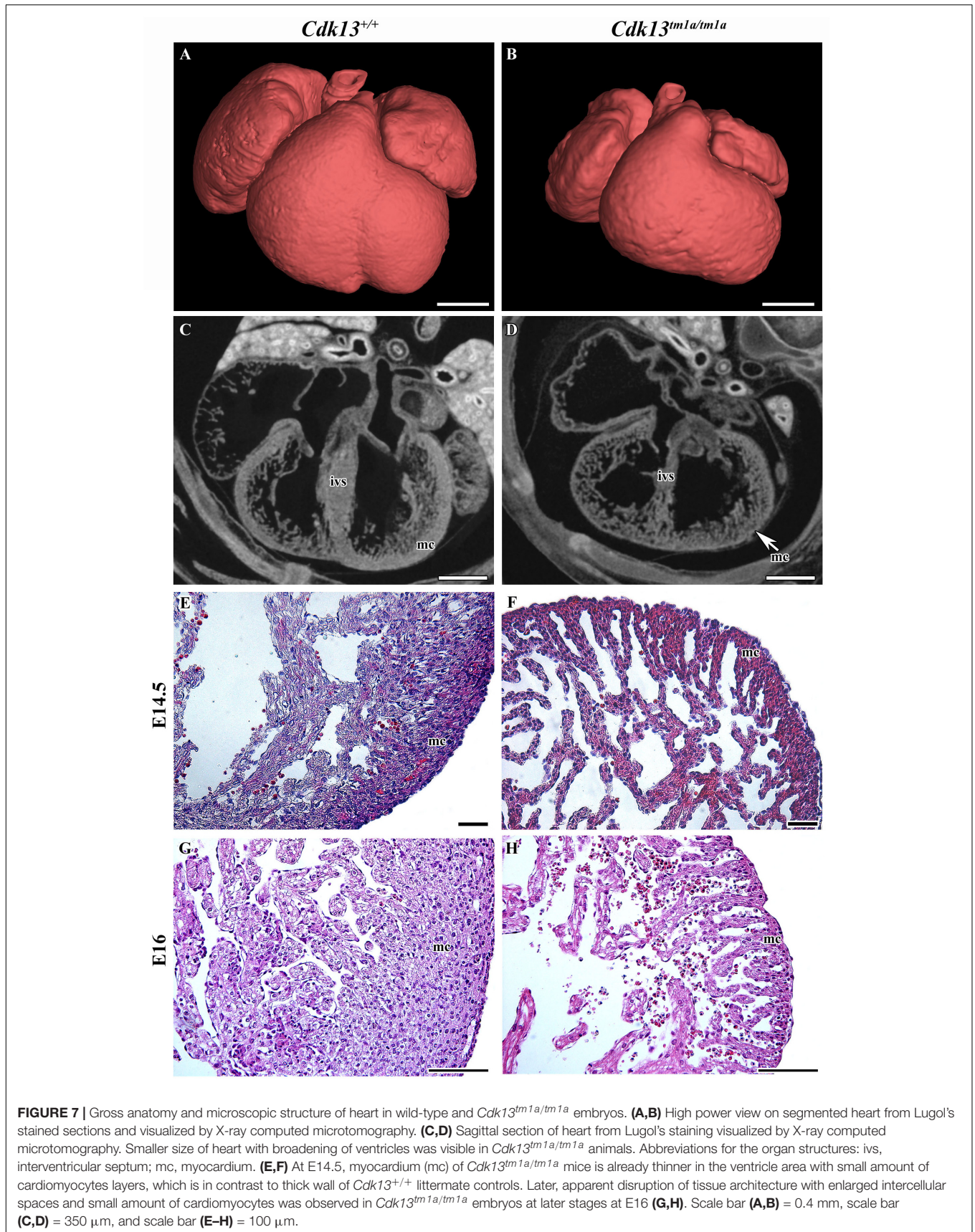


TABLE 2 | Summary of ultrasound scanned embryos at E14.5 and E15.5.

Stage	Number of embryos			Litters	Number of <i>Cdk13^{tm1a/tm1a}</i>	
	<i>Cdk13^{+/+}</i>	<i>Cdk13^{tm1a/+}</i>	<i>Cdk13^{tm1a/tm1a}</i>		Heart beating	Dying/dead
E14.5	11	27	9	6	8	1
E15.5	14	36	17	8	6	11

Comparison of *Cdk13^{tm1a/tm1a}* and *Cdk13^{tm1d/tm1d}* Mice at E13.5

Finally, the phenotype of *Cdk13^{tm1a/tm1a}* mice was compared to *Cdk13^{tm1d/tm1d}* mice (Figure 11 and Supplementary Figures S7, S8). High-contrast differentiation resolution by X-ray computed microtomography was used to assess gross morphology of the *Cdk13^{+/+}*, *Cdk13^{tm1a/tm1a}* and *Cdk13^{tm1d/tm1d}* embryos at E13.5. Both *Cdk13* mutants exhibited smaller body size with severe growth retardation in *Cdk13^{tm1d/tm1d}* animals (Figures 11A–D). Hypoplasia of midfacial structures was observed in *Cdk13^{tm1d/tm1d}* embryos (Figure 11, compare H to G). The hearts were smaller in both *Cdk13^{tm1a/tm1a}* as well as *Cdk13^{tm1d/tm1d}* embryos in comparison to littermate control mice with severe ventricle deficiency detected in *Cdk13^{tm1d/tm1d}* animals (Figure 11, compare J to I and L to K). Generally smaller liver were detected in *Cdk13^{tm1a/tm1a}* and *Cdk13^{tm1d/tm1d}* embryos in comparison to control *Cdk13^{+/+}* mice. Liver in *Cdk13^{tm1d/tm1d}* mice exhibited abrogated liver lobes arrangement (Figure 11, compare P to O and N to M). Kidneys in *Cdk13^{tm1d/tm1d}* mice do not follow right left kidney asymmetry (Figure 11, compare T to S).

DISCUSSION

Our analysis revealed a new function of *Cdk13* in the context of the mouse development and found that this protein is critical for proper development at later stages of embryogenesis. Loss of *Cdk13* affects negatively several organs and tissue structures during mouse development and its inactivation leads to late embryonic lethality.

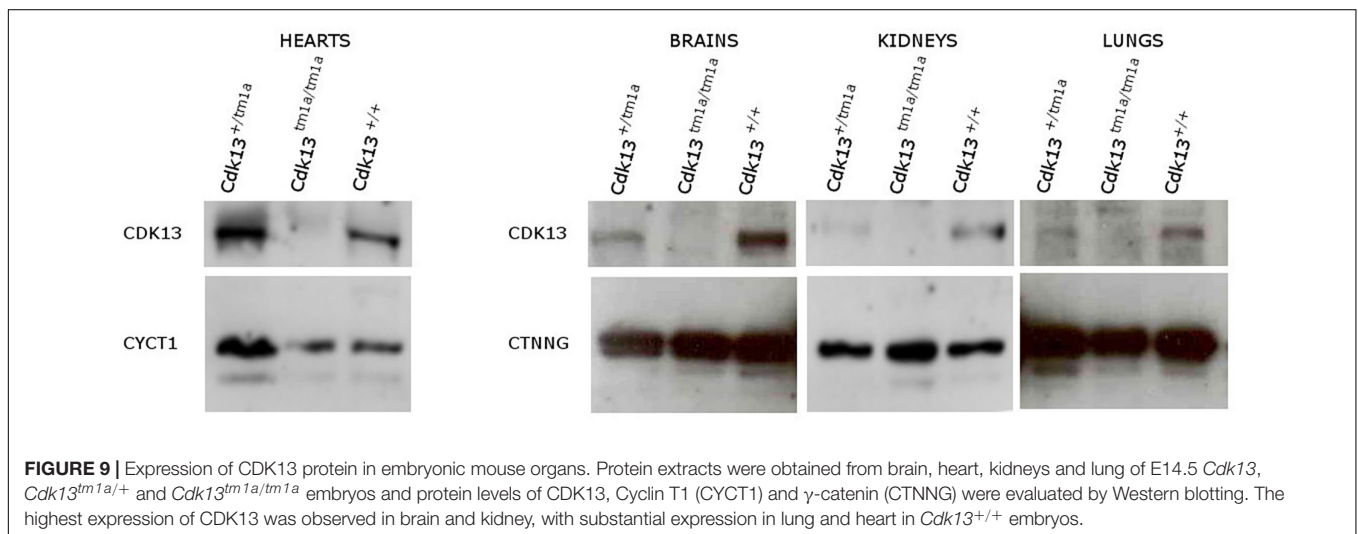
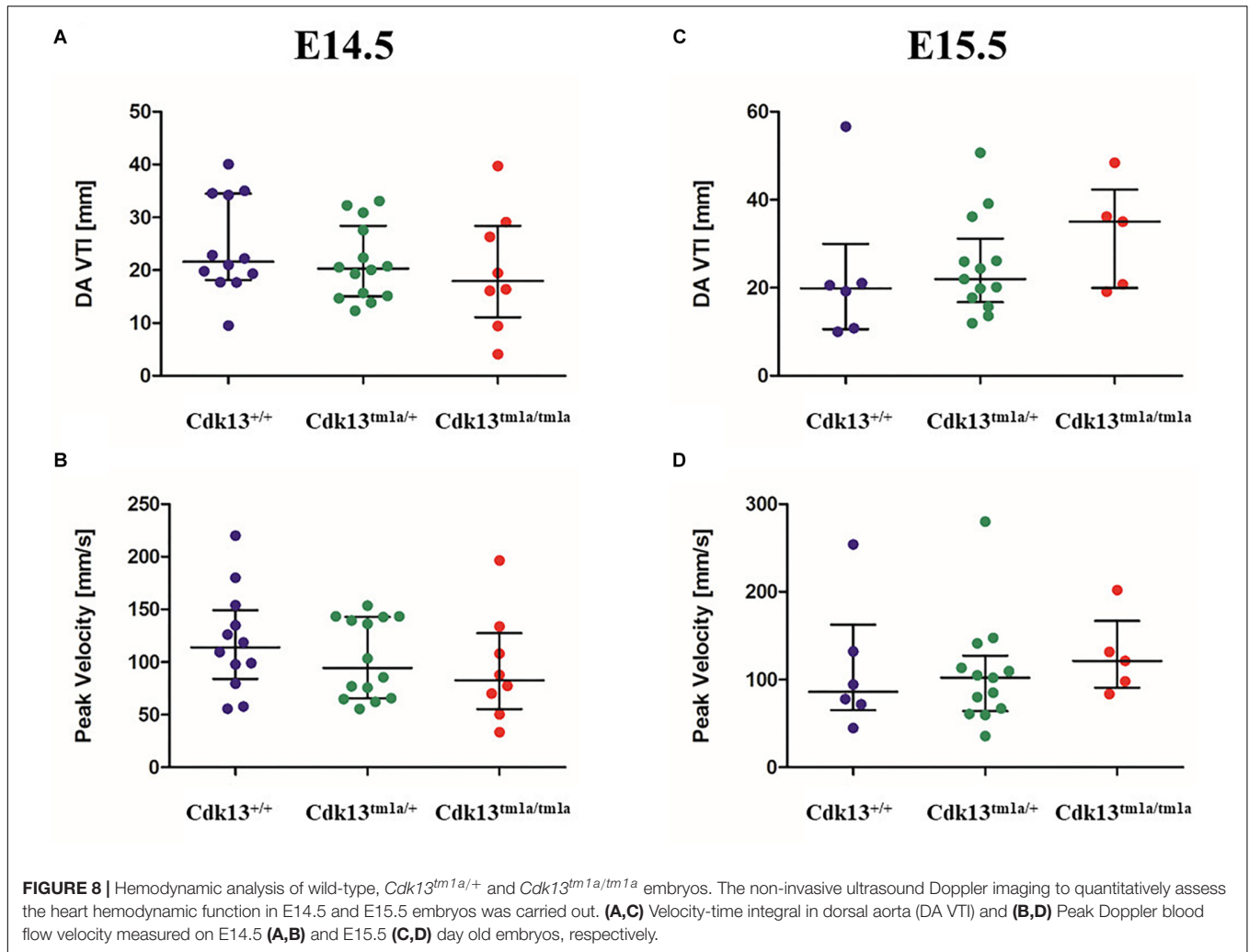
Animals with hypomorphic allele (*Cdk13^{tm1a}*) retained low residual expression of CDK13 and they were lethal by E16.5 most due to heart failure and delayed development of several organs was caused likely due to insufficient supply of oxygen and nutrients. Interestingly, several miRNAs able to target *Cdk13* mRNA for degradation were recently recognized during the acute myocardial infarctions (Wang et al., 2015) supporting the idea of CDK13 as a strategic molecule for optimal heart function. In addition, the expression of CDK13 was detectable not just in the heart, but also in other organs during embryonic development, such as craniofacial area or brain. However, the expression only cannot explain the complexity of phenotype exclusively in tissue autonomous manner or by insufficient nutrients and oxygen distribution. Thus, we assume that the organs with higher expression might be affected either by non-functional CDK13 in cell autonomous manner and/or by underdevelopment of

cardiovascular system and lack of nutrients, mostly by insufficient heart function. Importantly, the affected cardiovascular system is superior to development of other organ systems and can drive systemic developmental phenotype; the example of such phenotype is growth retardation in the whole embryo with no respect to local CDK13 expression levels, which is affecting size of all organs within the embryo body. Therefore, in organs where the expression of CDK13 is under detection limit, we suggest that the phenotype is caused mostly by failure of cardiovascular system development and its systemic influence.

It is also interesting why the *Cdk13^{tm1a}* allele exhibits the hypomorphic mutant phenotype. One possible explanation might be due to the insertion of neomycin selection cassette in non-coding region that has been shown to affect gene expression, both at the DNA and RNA levels (Pham et al., 1996; Meyers et al., 1998; Scacheri et al., 2001). Moreover, *in silico* analyses of post-transcriptional exon shuffling (PTES) events in humans revealed high PTES frequencies in *CDK13* gene enabling the formation of aberrant functional CDK13 transcripts (Al-Balool et al., 2011).

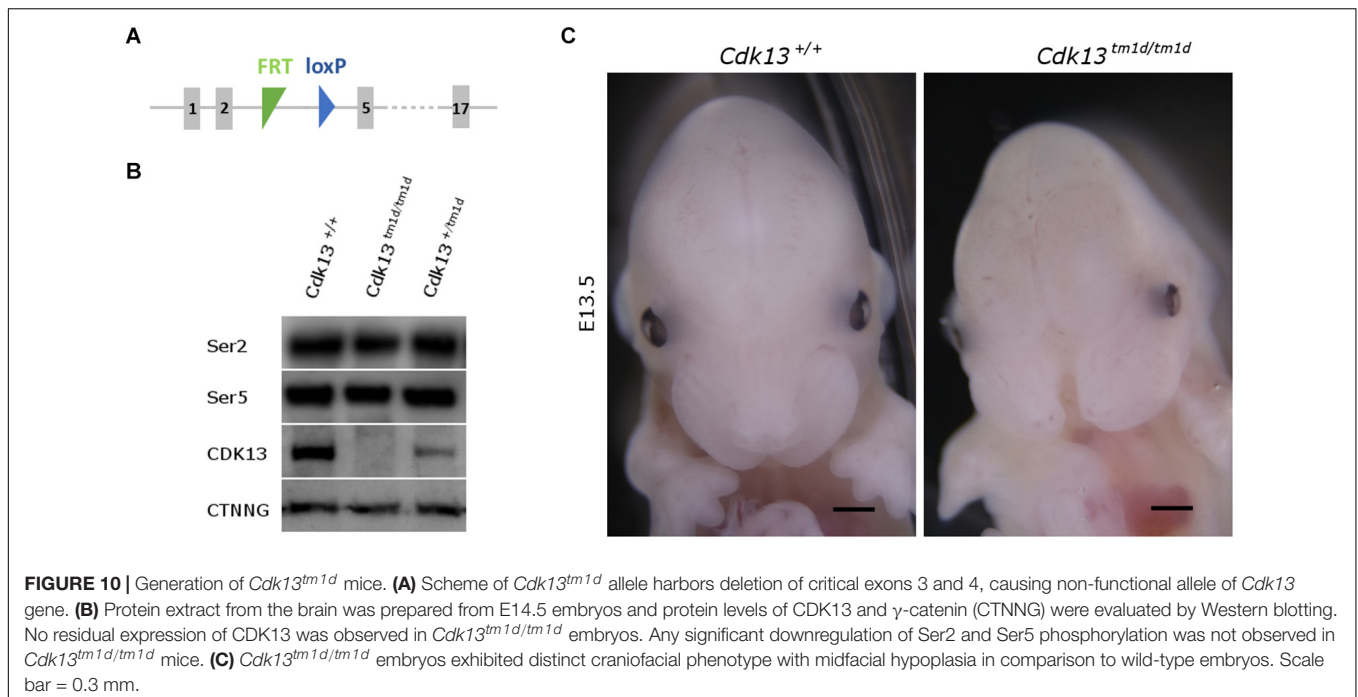
In contrast to our observations, genetic depletion of *Cdk12*, a kinase with high amino acid similarity to *Cdk13*, resulted in early developmental lethality at the blastocyst stage due to deregulated expression of DNA-damage repair genes leading to enhanced genomic instability (Juan et al., 2016). Importantly, KO of *CycK* resembled the same lethal phenotype at the blastocyst stage as *Cdk12* animals (Blazek et al., 2011). Besides clear effect of *CycK* during preimplantation stage, *CycK* is highly expressed in mouse embryonic stem cells and testes in a developmentally regulated manner (Dai et al., 2012). During neonatal spermatogenesis, *CycK* is highly expressed in gonocytes, spermatogonial stem cells and is absent in differentiating spermatogonia, spermatids and spermatozoa (Xiang et al., 2014). Similar expression in testes, ovary and uterus was also documented for CDK13 in our heterozygous mice.

Downregulation of *Cdk13* had also significant impact on brain development. It is known from previous studies that *CycK*, a *Cdk13* binding partner, has been identified in a genome-wide screen as one of the factors involved in the formation of the nervous system in *Drosophila* (Neumuller et al., 2011). In parallel, function of CDK12 in process of embryonic neural development was described in the conditional KO mouse model for this gene (Chen et al., 2014, 2017). When neuronal differentiation model of mouse embryonic carcinoma cell (P19) was employed, CDK12 and CDK13 kinases participated in the axonal elongation through a common signaling pathway that modulates protein expression of CDK5 (Chen et al., 2014). Recently, CDK13 was found remarkably dysregulated in hippocampus and suggested



as one of the hub genes useful to elucidate Alzheimer's disease (Pang et al., 2017). Importantly, studies of patients with *CDK13* mutations suggested their essential role in brain development. As

demonstrated in **Figure 5**, we were able to observe alteration of proliferation in neural tissue in *Cdk13^{tm1a}* mice (as analyzed by Ki67 expression) however overall changes in brain morphology



were not determined. On the other hand, observed proliferation changes can be also associated with developmental delay of *Cdk13^{tm1a}* animals and subventricular zone in brains may significantly expands later in development. However, it is also possible that a prominent role of CDK13 may be apparent in later stages of brain development, for instance, in the axon pathfinding, synapse formation and etc. Confirmation of this statement, however, has to be proven in future by employing the nestin-Cre or CreErt-Flox systems.

Importantly, developmental defects within craniofacial formation was documented for *Cdk13^{tm1a}* mice followed by complete loss of frontonasal part in *Cdk13^{tm1d}* mice. It is probably the most surprising observation in respect to patients with heterozygous mutation of *CDK13* gene (Sifrim et al., 2016; Bostwick et al., 2017; Carneiro et al., 2018; Hamilton et al., 2018). Moreover, gradual deregulation of CDK13 in mice resulted in enhanced craniofacial phenotype. The hypomorphic *Cdk13^{tm1a}* mice exhibited in the rostral area, altered shape of nasal septa and later at E15.5, incomplete formation of the secondary palate was observed in several animals, where palatal shelves

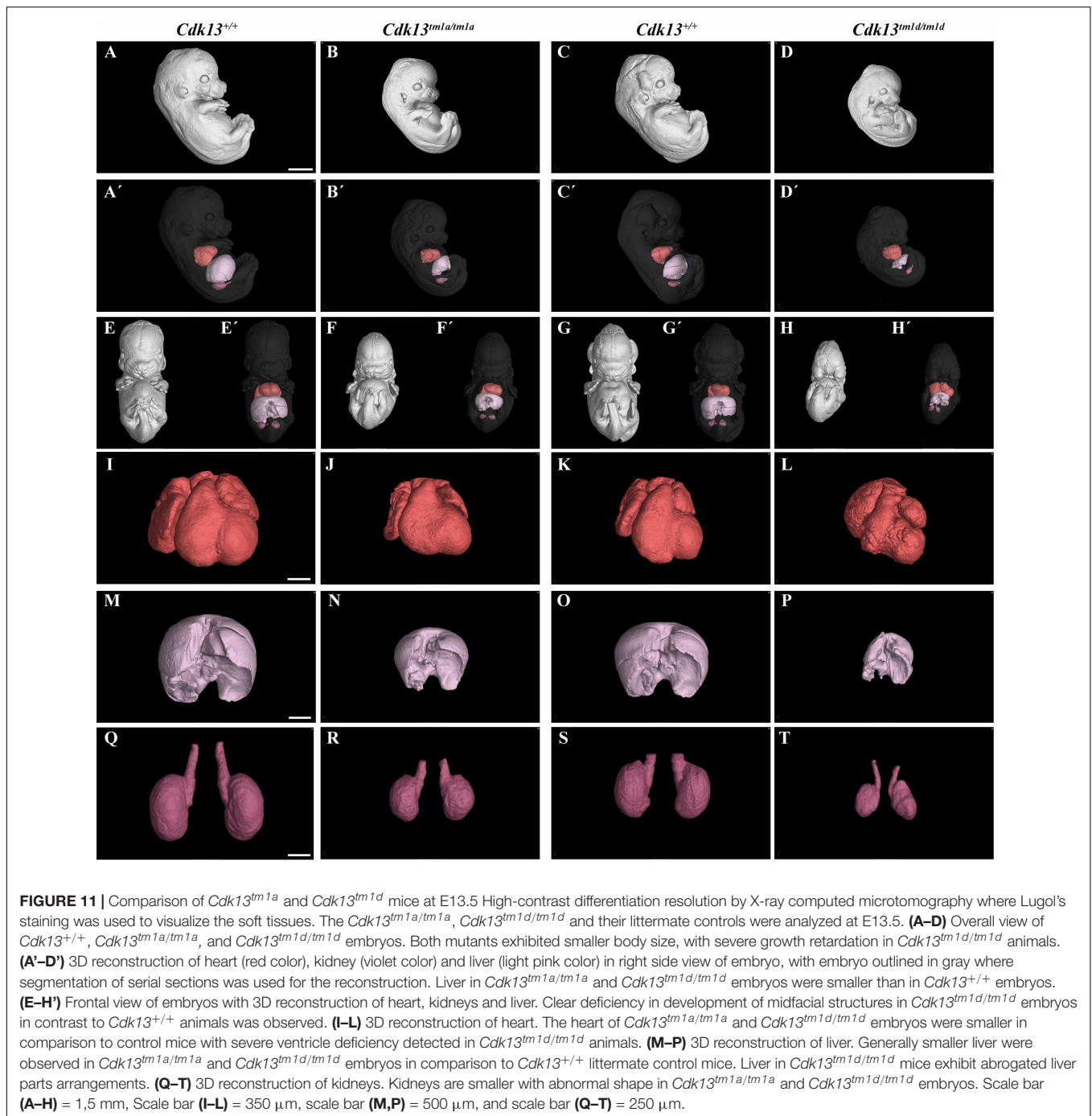
did not reach the midline, while control animals exhibited complete fusion of palatal processes. Nevertheless, complete depletion of CDK13 in the *Cdk13^{tm1d/tm1d}* mice led to ablation of the midline area of the head. There is a limited information regarding the role of CDK13 in this developmental process at the moment, yet. The association between SNP polymorphism rs373711932 located within *CDK13* gene and cranial base width was recently documented (Lee et al., 2017). Importantly, heterozygous copy number loss of *CCNK* gene in humans caused a syndromic neurodevelopmental disorder with distinctive facial dysmorphism (Fan et al., 2018). Therefore, it seems highly probable that CDK13 is indeed associated with craniofacial development, however, with unclear function, which will be necessary to uncover in the future.

From the functional point of view, it is surprising that only heterozygous mutation in one allele of the *CDK13* gene was sufficient to cause the CHDFIDD in human patients. Common feature in all studies depicting deleterious effect of pathogenic CDK13 in patients was presence of missense substitutions in the protein kinase domain around ATP-binding and magnesium binding sites (Sifrim et al., 2016; Bostwick et al., 2017; Hamilton et al., 2018). In addition, two nonsense variants and a frame-shift variant accompanying production of aberrant CDK13 transcripts have been identified (van den Akker et al., 2018). Based on crystal structure of CDK13/CycK complex, it is very possible that all these mutations most likely caused inactivation of catalytic activity of CDK13 or disrupted binding of CycK, its associating partner, leading to abrogated function of CDK13 (Kohoutek and Blazek, 2012; Greifenberg et al., 2016; Hamilton et al., 2018). Nevertheless, some of identified mutations in patients were predicted to retain binding to cyclin K with affected catalytic activity. If this is the case, then CDK13/CycK complex represents

TABLE 3 | Genotypes of offspring from *Cdk13^{tm1d/+}* intercross.

Stage	<i>Cdk13</i> ^{+/+}	<i>Cdk13</i> ^{tm1d/+}	<i>Cdk13</i> ^{tm1d/tm1d}	Litter	Empty decidua
	(25%)	(50%)	(25%)		
E12.5	33 (27.5%)	69 (57.5%)	18 (15%)*,#	18	24
E13.5	29 (31.5%)	52 (56.5%)	11 (12%)*,#	14	5
E14.5	24 (31.2%)	44 (57.1%)	9 (11.7%)*,#	10	4

*Growth retardation. #Dead embryos.



a dominant negative complex in cells (Hamilton et al., 2018). It is of note that two patients carrying stop codons at the end of the kinase domain represented milder phenotypes, although obvious genotype-phenotype correlation has not been recorded (van den Akker et al., 2018). From all these results, we can postulate that even loss of function of one *CDK13* allele is enough to interfere with developmental pathways and cause the CHDFIDD in humans, while complete abrogation of *CDK13* gene would lead to embryonic lethality as documented in our mouse model.

Currently, we can only speculate how CDK13 contributes to the developmental processes: if it participates in phosphorylation of Ser2 within CTD of RNAPII, it is highly probable that inhibition of CDK13 will block or dramatically affect ability of RNAPII to effectively synthesize nascent RNA. CDK13 was demonstrated to bind various splicing factors or proteins involved in splicing (Davidson et al., 2014; Bartkowiak and Greenleaf, 2015; Liang et al., 2015). Moreover, CDK13 was found to associate with ASF/SF2 factor, a member of the

spliceosome complex (Even et al., 2006). CDK13 was also identified in perinucleolar compartments enriched for proteins primarily implicated in pre-mRNA processing; therefore, lack of CDK13 could abrogate also RNA processing of given metazoan genes (Even et al., 2016). Thus, it is possible that a loss of kinase activity or associating potential of CDK13 will cripple proper splicing of transcribed RNA by RNAPII resulting in production of improperly spliced mRNA of proteins engaged in development processes.

It has been postulated that CDK13 phosphorylates Ser2 and Ser5 within CTD of RNAPII, if Ser7 is prephosphorylated at the C terminus of heptapeptide (Greifenberg et al., 2016). However, we were not able to detect any effect on Ser2 or Ser5, either in *Cdk13^{tm1a/tm1a}* or *Cdk13^{tm1d/tm1d}* animals with substantial decreased level of CDK13 in developing brain, where physiologically high level of CDK13 is present. Even though the global effect on Ser2 or Ser5 was not documented in *Cdk13^{tm1a/tm1a}* developing brains, CDK13 could still orchestrate phosphorylation of RNAPII at the specific sets of genes as earlier described for the CDK9/cyclin T2 or CDK12/cyclin K complexes in mouse and human cells (Zhu et al., 2009; Blazek et al., 2011; Johnson et al., 2016). When CDK13 was downregulated in HCT116 cells, gene ontology analysis revealed enrichment of functions connected to various extracellular and growth signaling pathways (Liang et al., 2015; Greifenberg et al., 2016). Similar *modus operandi* was implicated for CDK9 activation by MEK-1 and MSK1 in response to extracellular cues (Fujita et al., 2008; Smerdova et al., 2014). In addition, transcriptional kinase CDK8 was described to affect canonical Notch signaling by targeting activated *Notch* intracellular domain for proteasomal degradation (Fryer et al., 2004). In addition, CDK8 was suggested to stabilize β -catenin interaction with the promoter of WNT targets to achieve regulatory control (Firestein et al., 2008). Therefore, it is possible to envision that CDK13 regulates a specific set of genes at a specific developmental stage of embryonic development or in specialized cell types. Therefore, it will be critical in the near future to identify unique genes under control of CDK13 at given tissue or organ by employment of exome RNA-sequencing analyses in WT and *Cdk13*-deficient mice, which will be our next goal.

We believe that the *Cdk13^{tm1a}* hypomorphic mouse can be a very instrumental animal model to delineate cellular pathways or mechanisms participating in the onset or propagation of severe developmental cues in humans with mutated form of CDK13. Moreover, our *Cdk13^{tm1d}* mouse model with enhanced craniofacial phenotype may be invaluable for further clarification of molecular processes, which are responsible for clinical symptoms of human patients.

EXPERIMENTAL PROCEDURES

Mice, Genotyping, Breeding of *Cdk13^{tm1a}* Mice

Mouse embryos (*Cdk13^{tm1a}(EUCOM)Hmg*) bearing splicing acceptor, β -galactosidase and neomycine resistance gene both with poly A signals (Figure 1A) were obtained from

the Infrafrontier Research Infrastructure–Mouse disease Models¹. The acquired embryos carrying *Cdk13^{tm1a}* allele were transferred into pseudopregnant females of C57BL/6N mouse strain and the heterozygous *Cdk13^{tm1a}* mice were obtained at the Transgenic and Archiving Module, CCP (IMG, Prague, Czechia). Heterozygous mice for *Cdk13^{tm1a}* allele were bred and newborn mice were genotyped by PCR amplification (94°C, 30 s; 62°C/65°C, 20 s; 72°C, 30 s; 35 cycles) of *Cdk13* gene to distinguish WT (*Cdk13^{+/+}*) and *Cdk13^{tm1a/tm1a}* alleles. For PCR analysis, the following sets of primers were used for KO and WT alleles: (KOf, 5'-CCA GCT TTA AAG GCG CAT AAC-3'; KOr, 5'-TGA CCT TGG GCA AGA ACA TAA-3'; WtF, 5'-TAG CTG GCC AAT GAG CTT TC-3'; WtR, 5'-AGT CTA GGA AGC TGG GAA GAT- 3'). Primers KOf and KOr amplify a 257-bp fragment from *Cdk13^{tm1a}* allele while primers WtF and WtR amplify a 179-bp fragment from WT allele. Genomic DNA was isolated from mouse ears by NaOH extraction (Truett et al., 2000). Heterozygous mice carrying *Cdk13^{tm1a}* allele were bred and after mating, females were examined for vaginal plugs, embryonic day 0.5 (E0.5) was determined at noon at the day of vaginal plaque record. Embryos at various stages were obtained from uteri of pregnant heterozygous female mice, genotyped and the Mendelian ratios were defined.

To generate mouse carrying the *Cdk13^{tm1d}* allele, the *Cdk13^{tm1a/tm1a}* mice were crossed with the Flp-deleter mouse strain *Gt(ROSA)26Sor^{tm2}(CAG- β po,-EYFP)^{lcs}* (MGI: 5285396, Philippe Soriano) and Cre-deleter strain *Gt(ROSA)26Sor^{tm1}(ACTB-cre,-EGFP)^{lcs}* (MGI: 5285392, Philippe Soriano) in order to delete critical exons 3 and 4 within *Cdk13* gene. All animal procedures were performed in strict accordance to the Guide for the Care and Use of Laboratory Animals and approved by the Institutional Animal Care and Use Committee (Veterinary Research Institute, Brno, Czechia).

Western Blotting

Particular organ from *Cdk13^{tm1a/tm1a}*, *Cdk13^{tm1a/+}* and *Cdk13^{+/+}* embryos at E14.5 were lysed in lysis buffer (100 mM Tris, pH 7.4; 1% SDS; 10% glycerol) and sonicated. The brain from *Cdk13^{tm1d/tm1d}*, *Cdk13^{tm1d/+}* and *Cdk13^{+/+}* were lysed in lysis buffer (100 mM Tris, pH 7.4; 1% SDS; 10% glycerol) and sonicated. Concentrations of total proteins were determined with bicinchoninic acid (BCA). Lysates were diluted to the same concentration, mixed with the 3xLaemmli sample buffer and boiled for 5 min. Western blotting was performed using anti-mouse CDK13 polyclonal antibody (SAB1302350, Sigma-Aldrich), γ -catenin (CTNNG) antibody (2309, Cell Signaling Technology), cyclin T1 (CYCT1) (sc-10750, Santa Cruz Biotechnology) and anti-serine 2 (Ser2) and serine 5 (Ser5) rat monoclonal antibodies (clones 3E10 and 3E8 respectively, ChromoTek GmbH, Germany).

Histological Analysis

Wild-type and homozygous *Cdk13^{tm1a/tm1a}* embryos at E14.5 to E16.5 were fixed in 4% paraformaldehyde and dehydrated. After that hearts, brains, kidneys and livers were dissected,

¹<https://www.infrafrontier.eu/>

embedded in paraffin, and sectioned at 5 μm . Hematoxylin-eosin (H&E) staining was performed. Images were taken under bright field using a Leica compound microscope (DMLB2) with a Leica camera (DFC480) attached (Leica Microsystems, Wetzlar, Germany).

Immunohistochemistry

Proliferating cells were visualized on E14.5 brain sections by labeling of Ki67 (positive cells are brown). Sections were pretreated in Citrate buffer, pH6, 10 mM, 20 min/97°C in water bath and were labeled with Ki67 primary antibody (RBK027-05, Zytomed Systems). For primary antibody detection, specific secondary antibody and avidin-biotin complex were used (Vectastain kit, PK-6101, Vector laboratories). The signal was developed by DAB chromogen system (K3468, DAKO). Nuclei were counterstained by hematoxylin (blue). Mitotic index was counted as the ratio between Ki67-positive cells and total amount of cells in three biological samples for each group (three *Cdk13*^{+/+} embryos, three *Cdk13*^{tm1a/tm1a} embryos). Statistical significance in cell number differences between control and deficient mice were evaluated by unpaired *t*-test.

E14.5 heart sections were pretreated in DAKO Target Retrieval (32367, DAKO) solution for 15 min/97°C in water bath and labeled using primary antibodies against actin (sc-1615-R, Santa Cruz Biotechnology) and myosin (sc-32732, Santa Cruz Biotechnology). To detect primary antibodies, secondary Alexa Fluor antibodies (A11004, A11008, Invitrogen) were used. Nuclei were counterstained by DRAQ5TM (62251, Thermo Scientific). Images were captured on fluorescence confocal microscope Leica SP8 (Leica).

Micro-Computed Tomography (micro-CT)

The embryos at E13.5 or E15.5 were contrasted with Lugol's solution to visualize gross morphology of individual soft tissues by microCT. For the purpose of motion stabilization during the micro CT scan, mouse embryo was embedded in 1% agarose gel in Falcon conical centrifuge tube. The micro-CT scan was performed using - laboratory system GE Phoenix v| tome| x L 240 (GE Sensing & InspectionTechnologies GmbH, Germany), equipped with a 180 kV/15W maximum power nanofocus X-ray tube and high contrast flat panel detector DXR250 2048 px \times 2048 px with 200 μm \times 200 μm pixel size. The measurement was carried out in the air-conditioned cabinet (21°C) at acceleration voltage of 60 kV and X-ray tube current of 200 μA . Thousand nine hundred projections were taken over 360° with exposure time 900 ms resulting in 5.5 μm voxel resolution. The tomographic reconstruction was realized by software GE phoenix datos| x 2.0 (GE Sensing & Inspection Technologies GmbH, Germany). Reconstructed slice data were processed using VG Studio MAX 3.1 software (Volume Graphics GmbH, Germany) and segmentation of liver, kidneys and heart was completed manually.

Embryonic Ultrasound Imaging and Doppler Echocardiography

Pregnant females were anesthetized on gestational day 14.5 or 15.5 (before noon) with an isoflurane/oxygen mixture (anesthesia was initiated with 3–4%, and maintained with 1–2% isoflurane), and maintained on a temperature-controlled mouse platform (with sensors for monitoring of maternal electrocardiogram, respiration and core body temperature). Maternal temperature was maintained at 34–37°C, and maternal heart beat at \sim 400 beats/minute by adjusting the level of anesthesia. An incision of about 2–3 cm in the lower abdomen was made, and a uterine horn was externalized through the incision to provide imaging access. The number of fetuses in right and left uterine horns was counted from the mother's bladder and later during echocardiographic imaging, labeled as R1, R2, R3, etc (right side) and L1, L2, L3, etc (left side). Pre-warmed ultrasound gel (37°C) without bubbles was applied between the individual fetuses and the transducer. B-mode imaging scanning of the whole embryo with the focus on the heart and Color Doppler and PW Doppler measurements for heart aorta and dorsal aorta were obtained using a high-frequency ultrasound system (Vevo 2100, FUJIFILM VisualSonics, Inc., Toronto, ON, Canada) equipped with a MS-550S transducer operating at a center frequency of 44 MHz. At the end of imaging of all fetuses, the mother was sacrificed by cervical dislocation and a small piece of yolk sac of each fetus was taken for genotyping.

DATA AVAILABILITY

All datasets generated for this study are included in the manuscript and/or the **Supplementary Files**.

ETHICS STATEMENT

All animal procedures were performed in strict accordance to the Guide for the Care and Use of Laboratory Animals and approved by the Institutional Animal Care and Use Committee (Veterinary Research Institute, Brno, Czechia).

AUTHOR CONTRIBUTIONS

JKo conceptualized and supervised the project, acquired the funding, wrote the original draft, and administrated the project. MN conceptualized the project, contributed to formal analysis, investigation, and visualization, and wrote, review, and edited the manuscript. DV contributed to investigation and visualization. MH contributed to formal analysis, investigation, and visualization. JP contributed to conceptualization, formal analysis, supervision, and investigation and wrote, review, and edited the manuscript. SP and MP contributed to investigation and visualization. RS supervised the project. MK, TZ, and JKa contributed to software development and visualization. H-CJ contributed to investigation, and wrote, review, and edited the manuscript. M-JF and MB contributed to formal analysis, supervision, writing, review, and editing.

FUNDING

This research was supported by grants n. 16-24043J of the Czech Science Foundation to JKo, MN, and DV. The research for this manuscript was financially supported by the Ministry of Agriculture n. MZE-RO0518, by the Ministry of Education, Youth and Sports, n. LM2015040 and LQ1604 by, and by the Ministry of Education, Youth and Sports and European Fund for Regional Development n. OP RDE CZ.02.1.01/0.0/0.0/16_013/0001789 and n. OP RDI CZ.1.05/1.1.00/02.0109 and OP RDI CZ.1.05/2.1.00/19.0395 to JP, MP, SP, and RS. Work by MB and MH was supported by the Ministry of Education, Youth and Sports of the Czech Republic (CZ.02.1.01/0.0/0.0/15_003/0000460). The cooperation between MB and TZ labs is supported by the Czech Science Foundation (17-14886S). MicroCT analyses performed by MK, TZ, and JKa were carried out under the project CEITEC 2020 (LQ1601) with financial support from the Ministry of Education, Youth and Sports of the Czech Republic under the National Sustainability Program II. Work by H-CJ and M-JF was supported by Ministry of Science and Technology, Taiwan (MOST 106-2811-B-010-046 and MOST 105-2923-B-010 -002 -MY3).

ACKNOWLEDGMENTS

We would like to thank Assoc. Prof. S. Sevcikova for a critical comments to the manuscript and other members of the laboratory for helpful inputs.

SUPPLEMENTARY MATERIAL

The Supplementary Material for this article can be found online at: <https://www.frontiersin.org/articles/10.3389/fcell.2019.00155/full#supplementary-material>

FIGURE S1 | Truncated form of CDK13 protein. **(A)** Predicted amino acid sequence of truncated CDK13 protein due to transcriptional block mediated by two Poly A sites introduced into the intron 2 as part of trap vector in mice bearing *Cdk13^{tm1a}* allele. Black and Blue capital letters represent amino acids encoded within Exon 1 and Exon 2 of *Cdk13* gene, respectively. Predicted Molecular weight of truncated *CDK13* protein is 66.22 kDa (https://www.bioinformatics.org/sms/prot_mw.html). **(B)** Brain extracts were prepared from E14.5 embryos of given genotype and protein levels of wild-type and truncated form of CDK13 was evaluated by Western Blotting. The antibody used throughout our study recognizes N-terminal part of CDK13, which is expressed in both forms of Cdk13, wild-type as well as truncated one. The *Cdk13^{+/+}* mice contained only the wild-type CDK13 protein (WT-CDK13). The heterozygous *Cdk13^{tm1a/+}* mice

REFERENCES

- Al-Balool, H. H., Weber, D., Liu, Y., Wade, M., Guleria, K., Nam, P. L., et al. (2011). Post-transcriptional exon shuffling events in humans can be evolutionarily conserved and abundant. *Genome Res.* 21, 1788–1799. doi: 10.1101/gr.116442.110
- Bakre, A., Andersen, L. E., Meliopoulos, V., Coleman, K., Yan, X., Brooks, P., et al. (2013). Identification of host kinase genes required for Influenza virus replication and the regulatory role of MicroRNAs. *PLoS One* 8:e66796. doi: 10.1371/journal.pone.0066796

included wild-type (WT-CDK13) and truncated (TR-CDK13) forms of CDK13 protein. The *Cdk13^{tm1a}* expressed the truncated form of CDK13 and minor wild-type CDK13 as demonstrated by immunoblot.

FIGURE S2 | Comparison of gross morphology of *Cdk13*-deficient mice phenotype. **(A–H)** Wild-type *Cdk13^{+/+}*, **(I–P)** heterozygous *Cdk13^{tm1a/+}*, and **(Q–X)** *Cdk13^{tm1a}* embryos at various stages. Growth retardation of *Cdk13*-deficient mice was apparent from early developmental stages **(Q,R)**. Some embryos exhibited nuchal edema and peripheral hypervascularization **(U)** and abnormal craniofacial shape **(S,T)**. Developmental delay was observed at later stages **(V,W)**. At E16.5, each of the *Cdk13^{tm1a/tm1a}* embryos was undergoing resorption **(X)**. No morphological differences between wild-type and heterozygous embryos were observed. Scale bar = 0.1 mm.

FIGURE S3 | The 3D reconstruction of selected organs in micro-CT of control *Cdk13^{+/+}* and *Cdk13^{tm1a/tm1a}* embryos. Overall view on embryos of *Cdk13^{+/+}* **(A)** and *Cdk13^{tm1a/tm1a}* **(B)** with 3D reconstruction of heart, liver and kidney (left). Gross morphology is well visible on movable model on the right side. To visualize only one organ, click on the lower row and select heart (orange), liver (pink) or kidney (purple) organ only. Scale bar = 1 mm.

FIGURE S4 | Transversal sections of the head of control *Cdk13^{+/+}* and *Cdk13^{tm1a/tm1a}* embryos. Transversal sections through the mouse head with details of the nasal cavity area. At E14.5, no obvious differences were observed and only one epithelial protrusion (marked by arrow) were developed close to each nasal cavity (nc) (compare **A** to **D**). Later at E15.5, the number of nasal glands was reproducibly smaller in *Cdk13^{tm1a/tm1a}* mice in comparison to control animals (compare **B** to **E**). **(C,F)** Coronal section through the head of embryos at the level of the eyes. White arrows depict different complexity of the nasal cavity in wild-type, *Cdk13^{+/+}*, and *Cdk13^{tm1a/tm1a}* animals. Abbreviations nc – nasal cavity, arrowhead – nasal gland. Scale bar **(A,B,D,F)** = 100 μ m and scale bar **(C,F)** = 1 mm.

FIGURE S5 | Immunohistochemical detection of myosin and actin in the heart of *Cdk13^{+/+}* and *Cdk13^{tm1a/tm1a}* embryos. Sagittal sections through the mouse heart were prepared and immunohistochemical detection of myosin and actin was carried out with specific antibodies. Decreased expression of myosin was detected in ventricle myocardium, compare B and B' to E and E'. Scale bar **(A,D)** = 500 μ m; Scale bar **(B–F)**, without D) – 100 μ m.

FIGURE S6 | The expression of *Cdk13* in adult mouse organs visualized by β -galactosidase activity. The expression of *Cdk13* was examined by activity of β -galactosidase in adult mouse organs **(A)** eye, **(B)** heart, **(C)** thyroid gland, **(D)** urinary bladder, **(E)** kidney, **(F)** uterus, **(G)** gall bladder, **(H)** testes, and **(I)** ovary.

FIGURE S7 | Sagittal sections through heads of *Cdk13^{tm1a}* and *Cdk13^{tm1d}* and *Cdk13^{tm1a}* and *Cdk13^{tm1d}* mice. High-contrast differentiation resolution by X-ray computed microtomography where Lugol's staining was used to visualize the soft tissues. The *Cdk13^{tm1a/tm1a}*, *Cdk13^{tm1d/tm1d}* and their littermate controls are displayed at E13.5 to show overall developmental delay.

FIGURE S8 | Horizontal sections through heads of *Cdk13^{tm1a}* and *Cdk13^{tm1d}* mice. High-contrast differentiation resolution by X-ray computed microtomography where Lugol's staining was used to visualize the soft tissues. The *Cdk13^{tm1a/tm1a}*, *Cdk13^{tm1d/tm1d}* and their littermate controls are displayed at E13.5.

TABLE S1 | The prevalence of developmental defects in *Cdk13^{tm1a}* and *Cdk13^{tm1d}* transgenic mice.

- Bartkowiak, B., and Greenleaf, A. L. (2015). Expression, purification, and identification of associated proteins of the full-length hCDK12/CyclinK complex. *J. Biol. Chem.* 290, 1786–1795. doi: 10.1074/jbc.M114.612226
- Bartkowiak, B., Liu, P., Phatnani, H. P., Fuda, N. J., Cooper, J. J., Price, D. H., et al. (2010). CDK12 is a transcription elongation-associated CTD kinase, the metazoan ortholog of yeast Ctk1. *Genes Dev.* 24, 2303–2316. doi: 10.1101/gad.1968210
- Berro, R., Pedati, C., Kehn-Hall, K., Wu, W., Klase, Z., Even, Y., et al. (2008). CDK13, a new potential human immunodeficiency virus type 1 inhibitory

- factor regulating viral mRNA splicing. *J. Virol.* 82, 7155–7166. doi: 10.1128/JVI.02543-07
- Blazek, D., Kohoutek, J., Bartholomeeusen, K., Johansen, E., Hulinkova, P., Luo, Z., et al. (2011). The Cyclin K/Cdk12 complex maintains genomic stability via regulation of expression of DNA damage response genes. *Genes Dev.* 25, 2158–2172. doi: 10.1101/gad.16962311
- Bostwick, B. L., McLean, S., Posey, J. E., Streff, H. E., Gripp, K. W., Blesson, A., et al. (2017). Phenotypic and molecular characterisation of CDK13-related congenital heart defects, dysmorphic facial features and intellectual developmental disorders. *Genome Med.* 9:73. doi: 10.1186/s13073-017-0463-8
- Carneiro, T. N., Krepischi, A. C., Costa, S. S., Tojal da Silva, I., Vianna-Morgante, A. M., Valieris, R., et al. (2018). Utility of trio-based exome sequencing in the elucidation of the genetic basis of isolated syndromic intellectual disability: illustrative cases. *Appl. Clin. Genet.* 11, 93–98. doi: 10.2147/TACG.S165799
- Chen, H. R., Juan, H. C., Wong, Y. H., Tsai, J. W., and Fann, M. J. (2017). Cdk12 Regulates Neurogenesis and Late-Arising Neuronal Migration in the Developing Cerebral Cortex. *Cereb. Cortex* 27, 2289–2302. doi: 10.1093/cercor/bhw081
- Chen, H. R., Lin, G. T., Huang, C. K., and Fann, M. J. (2014). Cdk12 and Cdk13 regulate axonal elongation through a common signaling pathway that modulates Cdk5 expression. *Exp. Neurol.* 261, 10–21. doi: 10.1016/j.expneurol.2014.06.024
- Cheng, S. W., Kuzyk, M. A., Moradian, A., Ichu, T. A., Chang, V. C., Tien, J. F., et al. (2012). Interaction of cyclin-dependent kinase 12/CrkRS with cyclin K1 is required for the phosphorylation of the C-terminal domain of RNA polymerase II. *Mol. Cell. Biol.* 32, 4691–4704. doi: 10.1128/MCB.06267-11
- Dai, Q., Lei, T., Zhao, C., Zhong, J., Tang, Y. Z., Chen, B., et al. (2012). Cyclin K-containing kinase complexes maintain self-renewal in murine embryonic stem cells. *J. Biol. Chem.* 287, 25344–25352. doi: 10.1074/jbc.M111.321760
- Davidson, L., Muniz, L., and West, S. (2014). 3' end formation of pre-mRNA and phosphorylation of Ser2 on the RNA polymerase II CTD are reciprocally coupled in human cells. *Genes Dev.* 28, 342–356. doi: 10.1101/gad.231274.113
- Deciphering Developmental Disorders Study (2017). Prevalence and architecture of de novo mutations in developmental disorders. *Nature* 542, 433–438. doi: 10.1038/nature21062
- Even, Y., Durieux, S., Escande, M. L., Lozano, J. C., Peaucellier, G., Weil, D., et al. (2006). CDC2L5, a Cdk-like kinase with RS domain, interacts with the ASF/SF2-associated protein p32 and affects splicing in vivo. *J. Cell. Biochem.* 99, 890–904. doi: 10.1002/jcb.20986
- Even, Y., Escande, M. L., Fayet, C., and Genevriere, A. M. (2016). CDK13, a Kinase Involved in Pre-mRNA Splicing, Is a Component of the Perinuclear Compartment. *PLoS One* 11:e0149184. doi: 10.1371/journal.pone.0149184
- Fan, Y., Yin, W., Hu, B., Kline, A. D., Zhang, V. W., Liang, D., et al. (2018). De Novo mutations of CCNK cause a syndromic neurodevelopmental disorder with distinctive facial dysmorphism. *Am. J. Hum. Genet.* 103, 448–455. doi: 10.1016/j.ajhg.2018.07.019
- Firestein, R., Bass, A. J., Kim, S. Y., Dunn, I. F., Silver, S. J., Guney, I., et al. (2008). CDK8 is a colorectal cancer oncogene that regulates beta-catenin activity. *Nature* 455, 547–551. doi: 10.1038/nature07179
- Fryer, C. J., White, J. B., and Jones, K. A. (2004). Mastermind recruits CycC:CDK8 to phosphorylate the Notch ICD and coordinate activation with turnover. *Mol. Cell.* 16, 509–520. doi: 10.1016/j.molcel.2004.10.014
- Fujita, T., Ryser, S., Piuz, I., and Schlegel, W. (2008). Up-regulation of P-TEFb by the MEK1-extracellular signal-regulated kinase signaling pathway contributes to stimulated transcription elongation of immediate early genes in neuroendocrine cells. *Mol. Cell. Biol.* 28, 1630–1643. doi: 10.1128/mcb.01767-07
- Greenleaf, A. L. (2018). Human CDK12 and CDK13, multi-tasking CTD kinases for the new millennium. *Transcription* 10, 91–110. doi: 10.1080/21541264.2018.1535211
- Greifenberg, A. K., Honig, D., Pilarova, K., Duster, R., Bartholomeeusen, K., Bosken, C. A., et al. (2016). Structural and functional analysis of the Cdk13/Cyclin K complex. *Cell Rep.* 14, 320–331. doi: 10.1016/j.celrep.2015.12.025
- Hamilton, M. J., Caswell, R. C., Canham, N., Cole, T., Firth, H. V., Foulds, N., et al. (2018). Heterozygous mutations affecting the protein kinase domain of CDK13 cause a syndromic form of developmental delay and intellectual disability. *J. Med. Genet.* 55, 28–38. doi: 10.1136/jmedgenet-2017-104620
- Johnson, S. F., Cruz, C., Greifenberg, A. K., Dust, S., Stover, D. G., Chi, D., et al. (2016). CDK12 inhibition reverses de novo and acquired PARP inhibitor resistance in BRCA wild-type and mutated models of triple-negative breast cancer. *Cell Rep.* 17, 2367–2381. doi: 10.1016/j.celrep.2016.10.077
- Juan, H. C., Lin, Y., Chen, H. R., and Fann, M. J. (2016). Cdk12 is essential for embryonic development and the maintenance of genomic stability. *Cell Death Differ.* 23, 1038–1048. doi: 10.1038/cdd.2015.157
- Kim, H. E., Kim, D. G., Lee, K. J., Son, J. G., Song, M. Y., Park, Y. M., et al. (2012). Frequent amplification of CENPF, GMNN and CDK13 genes in hepatocellular carcinomas. *PLoS One* 7:e43223. doi: 10.1371/journal.pone.0043223
- Ko, T. K., Kelly, E., and Pines, J. (2001). CrkRS: a novel conserved Cdc2-related protein kinase that colocalizes with SC35 speckles. *J. Cell Sci.* 114, 2591–2603.
- Kohoutek, J. (2009). P-TEFb- the final frontier. *Cell Div.* 4:19. doi: 10.1186/1747-1028-4-19
- Kohoutek, J., and Blazek, D. (2012). Cyclin K goes with Cdk12 and Cdk13. *Cell Div.* 7:12. doi: 10.1186/1747-1028-7-12
- Lee, M. K., Shaffer, J. R., Leslie, E. J., Orlova, E., Carlson, J. C., Feingold, E., et al. (2017). Genome-wide association study of facial morphology reveals novel associations with *FREM1* and *PARK2*. *PLoS One* 12:e0176566. doi: 10.1371/journal.pone.0176566
- Liang, K., Gao, X., Gilmore, J. M., Florens, L., Washburn, M. P., Smith, E., et al. (2015). Characterization of human cyclin-dependent kinase 12 (CDK12) and CDK13 complexes in C-terminal domain phosphorylation, gene transcription, and RNA processing. *Mol. Cell. Biol.* 35, 928–938. doi: 10.1128/MCB.01426-14
- Meyers, E. N., Lewandoski, M., and Martin, G. R. (1998). An *Fgf8* mutant allelic series generated by Cre- and FLP-mediated recombination. *Nat. Genet.* 18, 136–141. doi: 10.1038/ng0298-136
- Neumuller, R. A., Richter, C., Fischer, A., Novatchkova, M., Neumuller, K. G., and Knoblich, J. A. (2011). Genome-wide analysis of self-renewal in *Drosophila* neural stem cells by transgenic RNAi. *Cell Stem Cell* 8, 580–593. doi: 10.1016/j.stem.2011.02.022
- Pan, J., Xue, Y., Chen, S., Qiu, H., Wu, C., Jiang, H., et al. (2012). Establishment and characterization of a new human acute myelomonocytic leukemia cell line J1H-3. *Leuk. Res.* 36, 889–894. doi: 10.1016/j.leukres.2012.01.012
- Pang, X., Zhao, Y., Wang, J., Zhou, Q., Xu, L., Kang, et al. (2017). The bioinformatic analysis of the dysregulated genes and microRNAs in entorhinal cortex, hippocampus, and blood for Alzheimer's disease. *Biomed. Res. Int.* 2017:9084507. doi: 10.1155/2017/9084507
- Pham, C. T., MacIvor, D. M., Hug, B. A., Heusel, J. W., and Ley, T. J. (1996). Long-range disruption of gene expression by a selectable marker cassette. *Proc. Natl. Acad. Sci. U.S.A.* 93, 13090–13095. doi: 10.1073/pnas.93.23.13090
- Scacheri, P. C., Crabtree, J. S., Novotny, E. A., Garrett-Beal, L., Chen, A., Edgemon, K. A., et al. (2001). Bidirectional transcriptional activity of PGK-neomycin and unexpected embryonic lethality in heterozygote chimeric knockout mice. *Genesis* 30, 259–263. doi: 10.1002/gene.1072
- Sifrim, A., Hitz, M. P., Wilsdon, A., Breckpot, J., Turki, S. H., Thienpont, B., et al. (2016). Distinct genetic architectures for syndromic and nonsyndromic congenital heart defects identified by exome sequencing. *Nat. Genet.* 48, 1060–1065. doi: 10.1038/ng.3627
- Smerdova, L., Smerdova, J., Kabatkova, M., Kohoutek, J., Blazek, D., Machala, M., et al. (2014). Upregulation of CYP1B1 expression by inflammatory cytokines is mediated by the p38 MAP kinase signal transduction pathway. *Carcinogenesis* 35, 2534–2543. doi: 10.1093/carcin/bgu190
- Truett, G. E., Heeger, P., Mynatt, R. L., Truett, A. A., Walker, J. A., and Warman, M. L. (2000). Preparation of PCR-quality mouse genomic DNA with hot sodium hydroxide and tris (HotSHOT). *Biotechniques* 29, 52, 54. doi: 10.2144/00291bm09
- Uehara, T., Takenouchi, T., Kosaki, R., Kurosawa, K., Mizuno, S., and Kosaki, K. (2018). Redefining the phenotypic spectrum of de novo heterozygous CDK13 variants: three patients without cardiac defects. *Eur. J. Med. Genet.* 61, 243–247. doi: 10.1016/j.ejmg.2017.12.004
- van den Akker, W. M. R., Brummelman, I., Martis, L. M., Timmermans, R. N., Pfundt, R., Kleefstra, T., et al. (2018). De novo variants in CDK13 associated with syndromic ID/DD: molecular and clinical delineation of 15

- individuals and a further review. *Clin. Genet.* 93, 1000–1007. doi: 10.1111/cge.13225
- Wang, Y., Pan, X., Fan, Y., Hu, X., Liu, X., Xiang, M., et al. (2015). Dysregulated expression of microRNAs and mRNAs in myocardial infarction. *Am. J. Transl. Res.* 7, 2291–2304.
- Xiang, X., Deng, L., Zhang, J., Zhang, X., Lei, T., Luan, G., et al. (2014). A distinct expression pattern of cyclin K in mammalian testes suggests a functional role in spermatogenesis. *PLoS One* 9:e101539. doi: 10.1371/journal.pone.0101539
- Zhu, H., Doherty, J. R., Kuliye, E., and Mead, P. E. (2009). CDK9/cyclin complexes modulate endoderm induction by direct interaction with Mix.3/mixer. *Dev. Dyn.* 238, 1346–1357. doi: 10.1002/dvdy.21920
- Conflict of Interest Statement:** The authors declare that the research was conducted in the absence of any commercial or financial relationships that could be construed as a potential conflict of interest.
- Copyright © 2019 Nováková, Hampl, Vrábek, Procházka, Petreselyová, Procházková, Sedláček, Kavková, Zikmund, Kaiser, Juan, Fann, Buchtová and Kohoutek. This is an open-access article distributed under the terms of the Creative Commons Attribution License (CC BY). The use, distribution or reproduction in other forums is permitted, provided the original author(s) and the copyright owner(s) are credited and that the original publication in this journal is cited, in accordance with accepted academic practice. No use, distribution or reproduction is permitted which does not comply with these terms.

APPENDIX 12

HAMPL, Marek, Nela JANDOVÁ, Denisa LUSKOVÁ, Monika NOVÁKOVÁ, Tereza SZOTKOWSKÁ, Štěpán ČADA, Jan PROCHÁZKA, **Jiri KOHOUTEK** and Marcela BUCHTOVÁ. Early embryogenesis in CHDFIDD mouse model reveals facial clefts and altered cranial neurogenesis. *Disease Models & Mechanisms*. 2024, 17(6), dmm050261.

Early embryogenesis in CHDFIDD mouse model reveals facial clefts and altered cranial neurogenesis

Marek Hampl^{1,2}, Nela Jandová^{1,2}, Denisa Lusková¹, Monika Nováková³, Tereza Szotkowská¹, Štěpán Čada², Jan Procházka^{4,5}, Jiri Kohoutek² and Marcela Buchtová^{1,2,*}

ABSTRACT

CDK13-related disorder, also known as congenital heart defects, dysmorphic facial features and intellectual developmental disorder (CHDFIDD) is associated with mutations in the *CDK13* gene encoding transcription-regulating cyclin-dependent kinase 13 (CDK13). Here, we focused on the development of craniofacial structures and analyzed early embryonic stages in CHDFIDD mouse models, with one model comprising a hypomorphic mutation in *Cdk13* and exhibiting cleft lip/palate, and another model comprising knockout of *Cdk13*, featuring a stronger phenotype including midfacial cleft. *Cdk13* was found to be physiologically expressed at high levels in the mouse embryonic craniofacial structures, namely in the forebrain, nasal epithelium and maxillary mesenchyme. We also uncovered that *Cdk13* deficiency leads to development of hypoplastic branches of the trigeminal nerve including the maxillary branch. Additionally, we detected significant changes in the expression levels of genes involved in neurogenesis (*Ache*, *Dcx*, *Mef2c*, *Neurog1*, *Ntn1*, *Pou4f1*) within the developing palatal shelves. These results, together with changes in the expression pattern of other key face-specific genes (*Fgf8*, *Foxd1*, *Msx1*, *Meis2* and *Shh*) at early stages in *Cdk13* mutant embryos, demonstrate a key role of CDK13 in the regulation of craniofacial morphogenesis.

KEY WORDS: Craniofacial development, Orofacial clefts, Axons, Neurite outgrowth, CDK13, Trigeminal ganglion

INTRODUCTION

CDK13 is one of the transcriptional kinases that regulates transcription via phosphorylation of RNA polymerase II (RNAPII) and controls alternative splicing (Bartkowiak et al., 2010; Blazek et al., 2011). Recently, a few case studies have described a variety of developmental defects in human patients carrying mutated *CDK13* (Hamilton and Suri, 2019). These patients exhibit delayed development, intellectual

disorders, heart and kidney defects, and craniofacial anomalies, features that – together – have been recognized as congenital heart defects, dysmorphic facial features and intellectual development disorder (CHDFIDD). In addition to the most common anomalies, patients suffer from brain anomalies, autism, seizures, limb and skeletogenesis anomalies, and other clinical presentations (Hamilton and Suri, 2019). To simulate anomalies presented in patients with *CDK13* mutations, we have developed mouse models that exhibit phenotypes similar to those observed in humans (Nováková et al., 2019). We observed that *Cdk13* deficiency in the mouse models causes embryonic lethality, delayed development, heart and brain abnormalities and a facial phenotype (Nováková et al., 2019).

Here, we screened the gene expression of *Cdk13* across several embryonic craniofacial tissues at different developmental stages, and evaluated the alteration of developmental processes in craniofacial structures in *Cdk13*-hypomorph (*Cdk13^{tm1a/tm1a}*) and *Cdk13*-knockout (*Cdk13^{tm1d/tm1d}*) mouse embryos, with the aim to uncover the mechanisms behind the observed developmental abnormalities. To determine the modification in molecular regulations caused by *Cdk13* deficiency, we also analyzed the gene expression of patterning proteins involved in craniofacial structure formation.

Moreover, previous *in vitro* approaches have uncovered the contribution of a *Cdk13* mutation to the alteration of neuronal differentiation and neurite outgrowth through regulation of the CDK5 pathway (Chen et al., 2014). These findings are in agreement with observations of neurodevelopmental disorders in human

Research Simplified

Congenital heart defects, dysmorphic facial features and intellectual development disorder (CHDFIDD) is a rare genetic disease, mostly reported in children. Reduced levels of CDK13 - a protein essential for the regulation of normal gene expression in human cells - have been implicated in some patients with CHDFIDD.

Understanding how CDK13 deficiency affects early development during pregnancy can help researchers devise therapeutics for CDK13-related CHDFIDD.

Since humans and mice share several developmental and anatomical similarities, the authors firstly used established laboratory mouse models with mutations in the CDK13-coding gene to mimic CDK13 deficiencies seen in humans with CHDFIDD. Mouse embryos with reduced CDK13 expression displayed structural defects in their heads, mostly in the face, as well as underdeveloped facial nerves. The authors find that these anomalies in CDK13-deficient mice were caused by lowered expression of genes with critical roles in the development of the face and in nerve growth.

This study tracked the expression of CDK13 during different developmental stages of the mouse embryo and confirmed the importance of this protein in craniofacial and neural development. Further research can facilitate the development of potential therapeutics for humans with CDK13-related CHDFIDD.

¹Laboratory of Molecular Morphogenesis, Institute of Animal Physiology and Genetics, Czech Academy of Sciences, 60200 Brno, Czech Republic.

²Department of Experimental Biology, Faculty of Science, Masaryk University, 60200 Brno, Czech Republic. ³Department of Chemistry and Toxicology, Veterinary Research Institute, 62100 Brno, Czech Republic. ⁴Laboratory of Transgenic Models of Diseases, Institute of Molecular Genetics, Czech Academy of Sciences, 14220 Prague, Czech Republic. ⁵Czech Centre for Phenogenomics, Institute of Molecular Genetics, Czech Academy of Sciences, 14220 Prague, Czech Republic.

*Author for correspondence (buchtova@iach.cz)

 M.H., 0000-0002-2824-1004; M.B., 0000-0002-0262-6774

This is an Open Access article distributed under the terms of the Creative Commons Attribution License (<https://creativecommons.org/licenses/by/4.0>), which permits unrestricted use, distribution and reproduction in any medium provided that the original work is properly attributed.

Handling Editor: Karen Liu

Received 24 April 2023; Accepted 12 March 2024

patients carrying mutations of *CDK13* (Trinh et al., 2019). Based on this evidence, we focused here on the analyses of cranial nerve growth and morphology in *Cdk13*-deficient animals, i.e. mice and chicken, that are associated with craniofacial structure formation, including palate morphogenesis. Further, we evaluated possible changes of neurogenesis-specific genes in *Cdk13*-deficient animals and tested the effect of the CDK12/13 inhibitor THZ531 on axon outgrowth from the embryonic trigeminal ganglion.

RESULTS

***Cdk13* deficiency causes craniofacial anomalies, including severe facial clefting**

In our previous study, we observed craniofacial developmental anomalies caused by *Cdk13* deficiency, which resulted either in a less severe phenotype in hypomorphic embryos [secondary palate dysmorphisms at embryonic day 15.5 (E15.5)] or in a more severe phenotype in knockout embryos (midfacial cleft at E13.5) (Nováková et al., 2019). The morphological difference between these two *Cdk13* genotypes was explained by the residual expression of CDK13 in hypomorphic embryos – probably caused either by insertion of a neomycin selection cassette into the non-coding region, which has been shown to affect gene expression at both RNA and DNA levels, or by a high frequency of post-transcriptional exon shuffling within *Cdk13*, enabling the formation of aberrant functional *Cdk13* transcripts – compared to undetectable expression of CDK13 in knockout embryos (Nováková et al., 2019). Thus, we decided to analyze all the crucial embryonic stages of *Cdk13^{tm1a/tm1a}* and *Cdk13^{tm1d/tm1d}* mice, all of which exhibited morphological anomalies of craniofacial structures including severe clefting (Fig. 1N).

Split facial prominences and, thus, a widely opened face (i.e. midfacial cleft) were detected in *Cdk13^{tm1d/tm1d}* embryos at E11.5, revealing also the development of telencephalon in the midline (Fig. 1A"). In *Cdk13^{tm1a/tm1a}* embryos at the same embryonic stage, we detected widely set facial prominences (Fig. 1A"). Measurements of distances between individual facial prominences revealed a significantly greater ratio of nasal pits distances and head width in maxillary prominence and lateral nasal prominence levels in both mutant genotypes (Fig. 2A-C). Widely set facial prominences at earlier embryonic stages then progress at E12.5 to median cleft lip in *Cdk13^{tm1a/tm1a}* embryos (Fig. 1B',H') but persisted in *Cdk13^{tm1d/tm1d}* embryos, leading to the development of midfacial cleft (Fig. 1B",H"). Delayed development of the palatal shelves (Fig. 1E',K',K") with cleft nasal septum (Fig. 1K',K") was detected in both mutant genotypes. Later, at E13.5 and E14.5, *Cdk13^{tm1a/tm1a}* embryos displayed thinner lips with increased distance between (Fig. 1F',I',G',J') and delayed development of the palatal shelves (Fig. 1F',L',G',M'), while *Cdk13^{tm1d/tm1d}* embryos exhibited a severe midfacial cleft (Fig. 1C",I",D",J") and persisting nasal septum cleft (Fig. 1L",M"). Less severe anomalies were detected in the caudal palate area, in which underdeveloped palatal shelves were the most prominent feature, especially in *Cdk13^{tm1d/tm1d}* embryos (Fig. S1E-G). For *Cdk13^{tm1a/tm1a}* embryos observed at the latest embryonic stage (i.e. E16.5), improperly fused lips in the midline as well as cleft palate persisted within the rostral and caudal areas, accompanied with necrotic tissue that was visible within all structures (Fig. S1B-B",D,D'). This confirmed embryonic lethality after E15.5, which had also been noticed previously (Nováková et al., 2019).

Based on craniofacial morphometrics, heads and individual facial prominences are generally smaller in *Cdk13*-deficient embryos. Thus, we quantified gene expression of *CyclinD1*, a gene responsible for cell cycle progression from G1 to S phase and used it as a marker of proliferation to see if there is a change in proliferation rates. Compared

with control embryos, *CyclinD1* expression was detected to be upregulated in almost all tissues isolated from facial prominences at E11.5 and E12.5 of *Cdk13*-deficient embryos (Fig. 2E). Although the palatal shelves in *Cdk13*-deficient animals were generally smaller and exhibited a different shape, there were no significant changes detected in *CyclinD1* expression in the palatal shelves of E12.5 *Cdk13^{tm1a/tm1a}* embryos. A slight downregulation of *CyclinD1* was detected in both palatal regions isolated from E14.5 *Cdk13^{tm1a/tm1a}* mice (Fig. 2E). Additional immunostaining for Ki-67 and TUNEL assays confirmed no significant changes in proliferation and apoptosis within the developing palatal shelves of *Cdk13^{tm1a/tm1a}* embryos (Fig. S2A-C).

Expression of *Cdk13* mRNA is dispersed through developing facial regions

As we observed distinct changes in facial and palatal morphogenesis in *Cdk13*-deficient embryos, we asked if there is localized expression of *Cdk13* mRNA within certain areas during craniofacial development. We evaluated gene expression of *Cdk13* on frontal sections to reveal possible differences in its distribution along the labio-lingual axis of the palatal shelves. In embryos between E12 and E14, the *Cdk13* signal was spread evenly within the palatal mesenchyme and epithelium of the palatal shelves (Fig. 3A-C). Later, at E15, we detected increased expression of *Cdk13* in the palatal mesenchyme, close to the region of fusion in the craniofacial midline (Fig. 3D). In the developing snout, intensity of the *Cdk13* signal was similar in the surface epithelium and mesenchyme. A visibly stronger signal was detected in the forebrain (Fig. 3F) and nasal epithelium at E11 (Fig. 3F",F"), and in the maxillary mesenchyme at E12 (Fig. 3G). At later stages (E13, E14), *Cdk13* mRNA was evenly spread in the developing snout in both mesenchyme and epithelium (Fig. S3). Quantification of relative *Cdk13* expression by qPCR revealed decreasing levels in the palatal area throughout the development (Fig. 3H) and increasing levels in the maxillary, mandibular and nasal prominences between E11.5 and E12.5 (Fig. 3I).

To uncover possible differences of *Cdk13* distribution along the rostral-caudal axis of the developing palate, we analyzed its expression in the sagittal sections. During earlier developmental stages (E11-E14), *Cdk13* was expressed in both rostral and caudal areas of the developing palatal shelves, with higher *Cdk13* signal intensity detected in the rostral region compared to that in caudal areas (Figs S4A-D and S5). Changes emerged in older embryos (E15-E16), where we observed strong expression of *Cdk13* in the palatal epithelium and adjacent mesenchyme, especially in the developing palatal rugae, both in the rostral and caudal regions (Fig. S4E,F).

CDK13 is located in cellular outgrowths as well as long neural processes

Next, we asked how CDK13 protein is distributed in cells *in vitro*. We analyzed its expression in cultured mouse embryonic fibroblasts (MEFs) and cells derived from DRGs (dorsal root ganglia) of adult mice as these cell types typically form long cytoplasmic processes.

In MEF cells, CDK13 was localized to the nuclear area and enriched in the cytoplasm around the nucleus (Fig. 4A). However, CDK13 protein was also detected within cellular outgrowths (Fig. 4A'-A"), including their most apical tips, where it was located together with actin filaments (Fig. 4A'). In cells isolated from DRGs, CDK13 was detected in the nuclear area, with highest levels detected in the cytoplasm adjacent to nuclei (Fig. 4B). As observed in cultured MEFs, we also detected CDK13 within long neural processes along the neurofilaments that were forming the outgrowths (Fig. 4B',B"). CDK13 in cytoplasm as analyzed by immunofluorescence staining was further evaluated by cellular fractionation followed by western

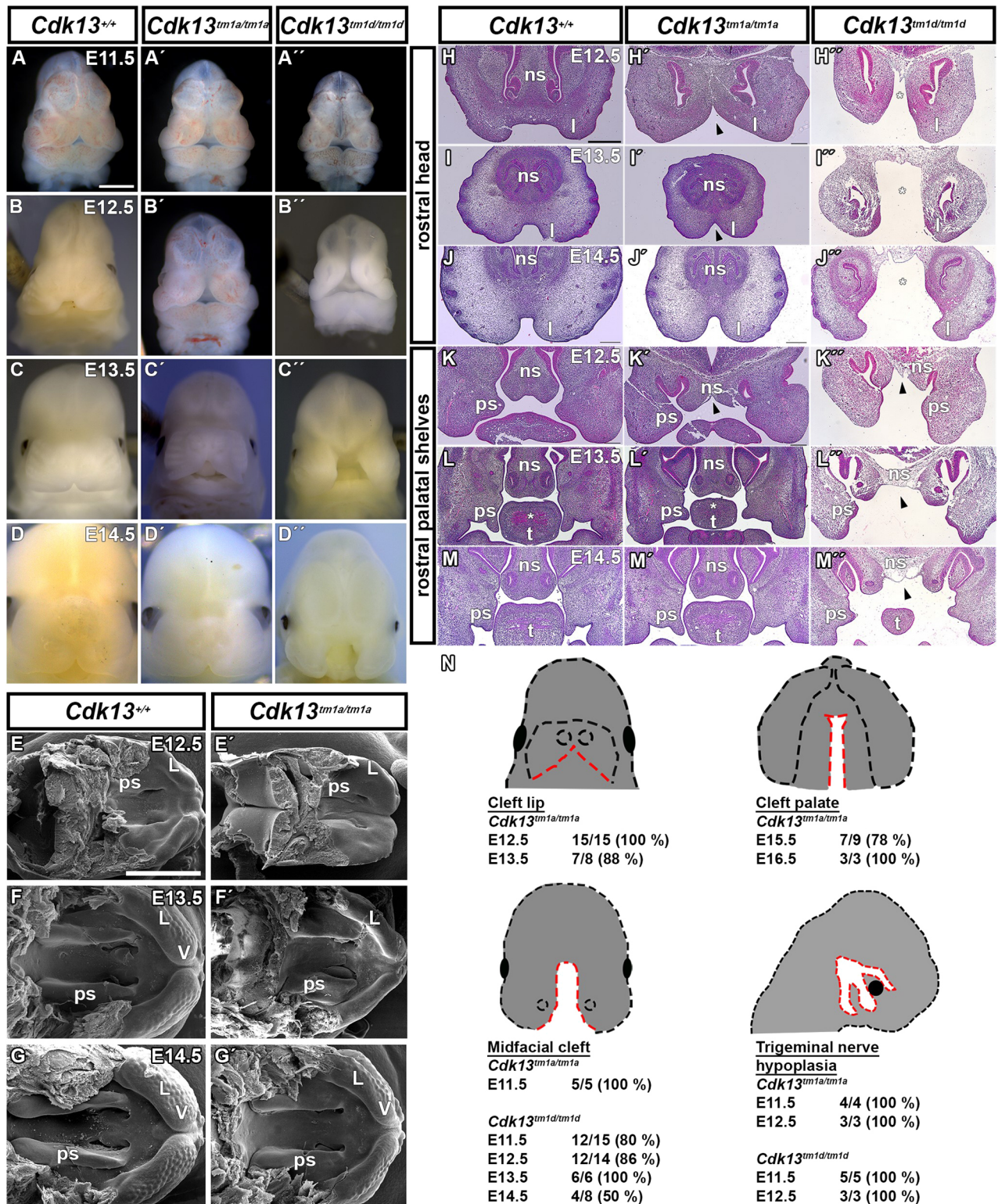


Fig. 1. *Cdk13*-deficient embryos display severe craniofacial clefting. (A-D'') Microscopy images showing external craniofacial phenotypes of WT (*Cdk13^{+/+}*), hypomorphic (*Cdk13^{tm1a/tm1a}*) and knockout (*Cdk13^{tm1d/tm1d}*) mouse embryos at different embryonic stages (E11.5-E14.5). Development of cleft lip typical for hypomorphic *Cdk13^{tm1a/tm1a}* embryos is shown in A'-D'. Development of midfacial cleft typical for knockout *Cdk13^{tm1d/tm1d}* embryos is shown in A''-D''. (E-G') Palatal view SEM images of WT and hypomorphic mouse embryos at E12.5, 13.5 and E14.5. Obvious morphological differences of the palatal shelves, as well as the formation of lips and vibrissae can be seen in hypomorphic (E'-G') compared to WT (E-G) embryos. (H-M'') H&E-stained images of mouse frontal head sections at E12.5 – E14.5. (H-J'') Arrowheads point to the cleft lip in *Cdk13^{tm1a/tm1a}* embryos and asterisks highlight the midfacial cleft in KO (*Cdk13^{tm1d/tm1d}*) embryos. (K-M'') Arrowheads point to cleft nasal septum in both hypomorph and KO embryos. The palatal shelf development in the rostral region is altered in both genotypes compared to WT embryos. Hypoplastic muscles in the tongue are marked by asterisks. (N) Schematic displaying the frequency of severe craniofacial phenotypes (cleft lip, cleft palate, midfacial cleft, hypoplasia of the trigeminal nerve) within individual genotypes and embryonic developmental stages. Red dashed lines contour anomalous structures. L, lip; ns, nasal septum; ps, palatal shelf; t, tongue; V, vibrissae. Scale bars: 1 mm (A-G'), 500 μ m (H-M'').

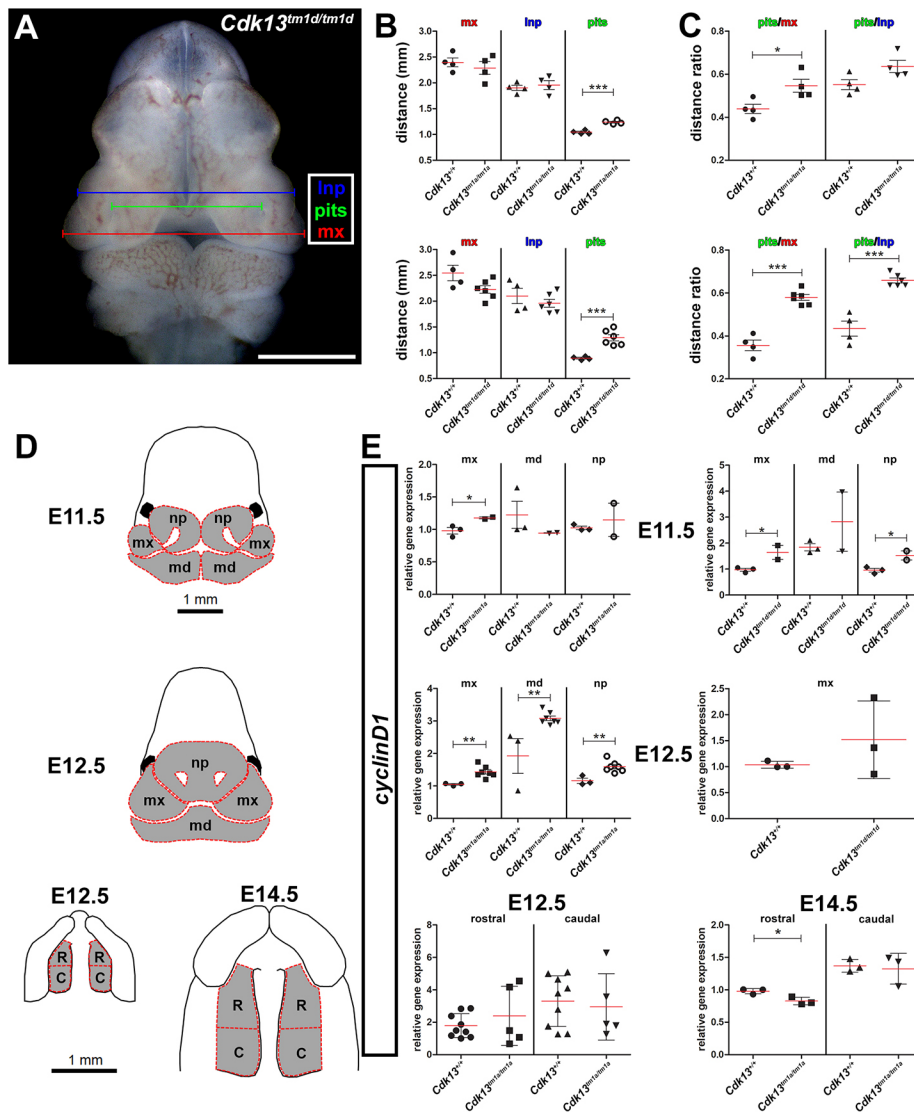


Fig. 2. Changes in facial morphometrics and cell proliferation in *Cdk13* mutant embryos. (A) Representative microscopy image of an embryonic *Cdk13^{tm1d/tm1d}* mouse head outlining the measurements performed at E11.5 in mice as indicated in B-C. Measured were the distances between edges of the lateral nasal prominences (blue), edges of the maxillary prominences (red) and nasal pits (green). (B,C) Individual graphs displaying the distance (B) (in mm) measured in WT, hypomorphic and knockout embryos at E11.5 and the ratio (C) calculated from these distances. (D) Schematics outlining how individual tissues were dissected to quantify *CyclinD1* gene expression in the mx, md and np, and R and C palatal shelves of mice at E11.5 and E12.5. (E) Quantification of the proliferation changes detected in the mx, md and np facial parts, and rostral and caudal palatal shelves of hypomorphic embryos at E12.5 and E14.5 by measuring the relative *CyclinD1* gene expression using qPCR. Student's *t*-test; error bars indicate \pm s.e.m. * $P < 0.05$, ** $P < 0.01$, *** $P < 0.001$. C, caudal palate; Inp, lateral nasal prominence; md, mandibular prominence; mx, maxillary prominence; np, nasal pits; R, rostral palate.

blotting for CDK13. As expected, CDK13 was detected in the nuclear fraction of primary MEF cells; however, significant levels of CDK13 were also detected in the cytoplasmic fraction (Fig. 4C). Moreover, the mouse fibroblast cell line NIH3T3 was used to assess the subcellular localization of CDK13, and CDK13 was found in both cytoplasmic and nuclear cellular fractions, with higher levels in the nuclear fraction (Fig. 4D).

Hypomorphic mutation causes production of a truncated form of CDK13, with preserved N-terminal domain (Nováková et al., 2019). This form of CDK13 aggregated in the cellular processes together with deposits of F-actin in E12.5 *Cdk13^{tm1a/tm1a}* MEFs (Fig. S6A). Similarly, aggregates of truncated CDK13 were located in protrusions of cells isolated from E12.5 *Cdk13^{tm1d/tm1d}* DRGs (Fig. S6B). Additionally, live cell imaging of MEF cells revealed different numbers of cellular protrusions per cell in *Cdk13^{tm1d/tm1d}* cells (Fig. S6C, top) compared to control cells. This was associated with the more-stretched morphology of cultured *Cdk13^{tm1d/tm1d}* cells (Fig. S6D), their weaker adherence to culture plates and easier release from plates during trypsin digestion (data not shown). However, cellular velocity (Fig. S6C, bottom) and the percentage of the cellular surface being protruded (Fig. S6C, middle) showed no statistically significant difference between either genotype in MEF cultures.

This specific cellular localization of the CDK13 to cellular protrusions indicates a potential cytoplasmic role of the CDK13 protein. However, when we performed detection of ICC signal by polyclonal anti-CDK13 antibodies, we revealed a reduction of the CDK13-specific signal in nuclei (see arrowheads in Fig. S6E) but not in the cytoplasm surrounding the nuclei or the cellular protrusions of *Cdk13^{tm1d/tm1d}* cells (Fig. S6E), indicating primary effect of *Cdk13* deficiency in nuclei.

***Cdk13* deficiency results in development of hypoplastic cranial nerves**

Development of the craniofacial region is closely associated with the development of cranial nerves. A large area is innervated by the trigeminal nerve comprising three main branches, i.e. the maxillary, mandibular and ophthalmic branch (Higashiyama and Kuratani, 2014). We detected complex spatial *Cdk13* gene expression in the developing maxillary nerve in cells that ensheath bundles of nerve fibers (Fig. S7A-E'). As the CDK13 has been demonstrated to regulate neurite outgrowth (Chen et al., 2014), we hypothesized that alteration of cranial nerve growth occurs during early craniofacial development in *Cdk13*-deficient animals.

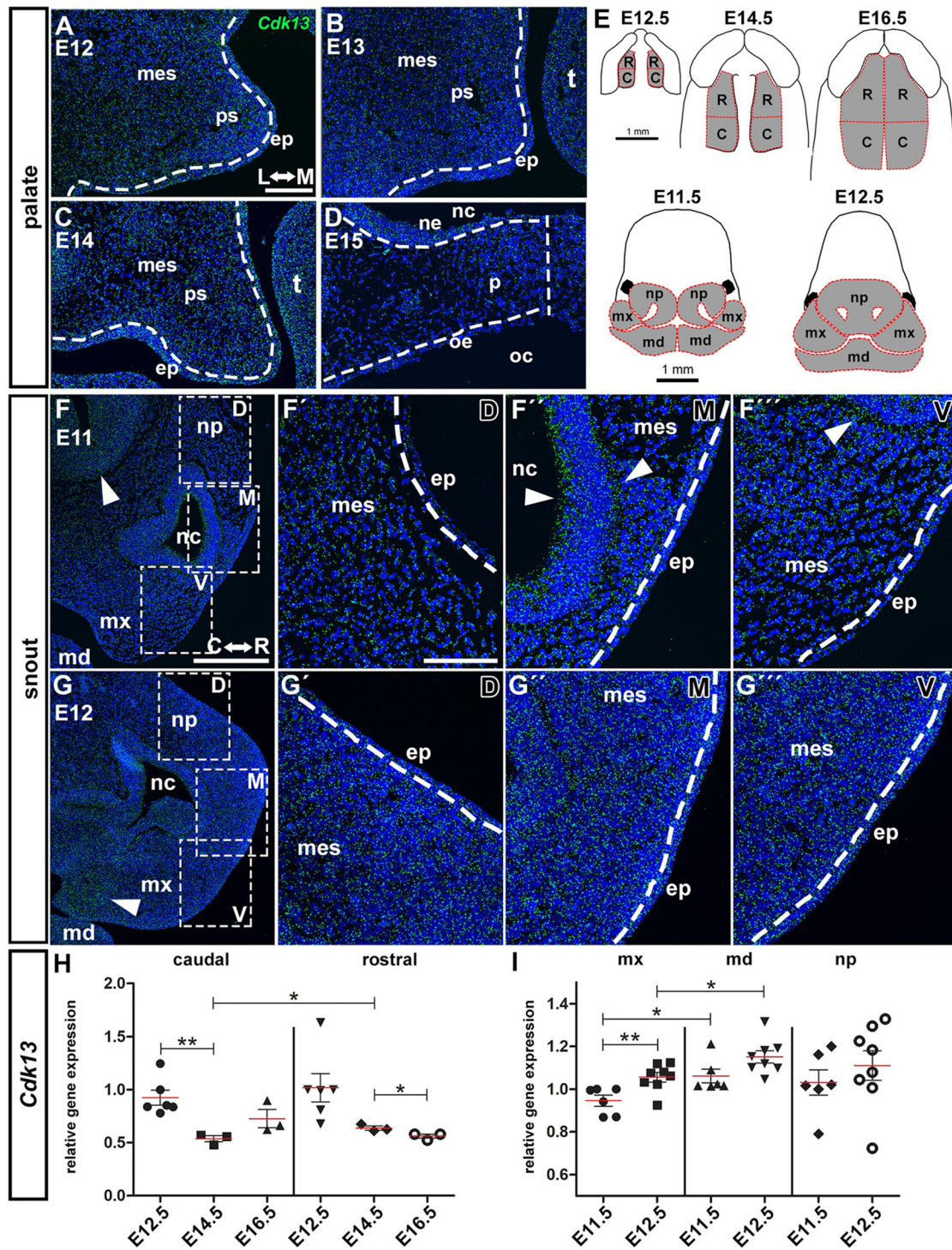


Fig. 3. Physiological gene expression of *Cdk13* within developing palatal tissues and snout detected by RNAScope and quantified by qPCR. (A–D) *Cdk13* (green) gene expression (RNA levels) in the developing palatal shelves of WT mice between E12 and E14, and in the fused secondary palate on transversal sections at E15. White dashed lines separate mesenchyme from epithelium. Vertical white dashed line (D) highlights the secondary palate midline at E15. L↔M, lateral↔medial. (E) Schematics showing how individual tissues were dissected to quantify *Cdk13* gene expression. RNA expression was quantified in tissues dissected from rostral (R) and caudal (C) palatal shelves or palates at E12.5, E14.5 and E16.5 and in tissues dissected from mx, md and np at E11.5 and E12.5. (F, G') Lower power magnification of *Cdk13* gene expression in the developing snout of WT embryos at E11 and E12. Boxed areas in F and G are shown at higher magnification in panels F'-F''' and G'-G''', respectively, which show dorsal (D); middle (M) and ventral (V) areas as indicated in the top right of each image. Arrowheads indicate higher *Cdk13* signal intensity in the developing forebrain (F) and nasal epithelium (F'', F''') at E11, and the developing maxillary prominence (G) at E12. Dashed lines separate mesenchyme and epithelium. Nuclei were counterstained with DAPI. C↔R, caudal↔rostral. (H) Quantification of *Cdk13* gene expression after using qPCR in palatal shelves at E12.5, E14.5 and E16.5. (I) Quantification of the *Cdk13* gene expression by qPCR in mx, md and np at E11.5 and E12.5. Unpaired two-tailed Student's *t*-test; **P*<0.05; ***P*<0.01; ****P*<0.001. C, caudal; ep, epithelium; md, mandibular prominence; mes, mesenchyme; mx, maxillary prominence; nc, nasal cavity; ne, nasal epithelium; np, nasal prominence; oc, oral cavity; oe, oral epithelium; p, palate; ps, palatal shelf; R, rostral; t, tongue. Scale bars: 100 μ m (A–D, F'–G'), 200 μ m (F', G').

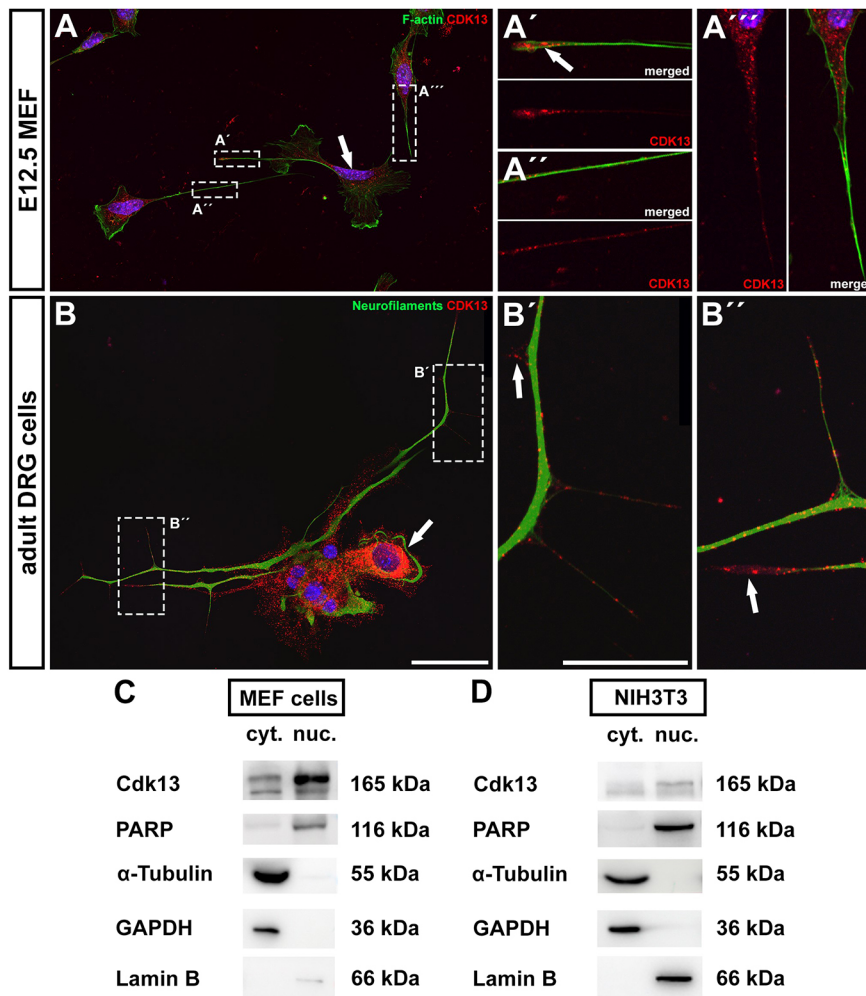


Fig. 4. CDK13 cellular localization using immunocytochemistry and western blotting. (A-A'') Immunofluorescence images of mouse embryonic fibroblasts (MEFs) isolated from embryonic bodies at E12.5, stained for CDK13 (red) and F-actin (green). Boxed areas indicate details of cellular outgrowths and are shown magnified in A'-A''' as indicated. Arrows point to the nuclear area (A) and cellular outgrowths (A') with increased CDK13 expression. (B-B'') Immunofluorescence images of primary cells isolated from dorsal root ganglia of adult mice stained for CDK13 (red) and neurofilaments (green; anti-neurofilament antibody 2H3). Boxed areas indicate neurite outgrowths and are shown magnified in B'-B'' as indicated. Arrows point to the nuclear area (B) and neurite outgrowths (B',B'') with CDK13 expression. Nuclei were counterstained with DAPI. Scale bars: 50 μ m (A,B), 20 μ m (A'-B''). (C,D) Western blotting for CDK13 in cytoplasmic (cyt.) and nuclear (nuc.) extracts from primary MEF cells (C) and NIH3T3 mouse fibroblasts (D), showing CDK13 levels in both nuclear and cytoplasmic fractions. Lamin B and PARP1 were used as positive loading controls for the nuclear fraction; α -tubulin and GAPDH were used as positive loading controls for the cytoplasmic fraction.

First, we visualized outgrowth of cranial nerves by whole-mount immunohistochemistry analysis of neurofilaments to uncover possible alterations of general morphology of trigeminal nerve and associated nerves. Alterations regarding the outgrowth of several cranial nerves were detected in *Cdk13^{tm1a/tm1a}* and *Cdk13^{tm1d/tm1d}* embryos (Fig. 5B,C'), with obvious hypoplasia of maxillary, mandibular and ophthalmic nerves, which were reduced in length. These nerves originate from the trigeminal ganglion (TG), which we also found to be abridged in the mutant embryos (Fig. 5B',C'). Only the frontal nerve (frN) was not morphologically altered (Fig. 5B',C'). This confirms that *Cdk13* deficiency negatively affects neurogenesis during embryonic development.

As observed by using whole-mount immunohistochemistry, changes of nerve protrusions were even more obvious on transversal sections of E11.5 *Cdk13^{tm1d/tm1d}* embryos. In the rostral region, we observed missing maxillary nerves in the developing maxillary prominence (Fig. 5D',E'; Fig. S8A',B'), hypoplastic MnNs in the mandibular prominence (Fig. 5E') and reduced size of the TG (Fig. S7F,G) confirming anomalies regarding nerve growth in *Cdk13*-deficient animals.

Changes in the expression of key developmental genes and proteins during early craniofacial development of *Cdk13*-deficient embryos

We also detected alterations in the expression patterns of genes and proteins strongly associated with craniofacial development, and

specifically enriched in mesenchymal (*SOX9*, *Msx1*, *Foxd1*) and epithelial structures (*SOX2*, *Meis2*, *Shh*) in this region. In E11.5 *Cdk13^{tm1d/tm1d}* embryos, we observed very low levels of the neural crest marker *SOX9* in the mesenchyme of lateral nasal prominences and maxillary prominences, including an area with undeveloped maxillary nerves (Fig. 5D'; Fig. S8A'). However, the pattern of *SOX2*, one of the regulators of neural cells differentiation and peripheral nervous system development (Adameyko et al., 2012), was similar to that in wild-type (WT) embryos, only missing in the area of the prospective maxillary nerve (Fig. 5E'; Fig. S8B'). Expression of *Meis2*, a gene involved in cranial neural crest development (Machon et al., 2015), was absent from the neural tube in the rostral area (Fig. 6A, see arrow at the top, indicating nt) and less expressed in the same tissue more caudally. Moreover, *Meis2* expression was detected caudally, close to the facial midline in knockout (Fig. 6A, asterisks) but not in WT mice. Conversely, *Meis2* was enriched in the mesenchyme of the rostral medial nasal prominences (Fig. 6A). *Msx1*, a key player in craniofacial development (Levi et al., 2006), was absent from the mesenchyme of the medial nasal prominences (asterisks) and also from the brain close to its midline (Fig. 6B). However, analysis of genes necessary for determination and development of facial primordia (Jeong et al., 2004), revealed that expression of *Shh* was enhanced in the ventral neural tube within the rostral region but also, to a similar extend, in the developing brain more caudally (Fig. 6C, arrows). Its altered expression pattern in the epithelium covering the forming stomodeal cavity was detected rostrally (Fig. 6C). Moreover,

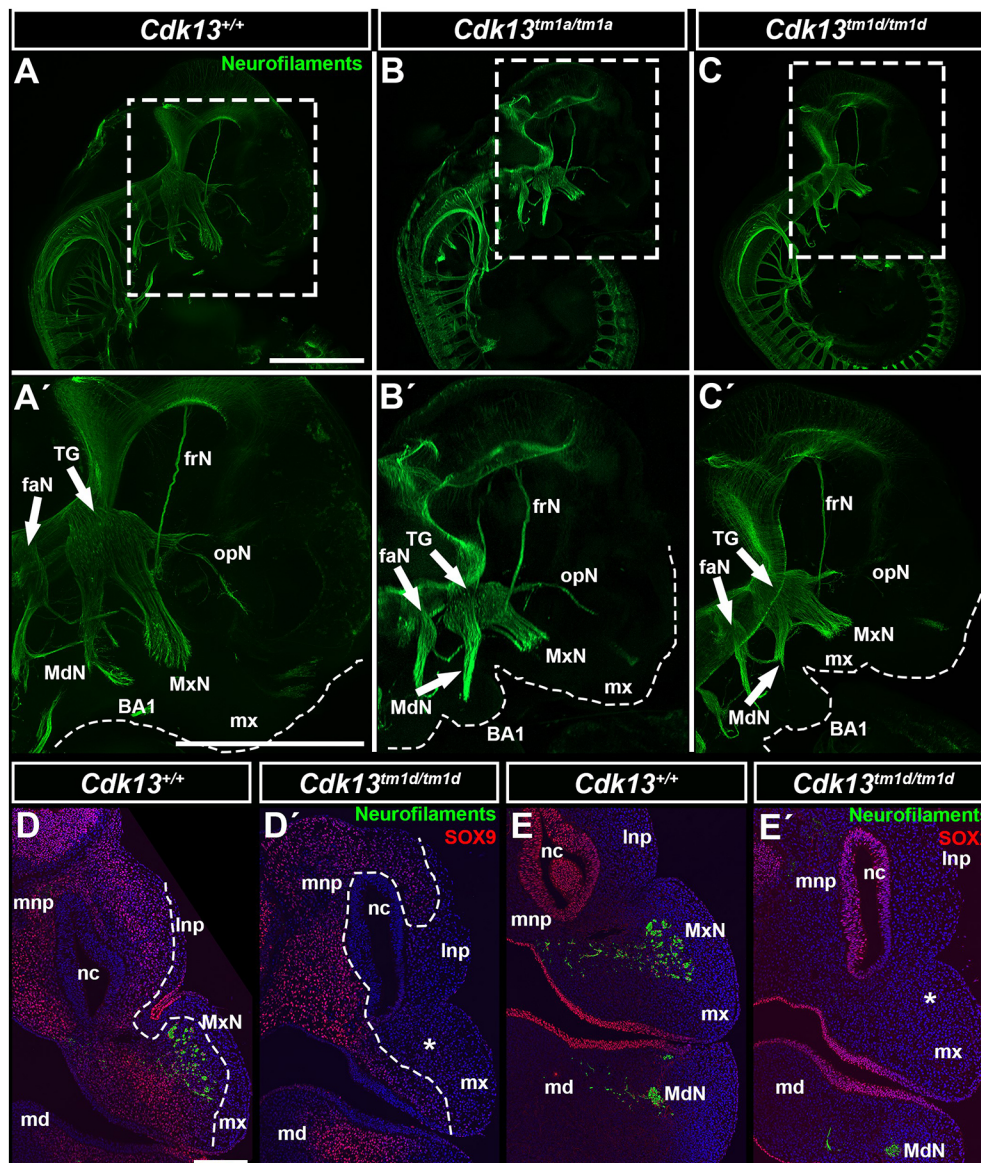


Fig. 5. Immunohistochemical detection of cranial nerves on whole-mount embryos and histological sections. (A-C') Whole-mount images stained to detect developing neurons (green) staining anti neurofilament antibody (anti-2H3) in WT, *Cdk13^{tm1a/tm1a}* and *Cdk13^{tm1d/tm1d}* embryos at E11.5. Dashed line rectangles highlight detail of the craniofacial region. Boxed areas are shown magnified in A'-C'. Detail displays the basis of the facial nerve, and divisions of the trigeminal nerve – mandibular, maxillary and ophthalmic nerves, including the frontal branch nerve of the ophthalmic nerve. Dashed lines indicate the edge of the maxillary prominences and the first branchial arch (BA1). Note underdeveloped and hypoplastic all three divisions of the trigeminal nerve in *Cdk13^{tm1a/tm1a}* (B') and especially in *Cdk13^{tm1d/tm1d}* (C') embryos. (D-E') Immunohistochemistry images stained to detect neurofilaments (green), as well as SOX9 and SOX2 (red) within frontal sections of E11.5 embryos. Missing maxillary nerves in *Cdk13*-deficient embryos are marked by asterisks in D' and E'. Dashed lines in D and D' indicate areas of SOX9 expression in D and D'. Scale bars: 1 mm (A-C'); 20 μm (D-E'). BA1, branchial arch 1; faN, frontal and acoustic nerve; frN, frontal branch of the ophthalmic nerve; Inp, lateral nasal prominence; md, mandibular prominence; MdN, mandibular branch of the trigeminal nerve; mx, maxillary prominence; MxN, maxillary branch of the trigeminal nerve; nc, nasal cavity; opN, ophthalmic branch of the trigeminal nerve; TG, trigeminal ganglion.

enhanced expression of *Foxd1*, which is expressed downstream of *Shh*, in the developing mandibular prominences points to altered development of the lower jaw (Fig. 6D). Finally, expression of *Fgf8* was absent in the epithelium of the developing primitive oral cavity close to the head midline (Fig. 6E, arrows and asterisks) and its expression was reduced in the developing brain (Fig. 6E, asterisks). This confirmed that *Cdk13* deficiency leads to deregulation of these key developmental genes already in early craniofacial development, subsequently resulting in severe facial clefting.

***Cdk13* deficiency alters expression of neurogenesis-specific genes and key morphogenic proteins in the developing secondary palate**

To further evaluate alterations in the expression of genes relevant to neurogenesis during palatogenesis in *Cdk13^{tm1a/tm1a}* embryos, we used PCR array analysis to simultaneously investigate the expression profile of 84 neurogenesis-specific genes. In separately dissected tissues from rostral and caudal palatal shelves (Fig. 7A), we first compared expression of neurogenesis-specific genes in rostral and caudal palatal regions (Table S1-S4).

Of all genes analyzed this way (Fig. 7A), 15 genes (*Ache*, *Apoe*, *Bmp2*, *Dcx*, *Fgf2*, *Heyl*, *Mef2c*, *Neurod1*, *Neurog1*, *Nog*, *Nrg1*, *Ntn1*, *Pou4f1*, *S100a6* and *Sox3*) were found to be significantly enriched in caudal compared to rostral palatal shelves in control (WT) embryos at E12.5 (Fig. 7B, top left panel). The same comparison between rostral and caudal palatal shelves in *Cdk13^{tm1a/tm1a}* embryos at E12.5 determined a preserved gene expression ratio only for *Bmp2* – probably caused by the downregulation of expression of caudal palatal shelf-dominant genes (*Ache*, *Dcx*, *Ntn1*, *Pou4f1*, *Bdnf*, *Bmp2*, *Ep300*, *Fgf2*, *Heyl*, *Mef2c*, *Kmt2a*, *Neurog1*, *Nfl*, *Nog*, *Notch2*, *Nrg1* and *S100a6*) in the caudal palatal shelves (Fig. 7C, right panel). By contrast, a change in ratio was detected for *Hey2* and *Ntn1*, whose expression was – conversely – enriched in the rostral palatal shelves (Fig. 7B, top right panel), caused by extreme upregulation of both genes in mutant embryos (Fig. 7C, left panel).

In control embryos at a later stage, i.e. at E14.5, ten genes were enriched in rostral palatal shelves (*Artn*, *Bcl2*, *Bmp2*, *Gdnf*, *Hey1*, *Neurog2*, *Pax3*, *Pou3f3*, *Slit2* and *Tgfb1*) and 15 genes in caudal palatal shelves (*Ache*, *Apoe*, *App*, *Cdk5r1*, *Dvl3*, *Fgf2*, *Map2*, *Ndn*, *Nfl*, *Ntf3*,

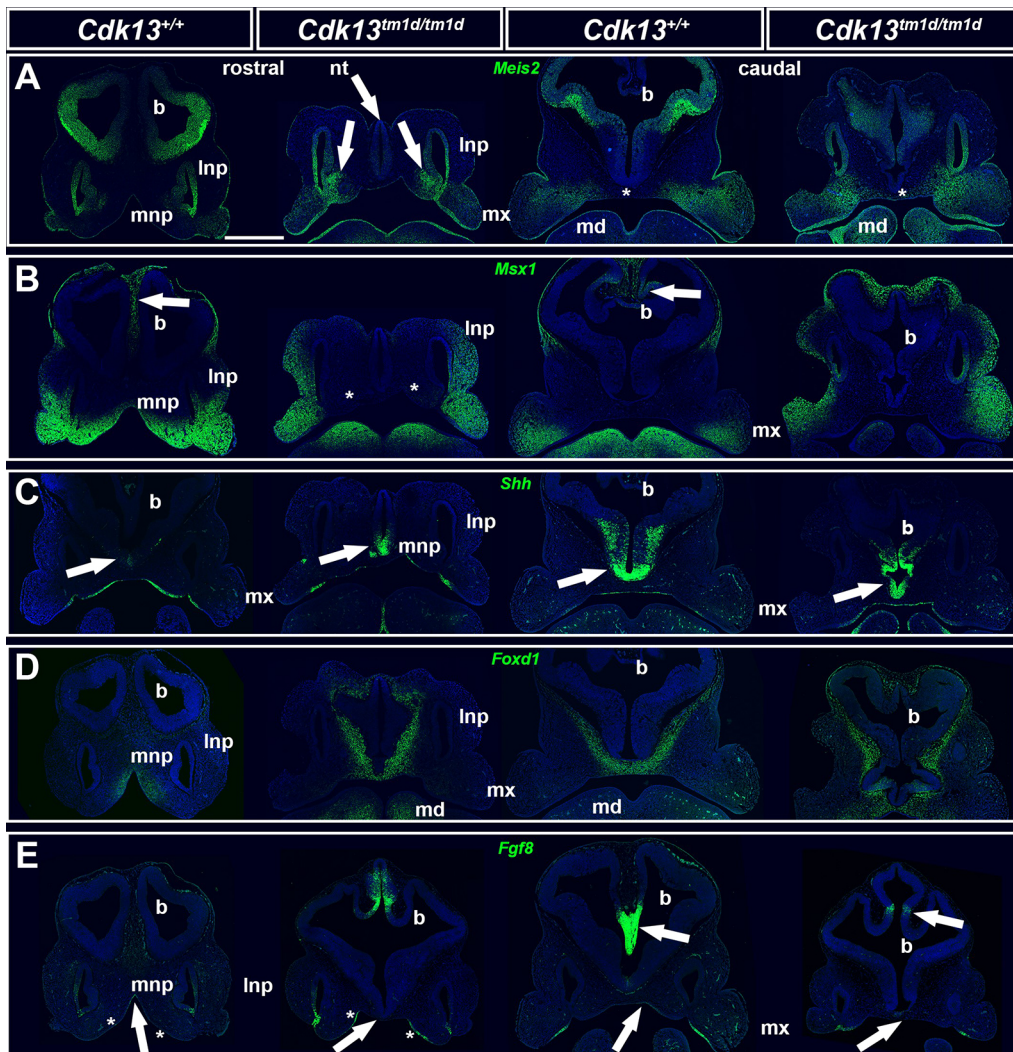


Fig. 6. RNAScope detection of *Meis2*, *Msx1*, *Shh*, *Foxd1* and *Fgf8* gene expression within frontal sections of WT and mutant mouse embryos at E11.5. RNAScope fluorescence images showing changes of gene expression patterns in the maxillary prominence (mx), mandibular prominence (md), lateral nasal prominence (lnp) and medial nasal prominences (mnp) and the developing brain from WT (*Cdk13*^{+/+}) and *Cdk13*-knockout (*Cdk13*^{tm1d/tm1d}) embryos. (A) *Meis2* gene expression. Arrows point to *Meis2* expression in the mesenchyme of the np and to lack of rostral expression in the nt of mutant. Asterisks indicate caudal differences in *Meis2* expression within the median mesenchyme. (B) *Msx1* gene expression. Arrows point to *Msx1* expression within WT brain. Asterisks indicate lack of *Msx1* expression in the mnp of mutant. (C) *Shh* gene expression. Arrows point to changes in the pattern of expression domains within the developing brain in WT and mutant. (D) *Foxd1* gene expression. Note the enhanced expression of *Foxd1* in mesenchyme around the nt in the rostral area of the *Cdk13* knockout compared to only trace amount around the brain in the WT embryo. (E) *Fgf8* gene expression. Arrows point to changes in *Fgf8* expression pattern in the epithelium, covering the middle area of the presumptive oral cavity, and the brain. Asterisks indicate changes in *Fgf8* expression pattern in the epithelium, covering the lateral area of the presumptive oral cavity within the rostral region. Individual gene expression patterns are shown in green. For each set of images, rostral sections are shown in the first two panels (from left) and caudal sections are shown in the last two panels (from left). Scale bar: 500 μ m. b, brain

Ntn1, *Pafah1b1*, *Pou4f1*, *Robo1* and *Rtn4*), (Fig. 7B, bottom left panel). Again, the same comparison between rostral and caudal palatal shelves, this time in E14.5 *Cdk13*^{tm1a/tm1a} embryos, revealed a preserved gene expression ratio for 11 genes (*Ache*, *App*, *Bcl2*, *Fgf2*, *Hey1*, *Nf1*, *Ntn1*, *Pax3*, *Pou3f3*, *Slit2* and *Tgfb1*) in E14.5 *Cdk13*^{tm1a/tm1a} embryos. Generally, deregulation of the neurogenesis-specific genes in the E14.5 palatal shelves was not as substantial (Fig. 7D) as was in case for E12.5 (Fig. 7C). But, in both observed embryonic stages, gene expression was generally downregulated in the caudal compared to the rostral region, whereas in the rostral region both up- and downregulation of gene expression was detected (Fig. 7C,D).

Moreover, altered expression patterns of palatal genes and proteins were detected later at E12.5 and E14.5. *Cdk13*-deficiency

leads to noticeable reduction of *Foxd1* expression in the mesenchyme of snout midline (Fig. 7F,G), *Msx1* reduction in the rostral palatal shelves (Fig. 7J,K) and also reduction of *Meis2* in the caudal palatal shelves (Fig. 7L,M), especially at E12.5. Levels and distribution of both SOX9 and SOX2 were similar to those observed for WT animals (Fig. 7H,I).

Cdk13* deficiency results in changes of RNAPII occupancy within promoters of *Pou4f1* and *Ntn1

To address the effect of CDK13 depletion on transcription, we performed chromatin immunoprecipitation (ChIP) with an antibody specifically recognizing RNA polymerase II (RNAPII) and IgG as a negative control (Fig. S9). For two genes selected from the PCR

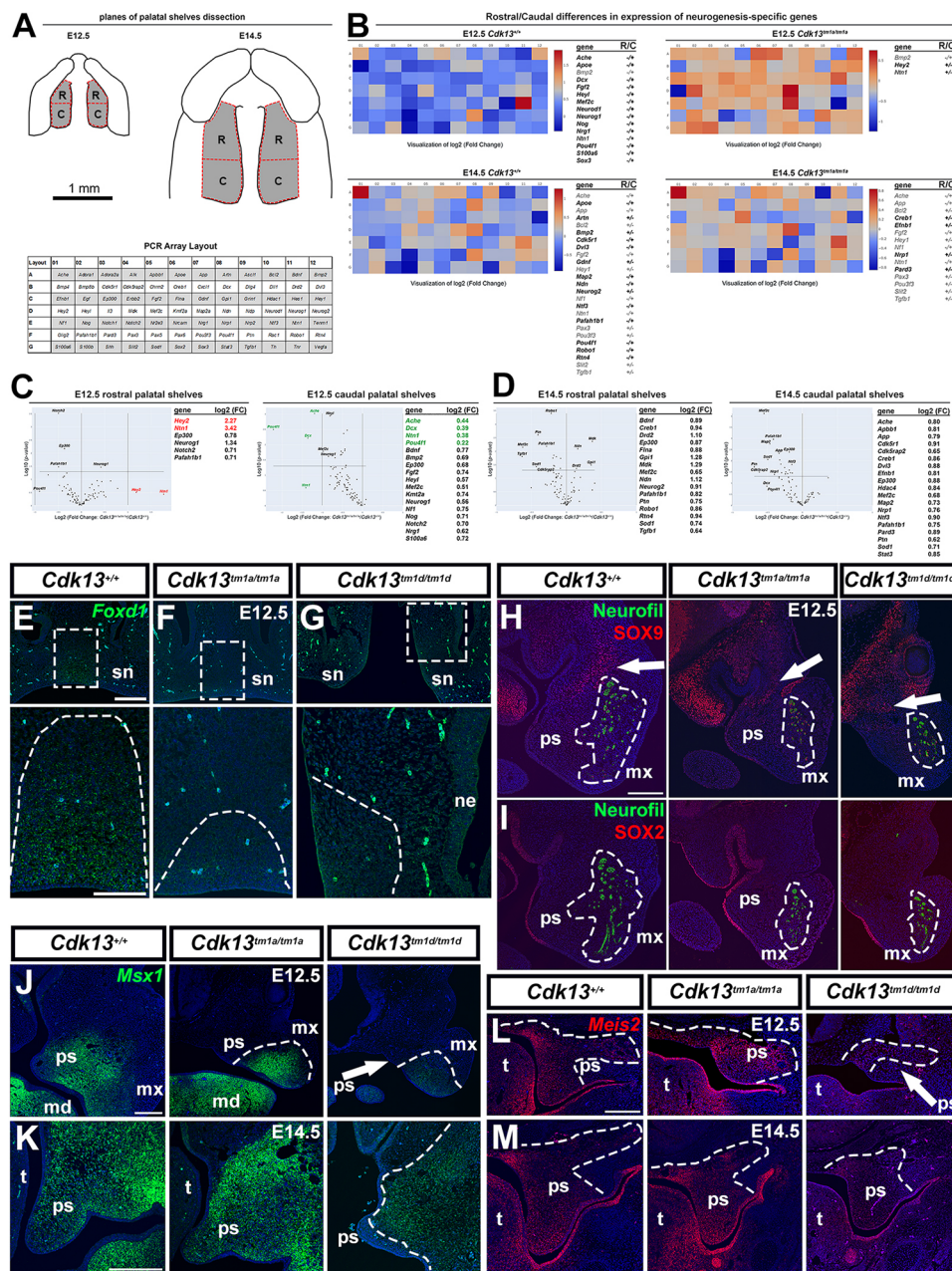


Fig. 7. Quantification of neurogenesis-associated gene expression in the palatal shelves of WT and *Cdk13^{tm1a/tm1a}* mice, and *in situ* gene and protein expression within sections obtained from WT and mutant mice. (A-D) PCR Array results for mouse neurogenesis-specific genes performed separately on tissues dissected from rostral and caudal palatal shelves of WT and *Cdk13^{tm1a/tm1a}* embryos at E12.5 and E14.5. (A) Schematics showing dissected rostral (R) and caudal (C) regions of the palatal shelves at E12.5 and E14.5, and the layout of the PCR array analysis of individual detected genes. (B) Heat maps and lists of genes presenting rostral/caudal differences in the expression of neurogenesis-specific genes in control (WT) embryos (left panels, top and bottom) and *Cdk13^{tm1a/tm1a}* embryos (right panels, top and bottom). Genes listed in black are enriched either in the rostral or caudal palatal shelves. Genes listed in grey are expressed in the palatal regions in similar extent. Notice the changed ratio of the gene expression polarity when comparing palatal shelves of WT and *Cdk13*-deficient mice, i.e. differences between genes expressed either in the rostral or caudal palatal shelves are much less in *Cdk13*-deficient tissues. (C,D) Volcano plots and log2-fold changes individually displaying significantly deregulated expression of neurogenesis-specific genes in *Cdk13*-deficient palatal shelves at E12.5 (C) and E14.5 (D). Genes listed in red are strongly upregulated and genes listed in green text are strongly downregulated in *Cdk13*-deficient embryos compared to control embryos. *P* values were calculated based on Student's *t*-test of replicate 2^{n-1} (Δ C_T) values for each gene in control and test groups. *P*-value calculation used was based on parametric, unpaired two-sample equal variance, two-tailed distribution. (E-G) RNAScope detection of *Foxd1* (green) *in situ* gene expression in sections of the rostral snout region of WT and mutant embryos as indicated, at E12.5. Boxed areas are shown magnified below the respective panel. Dashed lines in magnified images outline areas of *Foxd1* expression (H-I) Fluorescence images of rostral snout sections as described for panels E-G, stained for SOX9 (red) or SOX2 (red) and neurofilaments (green; anti-neurofilament antibody 2H3). Arrows point to regions enriched with SOX9-positive cells. Dashed lines surround neurofilaments, indicating developing maxillary nerves. (J-K) RNAScope detection of *Msx1* (green) *in situ* gene expression in sections of the rostral palate region of WT and mutant embryos as indicated, at embryos at E12.5 and E14.5. Dashed lines outline *Msx1*-positive regions. (L-M) RNAScope detection of *Meis2* (red) *in situ* gene expression in sections of the caudal palate region of WT and mutant embryos at E12.5 and E14.5. Dashed lines outline *Meis2*-positive regions. Scale bars: 200 μ m (E-G top row; H-M), 100 μ m (E-G magnified images, bottom row). md, mandibular prominence; mx, maxillary prominence; ne, nasal epithelium; ps, palatal shelves; sn, snout; t, tongue.

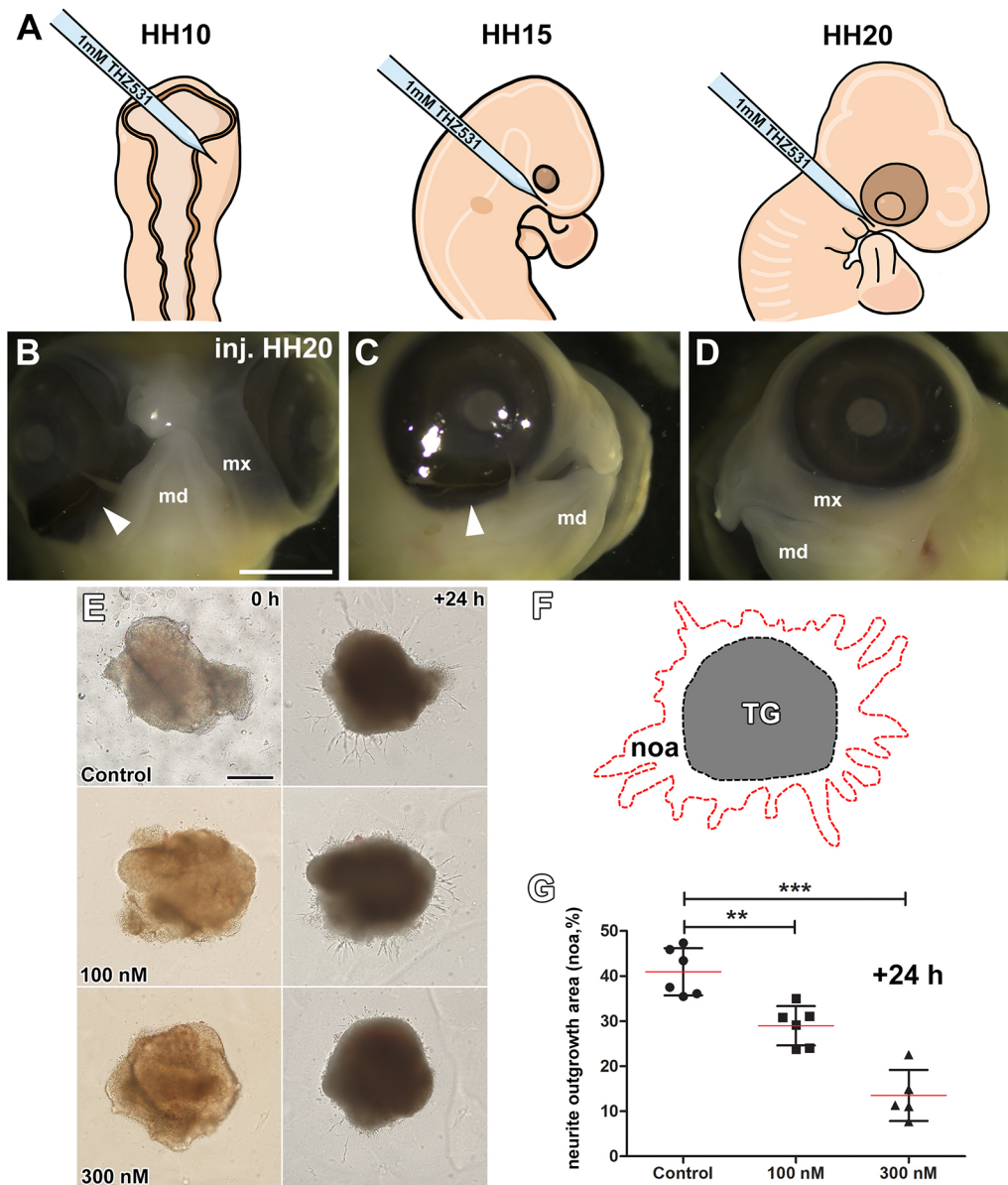


Fig. 8. Chemical inhibition of CDK12/CDK13 leads to embryonic facial malformations and altered neurite outgrowth in chicken and mouse.

(A) Schematics showing the injection side of the CDK12/CDK13 inhibitor THZ531 to the maxillary prominences in chicken at HH10, HH15 or HH20 followed by 4-6 days of incubation. (B-D) Macroscopic images showing the ventral and lateral regions of embryonic chicken heads that had either been injected (on the right side of the head) with THZ531 at HH20 (B,C) or not (D). White arrowheads indicate missing maxillary prominence in the ventral (B) and lateral (C) regions after inhibition of CDK12/CDK13. This anomaly is only present in heads that had been injected with THZ531 (D). Scale bar: 3 mm. md, mandibular prominence; mx, maxillary prominence. (E) General morphology of *ex vivo* trigeminal ganglia explants from E12 WT mouse embryos that had either been injected with THZ531 (100 nM or 300 nM) or not (Control). Images were taken at the beginning (0 h) and the end (+24 h) of cultivation. Notice the different length and number of neurite outgrowths under different conditions. Scale bar: 200 μ m. (F) Schematic showing the areas used to measure the differences in neurite outgrowth area (noa; surrounded by red dashed line) from the trigeminal ganglion (TG; grey area surrounded by black dashed line). (G) Bar graph showing the neurite outgrowth area (in %) in WT trigeminal mouse ganglia cultivated for 24 h without (control), or with 100 nM or 300 nM of the CDK12/CDK13 inhibitor THZ531. Unpaired two-tailed Student's *t*-test; error bars indicate \pm s.e.m.; ** P <0.01, *** P <0.001. Replicates: Control (n =6), 100 nM (n =6), 300 nM (n =5).

array analysis (Fig. 7), i.e. *Pou4f1* and *Ntn1*, we decided to evaluate the presence of RNAPII within their promoter regions in MEF cells obtained from *Cdk13*^{+/+} and *Cdk13*^{tm1d/tm1d} mice. Increased levels of RNAPII within either promoter of *Pou4f1* and *Ntn1* were observed in comparison to IgG control (Fig. S9A,B). In the case of the *Pou4f1* promoter, we detected less RNAPII in MEF cells obtained from *Cdk13*^{tm1d/tm1d} compared to those obtained from *Cdk13*^{+/+} mice (Fig. S9A). In contrast, RNAPII was associated more with the *Ntn1* promoter in *Cdk13*^{tm1d/tm1d} MEFs than in

Cdk13^{+/+} MEF cells (Fig. S9B). We then decided to compare the presence of RNAPII on these promoters as a percentage of RNAPII compared to IgG control. A slight decrease of RNAPII was observed for the *Pou4f1* promoter in *Cdk13*^{tm1d/tm1d} MEF cells compared with that in *Cdk13*^{+/+} MEFs (Fig. S9C). In contrast, higher occupancy of RNAPII was demonstrated for the *Ntn1* promoter in *Cdk13*^{tm1d/tm1d} MEFs when compared with *Cdk13*^{+/+} MEFs (Fig. S9D). Although the statistical difference for RNAPII occupancy at these promoters was not significant, the obtained

observation correlates with decreased and increased mRNA levels of *Pou4f1* and *Ntn1* genes as detected by using PCR expression screen (Fig. 7). However, future research regarding these findings will be necessary.

Chemical inhibition of the CDK13/CDK12 leads to embryonic facial malformations and altered neurite outgrowth

To confirm the effect of CDK13 deactivation on craniofacial structure formation, we used the synthetic CDK13 inhibitor THZ531 to treat early maxillary prominences of *Gallus gallus* embryos. It is necessary to note that THZ531 is also targeting CDK12, which shares several functions with CDK13 and, in developmental processes and under certain conditions, they can replace each other. Therefore, the usage of this inhibitor should prevent also compensatory mechanisms induced by CDK13 deficiency.

We injected 1 mM THZ531 into the craniofacial mesenchyme at Hamburger–Hamilton (HH) developmental stage 10 (HH10), the postoptic region at HH15 and into maxillary prominences at HH20. Then, chicken embryos were allowed to develop for 4–6 days (Fig. 8A). This led to the absence or deficiency of maxillary prominences, resulting in the unilateral cleft lip (Fig. 8B,C). Injection of THZ531 at earlier stages resulted in a stronger phenotype with high deficiency in craniofacial tissues (Fig. S10).

Furthermore, the effect of *Cdk13* deficiency on cranial nerve development as shown earlier (Fig. 5) was additionally tested by chemical inhibition of CDK13 (together with CDK12) in functional *ex vivo* cultivation experiment using TG explants (Fig. 8). TGs were dissected from E12 WT mouse embryos and cultured, while culture medium was supplemented with THZ531 (100 nM or 300 nM). A significant reduction in the formation of neurite outgrowths was observed in TGs when cultured with different concentrations of the CDK13 inhibitor THZ531 compared to control group (Fig. 8E–G), revealing the importance of both CDK13 and CDK12 in development of cranial nerves.

DISCUSSION

CDK13 controls craniofacial morphogenesis by regulating the expression of genes that are part of signalling pathways important during development

Here, we determined a key contribution of CDK13 to craniofacial morphogenesis and neurogenesis, where the phenotype of *Cdk13*-deficient animals included a smaller head and disturbed facial morphology, including facial clefts. In our mutants, we found altered expression patterns of *Msx1*, *Meis2*, *Shh*, *Foxd1* and *Fgf8* in craniofacial structures. Downregulation or upregulation of these genes or their downstream targets causes similar phenotypic craniofacial phenotypes, including facial clefts or reduced growth of facial nerves (Levi et al., 2006; Machon et al., 2015; Jeong et al., 2004). Pronounced similarities in the morphology of craniofacial structures with *Cdk13*-knockout embryos has previously been observed in mice embryos with reduced functional expression levels of *Fgf8*. These animals also exhibited abnormal midline separation with nasal prominences set widely apart (Griffin et al., 2013). Such morphological changes indicated insufficiency in the development of neural crest cells (NCCs), from which all these affected craniofacial structures originate – which we confirmed by identifying reduced protein expression of the NCC marker SOX9 in facial prominences of *Cdk13*-deficient animals. Moreover, we detected significant downregulation of *Mef2c* (in all the palatal shelves regions, except rostral E12.5 palatal shelves). Its conditional downregulation, specifically in NCCs, has previously been found to result in craniofacial anomalies and neonatal lethality (Verzi et al., 2007).

Anomalies in craniofacial morphogenesis and neurogenesis as a result of disrupted CDK-associated signaling

Similar to patients with mutations in *CDK13* or genes encoding other associated proteins, such as cyclin M, cyclin K, CDK10 (Colas, 2020) and CDK5RAP2 (Yigit et al., 2015), *Cdk13*-deficient mice produce neurogenic anomalies. These patients exhibit not just craniofacial anomalies but also affected neural tissues. Mutation in *cyclin M* results in optic nerve hypoplasia, mutation in *cyclin K* led to developmental delay and intellectual disabilities, and mutations in *CDK10* cause intellectual disabilities connected with language and learning disorders (Colas, 2020). Patients with loss-of-function mutation of *CDK5* display craniofacial anomalies other than facial clefts (short forehead, full cheeks, micrognathia), and also suffer of lissencephaly, cerebellar hypoplasia, microcephaly, intellectual disabilities, speech delay or autistic features (Colas, 2020), similar to patients with *CDK13* mutations (Hamilton and Suri, 2019).

CDK5 has a specific role in neural tissues physiology and regulates several neural processes, such as axonal transport, migration and synaptic vesicle endocytosis, and is also important for regulation of axon and neurite outgrowth (Shah and Rossie, 2018). Its knockout leads to perinatal lethality in mice, connected with deficient neuronal migration and impaired axonal transport of neurofilaments (Ohshima et al., 1996). Importantly, *in vitro* experiments using cortical neurons has demonstrated the role of CDK13 and also CDK12 in the regulation of neurite outgrowth through a common signaling pathway that involves modulation of *Cdk5* at RNA level (Chen et al., 2014). In our *Cdk13*-deficient models, we uncovered significant downregulation of genes encoding CDK5 regulatory subunits, such as *Cdk5rap2* and *Cdk5r1*, in the caudal palatal shelves at E14.5, confirming the CDK13-CDK5 functional association observed in *in vitro* experiments (Chen et al., 2014). Moreover, *CDK5RAP2* mutations in human patients cause Seckel syndrome, manifested by microcephaly and cognitive problems (Yigit et al., 2015), and *CDK5R1* was proposed to be a candidate gene in patients affected by NF1 microdeletion syndrome, which mutations lead to non-syndromic intellectual disability and undefined facial deformities (Venturin et al., 2006).

In this study, we found the CDK12/CDK13 inhibitor THZ531 to inhibit neurite outgrowths from the TG (Fig. 8E,G). Even though one could argue that the observed effect might be a result of CDK12 and CDK13 together, it is broadly accepted, that inhibition of CDK12 primarily targets DNA-damage response (DDR) pathways and pre-replication complex assembly (Pilarova et al., 2020). The process of neurite outgrowth takes place in nondividing differentiated cells of the TG; therefore, it is unlikely that altered outgrowth is the result of CDK12 inhibition due to blocking of the cell cycle in S-phase. Also, there is no significant impact of CDK12 inhibition of the DDR pathway since cells with lesser outgrowth of neurites do not exhibit any signs of DDR stress. Thus, the documented reduction in neurite outgrowth is likely a result of CDK13 inhibition through a different mechanism or, alternatively, a combinatory effect of CDK12 and CDK13 inhibition through regulation of CDK5 function in neural cytoskeleton organization; however, this needs further experimental evidence.

Effect of CDK13 on neurogenesis-specific gene expression and cranial nerve development

CDK13 is ubiquitously expressed in the murine snout, developing palatal shelves and cranial nerves and its mutation leads to prominent facial clefts. Craniofacial structures, including the palate, develop thanks to large contribution of NCCs. Growing peripheral nerves and glial cell types originate mostly from migrating NCCs and Schwann

cell precursors (SCPs) (Furlan and Adameyko, 2018) but there are few exceptions, among them sensory neurons, which innervate maxillary region including the palate. These neurons originate in mesencephalic trigeminal nucleus in the CNS, and their development is regulated by FGF8 and Pou4f1 (Hunter et al., 2001), in agreement to that study, expression of both genes was detected altered in *Cdk13*-deficient embryos by us.

Along with these findings, we detected deregulated expression of genes that are typically associated with the TG in the developing palatal shelves. Expression of *Nrg1* (Meyer et al., 1997), a gene encoding an EGF receptor ligand, which in turn induces axon growth (Onesto et al., 2021) was downregulated in the palatal shelves at E12.5. Interestingly, *Nrg1* deficiency in mice also leads to maxillary dysmorphology (Waddington et al., 2017), an alteration from which palatal shelves are developing. Another gene usually detected in the TG is the neural transcription factor *Neurog1* that previously has also been associated with the palatal shelves (Visel et al., 2007). Its downregulation in TGs was observed as a result of *Pou4f1* downregulation (Lanier et al., 2009). Similarly, we found *Pou4f1* and *Neurog1* deregulated in palatal shelves of mice at E12.5. However, deregulation of *Neurog1* expression corresponded with expression changes of *Ntn1*, a gene encoding a secreted factor that is responsible for the guiding of developing peripheral motor axons (Serafini et al., 1996), and the proposed risk factor for development of the non-syndromic cleft lip and cleft palate (Leslie et al., 2017). Expression of both genes was highly upregulated in rostral palatal shelves and strongly downregulated in caudal palatal shelves, which indicates a tendency to rescue nerve growth to rostral regions of the developing face. Fewer nerves and their reduced development in the facial region of *Cdk13*-deficient embryos is further accompanied with significantly downregulated expression of the *Ache* gene in the caudal palatal shelves at E12.5. *Ache* encodes an acetylcholinesterase necessary for the degradation of acetylcholine, leading to termination of signal transduction at neuromuscular junctions, which is also important for neurite outgrowth and its elongation (Olivera et al., 2003).

In *Cdk13*-deficient animals, we also determined changes in the expression of genes involved in neuronal migration, possibly leading to alteration of nerve growth. One of such genes, whose expression was detected to be downregulated in all analyzed palatal shelf regions, is *Pafah1b1*. This gene encodes a non-catalytic subunit of an enzyme responsible for activation of GTPases and actin polymerization at the leading edge of locomoting neurons making it important for neural migration (Kholmanskikh et al., 2003). Its mutation in humans frequently results in lissencephaly and Miller–Dieker syndrome (Liu et al., 2021), a disease with very phenotypic manifestations similar to those of *Cdk13* deficiency, including growth delay and cerebral, cardiovascular, facial and limb anomalies (Yingling et al., 2003).

Diverse levels of CDK13 action during embryonic development

CDK13 was originally discovered as a nuclear factor participating in the regulation of transcription. We were able to detect CDK13 in the nucleus by immunofluorescence and cellular fractionation; however, we also determined significant levels of CDK13 in the cytoplasm. This might seem a rather surprising observation but presence of CDK13 in the cytoplasm of various cancer cells has been already documented by another group (Wu et al., 2023). Importantly, CDK13 can phosphorylate the intracellular domain of the transmembrane protein SERINC5 within the cytoplasm (Chai et al., 2021). These observations indicate that CDK13 can be involved not just in

transcription or RNA processing but also in other cellular processes in cytoplasm – although this needs further analyses.

Deficiency in cell outgrowths as a potential cause of craniofacial anomalies

Our findings uncovered that *Cdk13*-deficiency triggers changes in the expression of neurogenesis-specific genes in the palatal shelves and the development of hypoplastic cranial nerves *in vivo*, confirming a previous *in-vitro* study using cortical neurons (Chen et al., 2014). However, a functional connection between anomalies in cranial nerve development, which, in turn, lead to facial malformations, has been detected only in few cases. Such non-canonical function of nerves as moderators of facial morphogenesis has been proven in Möbius syndrome, where either defective cranial nerves (Rizos et al., 1998; Tomas-Roca et al., 2015) or the entire defective rhombencephalon (Verzijl et al., 2003) can cause facial malformations. Other disorders of the peripheral nervous system that lead to facial anomalies are hereditary sensory and autonomic neuropathy type IV (HSAN IV) (Gao et al., 2013; Louryan et al., 1995; Nakajima et al., 2020) and Parry–Romberg syndrome with hemifacial atrophy accompanied by various neurological pathologies (Vix et al., 2015). Also, downregulated expression of the gene *Nrg1*, which was observed also by us, leads to altered maxillary development (Waddington et al., 2017), as this gene encodes neurogenin ligands with a positive axon growth potential. However, any functional association between the development of hypoplastic peripheral cranial nerves and the development of craniofacial clefts is still missing.

Conclusions

CDK13 is crucial for the development of several tissues and organs, including craniofacial structures. Here, we determined its role during development of facial structures in a mouse model of CHDFIDD, where loss-of-function in *Cdk13* results in cleft lip/palate and the formation of midfacial clefts, accompanied by the deregulated expression pattern of certain genes and of proteins indispensable for proper functioning of major signaling pathways. *Cdk13*-deficient animals exhibited altered neurogenesis accompanied with distorted expression of neurogenesis-specific genes leading to the development of hypoplastic cranial nerves. As our analyses uncovered the cytoplasmic localization of CDK13 *in vitro*, further investigation is necessary to explore its potential roles beyond transcriptional regulation.

MATERIALS AND METHODS

Embryonic material

Heterozygous hypomorphic (*Cdk13^{tm1a}(EUCOM)Hmgu*) and knockout (*Cdk13^{tm1d}*) mice were obtained from the Infrafrontier Research Infrastructure – Mouse disease Models (<https://www.infrafrontier.eu/services/rodent-model-generation/#MouseModelsGeneration>). Mice were generated at the Transgenic and Archiving Module, CCP (IMG, Prague, Czech Republic).

Breeding and genotyping protocols were performed as previously described (see Nováková et al., 2019). In summary, the *Cdk13^{tm1a}* allele consists of a splicing acceptor that is surrounded by two FRT sites within intron 2. Moreover, it has two *loxP* sites within intron 2 and one *loxP* site within intron 4. The *Cdk13^{tm1d}* allele lacks exons 3 and 4, resulting in a non-functional allele of the *Cdk13* gene (Nováková et al., 2019).

All animal procedures were performed in strict accordance with the Guide for the Care and Use of Laboratory Animals and approved by the Institutional Animal Care and Use Committee (Masaryk University, Brno, Czechia, No. MSMT-34505/2020-7).

Culture of MEF and NIH3T3 cells

Mouse embryonic fibroblasts (MEFs) were grown in conventional Dulbecco's modified Eagle medium (DMEM) supplemented with 4.5 g/l

glucose and 20% fetal calf serum (FCS), the NIH3T3 cells were grown in DMEM supplemented with 4.5 g/l glucose and 10% FCS. Cell cultures were maintained at 37°C under 5% CO₂.

Live cell imaging

MEF cells isolated from WT and KO mouse embryos were cultured in DMEM as explained above. Cells were seeded on ibidiTreat μ -Slide 8 Well (80826, Ibidi) at concentration 50000/ml. After adhesion of cells, DMEM was changed to Opti-MEM (11058021, Gibco, Thermo Fisher Scientific) without Phenol Red supplemented with 1% fetal bovine serum (FBS). Cells were stained with F-actin-specific dye and membrane-specific dye 30 min before scanning. Live Imaging was performed using a Leica SP8 Confocal microscope (Leica, Germany) equipped with a CO₂-controlled and tempered transparent chamber. Automated detection and tracking of filopodia, and automated quantification of cell migration was carried out as described by Barry et al. (2015). Final analysis was performed using GraphPad (GraphPad Software, Boston, MA, USA).

Scanning electron microscopy

Mouse embryos (control and *Cdk13^{tm1a/tm1a}*) were fixed in 4% paraformaldehyde, washed in distilled water and dehydrated through a graded series (30–100%) of ethanol solutions. Later, samples were dried out using the CPD 030 Critical Point Dryer (BAL-TEC) and shadowed by using gold in a metal shadowing apparatus Balzers SCD040 (Balzers, Liechtenstein). Images were taken with the TESCAN Vega TS 5136 XM scanning electron microscope (SEM) (Tescan, Czech Republic), using one embryo per stage (E12.5, E13.5, E14.5, E16.5) with the representative phenotype.

Measurement of facial proportions

Frontal images of E11.5 embryonic heads were taken using a Leica S6D stereoscope with the DFC295 camera (both Leica, Germany). Individual measurements (mx – distance between edges of the maxillary prominences; lnp – distance between edges of the lateral nasal prominences; pits – distance between individual nasal pits) were performed in AxioVision 4.8 software (Zeiss, Germany) using length measurement tool. Distance ratios were calculated as $\text{distance between nasal pits} \div \text{distance mx}$, and $\text{distance between nasal pits} \div \text{distance lnp}$. Graphs and statistical significance were performed in GraphPad (GraphPad Software, Boston, MA, USA). Measurements were performed in at least four different embryos of all three genotypes (*Cdk13^{+/+}*, *Cdk13^{tm1a/tm1a}* and *Cdk13^{tm1d/tm1d}*).

Immunofluorescence on slides

Mouse embryonic tissues were fixed in 4% PFA overnight. Specimens were then embedded in paraffin and cut in transverse and sagittal planes at 5 μ m sections. For immunohistochemistry staining, sections were deparaffinized in xylene and rehydrated in an ethanol series (100%, 96%, 70%). Antigen retrieval was performed either in 1% citrate buffer pH6 or in DAKO antigen retrieval solution pH9 (S1699, DAKO Agilent, USA) at 97.5°C.

For protein localization, we incubated sections with primary antibody (Table S5) for 1 h at room temperature or overnight at 4°C. Antibodies against the following proteins were used: 2H3 (1:50, Nefin, AB_2314897, Developmental Studies Hybridoma Bank), SOX2 (1:100, 2748s, Cell Signaling), SOX9 (1:100, HPA001758, Sigma), Ki67 (1:200, RBK027, Zytomed systems). Then sections were incubated with the following secondary antibodies (1:200) for 30 min at room temperature: anti-mouse Alexa-Fluor 488 (A11001), and anti-rabbit Alexa-Fluor 594 (A11037, both Thermo Fisher Scientific, USA). Ki-67-positive cells were detected by anti-rabbit secondary antibody, ABC binding (PK-6101, Vector laboratories) and followed by application of the DAB (K3468, Dako) chromogenic system.

For DNA staining (nuclei), sections were mounted using Fluoroshield with DAPI (F6057, Sigma, Merck, Germany). If DRAQ5 (62251, Thermo Fisher Scientific, USA) was used for nuclei staining, sections were mounted with Fluoroshield (F6182, Sigma, Merck, Germany). Pictures were taken on confocal microscopes Leica SP8 (Leica, Germany) and Zeiss LSM800 (Zeiss, Germany). Nuclei in DAB-stained sections were counterstained with

hematoxylin. Sections were photographed under bright-field illumination with the Leica DMLB2 compound microscope (Leica, Germany).

Mitotic index on Ki-67-stained sections in the palatal shelves, was counted as a ratio between Ki-67-positive cells (brown) and total number of cells (i.e. Ki-67-negative plus Ki-67-positive cells). Cells were counted independently in mesenchyme and epithelium of the palatal shelves. Cells were counted on four sections (both left and right palatal shelves) in three embryos for each genotype (*Cdk13^{+/+}* and *Cdk13^{tm1a/tm1a}*).

Immunocytochemistry on glass inserts

MEFs and cells from embryonic DRGs (dorsal root ganglia) were isolated from E12.5 embryonic mice. Tissues were enzymatically processed using Dispase II (D4693, Sigma, Merck, Germany) for 1 h at 37°C while shaking. Cells were then centrifuged, filtered through 40 μ m Cell strainer (431750, Corning), seeded on glass inserts and left to grow until 70–80% confluency in DMEM (D6546, Sigma, Merck, Germany). Adult DRG cells were isolated from DRGs from adult mice. DRGs were enzymatically processed using Collagenase IV (LS0004188, PAN Biotech) for 6 h at 37°C. Tissues were resuspended every hour by pipetting. Cells were then filtered through Cell strainer and seeded on glass inserts and left to grow and form long outgrowths in Neurobasal cultivation medium (21103-49, Gibco). Cells were then fixed in 4% PFA for 15 min.

For protein localization, we incubated cells on glass inserts with primary antibody for 1 h at room temperature. The following antibodies were used: anti-CDK13 (1:100, HPA059241, Sigma, Merck, Germany), anti-CDK13 N-TERM (1:100, SAB1302350, Sigma), anti-CDK13 (1:150, PA5-63692, Invitrogen, Thermo Fisher Scientific, USA), anti-F-actin (1:100, A12379, Alexa-Fluor 488™ phalloidin, Thermo Fisher Scientific), anti-2H3 (1:50, Nefin, AB_2314897, Developmental Studies Hybridoma Bank). Then sections were incubated with the following secondary antibodies (1:200) for 30 min at room temperature: anti-mouse Alexa-Fluor 488 (A11001), and anti-rabbit Alexa-Fluor 594 (A11037, both Thermo Fisher Scientific, USA). Glass inserts with cells were mounted on cells slides with Fluoroshield with DAPI (F6057, Sigma, Merck, Germany). Pictures were taken on confocal microscope Leica SP8 (Leica, Germany). Cells were cultivated from at least three different embryos of all three genotypes (*Cdk13^{+/+}*, *Cdk13^{tm1a/tm1a}* and *Cdk13^{tm1d/tm1d}*).

Whole-mount immunofluorescence

Mouse embryos were dissected, fixed in 4% PFA while rotating at 4°C for 4 h. Embryos were then postfixed in graded methanol dilutions (25%, 50%, 75%, 100%). Embryos were then bleached in a mixture of hydrogen peroxide, DMSO and methanol for 24 h, and postfixed in combination of DMSO and methanol. Embryos were incubated with primary antibody to stain neurofilaments (2H3, AB_2314897, Developmental Studies Hybridoma Bank) for 7 days while rotating, followed by secondary antibody incubation (anti-mouse Alexa-Fluor 488, A11001) for 2 days while rotating. Embryos were finally cleared in a mixture of benzyl benzoate and benzyl alcohol until they got transparent. For microscopy, embryos were placed on Nunc™ glass bottom dishes (150680, Thermo Fisher Scientific) and imaged by using a Zeiss AxioZoom.V16-Apoto2 (Zeiss, Germany) at CELLIM (Core Facility Cellular Imaging, CEITEC, Masaryk University, Brno, Czech Republic). Whole-mount immunodetection of the neurofilaments was performed in three different embryos of all three genotypes (*Cdk13^{+/+}*, *Cdk13^{tm1a/tm1a}* and *Cdk13^{tm1d/tm1d}*) at E11.5.

Cellular fractionation

MEF and NIH3T3 cells were cultured on a 100 mm culture plate until 75% confluency in a 37°C incubator under 5% CO₂. Cells were washed with ice-cold PBS and collected into 1 ml of ice-cold PBS with a scraper, transferred to a 1.5 ml Eppendorf tube and centrifuged at 300 g and 4°C for 4 min. Cell pellets were resuspended in 200 μ l of TMK buffer (25 mM Tris-HCl pH 7.4; 1 mM MgCl₂; 5 mM KCl) and 150 μ l TMK+1% NP-40 was added to the tube. Incubation on ice was for 5 min, followed by centrifugation at 250 g and 4°C for 5 min. Supernatant (cytoplasmic fraction) was transferred to the new 1.5 ml Eppendorf tube. Pellet (nuclei) was resuspended in 500 μ l of buffer S1 (0.25 M saccharose; 10 mM MgCl₂) and transferred to the new Eppendorf tube on top of 500 μ l of buffer S2 (0.35 M saccharose; 0.5 mM

MgCl₂), followed by centrifugation at 1400 *g* and 4°C for 5 min. Supernatant was removed and the pellet was resuspended in 50 µl of ice-cold PBS. Protein concentration was assessed for cytoplasmic and nuclear samples, and an appropriate volume of 3×Laemmli buffer was added to the given samples. The samples were boiled for 5 min at 100°C, followed by western blot procedure as published by Blazek et al. (2011). Antibodies used for western blotting were: CDK13 (Merck, cat. no.: HPA059241), PARP (Cell Signaling Technology, cat. no.: 9542S), α -Tubulin (Cell Signaling Technology, cat. no.: 7291S), Lamin B (Santa Cruz Technology, cat. no.: sc-6217) and GAPDH (Santa Cruz Technology, cat. no.: sc-23233).

Chromatin immunoprecipitation (ChIP)

We employed the same chromatin immunoprecipitation protocol as published by Blazek et al. (2011), with few modifications: MEF cells were washed with PBS and crosslinked with 1% formaldehyde/PBS solution for 10 min at room temperature. Crosslinking was quenched for 5 min with 125 mM glycine (final concentration). Cells were washed twice with ice-cold PBS and lysed in sonication buffer (0.5% SDS, 20 mM Tris-HCl pH 8.0, 2 mM EDTA, 0.5 mM EGTA, 0.5 mM PMSF, protease inhibitor). For immunoprecipitation, protein extracts were pre-cleared with ChIP Grade G agarose beads (Cell Signaling Technology, cat. no.: 9007S) and then incubated overnight with anti-RNAPII antibody [Cell Signaling Technology, Rpb1 NTD (D8L4Y), cat. no.: 14958S; 1:300], followed by 2 h incubation with ChIP Grade G agarose beads. The beads were washed once with low-salt buffer (0.1% SDS, 1% Triton X-100, 2 mM EDTA, 20 mM Tris-HCl pH 8.0, 150 mM NaCl) followed by triple washing with the same buffer containing 500 mM NaCl, one wash with lithium buffer (2 mM EDTA, 20 mM Tris pH 8, 250 mM LiCl, 1% NP-40 and 1% sodium deoxycholate) and two washes with TE buffer. We eluted the immunoprecipitates with 1% SDS and 100 mM sodium bicarbonate at room temperature for 15 min and crosslinking was reversed by incubation with 200 mM NaCl for 5 h at 65°C. Proteins were digested with proteinase K (Sigma), and DNA was extracted with phenol:chloroform:isoamyl alcohol (25:24:1) and precipitated with isopropanol overnight. A fraction of precipitated DNA was used in qPCR reactions with the KAPA SYBR FAST qPCR Master Mix (2×) optimized for LightCycler[®] 480 (Merck, KK4611). The amplifications were run using the Roche LC480II LightCycler under the following conditions: initial activation step at 94°C for 5 min, followed by 45 cycles at 95°C for 10 s, 60°C for 20 s and 72°C for 15 s. For the *Pou4f1* promoter, primers forward (Fw): 5'-AGAAA-TGCGCTGTGGATGAT-3' and reverse (Re): 5'-TCCCGAGTAGAAAAG-CACACA-3' were used as published by Tang et al. (2020). For the *Nm1* promoter, primers Fw: 5'-GTCCGGCAAATTTTCTCCAAA-3' and Re: 5'-GTTGCATCCTTTCACCCACT-3' were used as published by Kaneko et al. (2014).

PCR array analysis to investigate gene-expression profiles

PCR arrays analyses were performed on tissues isolated from embryonic mice, i.e. rostral and caudal parts of palatal shelves at E12.5 and E14.5. One sample was obtained by pooling tissue from two or three embryos, three biological replicates were used for each stage and genotypes were analyzed. Total RNA was extracted using the RNeasy Plus Mini Kit (74136, Qiagen, Germany) according to the manufacturer's instructions. Total RNA concentration and purity were measured using a NanoDrop One spectrophotometer (Thermo Fisher Scientific, USA). First-strand cDNA was synthesized using the gb Reverse Transcription Kit (3012, Generi Biotech, Czech Republic) according to the manufacturer's instructions. RT² Profiler[™] PCR Array Mouse Neurogenesis (330231, Qiagen, Germany) was performed according to the manufacturer's instructions on a LightCycler 96 (Roche, Germany). C_T values were exported to an Excel file to create a table of C_T values. This table was then uploaded on to the data analysis web portal at <http://www.qiagen.com/geneglobe>. Samples were assigned to controls and test groups. C_T values were normalized to *Gapdh* as a reference gene. The above data analysis web portal calculated fold change/regulation using the delta delta C_T method, in which delta C_T is calculated between gene of interest (GOI) and an average of reference genes (HKG), followed by delta-delta C_T calculations [delta C_T (Test Group)-delta C_T (Control Group)]. Fold Change was then calculated using 2^{Δ(-delta delta}

C_T) formula. *P* values were calculated based on a Student's *t*-test of the replicate 2^{Δ(-Delta C_T)} values for each gene in control and test groups. The *P*-value calculation used is based on parametric, unpaired, two-sample equal variance, two-tailed distribution.

RNAscope assay

Mouse embryos were fixed in 4% PFA and fixation time differed based on the stage. The tissues were then dehydrated in an ethanol series, embedded in paraffin, and 5 µm transverse sections were obtained. The sections were deparaffinized in xylene and dehydrated in 96% ethanol. To detect the expression of certain genes, we used RNA in situ hybridization assay (RNAscope Multiplex Fluorescent v2 Assay kit, 323 110, ACD Bio, USA) in formalin-fixed paraffin-embedded tissues according to the manufacturer's instructions. All reactions, which required incubation at 40°C, were carried out using the HyBEZ[™] II oven (ACD Bio, USA). Probes for *Cdk13* (895581), *Fgf8* (313411), *FoxD1* (495501), *Meis2* (436371), *Msx1* (421841) and *Shh* (314361) (all ACD Bio, USA) were used. For negative control staining, a probe diluent (300041; ACD Bio) was used instead of a probe. The hybridized probes were visualized using the TSA-Plus Cyanine 3 system (NEL744001KT, Perkin-Elmer, USA), according to the manufacturer's protocol. DAPI (323 108, ACD Bio, USA) was used to stain nuclei. Pictures were obtained with the Leica SP8 confocal microscope (Leica, Germany).

RNAscope[®] Probe Mm-*Cdk13* (#895581) binds to nucleotides 3312–4317 (last couple of exons and the 3'UTR) of mouse *Cdk13* (NM_001081058.2). If deletion of exons 3 and 4 (*Cdk13^{tm1d/tm1d}*) is unstable, it is possible to have a signal (some weak signal in the form of dots is present in both hypomorphic and knockout embryonic palatal shelves).

RT-PCR

Rostral and caudal parts of the palatal shelves at E12.5, E14.5 and E16.5, as well as maxillary (mx), mandibular (md) and frontonasal prominences (fnp) at E11.5 and E12.5 were dissected from WT mouse embryos to quantify the differences in *Cdk13* expression during development of the facial structures. Individual parts of the palatal shelves and facial prominences were dissected from at least three different embryos for each stage. Proliferation rate changes in the *Cdk13*-deficient embryos were assessed using *CyclinD1* gene expression in tissues isolated from rostral and caudal palatal shelves (*Cdk13^{tm1a}* E12.5, E14.5) and lips (*Cdk13^{tm1d}* E12.5). Total RNA was extracted using the RNeasy Plus Mini Kit (74136, Qiagen, Germany) according to the manufacturer's instructions. Total RNA concentration and purity was measured using a NanoDrop One (Thermo Fisher Scientific, USA). First-strand cDNA was synthesized using gb Reverse Transcription Kit (3012, Generi Biotech, Czech Republic) according to the manufacturer's instructions. TaqMan probe was used to quantify *Cdk13* (Mm01164725_m1, Thermo Fisher Scientific) and *CyclinD1* (Mm00432359_m1, Thermo Fisher Scientific) gene expression. The RT-PCR reaction was performed on LightCycler 96 (Roche, Germany). The comparative C_T method was used for analysis.

Injection of chicken embryos

Fertilized *Gallus gallus* (chicken) eggs were bought at a farm (Integra, Zabcice, Czech Republic) and incubated in a humidified incubator at 37°C. At Hamburger–Hamilton (HH) developmental stage 20 (HH20), 1 mM CDK12/13 inhibitor THZ531 (SML2619, Sigma Aldrich, Merck, Germany) was injected into the maxillary prominences (Fig. 8) using a glass capillary attached to an Eppendorf FemtoJet 4i Microinjector (Eppendorf, Germany) supplied with a manipulator (Leica, Germany). Moreover, we injected the inhibitor into the craniofacial mesenchyme and the postoptic region of chicken embryos at HH10 and HH15, respectively (Fig. 8). 10% Trypan Blue was used as a contrasting dye. After injections, embryos were incubated for another 96 h, and then killed and fixed in 4% paraformaldehyde. Frontal and lateral images were taken using a Leica S6D stereoscope with a DFC295 camera (both Leica, Germany).

MTT-Assay

The MTT test was used to establish the toxicity of the CDK12/13 inhibitor THZ531. Cells isolated from the trigeminal ganglion (TG) were cultivated for 4 days in 100 µl of DMEM supplemented with 10% FBS, 1% penicilin/

streptomycin, 1% L-glutamine in a 96-well plate (100,000 cells/ml). Cells were treated every day with different concentrations of THZ531 (i.e. 50, 100, 300, 500, 750, 1000 and 1500 nM). Untreated cells were used as controls. After 4 days, medium was discarded and replaced with 50 μ l of DMEM without FBS followed by addition of 50 μ l of MTT Reagent (MTT Cell Proliferation Kit Ab211091, Abcam), 50 μ l of common culture medium and 50 μ l of MTT Reagent were added to empty wells and used as background controls. The plate was then wrapped in foil and incubated for 3.5 h at 37°C under 5% CO₂. Afterwards, 150 μ l of MTT solvent (MTT Cell Proliferation Kit Ab211091, Abcam) was added to the samples. Absorbance was measured at 590 nm and cell survival rates were established as the absorbance index, with higher absorbance meaning better cell survival, lower absorbance meaning worse cell survival (Fig. S7H).

TG cultivation and neurite outgrowth assay

TGs were dissected from mouse embryos at E12 and washed in ice-cold Neurobasal medium (21103049, Gibco, Thermo Fisher Scientific, USA). Each TG was placed in a separate well on a culture well plate into 10 μ l drop of Matrigel (356231, Corning, USA) and left 20 min to polymerize in the tissue culture incubator. Neurobasal medium supplemented with 100 nM or 300 nM THZ531 (SML2619, Sigma Aldrich, Merck, Germany) was added. Images were taken after adding cultivation medium (0 h) and again after 24 h by using an Olympus IX71 inverted microscope (Olympus, Japan). Neurite outgrowth was measured using ImageJ software (NIH, USA) while comparing areas covered by neurites on pictures taken under different culture conditions.

Changes of the ability of TGs to produce neurite outgrowths (in %) were calculated as following: $\text{neurite outgrowth area} = (\text{total area} - \text{TG area}) / \text{total area} \times 100$.

Terminal deoxynucleotidyl transferase dUTP nick end labeling (TUNEL) assay

Apoptotic cells were detected by using the TUNEL assay (ApopTag Peroxidase In Situ Apoptosis Detection Kit, cat. no. S7101, Chemicon, Temecula, USA). Nuclei were counterstained with hematoxylin. Sections were photographed under bright-field illumination with a Leica DMLB2 compound microscope (Leica, Germany). TUNEL assays were performed using three different embryos of the *Cdk13*^{+/+} and *Cdk13*^{tm1a/tm1a} genotypes.

Statistical analyses

Data were evaluated for statistical significance in GraphPad (GraphPad Software, Boston, MA, USA) using unpaired two-tailed Student's *t*-tests. Differences were considered to be significant at **P*<0.05, ***P*<0.01 and ****P*<0.001. Errors are indicated as the \pm standard error of the mean (\pm s.e.m.).

Acknowledgements

We acknowledge the core facility CELLIM supported by the Czech-Biolmaging large RI project (LM2018129 funded by MEYS CR).

Competing interests

The authors declare no competing or financial interests.

Author contributions

Conceptualization: M.H., J.P., J.K., M.B.; Methodology: D.L.; Validation: M.B.; Formal analysis: M.H., N.J., M.N., T.S.; Investigation: M.N.; Resources: D.L., J.P.; Data curation: M.H., N.J., D.L., M.N., T.S., S.C.; Writing - original draft: M.H.; Writing - review & editing: N.J., J.P., J.K., M.B.; Visualization: M.H., N.J., T.S., S.C.; Supervision: M.B.; Project administration: M.B.; Funding acquisition: M.B.

Funding

This work was supported by the Czech Science Foundation (Grantová Agentura České Republiky; grant nos: 19-01205S, 22-02794S), by the MEYS CR (Ministerstvo Školství, Mládeže a Tělovýchovy; grant no.: CZ.02.1.01/0.0/0.0/15_003/0000460) and by the National Institute for Cancer Research (Programme EXCELES, ID Project No. LX22NPO5102) - Funded by the European Union - Next Generation EU. Deposited in PMC for immediate release.

Data availability

All relevant data can be found within the article and its [supplementary information](#).

First Person

This article has an associated First Person interview with the first author of the paper.

Special Issue

This article is part of the Special Issue 'Translating Multiscale Research in Rare Disease', guest edited by Monica Justice, Monkol Lek, Karen Liu and Kate Rauen. See related articles at <https://journals.biologists.com/dmm/collection/39/Rare-Disease>.

References

- Adameyko, I., Lallemand, F., Furlan, A., Zinin, N., Aranda, S., Kitambi, S. S., Blanchart, A., Favaro, R., Nicolis, S., Lübke, M. et al. (2012). Sox2 and Mif cross-regulatory interactions consolidate progenitor and melanocyte lineages in the cranial neural crest. *Development* **139**, 397-410. doi:10.1242/dev.065581
- Barry, D. J., Durkin, C. H., Abella, J. V. and Way, M. (2015). Open source software for quantification of cell migration, protrusions, and fluorescence intensities. *J. Cell Biol.* **209**, 163-180. doi:10.1083/jcb.201501081
- Barkowiac, B., Liu, P., Phatnani, H. P., Fuda, N. J., Cooper, J. J., Price, D. H., Adelman, K., Lis, J. T. and Greenleaf, A. L. (2010). CDK12 is a transcription elongation-associated CTD kinase, the metazoan ortholog of yeast Ctk1. *Genes Dev.* **24**, 2303-2316. doi:10.1101/gad.1968210
- Blazek, D., Kohoutek, J., Bartholomeeusen, K., Johansen, E., Hulinkova, P., Luo, Z., Cimermancic, P., Ule, J. and Peterlin, B. M. (2011). The Cyclin K/Cdk12 complex maintains genomic stability via regulation of expression of DNA damage response genes. *Genes Dev.* **25**, 2158-2172. doi:10.1101/gad.16962311
- Chai, Q., Li, S., Collins, M. K., Li, R., Ahmad, I., Johnson, S. F., Frabutt, D. A., Yang, Z., Shen, X., Sun, L. et al. (2021). HIV-1 Nef interacts with the cyclin K/CDK13 complex to antagonize SERINC5 for optimal viral infectivity. *Cell Rep.* **36**, 109514. doi:10.1016/j.celrep.2021.109514
- Chen, H. R., Lin, G. T., Huang, C. K. and Fann, M. J. (2014). Cdk12 and Cdk13 regulate axonal elongation through a common signaling pathway that modulates Cdk5 expression. *Exp. Neurol.* **261**, 10-21. doi:10.1016/j.expneurol.2014.06.024
- Colas, P. (2020). Cyclin-dependent kinases and rare developmental disorders. *Orphanet J. Rare Dis.* **15**, 203. doi:10.1186/s13023-020-01472-y
- Furlan, A. and Adameyko, I. (2018). Schwann cell precursor: a neural crest cell in disguise? *Dev. Biol.* **444** Suppl. 1, S25-S35. doi:10.1016/j.ydbio.2018.02.008
- Gao, L., Guo, H., Ye, N., Bai, Y., Liu, X., Yu, P., Xue, Y., Ma, S., Wei, K., Jin, Y. et al. (2013). Oral and craniofacial manifestations and two novel missense mutations of the NTRK1 gene identified in the patient with congenital insensitivity to pain with anhidrosis. *PLoS One* **8**, e66863. doi:10.1371/journal.pone.0066863
- Griffin, J. N., Compagnucci, C., Hu, D., Fish, J., Klein, O., Marcucio, R. and Depew, M. J. (2013). Fgf8 dosage determines midfacial integration and polarity within the nasal and optic capsules. *Dev. Biol.* **374**, 185-197. doi:10.1016/j.ydbio.2012.11.014
- Hamilton, M. J. and Suri, M. (2019). CDK13-related disorder. *Adv. Genet.* **103**, 163-182. doi:10.1016/bs.adgen.2018.11.001
- Higashiyama, H. and Kuratani, S. (2014). On the maxillary nerve. *J. Morphol.* **275**, 17-38. doi:10.1002/jmor.20193
- Hunter, E., Begbie, J., Mason, I. and Graham, A. (2001). Early development of the mesencephalic trigeminal nucleus. *Dev. Dyn.* **222**, 484-493. doi:10.1002/dvdy.1197
- Jeong, J., Mao, J., Tenzen, T., Kottmann, A. H. and McMahon, A. P. (2004). Hedgehog signaling in the neural crest cells regulates the patterning and growth of facial primordia. *Genes Dev.* **18**, 937-951. doi:10.1101/gad.1190304
- Kaneko, S., Son, J., Bonasio, R., Shen, S. S. and Reinberg, D. (2014). Nascent RNA interaction keeps PRC2 activity poised and in check. *Genes Dev.* **28**, 1983-1988. doi:10.1101/gad.247940.114
- Kholmanskikh, S. S., Dobrin, J. S., Wynshaw-Boris, A., Letourneau, P. C. and Ross, M. E. (2003). Disregulated RhoGTPases and actin cytoskeleton contribute to the migration defect in Lis1-deficient neurons. *J. Neurosci.* **23**, 8673-8681. doi:10.1523/JNEUROSCI.23-25-08673.2003
- Lanier, J., Dykes, I. M., Nissen, S., Eng, S. R. and Turner, E. E. (2009). Brn3a regulates the transition from neurogenesis to terminal differentiation and represses non-neural gene expression in the trigeminal ganglion. *Dev. Dyn.* **238**, 3065-3079. doi:10.1002/dvdy.22145
- Leslie, E. J., Carlson, J. C., Shaffer, J. R., Butali, A., Buxó, C. J., Castilla, E. E., Christensen, K., Deleyiannis, F. W., Leigh Field, L., Hecht, J. T. et al. (2017). Genome-wide meta-analyses of nonsyndromic orofacial clefts identify novel associations between FOXE1 and all orofacial clefts, and TP63 and cleft lip with or without cleft palate. *Hum. Genet.* **136**, 275-286. doi:10.1007/s00439-016-1754-7
- Levi, G., Mantero, S., Barbieri, O., Cantatore, D., Paleari, L., Beverdam, A., Genova, F., Robert, B. and Merlo, G. R. (2006). Msx1 and Dlx5 act independently in development of craniofacial skeleton, but converge on the regulation of Bmp signaling in palate formation. *Mech. Dev.* **123**, 3-16. doi:10.1016/j.mod.2005.10.007
- Liu, X., Bennison, S. A., Robinson, L. and Toyo-Oka, K. (2021). Responsible genes for neuronal migration in the chromosome 17p13.3: beyond. *Brain Sci* **12**, 56. doi:10.3390/brainsci12010056

- Louryan, S., Biermans, J. and Flegal, F. (1995). Nerve growth factor in the developing craniofacial region of the mouse embryo. *Eur. J. Morphol.* **33**, 415-419.
- Machon, O., Masek, J., Machonova, O., Krauss, S. and Kozmik, Z. (2015). Meis2 is essential for cranial and cardiac neural crest development. *BMC Dev. Biol.* **15**, 40. doi:10.1186/s12861-015-0093-6
- Meyer, D., Yamaai, T., Garratt, A., Riethmacher-Sonnenberg, E., Kane, D., Theill, L. E. and Birchmeier, C. (1997). Isoform-specific expression and function of neuregulin. *Development* **124**, 3575-3586. doi:10.1242/dev.124.18.3575
- Nakajima, K., Miranda, A., Craig, D. W., Shekhtman, T., Knoch, S., Bleyer, A., Szlinger, S., Kato, T. and Kelsoe, J. R. (2020). Ntrk1 mutation co-segregating with bipolar disorder and inherited kidney disease in a multiplex family causes defects in neuronal growth and depression-like behavior in mice. *Transl. Psychiatry* **10**, 407. doi:10.1038/s41398-020-01087-8
- Nováková, M., Hampl, M., Vrábel, D., Procházka, J., Petrezselyová, S., Procházková, M., Sedláček, R., Kavková, M., Zikmund, T., Kaiser, J. et al. (2019). Mouse model of congenital heart defects, dysmorphic facial features and intellectual developmental disorders as a result of non-functional CDK13. *Front. Cell Dev. Biol.* **7**, 155. doi:10.3389/fcell.2019.00155
- Ohshima, T., Ward, J. M., Huh, C. G., Longenecker, G., Veeranna, Pant, H. C., Brady, R. O., Martin, L. J. and Kulkarni, A. B. (1996). Targeted disruption of the cyclin-dependent kinase 5 gene results in abnormal corticogenesis, neuronal pathology and perinatal death. *Proc. Natl. Acad. Sci. USA*, **93**, 11173-11178. doi:10.1073/pnas.93.20.11173
- Olivera, S., Rodríguez-Ithurralde, D. and Henley, J. M. (2003). Acetylcholinesterase promotes neurite elongation, synapse formation, and surface expression of AMPA receptors in hippocampal neurons. *Mol. Cell. Neurosci.* **23**, 96-106. doi:10.1016/S1044-7431(03)00021-6
- Onesto, M. M., Short, C. A., Rempel, S. K., Catlett, T. S. and Gomez, T. M. (2021). Growth factors as axon guidance molecules: lessons from. *Front. Neurosci.* **15**, 678454. doi:10.3389/fnins.2021.678454
- Pilarova, K., Herudek, J. and Blazek, D. (2020). CDK12: cellular functions and therapeutic potential of versatile player in cancer. *NAR Cancer* **2**, zcaa003. doi:10.1093/narcan/zcaa003
- Rizos, M., Negrón, R. J. and Serman, N. (1998). Möbius syndrome with dental involvement: a case report and literature review. *Cleft Palate Craniofac. J.* **35**, 262-268. doi:10.1597/1545-1569_1998_035_0262_mbswdi_2.3.co_2
- Serafini, T., Colamarino, S. A., Leonardo, E. D., Wang, H., Beddington, R., Skarnes, W. C. and Tessier-Lavigne, M. (1996). Netrin-1 is required for commissural axon guidance in the developing vertebrate nervous system. *Cell* **87**, 1001-1014. doi:10.1016/S0092-8674(00)81795-X
- Shah, K. and Rossie, S. (2018). Tale of the good and the bad Cdk5: remodeling of the actin cytoskeleton in the brain. *Mol. Neurobiol.* **55**, 3426-3438. doi:10.1007/s12035-017-0525-3
- Tang, P. M., Zhang, Y. Y., Xiao, J., Tang, P. C., Chung, J. Y., Li, J., Xue, V. W., Huang, X. R., Chong, C. C., Ng, C. F. et al. (2020). Neural transcription factor Pou4f1 promotes renal fibrosis via macrophage-myofibroblast transition. *Proc. Natl. Acad. Sci. USA* **117**, 20741-20752. doi:10.1073/pnas.1917663117
- Tomas-Roca, L., Tsaalbi-Shtylik, A., Jansen, J. G., Singh, M. K., Epstein, J. A., Altunoglu, U., Verzijl, H., Soria, L., Van Beusekom, E., Roscioli, T. et al. (2015). De novo mutations in PLXND1 and REV3L cause Möbius syndrome. *Nat. Commun.* **6**, 7199. doi:10.1038/ncomms8199
- Trinh, J., Kandaswamy, K. K., Werber, M., Weiss, M. E. R., Oprea, G., Kishore, S., Lohmann, K. and Rolfs, A. (2019). Novel pathogenic variants and multiple molecular diagnoses in neurodevelopmental disorders. *J. Neurodev. Disord.* **11**, 11. doi:10.1186/s11689-019-9270-4
- Venturin, M., Moncini, S., Villa, V., Russo, S., Bonati, M. T., Larizza, L. and Riva, P. (2006). Mutations and novel polymorphisms in coding regions and UTRs of CDK5R1 and OMG genes in patients with non-syndromic mental retardation. *Neurogenetics* **7**, 59-66. doi:10.1007/s10048-005-0026-9
- Verzi, M. P., Agarwal, P., Brown, C., Mcculley, D. J., Schwarz, J. J. and Black, B. L. (2007). The transcription factor MEF2C is required for craniofacial development. *Dev. Cell* **12**, 645-652. doi:10.1016/j.devcel.2007.03.007
- Verzijl, H. T., Van Der Zwaag, B., Cruysberg, J. R. and Padberg, G. W. (2003). Möbius syndrome redefined: a syndrome of rhombencephalic maldevelopment. *Neurology* **61**, 327-333. doi:10.1212/01.WNL.0000076484.91275.CD
- Visel, A., Carson, J., Oldekamp, J., Warnecke, M., Jakubcakova, V., Zhou, X., Shaw, C. A., Alvarez-Bolado, G. and Eichele, G. (2007). Regulatory pathway analysis by high-throughput in situ hybridization. *PLoS Genet.* **3**, 1867-1883. doi:10.1371/journal.pgen.0030178
- Vix, J., Mathis, S., Lacoste, M., Guillevin, R. and Neau, J. P. (2015). Neurological manifestations in parry-romberg syndrome: 2 case reports. *Medicine (Baltimore)* **94**, e1147. doi:10.1097/MD.0000000000001147
- Waddington, J. L., Katina, S., O'tuathaigh, C. M. P. and Bowman, A. W. (2017). Translational genetic modelling of 3D craniofacial Dysmorphology: elaborating the facial phenotype of neurodevelopmental disorders through the "prism" of schizophrenia. *Curr. Behav. Neurosci. Rep.* **4**, 322-330. doi:10.1007/s40473-017-0136-3
- Wu, C., Xie, T., Guo, Y., Wang, D., Qiu, M., Han, R., Qing, G., Liang, K. and Liu, H. (2023). CDK13 phosphorylates the translation machinery and promotes tumorigenic protein synthesis. *Oncogene* **42**, 1321-1330. doi:10.1038/s41388-023-02653-2
- Yigit, G., Brown, K. E., Kayserili, H., Pohl, E., Caliebe, A., Zahnleiter, D., Rosser, E., Bögershausen, N., Uyguner, Z. O., Altunoglu, U. et al. (2015). Mutations in CDK5RAP2 cause Seckel syndrome. *Mol. Genet. Genomic Med.* **3**, 467-480. doi:10.1002/mgg3.158
- Yingling, J., Toyoko-Oka, K. and Wynshaw-Boris, A. (2003). Miller-Dieker syndrome: analysis of a human contiguous gene syndrome in the mouse. *Am. J. Hum. Genet.* **73**, 475-488. doi:10.1086/378096

APPENDIX 13

JANSOVA, Denisa, Veronika SEDMIKOVA, Fatima J. BERRO, Daria ALESHKINA, Michal DVORAN, Michal KUBELKA, Jitka REZACOVA, Jana RUTAROVA, **Jiri KOHOUTEK** and Andrej SUSOR. Absence of CDK12 in oocyte leads to female infertility. *Cell Death & Disease*. 2025, 16(1), 213.

ARTICLE OPEN



Absence of CDK12 in oocyte leads to female infertility

Denisa Jansova¹[✉], Veronika Sedmikova¹, Fatima J. Berro¹, Daria Aleshkina¹, Michal Dvoran¹, Michal Kubelka¹, Jitka Rezacova², Jana Rutarova², Jiri Kohoutek³ and Andrej Susor¹[✉]

© The Author(s) 2025

Transcriptional activity and gene expression are critical for the development of mature, meiotically competent oocytes. Our study demonstrates that the absence of cyclin-dependent kinase 12 (CDK12) in oocytes leads to complete female sterility, as fully developed oocytes capable of completing meiosis I are absent from the ovaries. Mechanistically, CDK12 regulates RNA polymerase II activity in growing oocytes and ensures the maintenance of the physiological maternal transcriptome, which is essential for protein synthesis that drives further oocyte growth. Notably, CDK12-deficient growing oocytes exhibit a 71% reduction in transcriptional activity. Furthermore, impaired oocyte development disrupts folliculogenesis, leading to premature ovarian failure without terminal follicle maturation or ovulation. In conclusion, our findings identify CDK12 as a key master regulator of the oocyte transcriptional program and gene expression, indispensable for oocyte growth and female fertility.

Cell Death and Disease (2025)16:213; <https://doi.org/10.1038/s41419-025-07536-w>

INTRODUCTION

Oocytes arise from primordial germ cells and develop in follicles. The periodic activation of primordial germ cells up to the preovulatory stage is defined by oocyte growth and cytoplasmic expansion, with the synthesis and storage of maternal components such as RNA and proteins in the cytoplasm [1]. The quality of oocytes and early embryos is based on the storage of maternal components, which is regulated by various signaling pathways [2–4]. During this period, the oocyte acquires meiotic competence, i.e. the ability to resume meiosis and to enter or arrest at metaphase II [5–9], and developmental competence, the ability to support early embryonic development [10, 11].

The regulation of transcription initiation by RNA polymerase II (POLII) is of central importance for the maintenance of the oocyte and early embryonic development. Transcriptional silencing occurs in a fully-grown oocyte and continues during meiotic maturation and after fertilization in the early embryo. The hyperphosphorylated form of POLII has been found in growing oocytes, while the hypophosphorylated form is typical of mature, transcriptionally inactive GV oocytes [12]. The transcription of protein-coding genes by POLII is tightly regulated to generate proper quantities and classes of mRNA. One of the principal factors participating in the regulation of POLII activity is Cyclin-dependent kinase 12 (CDK12). Complex of CDK12 and its binding partner Cyclin K controls transcription, by phosphorylating the C-terminal domain (CTD) of the large subunit of POLII [13]. Current evidence suggests that CDK12 has a wide range of biological functions, including DNA replication [14], regulation of the expression of DNA damage response genes and cell cycle genes [15], transcription elongation [16], pre-mRNA processing [17], RNA turnover [18] and the initiation of translation of mRNA subgroups

[15, 19, 20]. Blazek et al. have shown that the depletion of CDK12 leads to a reduced expression of 4% of genes [13]. CDK12 is one of the most frequently mutated genes in ovarian carcinoma [21] and these mutations lead to a loss of function [22]. Although the role of CDK12 in cancer has been broadly investigated, its specific role in oocyte development is unknown.

Based on this knowledge, we hypothesized that CDK12 is essential for maintaining the integrity of the maternal transcriptome and translome in growing oocytes. To test this hypothesis, we generated an oocyte-specific knockout mouse model lacking CDK12 expression. Our findings revealed that the absence of CDK12 disrupts transcription by impairing POLII regulation, leading to a dysregulated maternal transcriptome and defective translation in oocytes. This dysregulation adversely affects oocyte growth, thereby impairing folliculogenesis and ultimately resulting in female infertility.

RESULTS

CDK12 is essential for female fertility

To explore the requirement of Cyclin-dependent kinase 12 (CDK12) in female fertility, we performed a series of experiments using a conditional CDK12 knockout (cKO) mouse model. The aim of our study was to understand the effects of CDK12 depletion on oocyte development and overall fertility in female mice. The CDK12 cKO was generated by crossing *Cdk12^{lox/lox}* with a *Zp3^{Cre}* strain (Supporting Information 1A, B). The resulting experimental genotypes were labeled as wild-type (WT; CDK12^{+/+}; *Cdk12^{tm1c}*^{+/+} *Zp3-Cre*^{+/+}); heterozygote (HT; CDK12^{+/-}; *Cdk12^{tm1c}*^{+/-} *Zp3-Cre*^{+/+}) and homozygote (cKO; CDK12^{-/-}; *Cdk12^{tm1c}*^{-/-} *Zp3-Cre*^{+/+}) (Supporting Information 1A, B). Immunoblot analysis confirmed

¹Laboratory of Biochemistry and Molecular Biology of Germ Cells, Institute of Animal Physiology and Genetics of the Czech Academy of Sciences, Rumburska 89, 277 21 Libeňov, Czech Republic. ²Assisted reproductive center, Institute for Mother and Child Care, Podolske nabrezi 157, Prague, Czech Republic. ³Department of Experimental Biology, Faculty of Science, Masaryk University, 62500 Brno, Czech Republic. ✉email: jansova@iapg.cas.cz; susor@iapg.cas.cz

Edited by Massimiliano Agostini

Received: 21 November 2024 Revised: 18 February 2025 Accepted: 12 March 2025

Published online: 27 March 2025

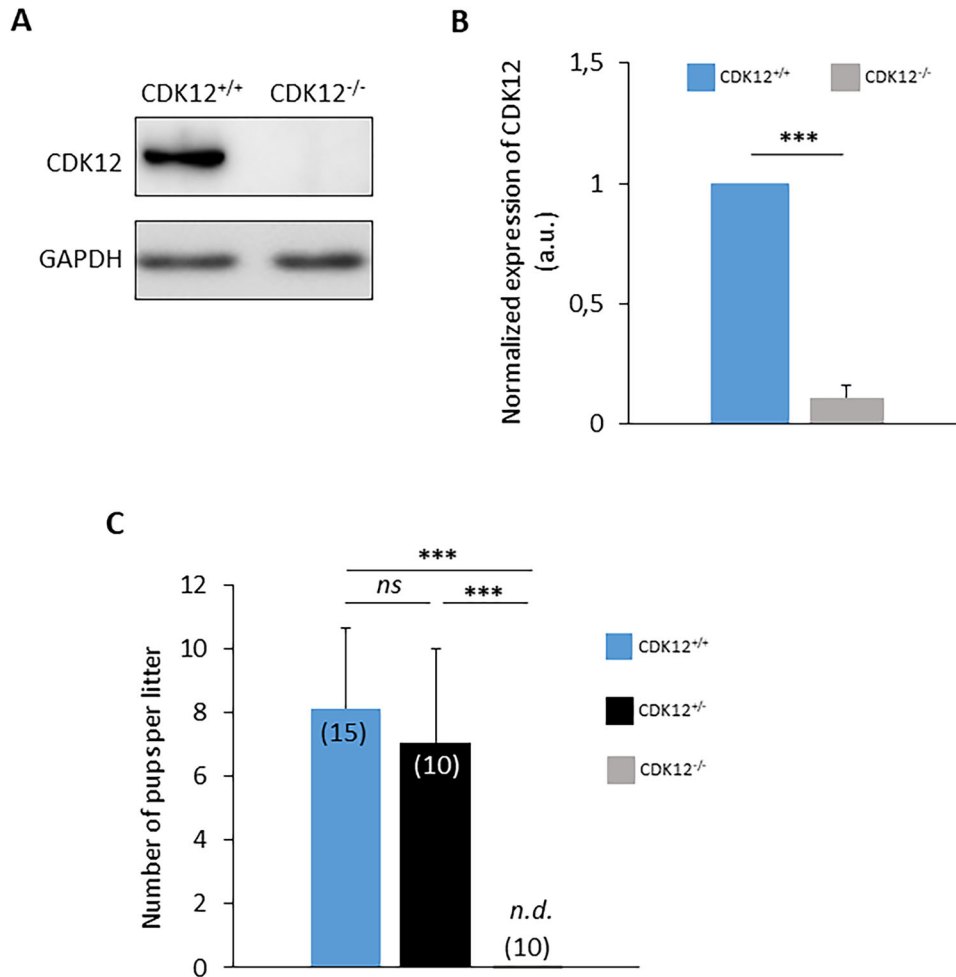


Fig. 1 CDK12 is essential for female fertility. **A** Western blot analysis of CDK12 expression in oocytes from wild-type (CDK12^{+/+}) and homozygous conditional knockout (cKO) females (CDK12^{-/-}). GAPDH was used as a loading control. Data from six independent biological replicates. For *Cdk12* mRNA expression analysis, see Fig. 5. For information about conditional KO generation and CDK12 localization and expression, see SI Fig. 1. **B** Quantification of CDK12 protein expression from (A) normalized to GAPDH. Data are presented as mean \pm SD; Student's *t*-test: ****p* < 0.001. **C** Analysis of fertility of females from different genotypes mated with proven breeder wild type males. Number of breeding pairs in parentheses. Data are presented as mean \pm SE; Student's *t*-test: *ns*, non-significant; ****p* < 0.001.

the absence of CDK12 protein in the CDK12^{-/-} GV oocytes (Fig. 1A, B and Supporting Information 1C, D). In addition, immunofluorescence experiments showed that CDK12 was localized to the nucleus of WT oocytes, while it was absent in CDK12^{-/-} oocytes (Supporting Information 1C, D). Breeding experiments with CDK12^{+/+} proven breeder males showed that females lacking CDK12 in their oocytes were completely sterile, while CDK12^{+/+} and CDK12^{+/-} females were normally fertile (Fig. 1C), suggesting that there is no haploinsufficiency for CDK12.

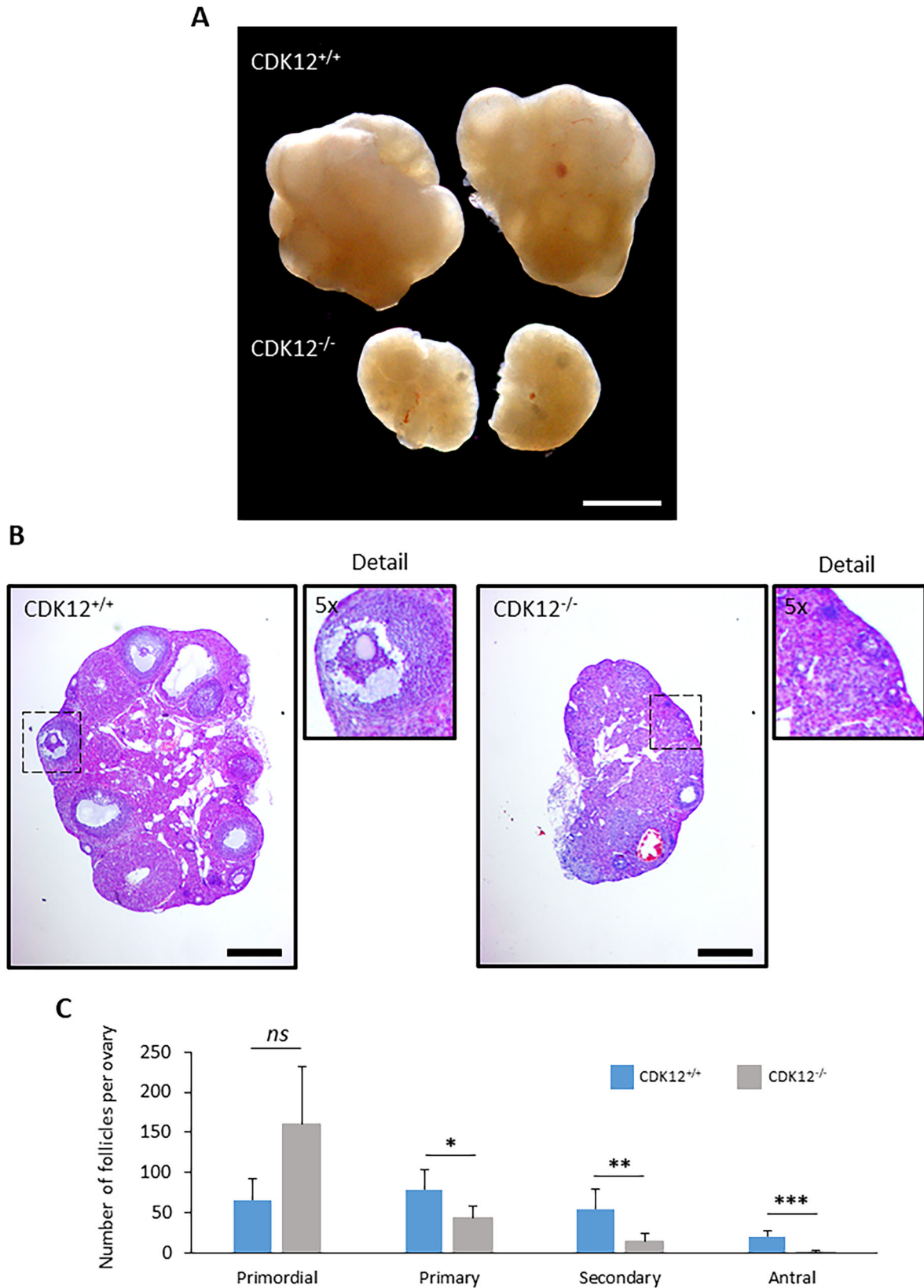
In conclusion, the results show that the absence of maternal CDK12 in oocytes leads to female sterility.

CDK12 is Essential to Oocyte Development and Maturation

Next, we investigated why absence of CDK12 in oocytes leads to female infertility. It is known that oocytes go through a series of developmental stages prior to fertilization, including oocyte growth, acquisition of meiotic competence and maturation into fertilizable MII oocyte. To understand the main cause of infertility in cKO mice, we analyzed the ovaries and oocyte quality. Following the standard procedure of superovulation, we examined the morphology of the ovaries. Despite the mice having the equal body size, the ovaries of cKO females were significantly smaller compared to those of WT

females (Fig. 2A and Supporting Information 2A). Histological analysis of cKO ovaries and quantification of follicles revealed a reduced number of primary follicles and almost no antral follicles (Fig. 2B, C), resulting in the premature ovarian failure (POF) phenotype. In addition, rare ovulations lead to the formation of the corpus luteum in the cKO ovaries, which shows that the ovaries respond to hormonal stimulation and ovulation (Supporting Information 2B). Next, we found that post PMSG stimulation most of the isolated oocytes from WT females were fully grown germinal vesicle (GV) (Fig. 3A, B). In contrast, oocytes from cKO females were predominantly growing GV oocytes (Fig. 3A, B). Following the standard procedure of superovulation, we obtained only a few ovulated oocytes in the oviduct of the cKO females, although the WT genotype ovulated a normal number of oocytes (Fig. 3B). In contrast, cKO females do not produce MII oocytes during scarce ovulation (Fig. 3C, D). Instead, the ovulated CDK12^{-/-} oocytes were devoid of polar body, with disorganized chromosomes and polymerized tubulin (Fig. 3C, D).

In summary, the absence of CDK12 in the oocyte leads to an interruption of oocyte development to fully grown GV stage and thus to a termination of folliculogenesis, resulting in female infertility.



The absence of CDK12 suppresses transcriptional activity in developing oocytes

Our results suggest that the main cause of infertility is impaired development of the growing oocytes. Previous reports indicated a

close link between CDK12 and the regulation of transcription via phosphorylation of RNA Polymerase II (POLII) [18]. We hypothesized that this regulatory function of CDK12 is critical for proper gene expression during oocyte growth. First, we found that CDK12

Fig. 2 Absence of CDK12 in the oocytes leads to decreased ovarian size via ceased folliculogenesis. **A** Representative image of pair of ovaries from CDK12^{+/+} and CDK12^{-/-} mice. Scale bar 1 mm. For measurement of the size of the ovaries, see SI Fig. 2. **B** Representative images of histological sections of ovaries stained with haematoxylin and eosin. The dashed squares correspond to 5-fold magnification of the ovarian cortex, showing representative antral follicle (CDK12^{+/+}) and primordial follicle (CDK12^{-/-}). Data from two independent biological replicates, $n = 6$ per group; scale bars 400 μm . For depiction of the corpus luteum in the ovaries, see SI Fig. 2. **C** Quantification of follicles from CDK12^{+/+} and CDK12^{-/-} mice. Data from three females for each genotype, data are presented as mean \pm SE; Student's *t*-test: *ns*, non-significant; * $p < 0.05$; ** $p < 0.01$; *** $p < 0.001$.

is predominantly localized in the oocyte nucleus (Supporting Information Fig. 1C). In addition, proximity ligation assay shows that CDK12 is localized together with its binding partner cyclin K (CCNK) in the nucleus of the mouse and human oocyte (Supporting Information 3). To assess overall transcription, we next labeled newly synthesized RNA with 5-ethynyluridine (EU) in growing oocytes. CDK12^{-/-} oocytes exhibited a 71% decrease in EU staining compared to CDK12^{+/+} oocytes, indicating a significant decrease in global transcription (Fig. 4A, B). In addition, the active form of RNA Polymerase II (Ser2), a marker for transcription elongation, was reduced by 39% in CDK12^{-/-} oocytes (Fig. 4C, D). Importantly, there were no differences in Pol II mRNA and protein levels between groups (Fig. 5A, B).

These results suggest that the absence of CDK12 leads to an abnormal transcriptional program that impairs the formation of the oocyte mRNA reserve and consequently prevents the development to fully grown GV oocytes and the depletion of the ovarian reserve.

The absence of CDK12 influences the expression of a subset of mRNAs in the oocyte

It is well known that oocyte development depends on proper gene expression. Given the significant reduction in transcription observed in CDK12^{-/-} oocytes (Fig. 4), we examined the expression of specific developmentally relevant classes of mRNAs encoding translational factors [15] (4E-BP1, eEF2, eIF4G1) and markers associated with premature ovarian failure [23–26] a phenotype observed in (Fig. 2) (POF; RPS26, FIGLA, GDF9, AIRE, FMRP1). Interestingly, qPCR data showed a significant 3.5-fold increase in mRNA of the translational repressor *4e-bp1* in CDK12^{-/-} oocytes (Fig. 5A). However, the mRNAs encoding the translation elongation factor *EEF2* were similar, and the mRNA encoding the translation initiation factor *eIF4G1* was significantly decreased in CDK12^{-/-} oocytes (Fig. 5A). In addition, all analyzed mRNAs encoding POF markers [24, 26, 27] were significantly reduced in CDK12^{-/-} oocytes (Fig. 5A). Further, we analyzed the expression of mRNAs encoding the homologous kinase CDK13 and the CDK12 binding partner CCNK (Supporting Information 3). The mRNAs of CDK12 and CDK13 were significantly decreased in CDK12^{-/-} oocytes, whereas the mRNAs of CCNK, POLII and HRPT were equally expressed in both groups (Fig. 5A).

Next, we analyzed the protein expression of selected candidate genes that had previously been examined by PCR (Fig. 5A). Immunoblotting analysis showed a positive correlation of the expression of POL II, 4E-BP1, eEF2, eIF4G1, RPS26, GDF9, CDK13 and CCNK with the corresponding mRNAs (Fig. 5B, C). To analyze the direct effect of CDK12 on the expression of candidate genes, we microinjected RNA encoding mouse CDK12 into CDK12^{-/-} oocytes. We restored the expression of CDK12 in the CDK12^{-/-} oocytes (Fig. 5D–F) and in such oocytes we observed decreased expression of the mRNA of the translational repressor *4e-bp1*. CDK12 expression increased the mRNAs of the *Eif4g1*, *Gdf9* and *Rps26* (Fig. 5D). Importantly, the presence of CDK12 in CDK12^{-/-} oocytes promoted the increase in POL II phosphorylation at serine 2, as well as the expression of eIF4G1 and the POF marker GDF9 (Fig. 5E, F).

In summary, the absence of CDK12 affects the expression of some selected mRNAs related to translation and the premature

ovarian failure phenotype. Furthermore, the addition of exogenous CDK12 to CDK12^{-/-} oocytes enhances POL II activity, leading to reorganization of the expression of translation factors and markers for POF.

Aberrant transcriptome of CDK12^{-/-} oocytes represses global translation and enhances expression of the translational repressor 4E-BP1

Considering that the absence of CDK12 promotes an aberrant maternal transcriptome and in particular, translational factors in the developing oocyte (Fig. 5A–C), we investigated, how protein synthesis was affected in CDK12^{-/-} oocytes. First, the ³⁵S-methionine incorporation assay showed that CDK12^{-/-} oocytes exhibited a 23% reduction in global protein synthesis compared to WT oocytes (Fig. 6A, B). Considering the reported effect of CDK12 on RNA polyadenylation [28, 29] and the impaired transcriptome/proteome (Fig. 5A–D) in CDK12^{-/-} oocytes, the polyadenylation directly correlates with the rate of protein synthesis of mRNA. We examined global polyadenylation by RNA FISH, which showed no difference between CDK12^{+/+} and CDK12^{-/-} oocytes (Fig. 6C and Supporting Information 4). In connection to overexpression of the translational repressor 4E-BP1 and reduced translation in CDK12^{-/-} oocytes (Fig. 5A, B), we analyzed polyadenylation of the mRNA encoding 4E-BP1. The PAT assay showed a visible poly(A) shift of the 3'UTR tail of *4e-bp1* in CDK12^{-/-} oocytes, while the poly(A) tail remained unchanged in *Cnot7* mRNA, which is translated after completion of meiosis I [30] (Fig. 6D, E).

In summary, we document that the absence of CDK12 leads to the stabilization of specific mRNAs, in particular *4e-bp1*, which is in the non-phosphorylated state (Supporting Information 5), thereby acting as a translational repressor and leading to reduced protein synthesis.

Our results clearly show that the absence of CDK12 leads to maternal infertility via the disruption of oocyte growth by a mechanism that impairs maternal transcriptome and translation (Graphical abstract). In addition, discontinued oocyte development leads to the failure of folliculogenesis, which is similar to the a-follicular form of premature ovarian failure that also occurs in humans [31].

DISCUSSION

We have summarized here the biological function of CDK12 with a focus on female reproduction. Interestingly, the absence of CDK12 in the oocyte results in the absence of fully developed oocytes, leading to complete female sterility. With Cre, CDK12 is down-regulated under the ZP3 promoter, which is activated in the growing 20 μm oocyte and reaches its maximum in the 50 μm oocyte [32]. This approach allows us to investigate the role of CDK12 in the transcriptionally active phase of oocyte development, which influences the early phase of oocyte growth and thus folliculogenesis. Although ovulation is promoted even in the absence of CDK12, it is only sparse and oocytes do not mature to a stage that can be fertilized and at least promote subfertility. Studies in mice have demonstrated that transcriptional activity and the transition of chromatin conformation from growing to fully grown GV oocyte are critical for oocyte maturation and

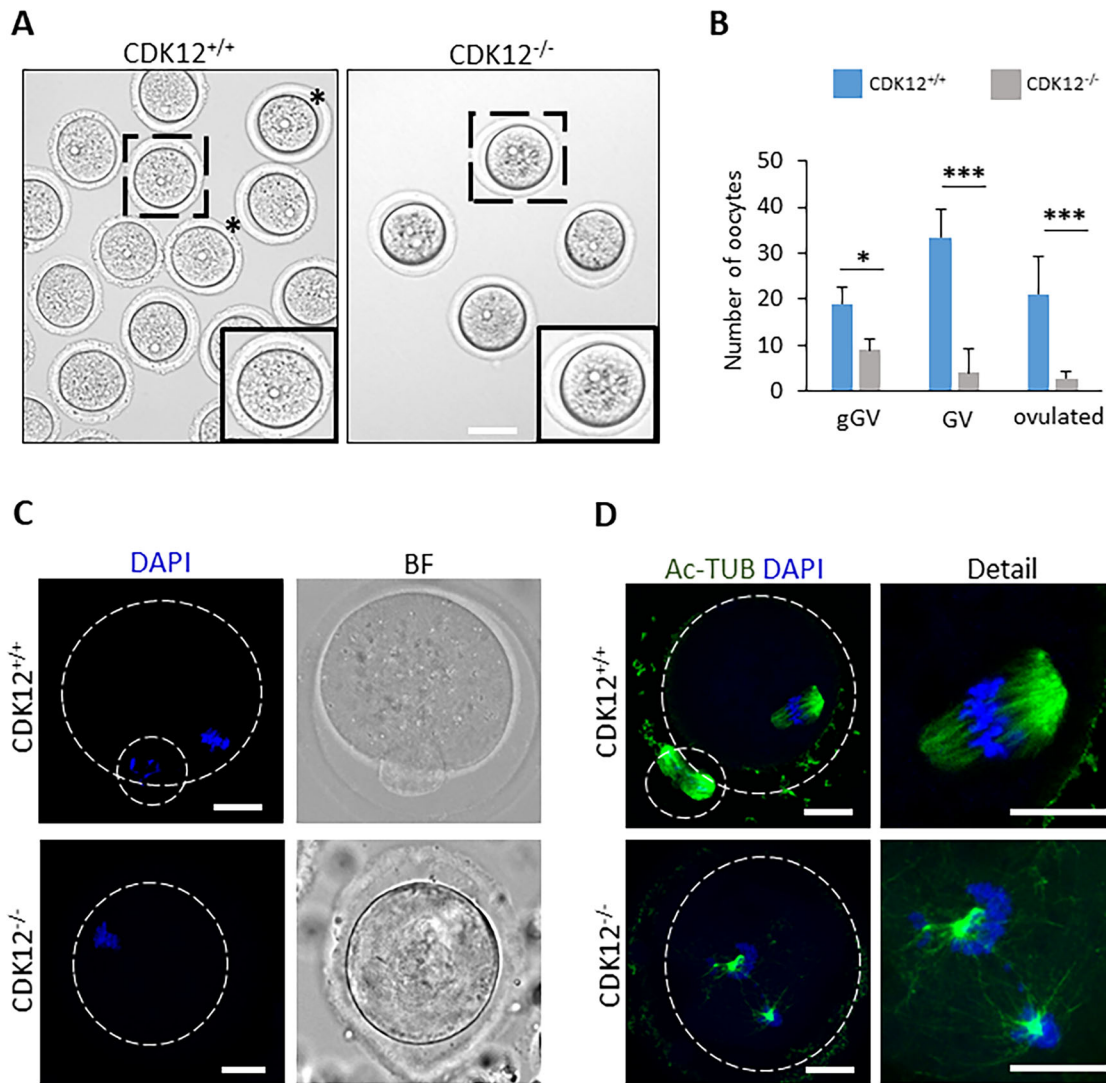
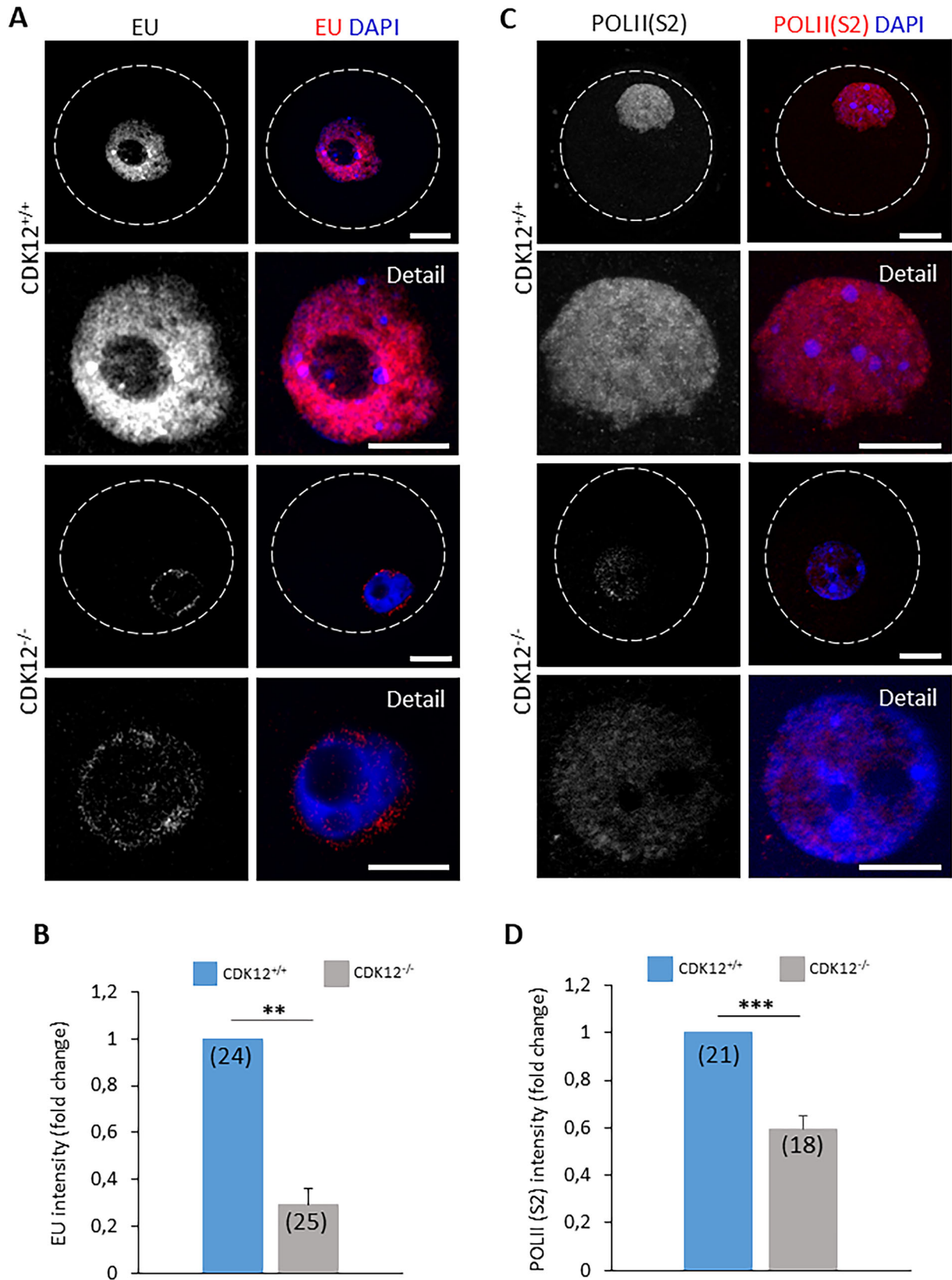


Fig. 3 CDK12 is Essential for oocyte development and maturation. **A** Representative images of morphology of CDK12^{+/+} and CDK12^{-/-} oocytes. Dashed squares show details of oocytes, asterisks show fully grown oocytes; scale bars 60 μ m. **B** Quantification of growing (gGV), fully-grown (GV) and ovulated (post hCG) oocytes isolated from ovaries. Data from five independent biological replicates. Data are presented as mean \pm SE; Student's t-test: * $p < 0.05$; *** $p < 0.001$. **C** Morphology of CDK12^{+/+} and CDK12^{-/-} ovulated oocytes. Data from three biological replicates and $n \leq 30$ cells per group. DAPI (blue), bright field (BF); the dashed line shows the cell cortex; scale bars 20 μ m. **D** Representative images of spindle morphology labeled with acetylated α -tubulin (Ac-TUB, green) in ovulated CDK12^{+/+} and CDK12^{-/-} oocytes. Data from three biological replicates and $n \leq 25$ per group. Details show the enlargement of the spindle area. DAPI (blue); the dashed line shows the cell cortex; scale bars 20 μ m.

subsequent embryo development [33–35]. Our analysis revealed a reduced number of antral follicles and an increased proportion of growing oocytes in CDK12-deficient mice. We hypothesize that the elevated proportion of growing CDK12^{-/-} oocytes results from their limited meiotic competence. A recent transcriptional profile analysis of human growing and fully grown oocytes showed that CDKs involved in transcription via POL II have higher expression in human growing oocytes, indicating the high activity characteristic of this developmental stage [35].

The CDK12/CCNK complex has been shown to be required for the promotion of transcription elongation by RNA polymerase II activation via the phosphorylation of its carboxyl-terminal domain [36]. CDK12 has sequences for nuclear localization [37]. In the oocyte, CDK12/CCNK complexes are abundant in the nucleus, supporting their biological function in transcription [13, 16]. Although CDK12 and CDK13 share a high degree of homology, they exhibit only partial redundancy in their roles in polymerase II-mediated transcription [16, 38]. In cancer cell lines, the genetic

deletion or chemical inhibition of CDK12 kinase activity has virtually no effect on CDK13 protein levels, and never leads to such a dramatic downregulation seen in growing oocytes [13, 39]. It is therefore difficult to decide whether the 69% decrease in global transcription is due to the absence of CDK12 or CDK13. In cancer cell lines, inhibition of the kinase activity of both kinases by several functionally different inhibitors affected transcription efficiency by 10–20% [13, 38]. One can speculate that the role of CDK12 and CDK13 in regulating transcription in cancer cell lines is different from that in primary cells such as oocytes. Not surprisingly, the decrease in global transcription was accompanied by a 39% decrease in the Ser2 phosphorylation detecting of elongating Pol II. Since we could still detect Pol II phosphorylated at Ser in the nucleus, it is very likely that CDK9 is the kinase responsible for the remaining Pol II(Ser2) signal, since CDK9 is active in the GVs of porcine oocytes [40]. Furthermore, the chemical inhibition of CDK12, CDK13 or both together affected up to 15% of all genes, clearly indicating that the transcriptional



program in growing oocytes is mainly the transcription of specialized and developmentally relevant genes [38]. Although we did not perform a global transcriptome analysis, we clearly found decreased mRNA for POF markers and translation factors

with the sole exception of the *4e-bp1* mRNA. Suggesting that the absence of CDK12 (i) promotes the transcription of specific genes, (ii) impairs a specific transcriptional program during the activation of the ZP3 promoter in the oocyte, and/or (iii) indirectly affects

Fig. 4 The absence of CDK12 suppress transcriptional activity in developing oocytes. A Detection of transcriptional activity with 5-Ethynyl Uridine (EU; gray and red) in CDK12^{+/+} and CDK12^{-/-} oocytes. Data from three independent biological replicates. Details show a magnification of the nucleus; DAPI (blue); the dashed line depicts the cell cortex; scale bar 20 μm. **B** Quantification of EU fluorescence in the nucleus from (A). The values from CDK12^{+/+} were set as 1. The number of cells is shown in parentheses. Data are presented as mean ± SE; Student's *t*-test: ***p* < 0.01. **C** Detection of phosphorylation of Polymerase II at Serine 2 (POLII(S2); gray and red) by immunocytochemistry. Data from three independent experiments. The details show an enlargement of the nuclear region. DAPI (blue); the dashed line depicts the cell cortex; scale bar 20 μm. **D** Quantification of POLII (S2) fluorescence intensity in the nucleus of CDK12^{+/+} and CDK12^{-/-} oocytes from the (C) experiment. The values from CDK12^{+/+} were set as 1. The number of cells is shown in parentheses. Data are presented as mean ± SE; Student's *t*-test: ****p* < 0.001.

transcription by altering the expression of factors that negatively modulate transcription. Our results show that the absence of CDK12 affects the transcriptome of the growing oocyte by interfering with the activity of Pol II, which in turn affects translation. Previous reports showed that the yeast ortholog of CDK12, Ctk1 [16, 41] stimulates mRNA translation globally [20, 42]. Similarly, we found an additional role of CDK12 that involves the stabilization of specific mRNA with increased polyadenylation, thereby promoting their translation. Indeed, CDK12 has been identified as a nuclear co-transcriptional polyadenylation factor that either ensures the processing of the 3'-end through a cleavage and polyadenylation mechanism, or blocks the premature cleavage and polyadenylation (PCPA) of hnRNA [29, 43]. Apart from the effect of CDK12 on the polyadenylation of 4E-BP1 mRNA, the deletion of CDK12 resulted in a moderate increase in the protein level of the 5'-cap-binding mRNA repressor 4E-BP1 in CDK12^{-/-} oocytes. Our previously published results provided evidence that expression of the inactive translational repressor 4E-BP1 leads to aberrant proteosynthesis in fully developed, transcriptionally silent oocyte [44]. Most mRNAs accumulated during oocyte growth are translationally repressed and are translated later when transcription is repressed [45, 46]. Therefore, 4E-BP1 may play a key role in mRNA storage process, and the overexpression of 4E-BP1 observed in CDK12^{-/-} oocytes suppresses the translation of already abnormally expressed mRNAs, the translation of which promotes oocyte growth. We previously reported that inactivation of 4E-BP1 occurs at later stages of oocyte development, after entry into the M phase [44], and similarly, CDK12 phosphorylates/inactivates 4E-BP1 and promotes the translation of specific mRNA of factors involved in mitotic spindle regulation and chromosome segregation [15]. Importantly, the translational repressor 4E-BP1 is inactivated by phosphorylation during the metaphase transition in cells and oocytes [15, 44]. The unphosphorylated form of 4E-BP1 is therefore present in growing GV oocytes. Nevertheless, we still do not know whether and how the mRNA stabilization and translation of 4E-BP1 is directly or indirectly influenced by CDK12. In addition, the reduced expression of the translation initiation factor eIF4G1 and aberrant transcriptome in CDK12^{-/-} oocytes, likely contribute to reduced global translation.

CDK12 is involved in the DNA-damage repair (DDR) pathway by regulating the expression of several DDR machinery components, including BRCA1, ATM, ATR, and Fanconi anemia (FANC) genes [13]. CDK12-deficient blastocysts exhibit abnormal morphology and developmental failure due to increased DNA damage within the inner cell mass [47]. Beyond its impact on transcription and translation in growing oocytes, the loss of CDK12 likely impairs the expression of DDR genes. Recent studies identifying factors responsible for primary and premature ovarian insufficiency (POI) have reported either dramatic downregulation or non-functional variants of several DDR pathway members, such as BRCA1, RAD51, ATR, MSH4, MSH5, and FANC genes [23, 48].

Long-term depletion of CDK12 leads to cell cycle arrest in the G2/M phase [27]. Moreover, novel deleterious mutations in the kinase domain of CDK12 (H857Y/R, F8787S, T893I) have been identified in ovarian cancer patients [49]. These mutations mimic a

loss-of-function phenotype, although their specific impact on fertility remains unknown. Interestingly, patients with CDK13-related disorders exhibit pregnancy complications in 29.4% of cases [50–53].

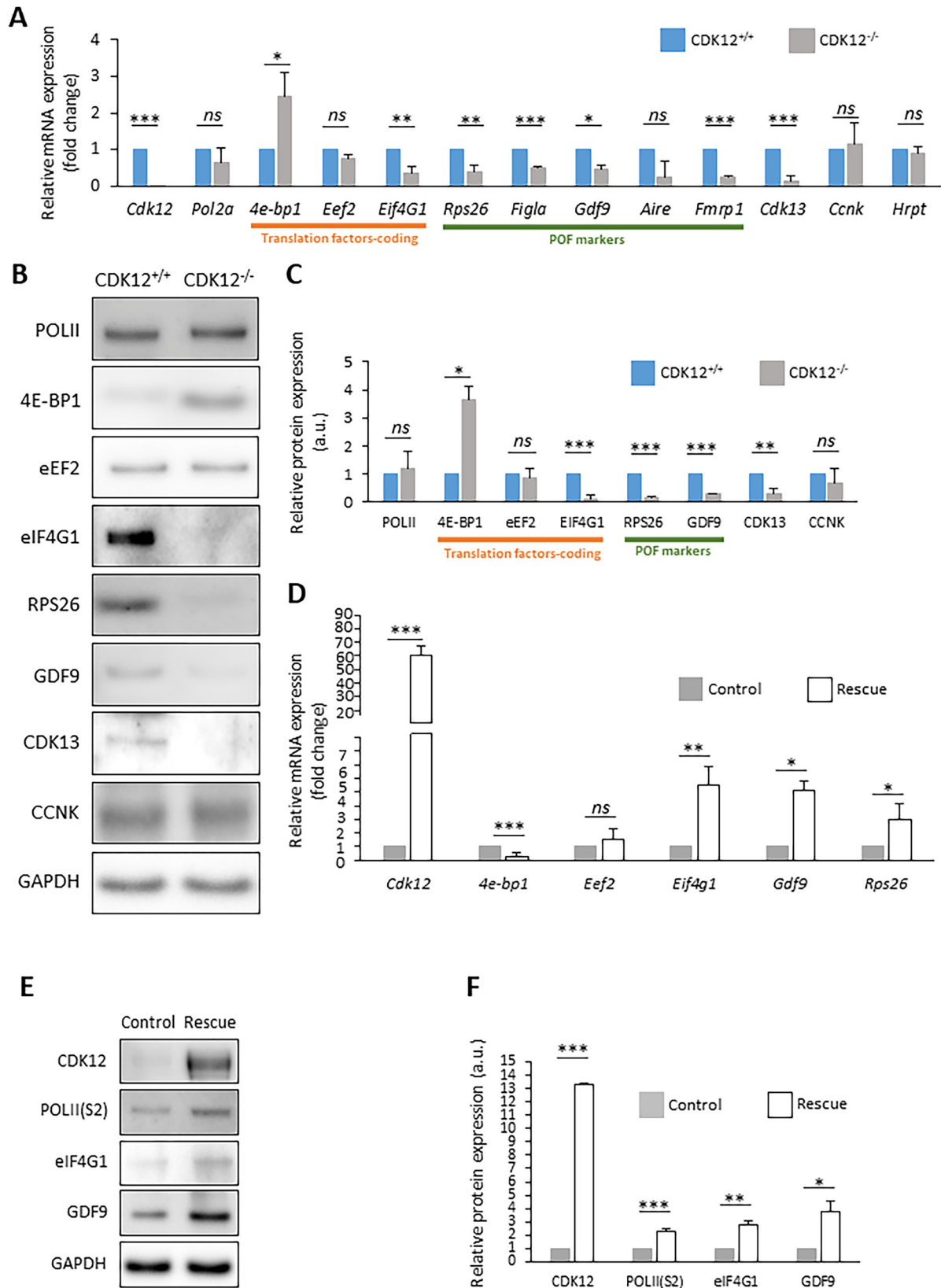
Among the downregulated transcripts and proteins, premature ovarian failure (POF) markers such as *Rps26*, *Figla*, *Gdf9*, *Aire* and *Fmrp1* [24, 25, 54–61] were detected, so the absence of CDK12 clearly resembles a POF phenotype [62–64]. We have compiled a list of genes linked to ovarian development and function in both human and mouse, which are regulated by CDK12 (Supplementary Table 1) [57, 65–67]. POF is a clinical disorder characterized by hypogonadism and amenorrhea, and affects 1–3% of women under 40 years of age [68–71]. The overall prevalence of familial POF ranges from 4% to 31% [70]. The appearance of the ovaries varies from the complete depletion of follicles to the presence of a variable population of follicles that fail to develop [68, 72]. The pregnancy rate among women with POF ranges from 2.2% to 14.2% [73]. GDF9 and RPS26 have been described as important factors for oocyte growth and the recruitment of a primordial follicle into the pool of growing follicles [25, 74]. GDF9, a protein secreted from the oocyte into the follicle, influences the proliferation, differentiation, steroid hormone synthesis, apoptosis and cumulus expansion of granulosa cells [75]. GDF9 levels increase dramatically with oocyte growth during preantral folliculogenesis and remain high until ovulation [74] in oocytes of various mammalian species, including humans [76], sheep [77], bovines [77] and rats [78], indicating the universality of the role of GDF9. In addition, CDK12 has been associated with follicular atresia (reduction in the number of ovulating follicles) and early menopause in humans [62, 64, 79]. CDK12 has been also shown to play a role in the PI3K/AKT/mTOR pathway, which is a critical signaling cascade involved in primary ovarian insufficiency (POI) [15, 65, 66, 80, 81].

Taken together, our results clearly demonstrate that the absence of CDK12 leads to an abnormal transcriptome and translome of the growing oocyte, which in turn results in the absence of a fully mature oocyte and leads to female infertility. In addition, we provide insight into the etiology of premature ovarian failure, in which CDK12 may also play an important role in humans, warranting further investigation.

METHODS

Oocyte isolation and cultivation

Experimental genotypes were designated as wild-type (WT; CDK12^{+/+}; *Cdk12*^{tm1c+/+} *Zp3-Cre*^{+/+}) and homozygotes (cKO; CDK12^{-/-}; *Cdk12*^{tm1c-/-} *Zp3*^{+/+}). Oocytes were obtained from C57BL/6 J mice that were at least 5 weeks of age. Females were stimulated with 5 IU of pregnant mare serum gonadotropin (PMSG; Folligon; Merck Animal Health) per mouse 46 h prior to oocyte isolation. To obtain MII, the mice were primed with 5 IU human chorionic gonadotropin (hCG, Pregnyl, N.V. Organon). Oocytes were isolated in transfer medium (TM) supplemented with 100 μM 3-isobutyl-1-methylxanthine (IBMX, Sigma Aldrich) to prevent the spontaneous resumption of meiosis. Selected oocytes were denuded and cultured in M16 medium (Millipore) without IBMX at 37 °C, 5% CO₂ for 0 h (GV) or 12 h (MII) [82]. All animal experiments were performed in accordance with the guidelines and protocols approved for the Laboratory



of Biochemistry and Molecular Biology of Germ Cells at the Institute of Animal Physiology and Genetics in the Czech Republic. All animal experiments were conducted in accordance with Act No. 246/1992 on the Protection of Animals from Cruelty, issued by the Ministry of

Agriculture under the number 67756/2020MZE-18134. Human oocytes not used for human reproduction were obtained from the Institute for the Care of Mother and Child in Prague. The project was approved and accredited by the Ethics Committee of the Institute for the Care of Mother

Fig. 5 The absence of CDK12 influences the expression of a subset of mRNAs in the oocyte. **A** Quantitative RT-PCR analysis of selected mRNAs. RNAs coding for translational factors (underlined in orange) and markers for premature ovarian failure markers (underlined in green). Data normalized to *Hrpt* mRNA. Data from three independent biological replicates. Values from CDK12^{+/+} oocytes were set as 1. Data are presented as mean ± SD; Student's *t*-test: *ns*, non-significant; **p* < 0.05, ***p* < 0.01; ****p* < 0.001. **B** Western blot analysis of candidate proteins selected from (A). Values from CDK12^{+/+} oocytes were set as 1. GAPDH was used as a loading control. Data from at least three independent biological replicates. For the phosphorylation of 4E-BP1, see Fig. 3. **C** Quantification of candidate proteins from (B). Data are presented as mean ± SE; Student's *t*-test: *ns*, non-significant; **p* < 0.05; ****p* < 0.001. **D** Quantitative RT-PCR analysis of the expression of selected mRNAs in control (microinjection of *H2b-Gfp* RNA into CDK12^{-/-} oocytes; gray) and in CDK12^{-/-} oocytes microinjected with *Cdk12* mRNA (rescue; white). Data from three independent biological replicates. Values were normalized to the number of oocytes per sample. Data are presented as mean ± SD; Student's *t*-test: *ns*, non-significant; **p* < 0.05. **E** Western blot analysis of selected proteins after CDK12 overexpression. GAPDH was used as a loading control. Data from three biological replicates. **F** Quantification of candidate proteins from (E). Data are presented as mean ± SE; Student's *t*-test: *ns*, non-significant; **p* < 0.05; ***p* < 0.01; ****p* < 0.001.

and Child (#1/3/4/2022; NU-23-07-0005). All patients gave informed consent to the use of their immature oocyte(s) this study.

Animals

Cdk12^{fx/fx} mice on a C57BL/6J genomic background were provided by Jiri Kohoutek. Cdk12^{fx/fx} mice were crossed with Zp3-Cre mice to generate the oocyte-specific Cdk12 knockout (CDK12^{-/-}). The target construct contains loxP sites in the 3 and 4th exon (8 nucleotides in the defective 4th exon and a stop codon inserted into the open reading frame). The primers used for PCR to genotype Cdk12^{fx/fx} were primer mCDK12 Flx-F—CTTCAGACAGTGCAGACCCTGGAGAAGC; primer mCDK12 Y3-R—CCTCTGACCTCCAATGTGTGCATGACAC; F-ZP3—GGTGGAGAATGTTAATC and R-ZP3—TATTCGGATCATCAGCTA. All experiments were performed according to the guidelines and with the approval of Institutional Animal Care. Pairs of 8-week-old female mice of genotypes CDK12^{+/+}, CDK12^{+/-} and CDK12^{-/-} were continuously mated with proven CDK12^{+/+} males to test the fertility of the females. The number of pups was recorded over a period of 8 months.

Histology of ovaries

Ovaries were fixed in 4% PFA solution (Sigma) for 48 h, then placed in 70% ethanol solution and subsequently placed in labeled histological cassettes. Samples were processed using an automated tissue processor (Leica ASP 6025, Leica Microsystems, Germany) and embedded in paraffin blocks using a Leica EG 1150H paraffin embedding station (Leica Microsystems, Germany). Sections of 3 µm were cut with a microtome (Leica RM2255, Leica Microsystems, Germany) on standard glass slides (Waldemar Knittel, GmbH, Germany), every 10th section was collected, 3–12 sections were collected per slide. Slides were stained with hematoxylin–eosin and mounted using a Leica ST5020 automated stainer in combination with a Leica CV5030 mounting frame. The number of follicles was quantified using a stereomicroscope (Zeiss Stemi 2000, Germany). The analysis of ovarian follicles was performed by two different investigators.

Oocyte microinjection

Experimental oocytes Cdk12^{-/-} were injected with an in vitro prepared *Cdk12* and *H2b-Gfp* RNAs diluted to a final concentration of 20 ng/µl, the control samples were injected with *H2b-Gfp* mRNA alone. Subsequently, the injected oocytes were incubated in IBMX at 37 °C and 5% CO₂ for 18 h. The oocytes were washed in PVA/PBS and frozen at –80 °C.

Measurement of Overall Protein Synthesis

To measure total protein synthesis, 50 mCi of ³⁵S-methionine (Perkin Elmer) was added to methionine-free culture medium, for 1 h and then oocytes were lysed in SDS-buffer and subjected to SDS–polyacrylamide gel electrophoresis. The labeled proteins were visualized by autoradiography with BasReader (FujiFilm). GAPDH was used as a loading control.

5-ethynyl uridine transcription assay

The 5-EU was added to the M16 medium with IBMX and incubated overnight with growing GV oocytes. Oocytes were then fixed in 4% paraformaldehyde/PBS for 15 min, permeabilized with 0.1% Triton X-100/PBS for 10 min at room temperature, and incubated for 1 h at room temperature in the dark with the Click-iT reaction cocktail (according to the manufacturer's instructions using Alexa A555 azide (ThermoFisher, A20012) and a commercial kit (Click-iT, ThermoFisher, C10276). After incubation, oocytes were washed once with PBS and mounted on slides

using DAPI in the presence of the anti-fade reagent Vectashield (H-1500, Vector laboratories). Images were captured using a confocal laser scanning microscope (Leica SP5, Leica Microsystems, Wetzlar, Germany). Images were quantified and compiled using FIJI software (version 1.8.0_172).

RNA isolation and RT-PCR

TRIzol reagent (Invitrogen) was used for RNA extraction according to the manufacturer's instructions. Reverse transcription was performed with a qPCR BIO cDNA Synthesis Kit (PCR Biosystems). qPCR was then carried out using QuantStudio 3 (Applied Biosystems) and Luna® Universal qPCR Master Mix (New England BioLabs) according to the manufacturer's protocols with an annealing temperature of 60 °C. The primers are listed in Supplementary Table 2.

Poly-A-tail length assay (PAT)

To obtain the total length of the poly(A) tail of each transcript, total RNA was extracted using the phenol-chloroform method according to the laboratory protocol. Elution was performed in 10 µl of water per sample. The isolated RNA was incubated with 1 µl of 20 mM oligo-dT annealing per sample for 5 min at 65 °C. Ligation was then carried out for 30 min at 42 °C. The ligation mix was prepared from the following components: T4 ligase (1 µl), Superscript IV 5x buffer (5 µl), 20U/µl RNase inhibitor (1 µl), 10 mM dNTP (1 µl), 10 mM ATP (1 µl), 1 M MgCl₂ (0.1 µl), 0.1 M DTT (2 µl), RNase-free water (2 µl). The cDNA synthesis was performed by adding 1 µl Superscript II Reverse Transcriptase with the following setup: 45 min at 45 °C, 10 min at 80 °C, hold at 4 °C. The prepared cDNA was subjected to PCR with gene-specific forward primers and anchoring reverse primer (Supplementary Table 2). PCR was performed with PPP Master Mix (Top-Bio) under the following conditions: 1 min at 95 °C, 35x (30 s at 95 °C, 20 s at 55 °C, 45 s at 72 °C). PCR products were analyzed on a 1.5% agarose gel stained with GelRed (41003, Biotinum) and run at 90 V for 45 min. The gels were detected with an Azure 600 Imager (Azure Biosystems).

RNA FISH of poly(A) mRNA

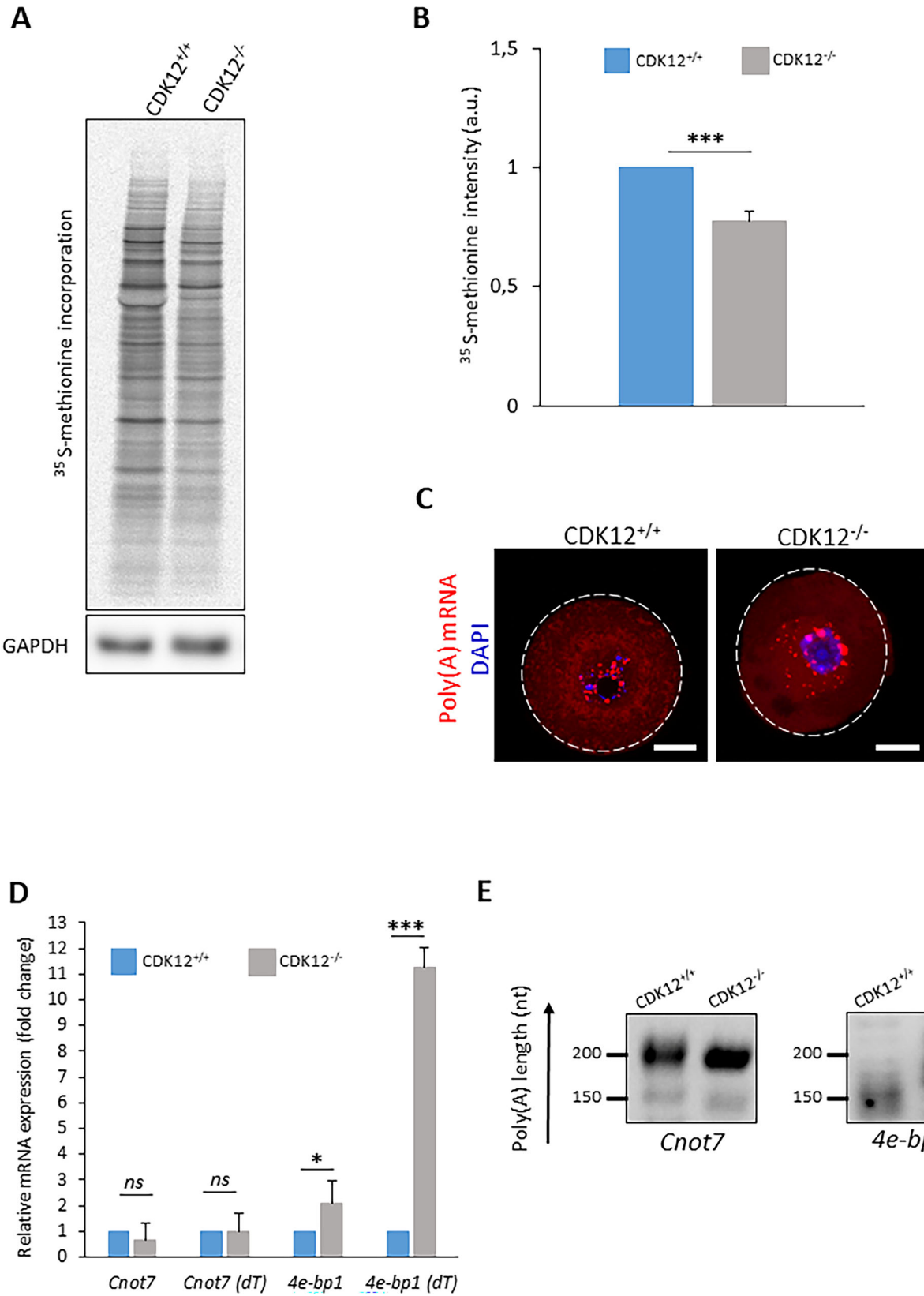
Oocytes were fixed in 4% paraformaldehyde for 15 min and permeabilized by protease III treatment (Biosearch Technologies). Samples were washed in wash buffer A (Biosearch Technologies) and incubated overnight at 42 °C in hybridization buffer (Biosearch Technologies) containing 75 nM oligo-d(T) probe with CalFluorRed635 (Biotec Generi). Samples were washed twice in wash buffer A and twice in 2x SSC (Sigma Aldrich). Samples were embedded in VectaShield medium with DAPI (H-1500, Vector Laboratories). A confocal laser scanning microscope was used for imaging (Leica SP5, Leica Microsystems, Wetzlar, Germany). Data from three biological replicates. The quantification of fluorescence intensity between CDK12^{+/+} and CDK12^{-/-} oocytes was performed using FIJI software (version 1.8.0_172).

Immunofluorescence

Fixed oocytes (15 min in 4% PFA, Sigma Aldrich) were permeabilized for 10 min in 0.1% Triton X-100, washed in PBS with polyvinyl alcohol (PVA, Sigma Aldrich), and incubated overnight at 4 °C with primary antibodies (Supplementary Table 2) diluted in PVA/PBS. Immunofluorescence analysis was performed according to a published protocol [83]. Image quantification and compilation was performed using FIJI software (version 1.8.0_172).

In situ proximity ligation assay (PLA)

The proximity ligation assay was performed according to the instructions of Naveni Triflex (Navinci). Oocytes were fixed in 4% PFA for 15 min and



permeabilized with 0.5% TritonX/PBS for 10 min. Oocytes were washed with TBS-T solution and then transferred into primary antibodies (CCNK and CDK12, Supplementary Table 2) 1.5: 100 dilution 1TF overnight at 4 °C. The oocytes were washed in TBS-T for 15 min. The oocytes were incubated

with Navenibody MTF and Navenibody RTF 1:10 dilution 2 for 1 h at 37 °C on a hot plate. The oocytes were washed every 15 min with TBS-T solution. A total of 40 µl of amplification reaction 1 was mixed according to the manufacturer's instructions, then added to the oocytes and incubated at

Fig. 6 The absence of CDK12 specifically affects the stability of the mRNA encoding the translational repressor 4E-BP1. **A** Analysis of global de novo proteosynthesis by incorporation of ^{35}S -methionine in CDK12 $^{+/+}$ and CDK12 $^{-/-}$ oocytes. Data from four independent biological replicates. GAPDH was used as a loading control. **B** Quantification of ^{35}S -methionine incorporation from (A). Values from CDK12 $^{+/+}$ oocytes were set as 1. Data from four independent experiments. Data presented as mean \pm SD; Student's *t*-test: ****p* < 0.001. **C** Representative confocal images of poly(A) mRNA in CDK12 $^{+/+}$ and CDK12 $^{-/-}$ oocytes. Data from three biological replicates (*n* \geq 15). Poly(A) mRNA (red); DAPI (blue); the dashed line depicts the cell cortex; scale bars 20 μm . For the quantification of fluorescence intensity, see SI Fig. 4. **D** Quantitative RT-PCR analysis of cDNA synthesized with hexamers or oligo(dT) primers in CDK12 $^{+/+}$ and CDK12 $^{-/-}$ oocytes. Data from three biological replicates. Data are normalized to the number of oocytes. Data are presented as mean \pm SD; Student's *t*-test: *ns*, non-significant; **p* < 0.05; ****p* < 0.001. **E** Polyadenylation test (PAT) to detect the poly(A) tail length of *4e-bp1* in CDK12 $^{+/+}$ and CDK12 $^{-/-}$ oocytes. Translationally inactive *Cnot7* mRNA was used as negative control. Data from three independent biological replicates. The length of the poly(A) tail is described on the left (nt).

37 °C for 30 min. It was then washed with TBS-T solution for 5 min. Reaction 2 was mixed according to the manufacturer's instructions. The oocytes were incubated in 40 μl of reaction 2, in a dish protected from light, for 1 h at 37 °C. Samples were washed for 5 min and then mounted on a concave-bottomed slide (cat. # 1216492, Marienfeld,) using Vectashield mounting medium with DAPI (H-1500, Vector Laboratories). A confocal laser scanning microscope was used for the images (Stellaris8).

Western Blotting

Oocyte lysates were analyzed on a 4–12% gradient acrylamide gel. Samples were transferred to a polyvinylidene fluoride membrane (Immobilon P; Merckmillipore) using a blotting system (Biometra GmbH) at 5 mA/cm 2 for 25 min. The membranes were blocked for 1 h at room temperature and then incubated overnight at 4 °C with the primary antibodies listed in Supplementary Table 2. Membranes were incubated with secondary antibodies for 1 h at room temperature. Proteins were visualised by chemiluminescence using ECL (Amersham) and imaged in an Azure 600 Imager (Azure Biosystems), and the acquired signals were quantified using ImageJ (<http://rsbweb.nih.gov/ij/>). Data from at least three biological replicates. To detect the phosphorylation shift, oocytes were dissolved in 20 μl of 1 \times NEB buffer containing 800 U of LPP enzyme (P0753, New England Biolabs) and incubated at 30 °C for 1 h.

Statistical analysis and data visualization

GraphPad Prism 8.3 was used for the statistical analysis. The statistical analysis included Student's *t*-tests to determine statistical significance between groups (labeled with an asterisk). **p* < 0.05; ***p* < 0.01, and ****p* < 0.001. Mean and standard error values were calculated in MS Excel (Microsoft).

DATA AVAILABILITY

All data generated or analyzed during this study are included in this published article and its supplementary information files.

REFERENCES

- Sternlicht AL, Schultz RM. Biochemical studies of mammalian oogenesis: Kinetics of accumulation of total and poly(A)-containing RNA during growth of the mouse oocyte. *J Exp Zool.* 1981;215:191–200. <https://doi.org/10.1002/jez.1402150209>.
- Ida Jentoft AM, Bäuerlein FJ, Welp LM, Urlaub H, Fernández-Busnadiego R, Jentoft IM, et al. Mammalian oocytes store proteins for the early embryo on cytoplasmic lattices. *Cell.* 2023;186:5308–27. <https://doi.org/10.1016/j.cell.2023.10.003>.
- Sha QQ, Dai XX, Dang Y, Tang F, Liu J, Zhang YL, et al. A MAPK cascade couples maternal mRNA translation and degradation to meiotic cell cycle progression in mouse oocytes. *Dev.* 2017;144:452–63. <https://doi.org/10.1242/dev.144410>.
- Leesch F, Lorenzo-Orts L, Pribitzer C, Grishkovskaya I, Roehsner J, Chugunova A, et al. A molecular network of conserved factors keeps ribosomes dormant in the egg. *Nature.* 2023;613:712 <https://doi.org/10.1038/S41586-022-05623-Y>.
- Wickramasinghe D, Albertini DF. Centrosome phosphorylation and the developmental expression of meiotic competence in mouse oocytes. *Dev Biol.* 1992;152:62–74. [https://doi.org/10.1016/0012-1606\(92\)90156-B](https://doi.org/10.1016/0012-1606(92)90156-B).
- Iyyappan R, Aleshkina D, Ming H, Dvoran M, Kakavand K, Anso VaDJ, et al. The translational oscillation in oocyte and early embryo development. *Nucleic Acids Res.* 2023;2023:2023 <https://doi.org/10.1093/NAR/GKAD996>.
- Yang F, Wang W, Cetinbas M, Sadreyev RI, Blower MD. Genome-wide analysis identifies cis-acting elements regulating mRNA polyadenylation and translation during vertebrate oocyte maturation. *RNA.* 2020;26:324–44. <https://doi.org/10.1261/RNA.073247.119/-/DC1>.
- Luo Y, Lee IW, Jo YJ, Namgoong S, Kim NH. Depletion of the LINC complex disrupts cytoskeleton dynamics and meiotic resumption in mouse oocytes. *Sci Rep.* 2016;6:1–11. <https://doi.org/10.1038/srep20408>.
- Sun H, Han L, Guo Y, An H, Wang B, Zhang X, et al. The global phosphorylation landscape of mouse oocytes during meiotic maturation. *EMBO J.* 2024. https://doi.org/10.1038/S44318-024-00222-1/SUPPL_FILE/44318_2024_222_MOESM28_ESM.PDF.
- Eppig JJ, Schroeder AC. Capacity of mouse oocytes from preantral follicles to undergo embryogenesis and development to live young after growth, maturation, and fertilization in vitro. *Biol Reprod.* 1989;41:268–76. <https://doi.org/10.1095/biolreprod41.2.268>.
- Sha QQ, Zhu YZ, Li S, Jiang Y, Chen L, Sun XH, et al. Characterization of zygotic genome activation-dependent maternal mRNA clearance in mouse. *Nucleic Acids Res.* 2020;48:879–94. <https://doi.org/10.1093/NAR/GKZ1111>.
- ABE K-I, INOUE A, SUZUKI MG, AOKI F. Global gene silencing is caused by the dissociation of RNA polymerase II from DNA in mouse oocytes. *J Reprod Dev.* 2010;56:502–7. <https://doi.org/10.1262/jrd.10-068a>.
- Blazek D, Kohoutek J, Bartholomeeusen K, Johansen E, Hulinkova P, Luo Z, et al. The cyclin K/Cdk12 complex maintains genomic stability via regulation of expression of DNA damage response genes. *Genes Dev.* 2011;25:2158–72. <https://doi.org/10.1101/gad.16962311>.
- Chirackal Manavalan AP, Pilarova K, Kluge M, Bartholomeeusen K, Rajecy M, Oppelt J, et al. CDK12 controls G1/S progression by regulating RNAPII processivity at core DNA replication genes. *EMBO Rep.* 2019;20:e47592 <https://doi.org/10.15252/embr.201847592>.
- Choi SH, Martinez TF, Kim S, Donaldson C, Shokhiev MN, Saghatelian A, et al. CDK12 phosphorylates 4E-BP1 to enable mTORC1-dependent translation and mitotic genome stability. *Genes Dev.* 2019;33:418–35. <https://doi.org/10.1101/gad.322339.118>.
- Bartkowiak B, Liu P, Phatnani HP, Fuda NJ, Cooper JJ, Price DH, et al. CDK12 is a transcription elongation-associated CTD kinase, the metazoan ortholog of yeast Ctk1. *Genes Dev.* 2010;24:2303–16. <https://doi.org/10.1101/gad.1968210>.
- Tien JF, Mazloomian A, Cheng SWG, Hughes CS, Chow CCT, Canapi LT, et al. CDK12 regulates alternative last exon mRNA splicing and promotes breast cancer cell invasion. *Nucleic Acids Res.* 2017;45:6698–716. <https://doi.org/10.1093/nar/gkx187>.
- Magnuson B, Bedi K, Narayanan IV, Bartkowiak B, Blinkiewicz H, Paulsen MT, et al. CDK12 regulates co-transcriptional splicing and RNA turnover in human cells. *IScience* 2022;25. <https://doi.org/10.1016/J.ISCI.2022.105030>.
- Ang HX, Sutiman N, Deng XL, Bartelt LC, Chen Q, Barrera A, et al. Cooperative regulation of coupled oncoprotein translation and stability in triple-negative breast cancer by EGFR and CDK12. *BioRxiv* 2021:2021.03.03.433762. <https://doi.org/10.1101/2021.03.03.433762>.
- Coordes B, Brünger KM, Burger K, Soufi B, Horenk J, Eick D, et al. Ctk1 function is necessary for full translation initiation activity in *Saccharomyces cerevisiae*. *Eukaryot Cell.* 2015;14:86 <https://doi.org/10.1128/EC.00106-14>.
- Bell D, Berchuck A, Birrer M, Chien J, Cramer DW, Dao F, et al. Integrated Genomic Analyses of Ovarian Carcinoma. *Nature.* 2011;474:609 <https://doi.org/10.1038/NATURE10166>.
- Ekumi KM, Paculova H, Lenasi T, Pospichalova V, Bösen CA, Rybarikova J, et al. Ovarian carcinoma CDK12 mutations misregulate expression of DNA repair genes via deficient formation and function of the Cdk12/CycK complex. *Nucleic Acids Res.* 2015;43:2575 <https://doi.org/10.1093/NAR/GKV101>.
- França MM, Mendonça BB Genetics of Primary Ovarian Insufficiency in the Next-Generation Sequencing Era. *J Endocr Soc* 2019;4. <https://doi.org/10.1210/JENDSO/BVZ037>.
- França MM, Funari MFA, Nishi MY, Narcizo AM, Domenice S, Costa EMF, et al. Identification of the first homozygous 1-bp deletion in GDF9 gene leading to

- primary ovarian insufficiency by using targeted massively parallel sequencing. *Clin Genet.* 2018;93:408–11. <https://doi.org/10.1111/CGE.13156>.
25. Liu XM, Yan MQ, Ji SY, Sha QQ, Huang T, Zhao H, et al. Loss of oocyte Rps26 in mice arrests oocyte growth and causes premature ovarian failure. *Cell Death Dis.* 2018;9. <https://doi.org/10.1038/S41419-018-1196-3>.
 26. Santos M, Cordts EB, Peluso C, Dornas M, Neto FHV, Bianco B, et al. Association of BMP15 and GDF9 variants to premature ovarian insufficiency. *J Assist Reprod Genet.* 2019;36:2163–9. <https://doi.org/10.1007/S10815-019-01548-0>.
 27. Wu J, Feng S, Luo Y, Ning Y, Qiu P, Lin Y, et al. Transcriptomic profile of premature ovarian insufficiency with RNA-sequencing. *Front Cell Dev Biol.* 2024;12. <https://doi.org/10.3389/FCELL.2024.1370772>.
 28. Dubbury S, Boutz P, Nature PS-, 2018 undefined. CDK12 regulates DNA repair genes by suppressing intronic polyadenylation. *NatureComSJ Dubbury, PL Boutz, PA SharpNature, 2018-natureCom n.d.*
 29. Krajewska M, Dries R, Grassetti AV, Dust S, Gao Y, Huang H, et al. CDK12 loss in cancer cells affects DNA damage response genes through premature cleavage and polyadenylation. *Nat Commun.* 2019;10:1–16. <https://doi.org/10.1038/s41467-019-09703-y>.
 30. Lamacova L, Jansova D, Jiang Z, Dvoran M, Aleshkina D, Iyyappan R, et al. CPEB3 Maintains Developmental Competence of the Oocyte. *Cells* 2024;13. <https://doi.org/10.3390/CELLS13100850>.
 31. Shestakova IG, Radzinsky VE, Khamoshina MB Occult form of premature ovarian insufficiency. *Gynecol Endocrinol.* 2016;1473–0766. <https://doi.org/10.1080/09513590.2016.1232676>.
 32. Philpott CC, Ringuette MJ, Dean J. Oocyte-specific expression and developmental regulation of ZP3, the sperm receptor of the mouse zona pellucida. *Dev Biol.* 1987;121:568–75. [https://doi.org/10.1016/0012-1606\(87\)90192-8](https://doi.org/10.1016/0012-1606(87)90192-8).
 33. Monti M, Zanoni M, Calligaro A, Ko MSH, Mauri P, Redi CA. Developmental arrest and mouse antral not-surrounded nucleolus oocytes. *Biol Reprod.* 2013;88:1–7. <https://doi.org/10.1095/bioreprod.112.103887>.
 34. Wu D Mouse Oocytes, A Complex Single Cell Transcriptome. *Front Cell Dev Biol.* 2022;10. <https://doi.org/10.3389/FCELL.2022.827937>.
 35. Zhang YR, Yin Y, Guo SM, Wang YF, Zhao GN, Ji DM, et al. The landscape of transcriptional profiles in human oocytes with different chromatin configurations. *J Ovarian Res.* 2024;17:99 <https://doi.org/10.1186/S13048-024-01431-2>.
 36. Böskén CA, Farnung L, Hintermair C, Schachter MM, Vogel-Bachmayr K, Blazek D, et al. The structure and substrate specificity of human Cdk12/Cyclin K. *Nat Commun.* 2014;5. <https://doi.org/10.1038/ncomms4505>.
 37. Cheng S-WG, Kuzyk MA, Moradian A, Ichu T-A, Chang VC-D, Tien JF, et al. Interaction of cyclin-dependent kinase 12/CrkR5 with cyclin K1 is required for the phosphorylation of the C-terminal domain of RNA polymerase II. *Mol Cell Biol.* 2012;32:4691–704. <https://doi.org/10.1128/MCB.06267-11>.
 38. Fan Z, Devlin JR, Hogg SJ, Doyle MA, Harrison PF, Todorovski I, et al. CDK13 cooperates with CDK12 to control global RNA polymerase II processivity. *Sci Adv.* 2020;6:eaz5041 <https://doi.org/10.1126/sciadv.aaz5041>.
 39. Niu T, Li K, Jiang L, Zhou Z, Hong J, Chen X, et al. Noncovalent CDK12/13 dual inhibitors-based PROTACs degrade CDK12-Cyclin K complex and induce synthetic lethality with PARP inhibitor. *Eur J Med Chem.* 2022;228:114012 <https://doi.org/10.1016/J.EJMECH.2021.114012>.
 40. Oqani RK, Lin T, Lee JE, Choi KM, Shin HY, Jin D. II. P-TEFb kinase activity is essential for global transcription, resumption of meiosis and embryonic genome activation in pig. *PLoS ONE.* 2016;11:e0152254 <https://doi.org/10.1371/JOURNAL.PONE.0152254>.
 41. Bowman EA, Kelly WG. RNA Polymerase II transcription elongation and Pol II CTD Ser2 phosphorylation: A tail of two kinases. *Nucleus.* 2014;5:224 <https://doi.org/10.4161/NUCL.29347>.
 42. Röther S, Sträßer K. The RNA polymerase II CTD kinase Ctk1 functions in translation elongation. *Genes Dev.* 2007;21:1409 <https://doi.org/10.1101/GAD.428407>.
 43. Ni Z, Ahmed N, Nabeel-Shah S, Guo X, Pu S, Song J, et al. Identifying human pre-mRNA cleavage and polyadenylation factors by genome-wide CRISPR screens using a dual fluorescence readthrough reporter. *Nucleic Acids Res.* 2024;52:4483–501. <https://doi.org/10.1093/NAR/GKAE240>.
 44. Jansova D, Koncicka M, Tetkova A, Cerna R, Malik R, del Llano E, et al. Regulation of 4E-BP1 activity in the mammalian oocyte. *Cell Cycle.* 2017;16:927–39. <https://doi.org/10.1080/15384101.2017.1295178>.
 45. Paynton BV, Rempel R, Bachvarova R. Changes in state of adenylation and time course of degradation of maternal mRNAs during oocyte maturation and early embryonic development in the mouse. *Dev Biol.* 1988;129:304–14. [https://doi.org/10.1016/0012-1606\(88\)90377-6](https://doi.org/10.1016/0012-1606(88)90377-6).
 46. De Leon V, Johnson A, Bachvarova R. Half-lives and relative amounts of stored and polysomal ribosomes and poly(A) + RNA in mouse oocytes. *Dev Biol.* 1983;98:400–8. [https://doi.org/10.1016/0012-1606\(83\)90369-X](https://doi.org/10.1016/0012-1606(83)90369-X).
 47. Juan HC, Lin Y, Chen HR, Fann MJ. Cdk12 is essential for embryonic development and the maintenance of genomic stability. *Cell Death Differ.* 2016;23:1038–48. <https://doi.org/10.1038/cdd.2015.157>.
 48. Federici S, Rossetti R, Moleri S, Munari EV, Frixou M, Bonomi M, et al. Primary ovarian insufficiency: update on clinical and genetic findings. *Front Endocrinol (Lausanne).* 2024;15:1464803 <https://doi.org/10.3389/FENDO.2024.1464803/BIBTEX>.
 49. Sokol ES, Pavlick D, Frampton GM, Ross JS, Miller VA, Ali SM, et al. Pan-Cancer Analysis of CDK12 Loss-of-Function Alterations and Their Association with the Focal Tandem-Duplicator Phenotype. *Oncologist.* 2019;24:1526–33. <https://doi.org/10.1634/THEONCOLOGIST.2019-0214/-/DC5>.
 50. Rouxel F, Relator R, Kerkhof J, McConkey H, Levy M, Dias P, et al. CDK13-related disorder: Report of a series of 18 previously unpublished individuals and description of an epigenetic signature. *Genet Med.* 2022;24:1096–107. <https://doi.org/10.1016/J.GIM.2021.12.016>.
 51. Wu Z, Zhang W, Chen L, Wang T, Wang X, Shi H, et al. CDK12 inhibition upregulates ATG7 triggering autophagy via AKT/FOXO3 pathway and enhances anti-PD-1 efficacy in colorectal cancer. *Pharmacol Res.* 2024;201. <https://doi.org/10.1016/J.PHRS.2024.107097>.
 52. Wang H, Wan H, Li X, Liu W, Chen Q, Wang Y, et al. Atg7 is required for acrosome biogenesis during spermatogenesis in mice. *Cell Res.* 2014;24:852–69. <https://doi.org/10.1038/CR.2014.70>.
 53. Castillo J, Knol JC, Korver CM, Piersma SR, Pham TV, de Goeij-de Haas RR, et al. Human Testis Phosphoproteome Reveals Kinases as Potential Targets in Spermatogenesis and Testicular Cancer. *Mol Cell Proteom.* 2019;18:5132 <https://doi.org/10.1074/MCP.RA118.001278>.
 54. Allingham-Hawkins DJ, Babul-Hirji R, Chitayat D, Holden JJA, Yang KT, Lee C, et al. Fragile X Premutation Is a Significant Risk Factor for Premature Ovarian Failure: The International Collaborative POF in Fragile X Study—Preliminary Data. *Am J Med Genet.* 1999;83:322. [https://doi.org/10.1002/\(SICI\)1096-8628\(19990402\)83:4<322::AID-AJMG17>3.0.CO;2-B](https://doi.org/10.1002/(SICI)1096-8628(19990402)83:4<322::AID-AJMG17>3.0.CO;2-B).
 55. Zhao H, Chen ZJ, Qin Y, Shi Y, Wang S, Choi Y, et al. Transcription Factor FIGLA is Mutated in Patients with Premature Ovarian Failure. *Am J Hum Genet.* 2008;82:1342–8. <https://doi.org/10.1016/J.AJHG.2008.04.018>.
 56. del Llano E, Masek T, Gahurova L, Pospisek M, Koncicka M, Jindrova A, et al. Age-related differences in the translational landscape of mammalian oocytes. *Aging Cell.* 2020:e13231. <https://doi.org/10.1111/accel.13231>.
 57. Ke H, Tang S, Guo T, Hou D, Jiao X, Li S, et al. Landscape of pathogenic mutations in premature ovarian insufficiency. *Nat Med.* 2023;29:483–92. <https://doi.org/10.1038/S41591-022-02194-3>.
 58. Luo W, Ke H, Tang S, Jiao X, Li Z, Zhao S, et al. Next-generation sequencing of 500 POI patients identified novel responsible monogenic and oligogenic variants. *J Ovarian Res.* 2023;16:1–13. <https://doi.org/10.1186/S13048-023-01104-6/TABLES/3>.
 59. Mok-Lin E, Ascano M, Serganov A, Rosenwaks Z, Tuschl T, Williams Z Premature recruitment of oocyte pool and increased mTOR activity in Fmr1 knockout mice and reversal of phenotype with rapamycin. *Sci Rep.* 2018;8. <https://doi.org/10.1038/S41598-017-18598-Y>.
 60. Jasti S, Warren BD, McGinnis LK, Kinsey WH, Petroff BK, Petroff MG. The Auto-immune Regulator Prevents Premature Reproductive Senescence in Female Mice. *Biol Reprod.* 2012;86:110 <https://doi.org/10.1095/BIOLREPROD.111.097501>.
 61. Liang LF, Soyal SM, Dean J. FIGa, a germ cell specific transcription factor involved in the coordinate expression of the zona pellucida genes. *Development.* 1997;124:4939–47.
 62. Day FR, Hinds DA, Tung JY, Stolk L, Styrkarsdottir U, Saxena R, et al. Causal mechanisms and balancing selection inferred from genetic associations with polycystic ovary syndrome. *Nat Commun.* 2015;6:1–7. <https://doi.org/10.1038/ncomms9464>.
 63. JSE L, JA V, AG U, WP V, JHJ. H Menopause: genome stability as new paradigm. *Maturitas n.d.*;92:15–23.
 64. Rodgers RJ, Laven JSE. Genetic relationships between early menopause and the behaviour of theca interna during follicular atresia. *Hum Reprod.* 2020;35:2185–7. <https://doi.org/10.1093/HUMREP/DEAA173>.
 65. Zhang C, Yu D, Mei Y, Liu S, Shao H, Sun Q, et al. Single-cell RNA sequencing of peripheral blood reveals immune cell dysfunction in premature ovarian insufficiency. *Front Endocrinol (Lausanne).* 2023;14. <https://doi.org/10.3389/FENDO.2023.1129657>.
 66. Liu D, Guan X, Liu W, Jia Y, Zhou H, Xi C, et al. Identification of transcriptome characteristics of granulosa cells and the possible role of UBE2C in the pathogenesis of premature ovarian insufficiency. *J Ovarian Res.* 2023;16:1–20. <https://doi.org/10.1186/S13048-023-01266-3/FIGURES/9>.
 67. Yu Z, Peng W, Li M. Exploring biomarkers of premature ovarian insufficiency based on oxford nanopore transcriptional profile and machine learning. *Sci Rep.* 2023;13:1–10. <https://doi.org/10.1038/s41598-023-38754-x>.
 68. Meskhi A, Seif MW. Premature ovarian failure. *Curr Opin Obstet Gynecol.* 2006;18:418–26. <https://doi.org/10.1097/01.GCO.0000233937.36554.D3>.
 69. Shelling AN. Premature ovarian failure. *Reproduction.* 2010;140:633–41. <https://doi.org/10.1530/REP-09-0567>.

70. Rossetti R, Ferrari I, Bonomi M, Persani L. Genetics of primary ovarian insufficiency. *Clin Genet*. 2017;91:183–98. <https://doi.org/10.1111/cge.12921>.
71. Coulam CB, Laws ER, Abboud CF, Randall RV. PRIMARY AMENORRHEA AND PITUITARY ADENOMAS. *Fertil Steril*. 1981;35:615–9. [https://doi.org/10.1016/S0015-0282\(16\)45551-2](https://doi.org/10.1016/S0015-0282(16)45551-2).
72. Kalantaridou SN, Davis SR, Nelson LM. PREMATURE OVARIAN FAILURE. *Endocrinol Metab Clin North Am*. 1998;27:989–1006. [https://doi.org/10.1016/S0889-8529\(05\)70051-7](https://doi.org/10.1016/S0889-8529(05)70051-7).
73. Fraison E, Crawford G, Casper G, Harris V, Ledger W. Pregnancy following diagnosis of premature ovarian insufficiency: a systematic review. *Reprod Biomed Online*. 2019;39:467–76. <https://doi.org/10.1016/j.rbmo.2019.04.019>.
74. Erickson GF, Shimasaki S. The role of the oocyte in folliculogenesis. *Trends Endocrinol Metab*. 2000;11:193–8. [https://doi.org/10.1016/S1043-2760\(00\)00249-6](https://doi.org/10.1016/S1043-2760(00)00249-6).
75. Dong J, Albertini DF, Nishimori K, Kumar TR, Lu N, Matzuk MM. Growth differentiation factor-9 is required during early ovarian folliculogenesis. *Nature*. 1996;383:531–5. <https://doi.org/10.1038/383531A0>.
76. Aaltonen J, Laitinen MP, Vuojolainen K, Jaatinen R, Horelli-Kuitunen N, Seppä L, et al. Human growth differentiation factor 9 (GDF-9) and its novel homolog GDF-9B are expressed in oocytes during early folliculogenesis. *J Clin Endocrinol Metab*. 1999;84:2744–50. <https://doi.org/10.1210/JCEM.84.8.5921>.
77. Bodensteiner KJ, Clay CM, Moeller CL, Sawyer HR. Molecular cloning of the ovine Growth/Differentiation factor-9 gene and expression of growth/differentiation factor-9 in ovine and bovine ovaries. *Biol Reprod*. 1999;60:381–6. <https://doi.org/10.1095/BIOLREPROD60.2.381>.
78. Jaatinen R, Laitinen MP, Vuojolainen K, Aaltonen J, Louhio H, Heikinheimo K, et al. Localization of growth differentiation factor-9 (GDF-9) mRNA and protein in rat ovaries and cDNA cloning of rat GDF-9 and its novel homolog GDF-9B. *Mol Cell Endocrinol*. 1999;156:189–93. [https://doi.org/10.1016/S0303-7207\(99\)00100-8](https://doi.org/10.1016/S0303-7207(99)00100-8).
79. Isola JVV, Ocañas SR, Hubbart CR, Ko S, Mondal SA, Hense JD, et al. A single-cell atlas of the aging mouse ovary. *Nat Aging*. 2024;4:145–62. <https://doi.org/10.1038/s43587-023-00552-5>.
80. Houles T, Lavoie G, Nourredine S, Cheung W, Vaillancourt-Jean É, Guérin CM, et al. CDK12 is hyperactivated and a synthetic-lethal target in BRAF-mutated melanoma. *Nat Commun*. 2022;13:1–16. <https://doi.org/10.1038/s41467-022-34179-8>.
81. Yagel S, Gullo G, Ospedaliera A, Riuniti Villa O, Cervello S, Gonfloni S, et al. Signaling pathway intervention in premature ovarian failure. *Front Med*. 2022;9:999440 <https://doi.org/10.3389/FMED.2022.999440>.
82. Tetkova A, Hancova M. Mouse Oocyte Isolation, Cultivation and RNA Microinjection. *BIO-PROTOCOL* 2016. <https://doi.org/10.21769/bioprotoc.1729>.
83. Jansova D, Aleshkina D, Jindrova A, Iyyappan R, An Q, Fan G, et al. Single Molecule RNA Localization and Translation in the Mammalian Oocyte and Embryo. *J Mol Biol*. 2021;433. <https://doi.org/10.1016/J.JMB.2021.167166>.

ACKNOWLEDGEMENTS

We wish to thank J. Supolikova and M. Hancova for technical assistance. We also thank to A. Jindrova, R. Iyyappan and K. Kakavand for critical reading of the manuscript. The authors used the services of the Czech Center for Phenogenomics at IMG supported by the Czech Academy of Sciences RVO 68378050 and the project

LM2023036. This work was supported by GACR 22-27301S, EXCELLENCE [CZ.02.1.01/0.0/0.0/15_003/0000460 OP RDE], Strategie VP38 AV21, Institutional Research Concept RVO67985904, National Institute for Cancer Research (Programme EXCELES, ID Project No. LX22NPO5102)—Funded by the European Union—Next Generation EU and V. Sedmikova by IGA from IAPG 2022.

AUTHOR CONTRIBUTIONS

D.J.: Supervision, Conceptualization, Investigation, Validation, Methodology, Writing—original draft, review & editing. Project administration. V.S.: Validation, Methodology, Investigation. F.B.: Validation, Methodology, Investigation, review & editing. D.A.: Validation, Methodology, Investigation. M.D.: Investigation. M.K.: Funding acquisition, editing. J.R.: Methodology. J.R.: Methodology. J.K.: Writing—original draft, review & editing. A.S.: Conceptualization, Supervision, Funding acquisition, Writing—original draft, review & editing.

COMPETING INTERESTS

The authors declare no competing interests.

ADDITIONAL INFORMATION

Supplementary information The online version contains supplementary material available at <https://doi.org/10.1038/s41419-025-07536-w>.

Correspondence and requests for materials should be addressed to Denisa Jansova or Andrej Susor.

Reprints and permission information is available at <http://www.nature.com/reprints>

Publisher's note Springer Nature remains neutral with regard to jurisdictional claims in published maps and institutional affiliations.



Open Access This article is licensed under a Creative Commons Attribution 4.0 International License, which permits use, sharing, adaptation, distribution and reproduction in any medium or format, as long as you give appropriate credit to the original author(s) and the source, provide a link to the Creative Commons licence, and indicate if changes were made. The images or other third party material in this article are included in the article's Creative Commons licence, unless indicated otherwise in a credit line to the material. If material is not included in the article's Creative Commons licence and your intended use is not permitted by statutory regulation or exceeds the permitted use, you will need to obtain permission directly from the copyright holder. To view a copy of this licence, visit <http://creativecommons.org/licenses/by/4.0/>.

© The Author(s) 2025